8524
P Wilson

SANDIA REPORT

SAND88—1008 • UC—92
Unlimited Release
Printed May 1988

Multiwell Experiment Final Report: II. The Paludal Interval of the Mesaverde Formation

Multiwell Experiment Project Groups,
at Sandia National Laboratories and CER Corporation

Prepared by
Sandia National Laboratories
Albuquerque, New Mexico 87185 and Livermore, California 94550
for the United States Department of Energy
under Contract DE-AC04-76DP00789

Issued by Sandia National Laboratories, operated for the United States Department of Energy by Sandia Corporation.

Printed in the United States of America
Available from
National Technical Information Service
U.S. Department of Commerce
5285 Port Royal Road
Springfield, VA22161

NTIS price codes
Printed copy: A24
Microfiche copy: A01

SAND88-1008
Unlimited Release
UC Category 92

MULTIWELL EXPERIMENT FINAL REPORT: II. THE PALUDAL INTERVAL OF THE MESAVERDE FORMATION

Compiled by the
Multiwell Experiment Project Groups
at
Sandia National Laboratories
Albuquerque, NM 87185
and
CER Corporation
Las Vegas, NV 89109
for the
U. S. Department of Energy

May 1988

ABSTRACT

The Department of Energy's Multiwell Experiment (MWX) is a field laboratory in the Piceance Basin of Colorado which has two overall objectives: to characterize the low permeability gas reservoirs in the Mesaverde Formation and to develop technology for their production. Different depositional environments have created distinctly different reservoirs in the Mesaverde, and MWX has addressed each of these in turn. This report presents a comprehensive summary of results from the paludal interval which lies between 6600 ft and 7450 ft at the MWX site. The interval is a complex, lower delta plain, fluvial depositional environment consisting of interbedded sandstone channels, carbonaceous siltstones and mudstones, and coals. Separate sections of this report are background and summary; site descriptions and operations; geology; log analysis; core analysis; in situ stress; well testing and analysis of one zone; well testing, stimulation, analysis and reservoir evaluation of another zone; supporting laboratory studies; hydraulic fracture diagnostics; and a bibliography. Additional detailed data, results, analyses, and data file references are given on microfiche in several appendices. Overall, the results show that the paludal is a complex and productive interval.

CONTENTS

		Page
1.0	BACKGROUND AND SUMMARY David A. Northrop, Sandia National Laboratories	
1.1	Introduction	1.1
1.2	Geologic Setting	1.2
1.3	MWX Description	1.4
1.4	The Paludal Interval	1.4
1.5	Activity Summaries	1.5
1.6	Significant Accomplishments	1.19
1.7	Acknowledgments	1.21
1.8	References	1.22
2.0	SITE DESCRIPTION AND OPERATIONS W. J. Mathis and F. Richard Myal, CER Corporation	
2.1	Well Drilling and Well Descriptions	2.1
2.2	Chronology of Paludal Operations	2.2
2.3	References	2.18
3.0	GEOLOGY J. C. Lorenz, Sandia National Laboratories	
3.1	Introduction	3.1
3.2	Lithology	3.1
3.3	Reservoir Sedimentology and Morphology	3.4
3.4	Organic Content and Maturation Level	3.7
3.5	Fractures	3.8
3.6	Fault in the MWX Area	3.8
3.7	References	3.9

4.0 LOG ANALYSIS

G. C. Kukal, CER Corporation

4.1	Database and Analysis Models	4.1
4.2	Fault at MWX Site	4.2
4.3	Formation Evaluation	4.3
4.4	Fracture Analysis	4.8
4.5	Mechanical Properties: Closure Stress	4.10
4.6	Cement Evaluation	4.10
4.7	Additional Information	4.11
4.8	References	4.11

5.0 CORE ANALYSIS

A. R. Sattler, Sandia National Laboratories

5.1	Introduction	5.1
5.2	Core Program	5.3
5.3	Core Handling and Preparation	5.4
5.4	Core Analyses, Results, and Discussion	5.5
5.5	Correlations with Borehole Televiewer and Caliper Data	5.10
5.6	References	

6.0 IN SITU STRESS

N. R. Warpinski, Sandia National Laboratories

6.1	Objective	6.1
6.2	In Situ Stress Measurements	6.1
6.3	Stress Tests Results	6.4
6.4	ASR Data and Results	6.10
6.5	Hydraulic Fracture Containment	6.14
6.6	Correlation with Rock Properties	6.14
6.7	Summary	6.15
6.8	References	6.16

7.0 WELL TESTING AND ANALYSIS, PALUDAL ZONE 2
P. T. Branagan, CER Corporation

7.1 Testing 7.1
7.2 Analysis 7.3
7.3 References 7.5

8.0 STIMULATION EXPERIMENT--ZONES 3 AND 4

8.1 Prefrac Testing, P. T. Branagan, CER Corporation

8.1.1 Description 8.1.1
8.1.2 Well Testing MWX-2 Fault 8.1.3
8.1.3 MWX-1 Production/Interference Testing 8.1.3
8.1.4 Reservoir Modeling--Homogeneous Model 8.1.5
8.1.5 Reservoir Modeling--Natural Fracture Model 8.1.6
8.1.6 References 8.1.9

8.2 Stimulation--Phase I, N. R. Warpinski, Sandia National Laboratories

8.2.1 Objectives 8.2.1
8.2.2 Design 8.2.1
8.2.3 Well Configuration and Instrumentation 8.2.2
8.2.4 Schedule 8.2.3
8.2.5 Step Rate Test 8.2.3
8.2.6 First Flowback Test 8.2.3
8.2.7 Pump-In/Flowback Test 8.2.4
8.2.8 Temperature Survey #1 8.2.5
8.2.9 Minifrac #1 8.2.5
8.2.10 Temperature Survey #2 8.2.6
8.2.11 Nolte Analysis of Minifrac #1 8.2.6
8.2.12 Minifrac #2 8.2.9
8.2.13 Temperature Survey #3 8.2.10

8.2.14 Analysis of Minifrac #2 8.2.10
8.2.15 Analysis Using Pressure History Matches 8.2.11
8.2.16 Discussion of Minifracs 8.2.15
8.2.17 References 8.2.15

8.3 Interim Well Testing, P. T. Branagan, CER Corporation

8.3.1 Well Testing 8.3.1
8.3.2 Analysis 8.3.2
8.3.3 Load Water Recovery 8.3.3
8.3.4 Reference 8.3.3

8.4 Stimulation--Phase II, N. R. Warpinski, Sandia National Laboratories

8.4.1 Objectives 8.4.1
8.4.2 Design 8.4.2
8.4.3 Well Configuration and Instrumentation 8.4.3
8.4.4 Treatment Procedure 8.4.4
8.4.5 Data 8.4.4
8.4.6 Nierode Analysis 8.4.6
8.4.7 Nolte Pressure Decline Analysis 8.4.8
8.4.8 Postfrac Surveys 8.4.8
8.4.9 Pressure History Match Analysis 8.4.9
8.4.10 Discussion of Stimulation Experiments 8.4.10
8.4.11 References 8.4.11

8.5 Remedial Treatment, P. T. Branagan, CER Corporation

8.5.1 Treatment 8.5.1
8.5.2 Injection Interference Testing 8.5.2
8.5.3 Treatment Results 8.5.3

8.6. Postfrac Well Testing, P. T. Branagan, CER Corporation

8.6.1 MWX-1 Production/Interference Testing 8.6.1
8.6.2 Reservoir Modeling and History Matching 8.6.3

8.7 Reentry Well Testing, P. T. Branagan, CER Corporation

8.7.1 Testing 8.7.1
8.7.2 Modeling and Analysis 8.7.3
8.7.3 Reference 8.7.4

8.8 Summary and Conclusions 8.8.1

9.0 LABORATORY STUDIES
Allan R. Sattler, Sandia National Laboratories

9.1 Introduction 9.1
9.2 Laboratory Studies before the Phase I Stimulation 9.2
9.3 Laboratory Studies before the Phase II Stimulation 9.4
9.4 Laboratory Studies after the Phase II Stimulation and the Remedial Treatment 9.7
9.5 Water Analysis 9.12
9.6 Integration of Results and Discussion of Damage Mechanisms 9.15
9.7 References 9.19

10.0 BOREHOLE SEISMIC ANALYSIS OF PALUDAL STIMULATION
Billy J. Thorne, Sandia National Laboratories

10.1 Phase I 10.1
10.2 Phase II 10.7
10.3 References 10.14

11.0 BIBLIOGRAPHY, Sharon J. Finley, Sandia National Laboratories 11.0

12.0 APPENDICES

12.1 Geophysics Final Report, C. A. Searls (Sandia)
12.2 Petrographic Data Sheets (Bendix)

12.3 Paludal Log Report, See
12.4 Core Laboratories Data Microfiche
12.5 Institute of Gas Technology (IGT) Data Inside Back
12.6 RESPEC Data Cover
12.7 Well Test Data (CER)
12.8 Phase II Liquid Recovery and Analyses (CER)
12.9 Paludal MWX Data File Entries, S. J. Finley (Sandia)

1.0 BACKGROUND AND SUMMARY

David A. Northrop
Sandia National Laboratories

1.1 INTRODUCTION

New and improved technology is required to enhance natural gas production from the low permeability reservoirs of the United States. This is a large potential resource with an estimated maximum recoverable resource of over 600 TCF.[1] The U.S. Government's efforts to stimulate production from these reservoirs began in the mid-1960's. The early work evaluated the use of nuclear explosives for fracturing, but this technique was abandoned in 1973. Efforts then focused upon massive hydraulic fracturing and several government-industry projects were conducted. The results were disappointing and did not result in either an improved technology or confident, commercial production. The basic shortcoming was that these past field tests provided insufficient data to define the critical factors affecting gas production from this resource.

The U. S. Department of Energy's Multiwell Experiment (MWX) was conceived as a field laboratory to obtain sufficient information on the geologic and technical aspects to unlock this resource. A key feature of MWX is three wells between 110 and 215 ft apart. Detailed core, log and well test data from such close spacings provide a detailed characterization of the reservoir. Interference and tracer tests as well as the use of fracture diagnostics in offset wells, give additional, out-of-the-ordinary information on stimulation and production. A second key is the synergism resulting from a broad spectrum of activities: geophysical surveys, sedimentological studies, core and log analyses, well testing, in situ stress determinations, stimulation, fracture diagnostics, and reservoir analyses. All these activities are further enhanced by the closely spaced wells. Thus, the Multiwell Experiment provides a unique opportunity for

understanding and developing economic production from tight gas reservoirs. The long-term research program under way at this facility is managed by DOE's Morgantown Technology Center.

Further discussion of the rationale, plans, objectives, and activities of MWX can be found in References 2-5. The intent of this report is to compile results from activities associated with one interval--the paludal--at the MWX site. A final report for the marine interval has been completed.[6] Similar final reports will be compiled for the coastal and fluvial intervals as well.

1.2 GEOLOGIC SETTING

The Multiwell Experiment's focus is the Mesaverde Formation in the Piceance basin of northwest Colorado. This thick sequence was deposited during the late Cretaceous age over a broad region of the western United States and contemporaneous formations are found in the Green River, Wind River, Uinta and San Juan basins. The great extent and thickness of these gas-containing deposits represent a significant natural gas resource.[1]

At the MWX site, the Mesaverde Formation lies at a depth of 4000 to 8250 ft, between the overlying Wasatch Formation and the underlying Mancos Shale (Figure 1.1). The Mesaverde is exposed in outcrop at Rifle Gap in the Grand Hogback, approximately 11 miles northeast of the MWX site, and the outcrops have given excellent insight into the subsurface geology at the site. The sandstones stand out clearly in outcrop and sedimentological studies have been performed on them. These studies show that the Mesaverde can be divided into five distinct intervals based upon different depositional environments and resulting sandstone morphologies.[7,8]

(1) The lowest interval, the marine, (7450-8250 ft) was formed immediately on either side of an oscillating coastline and is

composed of widespread shoreline-to-marine blanket sandstones, marine shales, and paralic coals. This interval contains the Corcoran, Cozzette, and Rollins Sandstones which are interspersed with Mancos Shale.

(2) The paludal interval (6600-7450 ft) lies above the Rollins Sandstone and contains thick, abundant coal deposits. These are interspersed with lenticular, distributary channel and splay sandstones formed in a lower delta plain environment. The sand percentage in this zone is markedly lower (26%) than other intervals (40%), and channel widths are probably 250-500 ft. This interval is the focus of this report.

(3) The coastal interval (6000-6600 ft) is characterized by distributary channel sandstones deposited in an upper delta plain environment. Most of these sandstones are probably 250-500 ft in width and are interbedded with carbonaceous mudstones and siltstones.

(4) The fluvial interval (4400-6000 ft) consists of irregularly shaped, multistory, composite sandstones which were deposited by broad meandering stream systems. These sandstones have widths on the order of 1000-2500 ft and contain abundant internal discontinuities.

(5) The uppermost interval, the paralic, (4000-4400 ft) is a zone of returned marine influence with more widespread, uniform sandstones. The interval is believed to be water-saturated at the MWX site.

Specific sandstones in the shoreline/marine, paludal, coastal and fluvial intervals have been the focus of separate MWX investigations.

1.3 MWX DESCRIPTION

The Multiwell Experiment field laboratory is located in the Rulison Field in the east central portion of the Piceance basin in northwestern Colorado. The site is located in the SW 1/4, NW 1/4, Sec. 34, T6S, R94W, Garfield County, and it is seven miles southwest of Rifle and just south of the Colorado River. Agreements on the lease and with landowners were obtained in mid-1981 and work at the site began in August of that year. A chronology of MWX activities is given in Figure 1.2.

Three wells were drilled: MWX-1 to a depth of 8350 ft in September-December 1981,[9] MWX-2 to a depth of 8300 ft in January-March 1982,[10] and MWX-3 to a depth of 7565 ft in June-August 1983.[11] Over 4100 ft of 4-in core, approximately 1135 ft of it oriented, were cut with a recovery of >99%. Numerous logging programs containing both standard and experimental logs were conducted. An overview of the coring and logging activities in all three wells in relation to the Mesaverde section at the site is given in Figure 1.3. The three wells are exceptionally straight as seen in Figure 1.4; relative separations are between 110 and 215 ft within the Mesaverde. Significant gas shows were encountered throughout the section in all three wells and mud weights as high as 15 lbs/gal were required to maintain well control. Wells were drilled as near balanced conditions as possible to minimize invasion.

The entire Mesaverde at the MWX site as seen by gamma ray logs in the three wells is shown in Figure 1.5.

1.4 THE PALUDAL INTERVAL

The paludal interval lies between 6600 and 7450 ft and is shown in detail in Figure 1.6. Initially, the paludal was not a specific interval of interest since it was not being produced in the vicinity of the MWX

site. However, based upon the gas shows encountered during drilling and the analyses of MWX-1 logs, the paludal interval became a major focus of MWX activities. Thus, core was taken in interesting zones encountered while drilling MWX-2 and MWX-3. Testing and stimulation activities were conducted in this interval over a 14-month period in 1983-84, and the interval was revisited and retested in 1986. This complex and potentially productive interval became an interesting and challenging target of the Multiwell Experiment.

This coal-bearing sequence in the Piceance basin is receiving considerable interest as a coal-bed methane resource. For example, the Deep Coal Seam Project sponsored by the Gas Research Institute has investigated the characteristics and gas production of the Cameo coal group at a site 2 miles east of Collbran, CO, about 18 miles SSW of the MWX site.[12] This project is currently active in the same coal group at Tenneco's East Divide Creek unit 8 miles SE of Silt, CO, about 18 miles ESE of the MWX site. The Cameo coal group is a sequence of coal seams and interbedded sandstones and shales directly relatable to the interval between 7000 and 7450 ft at MWX. It is interesting to note that in coal-bed methane technology, the coal seam is considered to be the reservoir which is bounded by sandstones and shales, where at MWX coal seams often abut the sandstone reservoir rock. The consequences of the possible interactions between these distinct reservoir types are not fully recognized or understood.

1.5 ACTIVITY SUMMARIES

The results of MWX activities conducted in the paludal interval of the Mesaverde are presented in separate sections of this report; each are authored by the principal investigator. Summaries of these sections are presented here.

1.5.1 Geology (Section 3.0)

The rocks of the paludal interval were deposited in environments of lenticular distributary channels and adjacent coal swamps. Sandstones occur as both channel fillings and splay (or flood) deposits adjacent to the channels. The swamps are recorded as mudstone, carbonaceous mudstone, and coal deposits. These environments were located on a prograding lower delta plain that was landward of the Rollins shoreline.

Five major sandstones were identified in the paludal interval and these were designated zone 1 (deepest) through zone 5 (shallowest). Core (where available) and log data from the three wells were analyzed from a sedimentological standpoint and these resulted in the following interpretations of the lithology and morphology for each of the five zones. Zone widths were estimated by correlation percentages between wells and by empirical relationships between channel thickness and width for this depositional environment as measured in outcrop.

- Zone 1 is a distributary channel. Channel margin deposits are present in all wells. The main channel probably runs E-W and lies south of the three wells. No well tests or stimulations were conducted in this relatively thin zone.

- Zone 2 is a distributary channel which abruptly overlies a coal seam. The thickest, most uniform sandstone is present in MWX-1, proximal levee deposits are present in MWX-2, and channel-margin deposits are present in MWX-3. The channel's width is estimated to be 550 ft and it probably runs NNE-SSW through MWX-1. Limited well tests were conducted in this relatively thick zone (Section 7.0).

- Zone 3 is also a distributary channel which abruptly overlies a coal seam. Main channel sandstones are present in all three wells, but are thinner in MWX-3. The channel's width is estimated to be 350 ft and it probably runs NE-SW through MWX-1 and MWX-2. Zone 3, together with zone 4, was the focus of extensive well testing and stimulation activities (Section 8.0).

- Zone 4 is a splay or floodplain deposit. The splay has about the same thickness in MWX-1 and MWX-3 and it thins significantly towards MWX-2. No size estimate is possible for this distinctly different deposit.

- Zone 5 is a distributary channel. Main channel sandstones are present in MWX-1 and MWX-2 and channel-margin deposits are present in MWX-3. The channel's width is estimated to be 200 ft and it runs probably WNW-ESE through MWX-1 and MWX-2.

Sandstone petrology (grain size, composition, and diagenetic history) is the primary control on reservoir porosity and matrix permeability. The sandstones are "dirty," and contain a high proportion of lithic fragments. The associated clays are primarily mixed-layer illite/montmorillonite, with some illite, and a trace of chlorite. Diagenesis includes, in approximate chronological order: early carbonate cementation, feldspar alteration, compaction, quartz precipitation, development of secondary porosity, later calcite precipitation, formation of authigenic clays, dolomitization, and later quartz precipitation.

The paludal is an organic-rich interval with significant coal beds, thinner coal seams and carbonaceous mudstones. The coals are low-volatile bituminous with rank increasing somewhat with depth. Isotopic and chemical gas analyses indicate that the gas in the paludal originated from the coals and organics within the interval itself.

Twenty-five mineralized fractures were observed in core from the paludal interval. While 19 of these occur in sandstones, only two were found in the thicker sandstone zones. Most are thin fractures which are completely filled with calcite. Several fractures contain an earlier phase of quartz deposition. Four fractures whose orientations are known have a general east-west strike.

Finally, there is evidence that a normal fault is present in MWX-2, most likely at 7055-7070 ft, and which dips to the southwest at an angle greater than 87°. Evidence includes a 10 ft shortening of the section in MWX-2 relative to the other two wells and a dipmeter log showing indications of possible drag deformation.

1.5.2 Log Analysis (Section 4.0)

Extensive logging programs were conducted during the drilling of the MWX wells. As seen in Figure 1.3, only a portion of the paludal section was logged more than once in each of the wells. The well logs were analyzed with TITEGAS, a tight gas sandstone log interpretation model developed in conjunction with the MWX log data base.[13]

Six sandstone units in the paludal section have good reservoir quality and thickness in at least two of the three wells. A summary of the log analyses for these zones is given in Table 1.1. It is difficult to make a uniform assessment for each zone due to the well-to-well variability. Based on these and core data, well tests were conducted in zone 2 in MWX-1, and a stimulation experiment and associated well tests were conducted in zones 3 and 4 together.

The log analyses included the opportunity to compare several natural fracture identification logs in MWX-3 and to indicate which zones appeared naturally fractured. Also, estimates for closure stresses were obtained from sonic log data.

1.5.3 Core Analysis (Section 5.0)

Limited 4-in diameter core was taken in the paludal interval: 230 ft at the top of the paludal (considerably above zone 5) in MWX-1, 298 ft in MWX-2 through zones 1-4, and 122 ft (oriented) in zones 3, 4 and 5 in MWX-3. Core samples were distributed to participants in a comprehensive core analysis program.[14] Both routine and special core analyses for reservoir properties were made at frequent intervals in the sandstones. Many analyses also extended above and below the sandstones so that properties are also available for the bounding lithologies.

A summary of the core-derived reservoir properties for the paludal sandstones is given in Table 1.2. Sandstone porosities are on the order of 8%-10%, water saturations are low at 25%-35%, and dry Klinkenberg permeabilities are 2-8 μd (at 2000 psi effective confining stress). The permeabilities are a strong function of water saturation and decrease somewhat with increasing net stress. The dry Klinkenberg permeabilities would be reduced by a factor of 3.5-3.7 at the measured water saturations; thus 0.5-2 μd is a realistic estimate of the true in situ matrix permeability. In addition, capillary pressures greater than 1000 psi were found at the prevailing water saturations.

The mechanical properties reflect the complex lithology of the paludal interval. Young's moduli (at 20 MPa (2850 psi) confining pressure) range from 18.4 to 40.3 GPa (2.6 to 5.8x10^6 psi), Poisson's ratios from 0.13 to 0.23, and fracture toughnesses from 0.4 to 1.5 MPa$\bullet m^{-1/2}$. However, it is difficult to make any firm correlations of the mechanical rock properties between sandstones and the confining shales; this is clearly seen in the observed moduli range for sandstones of 18-40 GPa and the "shales" of 18-30 GPa.

Other core analyses included vertical permeabilities, capillary pressure, caprock analyses, compressibility, triaxial tests for compressive strength, tensile strength, CEC, formation factor, and resistivity index. Several special analyses were also made upon coal core samples. Core samples were also used in other MWX activities such as sedimentology, mineralogy/petrology, natural fractures, in situ stress, and laboratory work supporting stimulation; these activities are reported in their respective sections of this report.

1.5.4 In Situ Stress Measurements and Analysis (Section 6.0)

Several different stress-related measurements were made in the paludal interval. Cased hole stress tests were conducted in MWX-2 and MWX-3 at a total of twelve depths in and between the different zones. These tests were repeated small volume hydraulic fractures (<100 gal) conducted through perforations under conditions where the instantaneous shut-in pressure is nearly equal to the minimum in situ stress.[15] Breakdowns of MWX-1 and MWX-3 and a flowback test in MWX-1 provided additional stress information. The measured minimum in situ stress and frac gradients are summarized in Table 1.3. The rapid variation of lithology, especially in the confining rocks, affects the quality of these measurements as compared to similar data in the marine interval. Generally there is no good correlation between rock type, rock properties, and the measured stresses. The data show that the selected stimulation interval, zones 3 and 4, have stresses some 1000-1200 psi lower than the confining rocks. The underlying high stress region is thick and offers a good containment feature for hydraulic fracturing, but the overlying region is relatively thin and offers less containment.

Anelastic strain recovery (ASR) measurements were made on oriented core.[16] The primary ASR result is the direction of the maximum horizontal in situ stress, which is the azimuth of a hydraulic fracture. Two

sandstone samples each from zones 3 and 5 in MWX-3 gave an azimuth of N54°W, respectively. (Borehole seismic instrumentation during stimulation of zones 3 and 4 gave an azimuth of N67±8°W[17] (Section 10.0).) Stress magnitudes were also calculated from ASR data via two different procedures: one a direct method of calculating stresses from the principal strains,[18] and the other a strain history method based on a least squares fit of a viscoelastic model to the entire strain data.[19] These data indicate the difference in horizontal stresses in the sandstones is 600-800 psi, whereas the difference in the shales is negligible.

1.5.5 Well Testing and Analysis, Paludal Zone 2 (Section 7.0)

A limited series of well tests were performed in zone 2 to determine its reservoir characteristics. The zone in MWX-1 was perforated between 7256 and 7284 ft and broken down with KCl water. A several day clean-up period was followed by two production-buildup cycles as seen in Figure 1.7. Sustainable rates after several days were on the order of 140-160 MCFD. Analysis of the buildup data by analytical and numerical techniques indicated: (1) the presence of a no-flow boundary that was consistent with the possible fault running near MWX-2 and parallel to the maximum horizontal stress direction (~N70°W), and (2) an average reservoir permeability of 50 μd. This permeability is significantly greater than 0.5-2 μd permeability of the matrix rock measured in core and indicates the paludal sandstones are naturally fractured.

1.5.6 Stimulation Experiment Zones 3 and 4 (Section 8.0)

The major focus of paludal activities was a stimulation experiment conducted in zones 3 and 4.[20] MWX-1 was the production/stimulation well. MWX-2 and MWX-3 were also perforated in each zone and served a interference/observation wells. The sequence of activities included: prefrac production/interference testing; Phase I stimulation tests; an

interim testing period; Phase II stimulation--a propped hydraulic fracture treatment--and cleanup; a remedial treatment and cleanup; postfrac production/interference testing; and a final production test when the interval was reentered after an 18 month shut-in. In addition, core, log, geologic, stress, laboratory and borehole seismic activities all supported the stimulation experiment.

Prefrac production/interference tests were conducted to obtain baseline reservoir behavior, and the data are shown in Figure 1.8. Sustainable production was approximately 250 MCFD at a bottomhole pressure around 800 psi. Horner analysis of the seven-day buildup data gave a bulk reservoir permeability of 36 μd, a value which indicated that interference should have been seen in the observation wells early in the test. However, no correlatable pressure changes were observed and reasons for the lack of interference must be considered. A series of parametric simulations with a homogeneous model failed to produce a lack of measurable interference. Thus, an advanced naturally fractured reservoir simulator was used,[21] and an anisotropic fracture permeability of 100:1 with a maximum permeability direction of N75°W provided a satisfactory match.[22] However, when all postfrac data were considered, the most consistent fit was found for a 10:1 anisotropy (5000 and 500 md fracture permeabilities) and a 1 μd matrix permeability.[23]

The Phase I stimulation tests were conducted to obtain design information for the main treatment (Phase II) and served as a first attempt to map fracture behavior in a lenticular reservoir via borehole seismic techniques. These tests conducted by Smith Energy Services over a four-day period in early December 1983 consisted of a step rate and flowback test, pump-in and flowback test, and two minifracs of different fluid and size (15,000 gal of 30 lb/1000 gal HPG-gelled fluid and 30,000 gal of 60 lb/1000 gal HPG-gelled fluid, each with a methanol prepad). The preliminary tests gave minimum stresses of 5800-6000 psi,

with slightly higher values with each succeeding test. Unexpectedly high fracturing pressures were attained during both minifracs: 900 and 1100 psi above the 5900 psi closure stress. Nolte pressure decline analysis of the shut-in data gave wing lengths of 242 and 440 ft for the two minifracs, leakoff coefficients of 0.0013 and 0.0007 ft/$\sqrt{}$min and good fluid efficiencies of 65% and 78%. Fracture height growth was limited as both temperature logs and borehole seismic data gave heights of 135 and 150 ft. Additional insight into the stimulation was obtained by matching the fracture pressure history with a fracture simulator based upon treatment parameters, stress data, and the inferred fractured geometry.

After a limited flowback period and twice-weekly flowing of MWX-1 during the winter shut-in, a month-long test period shown in Figure 1.9 was conducted prior to the Phase II stimulation. Sustainable production was approximately 200 MCFD at a bottomhole pressure of 600 psi. Horner analysis of the buildup data gave a kh of 0.64 md-ft and a skin of -3.8. These results indicate somewhat degraded performance (250 MCFD, 0.95 md-ft and a small positive skin of 0.59 had been measured during pre-Phase I testing), but the negative skin indicates a stimulated wellbore. Analytical type curve methods were used to assess the unpropped fracture: the derived fracture conductivity was 7.14 md-ft with an 80-100 ft wing length.

The Phase II stimulation was a single propped hydraulic fracture conducted on May 2, 1984 by the Western Company. The treatment consisted of a 7700 gal methanol prepad, 65,000 gal of cross-linked HPG-gelled fluid (at concentrations of 25-40 lb/1000 gel), and 193,000 lbs of 20/40 sand proppant (at concentrations of 1.5-5.5 lb/gal). The job was pumped in nine stages at a nominal 20 bbl/min. The design fracture height was 200 ft with a 500 ft propped wing length. Postfrac surveys provided limited data but were consistent with a 180 to 200 ft frac height. The pressure decline analysis indicated a very early frac closure, probably

due to the proppant settling out sooner than expected. This analysis, for a 180 ft frac height, gave a wing length of 520 ft, an average width of 0.59 in, a leakoff coefficient of 0.00123 ft/$\sqrt{}$min, and a fluid efficiency of 74%. A frac pressure history match (Figure 1.10) gives slightly greater estimates of length (600 ft) and height (250 ft). As before, very high treatment pressures were observed--as high as 7500 psi, or 1600 psi above closure, by the end of the treatment. Such high pressures could be the result of several factors such as complex fracturing, boundary-limited frac growth, back stresses, or higher stress regions. Whatever the cause, high pressures result in wider, shorter fractures and a higher leakoff and potential for damage.

Month-long attempts to flow back the well, along with several operational problems, resulted in poor additional fluid recovery and less than 50 MCFD production rates. Short buildup tests suggested a very short (~10 ft) fracture as if it were clogged or bridged. Analysis of the returned fluids indicated the possibility of unbroken gel. Thus, a remedial treatment of 6500 gal of KCl water containing a high breaker concentration (135 lb/1000 gal) and 1000 gal of 3% hydrogen peroxide was conducted at 1-2 bbl/min at pressures below 6000-6200 psi. (Interestingly, an almost-immediate, small (2-3 psi), but distinct, pressure increase was observed in MWX-2, which is most likely a poroelastic response.) Post-treatment response was again slow until the tubing was extended below the perforated interval and a packer inserted to control bottomhole pressures. This caused an immediate return of 50 bbl of liquid and significantly increased flow.

The subsequent postfrac production interference test period is shown in Figure 1.11. Sustainable flow rates were about 150 MCFD at bottomhole pressures of 1200-1500 psi. These rates are significantly less than the 250 and 200 MCFD rates observed during the prefrac and interim testing, respectively. Again, no directly correlatable pressure interference was

seen in the bottomhole pressures in the two observation wells. Analysis of the final buildup data indicted the presence of a fairly conductive fracture, but that it had only a 65-100 ft half length, considerably less than designed. A reservoir simulator was again applied to address questions of narrow channels, short frac lengths, and damage adjacent to the frac.[22] The results of several studies indicate that the reservoir permeability due to the natural fractures system (~35 μd) had probably been diminished to at least the matrix value of 1-2 μd. The extent of this damaged zone prevented any production increase due to the propped fracture. The fracture's productive wing length was estimated at 75 ft and its conductivity a minimum of 16 md-ft; however, this wing length could also be the half-width of the channel.

After these tests, bridge plugs were set in mid-August, 1984, above these paludal zones and MWX activities moved up to the coastal interval. However, in December 1985 paludal zones 3 and 4 were reentered with the intent of an extended production test during the winter site shutdown. High flows were observed for several days upon reentry. Unfortunately, pipeline access could not be obtained until mid-March 1986. A ten-week test began March 24, 1986 after essentially a 19-month shut-in; the reentry test data are shown in Figure 1.12. Gas production averaged 400 MCFD for the first 10 days and dropped to an average of 325 MCFD over 20-40 days. This significant improvement in production confirmed a transitory nature of the damage observed on stimulation.[23] Water production rates ranged from 20-40 bbl/day although little water was produced during the first five days of the test. The naturally fractured reservoir simulator was again used to analyze the test data. The best match indicated a fracture half-length of 100 ft with a fracture conductivity of 104 md-ft. Significantly, the match also showed that damage to natural fracture systems was no longer present. Further, the overall production by the hydraulic fracture was limited, since it propagated parallel to the direction of highest natural fracture permeability.

The well testing, stimulations, and analyses performed during the paludal stimulation experiment gave the following major results.

(1) The preservation of the gas permeability of the natural fractures intersected by a hydraulic fracture is critical to production enhancement.

(2) Damage to the natural fracture system can be due to liquid and/or fracturing fluid polymers, and their effects apparently decrease with time.

(3) The anisotropic nature of the natural fracture system in the paludal sandstones and the direction of the hydraulic fracture, parallel to the maximum permeability natural fractures, magnified the effects of damage and minimized the production enhancement possible by hydraulic fracture.

1.5.7 Laboratory Studies (Section 9.0)

A variety of laboratory studies was conducted to support the design of the Phase I and II stimulations which were performed by the two different service companies. These studies included mineralogy/petrology analyses, measurements of fluid system parameters, leakoff and matrix permeability degradation and recovery, and proppant embedment and crushing measurements. However, with the problems encountered after the Phase II stimulation, the scope of the laboratory studies was broadened considerably to help analyze stimulation performance and to gain insight into possible damage mechanisms.[24]

Emphasis was placed upon the frac fluid system and particularly breaker performance since relatively little breaker was used. It was shown that while a decrease in gel viscosity probably occurred shortly after the treatment, the molecular weight of the gel in the returned fluid remained

high and the gel had not "broken." The use of methanol and a formation temperature lowered by the treatment and postfrac operations further stabilized the gel. The possible effects of the very reactive remedial treatment were also studied in the laboratory and insight gained into the additional gel degradation, permeability damage, and well casing reactions caused by the treatment.

A unique explanation of the production problems is not possible, although the laboratory studies did eliminate several possibilities. However, the combination of field data and laboratory results strongly suggests that the damage was due to fluid effects upon the natural fracture system, and this damage was, at least in part, reversible with time. Fluid-matrix rock effects may have contributed to some extent, but the laboratory work shows that matrix permeability is eventually regained.

Numerous water analyses were made on samples collected during all paludal activities.[24] Three particular areas of interest were: (1) production of formation water, especially that from the adjacent coal seams; (2) concentration of ammonium thiocyanate, a tracer added to the Phase II fluid system; and (3) organic concentrations, as a measure of the state of the gel introduced into the formation.

1.5.8 Borehole Seismic Analysis (Section 10.0)

Microseismic activity was monitored during and immediately after the Phase I and II paludal stimulations in attempts to obtain diagnostic information on the created hydraulic fractures. Each time, special triaxial borehole seismic units were clamped in the two observation wells slightly above bridgeplugs which had been placed above the perforations. The units' orientations were determined by locating additional perforations fired in MWX-1 and by an air gun seismic source located over a mile away. Each unit could determine the location of the seismic source by combining the

direction obtained by hodogram analysis of the signal's polarization on the three geophone axes with the distance which was proportional to the difference in time of arrival of the p and s waves. Data from two units in separate wells would improve the estimate of a given source location.

During Phase 1, only data from MWX-3 was usable since there was apparently a gas leak in MWX-2 which caused an unacceptably high level of background noise. Nevertheless, 4, 15 and 56 analyzable seismic events were detected in the step rate test and the two minifracs, respectively. Analysis of these signals gave the locations shown in Figure 1.13.[25] The azimuth resulting from all points was N67°±8W; this direction is an excellent agreement with the estimate of the maximum horizontal stress direction as determined by ASR and other studies.[17] Vertical spread of the source locations was consistent with a fracture height of 160 ft. The minimum wing length northwest of MWX-1 was 375 ft; signal attenuation prevented detection of events beyond this distance.

Additional borehole seismic tests were conducted prior to Phase II, principally to assess system accuracy to air gun and perforation seismic sources. Data were obtained from borehole seismic units in both MWX-2 and MWX-3 during Phase II; a total of 340 events were recorded during 10 hours of monitoring. However, only 7 events during fracturing and 5 events during the subsequent shut-in were considered true seismic signals, recorded in both wells, and of sufficient quality for analysis. The two-well data indicated a location uncertainty on the order of ±50 ft. The signals indicated a northwest-southeast trend and 10 of the 12 events were within 110 ft of MWX-1. The major factor limiting the usefulness of seismic fracture diagnostics was found to be the low signal-to-noise ratio of the events. The complex velocity structure resulting from the complex geology and the possibility of nonuniform borehole seismic unit response also contribute to the difficulties.

1.5.9 Other Activities

Three geophysics-related experiments were conducted over the Mesaverde Formation at the MWX site: a three-dimensional surface seismic,[26,27] vertical seismic profiles (VSP),[26-29] and cross-well acoustic surveys.[26,30] (Reference 27 is reproduced as Appendix 12.1.) The focus of these studies was the lenticular sandstones of the paludal, coastal, and fluvial intervals. The coals in the paludal interval provide the largest relative impedance contrasts and, thus, the best potential for resolution of the reservoirs sandstones. However, analysis of the latest VSP survey show that only the gross thickness of the coal, shale, sandstone sequence in the paludal could be determined. Additionally, the uniform sine wave character of synthetic seismograms based upon log data is indicative of an unresolved fine structure; the seismic wavelengths of the 3D and VSP surveys are simply significantly greater than the paludal's lithologic features.[27] The cross-well acoustic surveys were focused on the coastal interval.

1.6 SIGNIFICANT ACCOMPLISHMENTS

Three wells have been drilled which penetrate the Mesaverde Formation in the Piceance basin at a site near Rifle, Colorado. These establish the Multiwell Experiment as a field laboratory for the study of the tight gas resource in this formation. The Mesaverde has been subdivided into distinct intervals based upon their depositional environments, which, in turn, strongly influence their reservoir characteristics. This report is the culmination of work in the second of the intervals--the paludal. (The marine final report has been completed;[6] similar reports on the coastal and fluvial intervals are in preparation.)

The paludal interval has been thoroughly characterized. It is a lithologically complex assortment of sandstones, mudstones and coals deposited in a lower delta plain environment. A comprehensive body of core,

log, stress, and geologic data has been compiled for this interval of the Mesaverde Formation and is available publicly as a result of the Multiwell Experiment.

The importance of natural fractures in gas production from these tight sandstone reservoirs continues to be demonstrated. While the sandstones have matrix permeabilities on the order of a microdarcy, average reservoir permeabilities were found to be 30-50 times higher.

Several stimulation-related activities were performed in zones 3 and 4. Data from step-rate and flow-back tests and two minifracs were shown to be very useful in stimulation designs and analysis. A 75,000 gal, 193,000 lb propped hydraulic fracture treatment was conducted. Unexpectedly high fracturing pressures were observed in the minifracs and main treatment. The resulting fractures were characterized by various diagnostic techniques, including postfrac pressure decline analyses and applying a new stimulation model to match the fracturing pressure history.

Gas production from individual unstimulated paludal zones is 100-200 MCFD, although breakdowns and additional clean-up time are required to achieve these rates. In zones 3 and 4 combined, prefrac production was 250 MCFD. However, this was reduced to 200 and 170 MCFD, as the result of the minifracs and main treatment, respectively. Yet, this reduction was transitory, as additional tests in the interval after 19 months of shut-in, gave a sustained production of 325 MCFD.

An advanced, naturally fractured, reservoir simulator was developed and used to successfully match pressure data from well tests conducted before, between, and after the stimulations. The successful matches clearly indicated the damage to the productive natural fracture system and the absence of damage upon reentry testing.

The preservation of the permeability of the natural fracture system intersected by a hydraulic fracture is critical to production enhancement. The fractures are susceptible to damage by liquids, fracturing fluid polymers and high fracture pressures. Further, the anisotropic nature of the natural fracture system and the direction of the hydraulic fracture parallel to the maximum natural fracture permeability direction, magnifies the effects of damage and minimizes the effectiveness of the hydraulic fracture.

Laboratory studies have provided insight into the possible damage mechanisms. In particular, several aspects of breaker performance and frac fluid stability have been shown to be important.

Borehole seismic diagnostics were used to map hydraulic fractures in conjunction with the paludal stimulations. A hydraulic fracture azimuth of N67°±8°W was determined; this was in excellent agreement with predictions. However, the low signal-to-noise ratios of the observed seismic events limited the range and detail of the resulting information.

Overall, the paludal has been shown to be an interesting and complex interval in the Mesaverde with a very good potential for natural gas production from both sandstone and coal reservoirs. The consequences of the possible interactions between these distinct reservoir types are not fully recognized or understood.

1.7 ACKNOWLEDGMENTS

A project of this magnitude is clearly the result of the efforts of a large number of people. The principal investigators express their appreciation for the assistance received from the MWX project personnel at Sandia National Laboratories and CER Corporation. Special thanks are extended to the CER field crew for their hard work and dedication in

maintaining the site and conducting the various tests often under difficult conditions.

We also acknowledge the contributions from many contractors and other participants in MWX who have helped us compile a unique, comprehensive set of data for this potential resource. The inputs of the U.S. Geological Survey have been particularly helpful.

The Multiwell Experiment is the major production technology project in the U.S. Department of Energy's Western Gas Sands Subprogram. DOE personnel responsible for MWX in the past have been C. H. Atkinson, A. B. Crawley, and J. K. Westhusing. For the past five years, the Western Gas Sands Subprogram has been managed by K-H. Frohne, at DOE's Morgantown Energy Technology Center.

1.8 REFERENCES

1. National Petroleum Council, "Unconventional Gas Sources--Volume V: Tight Gas Reservoirs, Part I," Library of Congress Card Number 80-82488, December 1980.

2. C. H. Atkinson, A. B. Crawley, D. A. Northrop, A. R. Sattler, R. L. Mann, and J. C. Schillo, "The Department of Energy's Western Gas Sands Project Multi-Well Experiment," SPE/DOE 9891, Proceedings of the 1981 SPE/DOE Symposium on Low Permeability Gas Reservoirs, Denver, CO, May 27-29, 1981, pp 577-582.

3. A. B. Crawley, D. A. Northrop, and A. R. Sattler, "The Department of Energy's Western Gas Sands Project Multi-Well Experiment Update," SPE 11183, the 57th Annual Society of Petroleum Engineer's Technical Conference and Exhibition, New Orleans, LA, September 26-29, 1982.

4. D. A. Northrop, A. R. Sattler, and J. K. Westhusing, "Multi-Well Experiment: A Field Laboratory for Tight Gas Sands," SPE/DOE 11646, Proceedings of the 1983 SPE/DOE Joint Symposium on Low Permeability Gas Reservoirs, Denver, CO, March 13-16, 1983, pp 393-398.

5. D. A. Northrop, A. R. Sattler, R. L. Mann, and K-H. Frohne, "Current Status of the Multiwell Experiment," SPE/DOE/GRI 12868, Proceedings of the 1984 SPE/DOE/GRI Unconventional Gas Recovery Symposium, Pittsburgh, PA, May 13-15, 1984, pp 351-358.

6. Multiwell Experiment Project Groups at Sandia National Laboratories and CER Corporation, "Multiwell Experiment Final Report: I. The Marine Interval of the Mesaverde Formation," Sandia National Laboratories Report, SAND87-0327, April 1987.

7. J. C. Lorenz, "Sedimentology of the Mesaverde Formation at Rifle Gap, Colorado and Implications for Gas-Bearing Intervals in the Subsurface," Sandia National Laboratories Report, SAND82-0604, March 1982.

8. J. C. Lorenz, "Reservoir Sedimentology in Mesaverde Rocks at the Multiwell Experiment Site," Sandia National Laboratories Report SAND83-1078, June 1983.

9. CER Corporation, "Multi-Well Experiment: MWX-1 As-Built Report," Sandia National Laboratories Contractor Report, SAND82-7201, July 1982.

10. CER Corporation, "Multi-Well Experiment: MWX-2 As-Built Report," Sandia National Laboratories Contractor Report, SAND82-7100, August 1982.

11. CER Corporation, "Multi-Well Experiment: MWX-3 As-Built Report," Sandia National Laboratories Contractor Report, SAND84-7132, February 1984.

12. T. L. Logan, J. C. Seccombe and A. H. Jones, "Hydraulic Fracture Stimulation and Open Hole Testing of a Deeply Buried Coal Seam in the Piceance Basin, Colorado," SPE 15251. Proceedings of the SPE Unconventional Gas Technology Symposium, Louisville, KY, May 1986.

13. G. C. Kukal, "A Systematic Approach for the Effective Log Analysis of Tight Gas Sands," SPE/DOE/GRI 12851, Proceedings of the 1984 SPE/DOE/GRI Unconventional Gas Recovery Symposium, Pittsburgh, PA, May 1984, pp 209-220.

14. A. R. Sattler, "The Multi-Well Experiment Core Program," SPE/DOE 11763, Proceedings of the 1983 SPE/DOE Joint Symposium on Low Permeability Gas Reservoirs, Denver, CO, March 13-16, 1983, pp 437-444.

15. N. R. Warpinski, P. Branagan, and R. Wilmer, "In Situ Stress Measurements at U.S. DOE's Multiwell Experiment Site, Mesaverde Group, Rifle, Colorado," Journal of Petroleum Technology, 37 (3), 527-536, March 1985.

16. L. W. Teufel, "Determination of In Situ Stress from Anelastic Strain Recovery Measurements of Oriented Core," SPE/DOE 11649, Proceedings of the 1983 SPE/DOE Joint Symposium on Low Permeability Gas Reservoirs, Denver CO, March 13-16, 1983, pp 421-430.

17. L. W. Teufel, C. M. Hart, A. R. Sattler, and J. A. Clark, "Determination of Hydraulic Fracture Azimuth by Geophysical, Geological and Oriented Core Methods at the Multi-Well Experiment Site, Rifle Colorado," SPE 13226, 59th Annual Technical Conference and Exhibition of the Society of Petroleum Engineers of AIME, Houston, TX, September 17-19, 1984.

18. T. L. Blanton, "The Relation between Recovery Deformation and In Situ Stress Magnitudes," SPE 11624, Proceedings of 1983 SPE/DOE Symposium on Low Permeability Gas Reservoirs, Denver, CO, March 1983, pp 213-218.

19. N. R. Warpinski and L. W. Teufel, "In Situ Stresses in Low-Permeability, Nonmarine Rocks," SPE/DOE 16402, Proceedings of the 1987 SPE/DOE Joint Symposium on Low Permeability Reservoirs, Denver CO, May 1987, pp 125-138.

20. N. R. Warpinski, P. T. Branagan, A. R. Sattler, J. C. Lorenz, D. A. Northrop, R. L. Mann and K-H. Frohne, "Fracturing and Testing Case Study of Paludal, Tight Lenticular Gas Sands," SPE/DOE 13876, Proceedings of the 1985 SPE/DOE Symposium on Low Permeability Gas Reservoirs, Denver, CO, May 1985, pp 267-278. Also as SPE Formation Evaluation, 2, 535-545, December 1987.

21. P. T. Branagan, C. Cipolla, S. J. Lee, and J. Chen, "Designing and Evaluating Hydraulic Fracture Treatments in Naturally Fractured Reservoirs," SPE/DOE 16434, SPE/DOE Symposium on Low Permeability Reservoirs, Denver, Colorado, May 1987.

22. P. T. Branagan, C. L. Cipolla, S. J. Lee, and R. H. Wilmer, "Comprehensive Well Testing and Modeling of Pre- and Post-Fracture Well Performance of the MWX Lenticular Tight Gas Sands," SPE 13867, presented at SPE/DOE 1985 Low Permeability Gas Reservoirs Symposium, Denver CO, May 19-21, 1985.

23. P. T. Branagan, C. L. Cipolla, S. J. Lee, and L. Yan, "Case History of Hydraulic Fracture Performance in the Naturally Fractured Paludal Zone: The Transitory Effects of Damage," SPE 16397, presented at 1987 SPE Low Permeability Reservoirs Symposium, Denver, CO, May 18-19, 1987.

24. A. R. Sattler, "Integration of Laboratory and Field Data for Insight on the Multiwell Experiment Paludal Stimulation," Sandia National Laboratories Report SAND86-0087, June 1986.

25. C. M. Hart, D. Engi, R. P. Fleming, and H. E. Morris, "Fracture Diagnostics Results for the Multiwell Experiment's Paludal Zone Stimulations," SPE/DOE/GRI 12852, Proceeding of the 1984 Unconventional Gas Recovery Symposium, Pittsburgh, PA, May 1984, pp 221-228.

26. C. A. Searls, M. W. Lee, J. J. Miller, J. N. Albright, J. Fried, and J. K. Applegate, "A Coordinated Seismic Study of the Multi-Well Experiment Site," SPE/DOE 11613 Proceedings of the 1983 SPE/DOE Joint Symposium on Low Permeability Gas Reservoirs, Denver, CO, March 13-16, 1983, pp 115-120.

27. C. A. Searls, "The Multiwell Experiment Geophysics Program; Final Report," Sandia National Laboratories Report, SAND85-1013, September 1985 (given as Appendix 12.1).

28. M. W. Lee, "Detection and Delineation of Lenticular-Type Sand Bodies by the Vertical Seismic Profiling Method," United States Geological Survey Open File Report, 84-757, November 1984, pp 121-134.

29. M. W. Lee, "Azimuthal Vertical Seismic Profiles at the Multiwell Experiment Site, Garfield County, Colorado," United States Geological Survey Open File Report, in progress.

30. J. N. Albright, D. A. Terry, and C. R. Bradley, "Pattern Recognition and Tomography Using Cross-well Acoustic Data," SPE/DOE 13854, Proceedings of the SPE/DOE Joint Symposium on Low Permeability Reservoirs, Denver, CO, March 1985, pp 55-64.

Table 1.1 LOG DERIVED RESERVOIR PROPERTIES

Zone	Well	Core Depth (ft)	Thickness (ft) Gross	Thickness (ft) Sand	ϕ (fraction)	S_w (fraction)	V_{cl} (fraction)	kh (md-ft)
5	MWX-1	6880.5-6892.5	12.0	12.0	0.087	0.537	0.105	0.45
	MWX-2	6883.0-6899.0	16.0	15.5	0.103	0.502	0.097	0.62
	MWX-3	not present						
4a	MWX-1	6997.5-7014.0	16.5	16.5	0.081	0.796	0.125	0.20
	MWX-2	not present						
	MWX-3	7003.0-7019.0	16.0	16.0	0.062	0.626	0.134	0.17
4	MWX-1	7071.0-7100.0	29.0	29.0	0.101	0.539	0.081	1.00
	MWX-2	7076.0-7087.5	11.5	4.5	0.036	0.761	0.173	-
	MWX-3	7079.0-7103.0	24.0	24.0	0.089	0.605	0.084	0.50
3	MWX-1	7119.5-7147.5	28.0	28.0	0.086	0.571	0.151	0.70
	MWX-2	7108.5-7133.0	24.5	24.0	0.094	0.526	0.143	0.65
	MWX-3	7123.5-7143.5	20.0	19.5	0.084	0.554	0.179	0.55
2	MWX-1	7240.0-7284.0	44.0	44.0	0.087	0.641	0.107	1.10
	MWX-2	7234.0-7274.0	40.0	28.5	0.068	0.685	0.126	0.18
	MWX-3	7273.0-7285.0	12.0	12.0	0.063	0.829	0.096	0.10
1	MWX-1	7315.5-7340.0	24.5	21.5	0.072	0.707	0.092	0.20
	MWX-2	7312.0-7326.5	14.5	14.5	0.089	0.593	0.150	0.25
	MWX-3	7328.5-7340.0	11.5	11.5	0.082	0.646	0.125	0.32

Table 1.2 SUMMARY OF CORE-DERIVED RESERVOIR PROPERTIES

Well	Zone	Porosity (%) Ave	Porosity (%) Range	Water Saturation (%) Ave	Water Saturation (%) Range	Permeability* (μd) Ave	Permeability* (μd) Range
MWX-2	1	8.0	5.0- 9.2	26.5	21-34	2.4	1.1-10.0
	2	8.0	5.4- 9.9	31.8	25-50	3.1	1.4- 8.3
	3	10.9	7.1-13.8	27.1	18-45	7.1	0.2-25.5
MWX-3	3	8.7	4.0-12.4	~53	48-62	7.2	0.3-25.2
	4	9.2	3.8-11.2	~55	50-66	7.7	0.6-14.4
	5	4.7	3.5- 5.8	-	-	2.6	1.6- 3.6

*Dry Klinkenburg permeabilities at 2000 psi effective confining stress.

Well	Zone	Core Depth (ft)	Young's Modulus* (GPa)	Poisson's* Ratio	Lithology: sand-stone	silty sand-stone	silt-stone	carb. mud-stone	shale
MWX-2	1	7308.5	28.4	0.20				x	
	1	7322.5	29.6	0.23		x			
	1	7343.4	30.1	0.19				x	
	1	7361.5	18.9	0.13		x			
MWX-2	2	7253.5	29.2	0.22			x		
	2	7269.1	25.7	0.21		x			
	2	7281.0	36.8	0.23	x				
MWX-2	3	7113.3	25.5	0.23	x				
	3	7171.6	28.2	0.22			x		
MWX-3	3	7112.7	24.3	0.23					x
	3	7133.3	28.1	0.22	x				
MWX-2	4	7085.8	40.3	0.22	x				
	4	7108.0	18.4	0.13			x		
MWX-3	4	7076.5	22.8	0.21					x
	4	7095.5	23.9	0.19	x				
	4	7112.7	24.5	0.23					x

* Calculated between 20% and 60% of ultimate axial stress, and at 20 MPa confining pressure.

Table 1.3 SUMMARY OF IN SITU STRESS MEASUREMENTS

Well	Depth (ft)	Lithology	Stress (psi)	Gradient (psi/ft)	Test Type
MWX-1	7076-7144	Sandstone	5900 ± 50	0.83	Flowback
	7256-7284	Sandstone	6300 ± 50	0.87	Breakdown
MWX-2	6928-6930	Mudstone	5830 ± 100	0.84	Stress Test
	6963-6965	Sandstone	5745 ± 50	0.82	Stress Test
	7010-7012	Mudstone	6325 ± 50	0.90	Stress Test
	7169-7171	Mudstone	7000 ± 30	0.98	Stress Test
	7206-7208	Siltstone	6900 ± 30	0.96	Stress Test
	7263-7265	Sandstone	6755 ± 50	0.92	Stress Test
	7303-7305	Mudstone	6430 ± 30	0.88	Stress Test
	7394-7396	Siltstone	6720 ± 150	0.91	Stress Test
	7423-7425	Coal	6865 ± 75	0.92	Stress Test
MWX-3	7032-7034	Mudstone	6800 ± 100	0.97	Stress Test
	7048-7050	Coal	7200 ± 100	1.02	Stress Test
	7068-7070	Mudstone	5780 ± 50	0.82	Stress Test
	7080-7142	Sandstone	5805 ± 50	0.82	Breakdown

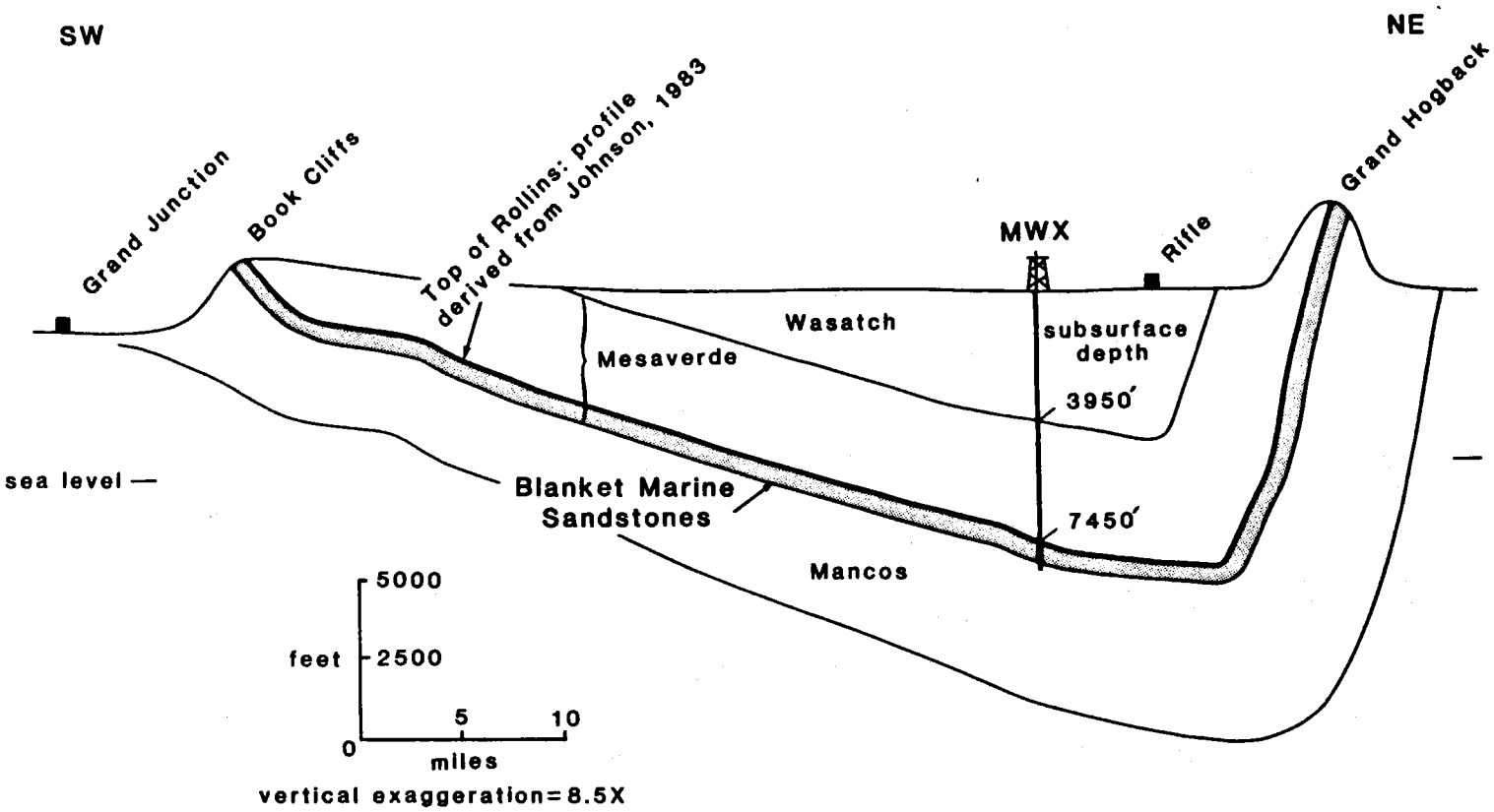

Figure 1.1 General Structure of the Mesaverde Formation in the Piceance Creek basin, Northwest Colorado.

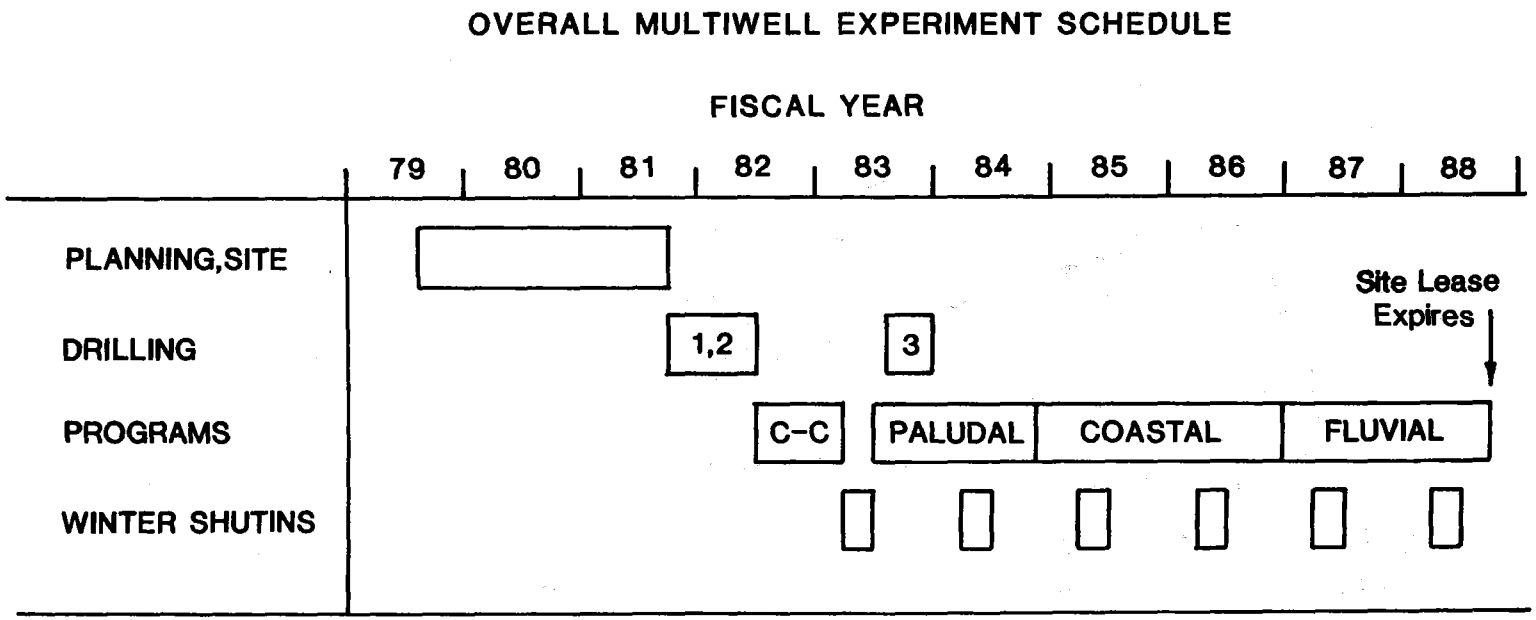

Figure 1.2 Overall Multiwell Experiment Schedule

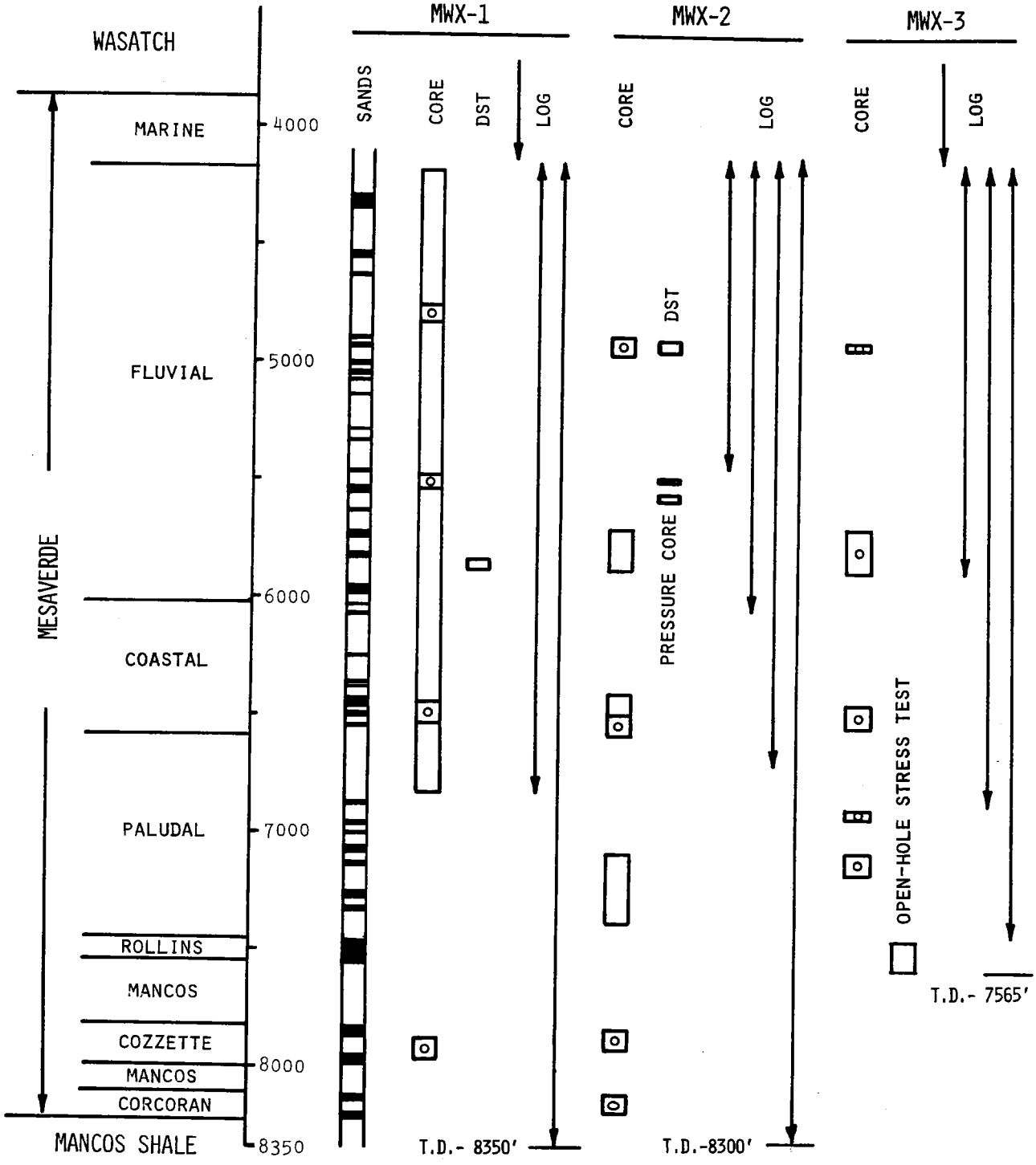

Figure 1.3 Summary of Coring and Logging Operations on the Three Multiwell Experiment Wells

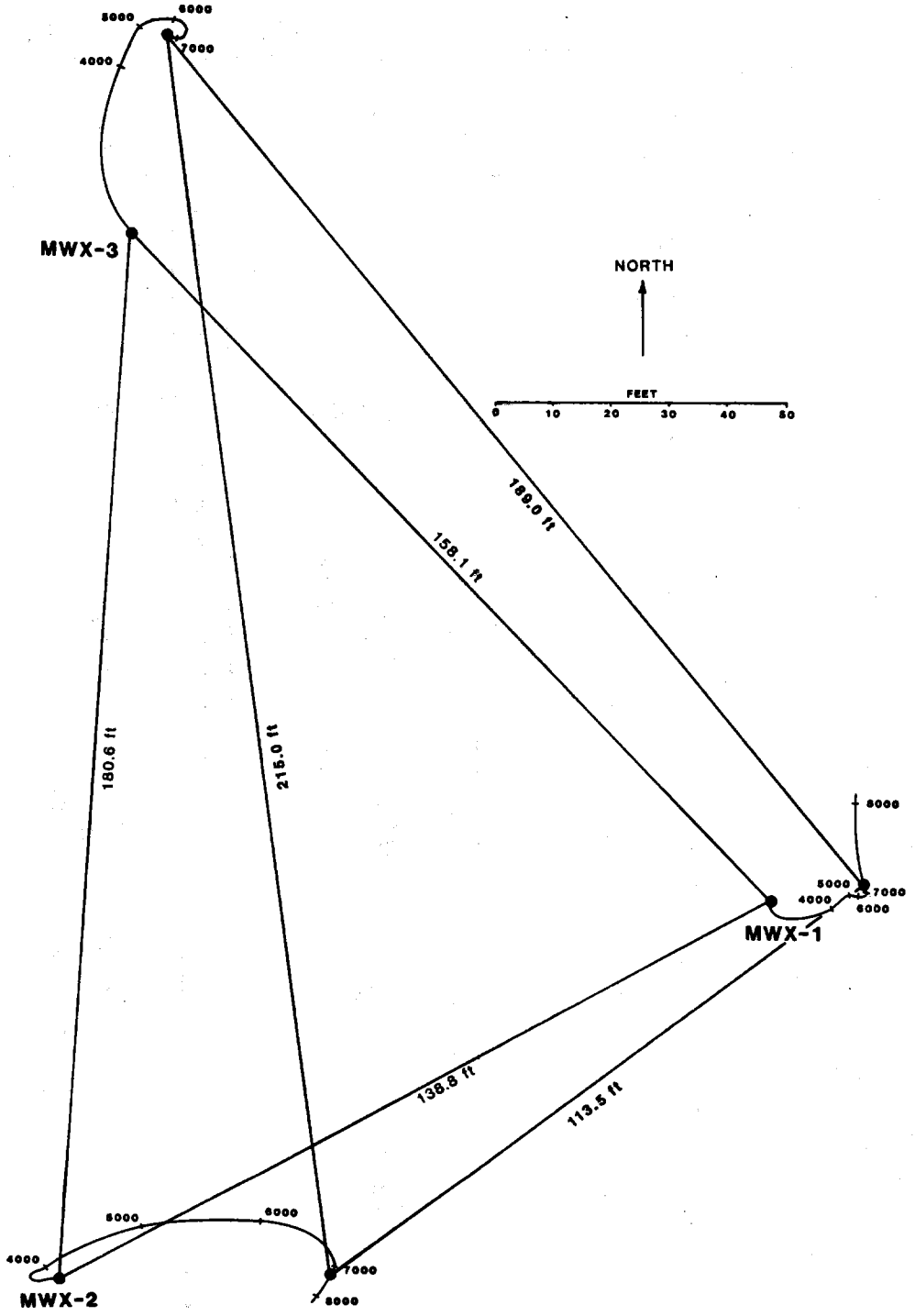

Figure 1.4 Relative Well Spacings at Surface and 7300 ft (the Deepest Survey in all Three Wells).

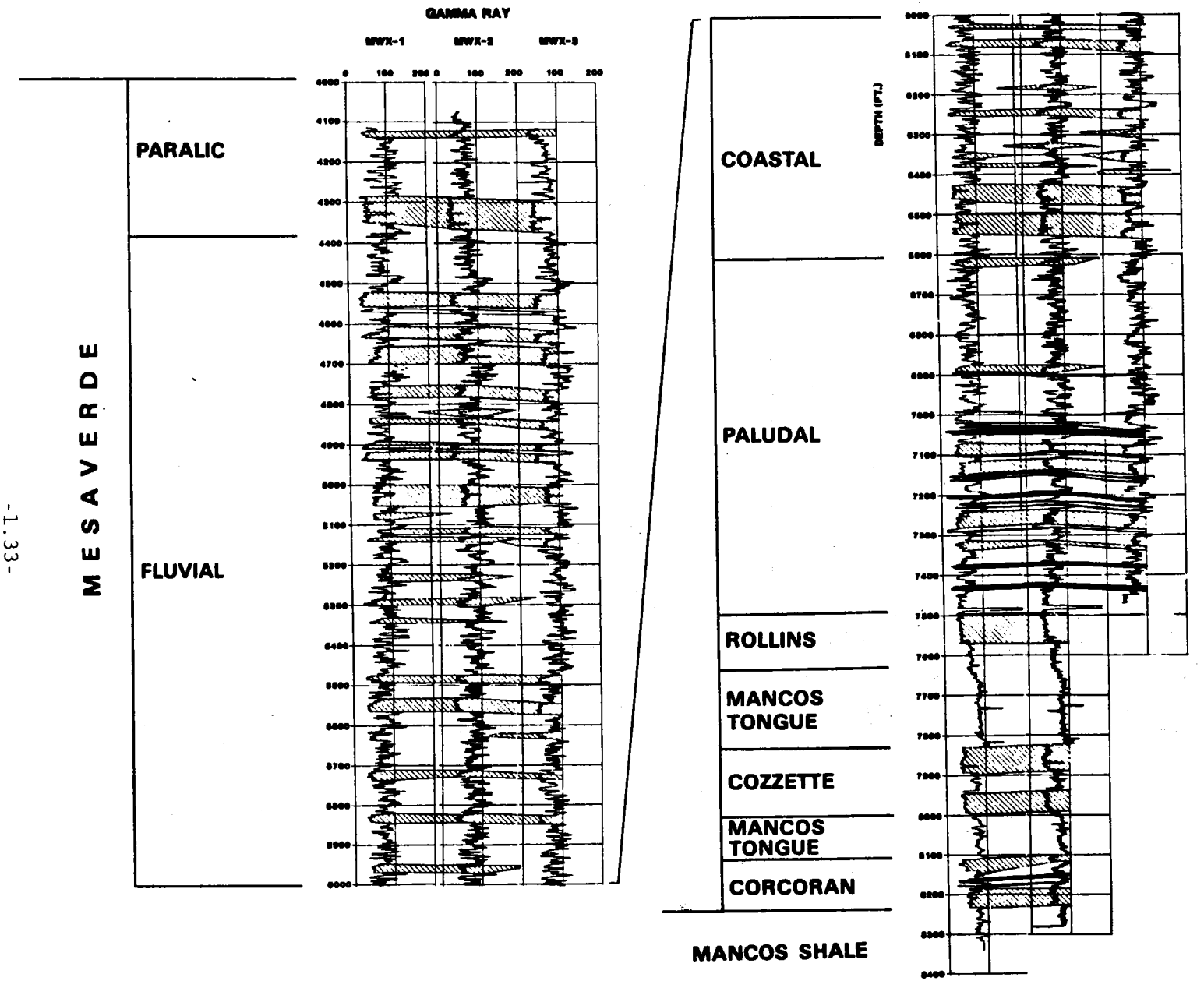

Figure 1.5 Gamma Ray Logs of the Three Multiwell Experiment Wells with Sands Identified

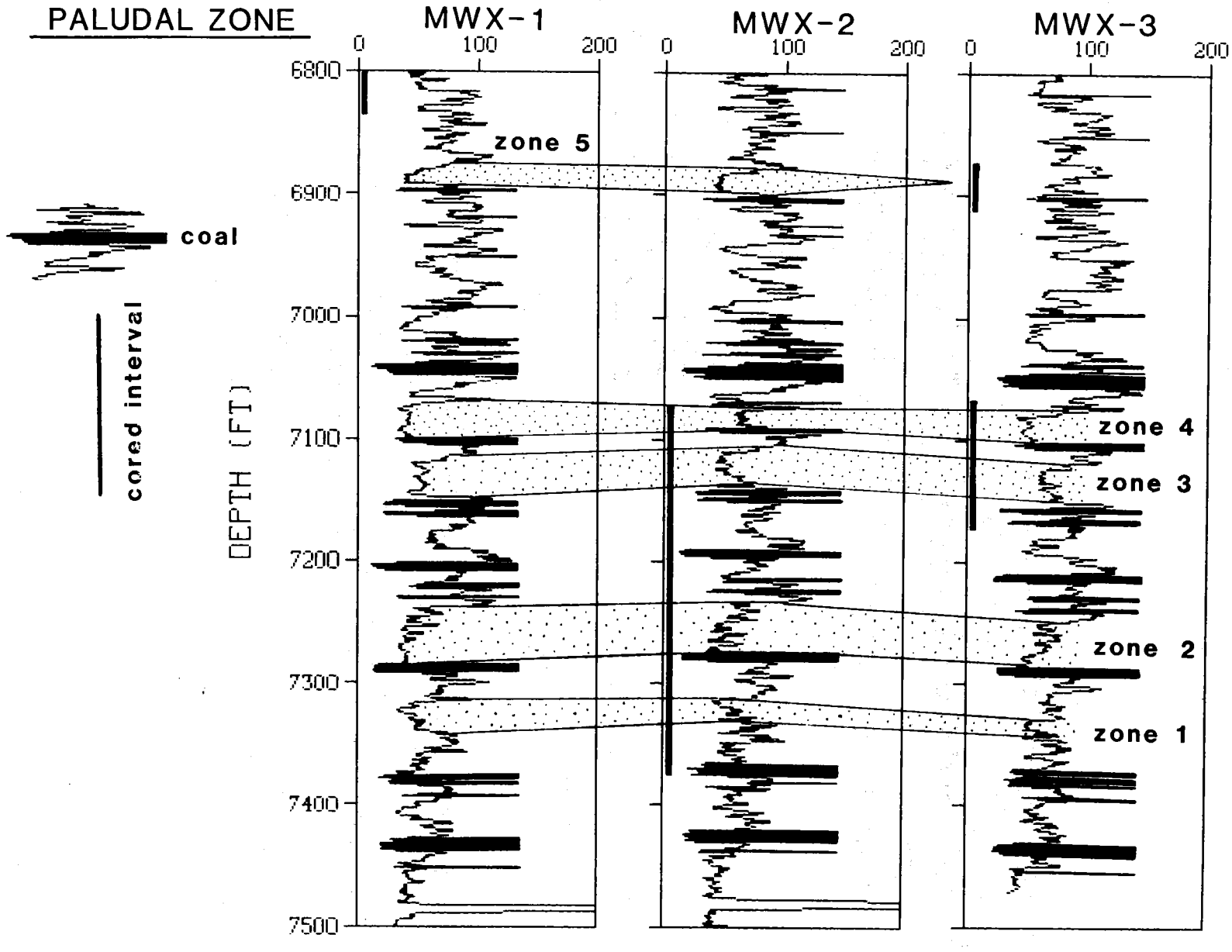

Figure 1.6 The Paludal Interval Showing the Region of Primary Interest

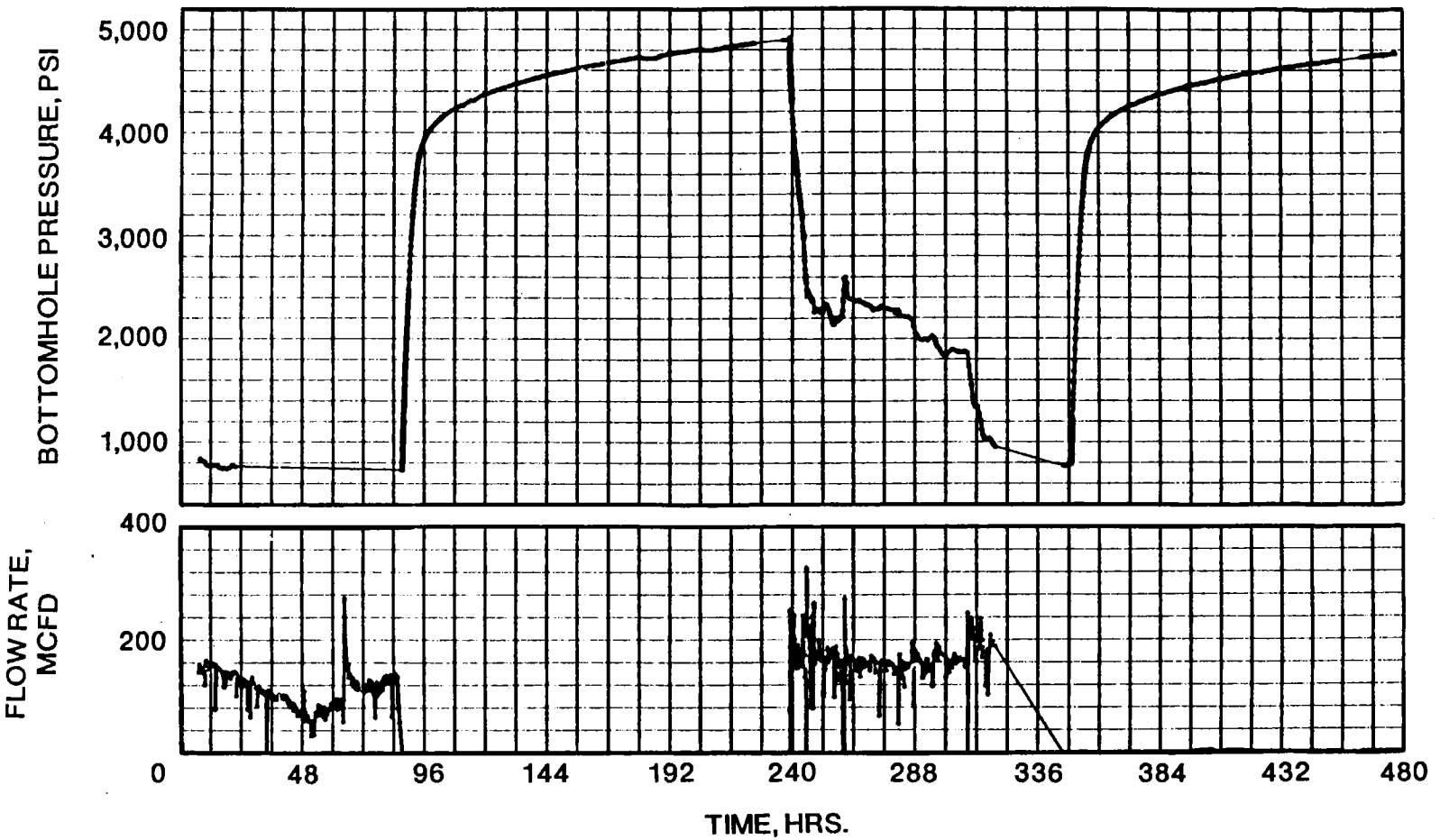

Figure 1.7 Production for the Zone 2 Test Period

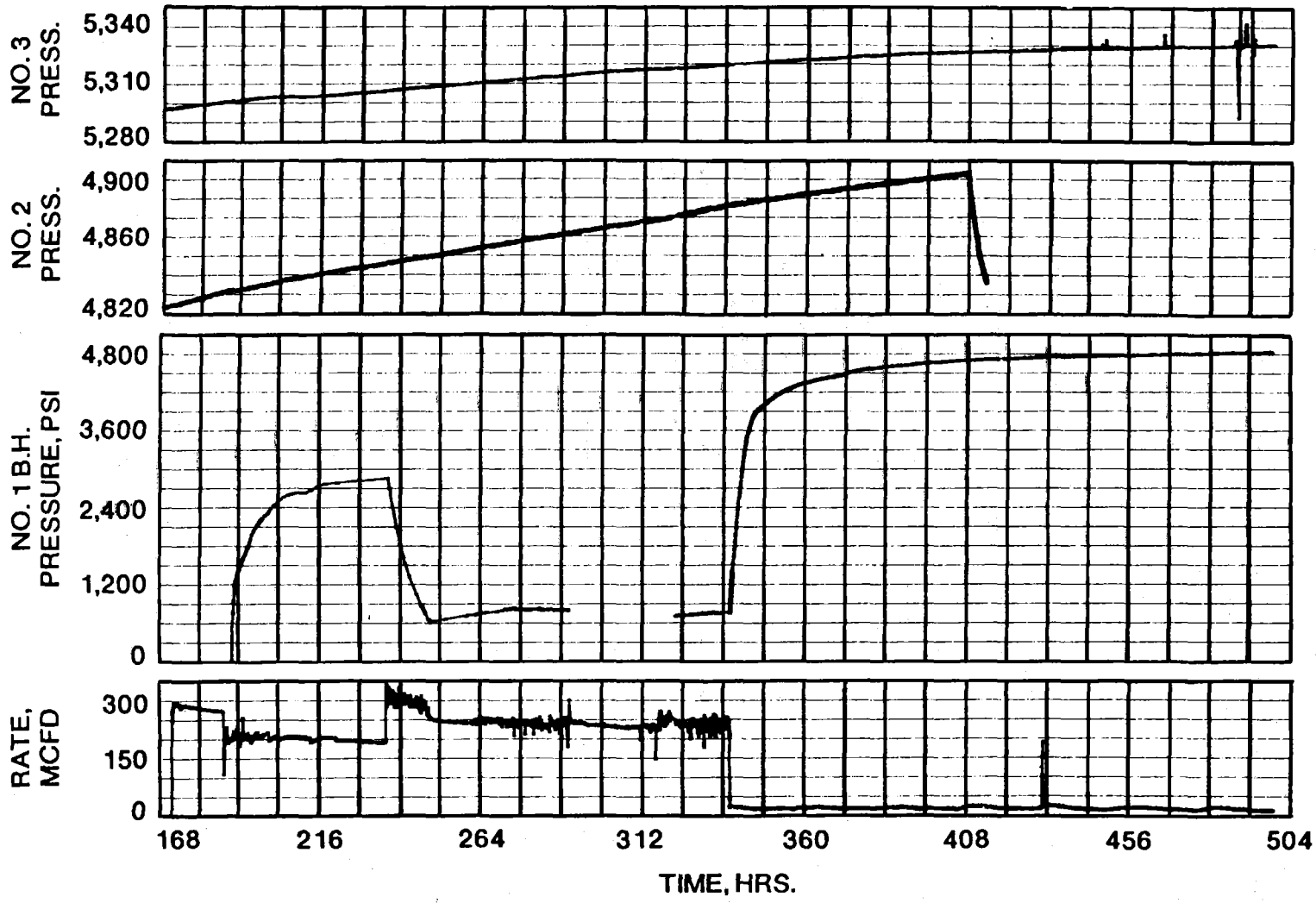

Figure 1.8 Pre-Frac Well Testing Flow Rate and Bottomhole Pressure Data for MWX-1 and Shut-In Bottomhole Pressure for Observation Wells MWX-2 and MWX-3

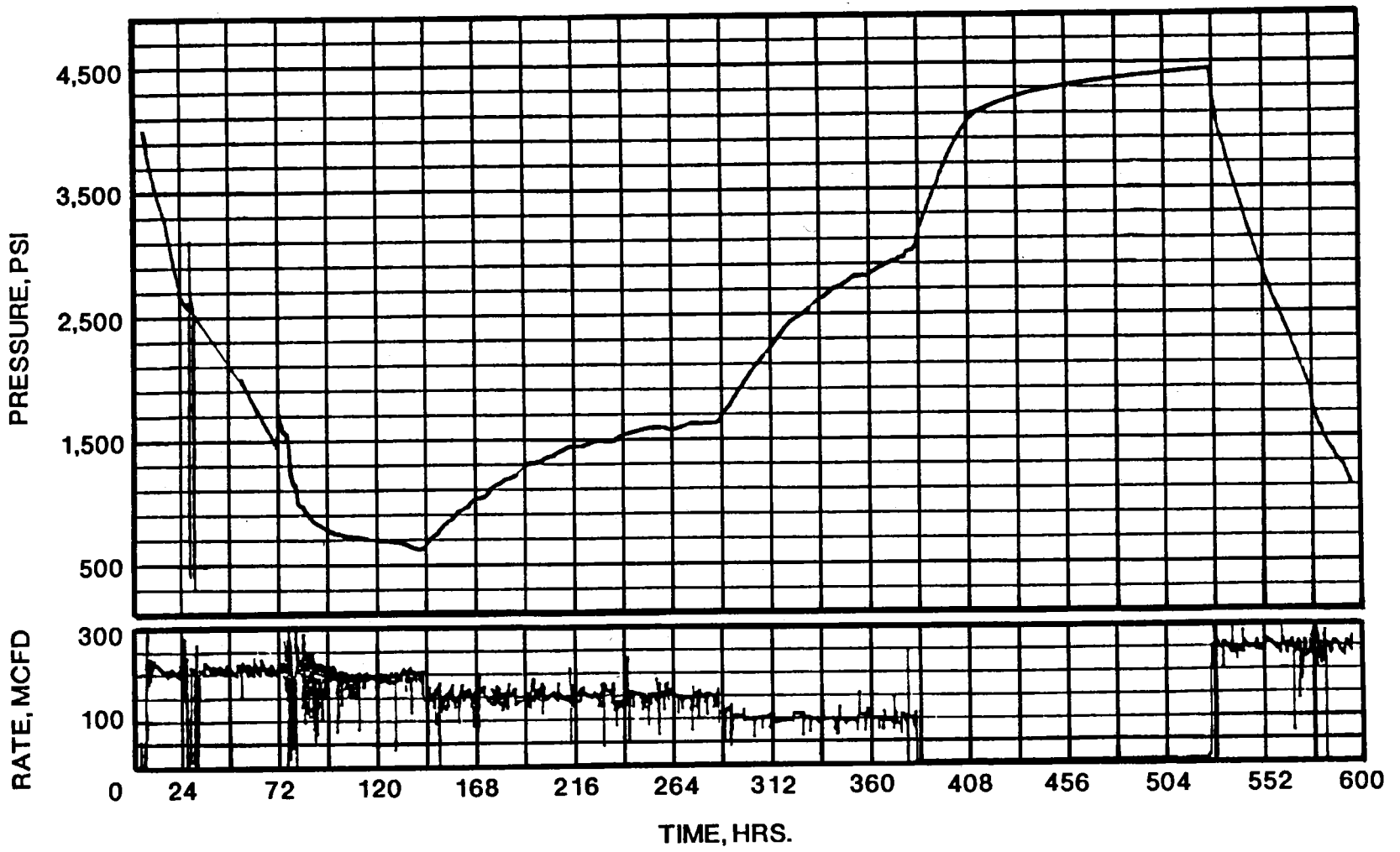

Figure 1.9 MWX-1 Post Phase I Well Testing, Flow Rate and Bottomhole Pressure

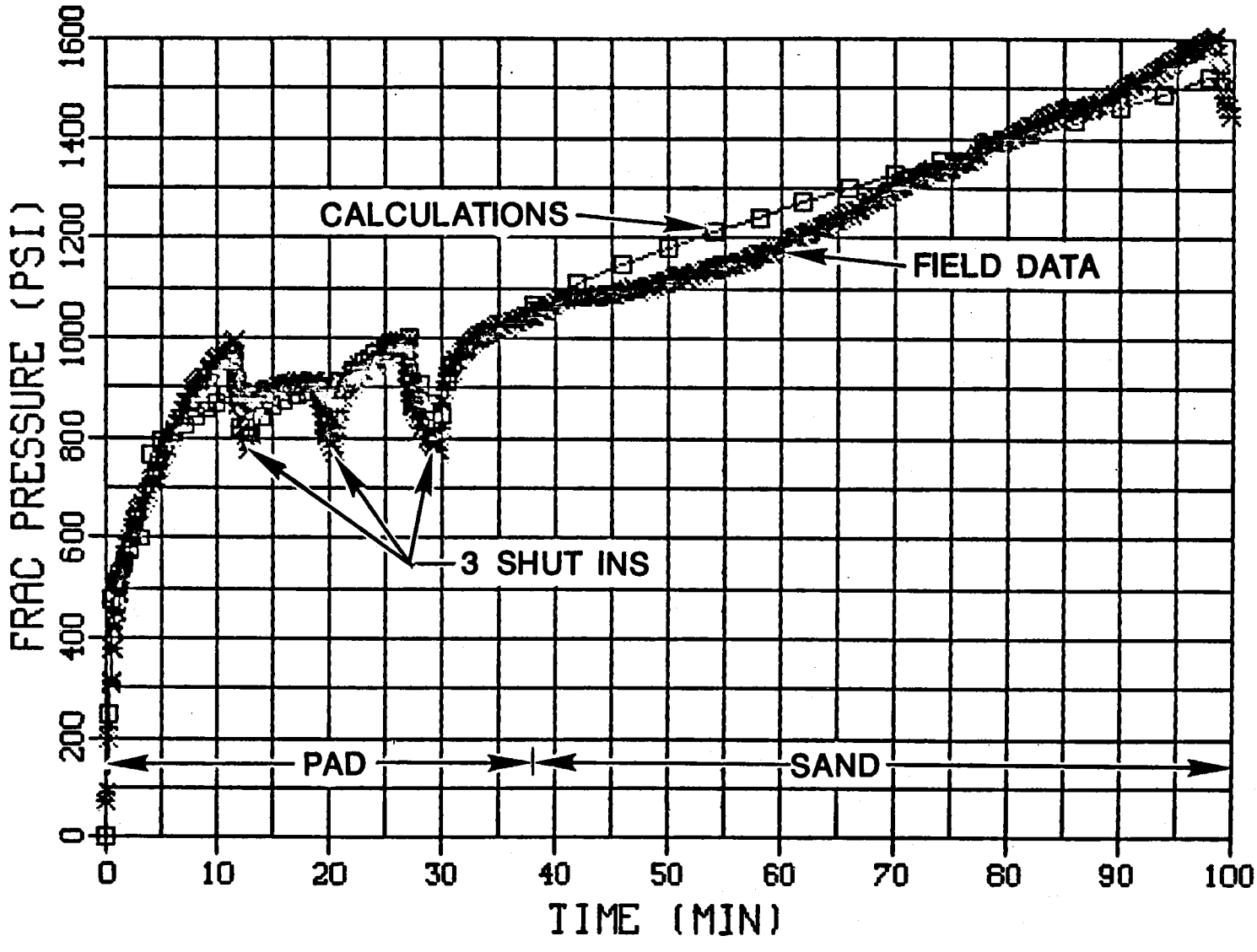

Figure 1.10 Fracturing Pressure History Match of Phase II Stimulation

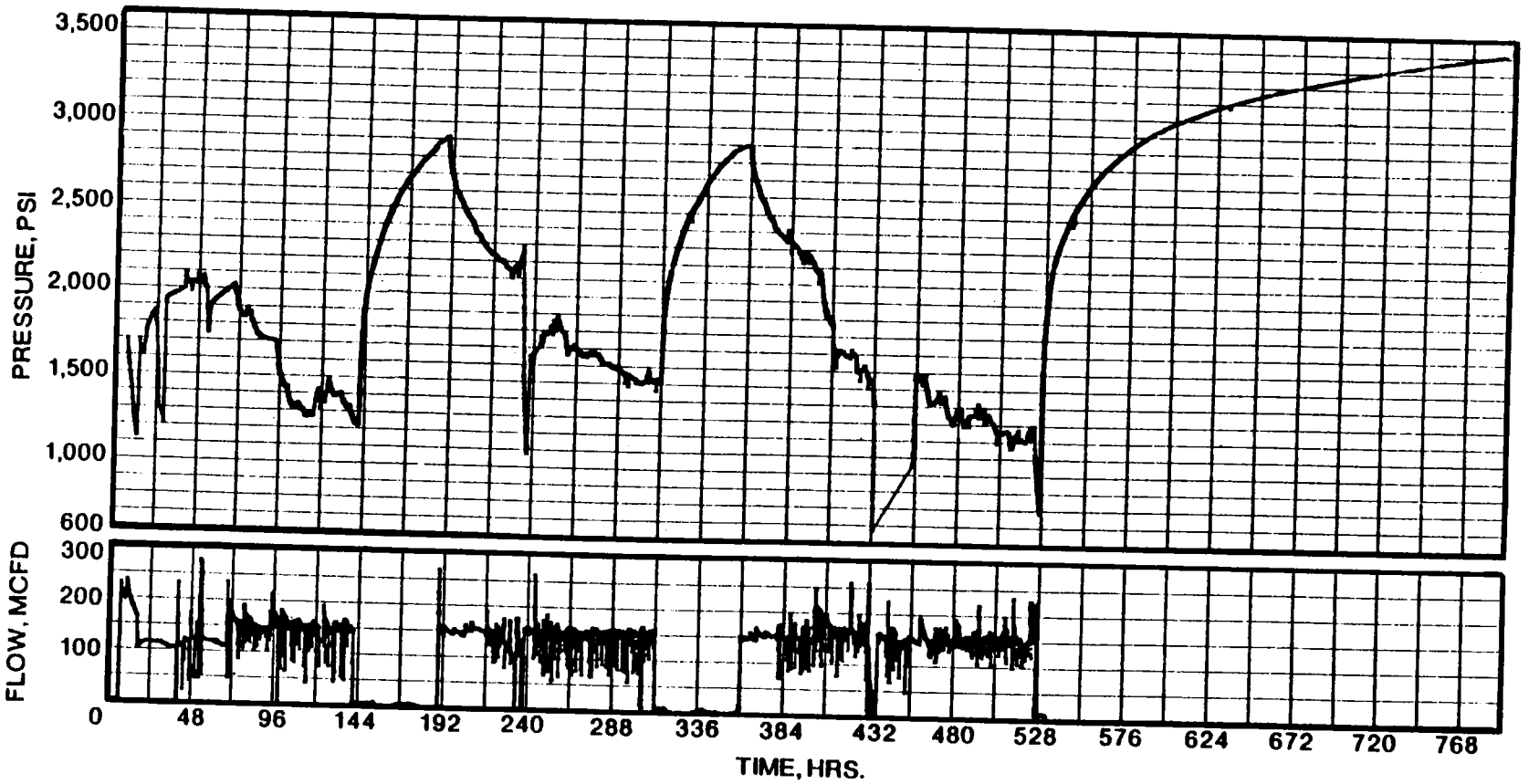

Figure 1.11 Post Phase II Well Testing Surface Flow Rate and Bottomhole Pressure

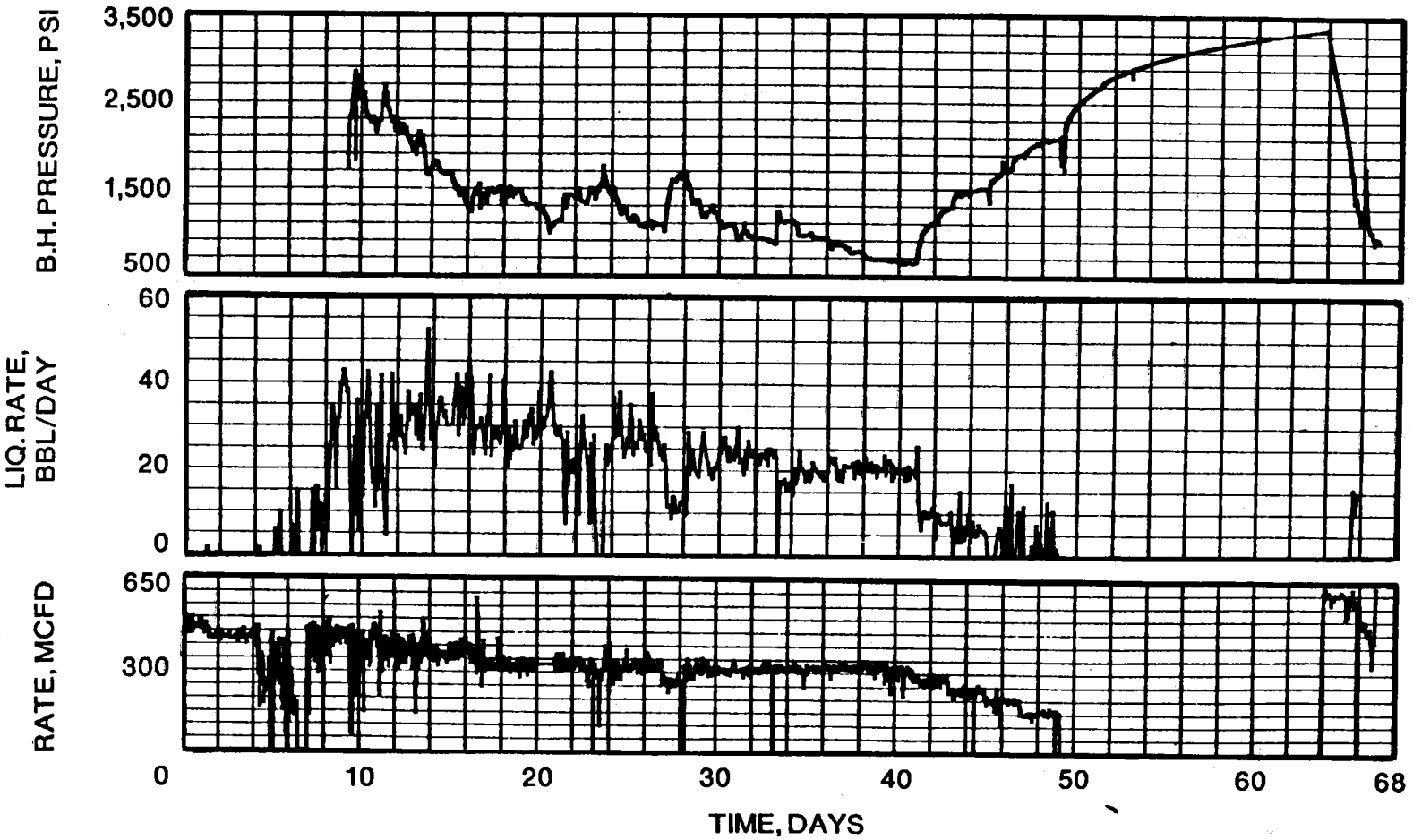

Figure 1.12 Re-Entry Well Test Data from Paludal Sands 3 and 4

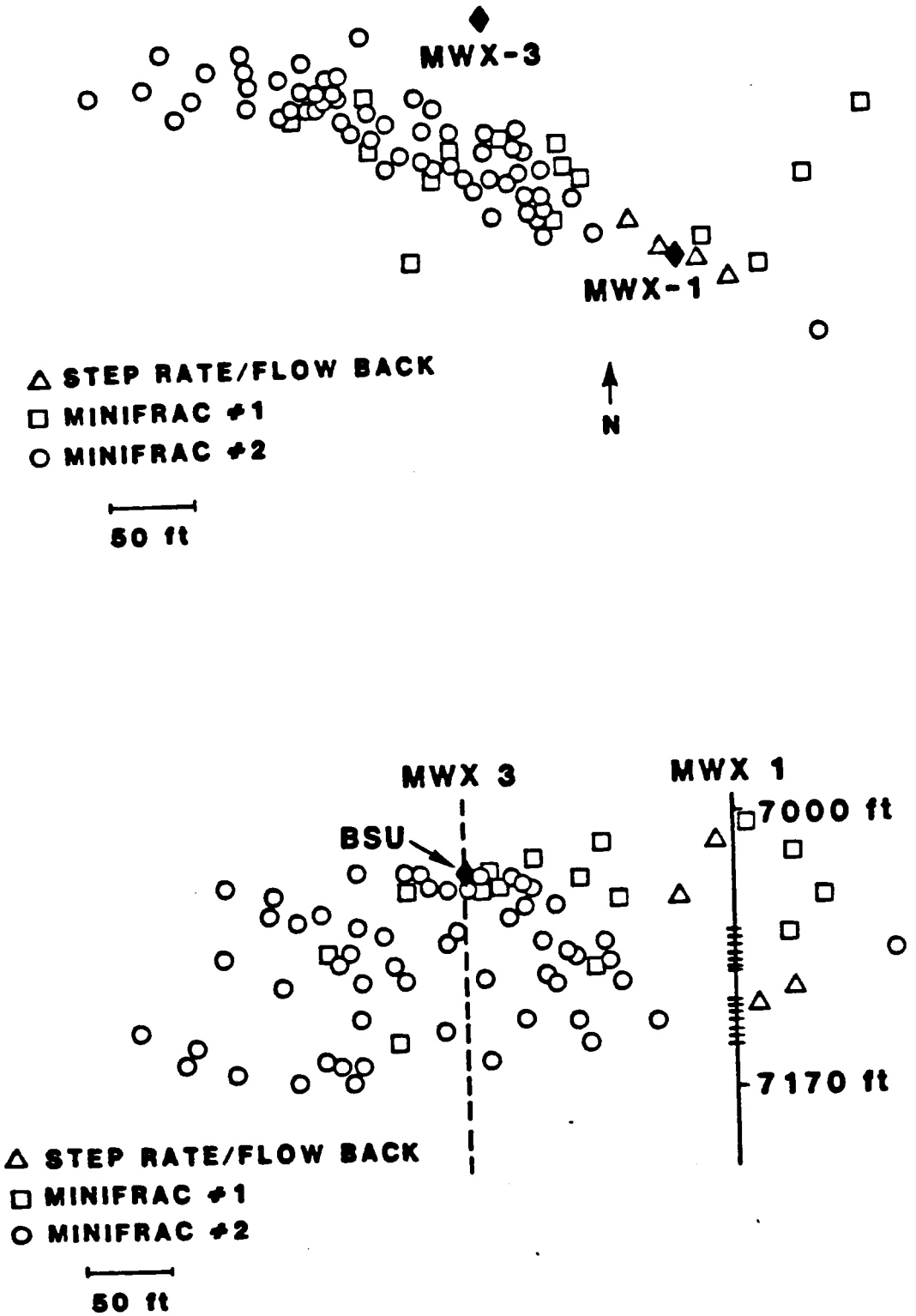

Figure 1.13 Seismic Event Locations During Phase I: (top) Projected onto Horizontal Plane, (bottom) Projected onto N67°W Plane

2.0 SITE DESCRIPTION AND OPERATIONS

W. J. Mathis and F. Richard Myal
CER Corporation

2.1 WELL DRILLING AND WELL DESCRIPTIONS

As shown in Figure 2.1, the Multiwell Experiment (MWX) is located in the southeastern portion of the Piceance Basin in Colorado. The site is located in the SW1/4 NW1/4 Sec. 34, T6S, R94W, Garfield County, and is about 7 miles southwest of Rifle.

An agreement was reached with Superior Oil Company in mid-1981 and all necessary drilling and operating permits were acquired. Drilling of MWX-1 began in mid-September 1981, achieving total depth at 8350 ft. The well was drilled through the blanket Mesaverde sections and 7-in, 29-lb N-80 casing was run and cemented. As shown in Figure 2.2, a total of 2747 ft of the Mesaverde group was cored and recovered, including 470 feet of oriented core.

The rig was moved to the adjoining location and the second well was spudded on December 31, 1981. MWX-2 was also drilled through the blanket marine Mesaverde to a depth of 8300 ft with 915 ft of formation cored and recovered, as shown in Figure 2.3. The MWX-2 casing program was similar to the first well. The casing was run and cemented and the rig released on March 30, 1982.

The third well, MWX-3, was spudded on June 7, 1983, and was drilled to a depth of 7564 ft. As shown in Figure 2.4, it penetrated the Rollins Formation but not the Corcoran/Cozzette. "As-built" reports have been published on all three wells.[1,2,3] An approximate geologic section and the formation tops in MWX-1 are shown in Figure 2.5.

During the drilling of the three MWX wells, it was noted that a gradual increase of formation pressure was encountered starting at approximately 5600 ft. Mud weight had to be continually increased with depth from 9.0 lb/gal at 5600 ft to over 15.0 lb/gal at 8350 ft, as shown in Figure 2.6. The Cozzette required a pressure gradient of 0.71 psi/ft and the Corcoran 0.75 psi/ft to control the formation pressure during drilling. From these data and subsequent test data, it is apparent that the lower Mesaverde formations are substantially overpressured.

Detailed direction surveys were also run in the wells to determine the relative well spacing at various depths, as well as at the surface. The wells were drilled with very little directional deviation so the relative spacing with depth does not change significantly. Figure 2.7 shows the relative locations of the three wells at the surface and at 7300 ft.

Complete logging suites were run on all three wells and the logs and analyses for the paludal interval are given in Section 4.0. A temperature log for MWX-1 is shown in Figure 2.8.

2.2 CHRONOLOGY OF PALUDAL OPERATIONS

Activities in the paludal interval of the Mesaverde Formation were initiated May 20, 1983 and were completed on August 14, 1984. Following 19 months shut-in, a second round of production tests in zones 3 and 4 was undertaken from March 24, 1986 to May 30, 1986. The chronology of events presented herein is a topical account of all paludal activities undertaken at the Multiwell Experiment Site. This information is presented in graphical format on Figure 2.9.

2.2.1 Stress Tests in MWX-2 (June 7-10, 1983)

June 7, six paludal intervals were perforated in MWX-2 with four 14-gm

jet shots per foot (JSPF) in preparation for stress testing: 7303-7305 ft, 7318-7320 ft, 7342-7344 ft, 7369-7371 ft, 7394-7396 ft, 7423-7425 ft.

Stress tests at 7423-7425 ft proceeded as planned. However, stress tests attempted at 7394-7396 ft indicated communication uphole to the stress test perfs at 7369-7371 ft and at 7342-7344 ft. The packer assembly was then reset over the perfs at 7303-7305 ft and the interval was successfully stress tested. Following this successful test, the stress test assembly was pulled from the well, both packers replaced, and a 28-ft tubing sub was placed between the packers to straddle the perfs at 7318-7320 ft and 7342-7344 ft. The casing-tubing annulus was then pressured to 1000 psi and a stress test was attempted on the combined interval. Communication to the annulus developed at 1700 psi. Stress testing below 7300 ft in MWX-2 ended on June 10.

2.2.2 Perforate, Breakdown, and Test Zone 2 in MWX-1 (July 10-August 14, 1983)

July 8, the Cozzette interval in MWX-1 was permanently abandoned by setting a G.O. Elite, wireline-set, cast iron bridge plug (CIBP) at 7770 ft. The 7-in. casing was then loaded with 220 bbl of 2% KCl water and zone 2 was perforated from 7256 ft to 7284 ft with two 14-gm JSPF.

July 12, zone 2 was stress tested down 2-7/8-in tubing, below a packer, by Dowell Schlumberger. This was immediately followed by a 68 bbl 2% KCl water breakdown of the interval, down tubing. The maximum treating pressure was 5400 psi, final treating pressure was 4900 psi, and the average treating pressure was 5000 psi. The average treating rate was 7.9 BPM, the instantaneous shut-in pressure (ISIP) was 3700 psi, and the 15-minute shut-in pressure was 3100 psi. The formation breakdown was followed by a second stress test using the stress test pump. During flowback of the breakdown fluid, a strong show of gas was indicated. Well tests were conducted for approximately a month in this zone (Section 7.0).

August 14, zone 2 in MWX-1 was permanently abandoned by setting a G.O. Elite, wireline-set cast-iron bridge plug (CIBP) at 7200 ft. This terminated all zone 2 operations in MWX-1.

2.2.3 Perforate, Breakdown, and Stress Test Zones 3 and 4 in MWX-1 (August 14-23, 1983)

August 14, zones 3 and 4 were perforated in MWX-1. Zone 3 was perforated from 7120 ft to 7144 ft (24 ft) and zone 4 was perforated from 7076 ft to 7100 ft (24 ft) with two 14-gm JSPF. The 2-7/8-in. tubing and a packer with one joint of tailpipe were then run in the well. The packer was set at 7038 ft with the tailpipe at 7049 ft.

August 22, zones 3 and 4 were stress tested together in MWX-1. The ISIP, measured bottomhole, was 5750 psi for the commingled test. The next day zones 3 and 4 were broken down with approximately 60 bbl of 2% KCl water. The average injection rate was 6.4 bpm at an average treating pressure of 4500 psi.

2.2.4 Cleanup and Single Well Test Zones 3 and 4 in MWX-1 (August 24-September 16, 1983)

Following cleanup after August 23 breakdown, retrieval of an HP gauge lost in the tubing during formation breakdown, and repairs to the wellhead assembly on MWX-1, a production test of zones 3 and 4 was initiated September 1, 1983 at a rate of 110 MCFD and 1397 psi flowing bottomhole pressure.

2.2.5 Perforate Zones 3 and 4 in MWX-3 (September 12, 1983)

September 12, zones 3 and 4 in MWX-3 were perforated with two 14-gm JSPF from 7126 ft to 7142 ft (16 ft) and 7080 ft to 7102 ft (22 ft),

respectively. Following perforation, the well was equipped with a packer and a bottomhole shut-off assembly run on 2-7/8-in tubing. The packer was set at 7052 ft, the wellhead assembly installed, and the casing-tubing annulus was pressure tested to 2000 psi. The well was now ready to serve as an interference test observation well.

2.2.6 Stress Tests in MWX-2 (September 13-16, 1983)

September 13, three intervals below zone 3 were perforated with four 14-gm JSPF in preparation for stress testing: 7263-7265 ft, 7206-7208 ft, and 7169-7171 ft. September 15 and 16, the three intervals were successfully stress tested. Then, a GO Elite, wireline-set, CIBP was set at 7160 ft to permanently abandon the stress test intervals below 7169 ft.

2.2.7 Production/Interference Test Zones 3 and 4; MWX-2 Producer (September 16-October 15, 1983)

September 16, zones 3 and 4 in MWX-2 were perforated with two 14-gm JSPF from 7107 ft to 7131 ft (24 ft) and 7060 ft to 7088 ft (28 ft), respectively. Following perforation, the well was equipped with a packer and bottomhole shutoff assembly run on 2-7/8-in tubing. The packer was set at 7038 ft, the wellhead assembly was installed, and the casing-tubing annulus was pressure tested to 1000 psi. The well was now ready for production. MWX-1 and MWX-3 served as interference measurement wells, with each containing downhole shut-off tools and HP quartz pressure transducers.

Production testing of MWX-2 was initiated at 125 MCFD at 12:00 noon September 23, and was completed at 9:30 pm, September 28.

2.2.8 Production/Interference Test, Zones 3 and 4; MWX-1 Producer (October 1-November 1, 1983)

Following two weeks of pressure buildup in the three MWX wells, and an additional week of trouble-shooting the HP gauges, the production testing in

MWX-1 was initiated at 1:30 pm, October 22. The well initially failed to flow and was subsequently shut in. Three soap sticks were dropped October 23, and approximately 10 bbls of load fluid were recovered. The well was then produced at a steady rate of 220 MCFD against 200 psi separator pressure. The flow test in MWX-1 and interference measurement in MWX-2 and MWX-3 were concluded at 1:45 pm November 1.

2.2.9 Stress Tests in MWX-2 (November 2-11, 1983)

November 8, an unsuccessful attempt as made to stress test zone 3 separately from zone 4. Communication apparently developed during breakdown of zone 3 outside the casing between the zone 3 perforations (7060-7088 ft) and the zone 4 perforations (7107-7131 ft). The two zones were then combined for stress testing by moving the packer to 7030 ft and pressuring the casing-tubing annulus to 2200 psi. The combined interval could not be broken down at 1.5 bpm and 3100 psi surface pressure due to rate limitations on the stress test pump.

November 9, three zones above zone 4 in MWX were perforated with four 14-gm JSPF in preparation for stress testing: 6928-6930 ft, 6963-6925 ft, and 7010-7012 ft. The next day, the interval at 7010-7012 ft was stress tested and, following unseating of the GRC tool, began flowing gas. November 11, the intervals at 6963-6965 ft and 6928-6930 ft were also successfully stress tested. No gas flow was noted from these two intervals following stress testing.

2.2.10 Fracture Diagnostics Tests and Frac Preparations (November 12-December 2, 1983)

November 12, the tubing and packer were pulled from MWX-2 and laid down to prepare the well for geophysical observation. The BOP's were closed and

the rig was moved to MWX-3. November 14, the tubing and packer were pulled from MWX-3 and laid down to prepare the well for geophysical observation. A Baker wireline-set, retrievable bridge plug was set at 7060 ft and the well was loaded with 2% KCl water and the casing was pressure tested to 2000 psi. The 7-in. lubricator was installed and the rig was moved to MWX-1. The well was now ready for the Sandia borehole seismic tools.

November 16, the tubing and packer were pulled from MWX-1 in preparation for fracture diagnostics. The BOP's and the rig remained on the well. The Sandia borehole seismic tools were set in MWX-2 and MWX-3 at a depth of 2000 ft. November 17, the tools were calibrated, using surface Vibroseis equipment, and then removed from the wells.

November 19 and 20, the borehole seismic tools in MWX-2 and MWX-3 were lowered and clamped around 7000 ft and were oriented by firing a series of 2-gm charges in a shrouded hollow steel carrier positioned at various depths between 6900 ft and 7200 ft in MWX-1. The tools were removed from the wells after these tests.

November 24, the stress test perfs in MWX-2 at 6928-6930 ft, 6953-6955 ft, and from 7010-7012 ft were bradenhead squeezed with 65 sacks of Class H cement, containing 0.8% Halad 9 and 0.1% HR-3, in an attempt to prevent gas flow which was causing undesirable seismic noise in the well. The cement squeeze was staged in small increments to 5500 psi. On November 27, drill-out operations were initiated. Solid cement was drilled from 6800 ft to 7050 ft. No gas was observed while drilling through the squeezed interval. Following completion of the drillout operations and laying down of the tubing, the 7-in. lubricator was installed. December 2, the borehole seismic tools were repositioned in both MWX-2 and MWX-3 just above the bridge plugs. Twelve 2-gm shots were select fired in zones 3 and 4 in MWX-1 to orient the borehole seismic tools in MWX-2 and MWX-3.

2.2.11 Phase I Frac Week: Steprate, Flowback, and Minifracs in MWX-1 (December 5-9, 1983)

December 6, an additional 16 orientation shots were select fired in MWX-1. In addition, water hammer tests, a steprate/flowback test, and two pump-in/flowback tests were conducted using Smith Energy Services equipment.

December 7, Smith Energy Services conducted the first of two minifracs in zones 3 and 4 to monitor fracture behavior as a function of treatment volume. The first minifrac consisted of a 2100 gal methanol prepad to assist with liquid recovery, followed by 15,000 gal of gelled 2% KCl water. The gelling agent was Smith WGA-2, a noncrosslinked HPG material at a 30 lb/1000 gal concentration. The job was pumped at a rate of 10 bpm at 3780 psig surface pressure.

December 9, an additional 18 orientation shots were fired in MWX-1 to reorient the Sandia borehole seismic tools installed in MWX-2 and MWX-3. (The tools had been removed for maintenance after the first minifrac.) Then a second, larger, minifrac was conducted by Smith Energy Services in the same zone 3 and 4 interval in MWX-1. The minifrac consisted of a 4500 gal methanol prepad to assist with liquid recovery, followed by 3600 gal of gelled 2% KCl water, a shut-down for a water hammer test, and then an additional 26,400 gal of gelled 2% KCl water. The gelling agent was Smith WGA-2, a noncrosslinked HPG material at a concentration of 60#/1000 gal. The job was pumped at a rate of 10 bpm at a maximum surface treating pressure of 4160 psi. The ISIP was 3820 psi, and the 10-minute shut-in pressure was 3500 psi.

2.2.12 Flowback and Site Shutdown (December 10-16, 1983)

At 10:00 am, December 10, flowback operations were initiated at MWX-1. By December 15, a total of 720 bbls of load fluid (out of 1490 bbls total

fluid) had been recovered. The well was shut in, the tree filled with diesel, and MWX-1 was secured for the winter. December 13, the tubing was rerun in MWX-2, the tree was installed and filled with diesel, and the well was secured for the winter. Similar operations the next day in MWX-3 secured the well for the winter.

2.2.13 Winter Shutdown (December 16, 1983-March 22, 1984)

During the winter shutdown, MWX-1 was flowed twice weekly to the flowback tank to assist with liquids removal from the well. Maintenance and repair of wellsite equipment was also undertaken during this time. Reactivation of the site began in early March.

2.2.14 Flow Tests in MWX-1 (March 26-April 21, 1984)

The postfrac testing of zones 3 and 4 began March 26. The primary objective of the testing was to determine the effects of the nonpropped hydraulic fracture in zones 3 and 4 on the productive capacity of these reservoirs, while a secondary objective was to derive the fracture characteristics. The testing consisted of three consecutive drawdown periods, a shut-in period, and a final drawdown. MWX-1 was shut in at approximately 8:00 am, April 11, for a pressure buildup test. The well was placed on production at 8:00 am, April 17, at a rate of 250 MCFD and 1928 psi FBHP. The well was shut in at 4:00 pm. Early analysis of the drawdown data indicated a reduced productive capacity for the interval.

2.2.15 Vertical Seismic Profiles in MWX-2 and MWX-3 (April 1-14, 1984)

From April 1 to April 14, Sandia , in conjunction with the US Geological Survey, conducted vertical seismic profiles in MWX-2 and MWX-3 using a seismic source (an air gun truck) positioned at one of three sites located either 3000 ft northeast, 3000 ft west, or 3400 ft southeast of the

Multiwell Experiment site. This work was undertaken in an effort to study the sand lens morphology and the magnitude of natural fracture system anisotropy in the lenticular Mesaverde sands.

2.2.16 Fracture Diagnostics Tests and Frac Preparations (April 24-May 1, 1984)

April 24, a fishing operation was initiated to recover a cable head, three sinker bars, and an HP gauge lost in MWX-1. Fishing operations were successfully concluded at 11:00 am, April 27. April 28, the 2-7/8-in. tubing was run in the well to 6747 ft and landed. The wellhead was installed and pressure tested to 5000 psi. A 2-1/8 in, select fire, tubing gun was run to zones 3 and 4. Three 6-gm shots were select fired in zone 3 and nine 6-gm shots were select fired in zone 4 to orient the Sandia borehole seismic tools in MWX-2 and MWX-3. (The Sandia borehole seismic tools remained clamped in MWX-2 and MWX-3 during this period with intermittent equipment troubleshooting of minor mechanical and electrical problems.)

2.2.17 Phase II Stimulation (May 2, 1984)

A sand-propped hydraulic fracture treatment was performed in zones 3 and 4 on May 2, by the Western Company using 75,479 gal of 3% KCl treatment fluid that was composed primarily of cross-linked HPG gels and 190,000 lbs of Ottawa sand. Ammonium thiocyanate was utilized as a liquid tracer and mixed with the HPG gels at a concentration of 100 ppm. Resin coated sand containing radioactive iodine^{131} and iridium^{192} were mixed with the slurry during treatment as a proppant tracer. The frac treatment consisted of a 7700 gal methanol prepad to assist with liquid recovery, followed by a 20,400 gal Apollo 40 pad, 46,000 gal of Apollo 35 gel containing 184,500 lbs of 20/40 sand at sand concentrations ranging from 1.5 ppg to 5.5 ppg, 1000 gal of Apollo 25 gel containing 5500 lbs of 12/20 sand at 5.5 ppg, and

an 8778 gal flush. The maximum treating pressure was 4400 psi, and the average pressure was 3600 psi. The average treating rate was 20 bpm down the annulus between the 7-in., 29-lb., N-80 casing and the 2-7/8-in., 6.5-lb., N-80 tubing. The ISIP was 4000 psi, and the 15-minute shut-in pressure was 3600 psi. The pumping time was approximately 2 hours. The total load fluid to recover was 2253 bbls, of which 2005 bbls were frac load fluid and the remaining 248 bbls were wellbore volume.

2.2.18 Flowback, Washing, and Fishing in MWX-1 (May 3-June 4, 1984)

May 3, the Sandia borehole seismic tools were removed from MWX-2 and MWX-3. MWX-1 was returned to production at 9:00 am May 3, and by May 7, 1267 bbls of frac load had been recovered.

May 4, sand fill was discovered at 7068 ft while attempting to run a postfrac gamma ray log. Sand cleanout operations in MWX-1 were initiated May 8. A workover rig was moved in, BOPs installed, and tubing was added to reach the top of the sand fill at 7065 ft. A power swivel was used to rotate the tubing while reverse circulating the sand fill out of the well, down to the depth of the bridge plug at 7200 ft. The well started to unload while reversing the sand fill from the hole. The well was killed with 40 bbls 2% KCl water, 14 joints of tubing were laid down, and the tubing was landed at 6744 ft. The BOPs were removed, the wellhead installed, and flowback of load fluid resumed at 8:30 am., May 9.

May 11, MWX-1 was dead on the tubing and had 650 psi on the casing. A workover rig was again moved on the well, BOPs installed, and the tubing was lowered to check for sand fill. Approximately 12 ft of sand fill was found on the bridge plug at 7200 ft, which was 44 ft below the lowermost perforation. The tubing was then pulled from the well. A 10-ft perforated sub and a No-Go device were then run below the retrievable packer on the tubing with the packer element set at 6880 ft and the tubing sub landed at

6897 ft. The wellhead was reinstalled and the well was shut in overnight May 12 to build pressure. On May 13, flowback of load fluid resumed with the well flowing sand and water.

May 23, a temperature survey attempted in MWX-1 would not go below 7085 ft due to suspected sand fill. A workover unit was moved onto the well May 24, BOPs installed, and the tubing was picked up to release the packer. The packer would not release. The following day Gearhart cut off the tubing at 6875 ft, the tubing was tripped from the well, and the cut-off joint was laid down. May 26, a fishing assembly consisting of a combination overshot-mill, mechanical and hydraulic jars, and five drill collars, were run in the well on 2-7/8-in. tubing to try and recover the remaining fish. The tubing stub was milled over and worked for several hours, came free, and was recovered along with the collar at the top of the packer mandrel. May 27, the same fishing assembly was run in the well on 2-7/8-in. tubing and successfully milled over the top of the packer mandrel. The packer came loose after 15 minutes jarring and was recovered from the well along with the 10 ft tubing sub and the No-Go device. May 29, the 2-7.8-in. tubing was run in the well, sand fill was tagged at 7150 ft and was reverse circulated from the well to 7192 ft. The tubing as then raised to 7064 ft, 12 ft above the top perforation, landed, the tree installed, and the well returned to flowing status to the 400 bbl tank.

From May 30 until June 6, the well was intermittently flowed to the 400 bbl tank and shut in to build pressure to facilitate liquid removal from the well.

2.2.19 Set Bottomhole Gauges in MWX-2 and MWX-3 (May 18-21, 1984)

May 18, MWX-2 was equipped for interference testing in zones 3 and 4. A 20-ft perforated sub, retrievable packer, and a CER downhole shut-in device, were run on 2-7/8-in. tubing with the packer being set at 7041 ft and the

downhole shut-in tool at 7994 ft. The next day, MWX-3 was equipped for interference testing in zones 3 and 4. A 12-ft, perforated sub, retrievable packer, and a CER downhole shut-in device, were run on 2-7/8-in. tubing with the packer being set at 7055 ft and the downhole shut-in tool at 7019 ft. The HP gauges were set in MWX-2 and MWX-3 on May 21.

2.2.20 Remedial Treatment in MWX-1 (June 6)

June 6, a chemical breaker treatment was conducted by the Western Company in zones 3 and 4 in MWX-1 to attempt to break the viscosity of the crosslinked HPG gel used during the May 2nd stimulation. This remedial treatment was undertaken in response to the inability of the well to return to the level of gas production achieved prior to stimulation. The well was loaded with 245 bbls of 3% KCl water. Forty bbls of treatment fluid were spotted across the perfs. A total of 6500 gal of 3% KCl water containing 1000 gals of 3% hydrogen peroxide and 975 lbs of ammonium persulfate breaker (at a concentration of 175 lb/1000 gal) were then displaced into the perforations down the tubing at rates of 1 to 2 bpm and flushed with 40 bbls of 3% KCl water. The maximum treatment pressure was 3150 psi, minimum treatment pressure was 2900 psi, and the average treating pressure was 3000 psi. The ISIP was 3000 psi and the 15-minute shut-in was 2400 psi. The total load fluid to recover from this remedial treatment was 423 bbls. The total pumping time was approximately 2 hours. The well was shut in at 12:40 pm and remained shut in until 8:15 am, June 7, when flowback was initiated.

2.2.21 Cleanup of Remedial Treatment in MWX-1 (June 7-July 10, 1984)

From June 7 until July 10, MWX-1 was alternately flowed to recover treatment fluid, and shut in to build pressure to try and maximize load fluid recovery. The well did not respond to the stimulation of May 2, 1984 or to the remedial treatment of June 6, 1984, sufficiently to be able to clean itself up and unload liquids on a continuous basis.

July 10, a workover unit was moved on to MWX-1 and the well was re-entered to recover a Kuster gauge and 3200 ft of slick line lost in the well. The slick line was recovered from the tubing without incident but the Kuster gauge remained on the No-Go device on the bottom of the tubing. The tubing was picked up and was lowered to 7188 ft, 44 ft below the lowermost perforation without encountering sand fill. The measurement for the downhole assembly tripped out of the well, including 2-7/8-in. tubing, No-Go nipple, and locator sub, was 7062 ft. The downhole assembly run back in the well, including 2-7/8 in. tubing, retrievable packer, tailpipe, CER downhole shut-in tool, and the No-Go nipple, measured 7179 ft. The tubing tail was landed 35 ft below the lowermost zone 3 perforation.

2.2.22 Production/Interference Tests, Zones 3 and 4; MWX-1 Producer (July 11-August 13, 1984)

Postfrac pressure drawdown and buildup testing was initiated in zones 3 and 4 on July 11. HP instruments were installed bottomhole in MWX-2 and MWX-3 for interference measurement, and in MWX-1 for monitoring the flowing bottomhole pressure. Bottomhole shut-in tools were used in all three wells to minimize the effect of wellbore storage during the testing. At 7:00 am, July 11, production was initiated at 150 MCFD from MWX-1 for a 134-hr, constant rate, pressure drawdown test which ended at 9:00 pm, July 16. This was followed by a 48-hr pressure buildup which ended at 9:00 pm July 18, when production was again initiated at 150 MCFD to begin a second constant rate, pressure drawdown test. This test ended after 123 hours of flow at 12:00 midnight, July 24, and it was followed by a 48-hr pressure buildup. At 12:00 midnight July 26, a third pressure drawdown was initiated at MWX-1 at a constant rate of 150 MCFD and terminated after 139 hrs flow at 7:00 pm, July 31. MWX-1 was shut in at that time for a 264 hr pressure buildup that ended at 7:00 pm, August 13. No distinct changes were observed in the bottomhole pressure of observation wells MWX-2 and MWX-3 due to the testing in MWX-1.

2.2.23 Stress Tests in MWX-3 (August 6-12, 1984)

August 6, three intervals in MWX-3 were perforated with four 14-gm JSPF in preparation for stress testing: 7032-7034 ft, 7048-7050 ft, and 7068-7070 ft. Two days later, stress testing was initiated at 7068-7070 ft, but testing was suspended due to communication around the sealing element in the top packer of a dual packer assembly. Several days were lost getting replacement parts to the site. On August 11, stress testing was successful, using a downhole assembly consisting of a retrievable bridge plug and one retrievable packer, on the 7032-7034 ft and 7068-7070 ft intervals. The coal zone, 7048-7050 ft, was successfully stress tested using the same downhole assembly on August 12.

2.2.24 End Paludal Stimulation Experiment (August 14-16, 1984)

August 14, the stress test assembly was pulled from MWX-3 and laid down. A G.O. Elite, wireline set, CIBP was set at 7020 ft and 2 sacks of sand were placed on top. The new plug-back depth was 7014 ft. The next day the tubing and packer were pulled from MWX-2 and laid down. A G.O. Elite, wireline-set, CIBP was set at 6920 ft and 2 sacks of sand were placed on top. The new plug-back depth was 6914 ft.

August 16, the tubing, packer, and tailpipe were pulled from MWX-1. The packer and tailpipe were laid down. A G.O. Elite, wireline set, CIBP was set at 7060 ft and the well was shut in overnight. Pressure built to 1500 psi in 13 hrs indicating the bridge plug was leaking. A casing scraper was run to 7050 ft, the tubing and scraper were pulled from the well and laid down, and a second wireline set, CIBP was run and set at 7040 ft. Two sacks of sand were dumped on the bridge plug, and the hole was loaded with 3% KCl water. The plug was successfully pressure tested to 3000 psi.

2.2.25 Workover and Reentry of MWX-1 (December 7-12, 1985)

Paludal zones 3 and 4 were to be connected to the pipeline for 1985 winter gas production. This interval was selected primarily to evaluate the effects of time and reservoir equilibrium on the damage that resulted from the stimulation during the summer of 1984.

December 6, a workover rig was moved to MWX-1, and preparations were made to begin drilling out the two CIBP's previously set at 7040 ft and 7060 ft in the well. The next day, a downhole assembly, consisting of a 5-3/4-in. drag tooth mill, a crossover sub, 14 4-3/4-in. drill collars, and 199 joints of 2-7/8-in. tubing, was run in the well to 7035 ft and reverse circulated to remove the sand from the bridge plug at 7040 ft. A considerable amount of rubber, but no sand, was recovered from the well. December 8, the CIBP at 7040 ft was drilled through and its remains pushed downhole on top of the CIBP at 7060 ft. Drilling proceeded on the second plug until an increase in gas rate was observed. Milling operations were shut down at 6:30 pm for the night.

At 7:00 am, December 9, following 14 hrs shut-in, wellhead pressure had built to 3300 psi. The well was blown down, the hole loaded with 3% KCl water, drilling resumed, and the second bridge plug was drilled up. The remains of the second bridge plug were pushed downhole to 7180 ft. The well was then flared to the pit on a 3/4-in. choke, overnight, to clean up.

December 10, the downhole drilling assembly was stripped from the well. The production string, consisting of a 10-ft perforated sub, 4 joints of 2-7/8-in. tailpipe, a retrievable packer, and 212 joints of 2-7/8-in. tubing, was then stripped into the well. The tailpipe was landed at 7145 ft, the packer was set at 6998 ft, and the well was made ready for production. The workover rig was moved off MWX-1 on December 12.

2.2.26 Limited Production Tests in MWX-1 (December 12-23, 1985)

December 12, MWX-1 was production tested for a period of four hours at 350 MCFD to test the surface equipment. The well was equipped with Kuster bottomhole pressure instruments on December 13, and was shut in at 5:00 pm for a pressure buildup. The well remained shut in until 12:00 noon December 18, when Western Slope Natural Gas Company turned the well to the pipeline at a rate of 400 MCFD. However, at 2:00 pm, December 23, Western Slope shut in the well due to lack of market demand for the gas.

2.2.27 Winter Shut-in (December 23, 1985-March 24, 1986)

MWX-1 remained shut in from December 23, 1985 to March 24, 1986, due to lack of demand for the gas in Western Slope's service area.

2.2.28 Production Tests in Paludal Zones 3 and 4 in MWX-1 (March 24-May 30, 1986)

Western Slope resumed taking gas production from MWX-1 at 9:00 am, March 24, at a rate in excess of 450 MCFD. Gas rates during the first ten days of production exceeded 400 MCFD, while the next thirty days of production averaged about 325 MCFD. The water production during this test averaged 20 to 40 bpd. Volumetric accounting of injected and recovered liquids indicated the produced liquids were well in excess of the injected fracture liquids, thus formation water was being produced.

Following about 48 days of production, the well was shut in at 3:00 pm May 12, for a pressure buildup test. The well remained shut in until 9:00 am May 27, when the well was returned to production at a rate of 600 MCFD to bleed off pressure from this interval preparatory to its abandonment.

2.2.29 Set Bridge Plug over Paludal Interval (May 30-June 12, 1986)

May 30, a tubing plug was set in the 2-7/8-in., 6.5-lb tubing in MWX-1 at 6950 ft and zones 3 and 4 were isolated from the wellbore ending the paludal reentry test. A short test of a shallower coastal zone was conducted. Finally, on June 12, a service rig was moved onto the well, the tubing and packer were pulled from the well, and the packer was laid down. A G.O. Elite, wireline set, CIBP was run in the well and set at 7050 ft, permanently abandoning the paludal interval.

2.3 REFERENCES

1. CER Corporation, "Multi-Well Experiment: MWX-1 As-Built Report," Sandia National Laboratories Contractor Report, SAND82-7201, July 1982.

2. CER Corporation, "Multi-Well Experiment: MWX-2 As-Built Report," Sandia National Laboratories Contractor Report, SAND82-7100, August 1982.

3. CER Corporation, "Multi-Well Experiment: MWX-3 As-Built Report," Sandia National Laboratories Contractor Report, SAND84-7132, February 1984.

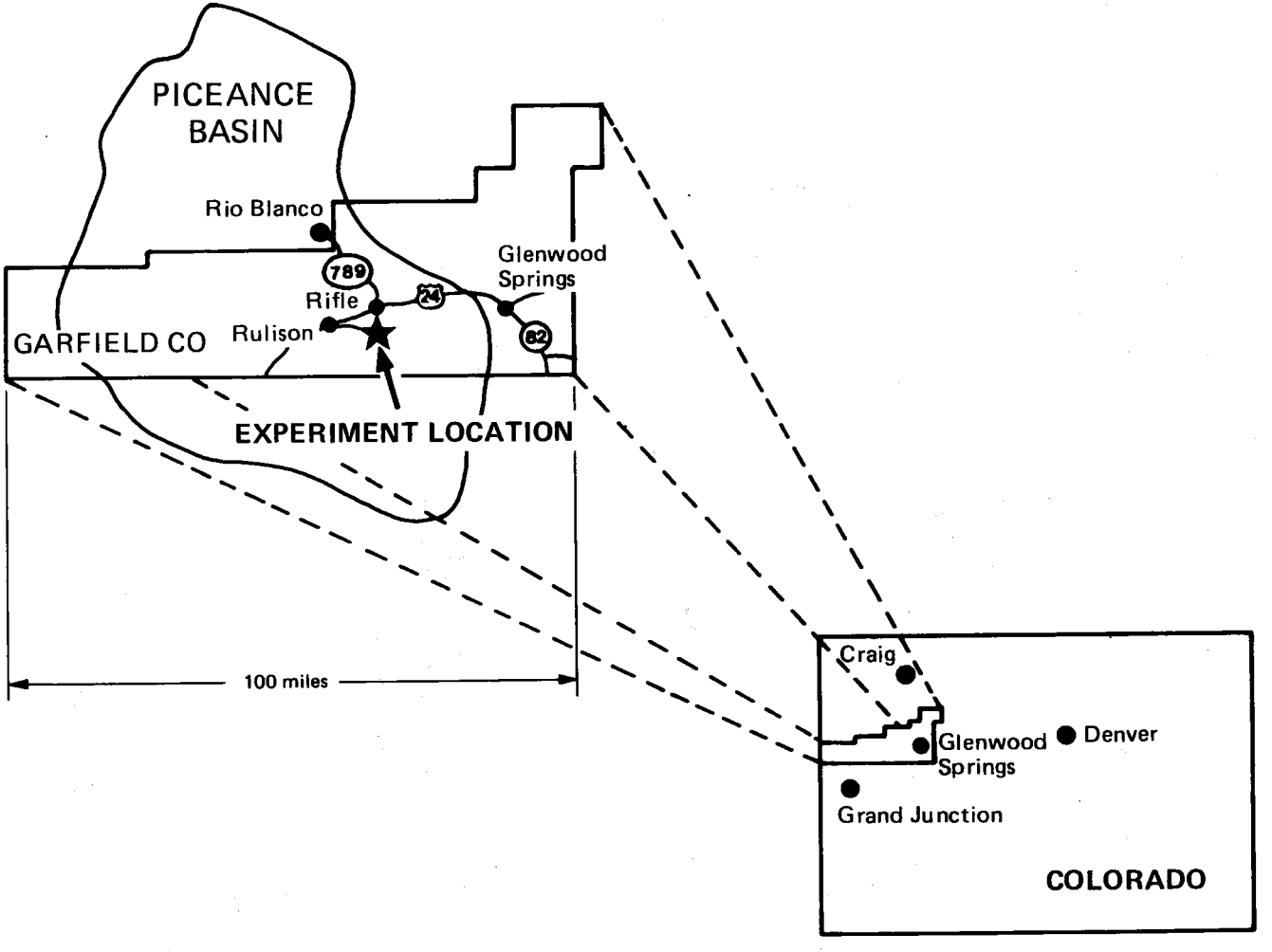

Fig. 2.1 Multiwell Experiment Location

MWX-1

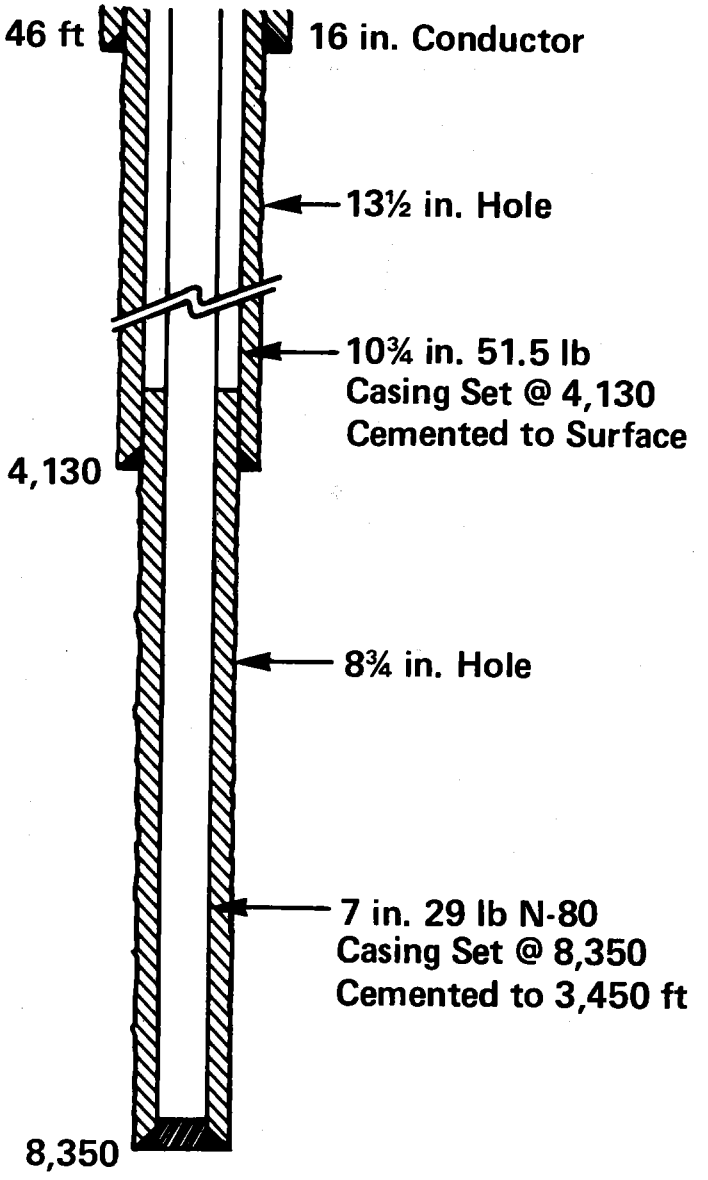

CORES

4,170 - 6,827 ft	2,657 ft
7,870 - 7,960	90 ft
Total	2,747 ft
Oriented	470 ft

LOGS

4,130 - Surface
4 Logs - comb.

6,827 - 4,130 ft
11 logs - comb.

8,350 - 4,130 ft
18 logs - comb.

DSTs

5,885 - 5,830 ft

RFTs

8,135 -4,535 ft
12 tests

Spud Date: Sept. 13, 1981
Rig Released: Dec. 21, 1981

Fig. 2.2 MWX-1 Well Information

MWX-2

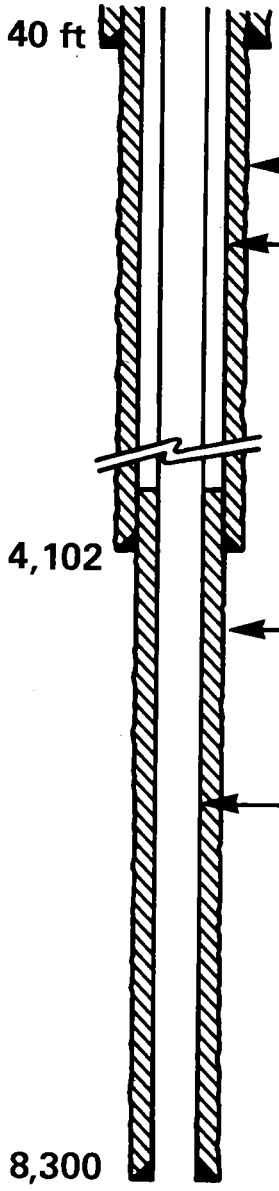

CORES

4,870 - 4,956 ft
5,485 - 5,581 Pressure Core
5,700 - 5,880
6,390 - 6,568
7,030 - 7,385
7, 817 - 7,907
8,100 - 8,141

915 ft of Core
395 ft Oriented

LOGS

5,438 - 4,094 ft
3 logs - comb.

6,050 - 4,094 ft
3 logs

6,688 - 4,094 ft
9 logs - comb.

8,300 - 4,094 ft
15 logs - comb.

DST

4,895 - 4,955 ft

Spud Date: Dec. 31, 1981
Rig Released: Mar. 30, 1982

91 days

Fig. 2.3 MWX-2 Well Information

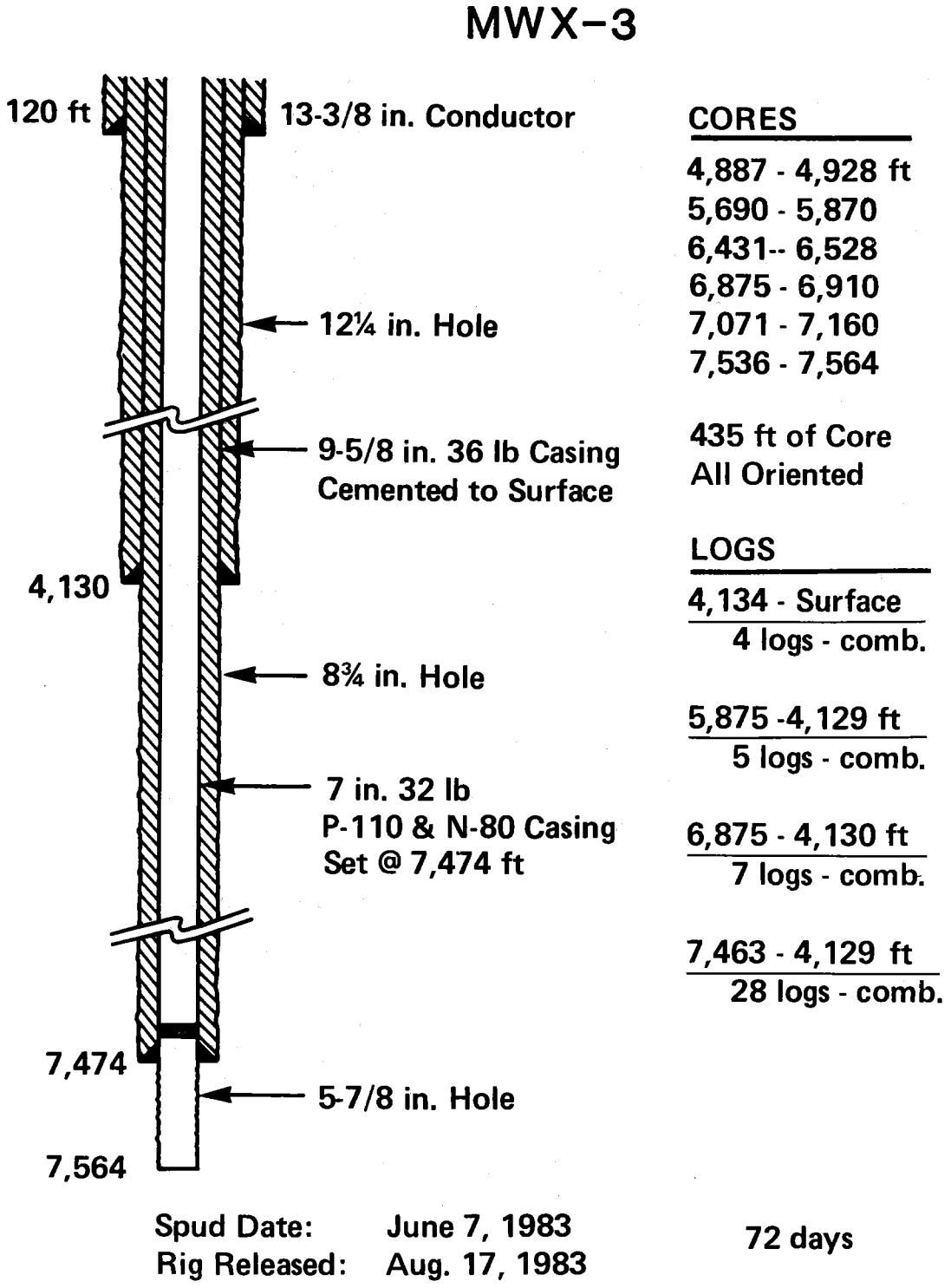

Fig. 2.4 MWX-3 Well Information

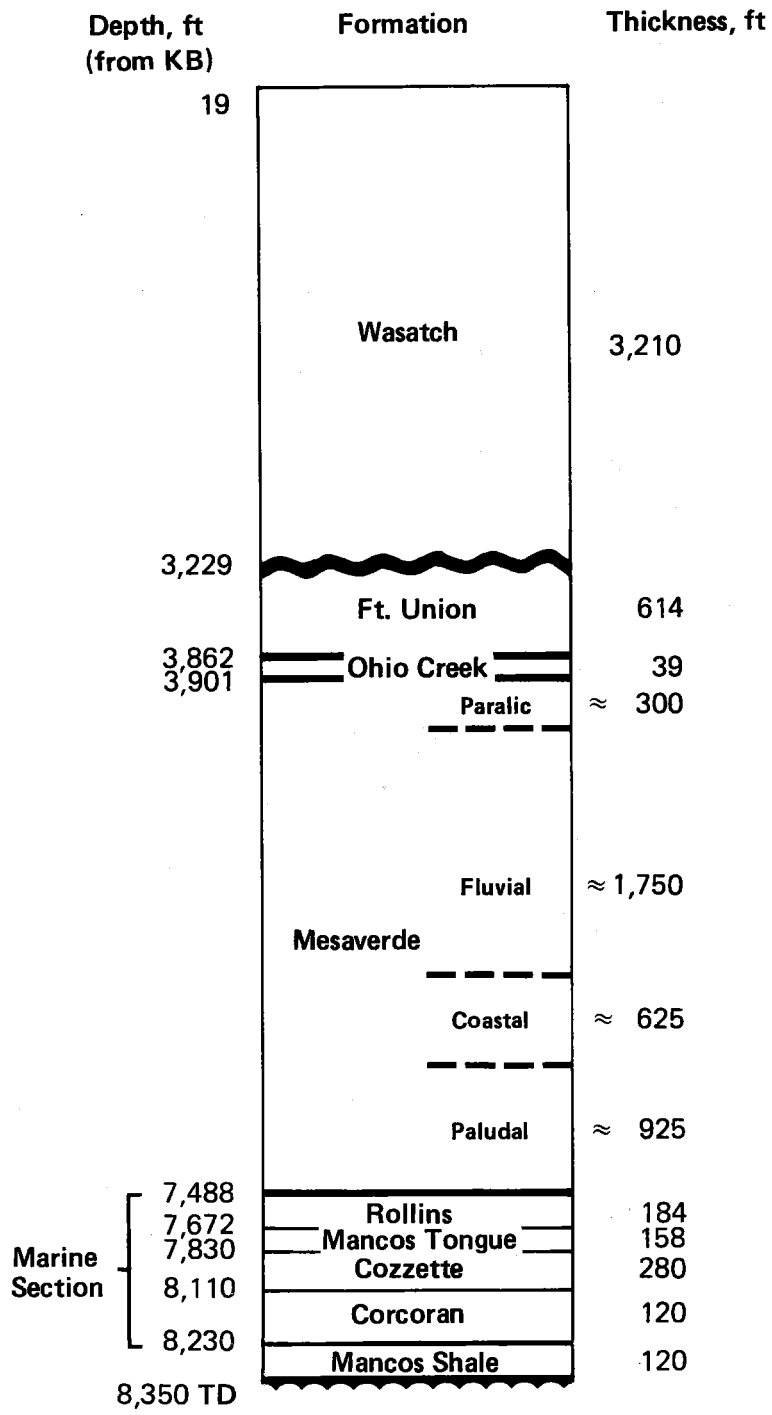

Fig. 2.5 Geologic Cross-section of MWX-1

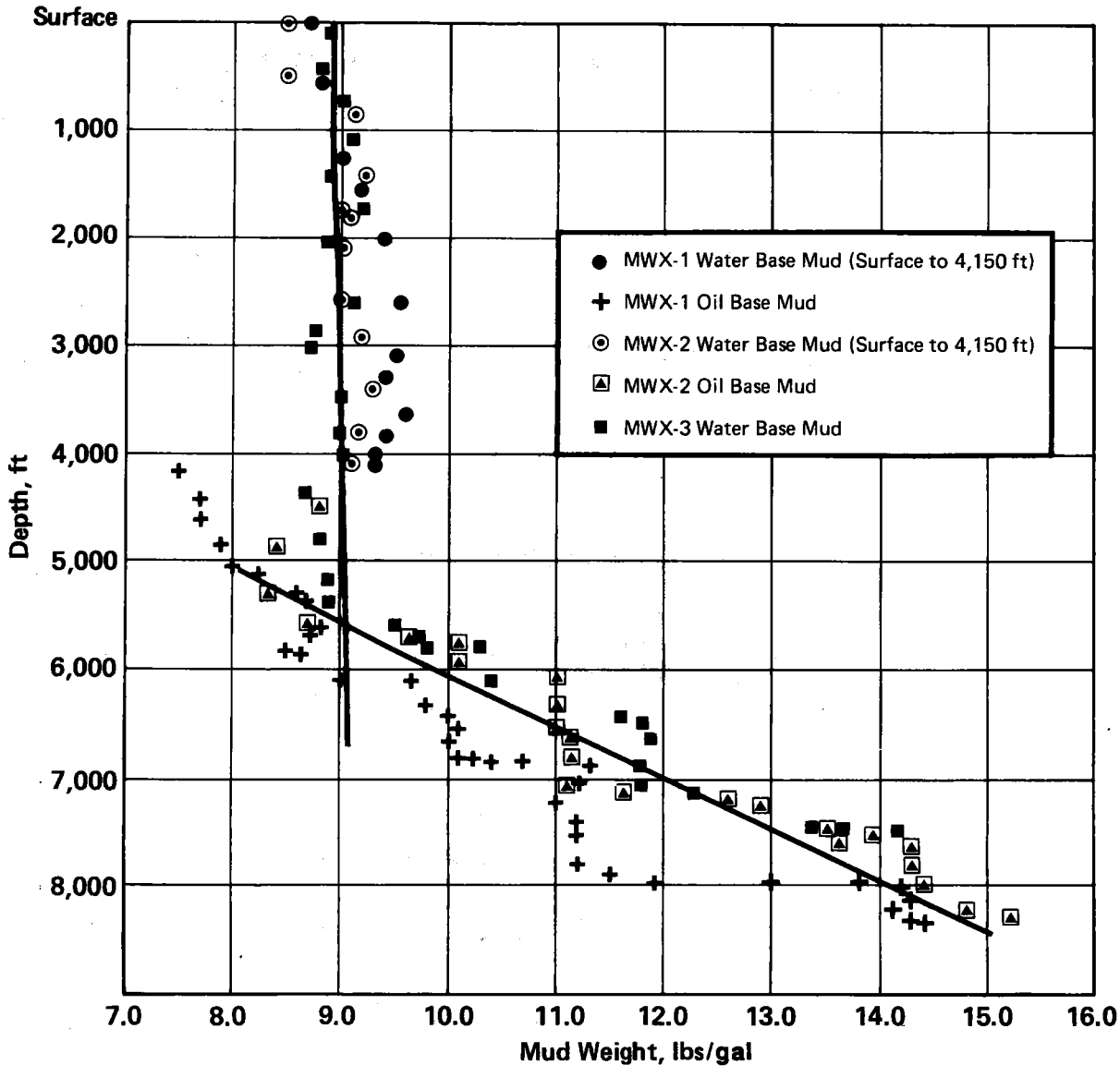

Fig. 2.6 Mud Weight Versus Depth

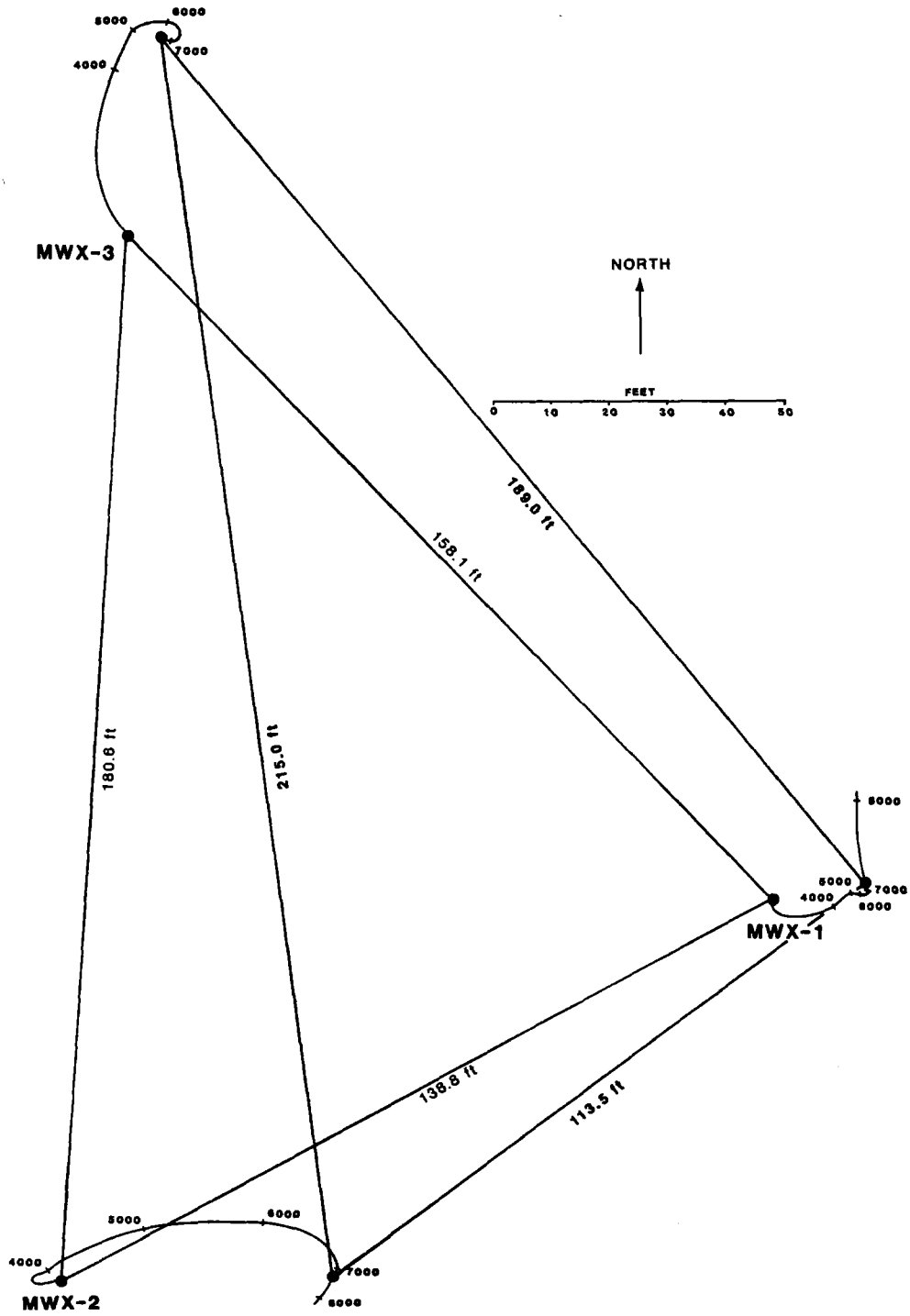

Figure 2.7 Relative Well Spacings at Surface and at 7300 ft (the deepest survey in all three wells).

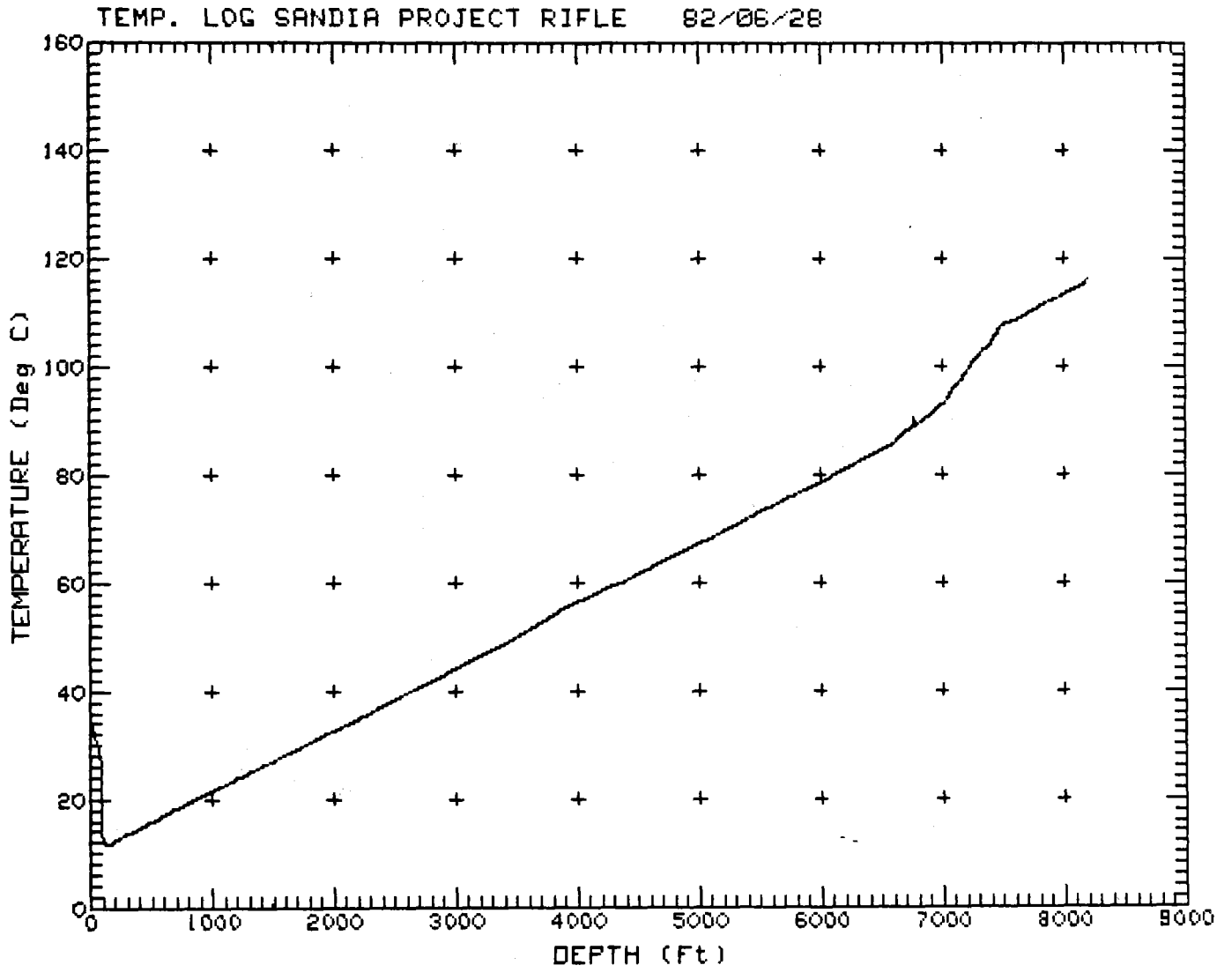

Figure 2.8 Temperature Log of MWX-1.

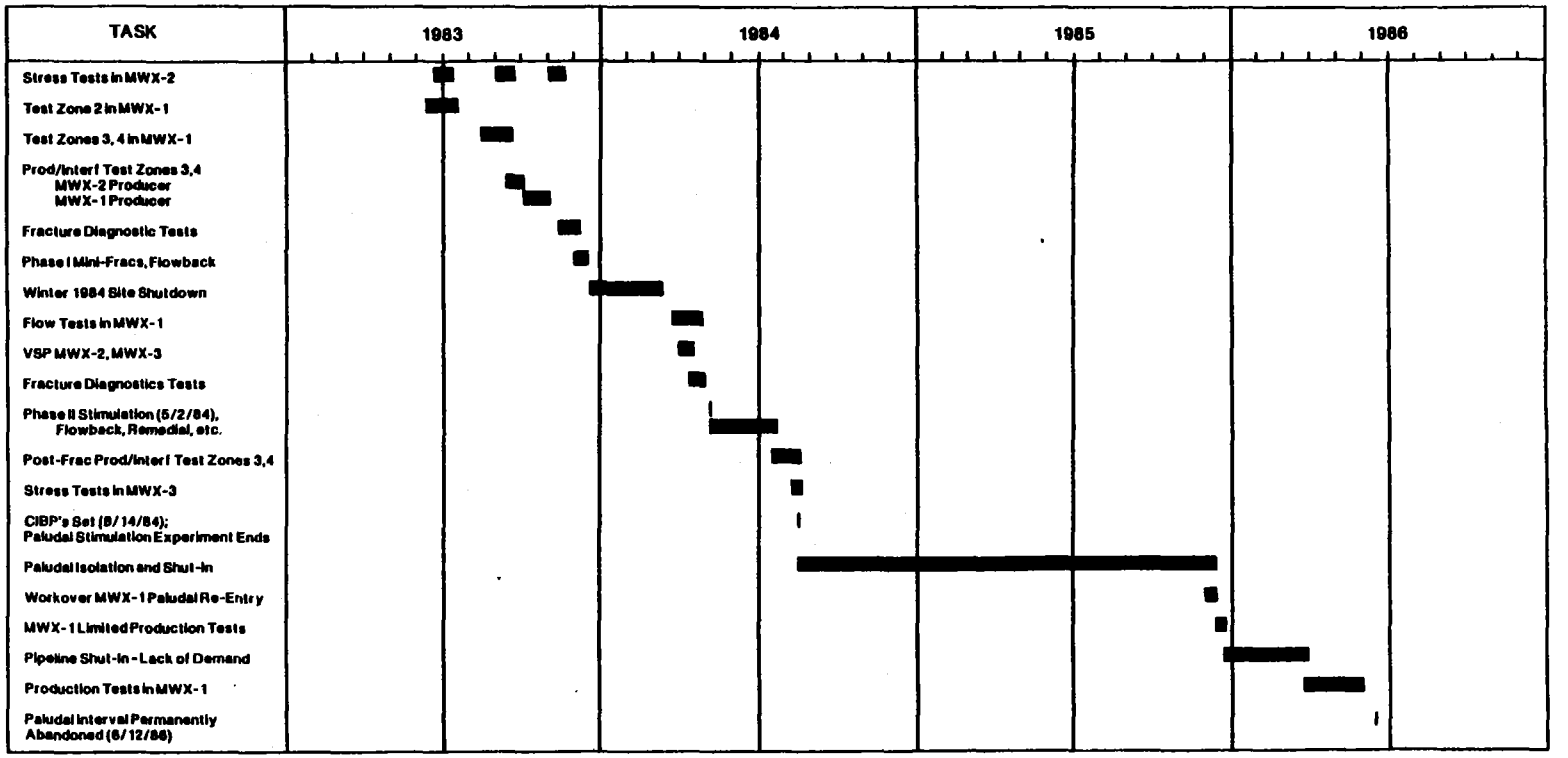

Figure 2.9 Chronology of Paludal Operations

3.0 GEOLOGY

John C. Lorenz
Sandia National Laboratories

3.1 INTRODUCTION

The paludal deposits are found at depths of 6600 to 7455 ft at the MWX site. The rocks of this interval were laid down in environments of lenticular distributary channels and adjacent coal swamps.[1,2] Sandstones occur as both channel fillings and splay (flood) deposits adjacent to the channels. The swamps are recorded as mudstone, carbonaceous mudstone, and coal deposits. These environments were located on a prograding lower delta plain, landward of the Rollins shoreline. The resulting deposits were penetrated by all three MWX wells, and are exposed in outcrops along the Grand Hogback (specifically at Rifle Gap).

The general structure of the Mesaverde Formation in the Piceance basin (Figure 3.1) is that of a gentle northeasterly dip toward the Grand Hogback.[3] There the dip abruptly reverses to a steep southwesterly trend due to uplift of the adjacent White River Plateau. There is no significant structural alteration of this gentle northeasterly dip in the paludal zone at MWX (Figure 3.2). However, ten feet of "missing" section in MWX-2 suggests that a high-angle, normal fault might cut through that well at about the 7060 foot depth (Section 3.6 and 4.2).[4,5]

3.2 LITHOLOGY

3.2.1 Core Lithology: Paludal Sandstone Reservoirs in the MWX Wells

Five major sandstones of the paludal zone, designated Zone 1 (lowest) to Zone 5 (highest) were penetrated in the MWX wells (Figure 3.3). Zones 1, 2, 3, and 4 were cored in MWX-2, and Zones 3, 4, and 5 were cored in MWX-3.

Zone 1 core in MWX-2 shows a sequence of alternating thin beds of mudstone, siltstone and sandstone. The main reservoir rock is only about 8 ft thick. It is found near the top of the interval, and consists of apparently massive sandstone with some carbonaceous material. The other, thinner sandstones display crossbedding and ripples, and also contain carbonaceous material as well as ripup clasts of claystone.

Zone 2 directly overlies a coal seam. MWX-2 core contains a suite of sandstones with carbonaceous zones and abundant mudstone ripup clasts and numerous internal scour surfaces. The sandstones are most commonly massive, but several thin crossbedded zones occur. This lithology constitutes the lower 21 ft of the reservoir in MWX-2, above which thin-bedded sandstones, siltstones, and mudstones are present.

Zone 3 also overlies a coal seam, but the main reservoir facies, cored in both MWX-2 and MWX-3, is a much cleaner, crossbedded and rippled sandstone. It is about 22 feet thick in MWX-2, and about 15 feet thick in MWX-3. Thin-bedded sandstones, siltstones, and mudstones constitute the rest of the reservoir, both over- and underlying the cleaner sandstones in both wells.

The lithology of Zone 4 is significantly different from the other reservoirs in the paludal zone. Core from MWX-3 shows a thick sequence of rippled sandstone interrupted by a few coaly and silty to muddy partings. The sandstones of the lower half are relatively clean, whereas those of the upper half contain abundant carbonaceous material. Zone 4 splits into two sandy intervals in MWX-2. Only the lower one was cored, and it consisted of about 16 feet of very thinly bedded, carbonaceous, siltstones and mudstones.

Zone 5 was cored only in MWX-3, and the main reservoir sandstone was not penetrated. Only thin-bedded sandstones, siltstones, and carbonaceous mudstones were cored.

3.2.2 Outcrop Lithology

The paludal zone of the Mesaverde Formation outcrops along the Grand Hogback, but the interbedded coals are commonly burned and the reservoir-type sandstones are not well exposed. Lenticular distributary-channel sandstones and the more amorphous splay deposits can be seen at Rifle Gap in the Hogback, but better exposures of this interval are found in the less structurally deformed Mesaverde rocks in Coal Canyon west of Cameo, in the west-central part of the basin. Heterogeneous, lenticular sandstone reservoirs with internal lithologic discontinuities are common in outcrop. These reservoirs are encased in a variety of lithologies that include coals and thin-bedded, carbonaceous mudstones, siltstones, and sandstones.

3.2.3 Reservoir Sandstone Petrology

The reservoir sandstones of the paludal interval are "dirty," containing a high proportion of lithic fragments. They range from dolomitic sublitharenites to dolomitic feldspathic litharenites.[6-10] The petrology characteristics are summarized in Table 3.1 and Figure 3.4. The complete set of petrology data is given in Appendix 12.2. Sand grains are fine-grained to very fine-grained, moderately to well-sorted, and subrounded to subangular. The associated clays are primarily mixed-layer illite/montmorillonite and some illite, with a trace of chlorite.

Porosity is a variable characteristic, ranging from a trace to 24%. It is poorly developed in samples with a high content of carbonate cement. Open porosity is rare: most porosity occurs as microporosity in intergranular authigenic clays, or as secondary porosity created by the dissolution of unstable grains.

Diagenesis in the paludal zone includes (in approximate chronological order): stages of early carbonate cement precipitation, feldspar

alteration, compaction, quartz precipitation, development of secondary porosity, later stages of calcite precipitation, formation of authigenic clays, later stages of dolomitization of calcite, and later stages of quartz precipitation.

3.3 RESERVOIR SEDIMENTOLOGY AND MORPHOLOGY

The size and shape of the Mesaverde reservoirs in the MWX wells vary with the different depositional environment of each zone.[11] The paludal zone is interpreted to have been deposited on a lower delta plain: (a) the lenticular reservoir sandstones deposited in narrow distributary channels, (b) the more amorphous sandstones as flood-produced splay deposits adjacent to the channels, and (c) the coals, mudstones, and carbonaceous mudstones deposited in swampy (paludal) environments adjacent to the distributary channels. The thin-bedded sandstone-siltstone-mudstone sequences probably represent channel-margin levee deposits.

The type of reservoir (splay or distributary channel) can be determined by the suite of sedimentary structures observed in core. The sizes of splay deposits are poorly defined, but the width of a channel-type reservoir bears a rough correlation to its thickness. Thus, the thickness of a channel-type reservoir penetrated in the MWX wells can be used to calculate its minimum probable width.[2,12] (This is a minimum estimate because it cannot be determined that the maximum thickness of the lens was penetrated).

Spatial arrangements of depositional environments for each zone, provided by the triangular layout of the three MWX wells, helped to define possible lenticular reservoir orientations. For example, the trend of a reservoir that is present in two wells but not a third is probably aligned with the two wells. Sedimentological detail provides additional information (e.g., a well may penetrate either the edge or center portion of a channel).

3.3.1 Zone 1 (Figure 3.5)

MWX-2 core suggests a channel-margin sequence. Some core from the thickest sand area was removed prior to sedimentologic study but indications are that this unit may have been part of a channel margin. The coarsening-upwards nature suggests that the main channel was migrating toward MWX-2 prior to abandonment. The MWX-1 gamma ray log is sandier and may indicate the position of the associated main channel lens. The MWX-3 gamma ray log suggests a sandstone and mudstone distal channel-margin sequence similar to the lower part of the MWX-2 core, but without density log crossovers. The main channel for this zone probably runs generally east-west just south of the MWX site, although it is possible that it may edge into MWX-1.

3.3.2 Zone 2 (Figure 3.6)

MWX-2 core shows a distinctive, repetitive sequence of clay-ripup conglomerates in a sandstone matrix, with abundant scour surfaces. This suggests that the core penetrated a proximal levee/splay deposit, where each successive flood episode ripped up the veneer of clay left by the previous flood as it spewed sand over the top of the river banks into a coal swamp. The sequence grades up into lower-energy, rooted/massive sandstones and interlayered mudstones typical of a levee. The MWX-1 downhole gamma ray log is more uniform, with good density log crossovers, suggesting that the main channel was penetrated.

The MWX-3 density logs have no crossovers, and the gamma ray log suggests a sandstone and mudstone channel-margin sequence. The main channel of Zone 2 probably runs generally northeast-southwest through MWX- 1, only the feather edge being penetrated by MWX-2 and MWX-3. Based on outcrop height-to-width relationships in the coastal zone at Coal Canyon north of Debeque, and assuming that the 46-foot thickness penetrated by MWX-1 is the maximum channel thickness, this channel should be about 550 feet wide.

3.3.3 Zone 3 (Figure 3.7)

MWX-2 core shows a good sequence of crossbedded and rippled sandstones with few mudstones. This, plus the basal scour surfaces and clay-ripup conglomerates suggest a main channel was penetrated. Core from MWX-3 shows a similar but thinner sandstone which is probably also in the main channel but close to the edge. The MWX-1 gamma ray log indicates a sandy sequence as well, probably main channel. This channel probably runs east-northeast, generally parallel to and centered on the line between MWX-1 and MWX-2, but encompassing MWX-3 at its edge. Based on its 28-foot thickness, it should be on the order of 350 feet wide.

3.3.4 Zone 4 (Figure 3.7)

Core from MWX-3 consists almost entirely of rippled and carbonaceous sandstone, without any of the crossbedding indicative of main channels. This type of rippled sandstone occurs primarily in splays, the flood deposits adjacent to channels. Zone 4 is split in MWX-2 by a coaly zone; only the lower half was cored. This core displays the thinly laminated and extensively burrowed deposits which occur at the subaqueous toes of splays. The gamma ray log from MWX-1 is similar in shape and thickness to that of MWX-3. Thus, zone 4 is interpreted to be a thick splay deposit which thins in the direction of MWX-2, and the parent channel of which is probably within hundreds of feet to the north and east of the MWX site.

This splay is very thin in MWX-2, and there is the possibility that a fault with a 10 to 12 ft throw has mechanically reduced the thickness, creating a "missing section" in MWX-2. However, the available core shows no evidence of structural deformation as it approaches the suggested zone of the fault (the actual zone was not cored), and the apparent thinning of the reservoir can be explained by sedimentary facies changes. On the other hand, the continued 10 to 12 ft offset of correlation horizons

uphole from this area is more easily explained by a fault than by sedimentary processes.

3.3.5 Zone 5 (Figure 3.8)

The gamma ray logs for Zone 5 in MWX-1 and MWX-2 indicate sandy zones with density log crossovers, and are probably main channel deposits. Maximum thickness is 17 feet which suggests a channel width of 200 feet. The core of this zone in MWX-3 is a rippled sandstone and carbonaceous mudstone sequence of a channel-margin/floodplain environment. The Zone 5 channel probably runs east-west through MWX-1 and MWX-2, with MWX-1 being closer to the edge of the channel.

3.3.6 Permeability Breaks

Permeability discontinuities or "breaks" are common within the paludal zone reservoirs. As shown in Figures 3.5-3.8, the reservoirs are not homogeneous sandstones, but contain numerous abrupt changes in grain size, thin zones of mudstone ripup clasts, high densities of carbonaceous material, and some thin but complete partings of mudstone between sandstone units. These breaks control the permeability paths in the reservoir, both through the matrix sandstone and, because the natural fractures commonly terminate at such breaks, through the fractures. Permeability breaks, therefore, significantly affect the observed production characteristics in these reservoirs, although their distribution, extent, and exact effects are very difficult to define.

3.4 ORGANIC CONTENT AND MATURATION LEVEL

The paludal zone is an organic-rich interval, with at least eight significant coal beds, as well as numerous thinner coal seams and carbonaceous mudstone beds. The coal beds of this interval at MWX are low volatile bituminous in rank, and with rank increasing with

depth.[13,14] MWX coal samples tested for gas desorption produced between 200-300 cubic feet of methane per ton on average. Organic content is generally high in the highly carbonaceous mudstones and coals. (Details of coal characterization, vitrinite reflectance data, and gas analyses, are given in Section 5.0.)

3.5 FRACTURES

Twenty-five mineralized fractures are known in MWX core from the paludal zone (Table 3.2). Nineteen fractures occur in sandstones, although only two of these are found in the thick reservoir sandstones. The rest occur in the thin sandstones that are interbedded with siltstones and mudstones between the main reservoirs. Of the six remaining fractures, two occur in the siltstone/mudstone facies, and four are found in coals.

Six of the fractures, including three within sandstones, have a low-angle to horizontal orientation. The rest are essentially vertical. Only two fractures are in oriented core and both have an east-west strike. Two additional fractures were oriented by paleomagnetic techniques[15]: one fracture strikes east-west and the other strikes approximately westnorthwest-eastsoutheast.

Most of the fractures are (macroscopically) completely filled with calcite. Several fractures contain an earlier phase of quartz deposition, and some have unfilled porosity despite partial mineralization. None of the fractures of this zone have been tested for fracture-parallel permeability enhancement.

3.6 FAULT IN THE MWX AREA

There are several lines of evidence that suggest that normal fault is present in the paludal section of MWX-2. Initial evidence consisted of

an apparent shortening of section in MWX-2, by about ten feet, compared to the other two wells, between the depths of 7050 and 7092 ft.[5] Correlations indicate that the most likely locations for the fault are at either 7058 or 7090 ft, and the dipmeter log shows indications of possible drag deformation commonly associated with faults between 7054 and 7080 ft.[4]

Core from MWX-2 between 7072 and 7080 shows no indication of deformation near a fault, and much of the thinning of Zone 2 can be explained by sedimentary pinch-out (see Figure 3.7). The most likely position of the fault is at 7055-7070 ft, dipping to the southwest at an angle of greater than 87°.[4]

3.7 REFERENCES

1. Lorenz, J. C., 1983, Paludal Zone Sedimentology: Memorandum of Record, January 19, 1983.

2. Lorenz, J. C., 1985, Predictions of Size and Orientations of Lenticular Reservoirs in the Mesaverde Group, Northwestern Colorado: SPE/DOE 13851, SPE/DOE Symposium on Low-Permeability Gas Reservoirs, Denver, CO, pp 23- 31.

3. Johnson, R. C., "Structure Contour Map of the Top of the Rollins Sandstone Member of the Mesaverde Formation and Trout Creek Sandstone Member of the Iles Formation, Piceance Creek Basin, Colorado," US Geol. Survey Map MF-1667.

4. Northrop, D. A., "Fault Evidence," Memo to distribution, May 17, 1983.

5. Simons, K., "Possible Faulting in MWX-2 Paludal Zone, Zones 3 and 4," Memo to G. C. Kukal, May 5, 1983.

6. Bendix Field Engineering, series of contractor's reports on the petrologic characteristics of the sandstones in the MWX cores (unpublished), 1982- 1984. (See Appendix 12.2)

7. Finley, S. J., "Summary of MWX Bendix Reports," memo to D. A. Northrop, August 12, 1985.

8. Heinze, D. M., "Overview of Mineralogy/Petrology of MWX Paludal Zones 3 and 4 for Fracture Considerations," Memo to Distribution, November 8, 1983.

9. Pitman, J. A., and Spencer, C. W., "Petrology of Selected Sandstones in the MWX Wells (Northwest Colorado) and Its Relationship to Borehole Geophysical-Log Analysis and Reservoir Quality," USGS Open File Report 84- 757, pp 33-66, 1984.

10. Spencer, C. W., and Pitman, J. K., "USGS Analysis of Paludal Zone in CER #1 and #2 MWX," Memo to Distribution, July, 1983.

11. Lorenz, J. C., "Reservoir Sedimentology of the Rocks of the Mesaverde Group at the Multiwell Experiment Site and East Central Piceance Basin," Sandia National Laboratories Report, SAND87-0040, 1987

12. Lorenz, J. C., D. M. Heinze, J. A. Clark, and Searls, C. A., "Determination of Widths of Meander-Belt Sandstone Reservoirs from Vertical Downhole Data, Mesaverde Group, Piceance Creek Basin, Colorado," Bull. Am. Ass'n Petrol. Geol., v. 69, pp 710-721, 1985.

13. Nuccio, V. F., and R. C. Johnson, "Preliminary Thermal Maturity map of the Cameo and Fairfield or Equivalent Coal Zone in the Piceance Creek Basin, Colorado," US Geol. Survey map MF-1575, 2 sheets.

14. Hemmler, T., "MWX-1 and MWX-2 Cores: Vitrinite Reflectance Data," Letter Report to A. R. Sattler, Sandia National Laboratories, November 1982.

15. Geissman, J., "Paleomagnetic Orientation of MWX Core," Letter Report to J. C. Lorenz, November 1987.

Table 3.1. Petrologic Summary of Core From Zones 3 and 4*
(Ref. 6 as Summarized in Ref. 8)

PROPERTY	MWX-2 Zone 3		MWX-3 Zone 3		MWX-3 Zone 4	
Mean Grain Size (mm)	0.08	(0.06-0.10)	0.10	(0.02-0.41)	0.11	(0.03-0.34)
Quartz (%)	43.9	(35-52)	37.4	(24-52)	48.3	(28-62)
Silica Overgrowths (%)	3.4	(2-5)				
Potassium Feldspar (%) (mostly altered to carbonate)	~0.3	(tr.-1)	~0.3	-	~0.6	-
Plagioclase Feldspar (%) (sericitic alteration)	6.3	(4-9)	6.2	(3-9)	5.7	(3-9)
Chert (%)	~2.2	(tr.-5)	3.3	(1-6)	~2.3	(tr.-6)
Lithics (%) (mostly sedimentary)	5.6	(1-9)	11.9	(7-19)	7.4	(4-14)
Calcite (%) (mostly cement/replacement)	~2.3	(tr.-8)	~1.3	(tr.-8)	~2.5	(tr.-5)
Dolomite (%) (mostly grains)	11.6	(7-19)	13.5	(1-34)	14.4	(5-41)
Siderite (%)	-	(tr.-1)	2.8	(1-5)	3.5	(2-7)
Carbonate as Dolomite (%)	87.3	(58-98)	76.5	(14-99)	71.7	(41-98)
Clays - Nonimpregnated (%) (matrix recrystallized)	9.1	(5-16)	10.7	(tr.-42)	3.4	(1-15)
Clays in Voids - Impregnated (%)	13.6	(6-23)	8.6	(tr.-18)	12.5	(5-19)
Pyrite (%)	-	-	tr.	-	tr.	-
Carbonaceous Material (%) (stringers and along bedding)	-	(tr.-2)	1.6	(0-8)	~2.8	(0-8)
Trace Minerals (inconsistent):	anatase, goethite, muscovite, biotite, tourmaline, zircon, apatite, epidote, and unidentified opaques.					

*Average and range of values measured in thin sections.

Table 3.2. Natural Fracture Data from the Paludal Interval at MWX (continued)

Core Depth (ft)	Height In Core (ft)	Maximum Width (mm)	Mineralization Type	Mineralization Amount	True Strike	Dip	Rock Type	Terminations Top	Terminations Bottom	Comments
				MWX-2 (contd.)						
7315.2-15.6	0.4	0.2	calcite	partial	-	90°	sandstone	at shale	at shale	
7316.6-16.7	0.1	?	quartz & calcite	partial	-	5-30°	siltstone & mudstone	outcore	outcore	13
7348.4-48.9	0.5	0.2	calcite	complete	-	80-90°	sandstone	at shale	at shale	
7368.4-69.1	0.7	0.2	calcite	complete	-	90°	sandstone	at shale	in lith	
				MWX-3						
6887.1-87.3	0.2	0.2	calcite	complete	95°	90°	sandstone	at shale	at shale	
6897.4-97.6	0.2	0.5	calcite	complete	85°	90°	coal	in lith	in lith	14

*Paleomagnetic orientation.

1. Two parallel fracs.
2. Parallel to adjacent shear frac.
3. Three parallel fracs--fractures follow bedding.
4. Four irregular fracs, subhorizontal.
5. Frac barely within core.
6. Unfilled second frac parallels the top of this one for 2.6 ft.
7. Intersects a low-angle, dickite-coated shear fracture.
8. Occurs along organic lamination in sandstone.
9. Three parallel subhorizontal fractures.
10. Frac consists of 3 en echelon sub fracs, each multiple in itself.
11. Frac consists of 2 en echelon fracs, each about 1 ft long.
12. Frac consists of 3 en echelon fracs.
13. Irregular frac, follows bedding.
14. Four parallel mineralized coal cleats.

Table 3.2. Natural Fracture Data from the Paludal Interval at MWX (continued)

Core Depth (ft)	Height In Core (ft)	Maximum Width (mm)	Mineralization Type	Mineralization Amount	True Strike	Dip	Rock Type	Terminations Top	Terminations Bottom	Comments
				MWX-2 (contd.)						
7315.2-15.6	0.4	0.2	calcite	partial	-	90°	sandstone	at shale	at shale	
7316.6-16.7	0.1	?	quartz & calcite	partial	-	5-30°	siltstone & mudstone	outcore	outcore	13
7348.4-48.9	0.5	0.2	calcite	complete	-	80-90°	sandstone	at shale	at shale	
7368.4-69.1	0.7	0.2	calcite	complete	-	90°	sandstone	at shale	in lith	
				MWX-3						
6887.1-87.3	0.2	0.2	calcite	complete	95°	90°	sandstone	at shale	at shale	
6897.4-97.6	0.2	0.5	calcite	complete	85°	90°	coal	in lith	in lith	14

*Paleomagnetic orientation.

1. Two parallel fracs.
2. Parallel to adjacent shear frac.
3. Three parallel fracs--fractures follow bedding.
4. Four irregular fracs, subhorizontal.
5. Frac barely within core.
6. Unfilled second frac parallels the top of this one for 2.6 ft.
7. Intersects a low-angle, dickite-coated shear fracture.
8. Occurs along organic lamination in sandstone.
9. Three parallel subhorizontal fractures.
10. Frac consists of 3 en echelon sub fracs, each multiple in itself.
11. Frac consists of 2 en echelon fracs, each about 1 ft long.
12. Frac consists of 3 en echelon fracs.
13. Irregular frac, follows bedding.
14. Four parallel mineralized coal cleats.

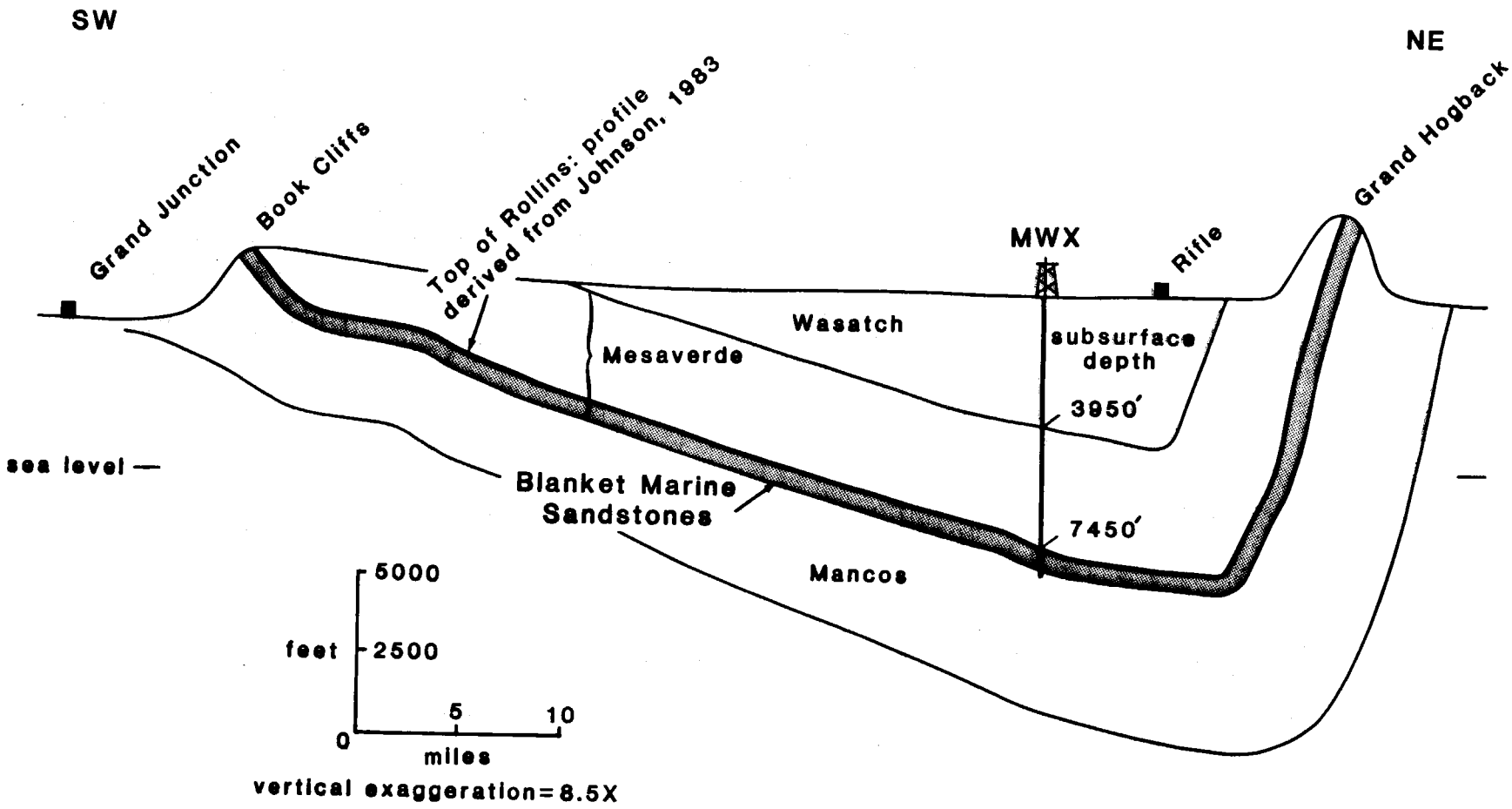

Figure 3.1 Generalized structure of the Mesaverde Formation in the Piceance basin. The paludal zone at the MWX site extends approximately 850 ft above the top of the Rollins Sandstone

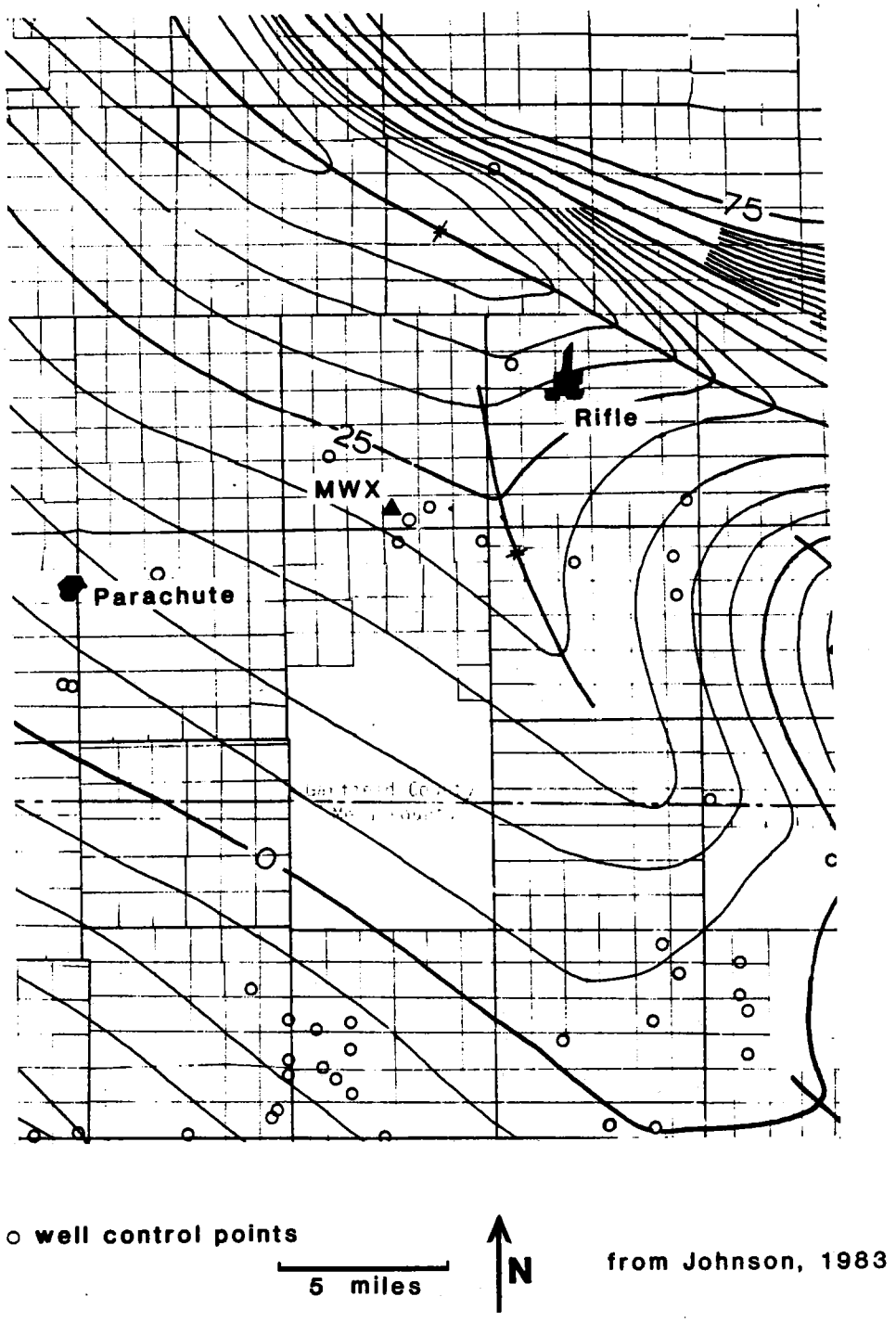

Figure 3.2 Structure contours on top of the Rollins Sandstone. Contours are in hundreds of feet above/below sea level (from Reference 3)

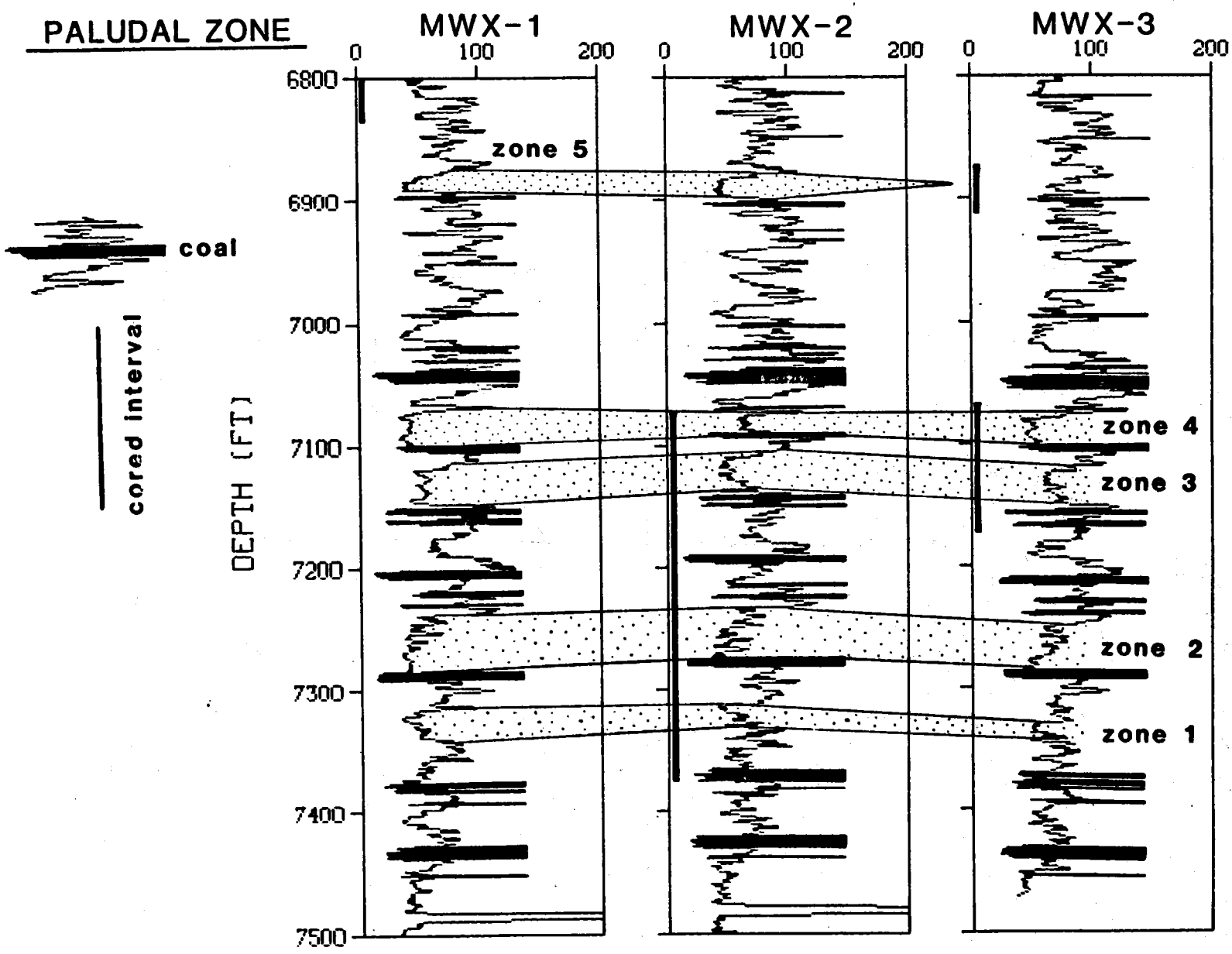

Figure 3.3 Three-well Correlation of Sandstones in Lower Paludal Interval at MWX

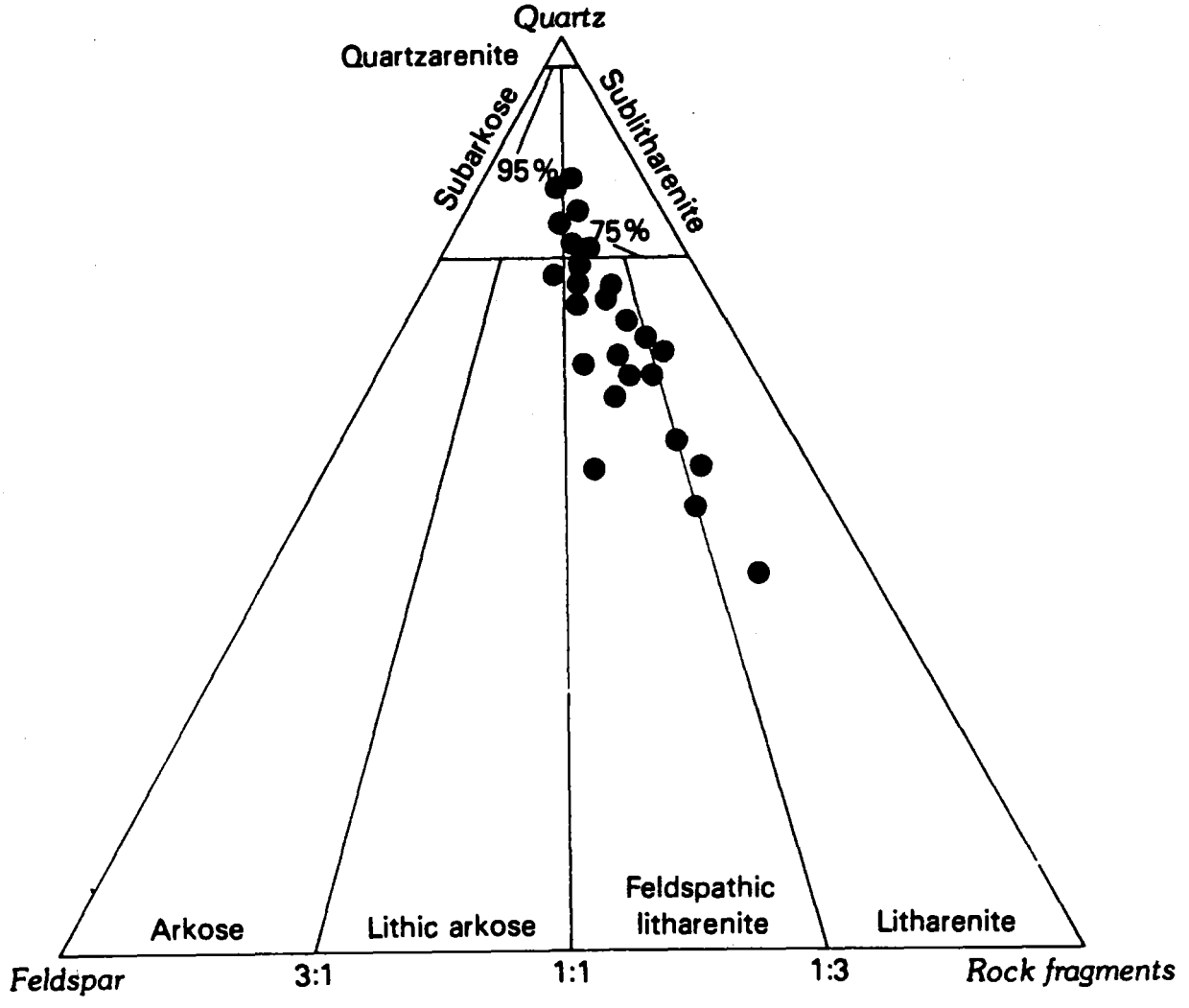

Figure 3.4 Ternary diagram showing mineralogic composition of sandstones in the paludal zone (from Reference 9, Figure 17)

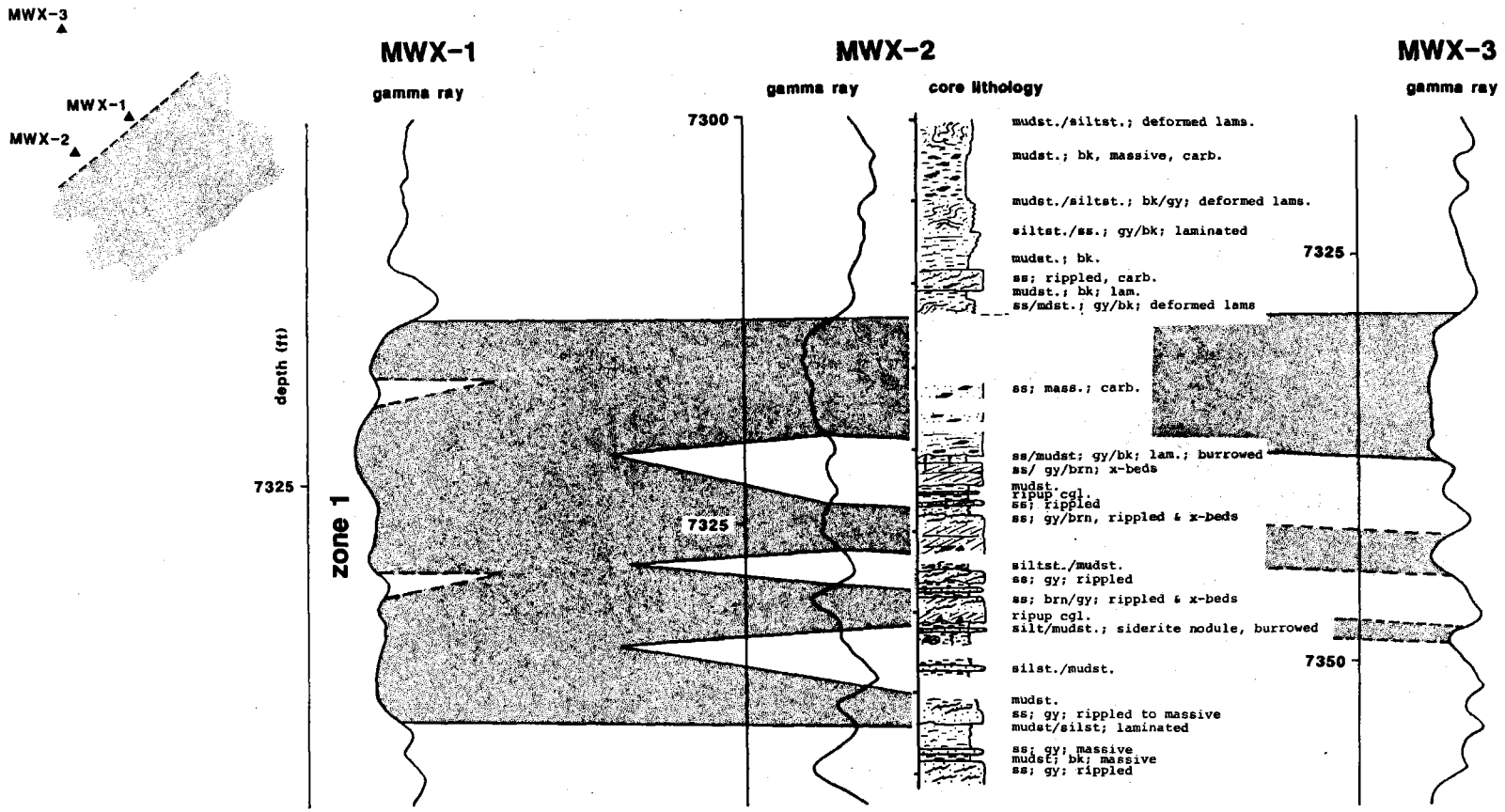

Figure 3.5 Gamma Ray and Core Logs of Zone 1 and Inferred Lens Orientation

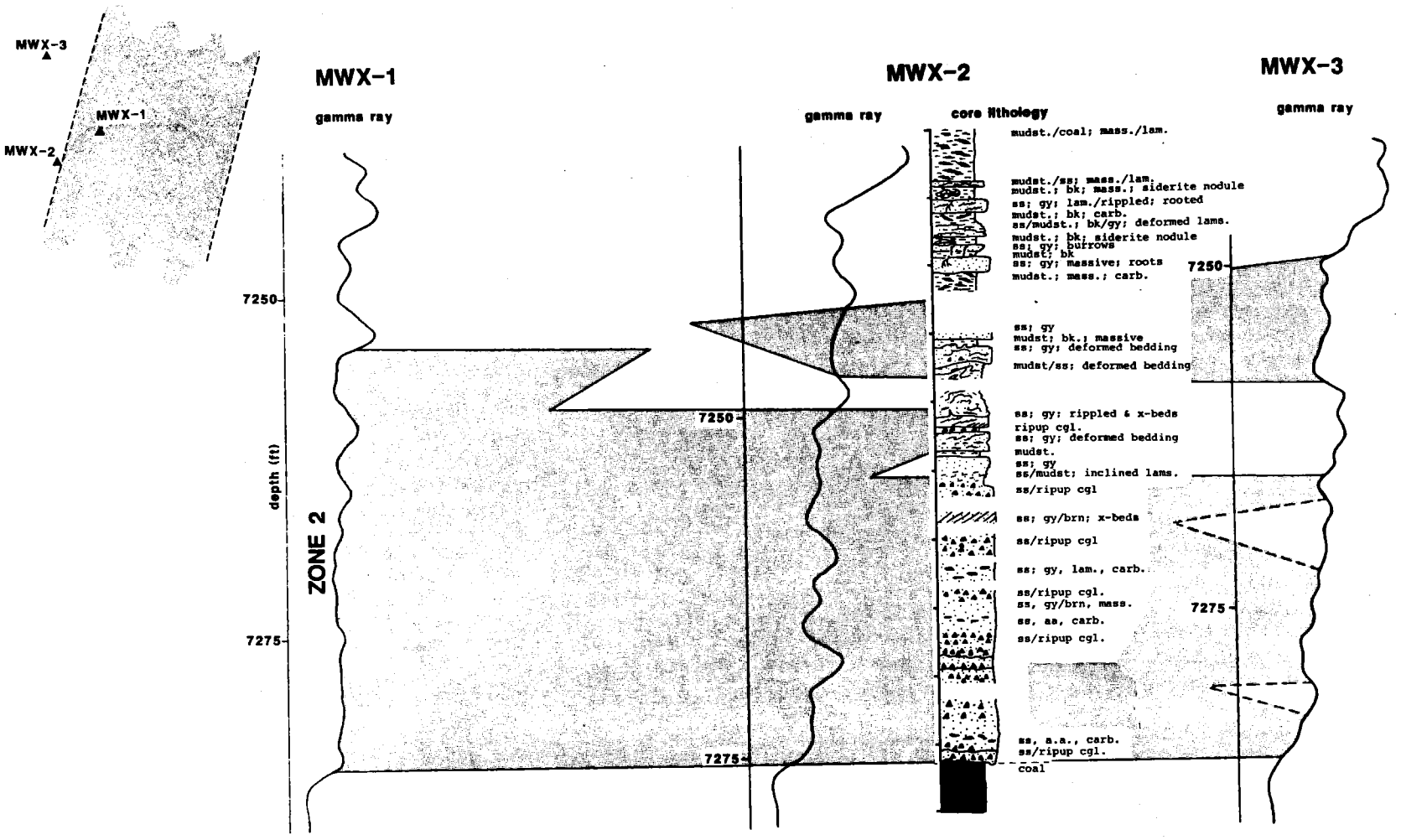

Figure 3.6 Gamma Ray and Core Logs of Zone 2 and Inferred Lens Orientation

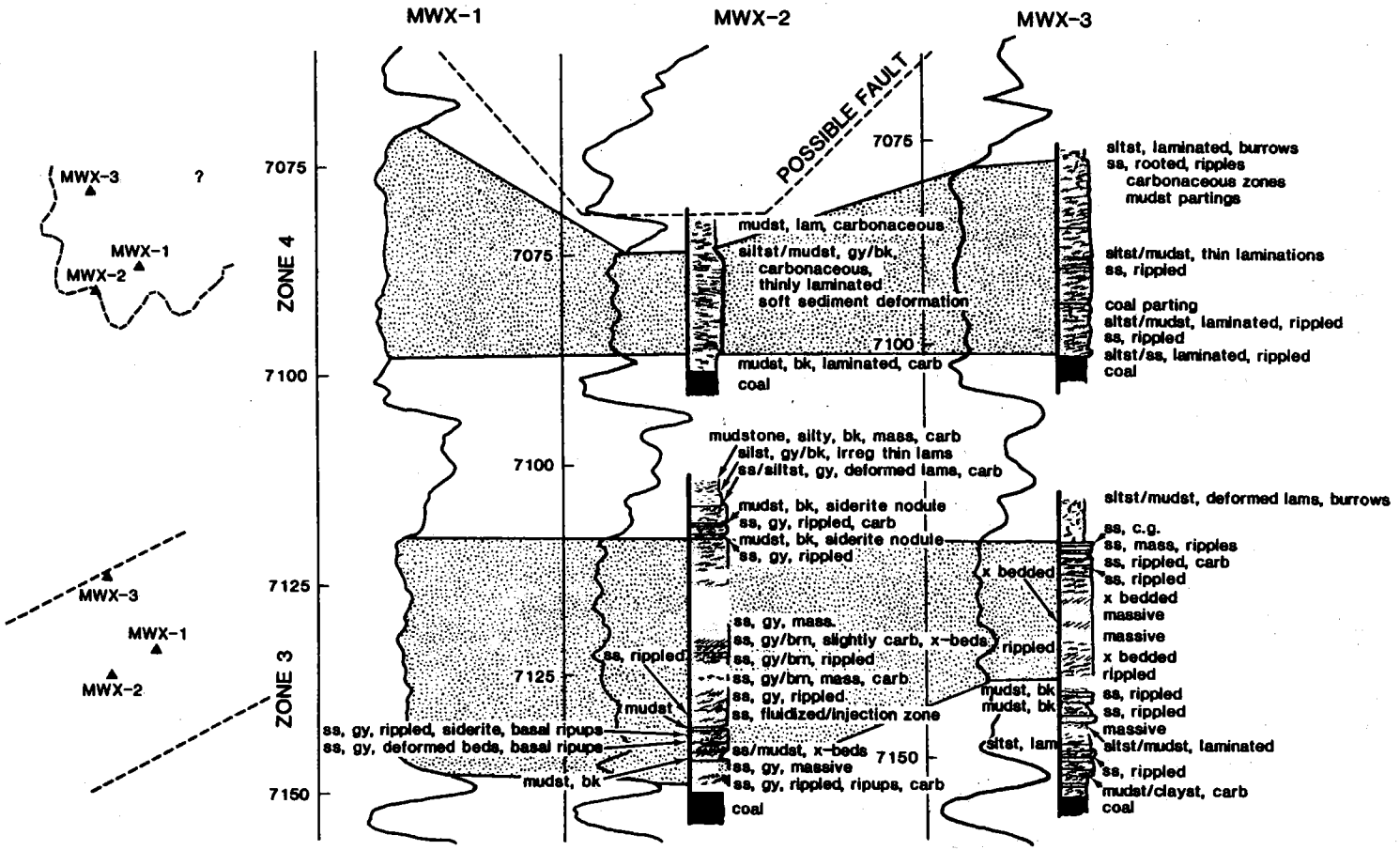

Figure 3.7 Gamma Ray and Core Logs of Zones 3 and 4 Inferred Lens Orientation. (Possible Fault could be anywhere between dashed line and 7056 ft.)

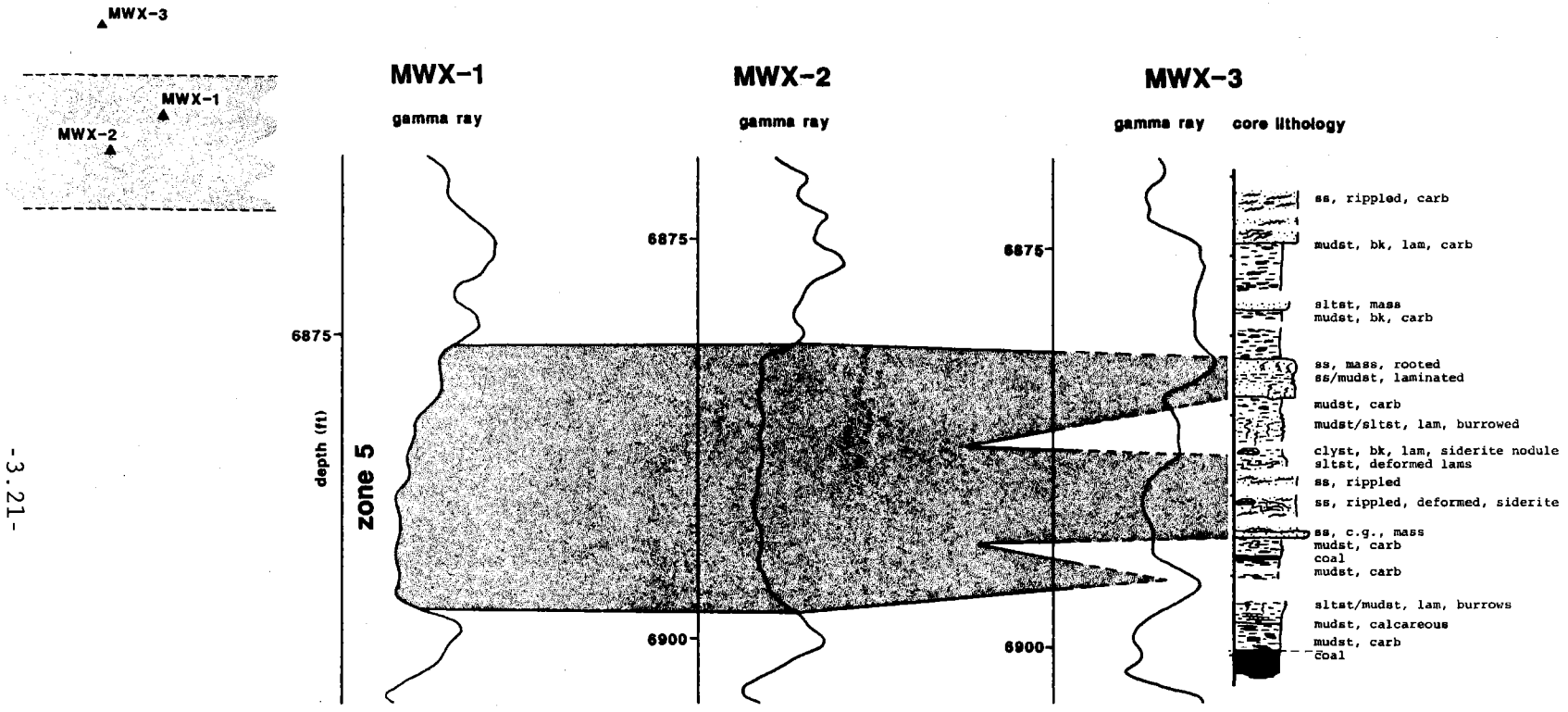

Figure 3.8 Gamma Ray and Core Logs of Zone 5 and Inferred Lens Orientation

4.0 LOG ANALYSIS

G. C. Kukal
CER Corporation

4.1 DATABASE AND ANALYSIS MODELS

Experimental wells MWX-1, MWX-2, and MWX-3 are located in Section 34 of Township 6 South, Range 94 West in the Rulison Gas Field, Garfield County, Colorado. The paludal section begins at approximately 7420 ft and extends to 6570 ft in the three wells. Because of the close well spacing and nearly horizontal sediments, the thickness and overall character of the entire paludal section does not vary much. On a smaller scale, however, the individual sandstone's quality and thickness between the wells may vary dramatically.

An extensive log data base was acquired from the logging programs shown in Table 4.1. The log suites were run to enable development of new log analysis techniques as well as to facilitate thorough analysis of the formation. Analysis of the paludal interval was performed with TITEGAS, a sandstone analysis system developed by CER.[1,2] The analysis model utilizes a bulk density log (FDC or LDT), neutron porosity log (CNL or SNP), resistivity log, standard gamma or spectral gamma ray log, caliper, and optionally: the electromagnetic propagation tool (EPT), the dielectric log, the shallow focused log (SFL) and the microspherically focused log (MSFL). The raw log data is corrected for environmental effects (and normalized if necessary) and then used to determine lithologic parameters as well as reservoir characteristics. These include volume clay, volume carbonate,[3] matrix density, total porosity, water resistivity, in situ intrinsic matrix permeability,[4] formation water saturation, and "invaded" or shallow zone water saturation.

A critical parameter for accurate log analysis is determining the salinity of formation waters correctly. The water salinity of the

formation is generally assumed to be constant except near the outcrop or where incursion of fresh meteoric waters occur downdip from the outcrop. Water resistivity (R_w) is directly related to salinity and also decreases with increasing temperature. Therefore, a linear trend of gradually decreasing R_w from surface to depth is generally assumed. At the MWX site, however, the paludal interval shows anomalously fresh formation water. The decrease in salinity coincides exactly with the increase in coals, and is postulated to be the result of dewatering of coal and other noncoal carbonaceous lithologies.[5] For log analysis of the paludal interval an R_w of 0.650 ohm-m at 75 degrees was used.

The basic logs are presented in Figures 4.1-4.12 in the following format:

	MWX-1	MWX-2	MWX-3
Resistivity	Figure 4.1	Figure 4.5	Figure 4.9
Density-Neutron	4.2	4.6	4.10
Bulk Density	4.3	4.7	4.11
Sonic	4.4	4.8	4.12

The TITEGAS computed logs for MWX-1, MWX-2, and MWX-3 are presented in Figures 4.13, 4.14, and 4.15, respectively. The spectral gamma logs and additional computed logs can be found in Appendix 12.3.

4.2 FAULT AT MWX SITE

MWX-2 logs show a discrepancy in the overall thickness of the paludal section.[6] This has been interpreted as a normal fault encountering the MWX-2 borehole somewhere between 7050 and 7100 ft, most probably at 7090 ft. Above the fault, sediments are on depth in the three wells; below the fault, MWX-2 sediments are roughly 10 to 12 feet higher than correlated points in MWX-1 and MWX-3. Figure 4.16 illustrates the missing section of MWX-2.

It was determined geometrically that the apparent fault, if it strikes parallel to the azimuth of most faults in the area (N75W to N81W), would have a minimum dip of 86 degrees to the northeast. The actual dip is probably greater. The fault is not apparent in either MWX-1 or MWX-3.

MWX-2 log evidence for the fault is limited. Except for the correlation discrepancy, no expression of a fault was apparent on MWX-2 logs. A core run beginning at 7072 ft (log depth) recorded near-horizontal fracture zones at 7072 ft and at 7092 ft, both of which are coaly zones.

Well testing of the zone believed to be faulted showed evidence of a high conductivity, linear flow system similar to a hydraulically fractured reservoir (Section 8.1). The pressure history observed differs substantially from other zones tested. The anomalous well test results are held to be evidence of a single, large, conductive fracture, or fault, in this zone.

4.3 FORMATION EVALUATION

Six sandstone units in the paludal section have relatively good reservoir quality and thickness in at least two of the three MWX wells. Log reservoir characteristics and core data for each zone in each well are listed in Table 4.2.

The upper 300 ft of the paludal interval consists of thin coals, shales and noncontinuous sandstones. No sandstones greater than 10 ft thick are present in this upper zone in any of the three wells. In the lower 550 ft of the paludal interval (6870 to 7420 ft), six significant sandstone units greater than 10 ft thick and present in at least two wells were identified. They are referred to as zones 1 through 5, with zone 1 being the deepest (Figure 4.17). At the time of the original zone

classification, a sandstone unit lying between zones 4 and 5 was not considered significant enough for detailed analysis; however, since it was encountered in the subsequently drilled MWX-3, it has been included and is referred to as zone 4a.

4.3.1 MWX-1 Analysis

Log quality of MWX-1 logs is excellent. The oil base mud maintained a gauge borehole with few washouts; consequently, almost all pad-type tool log data are valid. Unfortunately, the nonconductive oil base mud precluded some desirable measurements and rendered others unusable.

Zone 1 is interpreted to be a tight zone. Water saturation varies but is generally high. Porosity is relatively low throughout the zone. The permeability is low. There is localized high carbonate content, notably at 7321 to 7325 ft and 7332 to 7334 ft.

Zone 2 has a relatively high gas saturation and permeability is favorable, especially at 7256 to 7262 ft and 7268 to 7274 ft. Carbonate content is concentrated in two areas, 7254 to 7258 ft and 7268 to 7274 ft. The carbonate zones generally have lower clay content which is a factor in the permeability developed at 7268 to 7274 ft.

Zone 3 has low water saturation in the best developed portion from 7129 to 7136 ft. Again, there is carbonate cement within the interval of permeability development and clay content is relatively high. With this combination, it is likely that this unit is naturally fractured. Permeability is best developed at 7130 to 7136 ft.

Zone 4 has relatively low water saturation. Porosity is well developed, and permeability is relatively high throughout the zone. Carbonate content is high from 7075 to 7079 ft and 7089 to 7095 ft. Clay content is relatively low throughout the zone and is lowest where there is carbonate cement.

Zone 4a has unattractive reservoir characteristics.

Zone 5, although thin in this well, has good reservoir characteristics.

In summary, the paludal reservoirs in MWX-1 look like potentially productive units, excluding zones 1 and 4a. Each zone contains localized high-carbonate areas. MWX-1 is the cleanest of the three wells; its average clay volume in the sandstones is the lowest. The total thickness of sandstone with less than 25 percent clay (in 6 zones present) is 151 ft, greatest of the three wells.

Five of the six paludal zones (all but zone 1) exhibit some degree of mud filtrate invasion, and the same zones have moderate to good permeability. There appears to be a direct relationship between permeability and invasion. When adequate time and differential pressure exists, invasion will occur in more permeable zones.

Small to moderate gas shows were recorded for zones 2 through 5 on the MWX-1 mud log. Figure 4.18 is a modified mud log for the MWX-1 paludal interval from 6800 to 7400 ft which presents gamma response, natural fractures (interpreted from the long spaced sonic log and the variable density display of the CBL-VDL log), intervals with adequate cement bonding, cored intervals, total gas recorded by the mud logger, and mud weight.

4.3.2 MWX-2 Analysis

As with MWX-1, log quality is excellent. MWX-2 also had an oil-base mud system, thus borehole washouts are rare. One difference of note in this well is the absence of an LDT log, which precludes carbonate volume estimates. (Table 4.1 listed the log suite available for MWX-2.)

Zone 1 appears to have relatively high matrix permeability, but inspection of core permeability and porosity reveals erroneous log porosity estimates, possibly due to natural fractures. Matrix permeability is lower than indicated, but fracture permeability may exist. The unit is thin, but other characteristics are good. Porosity is relatively high, and both water saturation and clay content are moderate.

Zone 2 has low permeability. Porosity is moderate but water saturation is high.

Zone 3 has good matrix permeability which is slightly less at the top of the zone. Porosity and gas saturation are good and clay content is moderate; permeability is relatively high. A one-ft vertical fracture was noted on the core at 7115 ft (log depth).

Zone 4, through which a fault passes in MWX-2, is a poor reservoir. It is thin, has low porosity, very low permeability and high water saturation. Log quality is not consistent through the zone.

Zone 4a is not developed in MWX-2. The unit degrades into siltstone and shale, interbedded with thin sand stringers.

Zone 5 has attractive reservoir parameters. This zone has the best permeability development in the MWX-2 paludal section.

In general, MWX-2 paludal sandstones are not as good reservoirs as MWX-1 sandstones. Total footage of sand cleaner than 25 percent clay is 87 ft (5 zones present). Petrographic data indicate that carbonate cement is common and is predominantly dolomite.

Figure 4.19 is a composite mud log for the MWX-2 paludal interval from 6800 to 7400 ft, which shows total gas, gamma ray response, cement bonding, mud weight, cored intervals and fracture data interpreted (from the long-spaced sonic log and the VDL display on the CBL-VDL log). All of the zones exhibited moderate to good gas shows during drilling. Zones 1 through 4 have core data that indicate the presence of natural fractures. Zone 5 may or may not be fractured. In this well, zones 3 and 5 have relatively good permeability development and have the best production potential.

4.3.3 MWX-3 Analysis

MWX-3 has the most extensive log suite of all the Multiwell Experiment wells (Table 4.1). The well was drilled with a water-base mud which enabled many logs to be run that could not be run in the oil- base mud. The water-base mud created some borehole enlargements which affected some of the logging measurements; however, the overall log quality was excellent. The additional log data were used to detect naturally fractured intervals.

Zone 1 has marginal matrix permeability. The zone has moderate water saturation and variable porosity. Clay content is low, probably due to the high carbonate content. The unit is thin and is therefore unattractive for completion.

Zone 2 is interpreted to be naturally fractured. However, matrix permeability is low and the zone has low porosity, high water saturation and high carbonate content. Overall it does not appear to be an attractive zone.

Zones 3 and 4 have good matrix permeability and are interpreted to be naturally fractured. Both have good porosity, moderate water saturation, and moderate clay content. Zone 3 has high carbonate content localized at 7128 to 7136 ft. Zone 4 has a calcareous development at 7077 to 7083 ft. Both zones have good sand thickness developed and matrix permeability is relatively well developed. Zones 3 and 4 are judged the best units in the MWX-3 paludal interval.

Zone 4a is interpreted to be naturally fractured, but other reservoir parameters are unattractive. Matrix permeability is low.

Zone 5 deteriorates to nonreservoir quality in MWX-3. The sandstone correlates lithologically, but has poorer character than in MWX-1 and MWX-2.

MWX-3 has the least sand footage (83 ft) of the three wells and the sandstones contain more clay than those in MWX-1 and MWX-2. Each of the five zones analyzed contained some carbonate, usually localized rather than evenly distributed. Most zones are naturally fractured. It is noteworthy that fractures identified from the well logs correspond closely to the presence of carbonate volume. Zone 4 is a good example of this relationship.

Figure 4.20 is a composite mud log for the MWX-3 paludal interval from 6800 to 7400 ft which includes gas shows, cement bonding, mud weight and fracture information (derived from MWX-3 fracture logs). The best gas show on the mud log occurs through zones 3 and 4. MWX-3 logs indicate that the paludal interval in this well will be the least productive of the three wells.

4.4 FRACTURE ANALYSIS

MWX-3 presented a unique opportunity to run several fracture identification logs and to compare the various techniques. Logs run in

MWX-3 to identify fractures were: borehole televiewer (BHTV), circumferential acoustilog (CMA), fracture identification log (FIL), borehole acoustic fraclog (BHCAF), variable density log with 3-ft spacing (VDL), and fracture probability log (FPL).

Generally, there does not appear to be one specific fracture log which can be used to detect fractures throughout the paludal interval. The better fracture indicator logs are the CMA, BHCAF and VDL. The poorest indicator of fractures was the FPL. For a physical description of the fracture, the BHTV is the best. Both the BHTV and the FIL measure the azimuth of the fracture. Of the five zones where both the BHTV and FIL indicated fractures, four zones had corresponding directional measurements. There does not appear to be a preferential direction for the fractures to occur.

Zones 3 and 4 of the paludal interval in MWX-3 are naturally fractured. In addition, other fractured sand intervals are 6979 to 6986 ft and 6808 to 6816 ft. In these zones, four or more of the fracture logs listed above indicated a fracture. In addition, the following zones in MWX-1 and MWX-2 are interpreted to be fractured based upon analyses from the variable density logs (VDL) run in cased hole:

MWX-1	MWX-2
6958-6966 ft	6961-6968 ft
7086-7092	7109-7133
7128-7132	7167-7176
7322-7325	7318-7322

A more complete discussion of the fracture identification logs can be found in Appendix 12.3. A description of the natural fractures observed in core is given in Section 3.5.

4.5 MECHANICAL PROPERTIES: CLOSURE STRESS

The following analysis is from Schlumberger's closure stress log run in MWX-3. This log is computed from the digital sonic log. Zone 1 has a low closure stress while the shales above and below have a medium closure stress. Zone 2 has a medium closure stress slightly less than the adjacent shales. A low closure stress is calculated for both zones 3 and 4. Directly above zone 4, the shale has a moderately high to high closure stress. Zone 5 has a high closure stress, as do the shales above and below it.

A closure stress curve was calculated for MWX-1 from the Long Spaced Sonic digitized waveforms. For zone 1, a medium closure stress is shown with a moderately high stress interval at 7322 to 7324 ft. Below zone 1, the shale has a slightly higher closure stress. Zone 2 had a medium closure stress while the shales above and below are shown to have only a slightly higher closure stress. Directly below zone 3, 7151 to 7155 ft has a moderately high closure stress. Zones 3 and 4 have a medium closure stress, while the shale between zones 3 and 4 shows a slightly higher closure stress. The interval 7100 to 7104 has a moderately high closure stress. The shales above zone 4 have a moderately high closure stress. Zone 5 has a medium closure stress while the shales above and below have a slightly higher closure stress.

These calculated stresses can be compared with the measured stress data for the paludal interval found in Section 6.0.

4.6 CEMENT EVALUATION

Throughout most of the paludal interval in MWX-3, the casing cement was contaminated with formation gas, which greatly reduced its compressive strength. This contamination stops at 6660 ft. From 6660 to 6560 ft, bonding is excellent. Below 6660 ft, neither the cement evaluation log nor the cement bond log/variable density log show

continuous good bonding. Figures 4.18-4.20 show intervals with adequate cement bonding in each of the three wells.

4.7 ADDITIONAL INFORMATION

The information presented herein is designed to provide all pertinent information required by the general reader. If more detailed information is required it may be found in the "Well Log Analysis of Paludal Interval MWX-1, MWX-2 and MWX-3," an unpublished project report given in its entirety as Appendix 12.3.

4.8 REFERENCES

1. Kukal, G. C., "A Systematic Approach for the Effective Log Analysis of Tight Gas Sands," SPE 12851, Proceedings of the 1984 SPE/DOE/GRI Unconventional Gas Recovery Symposium, Pittsburgh, PA, May 1984, pp 209-220 (included as appendix 4 in Appendix 12.3).

2. Kukal, G. C., "Log Analysis in Low Permeability Gas Sand Sequences--Correcting for Variable Unflushed Gas Saturation," Paper F, Transactions of the SPWLA 24th Annual Logging Symposium, Calgary, Canada, June 1983.

3. Kukal, G. C. and R. E. Hill, "Improved Shaly Sand Analysis in Heavy Drilling Muds: A Simple Technique for Using the Photoelectric Measurement," Paper U, Transactions of the SPWLA 26th Annual Logging Symposium, Dallas, TX, June 1985.

4. Kukal, G. C. and K. E. Simons, "Log Analysis Techniques for Quantifying the Permeability of Submillidarcy Sandstone Reservoirs," SPE 13880, SPE Formation Evaluation, December 1986, pp 609-622.

5. Law, B. E., J. R. Hatch, G. C. Kukal, and C. W. Keighin, "Geologic Implications of Coal Dewatering," AAPG Bulletin Vol. 67, No. 12, December 1983, pp 2255-2260.

6. Simons, K., "Possible Faulting in MWX-2 Paludal Zone, Zones 3 and 4," memo to G. C. Kukal, May 5, 1983.

Table 4.1. MWX Log Database.

MWX-1 LOGS

4,130 ft to Surface

Borehole Compensated Sonic/Gamma Ray/Caliper/
Dual Induction

6,827 to 4,130 ft

Dual Induction/Gamma Ray
Lithodensity/Caliper
Compensated Formation Density
Compensated Neutron/Gamma Ray/Caliper
Natural Gamma Spectroscopy
Long Spaced Sonic
Repeat Formation Tester

8,350 to 4,130 ft

Dual Induction/Gamma Ray/SP
Lithodensity/Compensated Neutron/Gamma Ray/
Caliper
Long Spaced Sonic
Epithermal Sidewall Neutron/Gamma Ray/Caliper
Electromagnetic Propagation/Gamma Ray/Caliper
Amoco Sonic Tool
Dipmeter - Structural and Stratigraphic
Computed Logs
Geo Dip
Standard Cluster
Directional Survey
Fracture Identification Log
Repeat Formation Tester (12 tests)

MWX-2 LOGS

5,438 to 4,094 ft

Formation Density/Compensated Neutron/GR/
Caliper

6,692 to 4,094 ft

Dual Induction/GR/SP
Formation Density/Compensated Neutron/GR/
Caliper
Litho Density/GR/Caliper
Sidewall Neutron/GR/Caliper
Natural Gamma Spectroscopy

8,291 to 4,094 ft

Dual Induction/GR/SP
Circumferential Micro Sonic/GR
Digitized Waveforms
Formation Density/Compensated Neutron/
Natural Gamma Spectroscopy/Caliper
Long Spaced Sonic
Digitized LS Waveforms
Amoco Multiple Spaced Sonic/Waveforms
Sidewall Neutron/GR/Caliper
Dipmeter
Fracture Identification Log

Table 4.1 (Cont.)

MWX-3 LOGS

4,134 ft to Surface

Borehole Compensated Sonic/Gamma Ray/Caliper
Formation Density/Compensated/Gamma Ray/Caliper

5,875 to 4,129 ft

Litho Density/Compensated Neutron Log/Gamma Ray/Caliper

5,840 to 4,900 ft

Borehole Televiewer

6,875 to 4,130 ft

Litho Density/Compensated Neutron Log/Gamma Ray/Caliper
Micro SFL/SP/Caliper

7,474 to 4,129 ft

Dual Induction Log/Gamma Ray/SP
Litho Density Tool/Compensated Neutron Log/Natural Gamma Spectroscopy/Caliper
Sidewall Neutron Porosity/Gamma Ray/Caliper
High Resolution Dipmeter/Gamma Ray/Calipers
Fracture Identification Log/Gamma Ray/Caliper
Borehole Compensated Sonic (Digital Sonic) Shear and Compressional Travel Times
Variable Density Log (3 ft spacing)
Mechanical Properties Quick Look (Computed Log)
Dual Laterolog/Microspherically Focused Log/Gamma Ray/Caliper
Electromagnetic Propagation Tool/Gamma Ray/Caliper
Dual Porosity Compensated Neutron Log (CNT-G)/Gamma Ray/Micro Log
Formation Density Compensated/Gamma Ray/Caliper
Amoco Multiple Spaced Sonic
Mobil Multiple Spaced Sonic
Mobil Borehole Televiewer
Spectralog
Borehole Compensated Acoustilog/Gamma Ray/Caliper
BHC Acoustic Fraclog/Gamma Ray/Caliper
Sonic Waveforms Digitized
Dielectric Constant Log
Circumferential Acoustilog

7,300 to 4,130 ft

Cement Bond Log/Variable Density Log/Gamma Ray/Casing Collar Locator
Cement Evaluation Log/Gamma Ray
Compensated Neutron Log
Thermal Decay Tool/Gamma Ray/Casing Collar Locator

Table 4.2. MWX Paludal Reservoir Characteristics

	MWX-1	MWX-2	MWX-3
ZONE 1	7,315.5 - 7,340.0	7,312.0 - 7,326.5	7,328.5 - 7,340.0
Zone Thickness (h), ft	24.50	14.50	11.50
Sand Thickness (hsd), ft	21.50	14.50	11.50
Porosity (ϕ), %	7.23	8.92	8.18
Water Saturation (S_W), %	70.70	59.25	64.57
Shallow Zone S_W (S_{XO}), %	71.40	66.55	73.04
S_{XO}–S_W (ΔS_W), %	0.70	7.30	8.47
Volume Clay (V_{Cl}), %	9.23	15.00	12.53
Volume Carbonate (VCO_3), %	6.04	–	22.93
Core Porosity, %	–	7.59	–
Core Permeability, md	–	0.03	–
Core Water Saturation, %	–	25.51	–
Core Grain Density, gm/cc	–	2.68	–
Cation Exchange Capacity, meq/100 gm	–	1.54	–
Permeability-feet (kh), md-ft	0.20	0.25	0.32
ZONE 2	7,240.0 - 7,284.0	7,234.0 - 7,274.0	7,273.0 - 7,285.0
Zone Thickness, ft	44.00	40.00	12.00
Sand Thickness, ft	44.00	28.50	12.00
Porosity, %	8.74	6.84	6.25
Water Saturation, %	64.07	68.46	82.90
Shallow Zone S_W, %	67.60	78.46	85.47
S_{XO}–S_W, %	3.53	10.18	2.57
Volume Clay, %	10.68	12.56	9.62
Volume Carbonate, %	2.30	–	15.60
Core Porosity, %	–	5.07	–
Core Permeability, md	–	0.02	–
Core Water Saturation, %	–	55.95	–
Core Grain Density, gm/cc	–	2.67	–
Cation Exchange Capacity, meq/100 gm	–	3.83	–
Permeability-feet, md-ft	1.10	0.18	0.10

Table 4.2 (Cont.)

	MWX-1	MWX-2	MWX-3
ZONE 3	7,119.5 - 7,147.5	7,108.5 - 7,133.0	7,123.5 - 7,143.5
Zone Thickness, ft	28.00	24.50	20.00
Sand Thickness, ft	28.00	24.00	19.50
Porosity, %	8.55	9.41	8.42
Water Saturation, %	57.06	52.61	55.43
Shallow Zone S_w, %	61.71	65.15	77.15
$S_{xo}-S_w$, %	4.65	12.54	21.72
Volume Clay, %	15.12	14.28	17.88
Volume Carbonate, %	5.65	–	8.85
Core Porosity, %	–	9.53	9.57
Core Permeability, md	–	0.04	0.05
Core Water Saturation, %	–	27.31	58.96
Core Grain Density, gm/cc	–	2.68	2.69
Cation Exchange Capacity, meq/100 gm	–	1.67	–
Permeability-feet, md-ft	0.70	0.65	0.55
ZONE 4	7,071.0 - 7,100.0	7,076.0 - 7,087.5	7,079.0 - 7,103.0
Zone Thickness, ft	29.00	11.50	24.00
Sand Thickness, ft	29.00	4.50	24.00
Porosity, %	10.06	3.60	8.88
Water Saturation, %	53.93	76.05	60.52
Shallow Zone S_w, %	69.03	92.04	79.59
$S_{xo}-S_w$, %	15.10	15.99	19.07
Volume Clay, %	8.09	17.32	8.43
Volume Carbonate, %	11.90	–	8.85
Core Porosity, %	–	3.00	9.41
Core Permeability, md	–	0.01	0.07
Core Water Saturation, %	–	26.78	63.21
Core Grain Density, gm/cc	–	2.70	2.69
Cation Exchange Capacity, meq/100 gm	–	–	–
Permeability-feet, md-ft	1.0	–	0.50

Table 4.2 (Cont.)

	MWX-1	MWX-2	MWX-3
ZONE 4a	6,997.5 - 7,014.0	Not Present	7,003.0 - 7,019.0
Zone Thickness, ft	16.50	–	16.00
Sand Thickness, ft	16.50	–	16.00
Porosity, %	8.06	–	6.42
Water Saturation, %	79.55	–	62.57
Shallow Zone S_w, %	77.35	–	66.05
$S_{xo}-S_w$, %	–	–	3.48
Volume Clay, %	12.53	–	13.38
Volume Carbonate, %	6.45	–	5.93
Core Porosity, %	–	–	–
Core Permeability, md	–	–	–
Core Water Saturation, %	–	–	–
Core Grain Density, gm/cc	–	–	–
Cation Exchange Capacity, meq/100 gm	–	–	–
Permeability-feet, md-ft	0.20	–	0.17
ZONE 5	6,880.5 - 6,892.5	6,883.0 - 6,899.0	Not Computed
Zone Thickness, ft	12.00	16.00	–
Sand Thickness, ft	12.00	15.50	–
Porosity, %	8.68	10.26	–
Water Saturation, %	53.68	50.20	–
Shallow Zone S_w, %	65.39	71.77	–
$S_{xo}-S_w$, %	11.71	21.57	–
Volume Clay, %	10.46	9.69	–
Volume Carbonate, %	8.36	–	–
Core Porosity, %	–	–	–
Core Permeability, md	–	–	–
Core Water Saturation, %	–	–	–
Core Grain Density, gm/cc	–	–	–
Cation Exchange Capacity, meq/100 gm	–	–	–
Permeability-feet, md-ft	0.45	0.62	–
Total Sand Thickness, All 6 Zones	151.00 ft	87.00 ft	83.00 ft

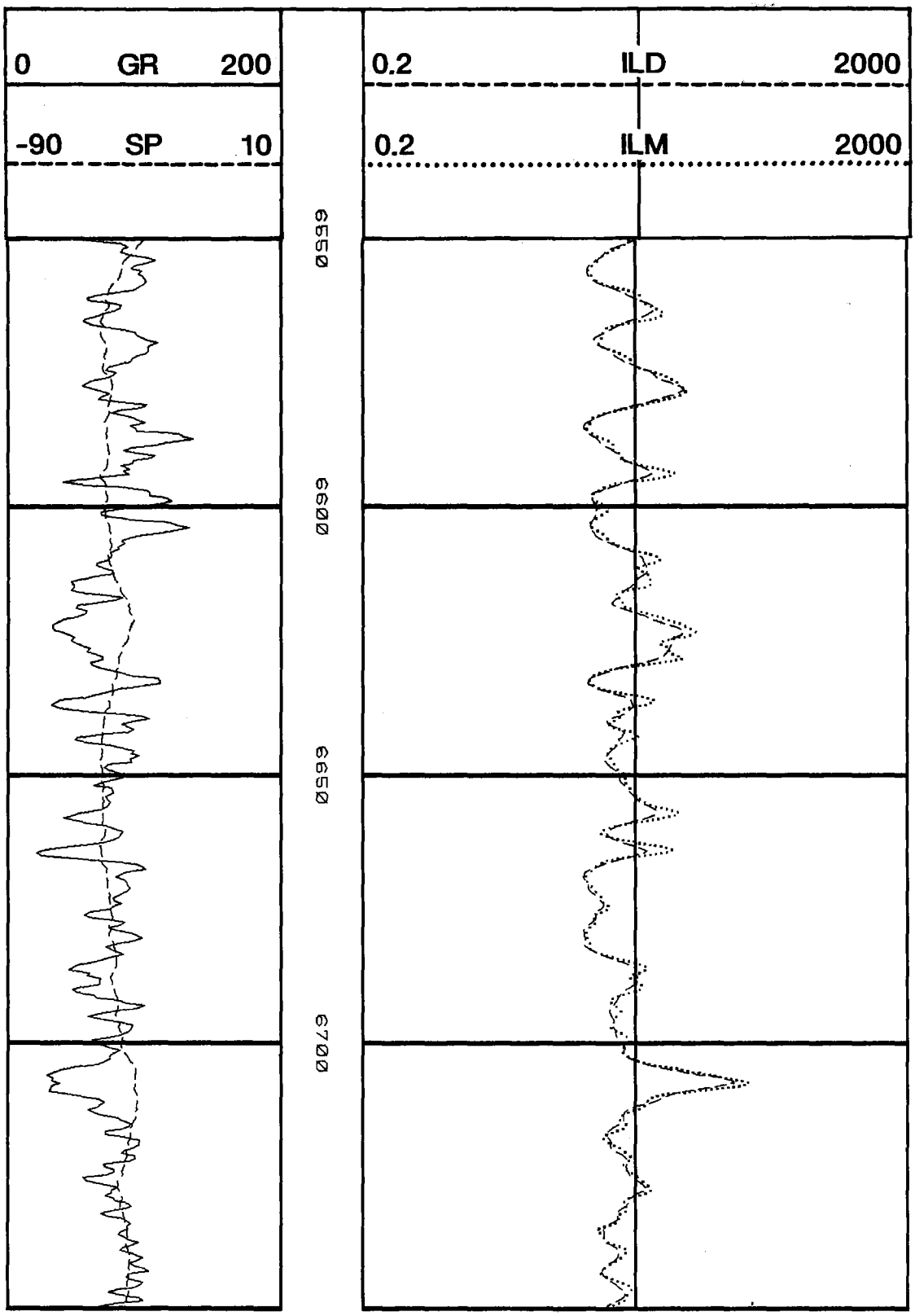

Figure 4.1 Resistivity Log, MWX-1

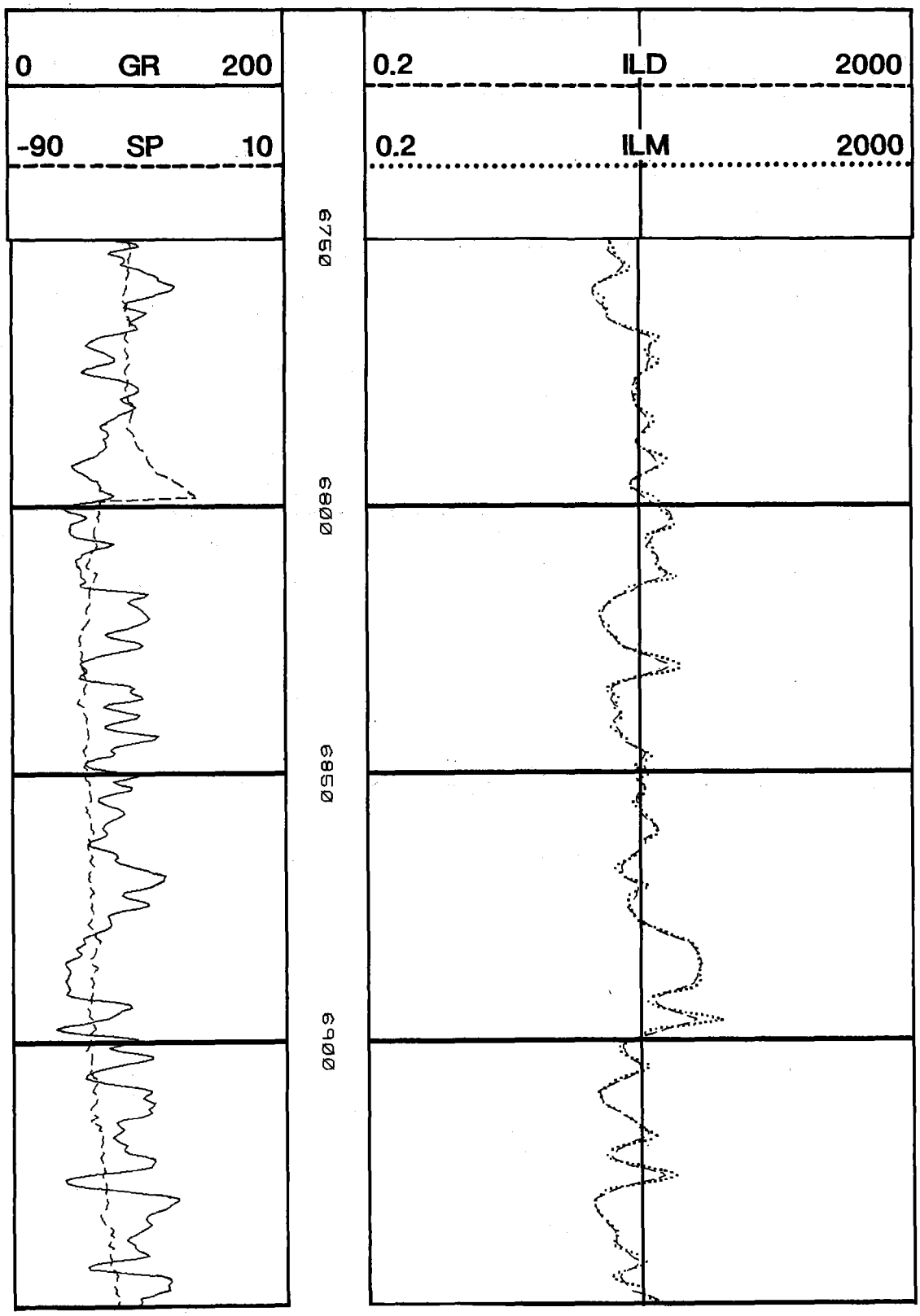

Figure 4.1 Resistivity Log, MWX-1 (continued)

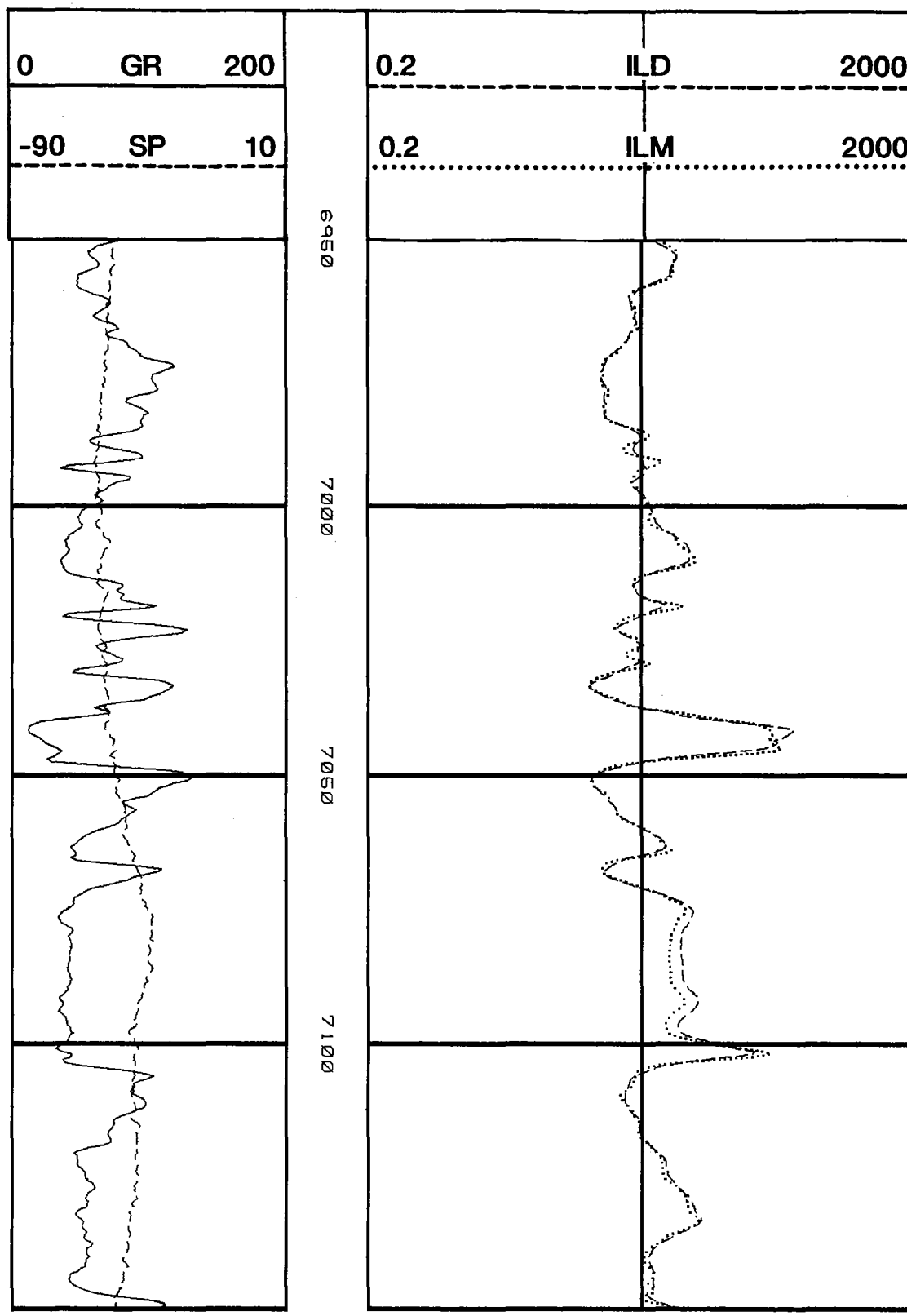

Figure 4.1 Resistivity Log, MWX-1 (continued)

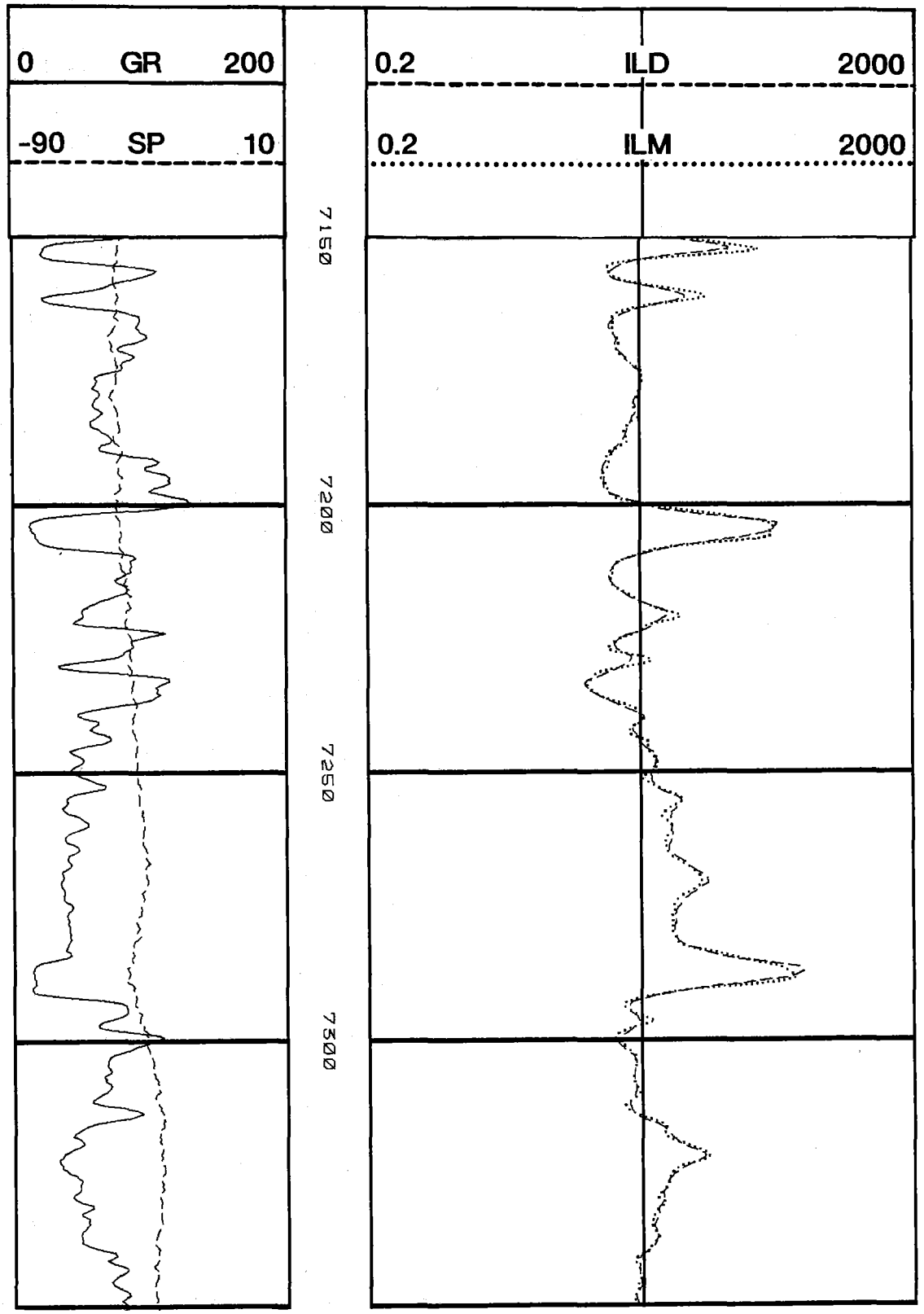

Figure 4.1 Resistivity Log, MWX-1 (continued)

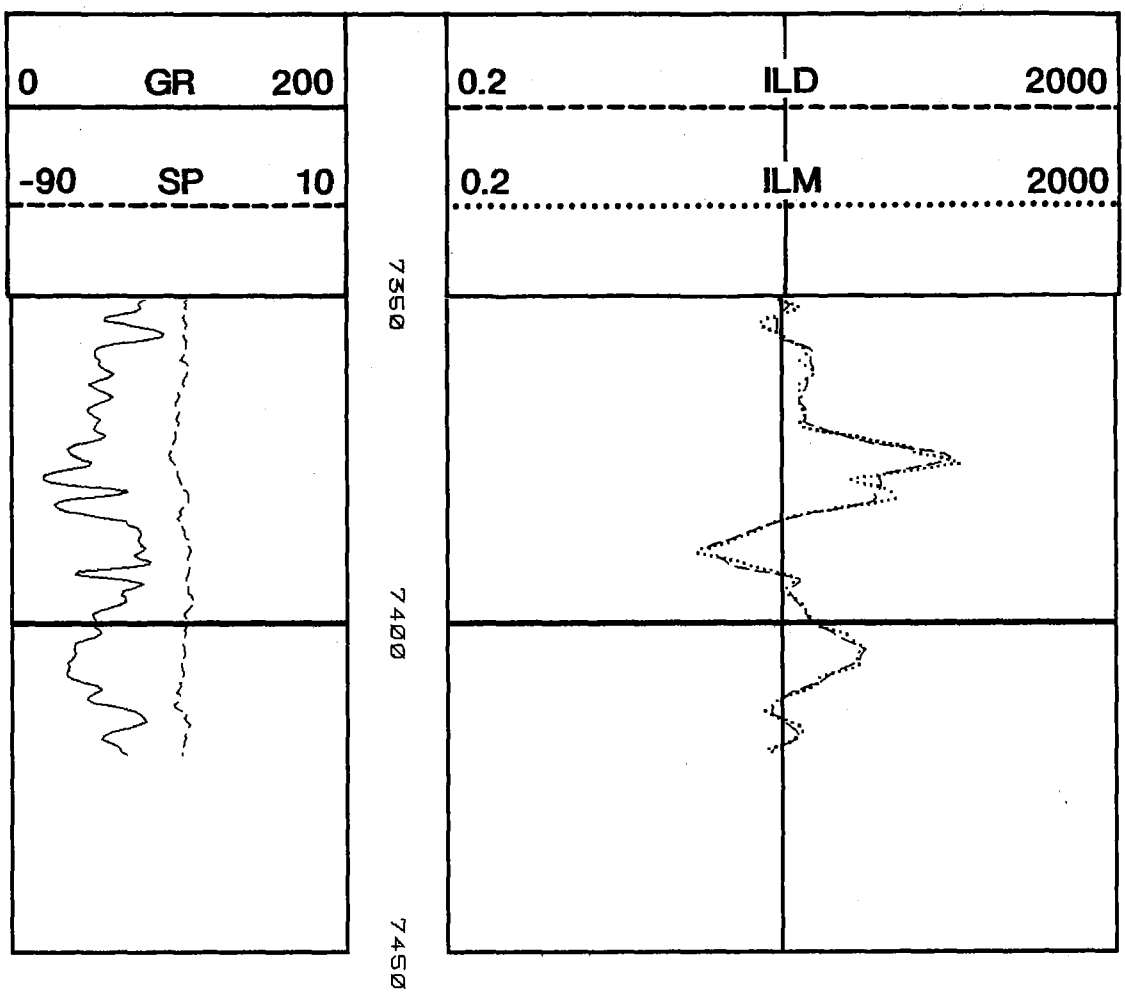

Figure 4.1 Resistivity Log, MWX-1 (continued)

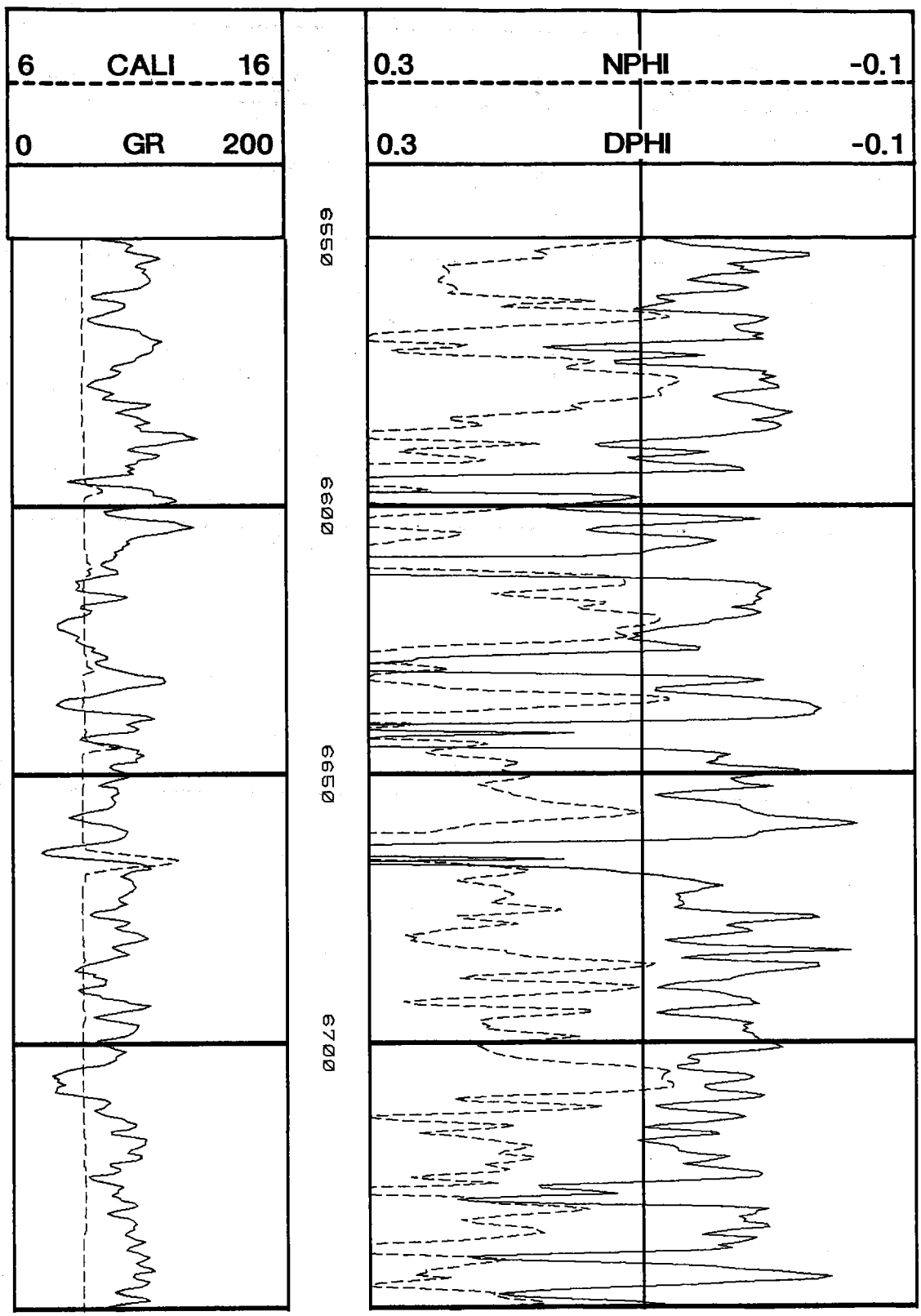

Figure 4.2 Density-Neutron Log, MWX-1

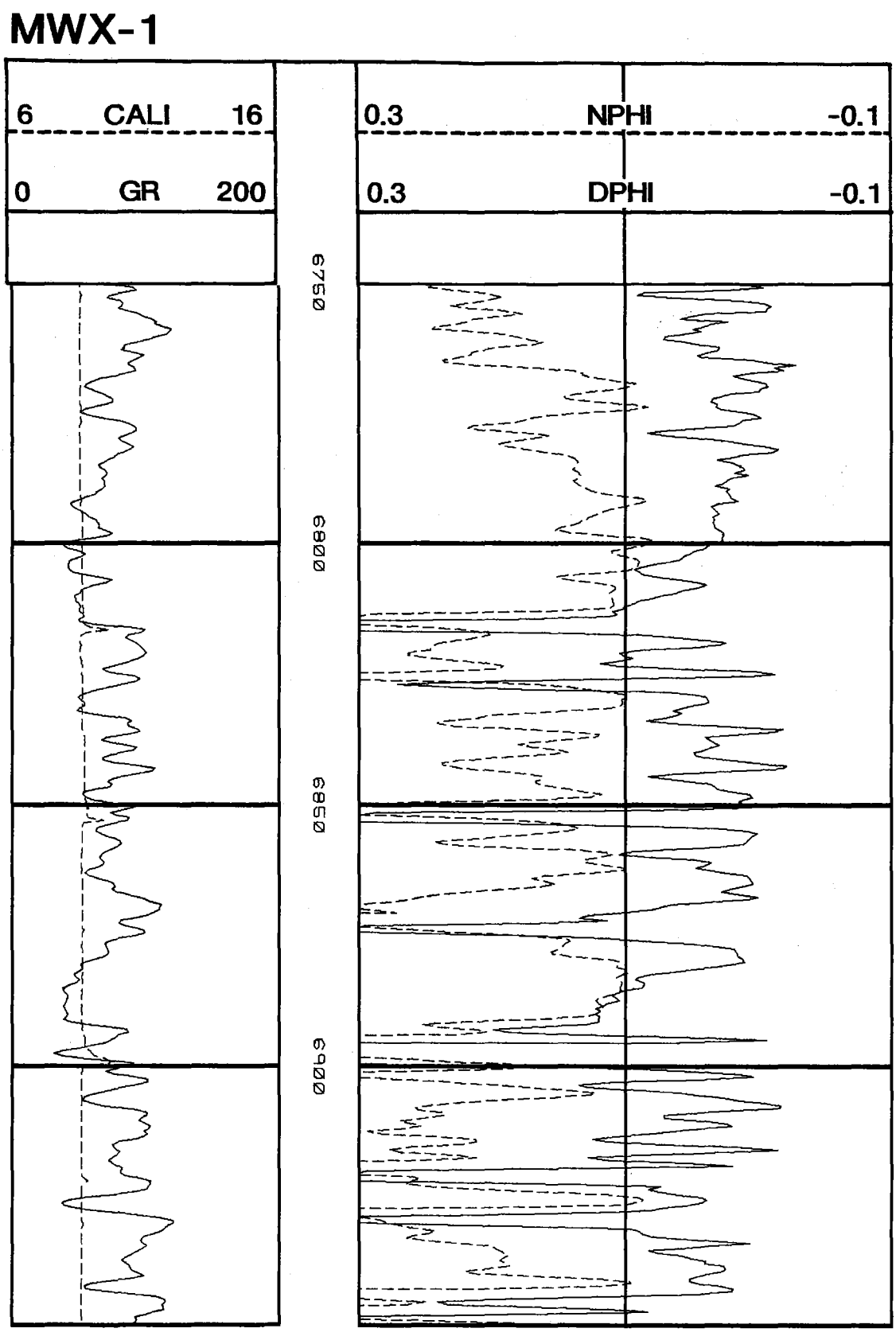

Figure 4.2 Density-Neutron Log, MWX-1 (continued)

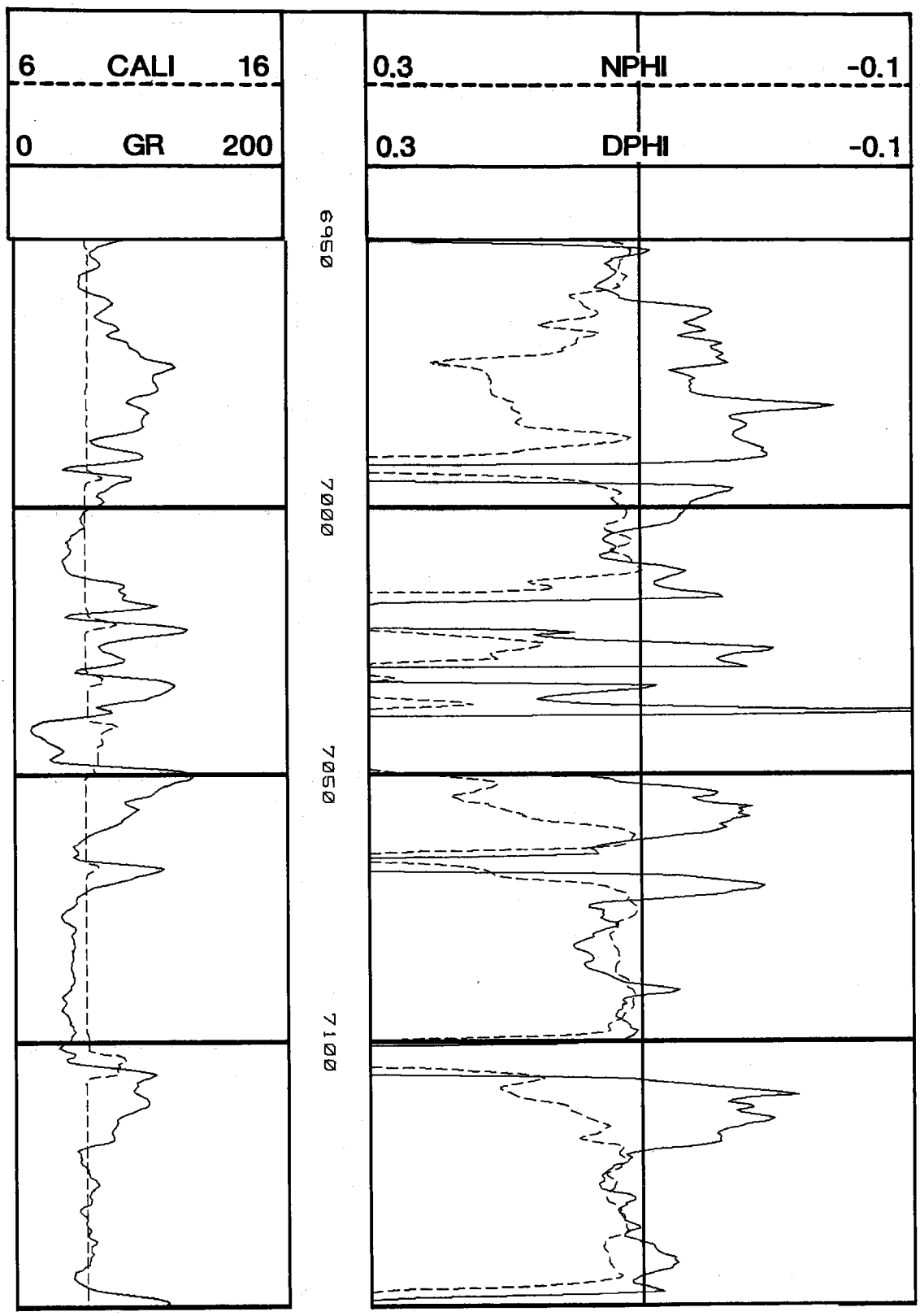

Figure 4.2 Density-Neutron Log, MWX-1 (continued)

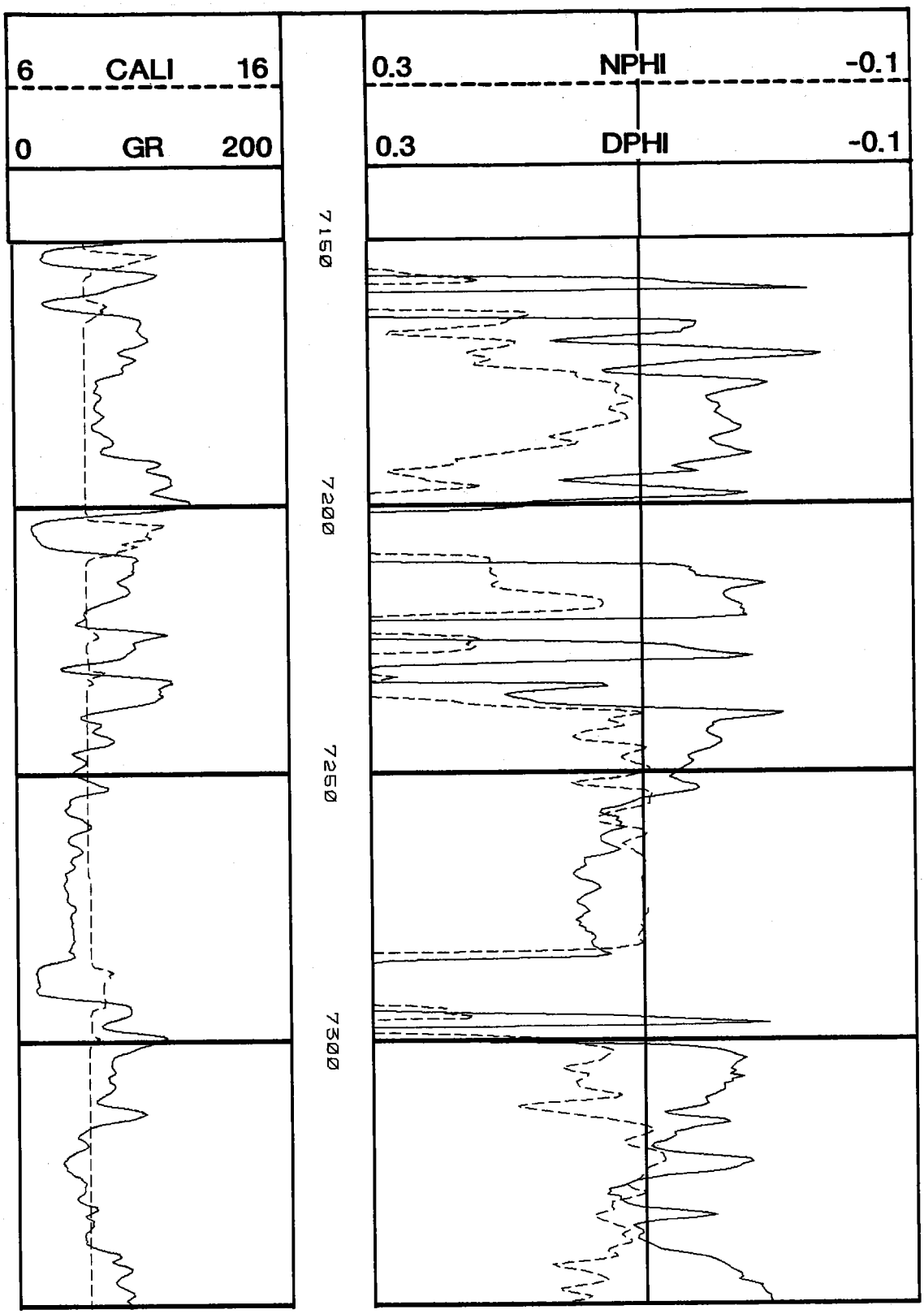

Figure 4.2 Density-Neutron Log, MWX-1 (continued)

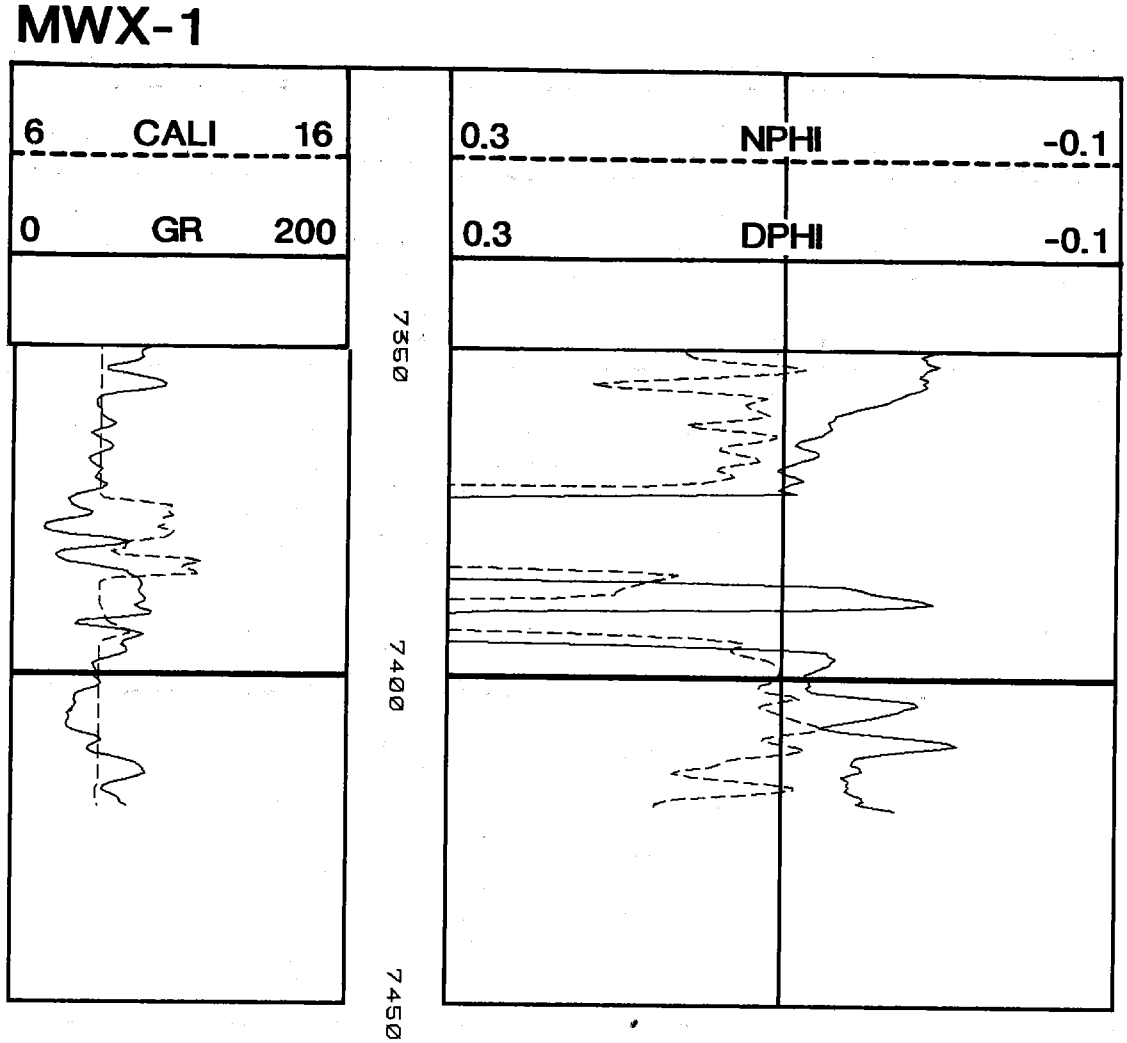

Figure 4.2 Density-Neutron Log, MWX-1 (continued)

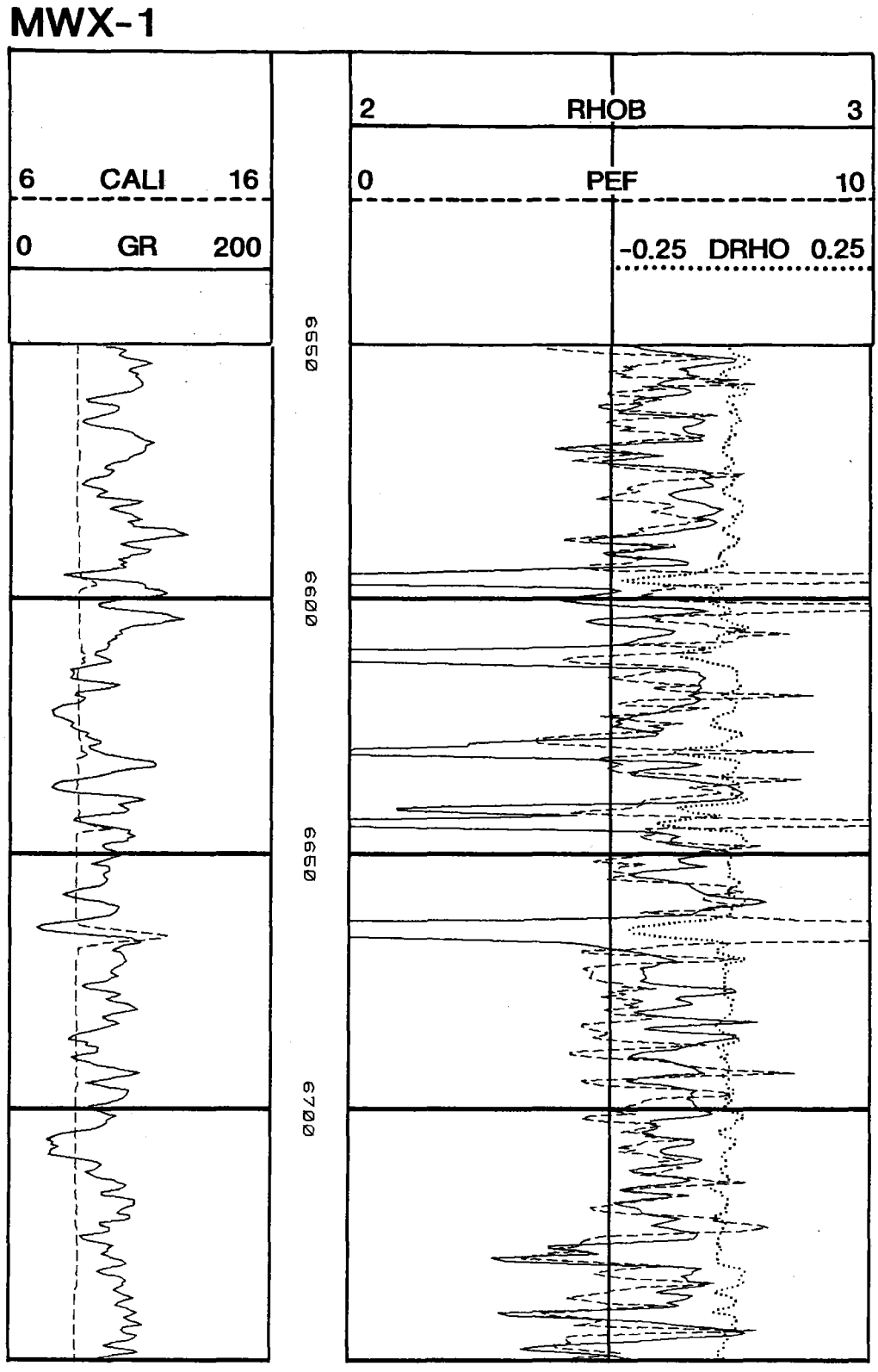

Figure 4.3 Bulk Density Log, MWX-1

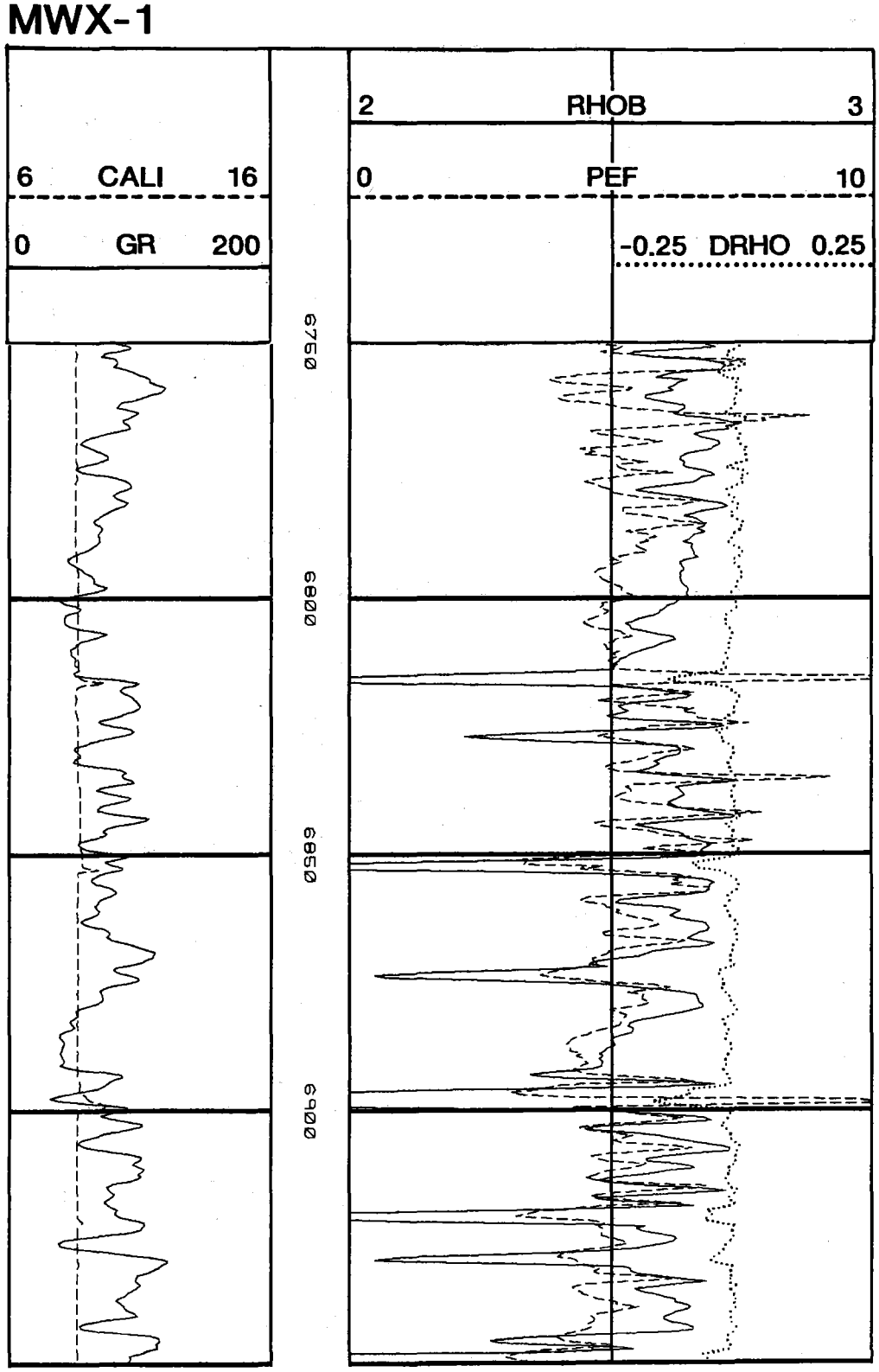

Figure 4.3 Bulk Density Log, MWX-1 (continued)

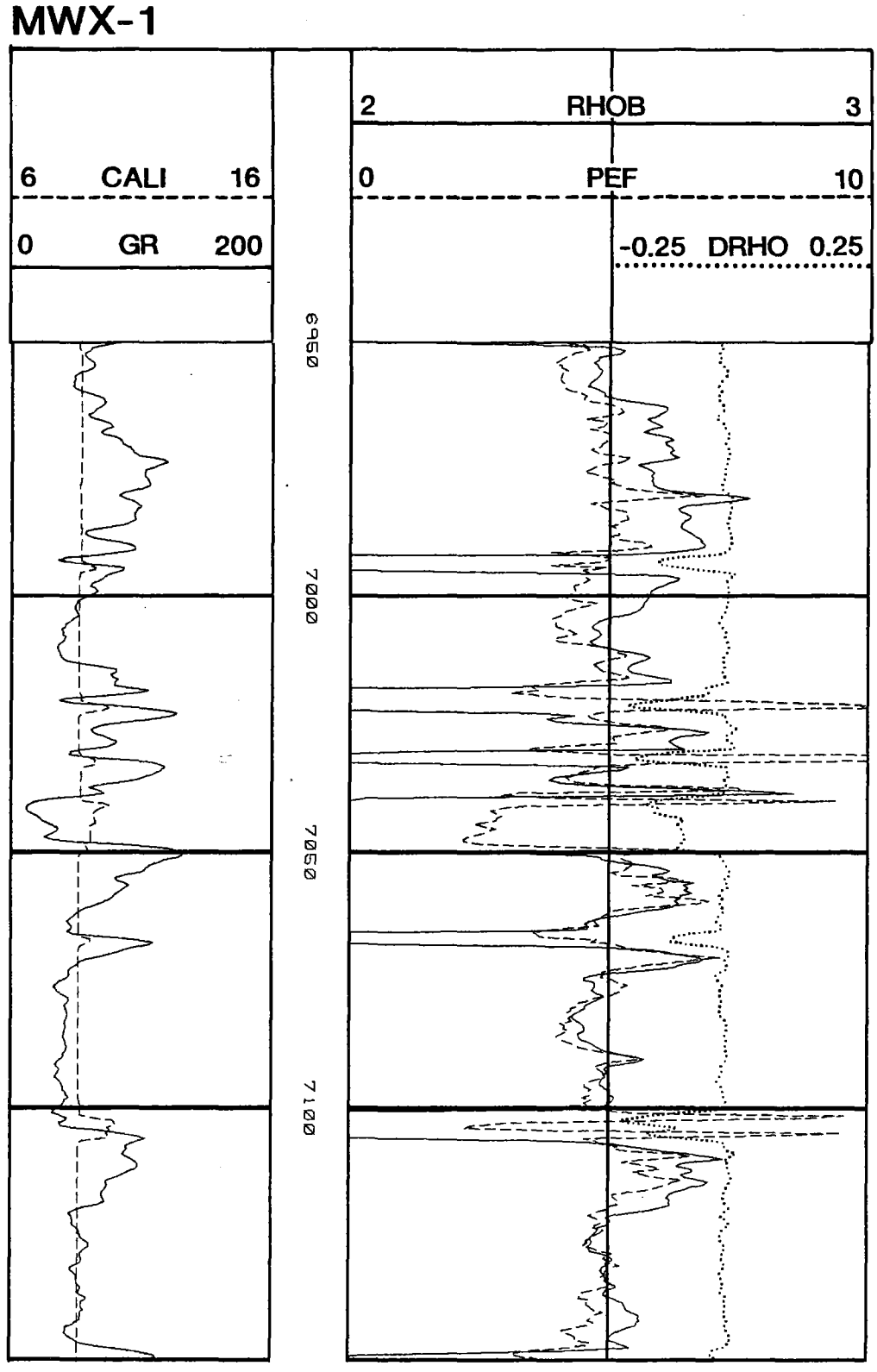

Figure 4.3 Bulk Density Log, MWX-1 (continued)

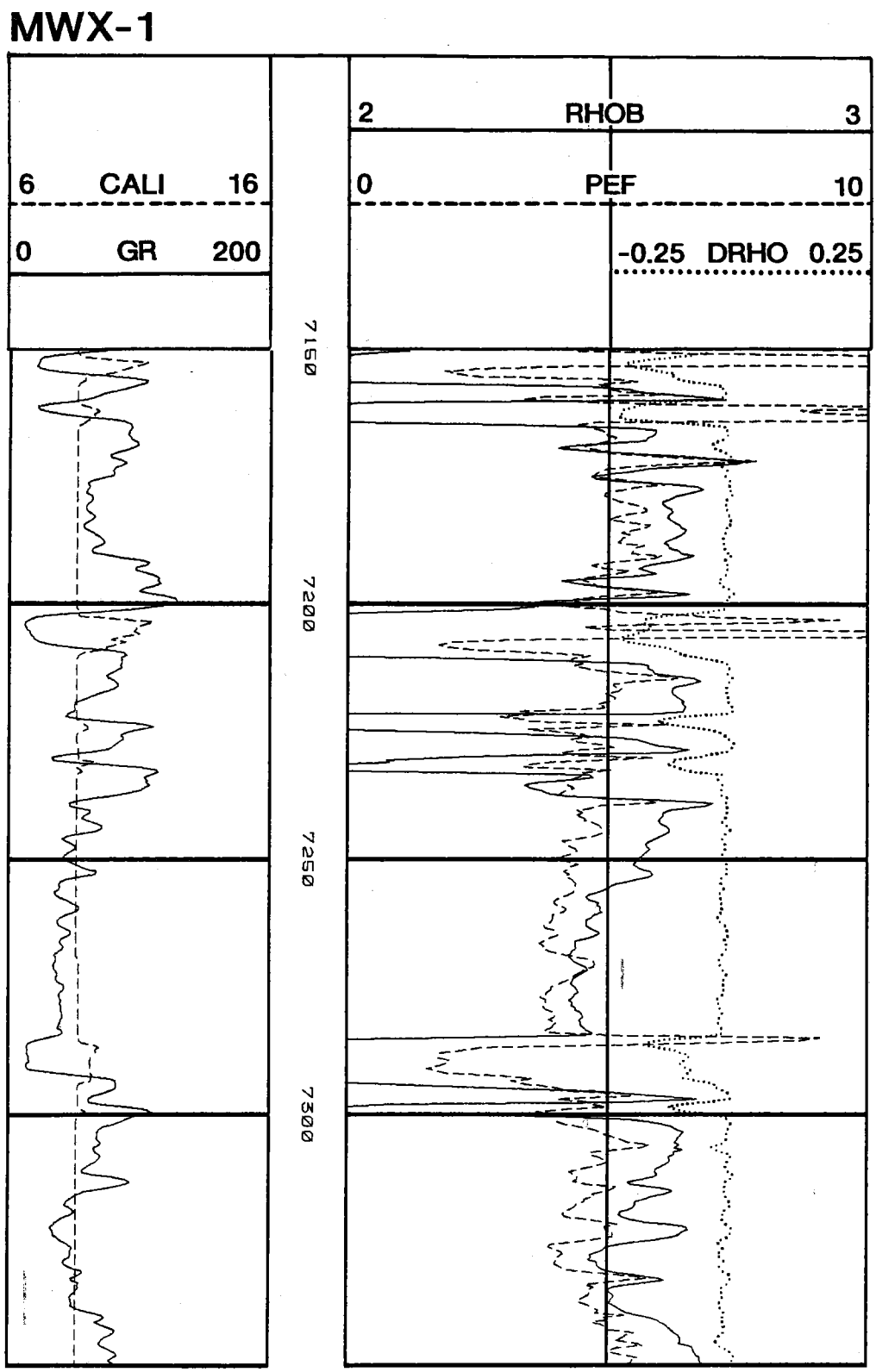

Figure 4.3 Bulk Density Log, MWX-1 (continued)

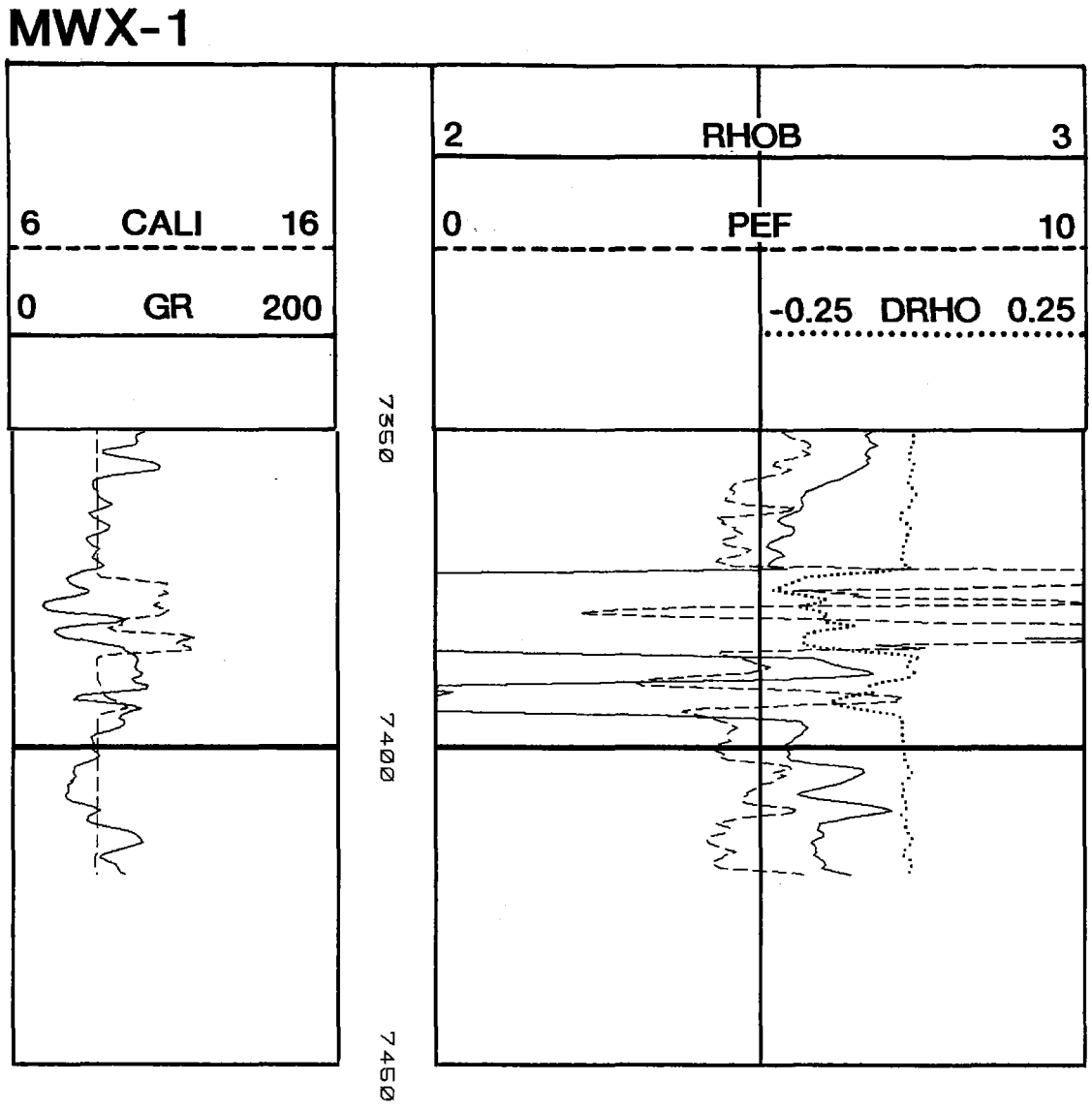

Figure 4.3 Bulk Density Log, MWX-1 (continued)

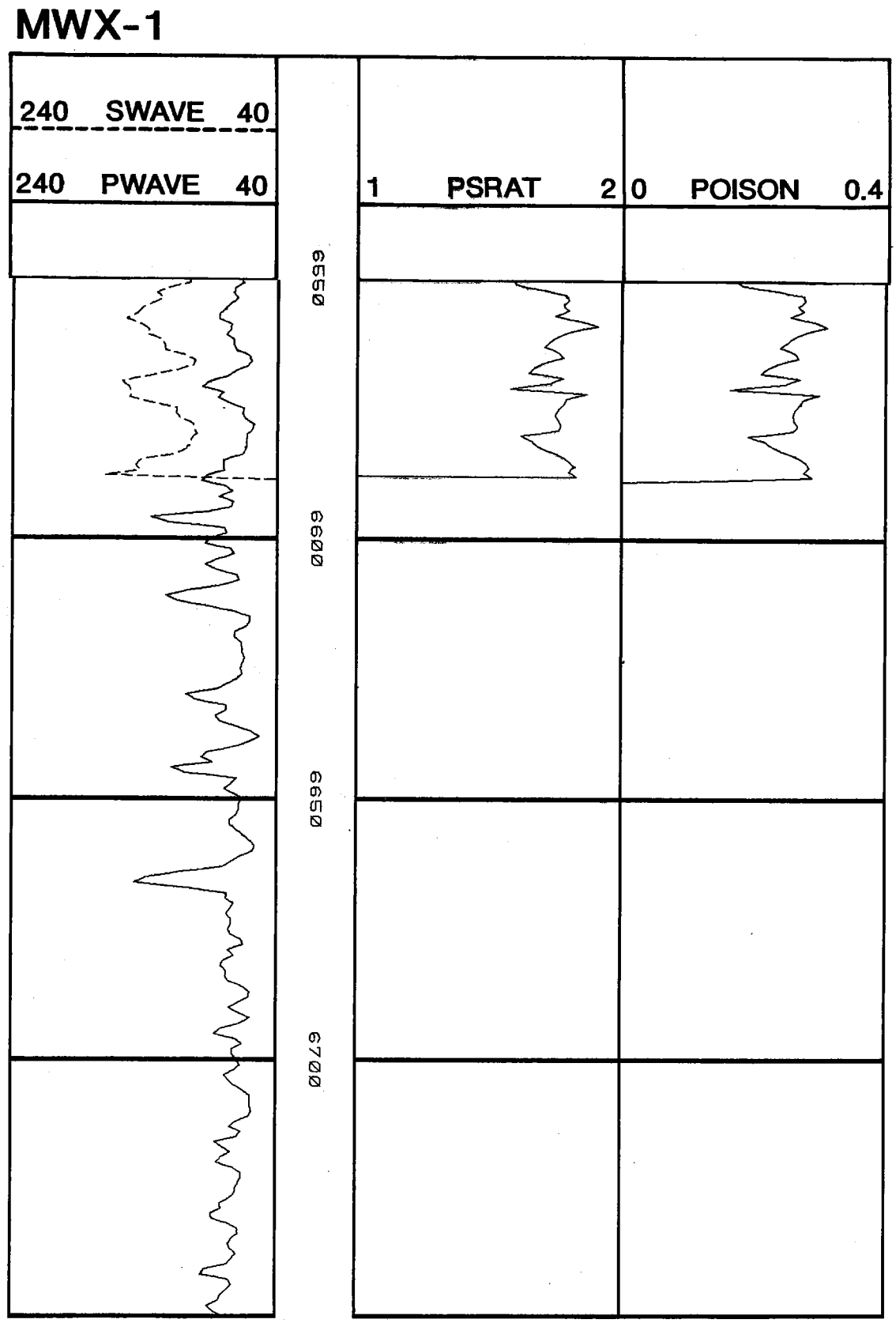

Figure 4.4 Sonic Log, MWX-1

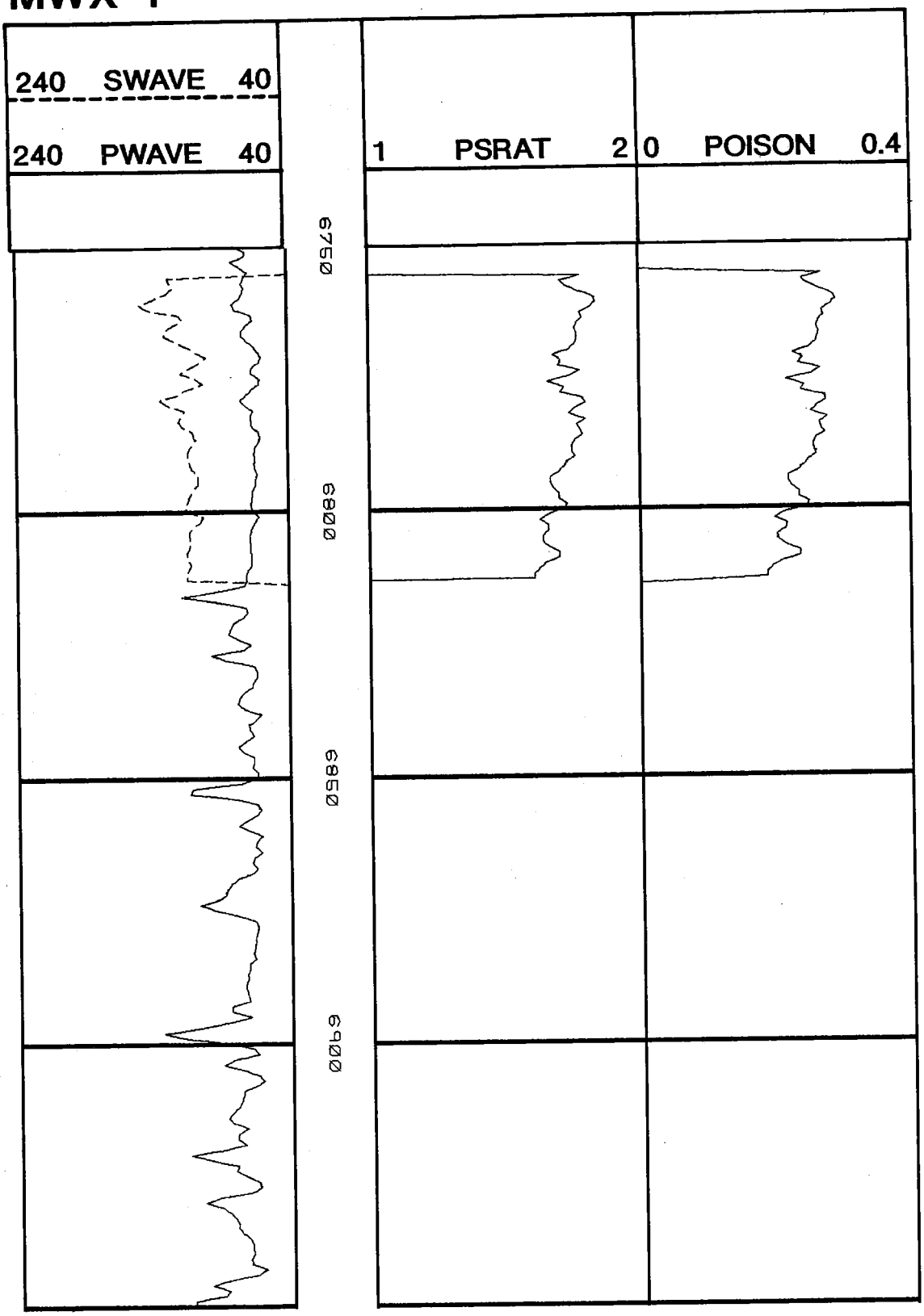

Figure 4.4 Sonic Log, MWX-1 (continued)

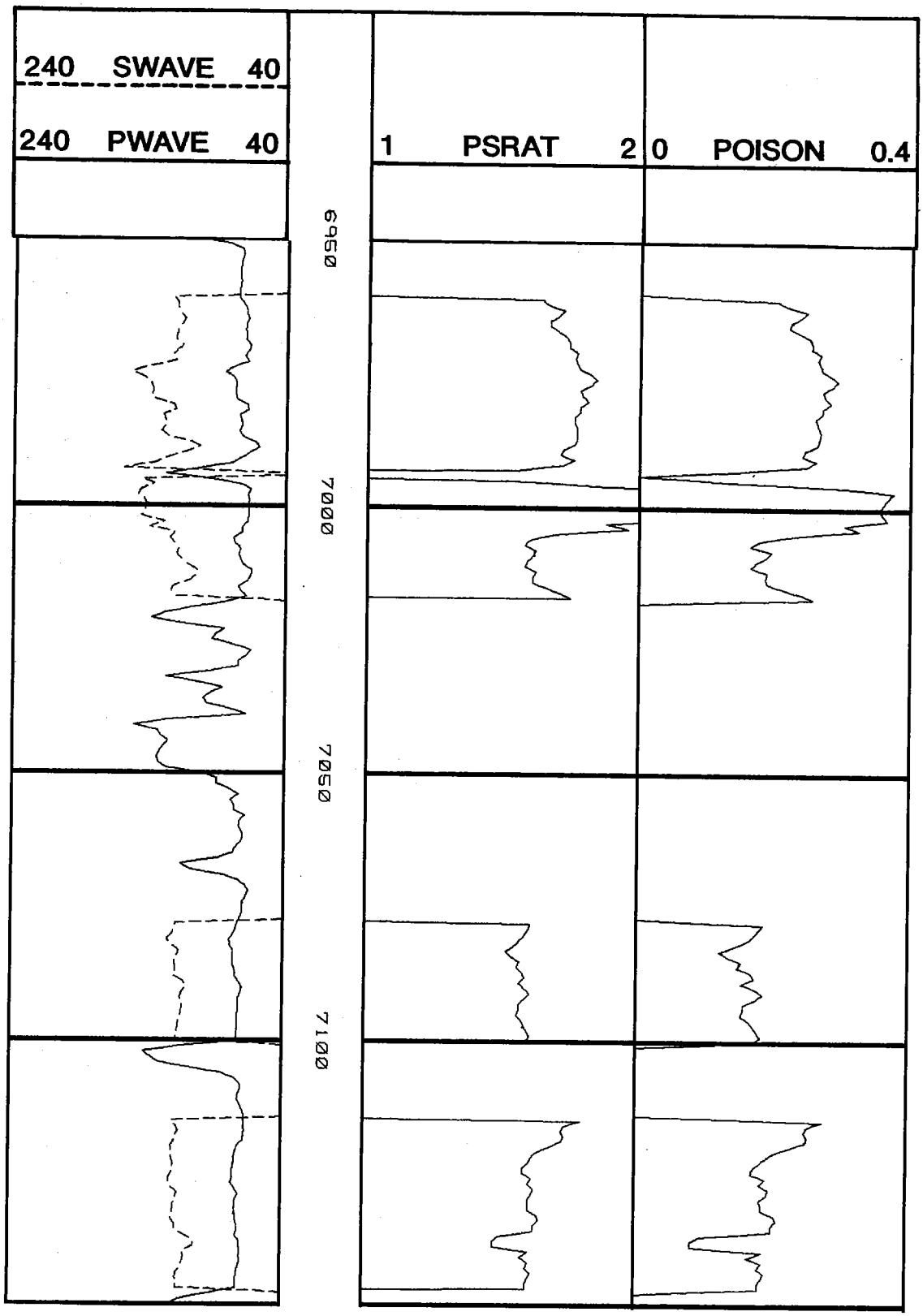

Figure 4.4 Sonic Log, MWX-1 (continued)

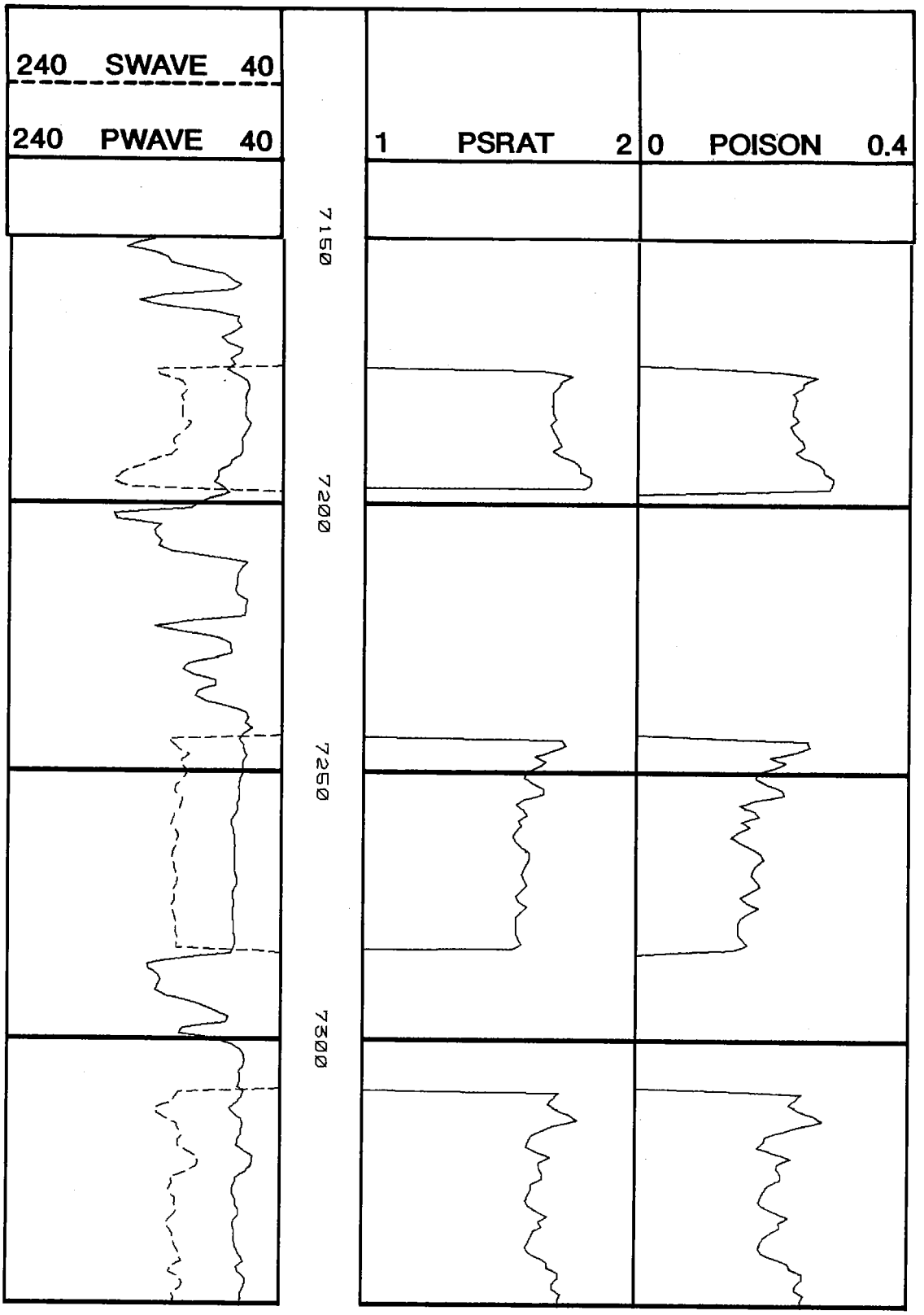

Figure 4.4 Sonic Log, MWX-1 (continued)

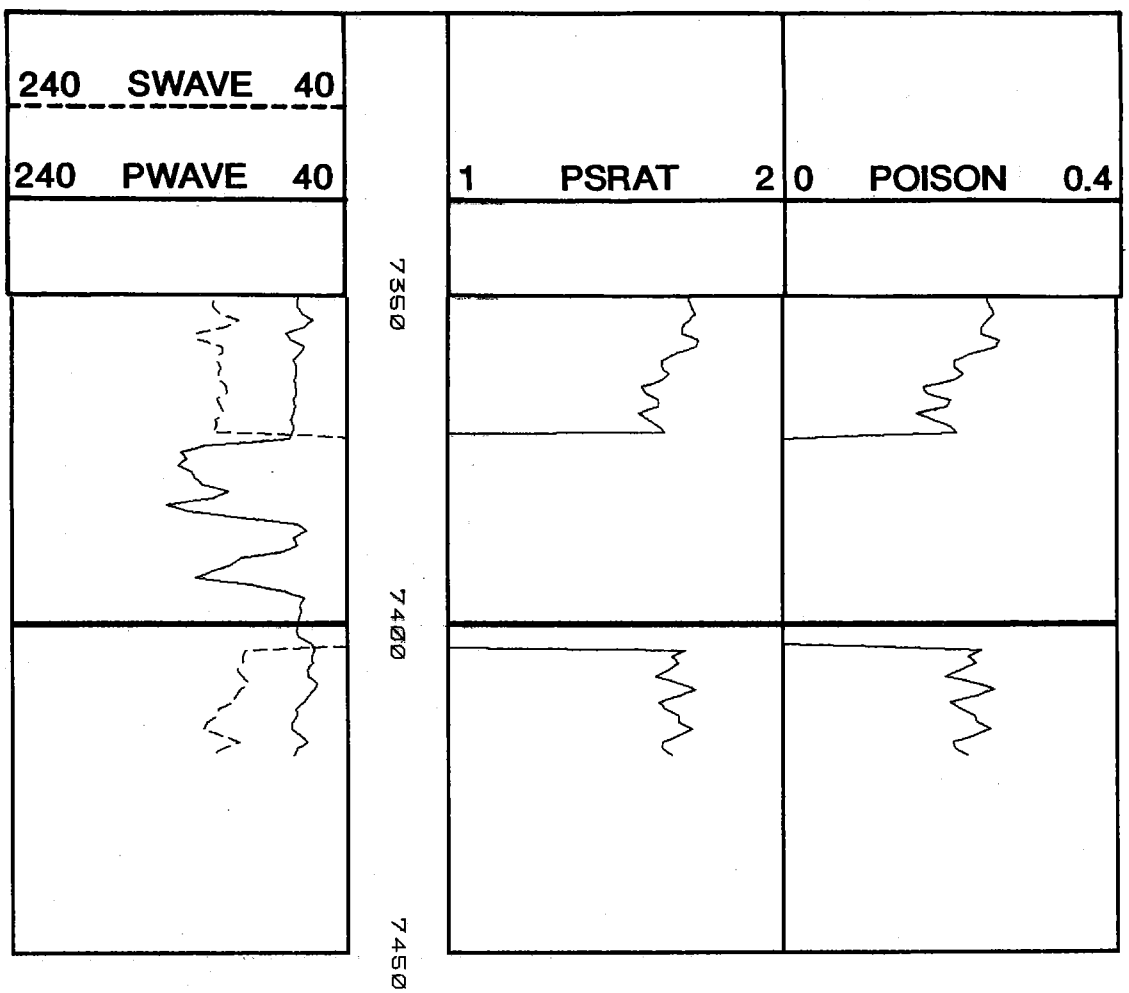

Figure 4.4 Sonic Log, MWX-1 (continued)

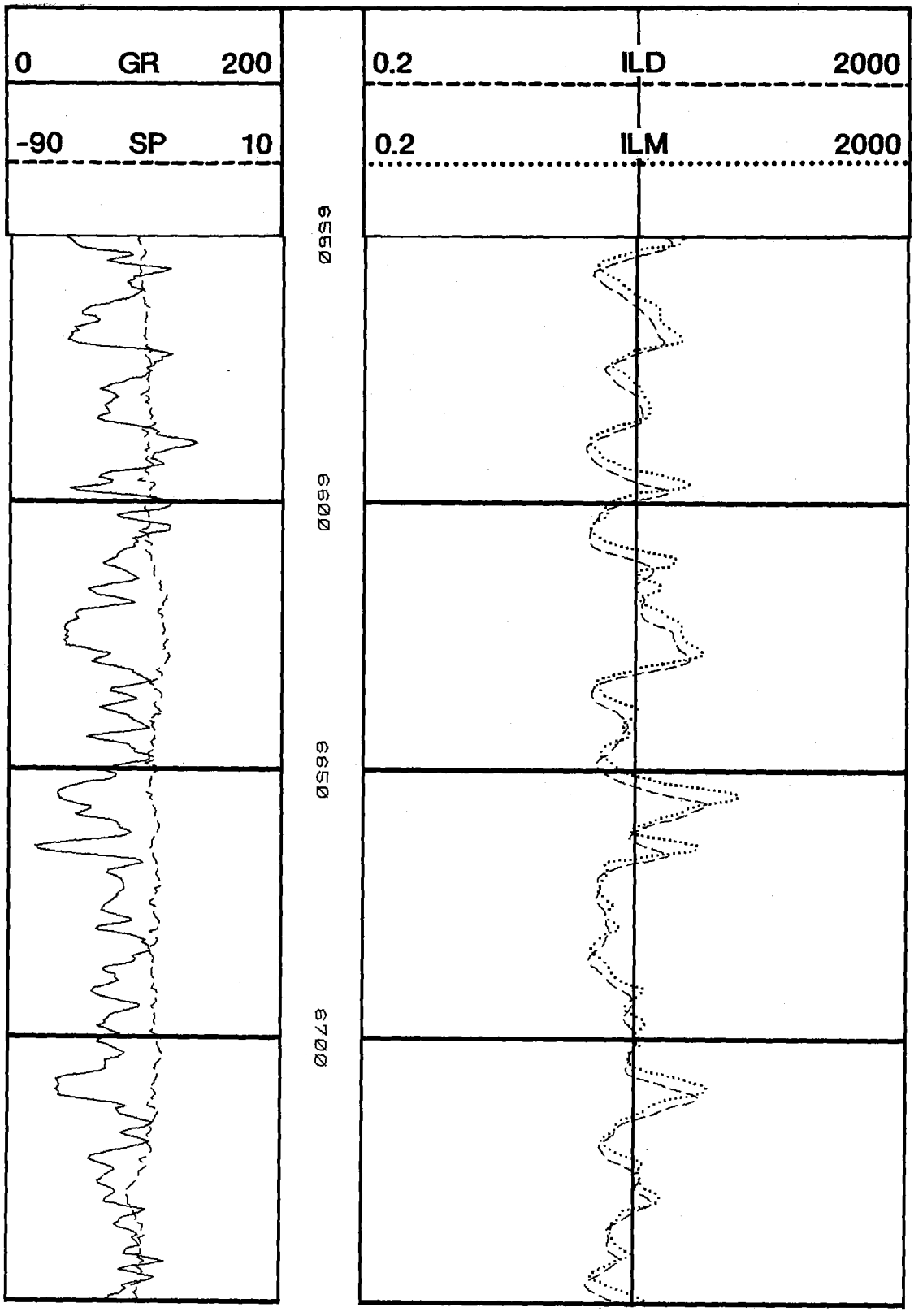

Figure 4.5 Resistivity Log, MWX-2

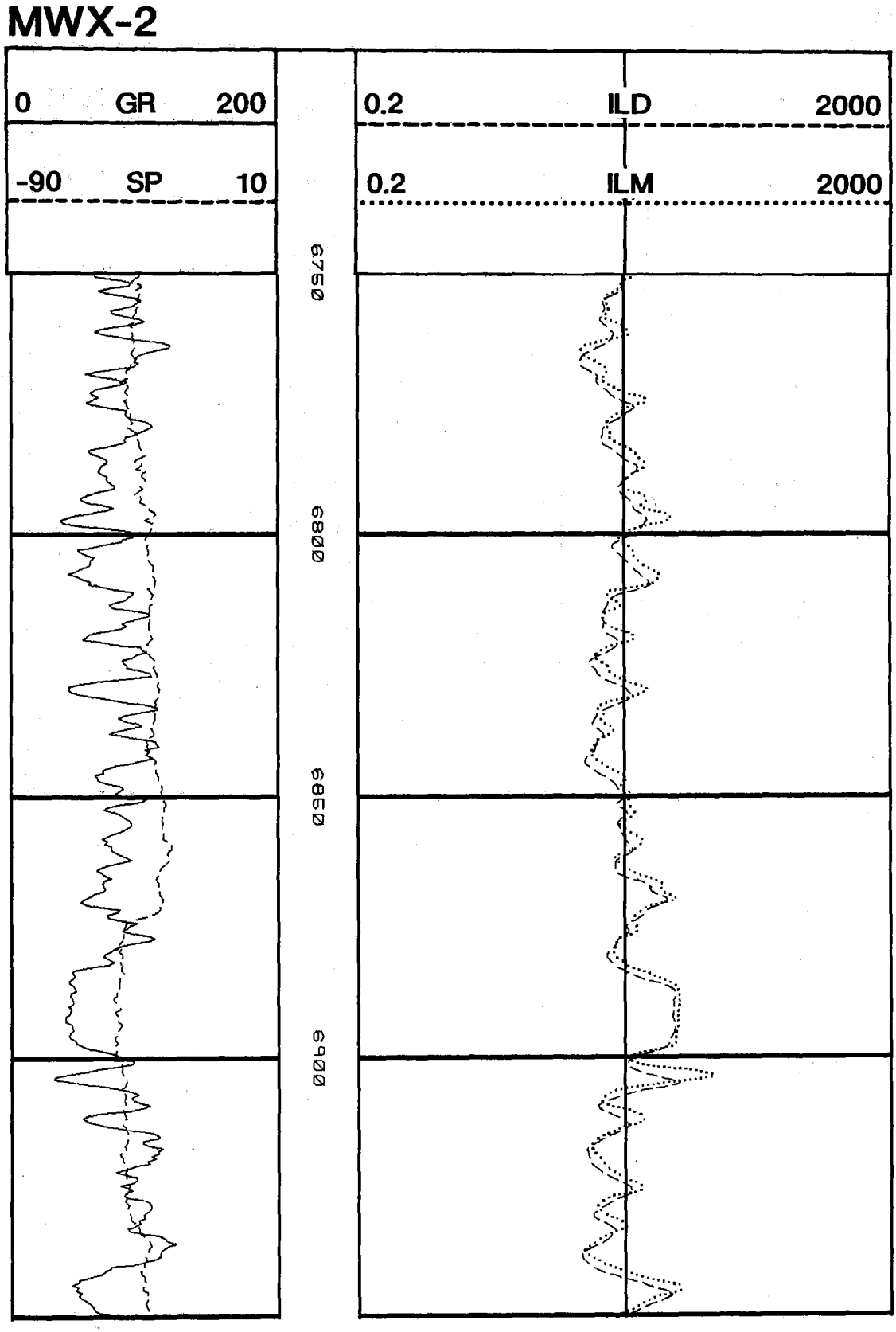

Figure 4.5 Resistivity Log, MWX-2 (continued)

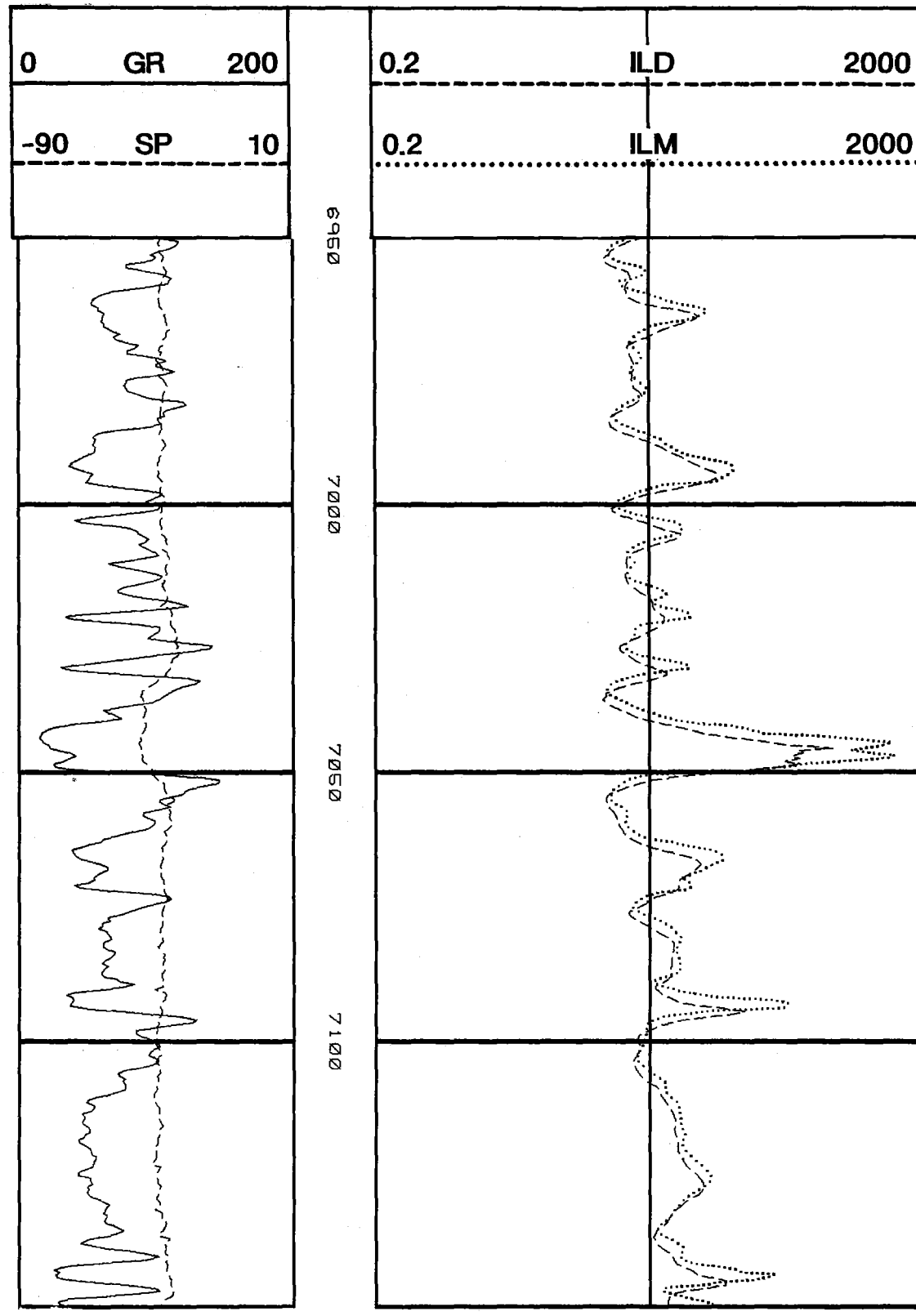

Figure 4.5 Resistivity Log, MWX-2 (continued)

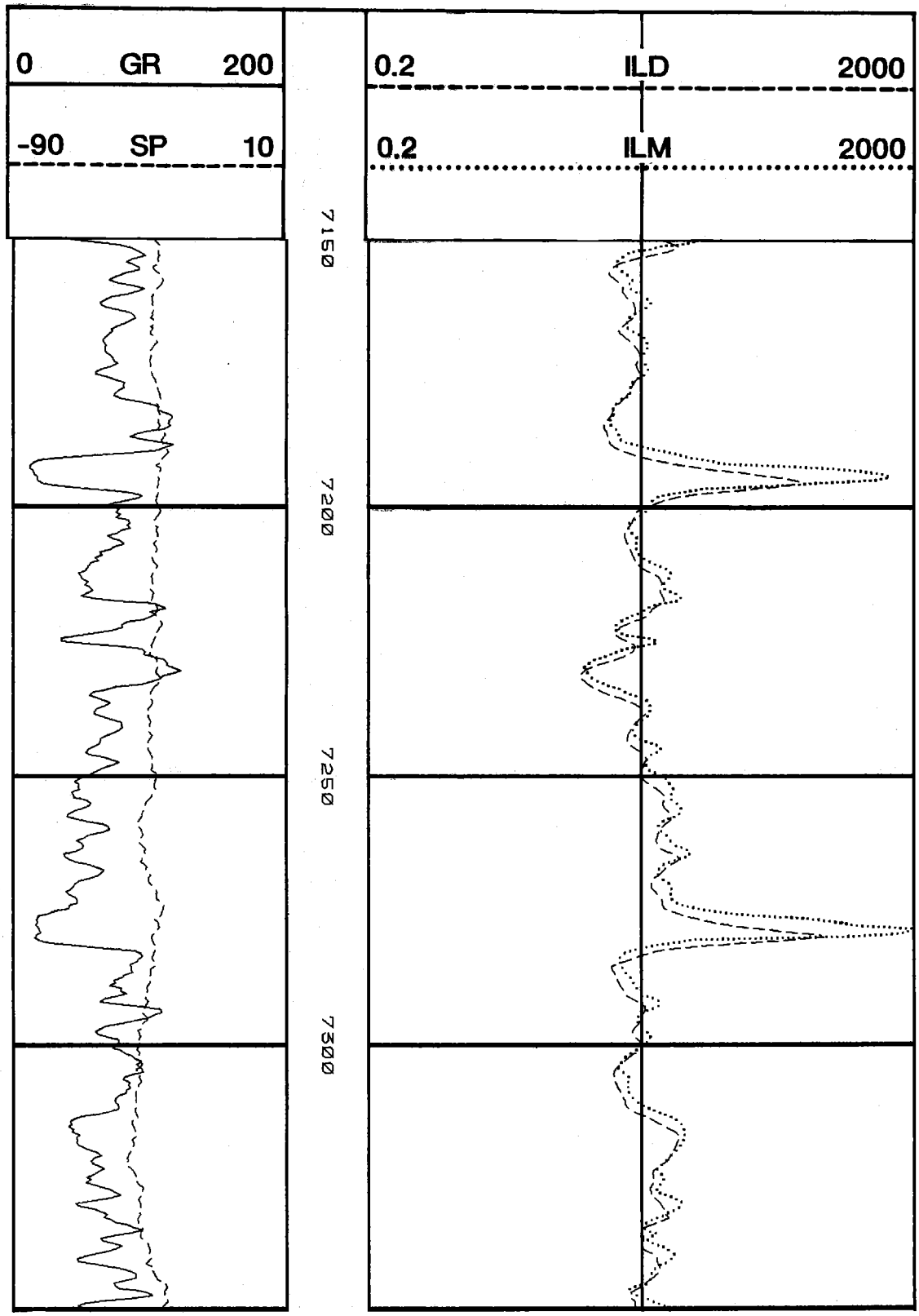

Figure 4.5 Resistivity Log, MWX-2 (continued)

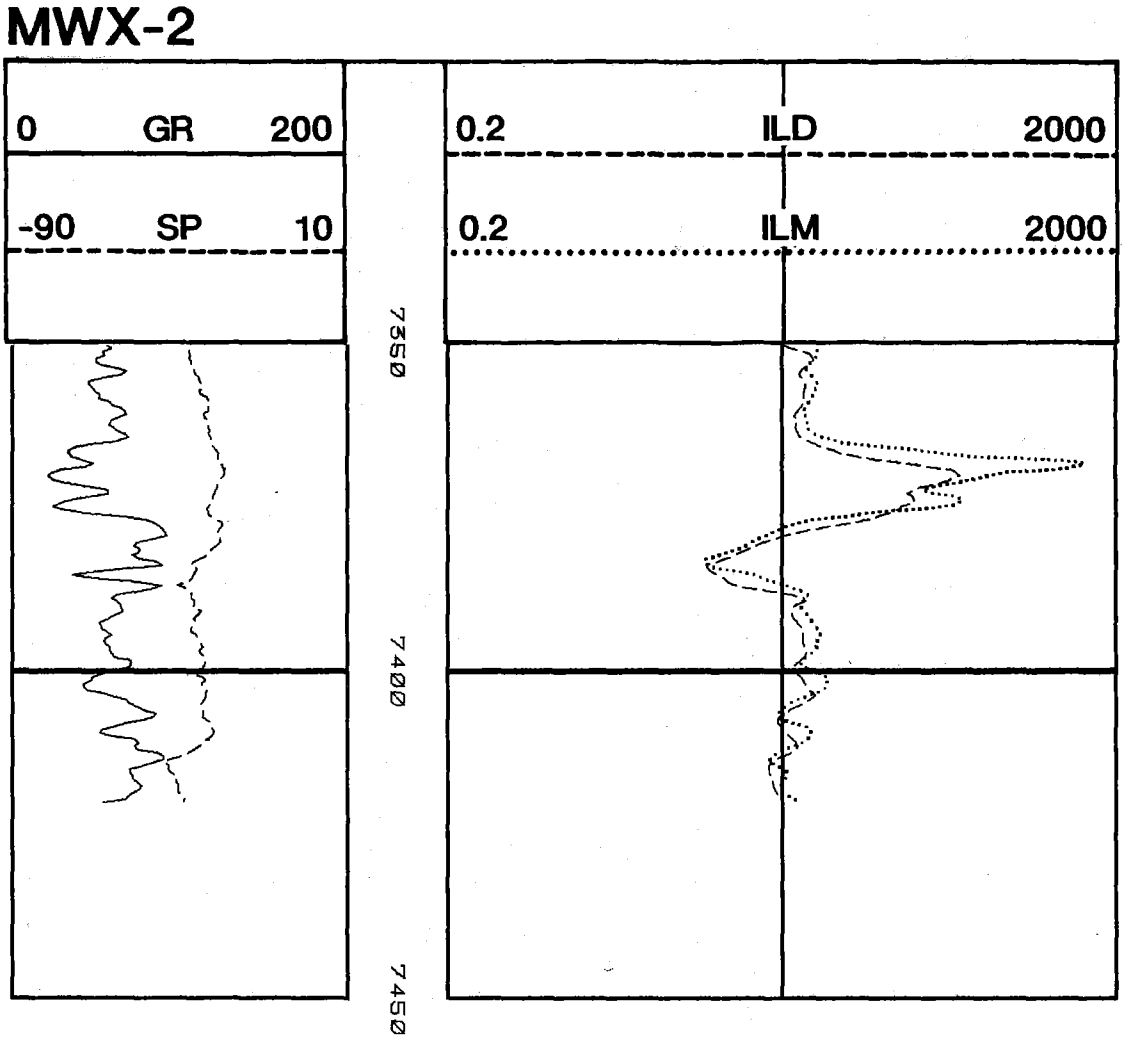

Figure 4.5 Resistivity Log, MWX-2 (continued)

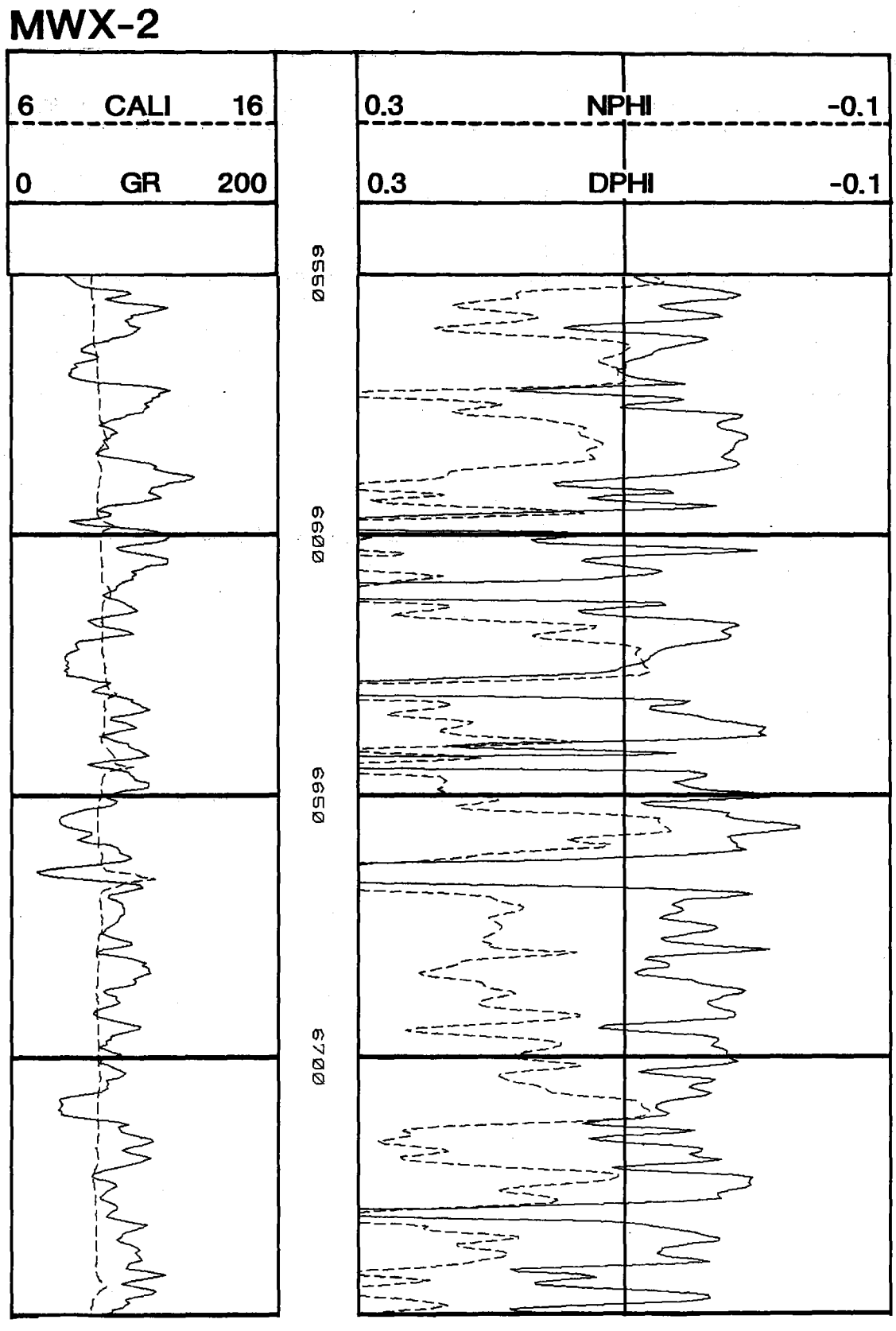

Figure 4.6 Density-Neutron Log, MWX-2

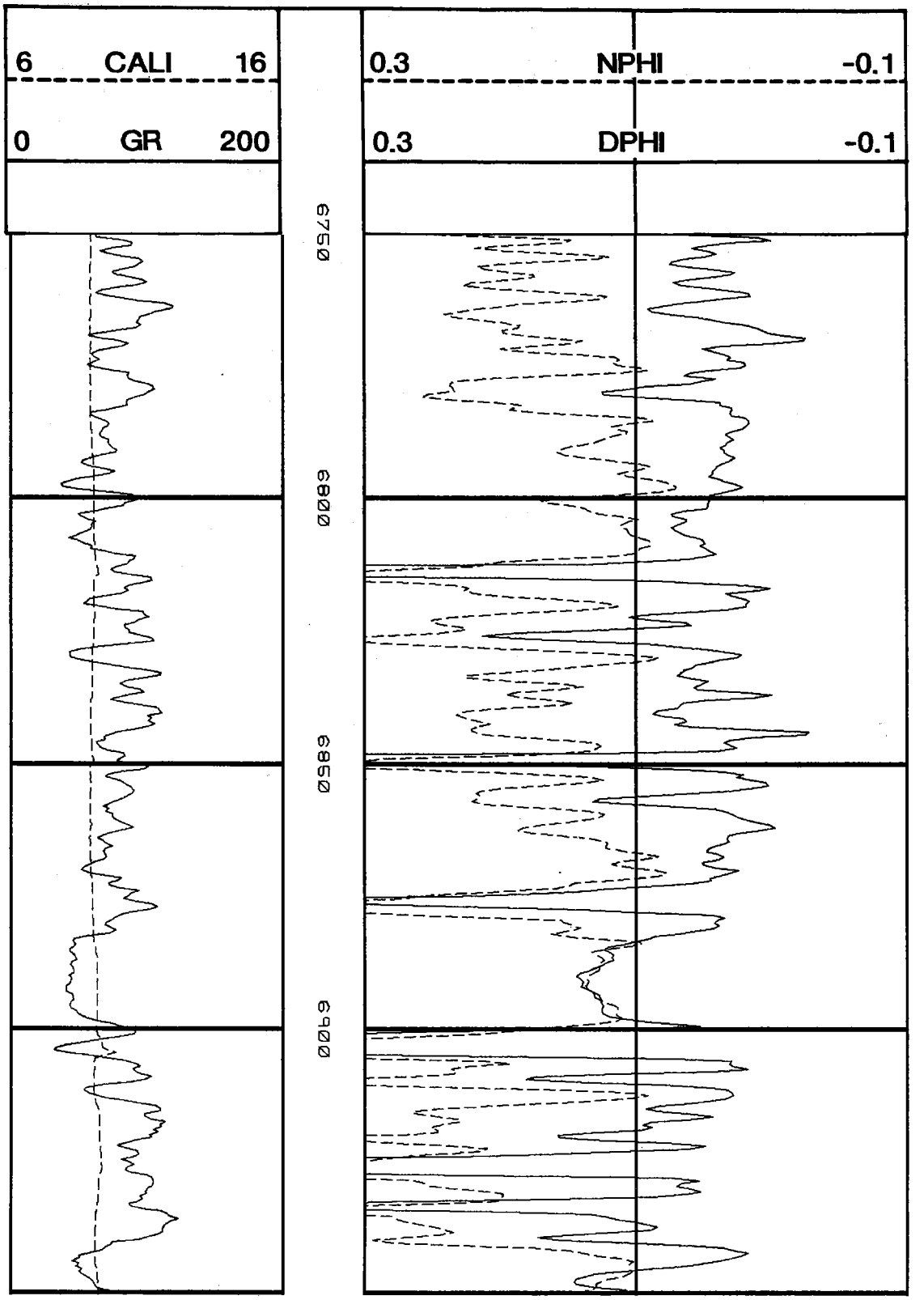

Figure 4.6 Density-Neutron Log, MWX-2 (continued)

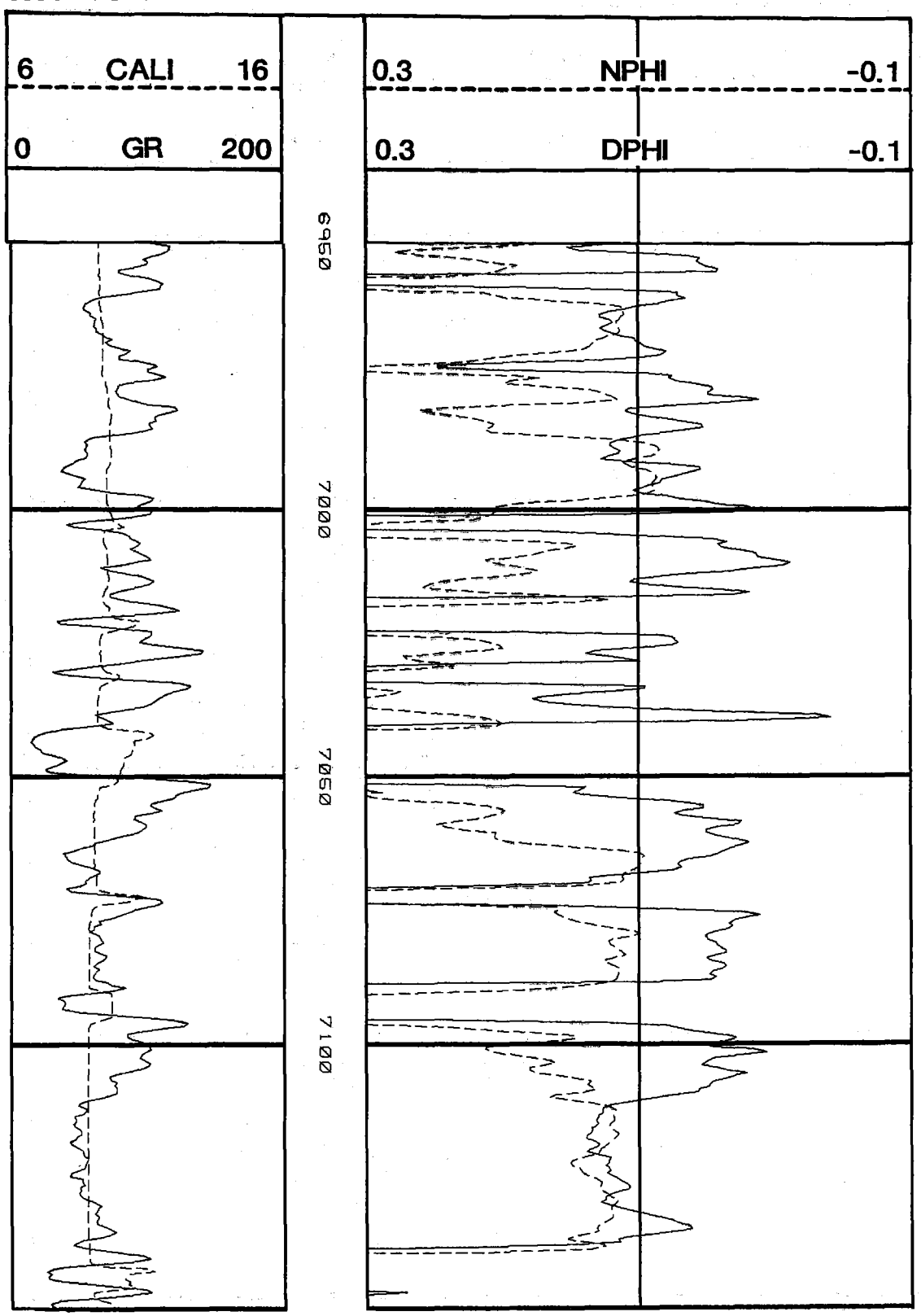

Figure 4.6 Density-Neutron Log, MWX-2 (continued)

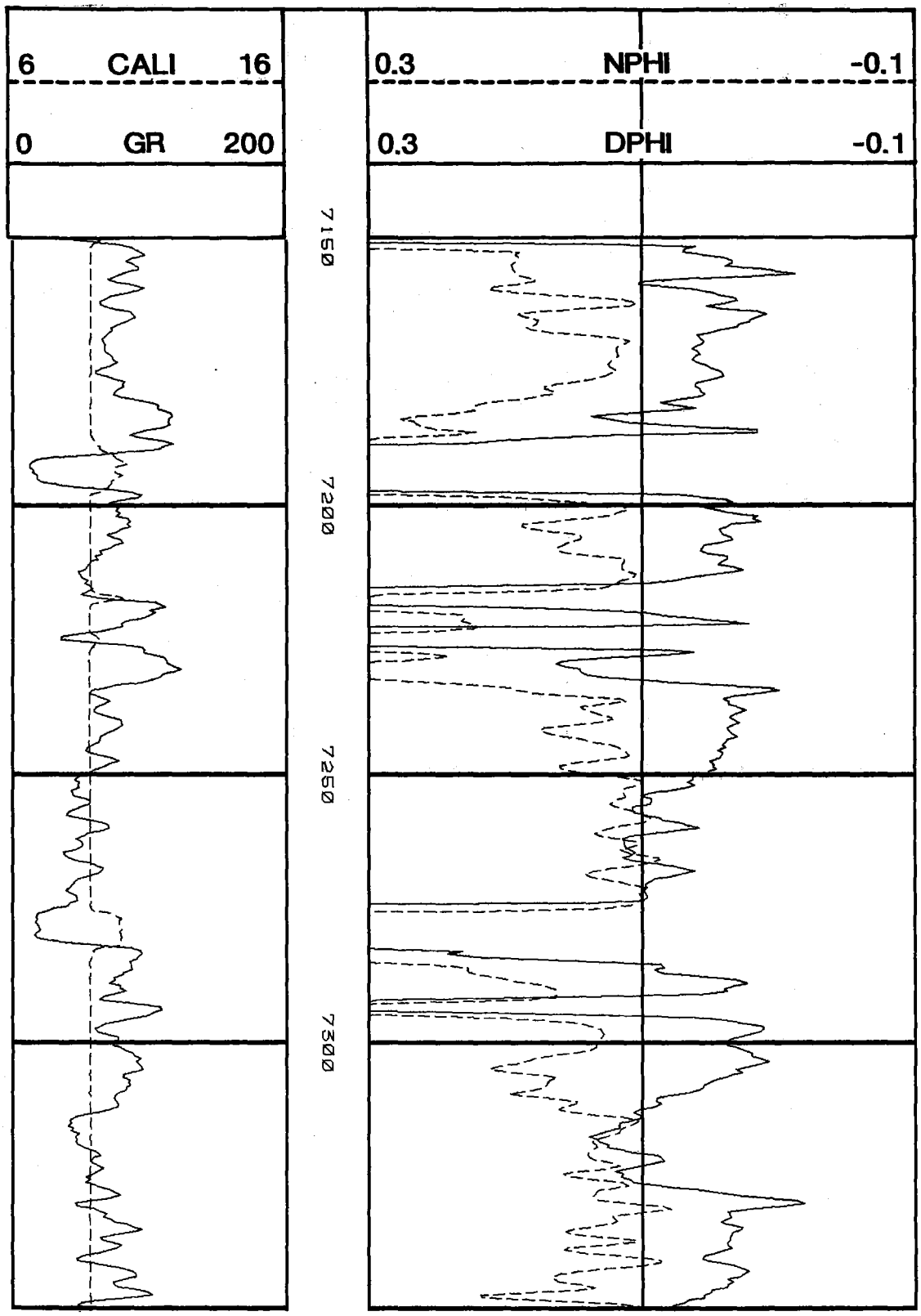

Figure 4.6 Density-Neutron Log, MWX-2 (continued)

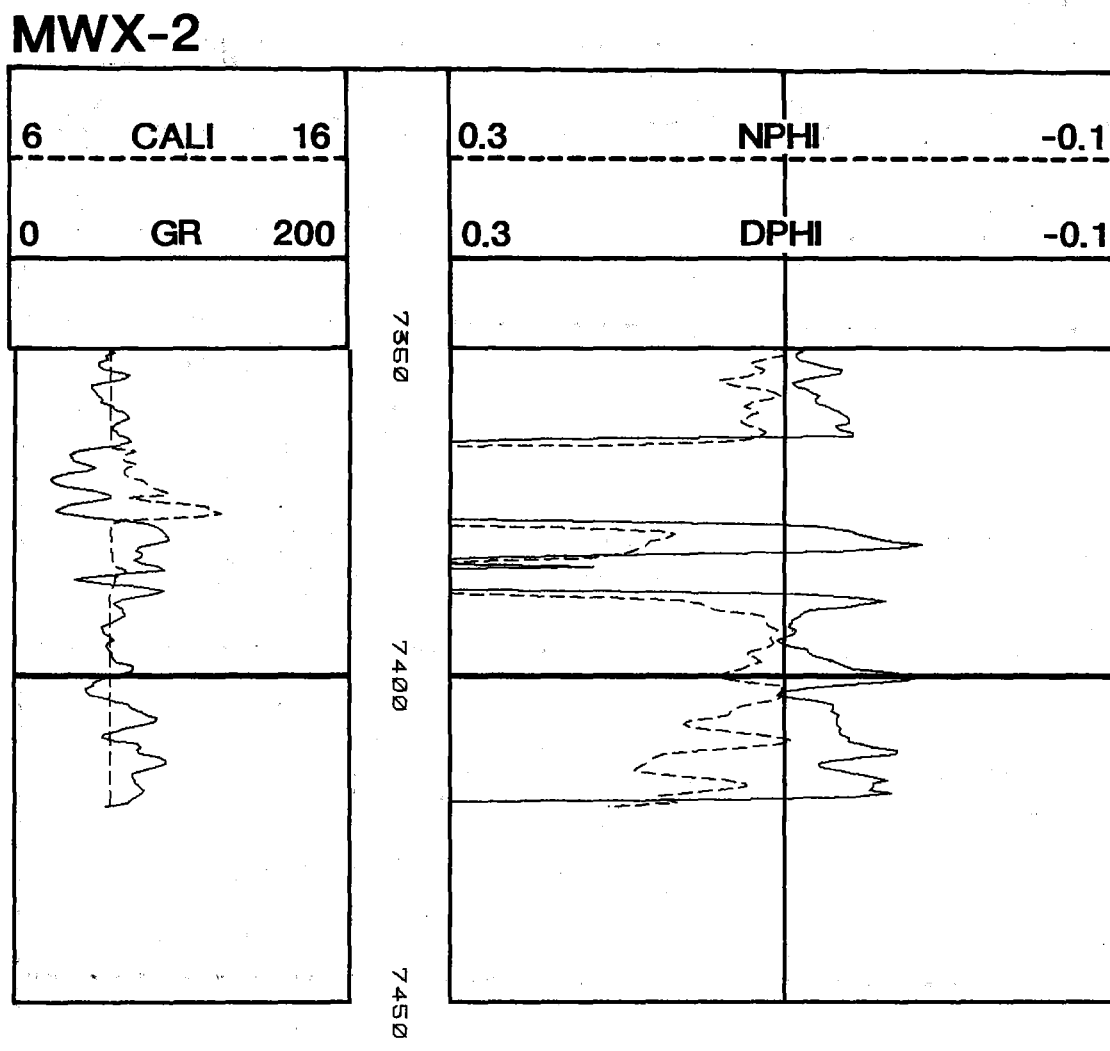

Figure 4.6 Density-Neutron Log, MWX-2 (continued)

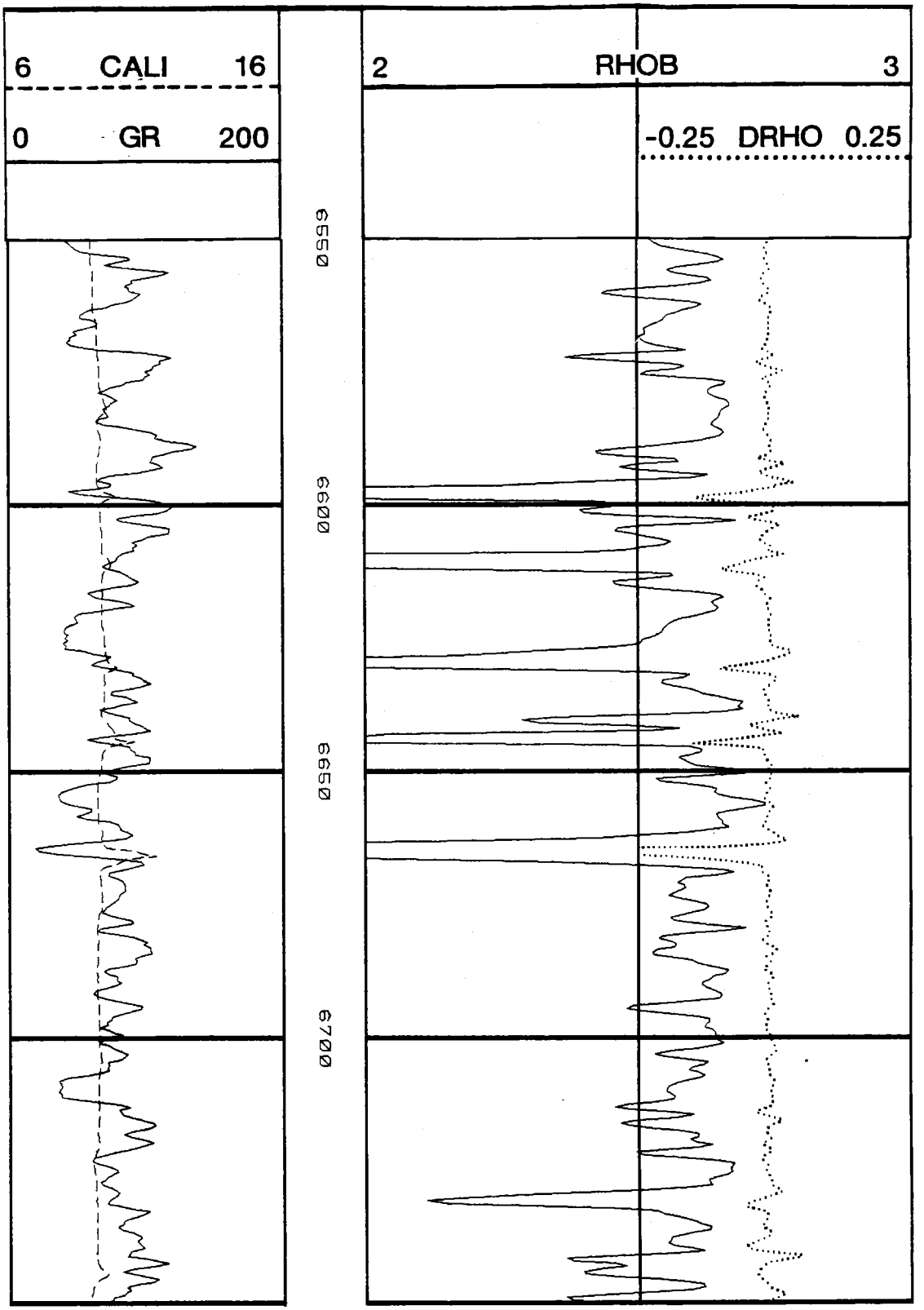

Figure 4.7 Bulk Density Log, MWX-2

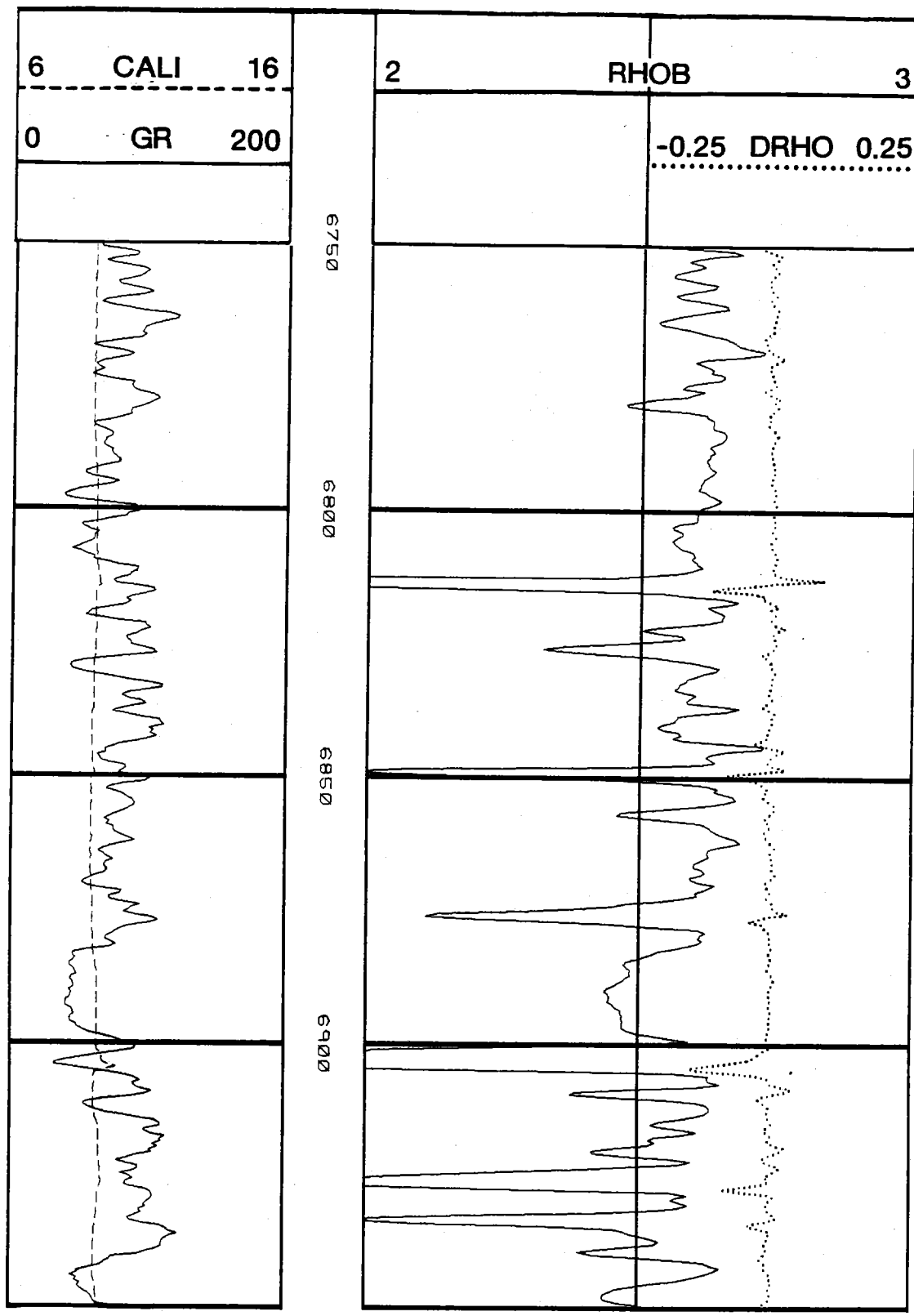

Figure 4.7 Bulk Density Log, MWX-2 (continued)

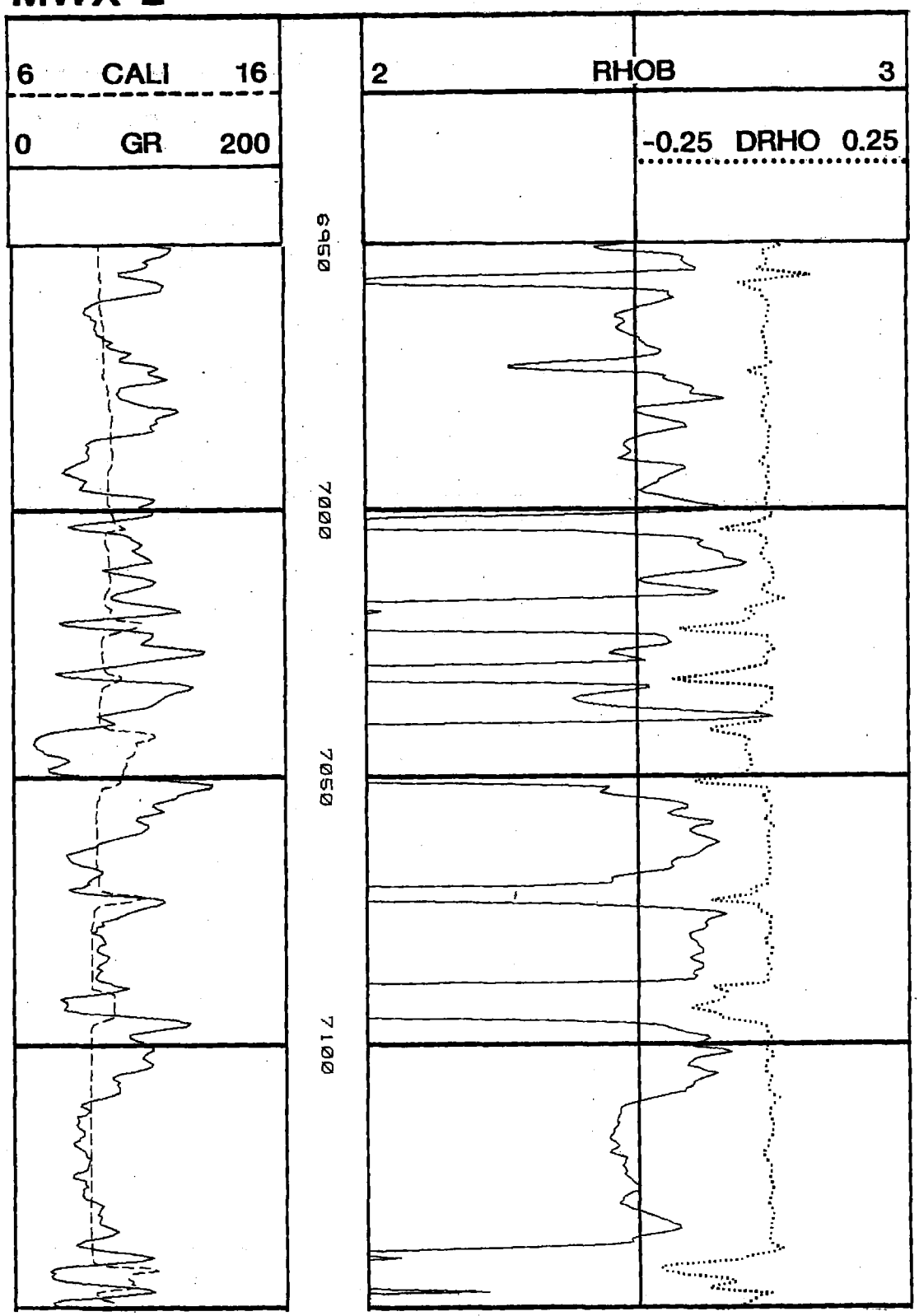

Figure 4.7 Bulk Density Log, MWX-2 (continued)

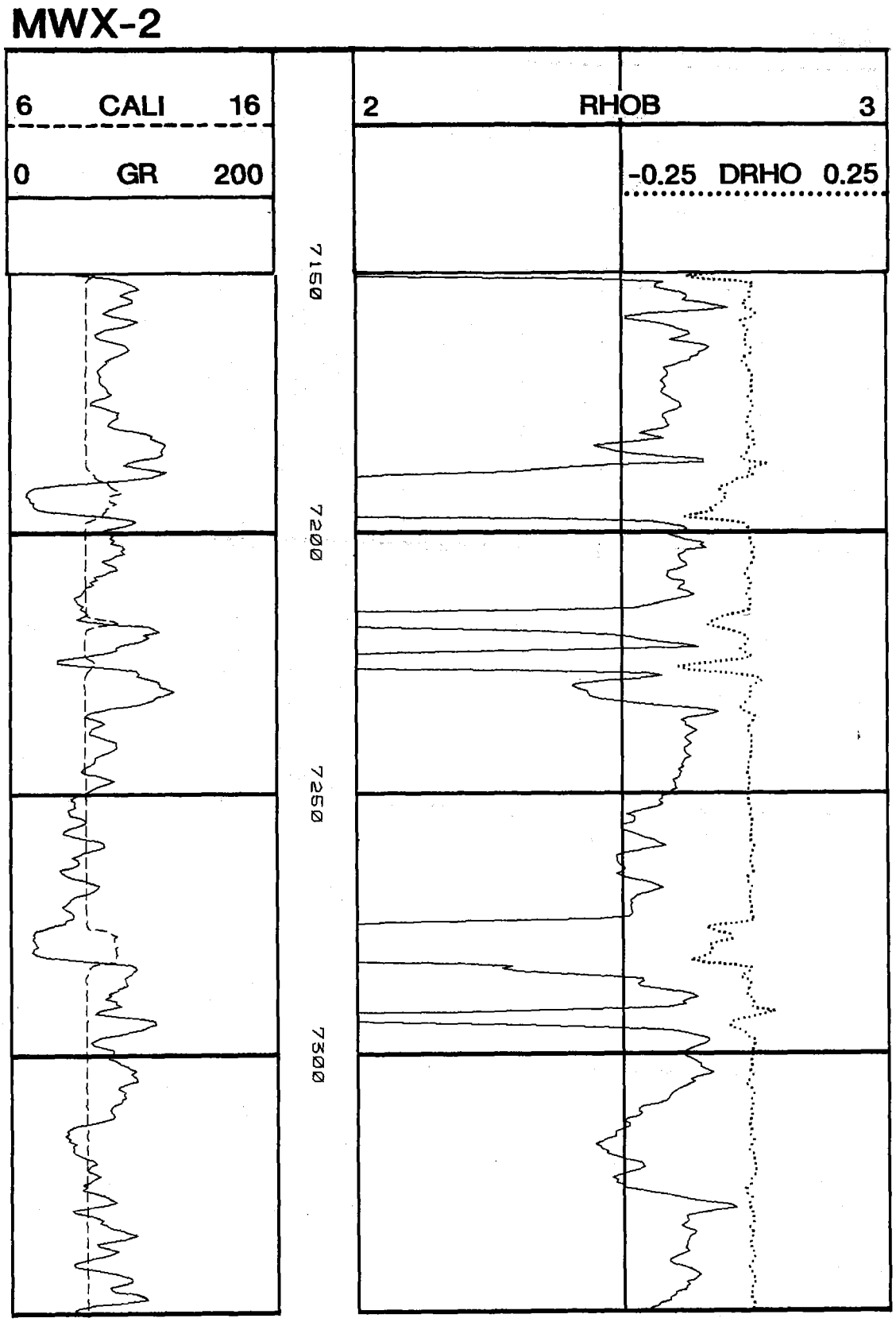

Figure 4.7 Bulk Density Log, MWX-2 (continued)

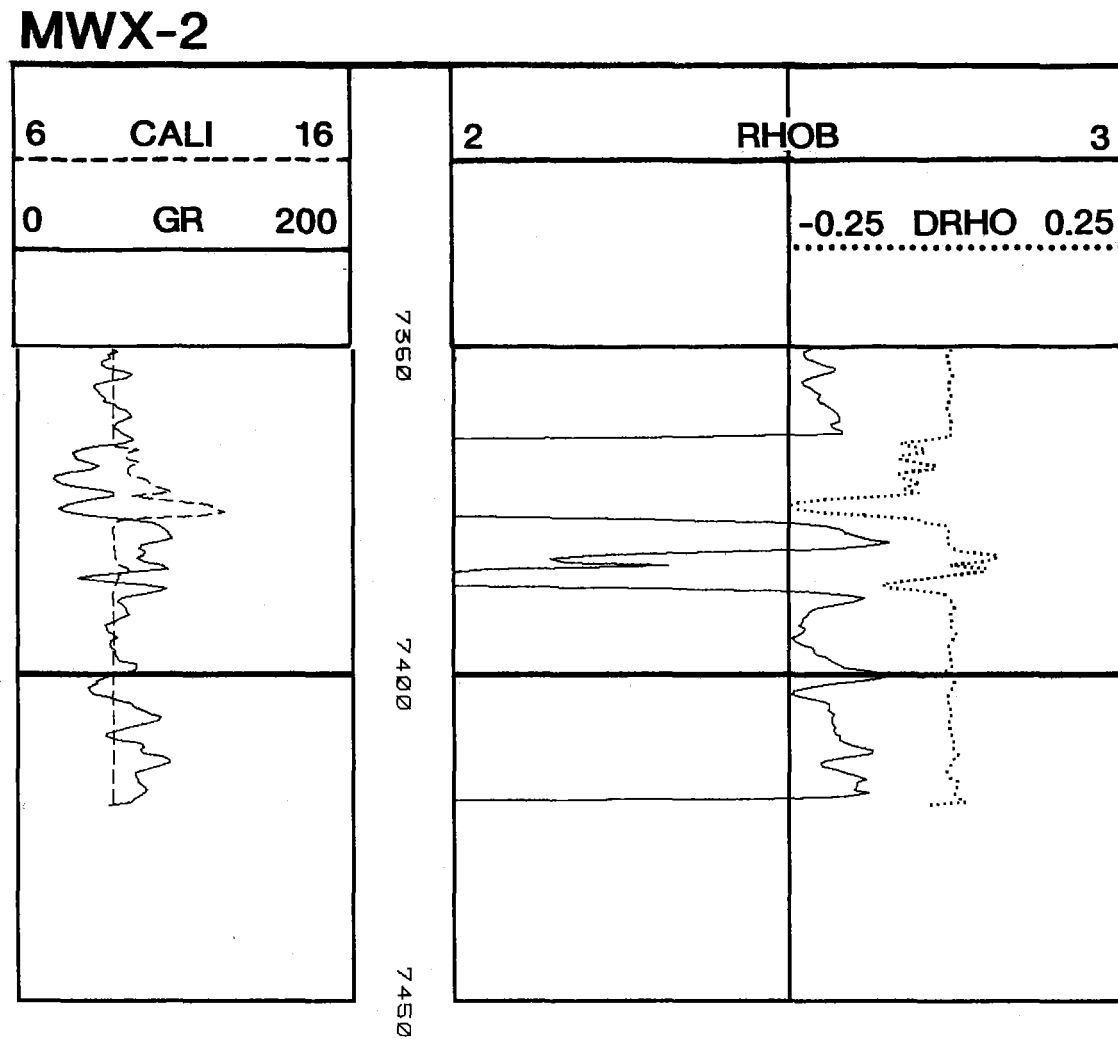

Figure 4.7 Bulk Density Log, MWX-2 (continued)

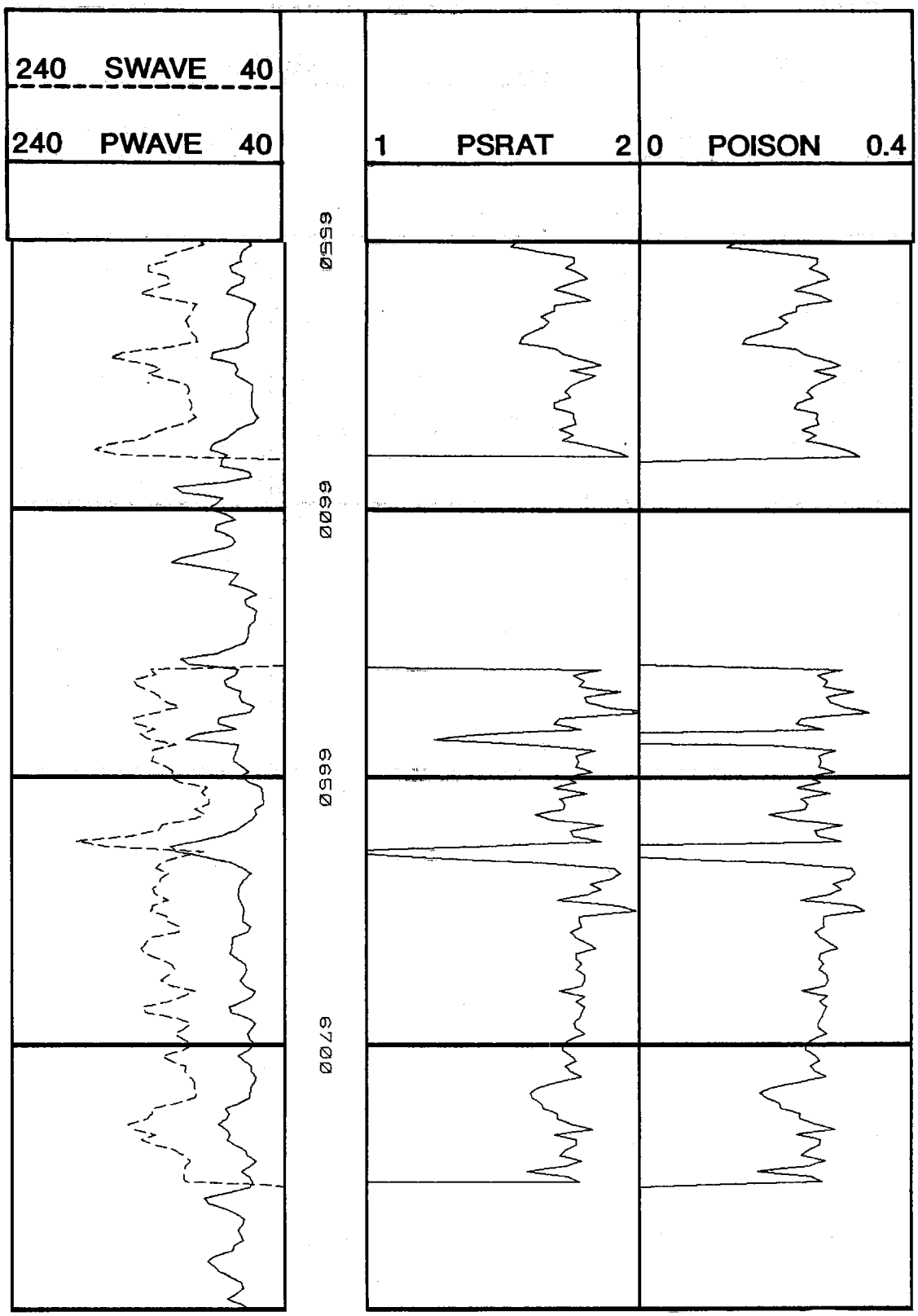

Figure 4.8 Sonic Log, MWX-2

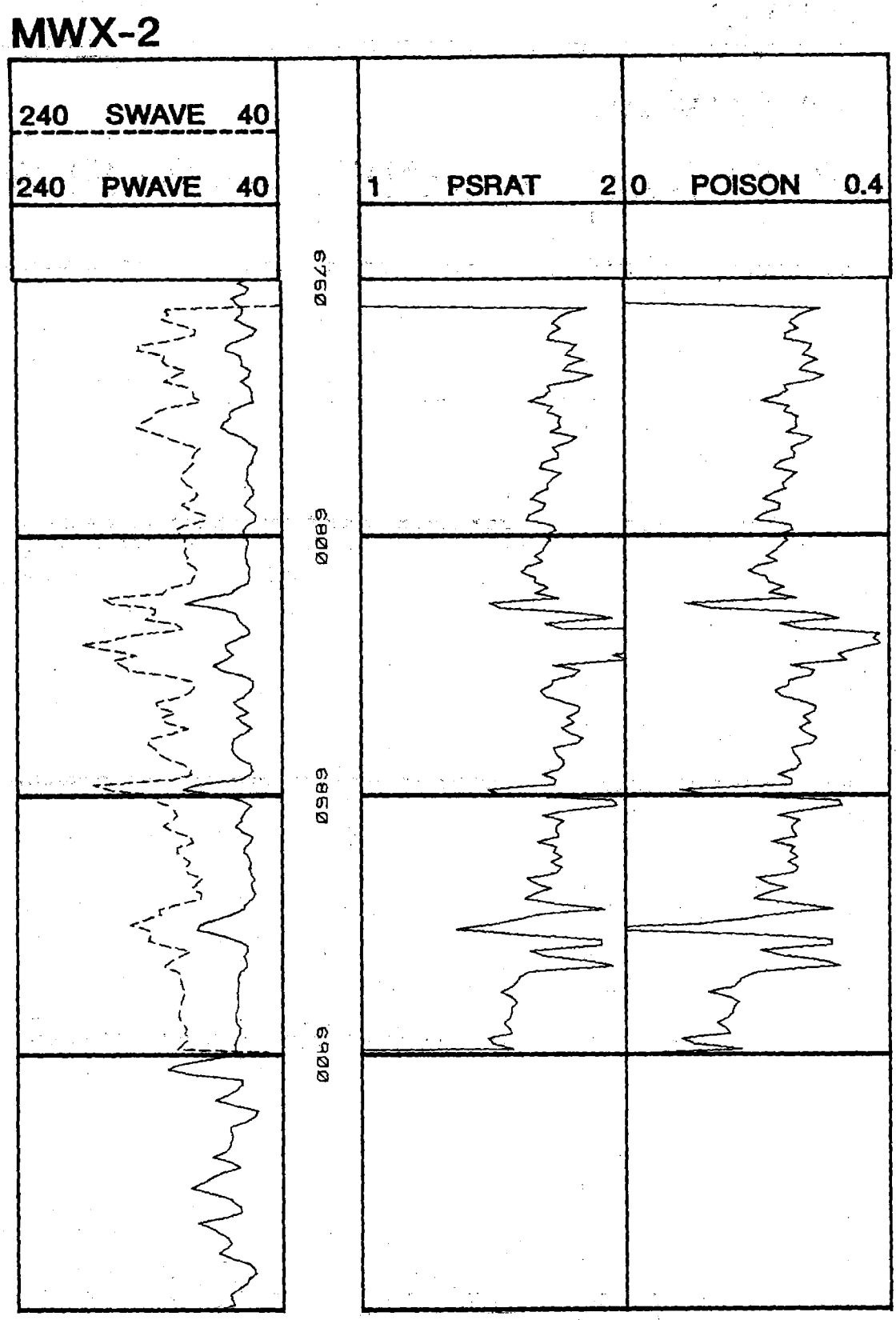

Figure 4.8 Sonic Log, MWX-2 (continued)

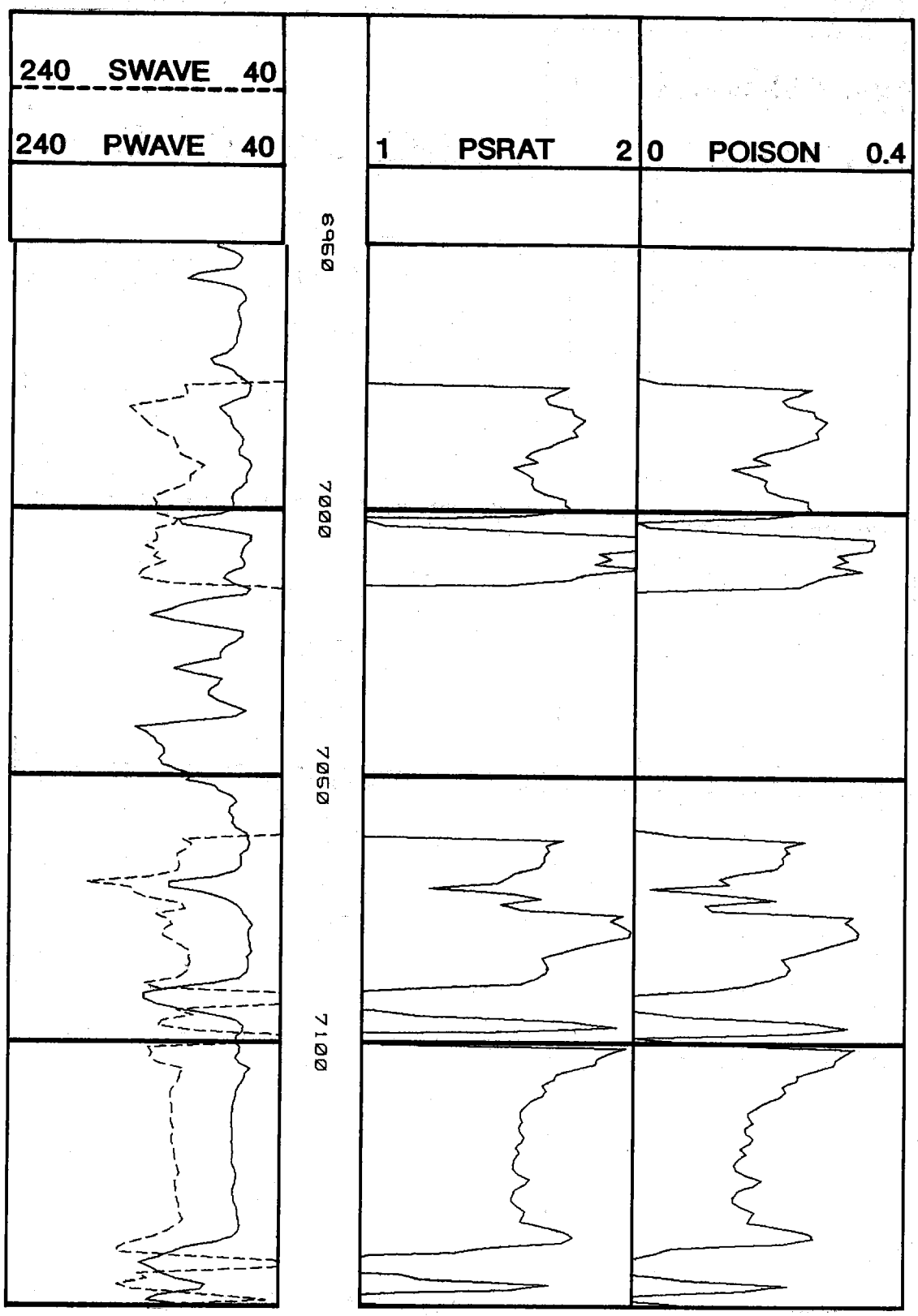

Figure 4.8 Sonic Log, MWX-2 (continued)

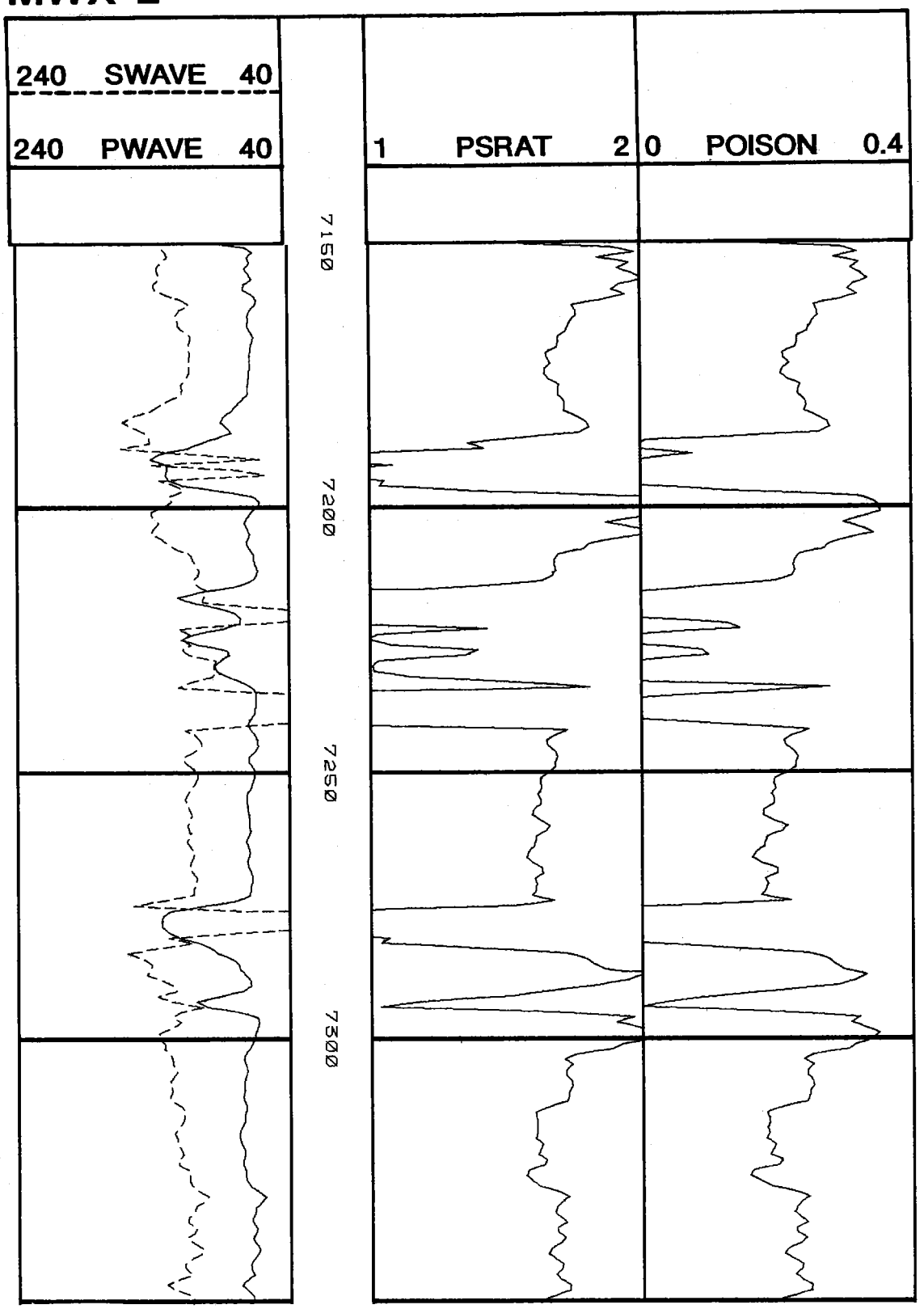

Figure 4.8 Sonic Log, MWX-2 (continued)

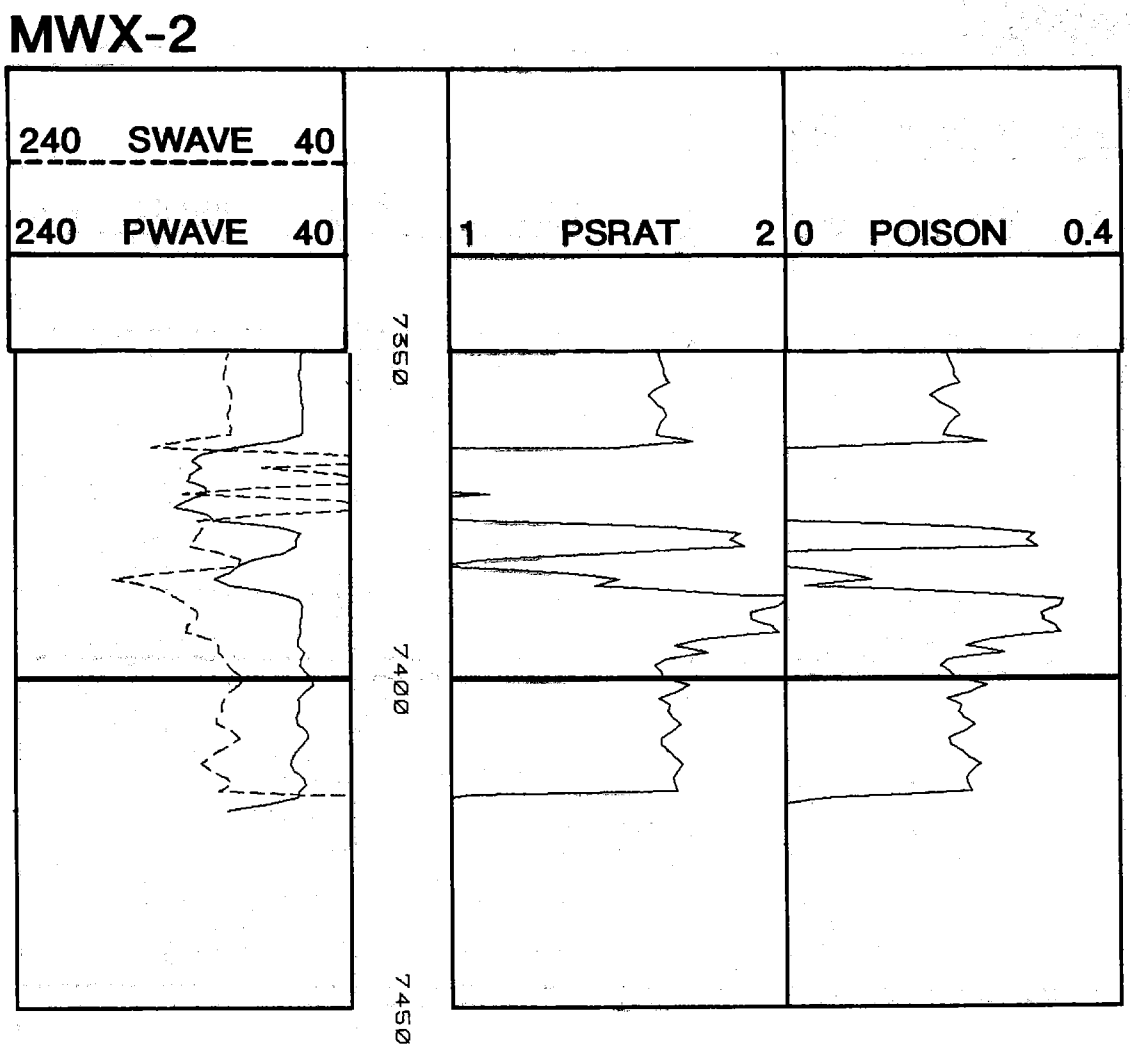

Figure 4.8 Sonic Log, MWX-2 (continued)

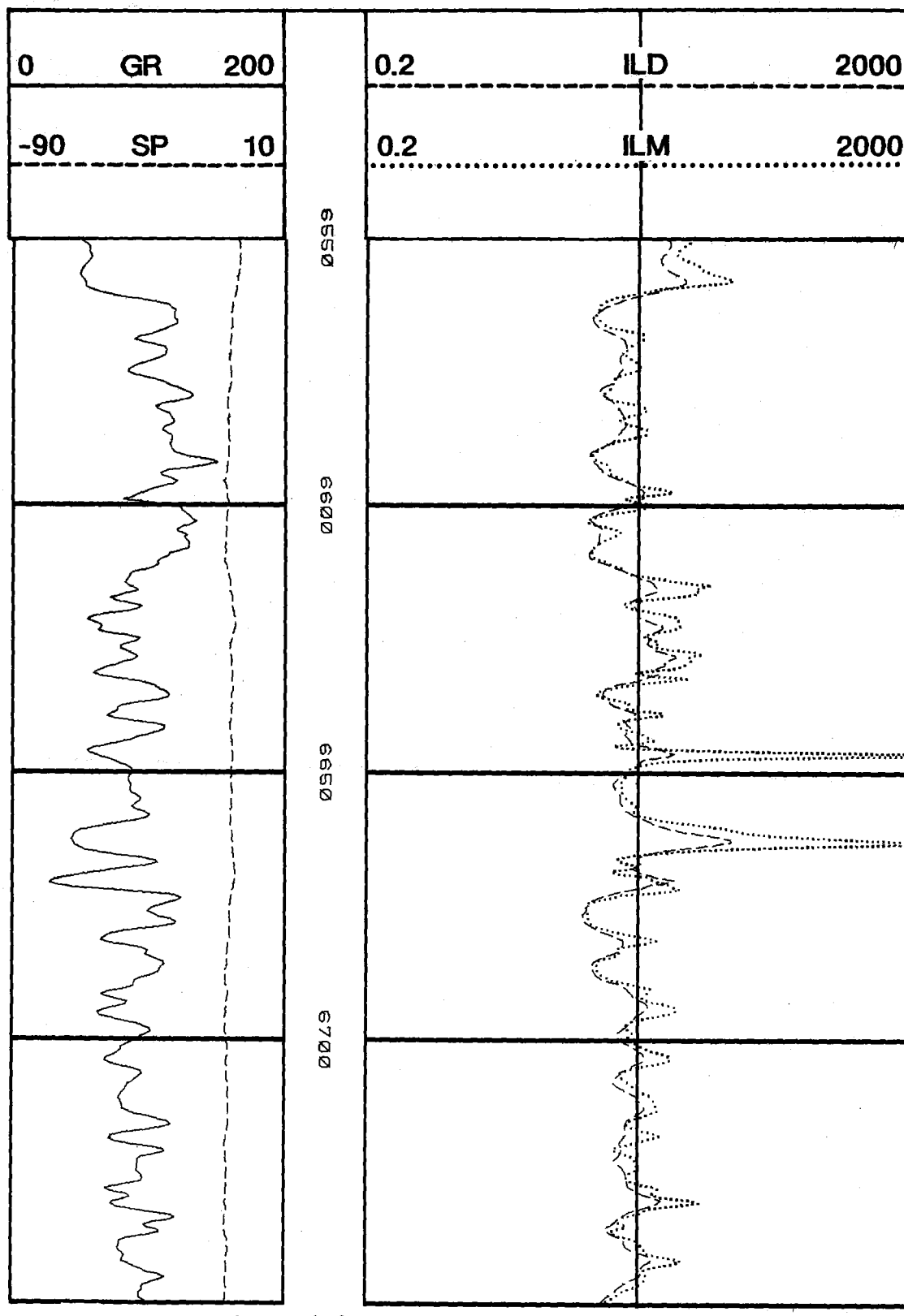

Figure 4.9 Resistivity Log, MWX-3

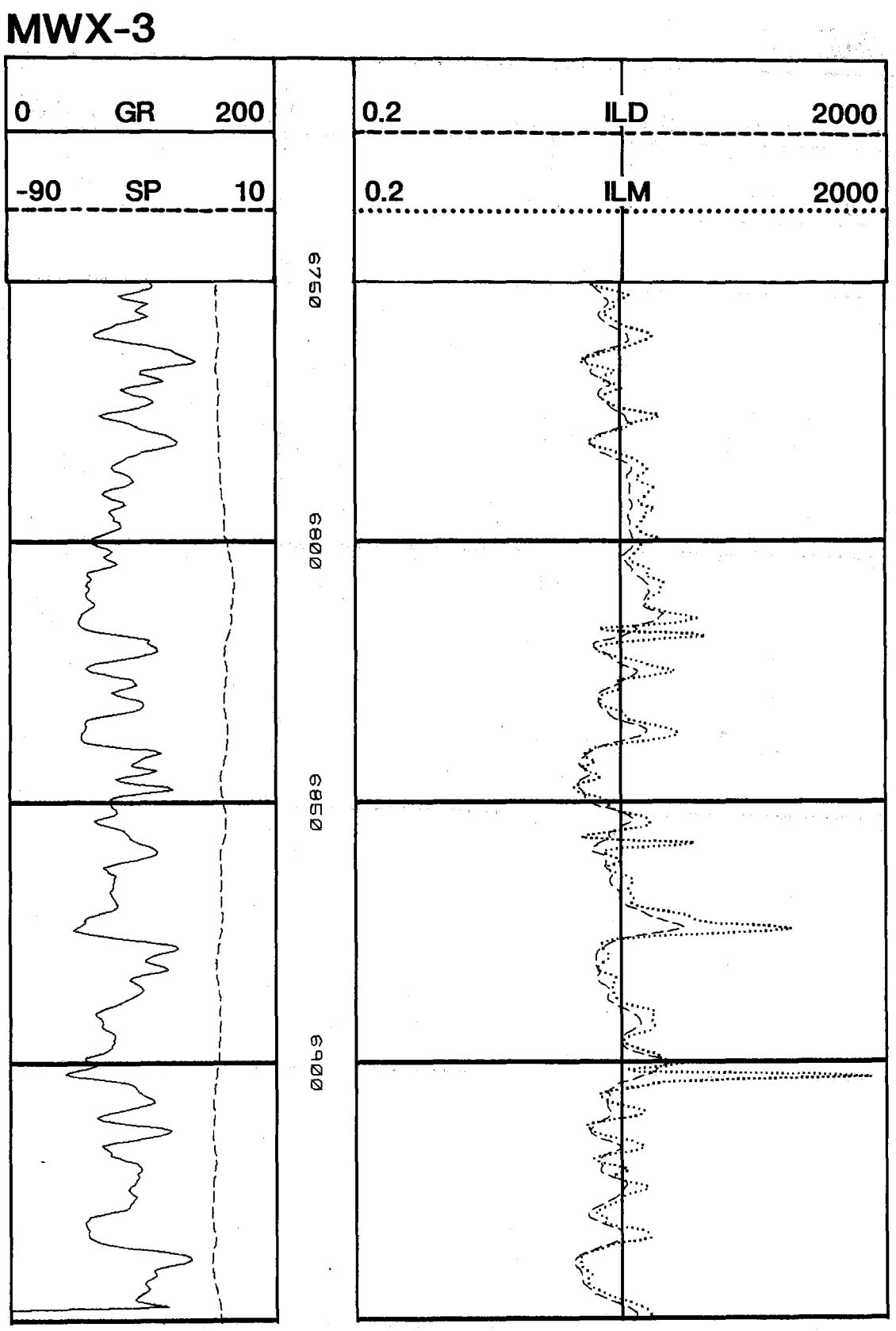

Figure 4.9 Resistivity Log, MWX-3 (continued)

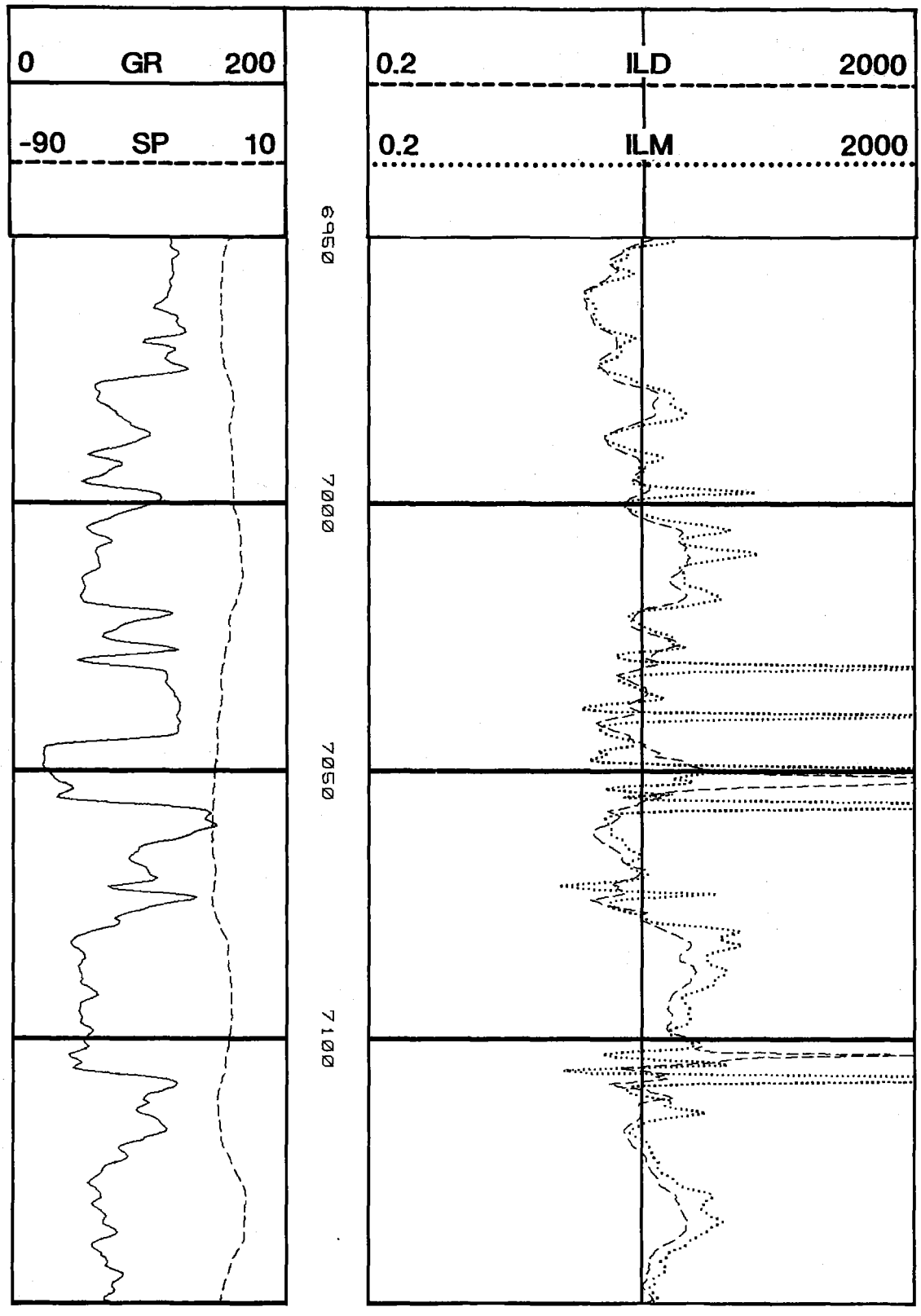

Figure 4.9 Resistivity Log, MWX-3 (continued)

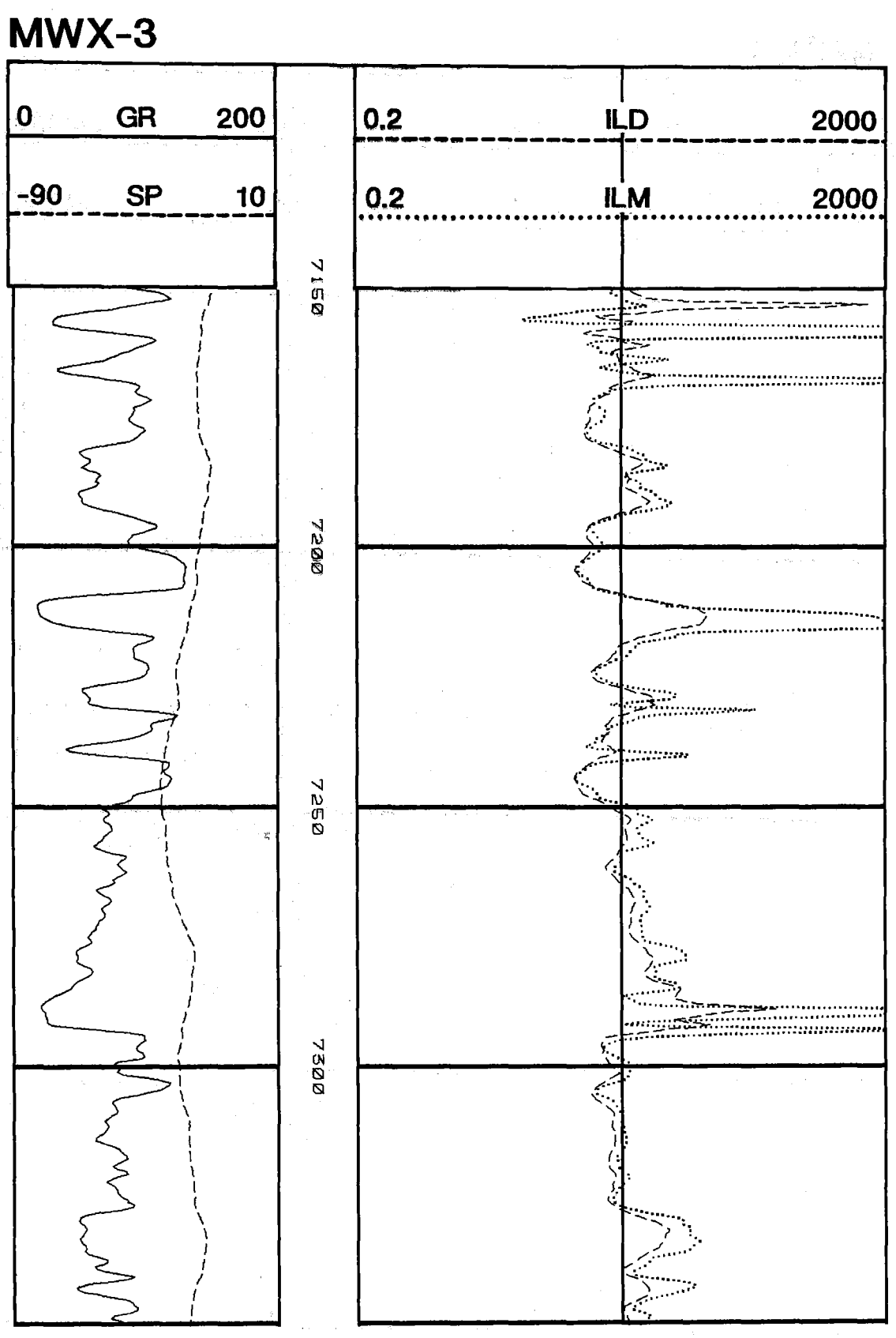

Figure 4.9 Resistivity Log, MWX-3 (continued)

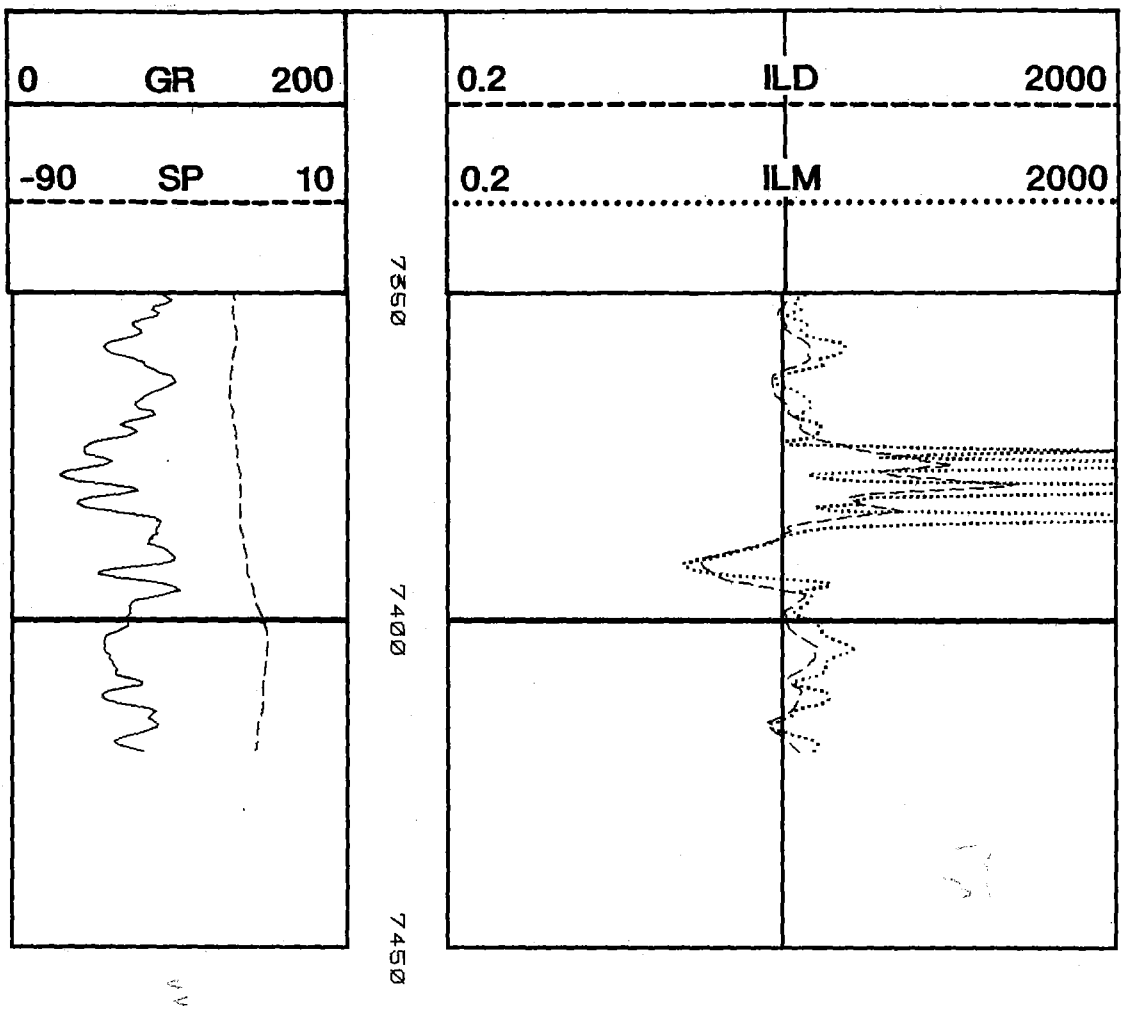

Figure 4.9 Resistivity Log, MWX-3 (continued)

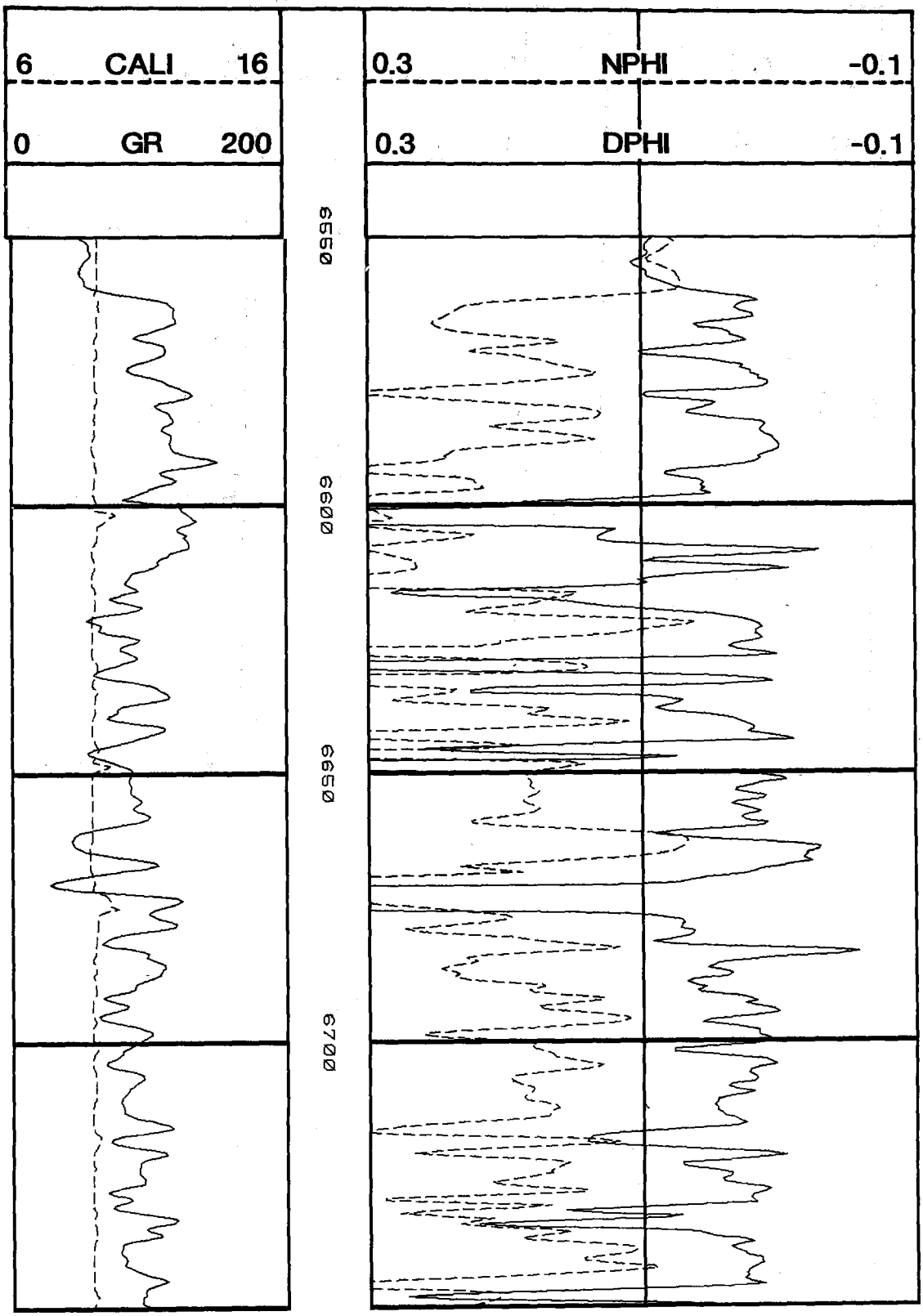

Figure 4.10 Density-Neutron Log, MWX-3

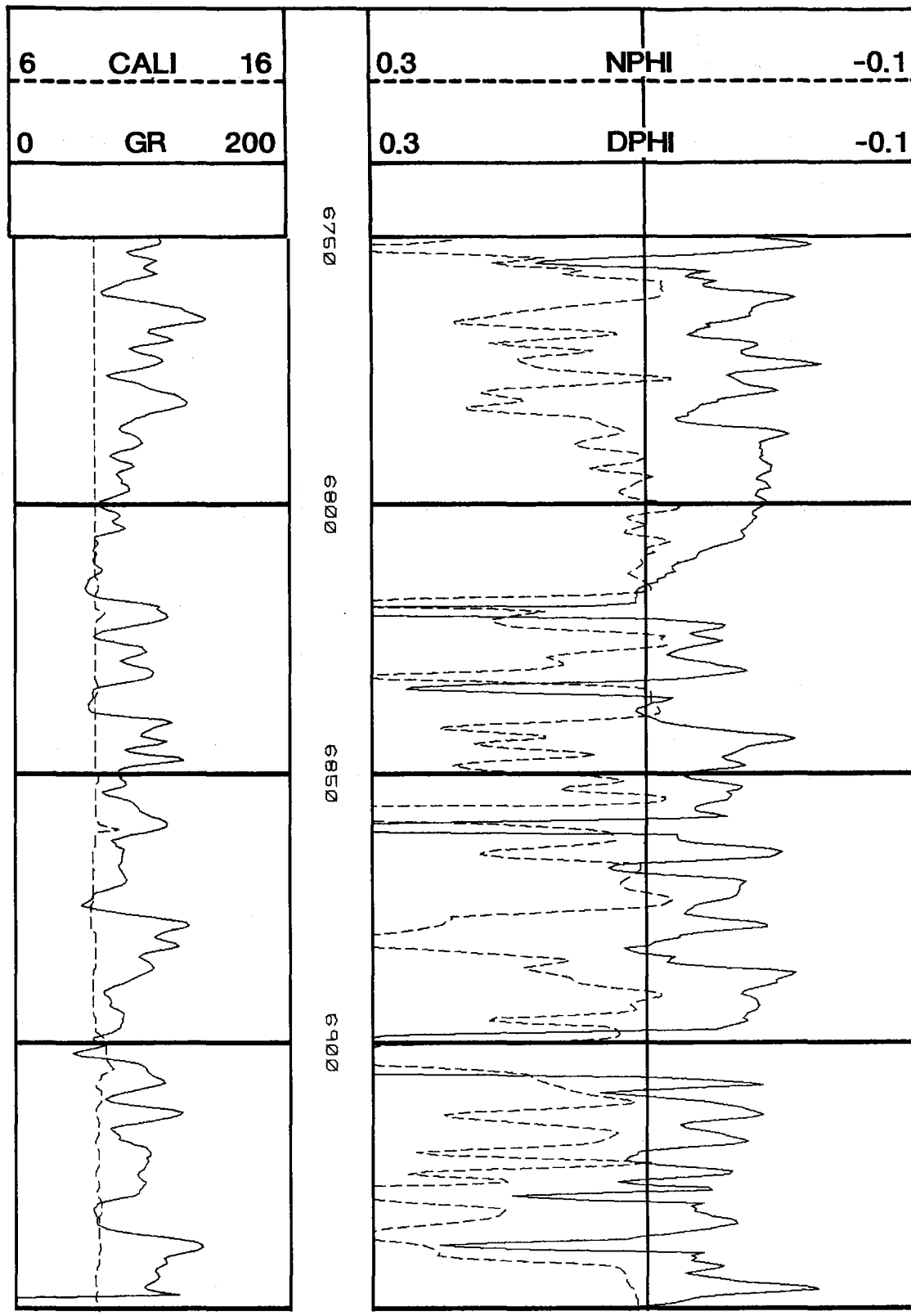

Figure 4.10 Density-Neutron Log, MWX-3 (continued)

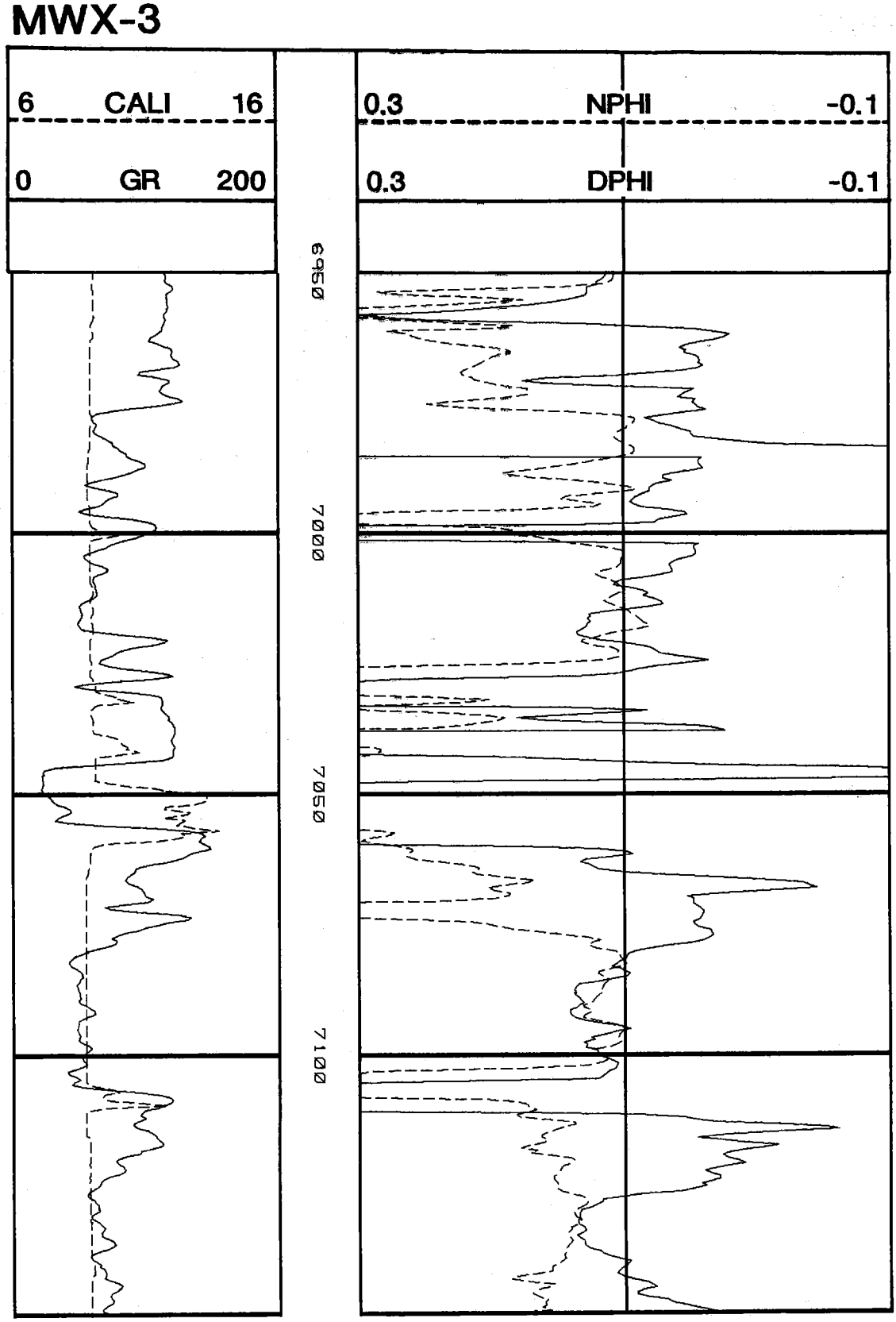

Figure 4.10 Density-Neutron Log, MWX-3 (continued)

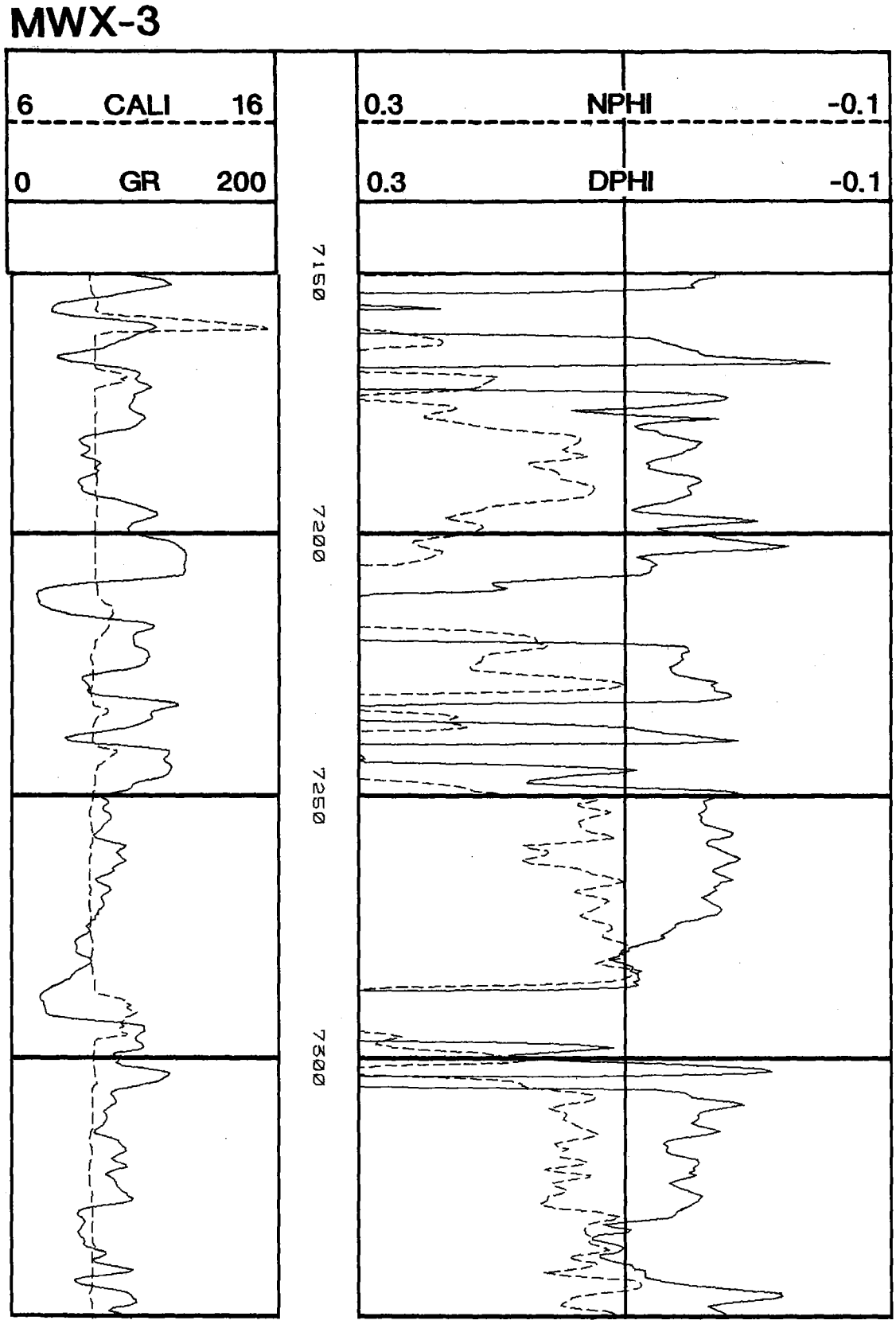

Figure 4.10 Density-Neutron Log, MWX-3 (continued)

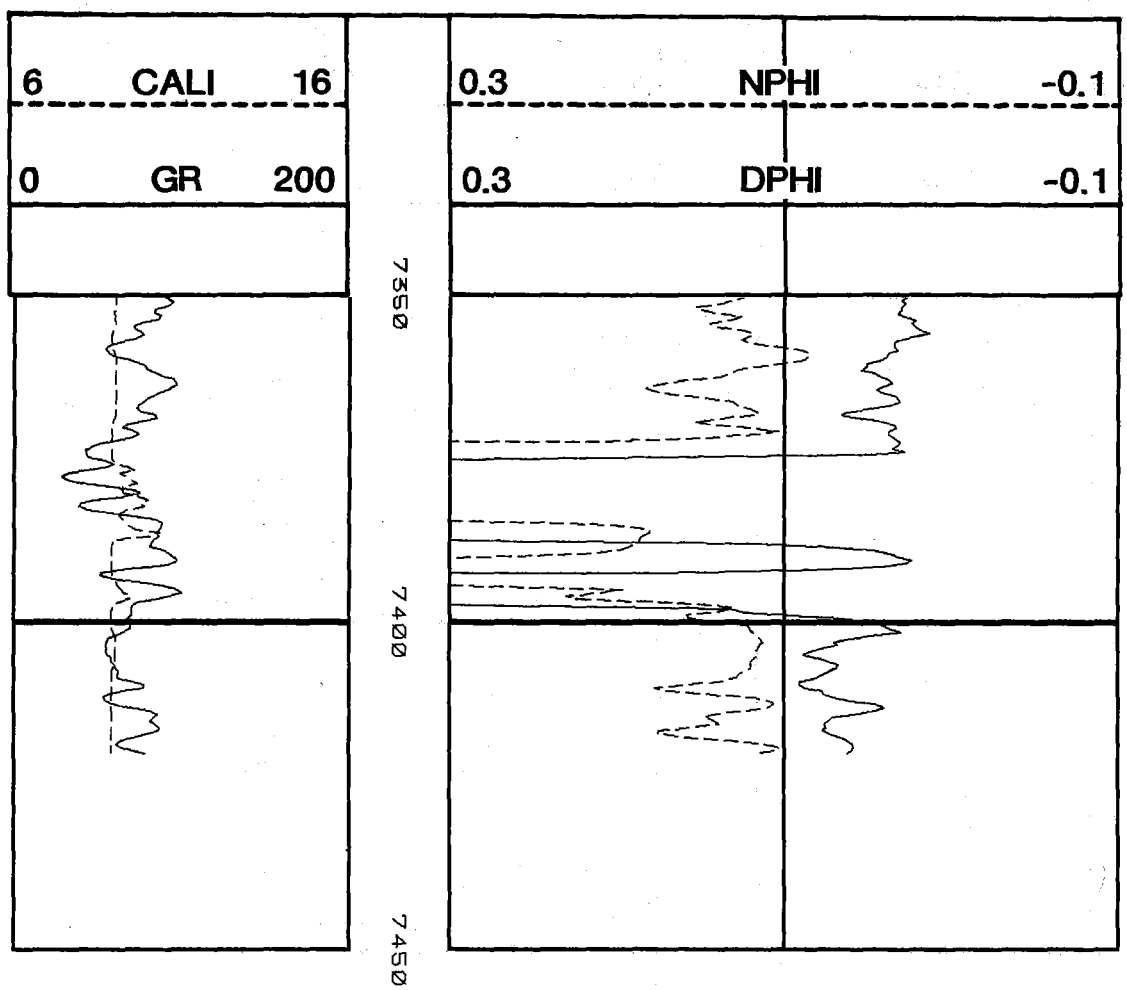

Figure 4.10 Density-Neutron Log, MWX-3 (continued)

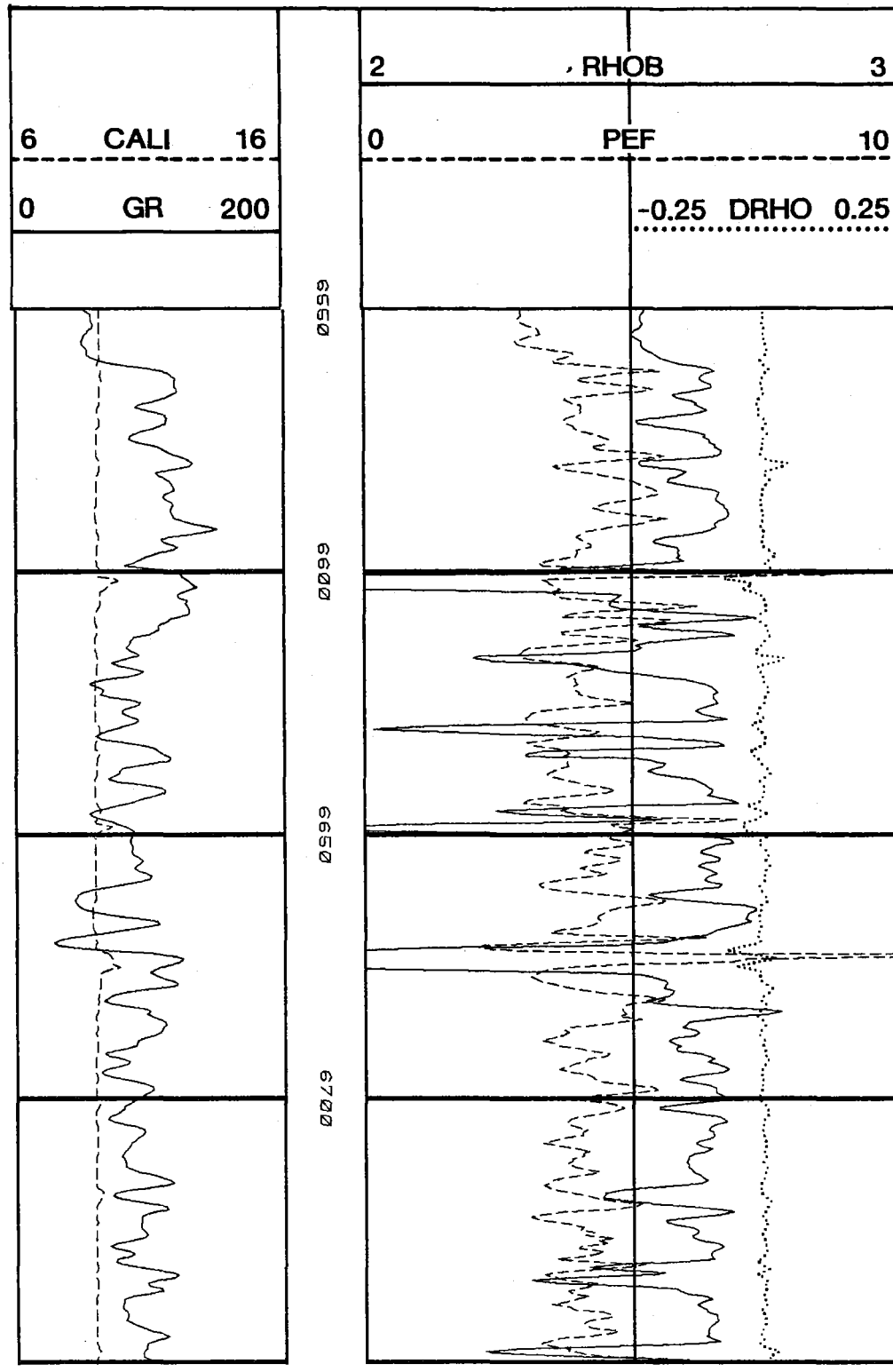

Figure 4.11 Bulk Density Log, MWX-3

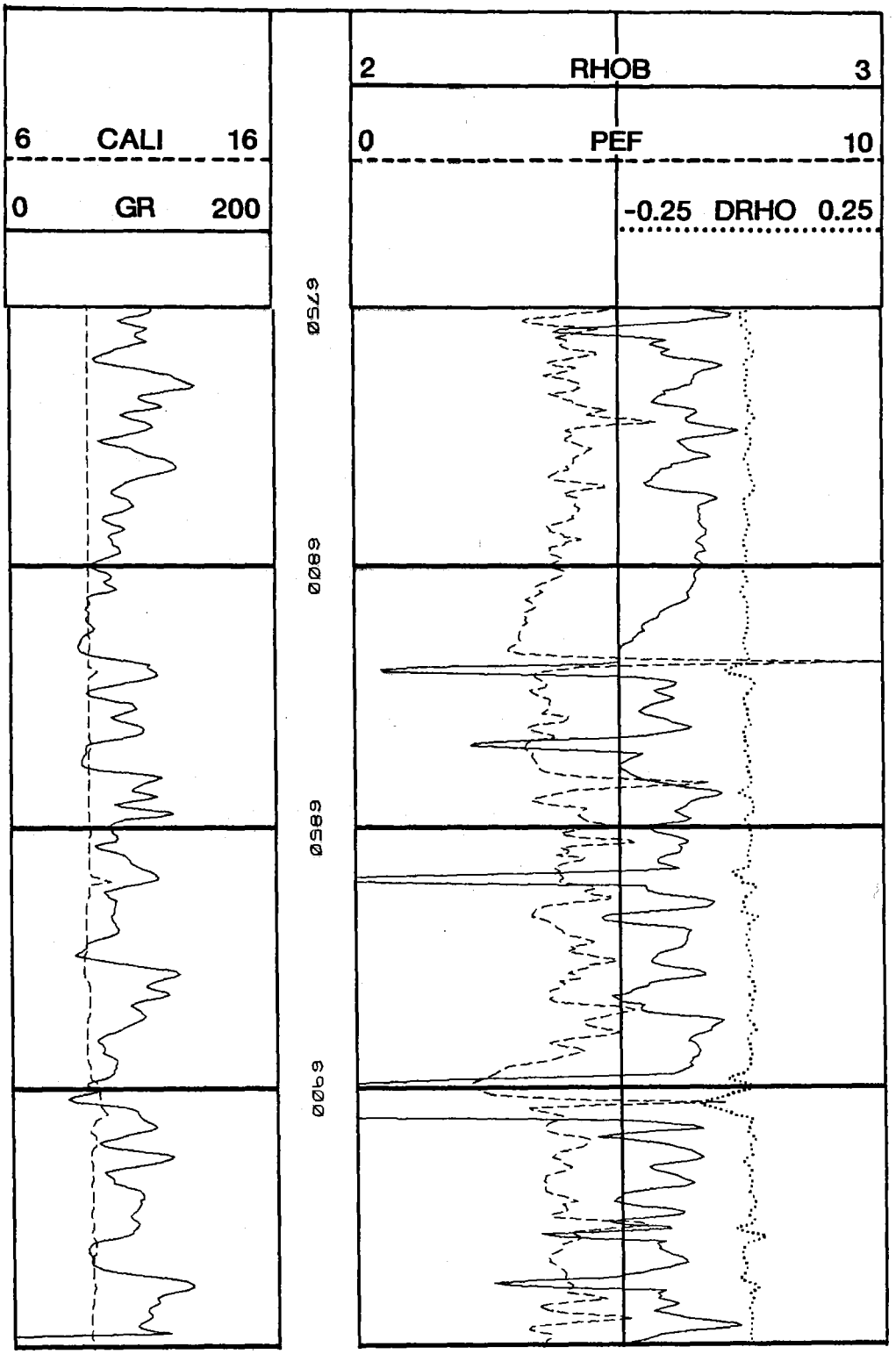

Figure 4.11 Bulk Density Log, MWX-3 (continued)

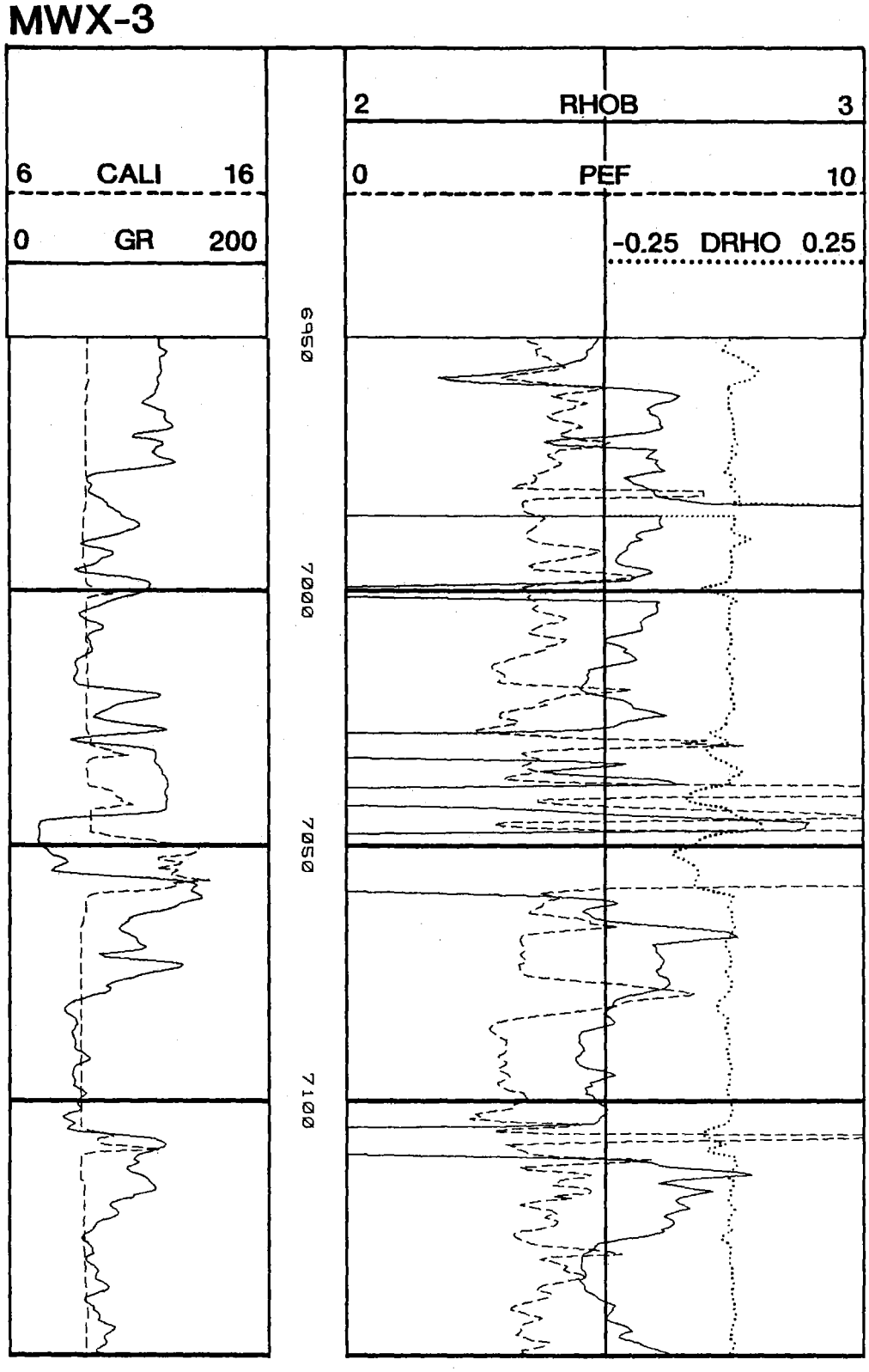

Figure 4.11 Bulk Density Log, MWX-3 (continued)

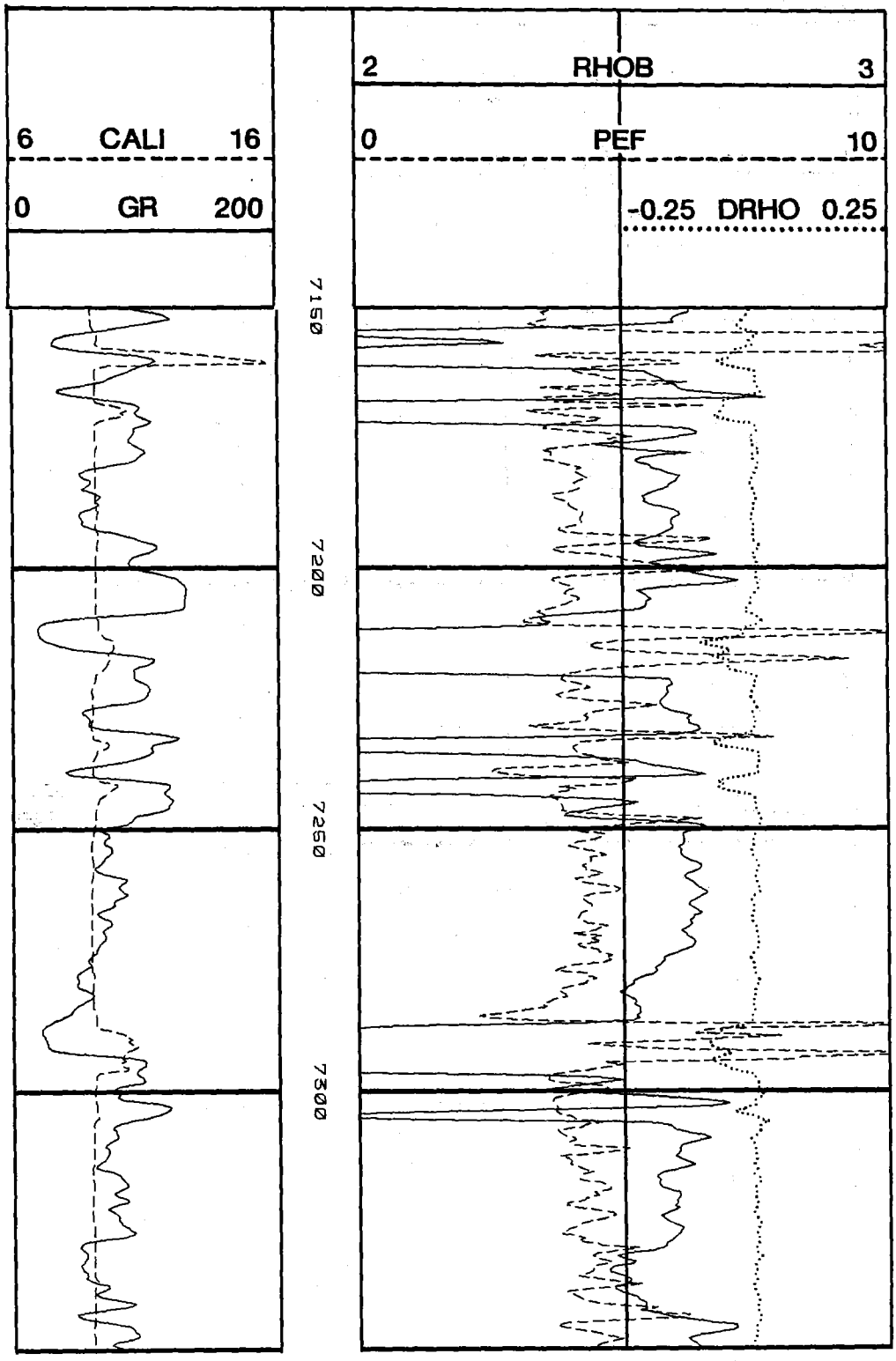

Figure 4.11 Bulk Density Log, MWX-3 (continued)

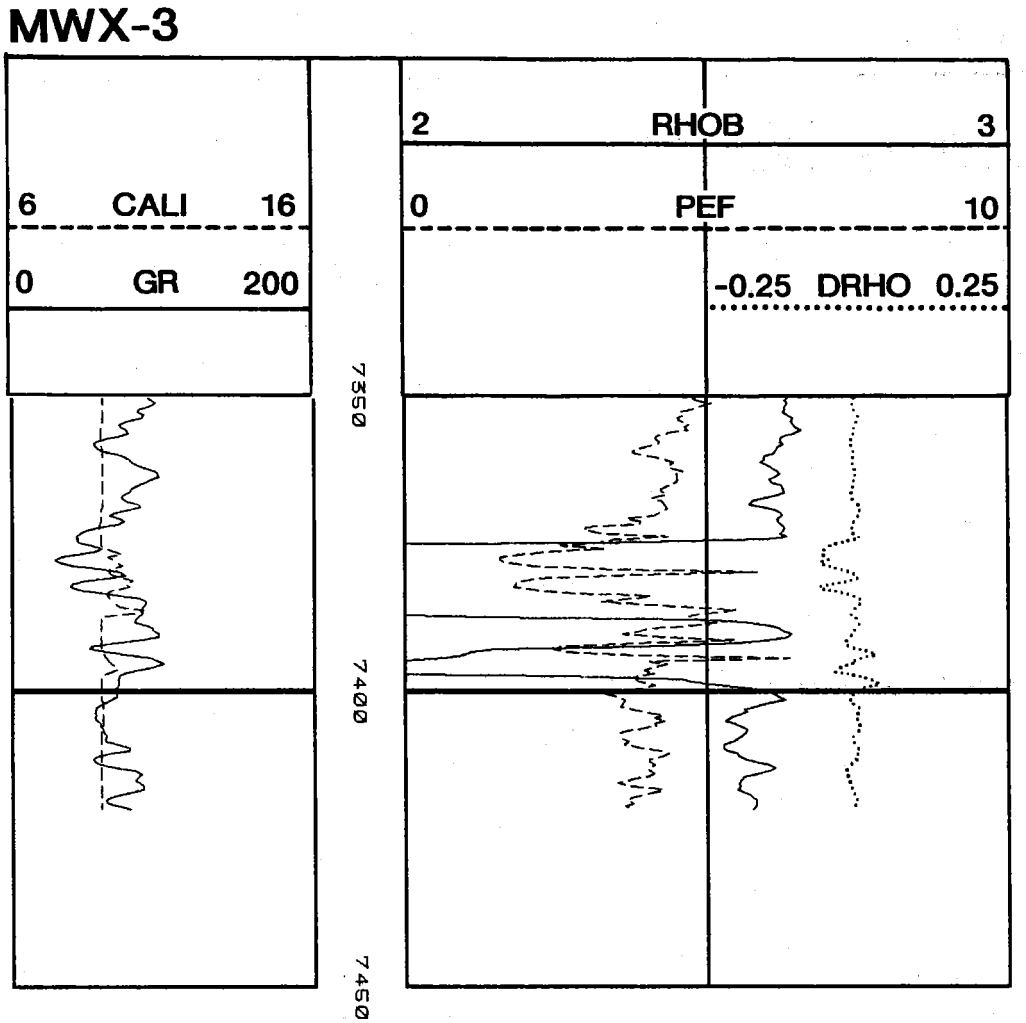

Figure 4.11 Bulk Density Log, MWX-3 (continued)

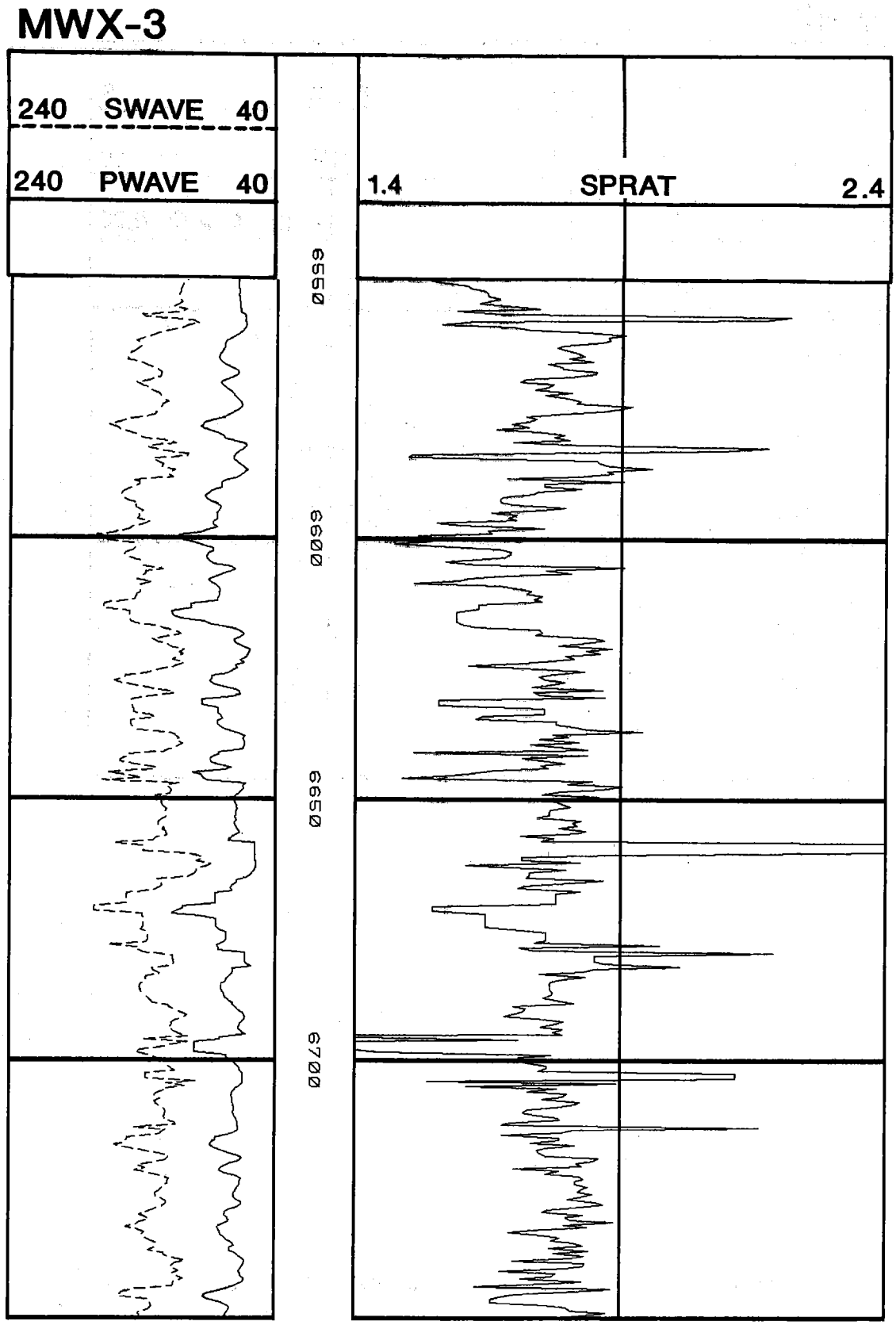

Figure 4.12 Sonic Log, MWX-3

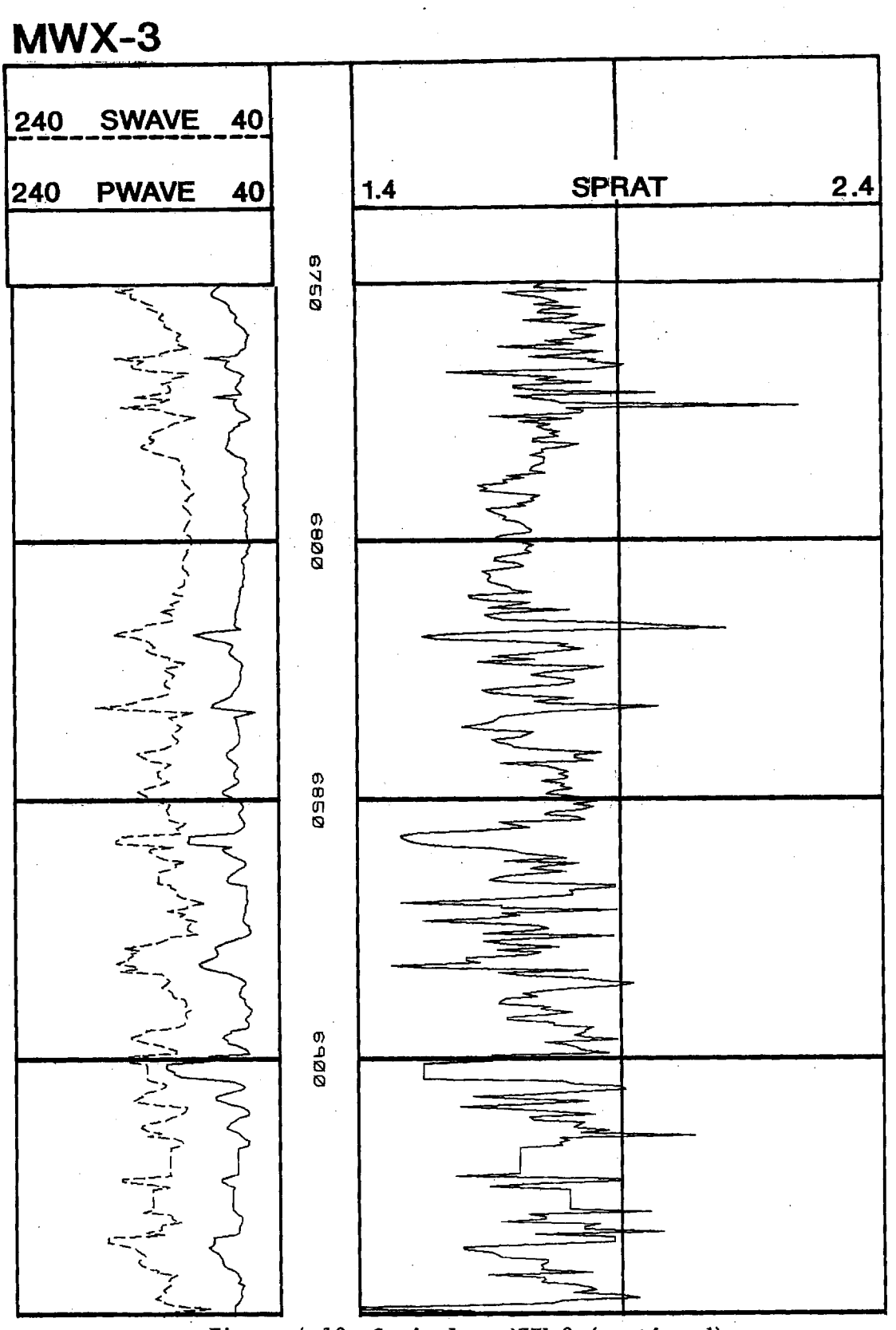

Figure 4.12 Sonic Log, MWX-3 (continued)

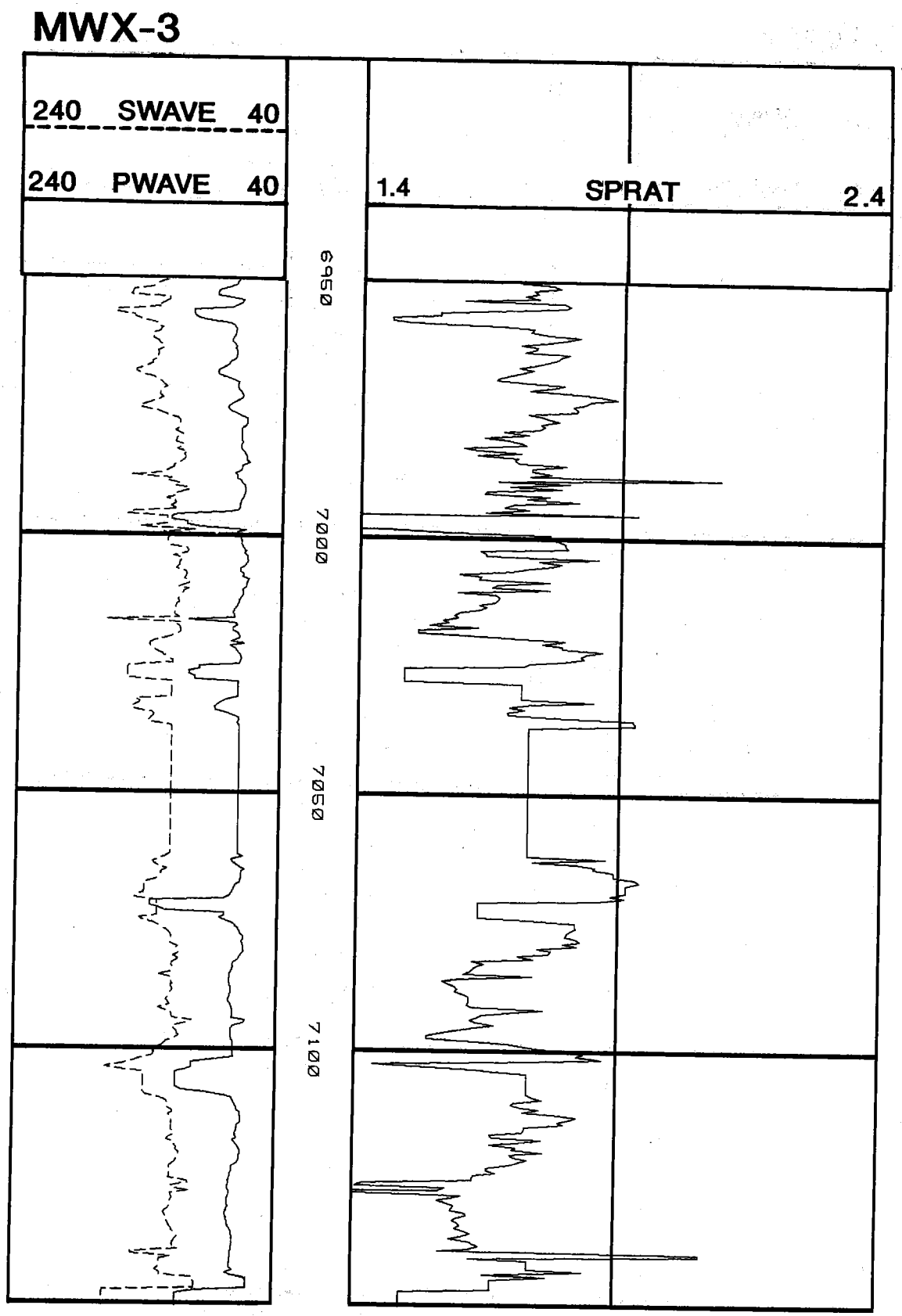

Figure 4.12 Sonic Log, MWX-3 (continued)

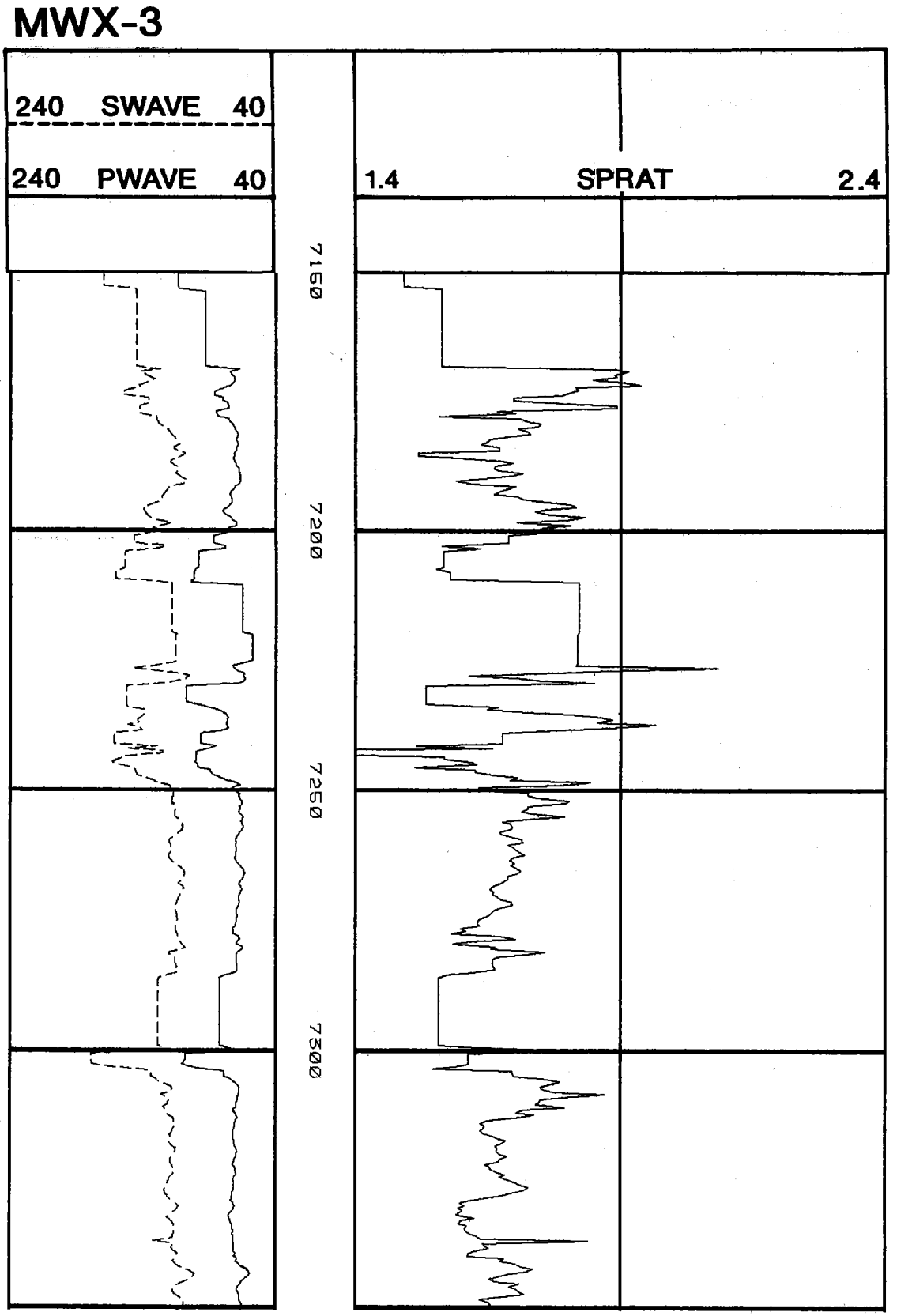

Figure 4.12 Sonic Log, MWX-3 (continued)

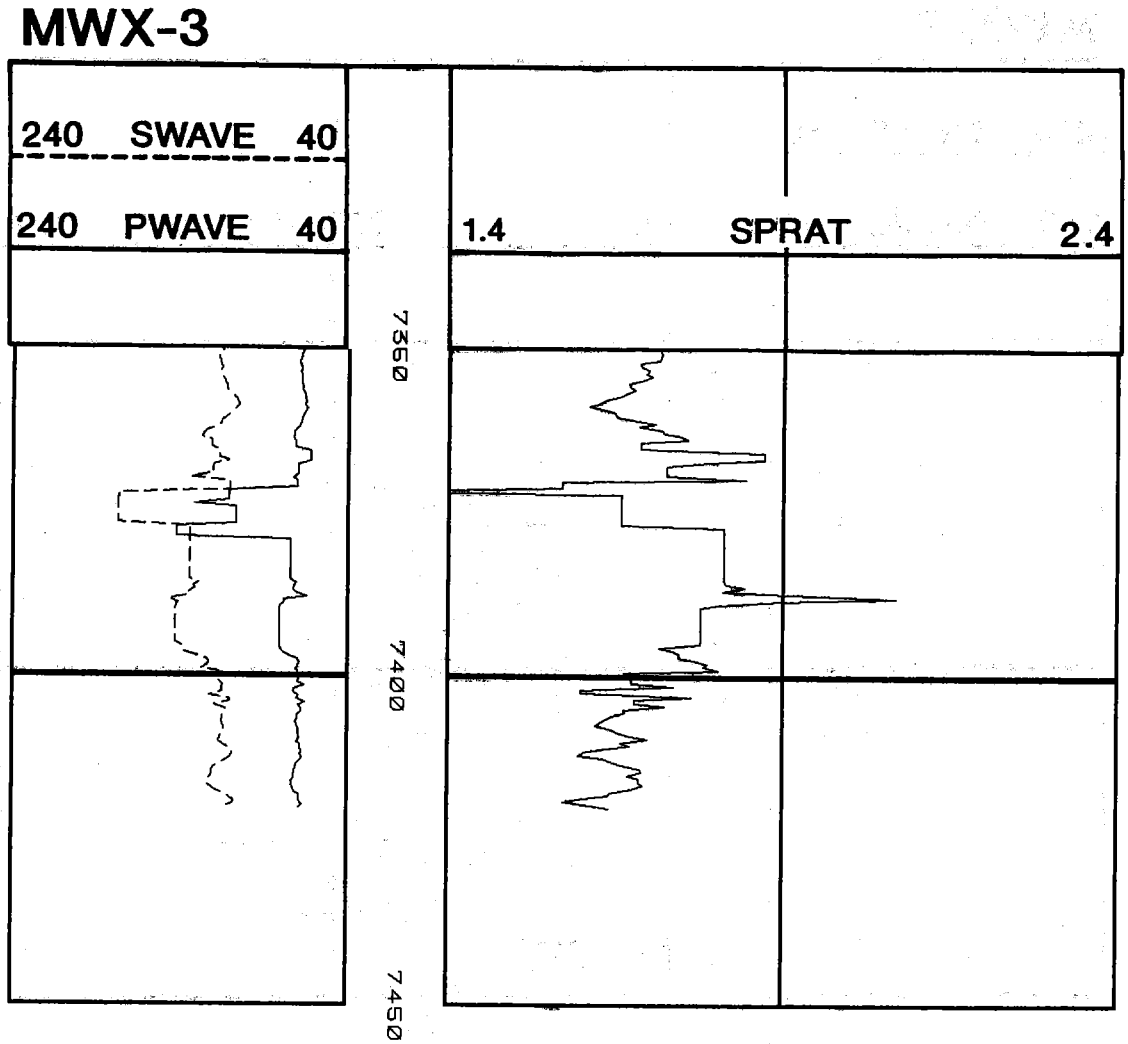

Figure 4.12 Sonic Log, MWX-3 (continued)

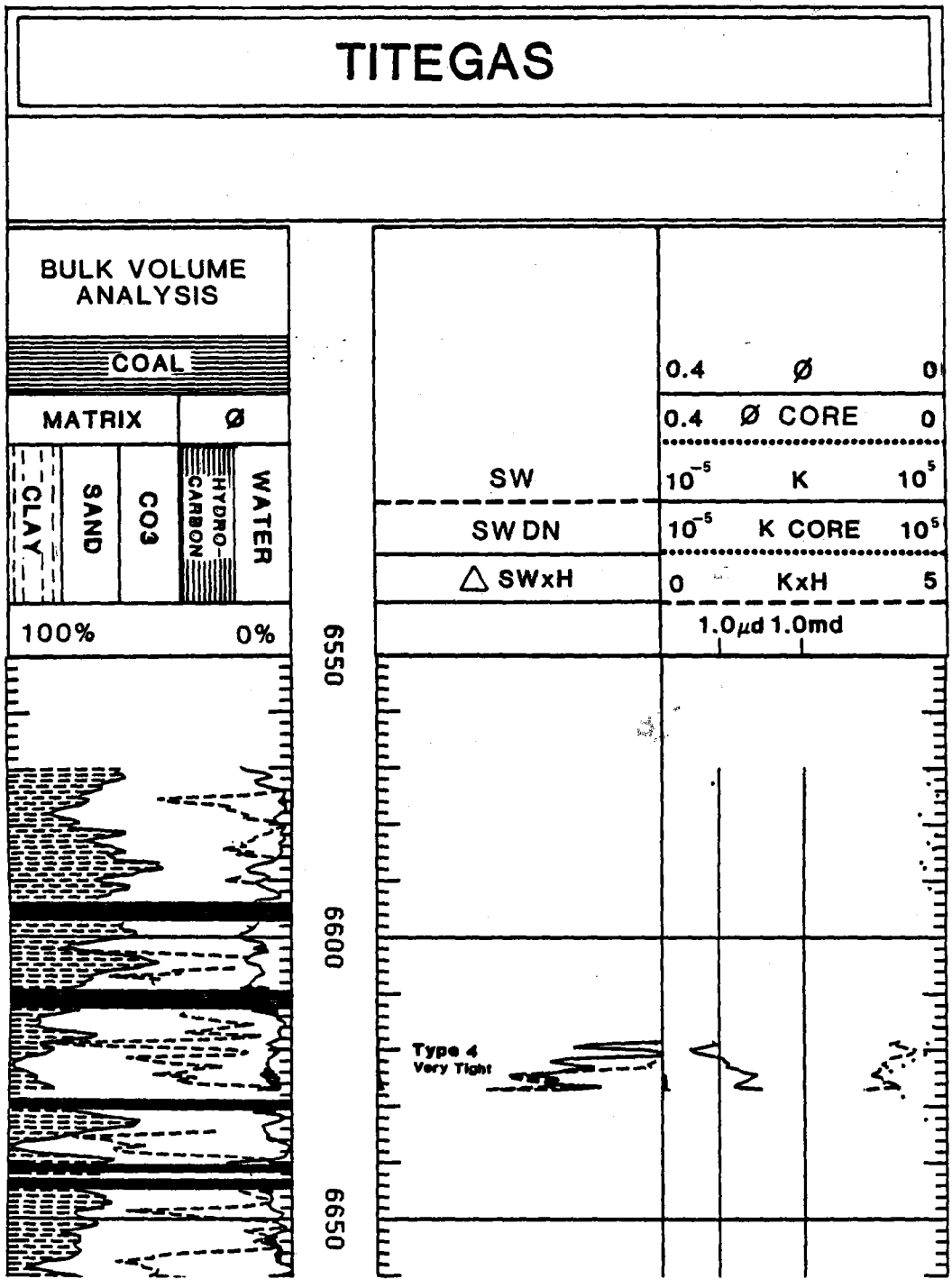

Figure 4.13 TITEGAS Computed Log, MWX-1

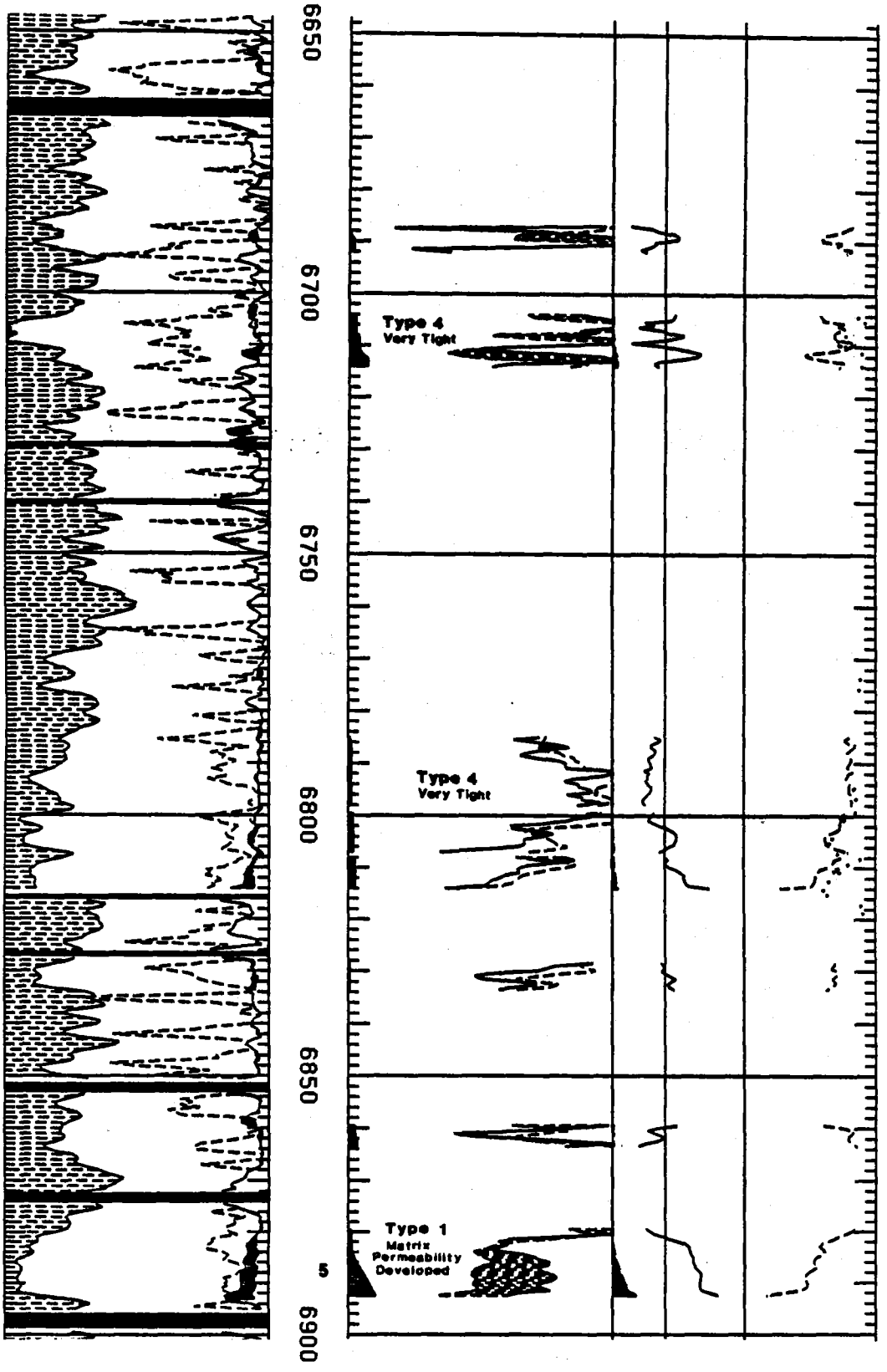

Figure 4.13 TITEGAS Computed Log, MWX-1 (continued)

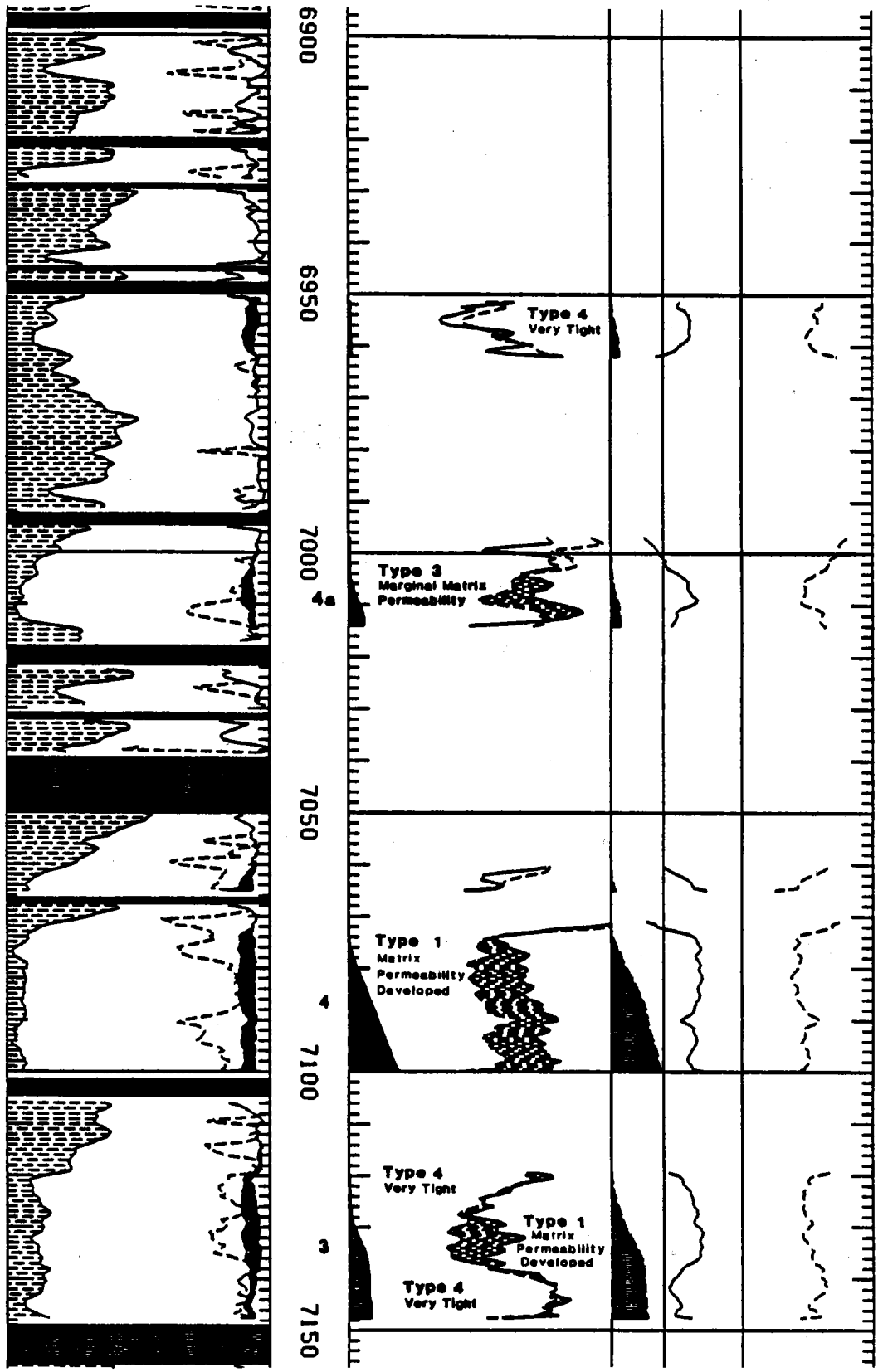

Figure 4.13 TITEGAS Computed Log, MWX-1 (continued)

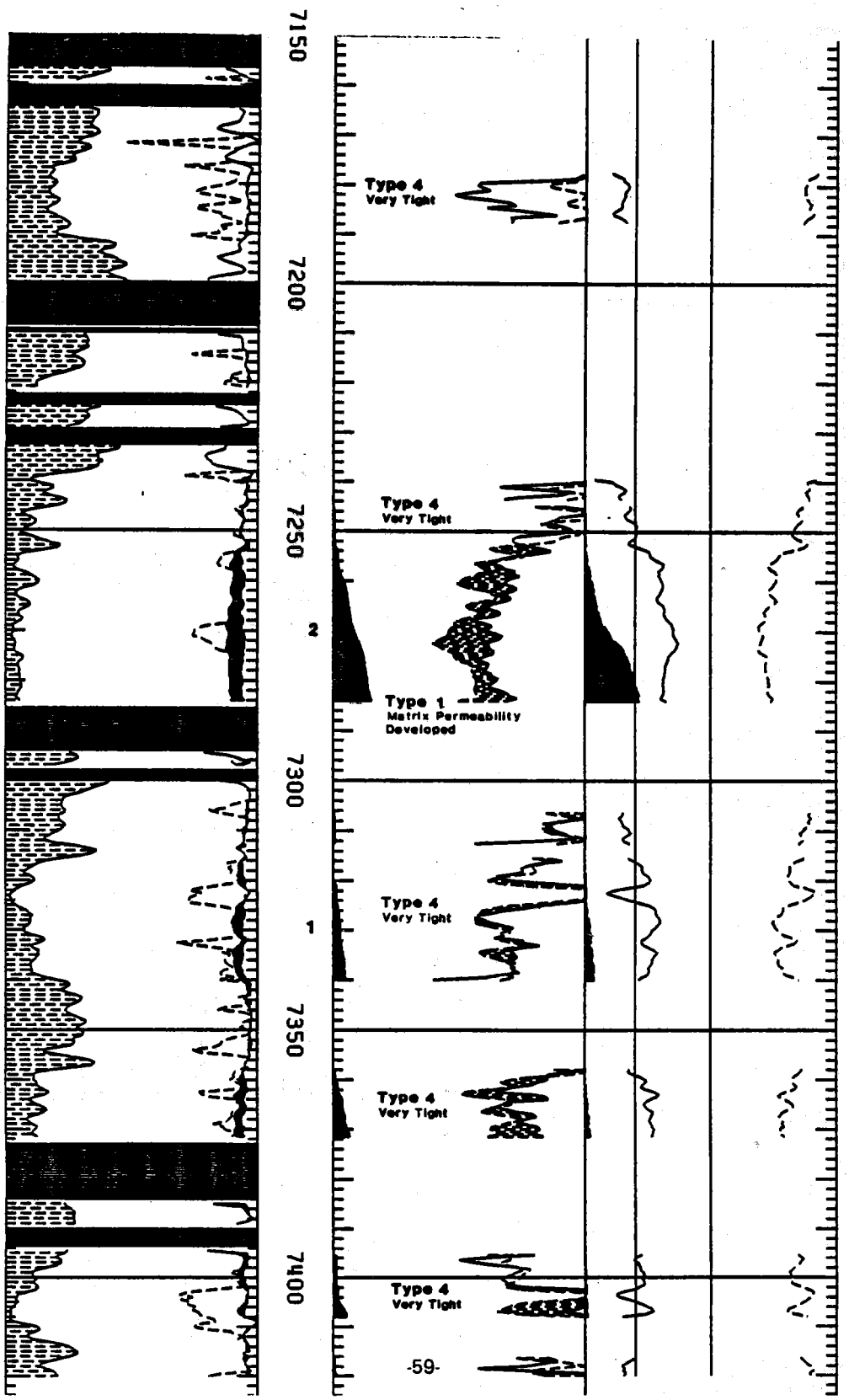

Figure 4.13 TITEGAS Computed Log, MWX-1 (continued)

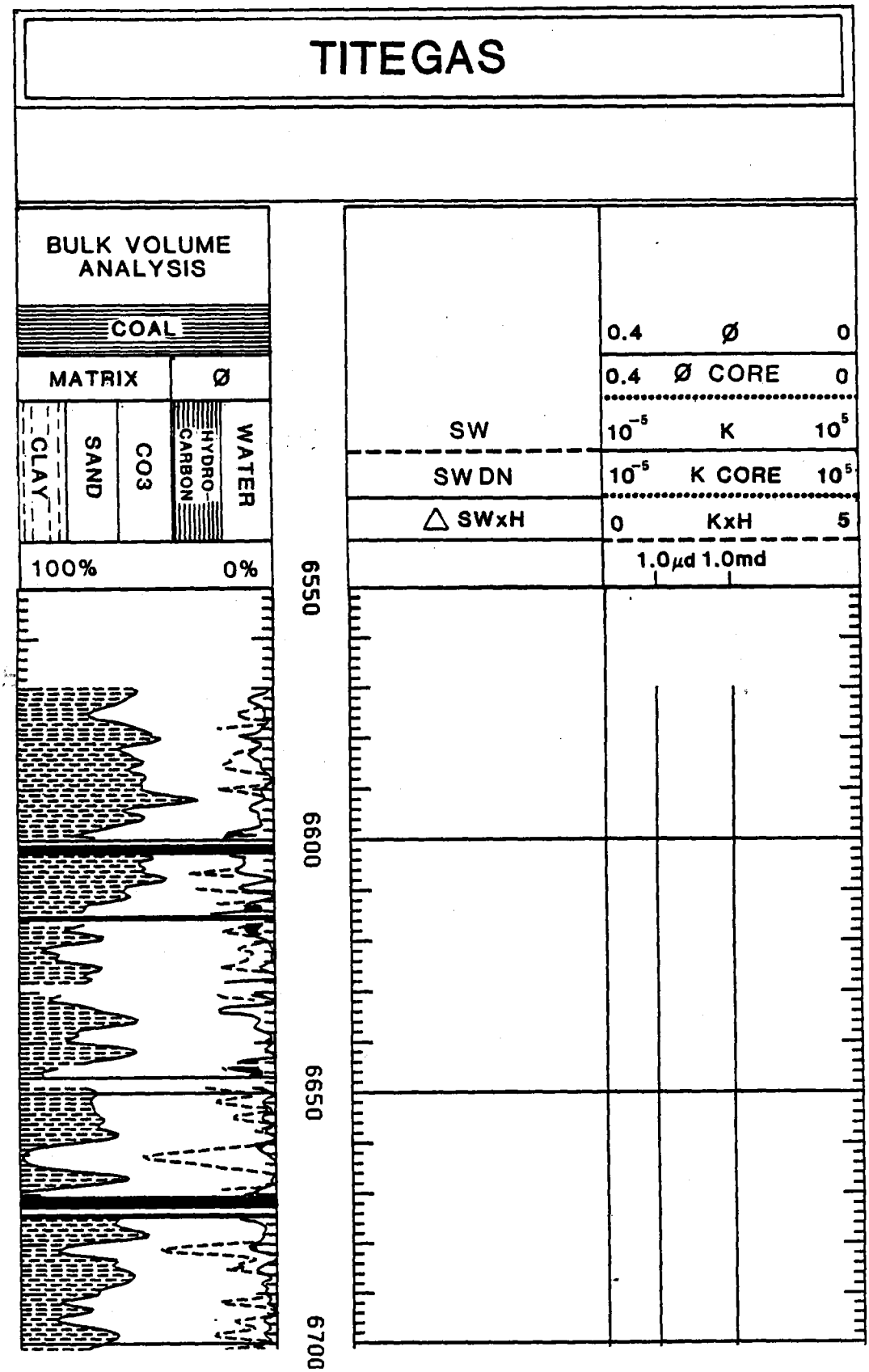

Figure 4.14 TITEGAS Computer Log, MWX-2

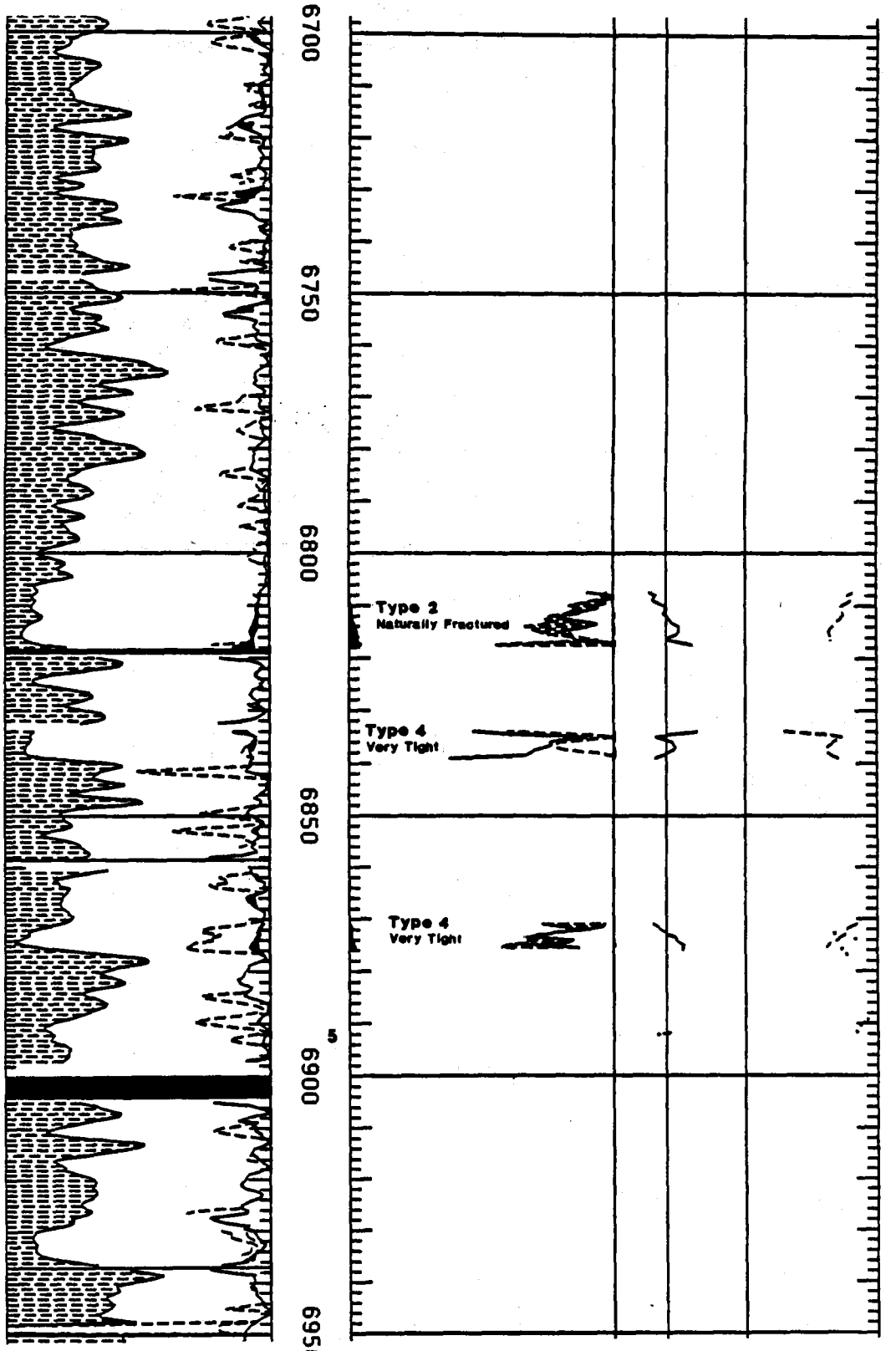

Figure 4.14 TITEGAS Computed Log, MWX-2 (continued)

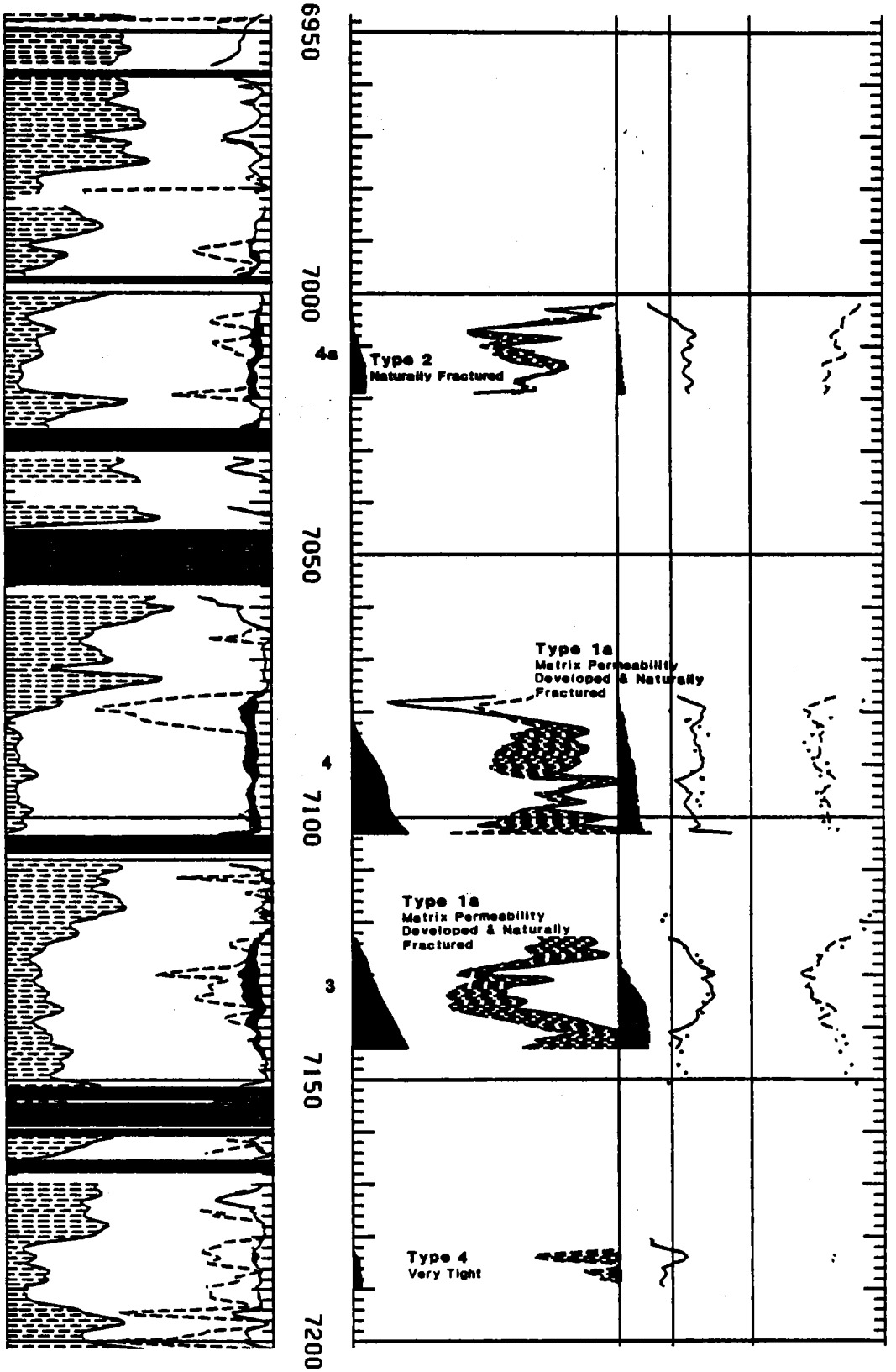

Figure 4.14 TITEGAS Computed Log, MWX-2 (continued)

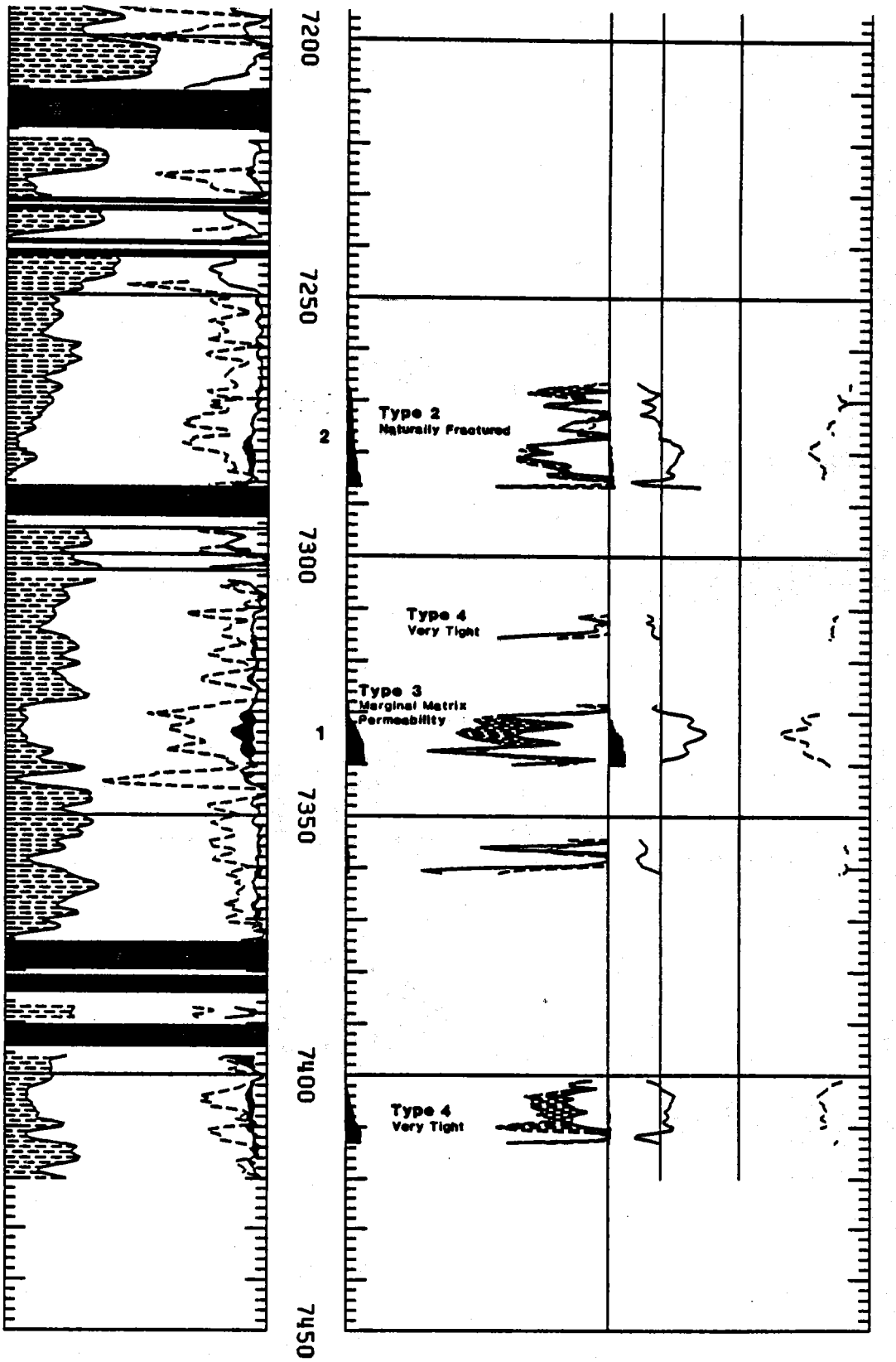

Figure 4.14 TITEGAS Computed Log, MWX-2 (continued)

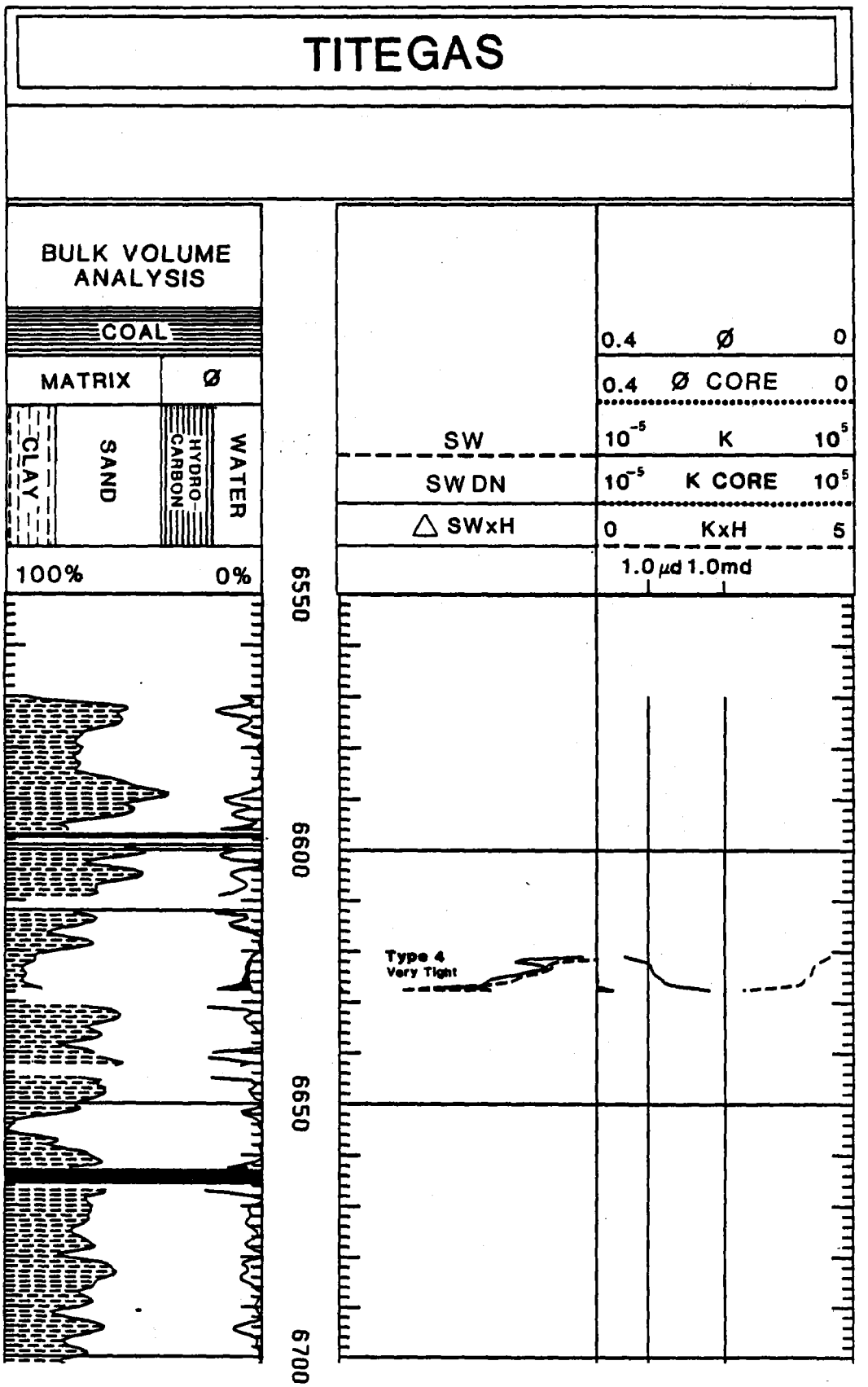

Figure 4.15 TITEGAS Computer Log, MWX-3

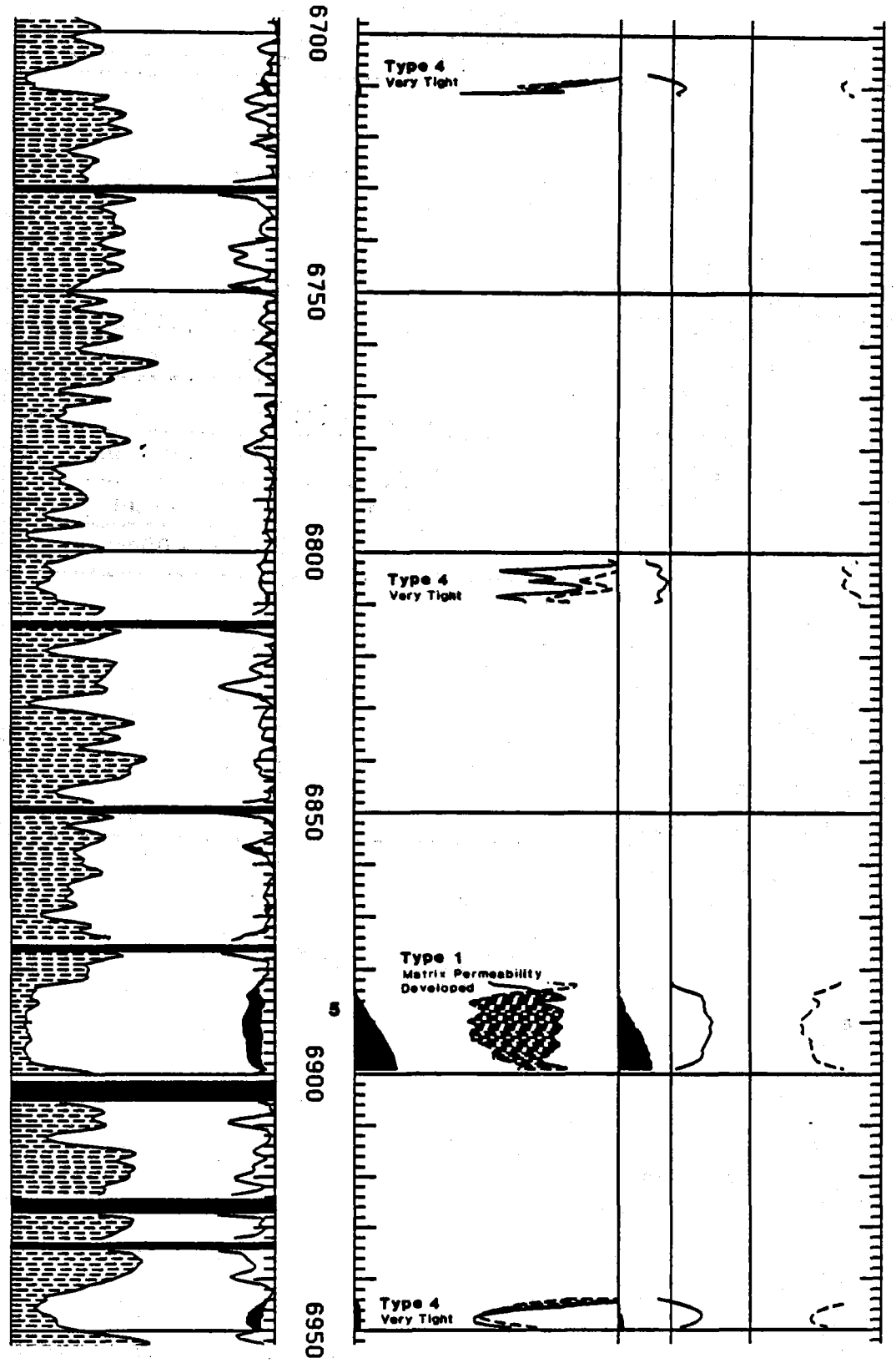

Figure 4.15 TITEGAS Computed Log, MWX-3 (continued)

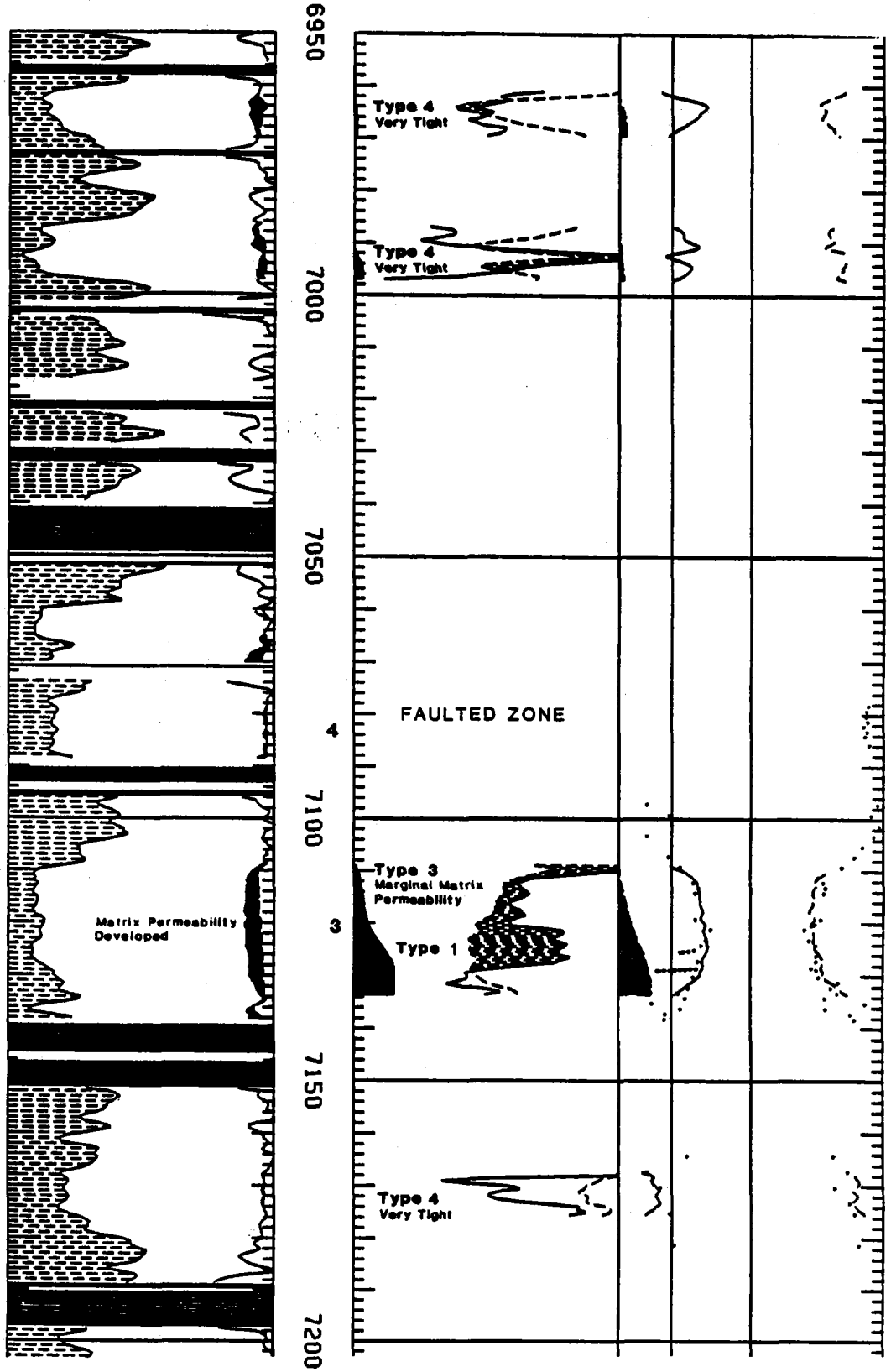

Figure 4.15 TITEGAS Computed Log, MWX-3 (continued)

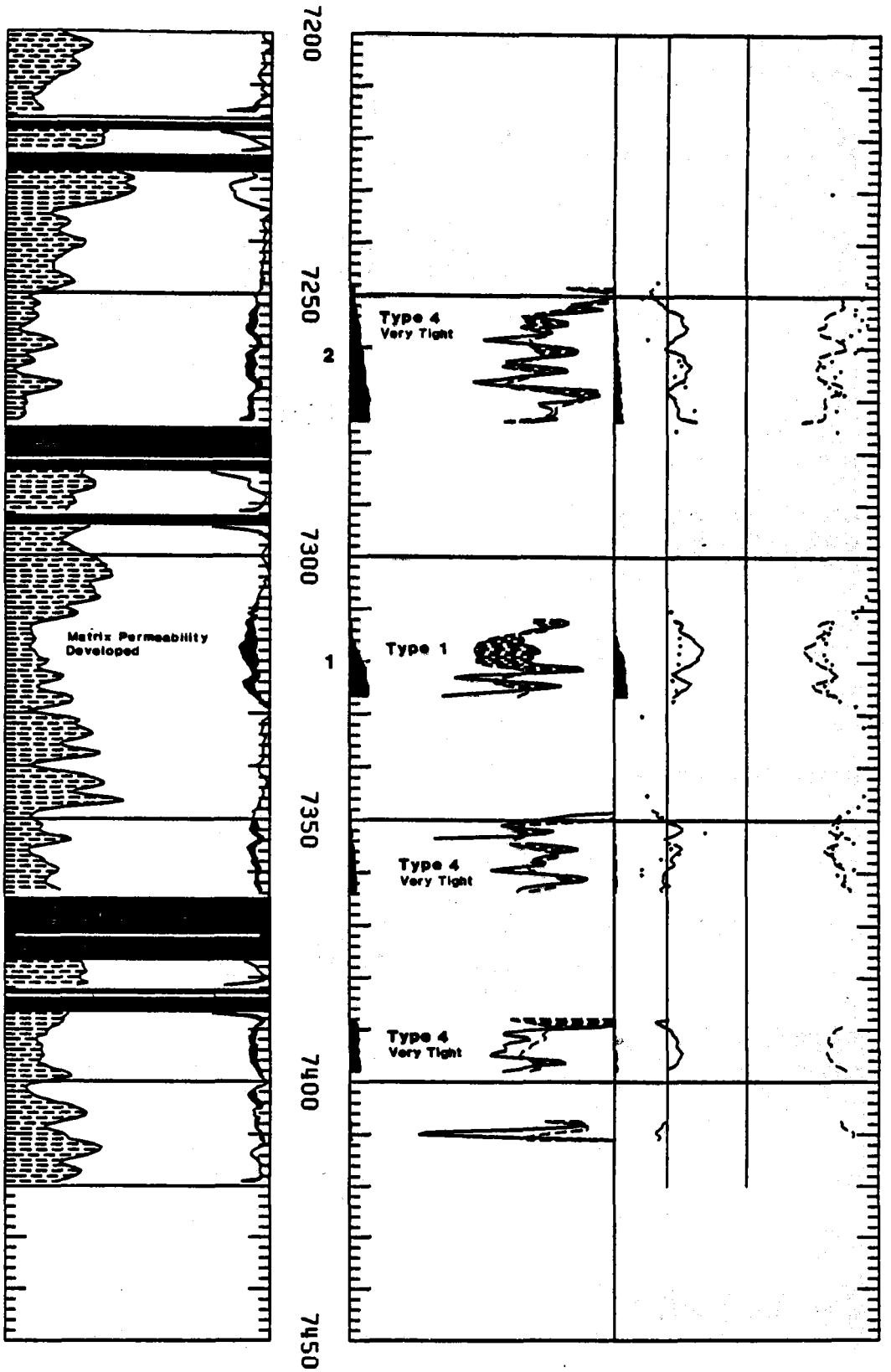

Figure 4.15 TITEGAS Computed Log, MWX-3 (continued)

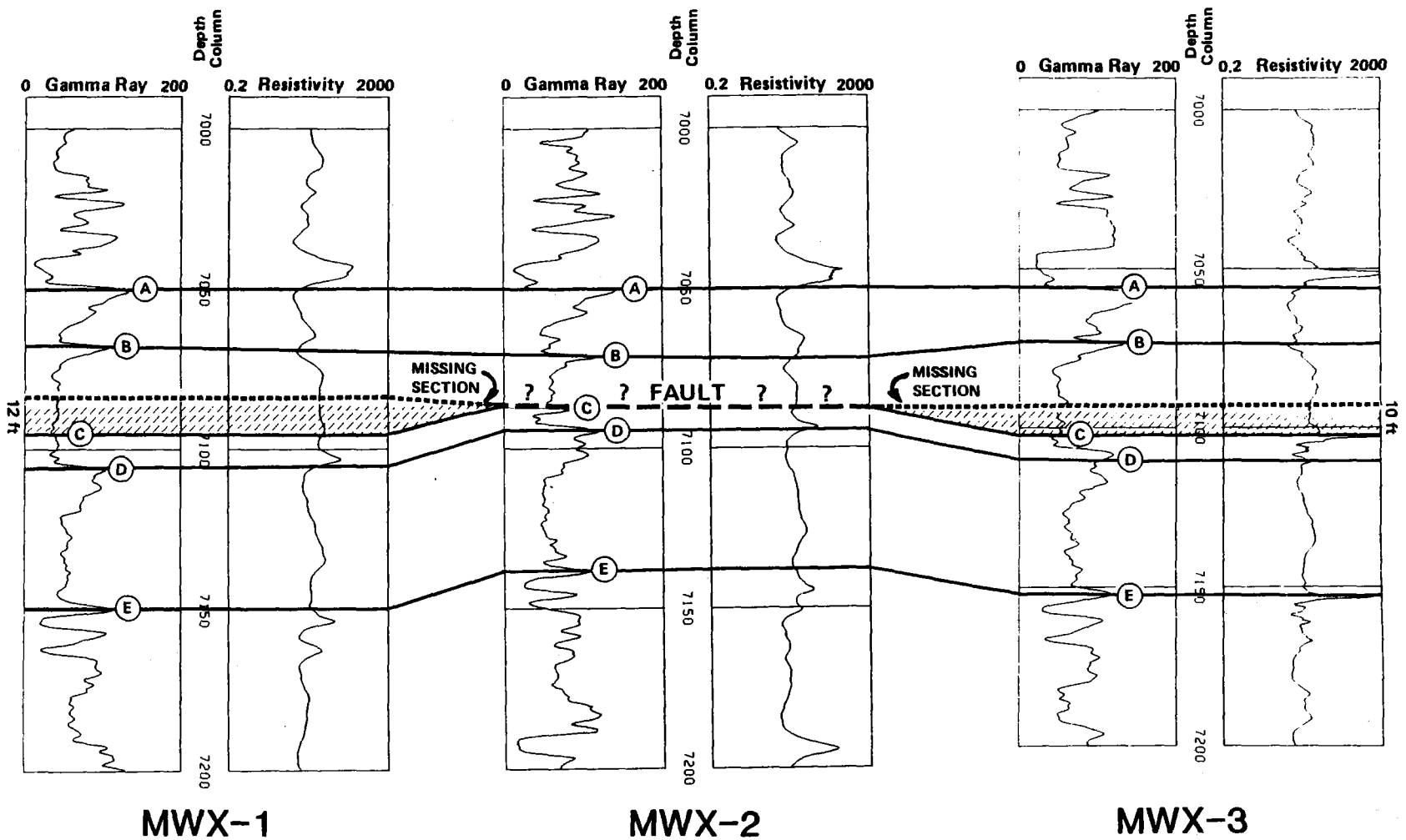

Figure 4.16 Missing Section in MWX-2 and Probable Fault Location

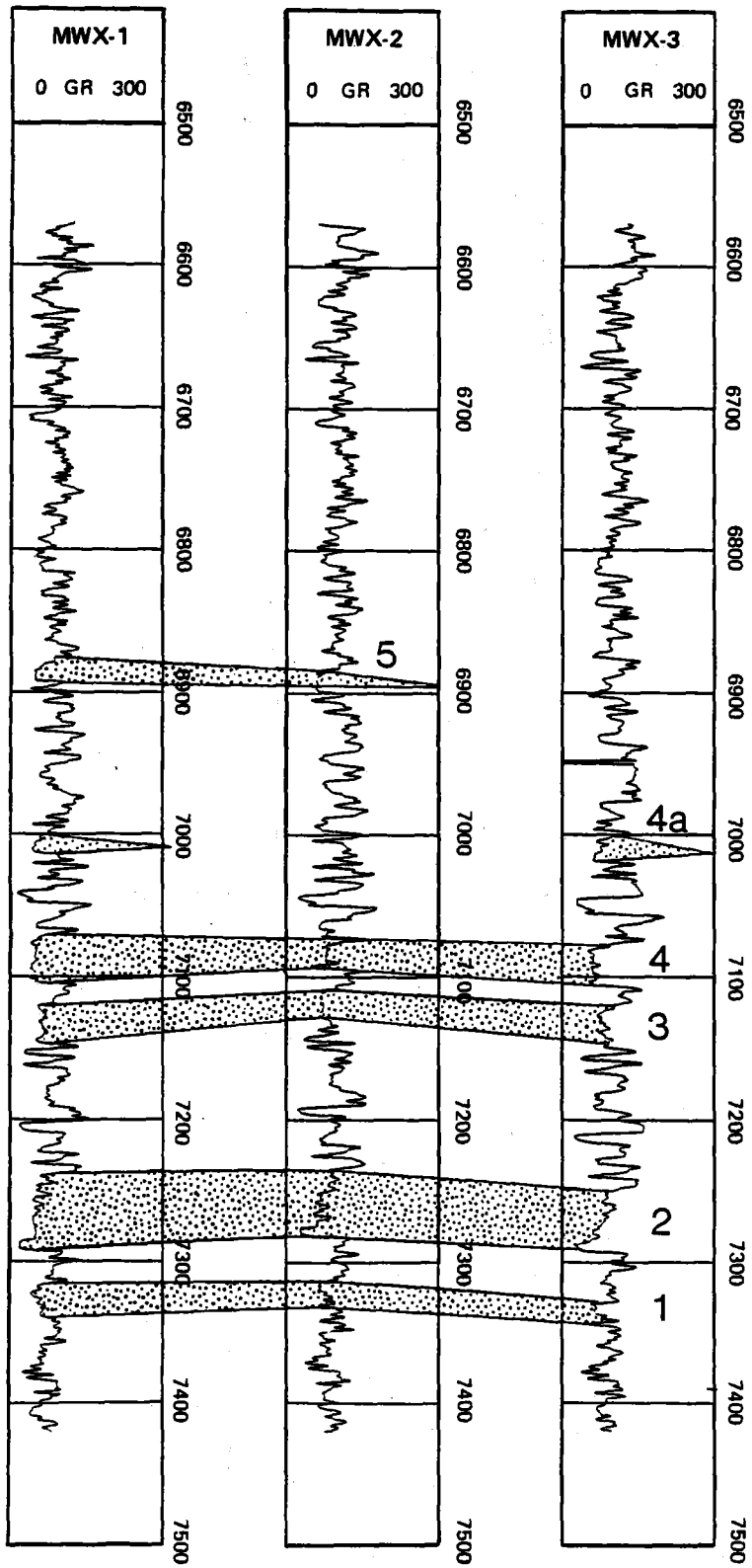

Figure 4.17 Zone Correlations of Paludal Interval

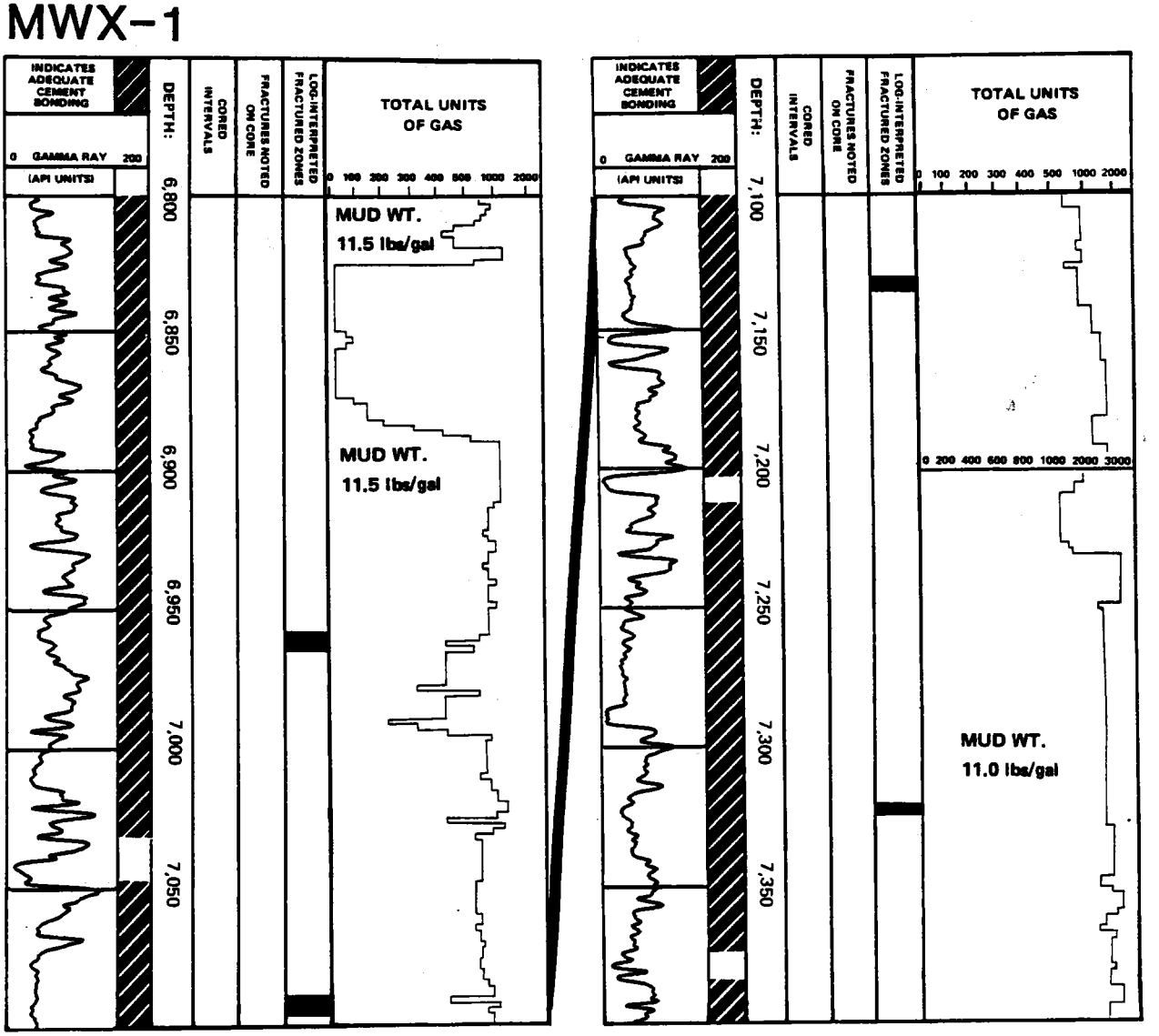

Figure 4.18 MWX-1 Mud Log from Paludal Interval

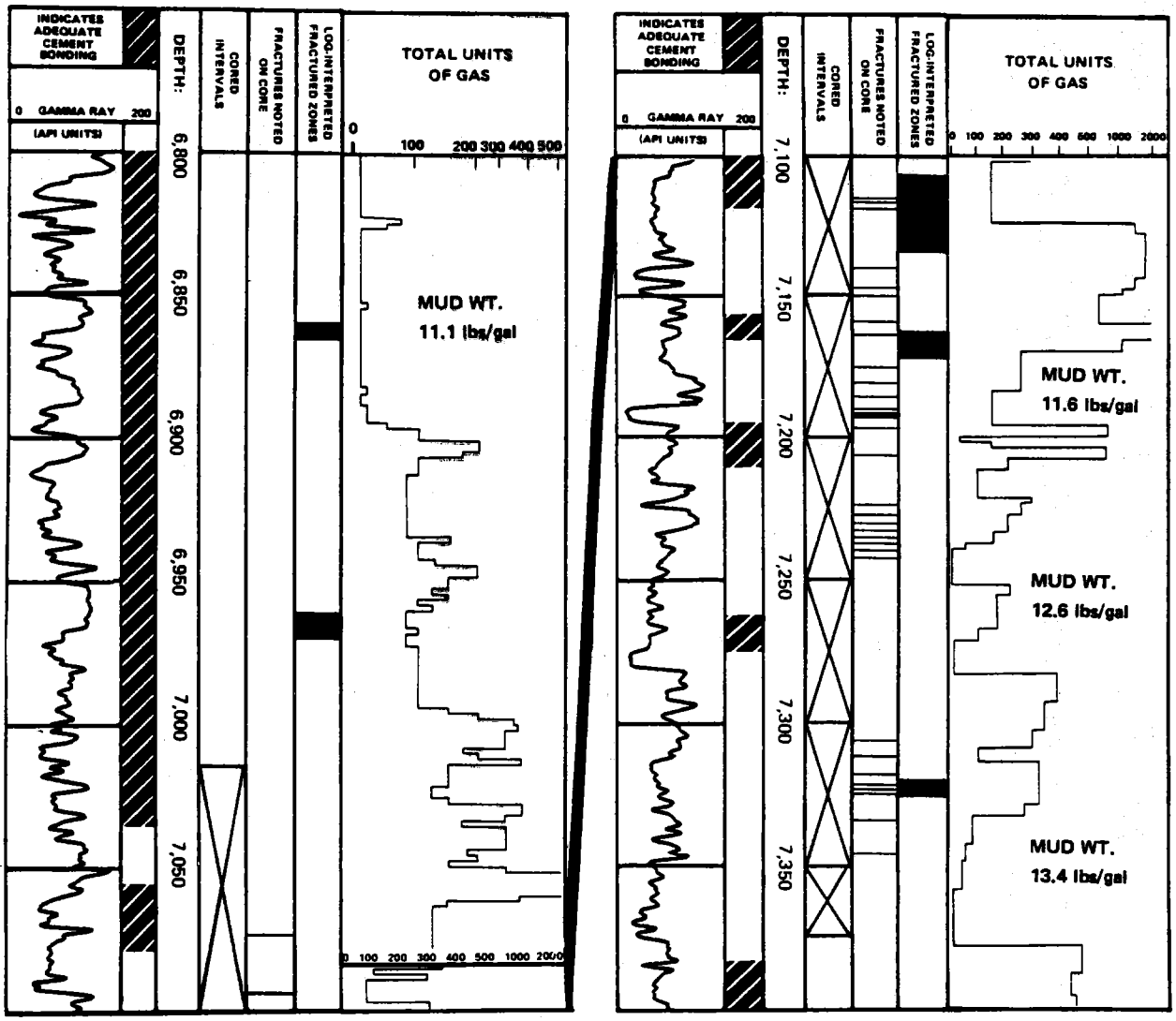

Figure 4.19 MWX-2 Mud Log from Paludal Interval

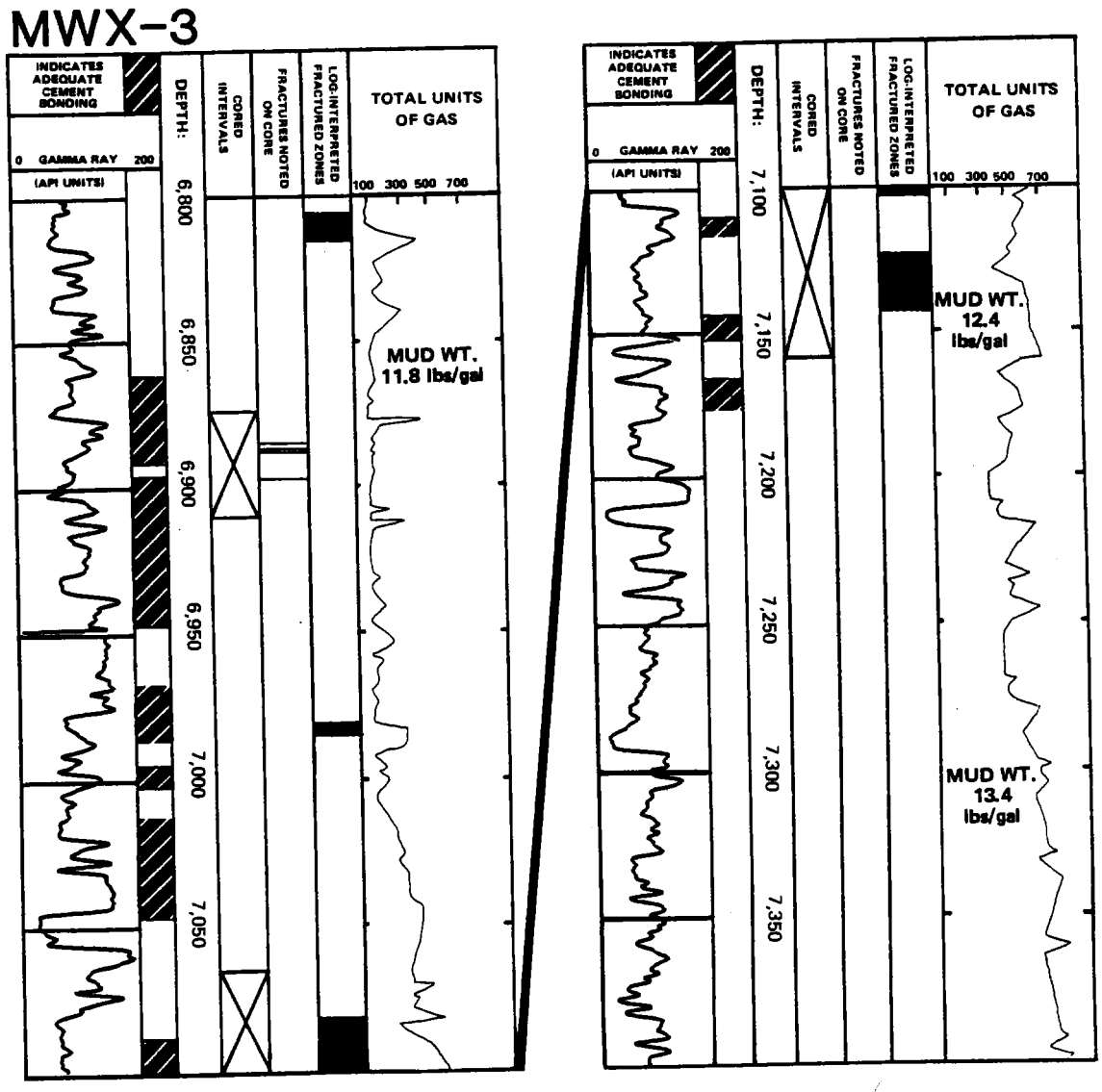

Figure 4.20 MWX-3 Mud Log from Paludal Interval

5.0 CORE ANALYSIS

A. R. Sattler
Sandia National Laboratories

5.1 INTRODUCTION

The paludal zone occurs at a depth of about 6600 to 7450 ft at the MWX site (Figure 5.1). The core data help describe the formations, the reservoir, and they provide input data to all MWX activities. In this section examples of the core data are presented and discussion is given to put the data in perspective. Specifically these remarks indicate:

- what core was taken and what analyses were made;
- typical values of reservoir parameters, rock properties and other measurements;
- implications of the core data; and
- some comparisons of the core data with that of other geologic sections of interest in the Mesaverde.

As described in section 3.0, the paludal zone is at the lower part of a delta plain. This interval contains several thick coal deposits and abundant carbonaceous shells. These coal deposits are interspersed with lenticular, distributary channel and splay sandstones formed in a lower delta plain environment. The sand percentage in this zone is markedly lower than other intervals of the Mesaverde at MWX. This is an extremely organic-rich section, and many of the noncoal members of this section are carbonaceous--even the sandstones are laced with carbonaceous stringers. The sandstones in this zone contain about 45 BCF of gas per square mile vs about 156 BCF per square mile for all Mesaverde sands. The coals in the paludal zone may contain about the same amount of gas as the sandstones.

The paludal zone has generally not been exploited for production in the vicinity of the MWX site. Prior to drilling MWX-1, we had studied the logs of neighboring wells and had decided that this zone would not be of great interest to MWX. Thus, little core was planned from the paludal zone in the first well. However, based upon MWX-1 results, a fairly extensive amount of core was taken in the paludal zone during the drilling of MWX-2 and MWX-3. The paludal has become one of the most interesting intervals in the Mesaverde.

These intervals of the paludal zone were cored:

(1) MWX-1, 6600-6830 ft, 4-in. core: This interval does not include any sandstones of interest. MWX-1 had been cored continuously from 4200 ft down to this interval. No sandstones of real interest below the lower coastal zone at 6550 ft were encountered. A decision was made to discontinue coring at this 6830-ft depth until the marine blanket sandstones were encountered.

(2) MWX-2, 7090-7388 ft, 4-in. core: After the drilling and logging of MWX-1 was completed, study of the MWX-1 logs revealed that there were a number of interesting sandstones in this paludal zone. On the basis of these logs a decision was made to make the paludal zone one of the principal coring targets in MWX-2. From these logs the major sandstones of interest were labeled zones 1-5, and all but zone 5 were included in the MWX-2 coring interval. Reasonable sand thicknesses were found in zones 1-3; zone 4 had effectively "shaled out."

(3) MWX-3, 6875-6910 ft, 7071-7158 ft, 4-in core, all oriented: Zones 3 and 4 were still our primary coring targets in this well. Core was also taken from zone 5. This particular zone had looked quite promising on both the MWX-1 and -2 logs; but was essentially nonexistent in MWX-3.

5.2 CORE PROGRAM

The MWX core analysis program is described in detail in elsewhere.[1,2] The results of analyses presented in this section have been taken from the reports submitted by the participants. These reports are specifically referenced where used in this section, and more comprehensive listings are found in Section 11.0 and Appendix 12.9. This section presents reservoir, mechanical, and organic properties obtained from core. Other core-derived properties are reported in other sections: lithology (3.2), mineralogy/ petrology (3.2.3), sedimentology (3.3), natural fractures (3.5), and estimates of in situ stresses from core (6.4). Core-log correlations are displayed with the log analyses formalisms in Section 4, although correlations made with respect to the televiewer and caliper logs are in Section 5.5.

There were over 25 participants in the core program. The major ones were Core Laboratories, Institute of Gas Technology (IGT), and New Mexico Petroleum Recovery Research Center (PRRC) (reservoir properties, caprock analysis); RE/SPEC (mechanical rock properties); Bendix Field Engineering Corp. and the US Geological Survey (mineralogy/petrology); and Colorado Geological Survey, USGS, TRW, and Amoco (organic maturation). Much of the core analysis data from Core Laboratories, IGT, and RE/SPEC are given as Appendices 12.4, 12.5, and 12.6, respectively.

In many core studies, analyses are confined to the reservoir rock only. In this case, however, the material abutting the sands was studied to obtain properties useful for hydraulic fracture design and analyses of stress test data; for example, mechanical property measurements were made on both sandstone and confining rock samples. In addition, caprock analyses and cation exchange capacity (CEC) measurements were often made to help determine the extent of the reservoir.

5.3 CORE HANDLING AND PREPARATION

A special core processing facility was established in a building at the Department of Energy's Anvil Points Facility across the Colorado River and about 15 miles from the MWX site. When the core came to the surface, it was removed from the core barrel by project geologists and placed in trays. After a quick preliminary inspection and removal of samples for special measurements, such as anelastic strain recovery (ASR), the core was first covered with plastic to prevent evaporation, and then with thick canvas to protect it from the elements. The core was then transported to Anvil Points for processing. Field processing of the core entailed many nonstandard procedures that included the following:

- Construction and use of a six-detector core gamma assembly. The core gamma assembly provided for well control during drilling and for core-log depth correlations after logging. The core gamma assembly also had better spatial resolution than the open-hole gamma ray log.

- Marking the positions and magnitude of scribe line deviation and locations of connections and other breaks in core.

- Photographing the entire amount of core in color.

- A special no-freeze freight service was used in the winter to ship samples selected for measurements of reservoir parameter or mechanical rock properties.

Because there were so many conflicting requirements for the MWX core, many of the routine and special core analyses were performed on plugs. This allowed most of the whole core to be available for studies of sedimentology and depositional environment, mechanical rock properties, and organic maturation. Thin sections were taken by facing off the ends of the same core plugs. Preference for thin section analyses was given to the plug ends corresponding to the plugs selected for the restored state permeability measurements. This allowed correlations of sandstone reservoir properties

with mineralogy/petrology. Since properties can often vary rapidly in a lenticular sequence, it was necessary to make the correlations from the same sample.

5.4 CORE ANALYSES, RESULTS, AND DISCUSSION

5.4.1 Reservoir Properties

Reservoir parameter measurements were made at frequent intervals in the sands. Routine core analyses were made on plugs taken every foot.[3-5] Restored pressure state permeabilities and CEC analyses were made every two or three feet, mainly in zones 3 and 4,[6-12] which were the stimulation targets in this zone.

Much of this core reservoir data is displayed in Table 5.1 and Figures 5.2-5.5. The water saturations were made with the Dean Stark distillation method. (The oil-based mud used in drilling MWX-1 and MWX-2 contributed to good water saturation data. However, MWX-3 was drilled with a water-based drilled fluid; even though drilled at or near balanced conditions, MWX-3 water saturations may be 5-15 percentage points high due to invasion.) Porosities were determined by Boyles Law method with helium. Core Laboratories used the nonsteady-state, pulsed method to determine their restored pressure Klinkenberg (gas slippage corrected) permeabilities. IGT used the steady-state method to determine their restored pressure Klinkenberg permeabilities. Core Laboratories subjected each of the core plugs to toluene extraction to remove any residue from the oil-based drilling fluid and they leached any salts out of the pores using hot methyl alcohol. IGT made their restored pressure state permeabilities without cleaning procedures. In some cases, the IGT permeability data may appear a little lower than the Core Laboratories data. However, when both are corrected to the same confining pressures, the IGT and Core Laboratories data are generally in good agreement.

The core in zones 3 and 4 exhibits a higher average permeability and porosity than other Mesaverde intervals studied at MWX (Corcoran, Cozzette, coastal and fluvial zones). Maximum permeabilities are in excess of 20 microdarcies at 2000 psi confining pressure. Average permeabilities when corrected for water saturation are in the 2-3 microdarcy range; this is one of the few zones where formation permeabilities corrected for water saturation are above a microdarcy. Since formation permeabilities from well testing range from around 40-200 microdarcies, the strong influence of natural fractures in production has been postulated even though few natural fractures have been seen either in core from paludal reservoir rock (Section 3.5) or in the borehole televiewer log (Section 5.5). However, it would take only a few natural fractures, cracks or joints to raise formation permeabilities above the 2-3 microdarcy range.

Permeabilities were also measured as a function of stress and water saturation[12,14-17] (Table 5.2 and Figures 5.6-5.8). The permeabilities of paludal sandstones depend on effective stress, although apparently to less extent than in other zones of the Mesaverde, as seen in Figure 5.6. Well test data indicate that the pore pressures in the paludal zone are 5200-5400 psi. Thus, initial in situ confining stresses are around 2000 psi and could increase if the reservoir is drawn down. Restored state permeability measurements were made at 1000, 2000 and 3000 psi. Although not shown, there is little dependence of permeability with temperature.

In addition, permeabilities were made over a range of both net confining stresses and water saturations (Figure 5.7-5.8). Increasing the water saturation from 0% to 50% decreases permeabilities by about an order of magnitude. This effect is less severe at lower confining pressures. Based on these results, dry Klinkenberg permeabilities at 2000 psi should be reduced by a factor of about 3.5 to obtain an estimate of in situ permeabilities at in situ stress and water saturation.

A few vertical permeabilities were run (Table 5.3).[14] Vertical permeabilities are about the same magnitude as the horizontal permeabilities.

Maximum porosities exceed 12%. Porosities vary little with confining pressure (Table 5.4).[18]

Capillary pressure measurements were made on several samples[8-11,18-19] (Table 5.5 and Figure 5.9). Capillary pressures are several hundreds of psi or higher. These capillary pressures may keep the naturally occurring microfractures free of water at reservoir conditions and may also help reduce effects of water damage to these fractures after stimulation treatment.

5.4.2 Caprock Analysis

Caprock analyses were used in MWX-2 and MWX-3 in an attempt to determine how good the materials abutting the sandstones were in containing the gas[20-22] (Table 5.6). These measurements included permeability to brine and the minimum gas threshold necessary to displace water. A combination of very low permeability plus a large threshold displacement pressure would indicate good caprock. These tests indicate that these abutting materials are probably adequate for caprocks. The caprock permeabilities are generally in the subnanodarcy range and the water displacement threshold were in the range of hundreds of psi. These measurements must be considered qualitative, since the test apparatus could not go to the range of existing pore pressures.

5.4.3 Cation Exchange Coefficient (CEC)

CEC analyses were performed on a trimmed core plug end using the adsorbed water method[6] (Figures 5.2-5.5). CEC values are used as corrections to the formation factor determination in the Waxman-Smits-Thomas/Archie's Law formalisms. The formalisms themselves are used in log analyses for the determination of resistivity and water saturation. The CEC data can be used to obtain a rough estimate of clays across a zone on a relative basis. Formation factor and resistivity index measurements were run on samples of paludal core[23] (Table 5.7 and Figures 5.10 and 5.11).

CEC values in the paludal sandstones are around 1.5 meq/100 g. These are higher than those in the Cozzette pyrobitumen zone (1.3 meq/100 g), Cozzette productive sandstone (0.5 meq/100 g), and Corcoran sandstone (0.9 meq/100 g). Paludal sandstones are not as clean as the blanket sandstones; they have a higher clay content. The shales have considerably higher CEC values than their abutting sandstones; for example, the shales below zone 3 at 7107-7111 ft have an average CEC value of 6.2 meq/100 g. The derived composite cementation exponents (m, m*; clay-corrected) appear to be independent of depositional environment (Table 5.8).

5.4.4 Mechanical Rock Properties.

Mechanical rock property measurements were made on selected samples not only in the sandstones but in the rock abutting them: carbonaceous siltstones, mudstones, and shales[24-27] (Figures 5.12-5.17). These measurements were made throughout all paludal coring intervals. Young's modulus and compressive strength are given at various confining pressures, Poisson's ratio, and tensile strength. Limited fracture toughness data are given in Table 5.9.

Young's moduli, E, range from 18-37 GPa in the sandstones and 18-30 GPa for the "shales," respectively, Poisson's Ratios, ν, range from 0.19-0.22 and 0.13-0.27, and fracture toughness ranges from 0.69-1.69 and 0.43-1.25 MPa$\sqrt{m}$ for the two respective lithologies. It is difficult to make strong correlations between any differences in mechanical rock properties between the sandstones and the abutting rocks in this very complex lithology. For example, carbonaceous mudstones sometimes have higher moduli than the sandstones and noncarbonaceous mudstones have lower moduli than the sandstones. Generally, the lithology may vary rapidly over a few feet vertically and variations are seen in horizontal distances of the order of well spacing (~100-200 ft).

5.4.5 Organic Analyses

Because there are a number of fairly large coals in the paludal zone at MWX a number of special studies were run on these paludal zone coals and other rock. Vitrinite reflectance measurements[28,29] (Figure 5.18) were made not only in the coals but were also made on rock containing organic material. Both Amoco and the USGS vitrinite reflectance data are in good agreement. These data support a time-dependent paleotemperature model developed by the USGS and infer basinal heat flow. Similar reflectance values are found in other places in the region. The data suggest intense regional heating. Migration of gas found in channel sands is postulated.

Rock evaluation pyrolysis analyses were run on several samples to measure their organic content[30,31] (Table 5.10). Interestingly, a few of the dark mudstones had an organic content that was not significantly higher than a control sample of apparently clean sandstone (MWX-3, depth 7135.9 ft).

Special analyses were run on the coals, which include methane content of coals from desorption[32,39] (Tables 5.11 and 5.12), some special lithologic descriptions of the coals[33-38] (Table 5.13), ultimate and proximate analyses, heating value and forms of sulfur[34,35] (Table 5.14), and palynology.[40] The desorption data from TRW[32] and the Colorado GS[38] seem in reasonable agreement, although an exact comparison is not possible. The TRW desorption data were carried from about 7200 ft to the bottom of the coals in MWX-2 where oil-based drilling fluid was used. The Colorado GS data were done over the paludal coals down to 7160 ft in MWX-3, where the water-based drilling fluid was used.

Produced gas analyses for molecular species[41-43] (Table 5.15) and isotopic species[44,45] were also made. The isotopic and chemical analyses of the gas from the paludal zone, not surprisingly, infer that the gas in the paludal zone sands emanated from the coals.

5.5 CORRELATIONS WITH BOREHOLE TELEVIEWER AND CALIPER DATA

This section presents the MWX-3 borehole televiewer and oriented caliper data and presents brief comments on the relevance of these data to the core data on natural fractures (Section 3.5) and in situ stress (Section 6). The televiewer data shown in Figure 5.19 suggest a lower natural fracture frequency in the paludal and coastal zones than in the fluvial zone. This is consistent, qualitatively at least, with the fracture frequency seen in core in these three zones. The interpretation of natural fractures from the televiewer log was rather difficult in the paludal zone. The display of fractures from the televiewer log shows a preferred azimuth somewhat north of west. This azimuth is in general agreement with the strain relaxation data (Section 6.4) and the fracture diagnostic data (Section 10). It appears as if the present-day direction of the maximum principal horizontal stress is about the same as the paleostress direction.

There appears to be little preferred orientation in the display of borehole breakouts from the televiewer log in the paludal zone (Figure 5.20). The appearance and directionality of borehole breakouts may be influenced by factors other than in situ stress--for example, rock fabric properties.

The ratio of the long to the short borehole axis taken from the MWX-3 oriented borehole caliper data is consistently closer to unity through the paludal zone that it is in the fluvial or coastal zone (Figure 5.21). It appears as if effective horizontal stress differences have not been great enough in the paludal zone to cause significant hole elongation. However, the azimuth of breakouts measured in the caliper log (Table 5.16) is generally consistent with the televiewer data (above) and ASR data (Section 6.4).

5.6 REFERENCES

1. Sattler, A. R., "The Multiwell Experiment Core Program," SPE 11763, Proceedings of the 1983 SPE/DOE Symposium on Low Permeability, Denver, CO, March 14-18, 1983.

2. Sattler, A. R., "The Multi-Well Experiment Core Program, II," SPE 11763, Proceedings of the 1984 SPE/DOE Unconventional Gas Recovery Symposium, Pittsburgh, PA, May 16-18, 1984.

3. Core Laboratories, Report RP-2-6714, November 1981.

4. Core Laboratories, Report RP-2-6806, March 1982.

5. Core Laboratories, Report 3806-7199, July 1983.

6. Core Laboratories, SCAL Report 203-82014, June 1983.

7. Core Laboratories, SCAL report 203-830070, November 1983.

8-10 Institute of Gas Technology, Project 65056 Reports, "Sandstone Permeability and Porosity Measurements," July 1982, August 1982, and October 1982.

11. Institute of Gas Technology, Project 61071 Report, "Special Dry Core Analyses of the Mesaverde Formation--US DOE Multiwell Experiment, Garfield County, Colorado," submitted to DOE, June 1984.

12. Wei, K. K. et al., "Effect of Fluid, Confining Pressure, and Temperature on Absolute Permeabilities of Low Permeability Sandstones," SPE Formation Evaluation, pp 413-424, August 1986.

13. Core Laboratories Report P83012, January 1984.

14. Core Laboratories SCAL Report 203-83005, March 1984.

15-16 Institute of Gas Technology, Project 6506 Reports, "Sandstone Permeability and Porosity Measurements: Relative Permeability Data," October 1982 and November 1981.

17. Institute of Gas Technology, Project 61071 Report, "Effects of Water and Stress upon Permeability to Gas of Paludal and Coastal Sands--US DOE Multiwell Experiment, Garfield, County, Colorado," April 1985.

18. Core Laboratories SCAL Report 203-830024, March 1984.

19. Ward, J. S. and N. R. Morrow, "Capillary Pressures and Gas Relative Permeabilities of Low Permeability Sandstones," SPE Formation Evaluation, pp 345-346, September 1987.

20-21 Institute of Gas Technology, Project 65056 Reports, "Caprock Analysis," June 1982 and September 1982.

22. Institute of Gas Technology, Project 61071 Report, "Analysis of Stratigraphic Barriers (Caprock) between Sands in the Cretaceous Mesaverde Formation--US DOE Multiwell Experiment, Garfield County, Colorado," June 1984.

23. Core Laboratories SCAL Report 203-840026, August 1984.

24. RE/SPEC Inc., Data Report RS1-0226, September 1983.

25. RE/SPEC Inc., Data Report RS1-0234, October 1983.

26. RE/SPEC Inc., Data Report RS1-0238, November 1983.

27. RE/SPEC Inc., Data Report, RSI(RCO)-046.2-84/227, February 1984.

28. Bostick, N. H. and Freeman, V. L., "Tests of Vitrinite Reflectance and Paleotemperature Model at the Multiwell Site, Piceance Creek Basin, Colorado," Chapter in USGS Open File Report 84-7577, 1984.

29. Hemmler, T., "MWX-1 and MWX-2 Cores; Vitrinite Reflectance Data," Letter report to A. R. Sattler, Sandia National Laboratories, November 1982.

30. Core Laboratories, Letter Report 84012, March 1984.

31. Core Laboratories, Letter Report 84137, August 1984.

32. Choate, R., "Methane Content in Mesaverde Coals," TRW Report, February 1983.

33-39 Tremain, C. L., Colorado Geological Survey Letter Reports to A. R. Sattler, Sandia National Laboratories; January 1982, March 1982, July 1982, November 1982, February 1983, March 1983, and January 1984.

40. R. E. Jones, Amoco Production Company Palynology Letter Report to J. C. Lorenz, Sandia National Laboratories, February 1983.

41-43 Core Laboratories, Reservoir Fluid Analyses Reports ARFL 860066 (Corrected), 860079, 860081, 1986.

44-45 Rice, D., USGS Letter Reports to Sandia National Laboratories, September 1982 and February 1983.

46. Kilmer, N. H., et al., "Pressure Sensitivity of Low Permeability Sandstones," Journal of Petroleum Science and Engineering 1, pp 55-81, 1987.

47. New Mexico Petroleum Research Recovery Center, New Mexico Institute of Mining and Technology, Project 2-75-7339 Reports for Morgantown Energy Technology Center, (Annual) 1987.

48. Soeder, D. J. and P. L. Randolph "Porosity Permeability and Permeability in Tight Mesaverde Sandstone, Piceance Basin Colorado," SPE Formation Evaluation, pp 129-136, June 1987.

Table 5.1 RESULTS FROM ANALYSIS OF DRY PALUDAL CORE (IGT)

MWX-2 Core Depth (ft)	Values at Net Confining Stress*						
	Lab Net Confining Stress* (psi)	Porosity (%)	As Received Water Sat. (%)	Klinkenberg Permeability (μd)	Klinkenberg "B" (psi/μd)	Pore Volume** Compressibility (microsips)	Mercury Capillary Entry Pressure (psia)
7125.0	4440	10.66	45	3.20	85.7	9.8	350
7130.0	4440	11.43	46	8.25	63.0	8.1	280
7144.7	4450	9.83	43	1.53	104.0	9.0	470
7265.5	4280	8.54	36	1.78	74.9	11.2	490
7329.2	4210	8.13	52	1.30	73.9	7.8	490
7366.3	4230	7.67	55	.59	119.0	9.1	680

* Calculated using (0.925) (sample depth) - (0.5) (pore pressure estimated from mud weight).

** Pore volume compressibility ($\Delta V/V\Delta P$) determined by fractional changes in pore volume per psi of stepwise increase in confining pressure on the first compression of the rock from about 2,000 psi net stress to the net stress used for testing. Lower values would probably result from cycling of net stress to the maximum that would be experienced in reservoir depletion.

Table 5.2 SELECTED PERMEABILITY DATA AS A FUNCTION OF OVERBURDEN PRESSURE AND WATER SATURATION (CORE LABORATORIES)

MWX-2 Core Depth (ft)	Permeability to Air (md)	Porosity (%)	Water Saturation (%)	Klinkenberg Permeability (md) at Effective Overburden Pressure of 1000 psi	2000 psi
7130.9	0.06	12.6	45	No Reading	
			30	.0063	.0050
			15	.0072	.0048
7133.1	0.04	11.6	45	No Reading	
			30	.0021	.0021
			15	.0031	.0029
7281.6	0.08	7.9	45	No Reading	
			30	.0025	.0005
			15	.0037	.0029
7331.1	0.02	8.1	45	No Reading	
			30	No Reading	
			15	.0043	.0020
7340.1	<0.01	1.4	45	No Reading	
			30	No Reading	
			15	.0010	.0002

Table 5.3 SUMMARY OF VERTICAL PERMEABILITY AS FUNCTION OF OVERBURDEN PRESSURE (CORE LABORATORIES)

MWX-3 Core Depth (ft)	Vertical Permeability to Air (md)	Porosity (%)	Vertical Klinkenberg Permeability (md) at Effective Overburden Pressure of		
			1000 psi	2000 psi	3000 psi
6894.7-94.9	0.03	7.9	0.0007	0.0004	0.0001
7083.3-83.6	0.03	6.5	0.0049	0.0034	0.0016
7094.0-94.6	0.03	7.8	0.0088	0.0078	0.0038
7129.0-29.5	0.02	6.4	0.0094	0.0068	0.0033
7541.4-41.9	0.03	4.8	0.0046	0.0027	0.0009

Table 5.4 POROSITY AS FUNCTION OF OVERBURDEN PRESSURE

MWX-2 Core Depth (ft)	Porosity (%) at Overburden Pressure of 200 psi	1000 psi	2000 psi	3000 psi	200 psi*
7121.0	4.1	4.0	3.9	3.8	4.0
7140.0	1.6	1.5	1.5	1.4	1.5
7365.9	11.1	11.0	11.0	10.8	11.0

*Returned to 200 psi

Table 5.5 SUMMARY OF CAPILLARY PRESSURE TEST RESULTS*

MWX-2 Core Depth (ft)	Permeability to Air (md)	Porosity (%)	Brine Saturation (% pore space) at Pressure (psi) of: 1	10	50	100	150	200	250	300	500	1000
7128.9	0.10	12.9	100.0	100.0	100.0	53.2	52.1	49.9	46.6	42.4	35.4	32.5
7138.3	0.07	13.3	100.0	100.0	100.0	50.0	43.8	40.1	38.5	37.0	34.4	32.1
7285.3	0.04	7.8	100.0	100.0	100.0	100.0	79.2	67.5	60.1	55.4	49.3	42.5
7328.1	0.02	9.6	100.0	100.0	100.0	100.0	64.9	58.9	57.7	51.0	46.6	40.4

* Fluid System: Air-Water
Test Method: High-Speed Centrifuge

Table 5.6 CAPROCK ANALYSES (IGT)

Well	Core Depth (ft)	Rock Type	Vertical K_w (nanodarcies)	Threshold Pressure (psi)	Effective Porosity* (%)
MWX-2	7116	Coaly Siltstone	<0.101	525	4.83
MWX-2	7259	Silty Shale and Siltstone	<0.105	750	3.61
MWX-2	7265	Black Shale and Siltstone	59.1	210	6.12
MWX-2	7318	Black Shale	0.747	750	3.70
MWX-2	7345**	Black Shale	60×10^3	0	4.01
MWX-3	6894	Shale	0.7	810	-
MWX-3	6899	Shale	0.3	790	-
MWX-3	7076	Shale	-	>1000	-
MWX-3	7115	Silty Shale	0.6	780	-
MWX-3	7153	Shale	-	>1000	-

* Fluid porosity, ϕ_w, measured at zero net stress and barometric pressure
** Affected by vertical fracture

Table 5.7 FORMATION RESISTIVITY FACTOR AND RESISTIVITY INDEX*

MWX-2 Core Depth (ft)	Permeability to Air (md)	Porosity (%)	Brine Saturation (% pore space)	Resistivity Index (n)	Overburden Pressure (psi)	Formation Resistivity Factor (m)	Corrected Porosity** (%)
7128.9	0.15	13.5	100.0	1.00			
			87.5	1.21			
			59.4	1.68			
			38.9	2.61			
					0	45.4	
					200	59.8	
					3600	68.2	11.7
7141.0	0.04	7.7	100.0	1.00			
			95.2	1.14			
			67.9	1.40			
			51.2	1.90			
					0	81.7	
					200	97.9	
					3600	120	7.3
7285.3	0.05	8.4	100.0	1.00			
			80.7	1.27			
			63.9	1.46			
			48.3	2.09			
					0	78.6	
					200	99.3	
					3600	119	8.4
7328.1	0.05	9.1	100.0	1.00			
			86.5	1.25			
			58.7	1.62			
			44.2	2.27			
					0	74.1	
					200	93.6	
					3600	112	8.9

* Saturant: 13,000 ppm NaCl with resistivity of 0.440 ohm-meters at 77°F.
** Corrected for pore volume reduction at pressure.

Table 5.8 DERIVED COMPOSITE, CLAY-CORRECTED CEMENTATION AND SATURATION EXPONENTS

Interval	Well	Effective Overburden Pressure (psi)	Cementation Exponent m	Cementation Exponent m*	Saturation Exponent n	Saturation Exponent n*
Fluvial	MWX-1	0	1.72	1.92	1.37	1.83
		200	1.79	2.00		
		3000	1.89	2.08		
Coastal	MWX-1	0	1.74	1.96	1.85	2.55
		200	1.79	1.98		
		3200	1.88	2.09		
Paludal	MWX-2	0	1.82	2.03	1.08	1.47
		200	1.92	2.12		
		3600	1.95	2.17		

Table 5.9 FRACTURE TOUGHNESS MEASUREMENTS

Well	Zone	Lithology	Core Depth (Log Depth) (ft)	Fracture Toughness ($MPa \cdot m^{-1/2}$)
MWX-3	4	Sandstone	7095.8-6.1 (7094.8-5.1)	1.03 ± 0.09
	3	Shale	7112.1-3.4 (7111.1-2.4)	0.86 ± 0.13
	3	Sandstone	7132.7-3.9 (7131.7-2.9)	0.69 ± 0.20
MWX-2	4	Sandstone	7085.6-7.0 (7100.3-0.9)	1.26 ± 0.16
	4	Siltstone	7107.6-8.3 (7100.3-0.9)	0.43 ± 0.25
	3	Sandstone	7121.0-1.7 (7113.0-3.7)	0.91
	3	Siltstone	7162.0-3.0 (7152.0-3.0)	0.78 ± 0.30
	2	Siltstone	7253.0-4.0 (7243.0-4.0)	1.10 ± 0.48
	2	Silty Sandstone	7268.8-9.5 (7258.8-9.5)	1.02 ± 0.90
	2	Sandstone	7280.5-1.5 (7270.5-1.5)	1.49 ± 0.29
	1	Carbonaceous Mudstone	7308.1-9.0 (7298.1-9.0)	1.25 ± 0.29
	1	Silty Sandstone	7322.1-2.8 (7312.1-2.8)	1.37 ± 0.30
	1	Carbonaceous Mudstone	7342.9-3.9 (7332.9-3.9)	1.11 ± 0.18
	1	Silty Sandstone	7360.9-2.0 (7350.9-2.0)	1.38 ± 0.26

Table 5.10 ROCK EVALUATION PYROLYSIS DATA
FROM THE PALUDAL INTERVAL

Depth (ft)	Description	Total Organic Carbon (%)	Gas Evolved* (mg/gm rock) S_1	S_2	S_3
MWX-2					
7081.0	carbonaceous mudstone	3.69	0.99	1.54	0.44
7100.0	coal	21.55	14.91	58.27	1.30
7148.0	coal	13.83	2.74	20.44	2.19
7228.0	coal	8.24	3.95	7.74	1.49
7241.0	carbonaceous mudstone	4.20	1.24	1.46	0.44
7290.0	coal	12.27	6.77	39.62	1.98
7313.0	carbonaceous mudstone	1.68	0.34	0.13	0.53
MWX-3					
6883.2	carbonaceous mudstone	8.09	1.23	4.62	0.20
6882.1	dark mudstone	1.85	0.20	0.70	0.18
6890.5	grey mudstone	1.04	0.28	0.42	0.16
6898.7	coal	8.56	1.40	7.03	0.23
6904.2	dirty coal	14.36	3.10	13.21	0.32
6906.6	coal	11.14	1.31	6.21	0.27
7071.2	carbonaceous silty mudstone	12.12	1.41	7.78	0.18
7072.3	coal	14.16	1.54	12.88	0.60
7077.3	coal	1.16	0.09	0.23	0.11
7079.8	silty mudstone	1.75	0.49	0.64	0.19
7084.6	carbonaceous sandstone	1.13	0.42	0.44	0.23
7100.3	carbonaceous sandstone	1.78	0.48	0.77	0.29
7105.5	coal	59.26	3.40	55.58	0.47
7108.8	coal	68.07	2.92	50.69	0.32
7110.5	carbonaceous siltstone	6.77	1.35	3.09	0.06
7115.4	dark mudstone	1.34	0.14	0.39	0.13
7121.4	carbonaceous mudstone	0.36	0.12	0.13	0.15
7135.9	sandstone	0.11	0.14	0.04	0.17
7147.1	mudstone	1.63	0.24	0.56	0.08
7153.2	carbonaceous mudstone	4.89	0.71	1.98	0.02
7154.5	carbonaceous mudstone	12.33	1.43	16.75	0.37
7154.0	coal	12.88	1.85	22.55	0.39

*S_1 Free hydrocarbons present
S_2 Hydrocarbons produced by thermal conversion of kerogen
S_3 Organic carbon dioxide produced by pyrolysis of kerogen

Table 5.11 METHANE DESORPTION RESULTS FOR CORE AND DRILL-CUTTING SAMPLES COLLECTED FROM DOE WELL MWX-2 (TRW)

SAMPLE NO.	CORE NO.	CANISTER NO.	CORING INTERVAL	CORE[6] DEPTH CORRECTION (ft)	SAMPLE TYPE	SAMPLE WEIGHT (gm)	GAS CONTENT[1]							
							LOST GAS		DESORBED GAS			RESIDUAL GAS	TOTAL GAS	
							cc	cc/gm	days[2]	cc	cc/gm	cc/gm	cc/gm	cu ft/ton
1	53	35	7203.7-7204.2	-8.0	core	1447	1866	1.29	271	11900	8.22	0.39	9.90	317[5]
2	53	28	7224.4-7224.7	-9.5	core	929	1894	2.04	214	7856	8.46	0	10.50	336[5]
3	53	14	7229.5-7229.8	-10.0	core	2269	932	0.41	271	6002	2.65	0.52	3.58	125[4]
4	--	25	7234-7236 7238-7242	-10.5 -10.5	drilling chips	2270	117	0.05	271	549	0.24	--	0.29	9[3]
5	54	43	7234.6-7234.9	-10.5	core	1465	2156	1.47	270	8979	6.13	1.34	8.94	286[5]
6	--	53	7374-7386	-10.0	drilling chips	2062	89	0.04	269	4175	2.02	--	2.06	65[3]
7	--	80	7374-7386	-10.0	drilling chips	2247	-20	-0.01	269	1006	0.45	--	0.45	14[3]
8	--	93	7374-7386	-10.0	drilling chips	2140	103	0.05	269	863	0.40	--	0.45	14[3]
9	55	152	7375.8-7376.1	-10.0	core	1257	1803	1.43	212	7761	6.17	1.04	8.64	303[5]
10	55	108	7380.3-7380.6	-10.0	core	1093	1856	1.70	212	7658	7.01	0	8.71	279[5]
11	55	89	7384.3-7384.6	-11.0	core	1545	1993	1.29	317	10495	6.79	0.35	8.43	295[5]
													Average (six samples[5])	303

Notes:
1. Final gas values; revised 2/1/83.
2. Number of days before desorption ceased.
3. Drill-cutting sample values are extremely low because cuttings were very fine and probably outgassed very fast while circulating uphole. Values are unadjusted for contamination by diesel-oil drilling fluid and noncoalbed water and rock chips. Also, crude and refined oil having high capacity for taking methane into solution probably also accounts for the low desorption values of the drilling-chip samples.
4. Sample comprised of highly broken pieces of core; lower value for desorbed gas indicates sample outgased quickly, before being sealed in canister, therefore, sample value is here considered to be suspect and non-representatively low.
5. These six samples are here considered to be good samples and as representative as can be practically obtained.
6. Correction value to correlate core depth with geophysical log depth.

Table 5.12 METHANE DESORPTION DATA FROM MWX-3
(COLORADO GEOLOGICAL SURVEY)

Sample Depth (feet)	Desorbed and Lost Gas	
	(Cubic feet/ton)	(Standard cubic feet/ton)
6883.9-6884.2	112	Standard not yet calculated.
6903.0-6903.6	27	
6905.6-6906.0	127	
7072.8-7073.3	479	384
7106.6-7106.9	376	302
7158.0-7158.6	206	165
7159.4-7159.9	302	243

Table 5.13 COAL LITHOLOGY OF MWX PALUDAL ZONE SAMPLES

MWX-2 Core Depth (ft)	Sample Description
7099.7-7100.8	dull carbonaceous shale with minute coal stringers
7152.7-7153.5	dull carbonaceous shale with traces of coal
7201.9-7202.2	dull carbonaceous shale with lenses of coal
7226.0	dull carbonaceous shale with minute coal stringers
7235.3-7235.6	shiny black coal
7241.8-7241.9	shiny black coal
7290.0-7290.5	shiny black coal
7380.6-7381.3	shiny black coal; petroleum-based mud

Table 5.14 ANALYSES OF MWX-2 COALS (AS RECEIVED)

	Sample Depth (ft)				
	7100	7153	7202	7242	7381
Proximate Analysis (%)					
Moisture	0.66	1.23	0.90	1.63	1.18
Ash	7.19	47.73	4.96	88.46	7.91
Volatile Matter	16.34	12.01	16.85	5.24	21.08
Fixed Carbon	75.81	39.03	74.29	4.73	69.83
Ultimate Analysis (%)					
Hydrogen	4.24	2.71	4.04	0.86	4.02
Carbon	22.85	43.35	85.16	5.39	82.77
Nitrogen	1.61	0.89	1.65	0.20	1.51
Sulfur	1.12	0.40	0.90	0.50	0.95
Oxygen	2.99	4.92	3.29	4.65	2.84
Ash	7.19	47.73	4.96	88.40	7.91
Heating Value (Btu/lb)	14,334	7,338	14,696	799	14,279
Forms of Sulfur	Mostly Organic	Mostly Organic	Mostly Organic	Mostly Organic	Mostly Organic
Rank	LVB*	LVB	LVB	LVB	LVB

*Low Volatile Bituminous

Table 5.15 REPRESENTATIVE PRODUCED GAS ANALYSIS FROM PALUDAL REENTRY (MWX-1, MARCH 26, 1986)

Component	Mol Percent
Hydrogen Sulfide	0.00
Carbon Dioxide	5.89
Nitrogen	0.05
Methane	91.29
Ethane	2.54
Propane	0.16
iso-Butane	0.03
n-Butane	0.01
iso-Pentane	0.01
n-Pentane	trace
Hexanes	trace
Heptanes plus	0.02
	100.00

Calculated gas gravity (air = 1.000) = 0.626

Calculated gross heating value = 995 Btu per cubic foot of dry gas at 15.025 psia and 60°F.

Laboratory opening pressure = 60 psig at 75°F.

Table 5.16 ORIENTATION OF WELLBORE BREAKOUTS DERIVED FROM ORIENTED CALIPER LOG RUN IN MWX-2 PALUDAL ZONE

Depth (ft)	Eccentricity (Minor/major axis)	Orientation (degrees from north)
6600	0.98	180
6675	0.98	140
6700	0.99	276
6750	0.99	178
6850	0.99	168
7050	0.8*	180
7225	0.98	248
7275	0.98	241
7300	0.98	187
7375	0.8*	210

*Coaly Region

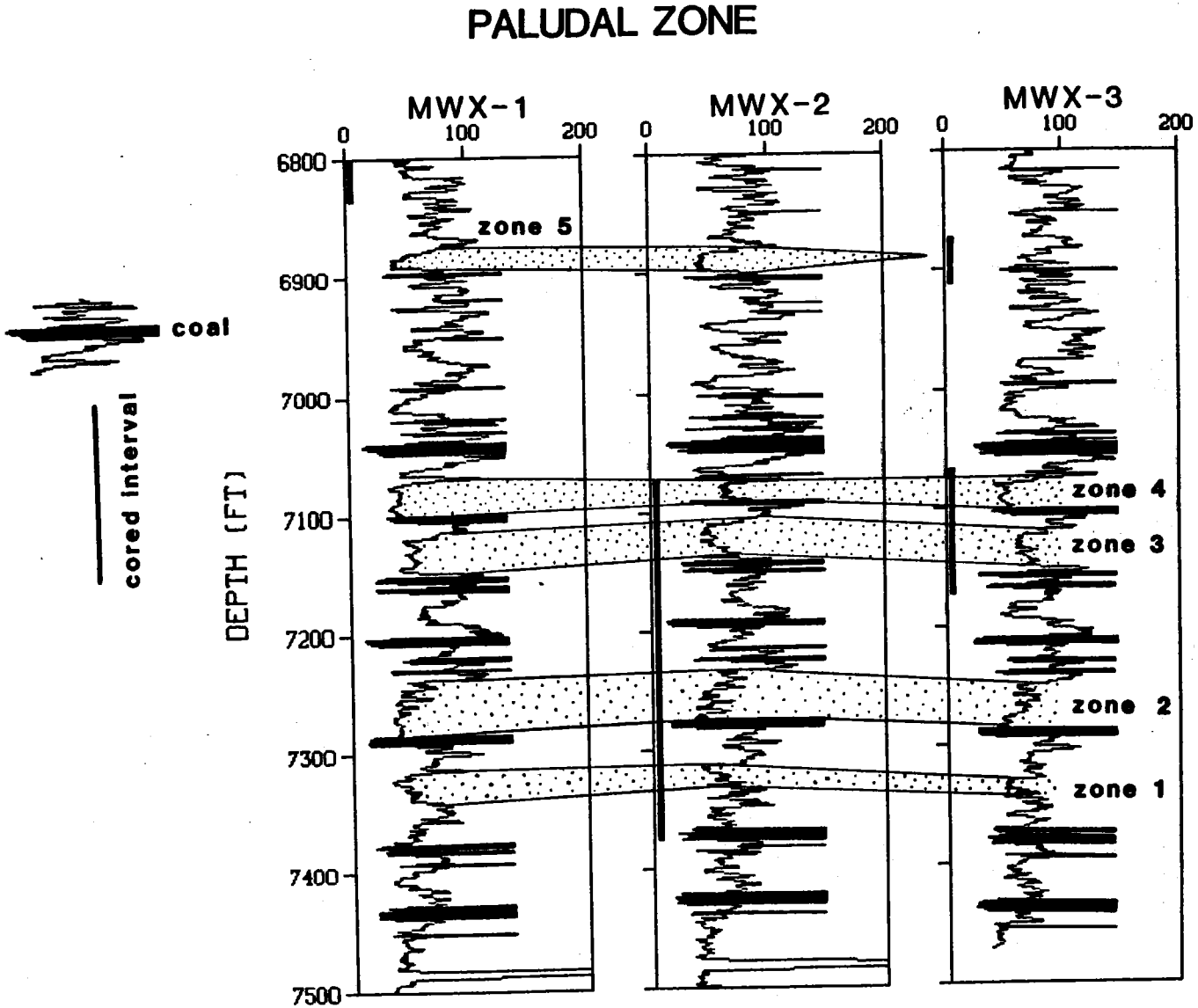

Figure 5.1 The Paludal Interval in the Three Wells

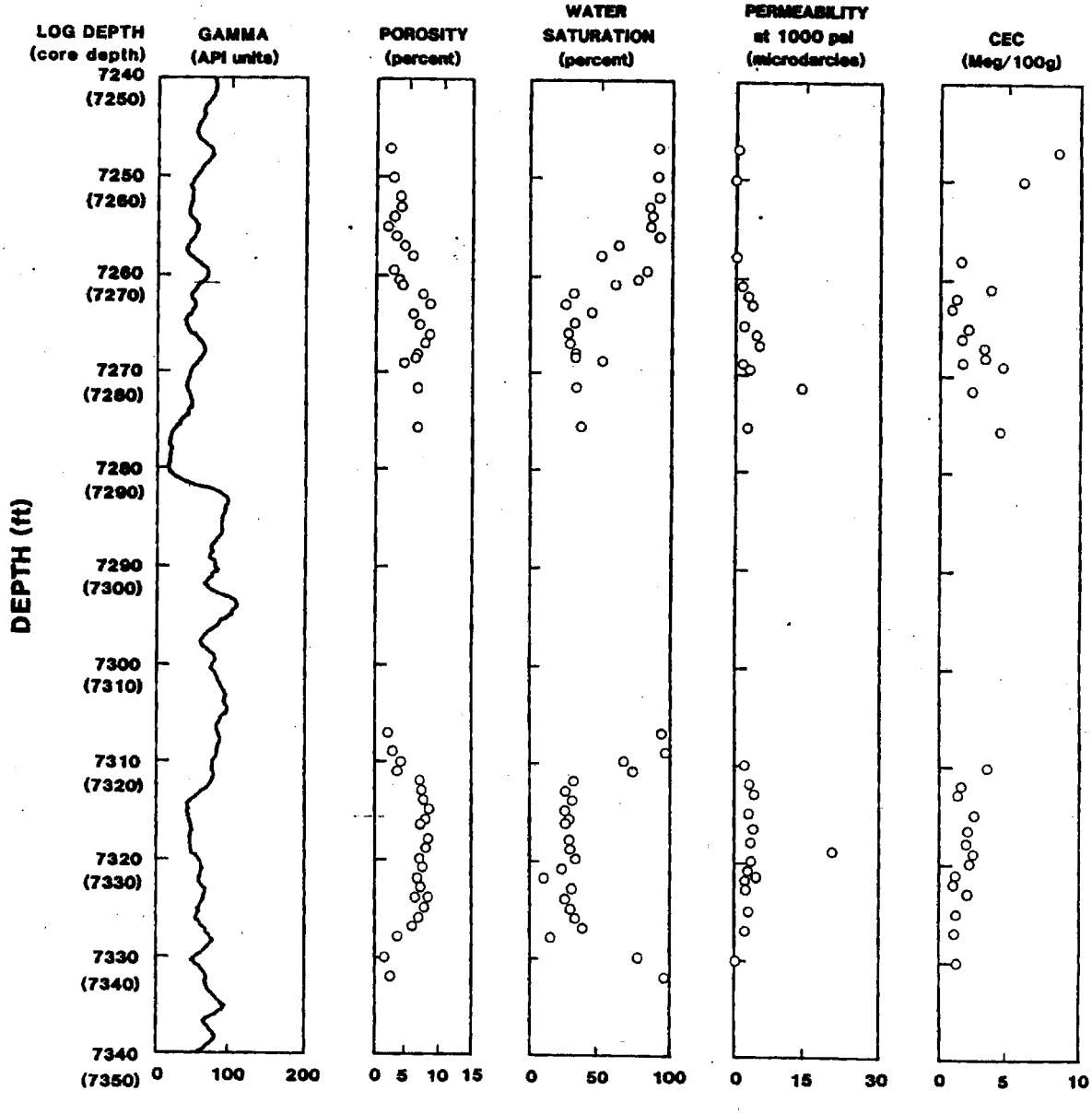

Figure 5.2 Reservoir Properties of Zones 1 and 2 in MWX-2

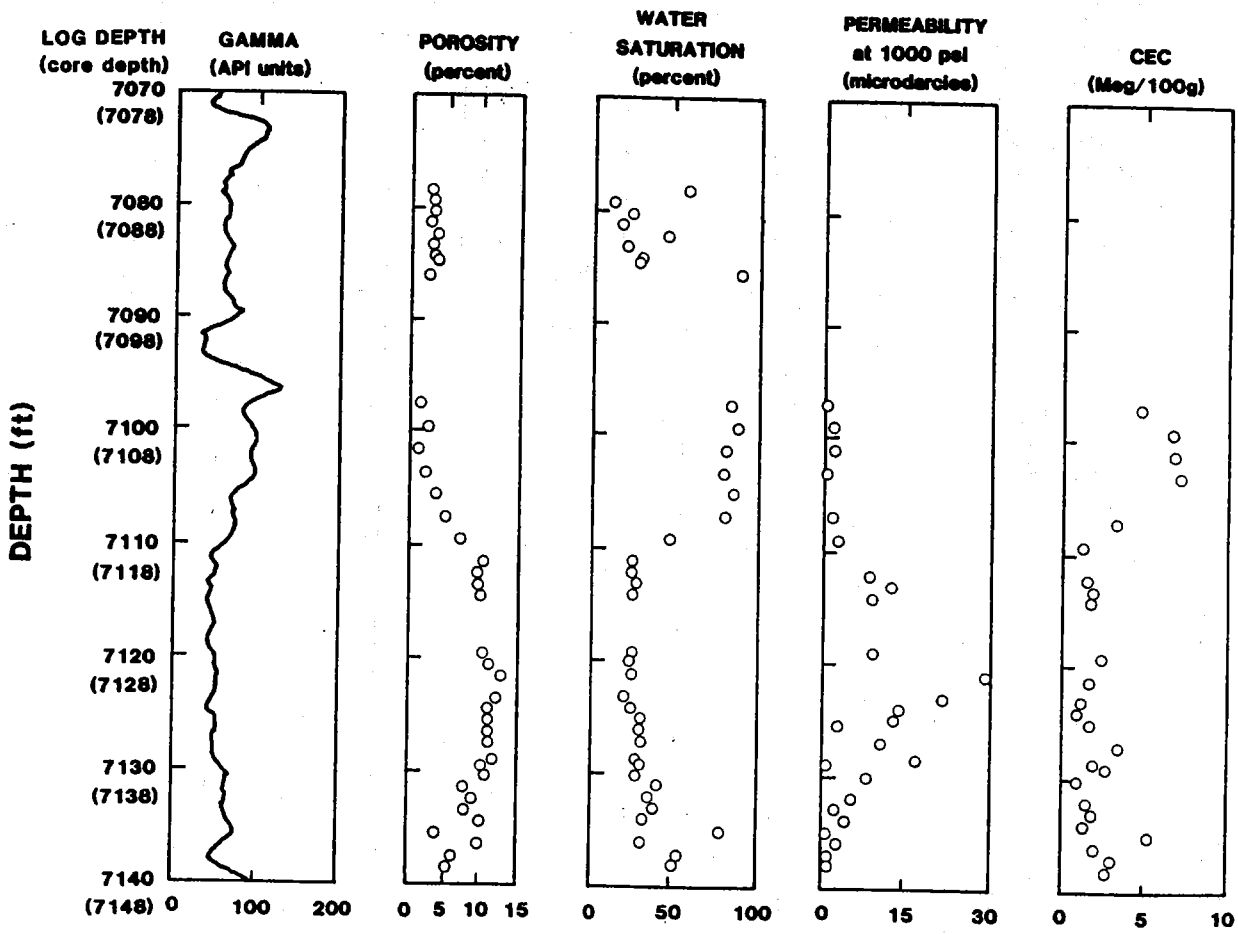

Figure 5.3 Reservoir Properties of Zones 3 and 4 in MWX-2

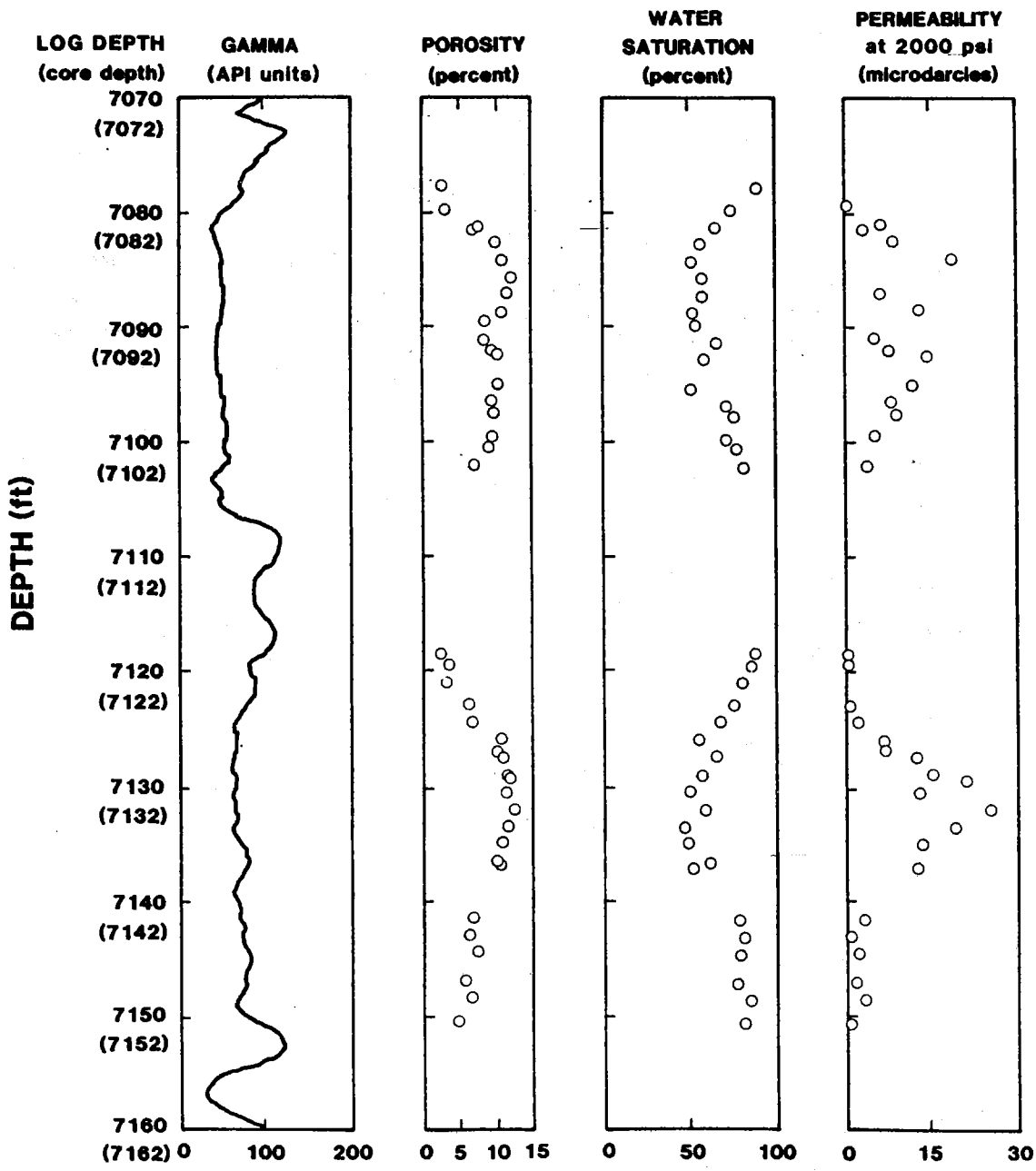

Figure 5.4 Reservoir Properties of Zones 3 and 4 in MWX-3

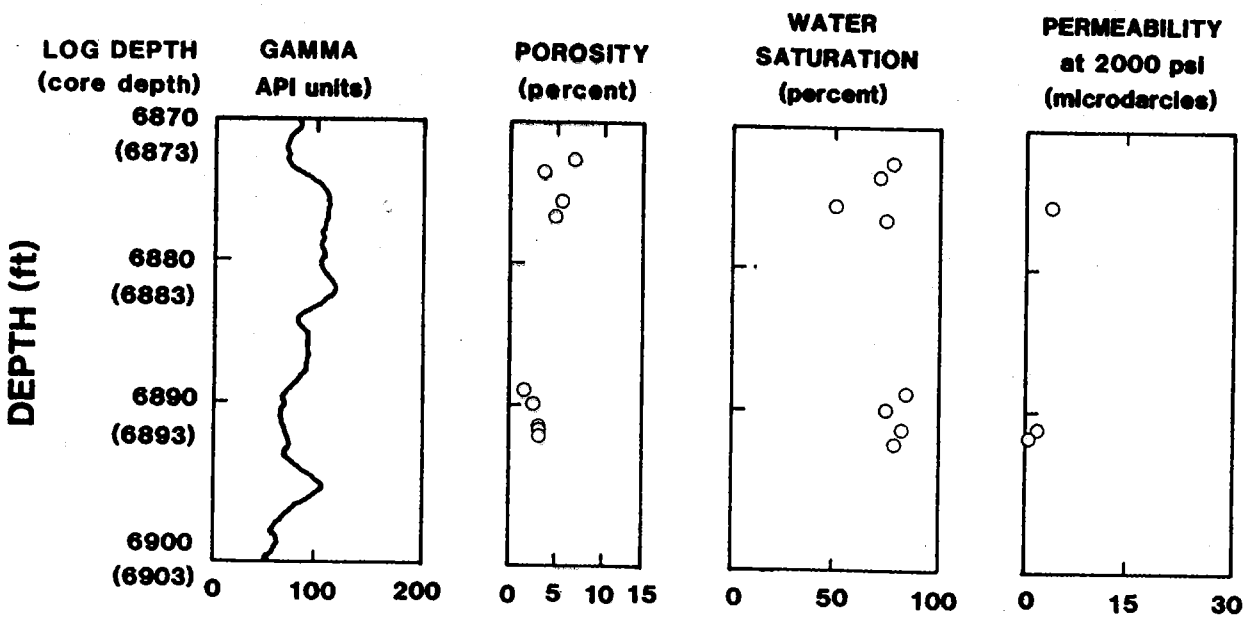

Figure 5.5 Reservoir Properties of Zone 5 in MWX-3

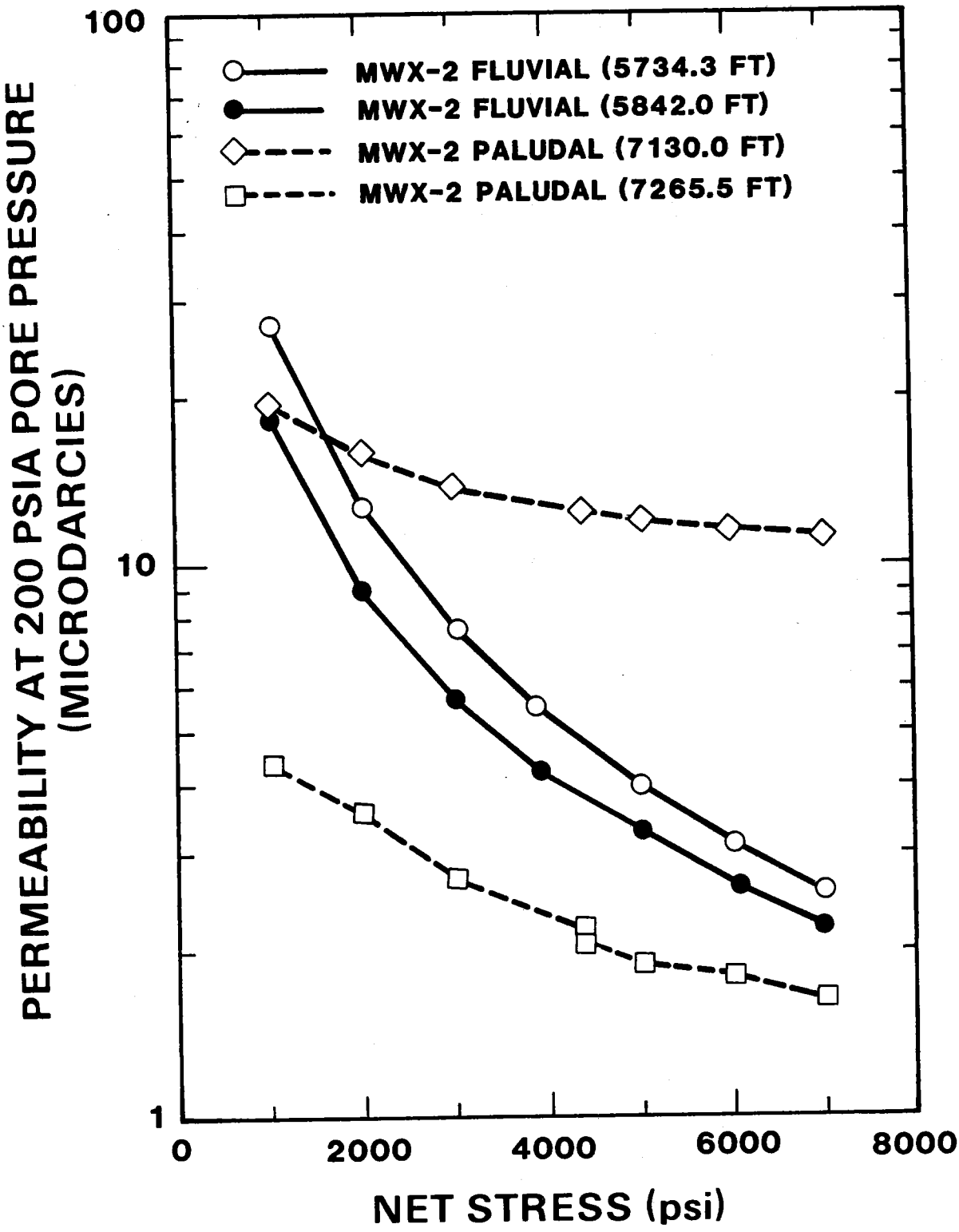

Figure 5.6 Permeability as a Function of Net Stress

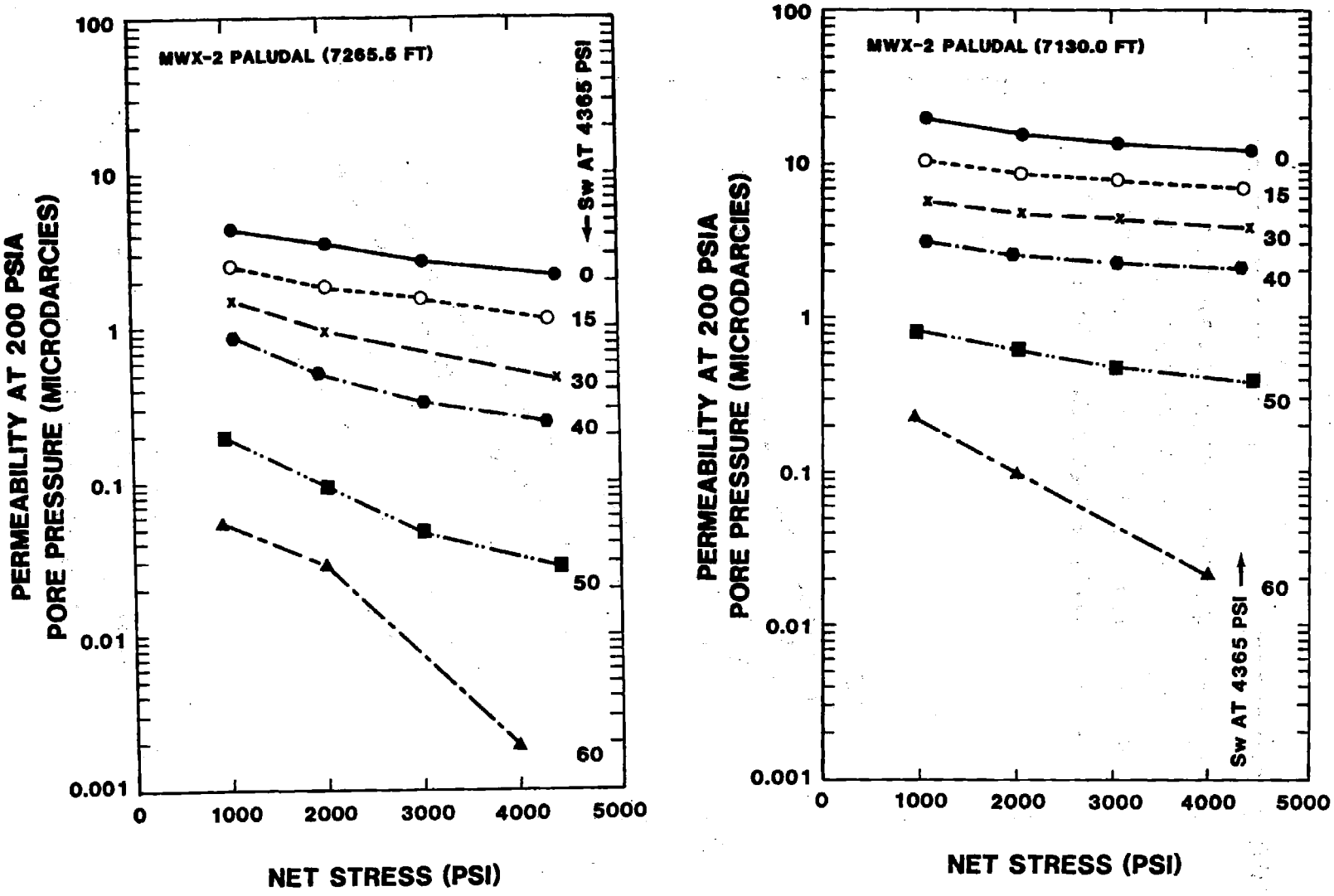

Figure 5.7 Permeability as a Function of Net Stress and Water Saturation: (a) Zone 2, (b) Zone 3

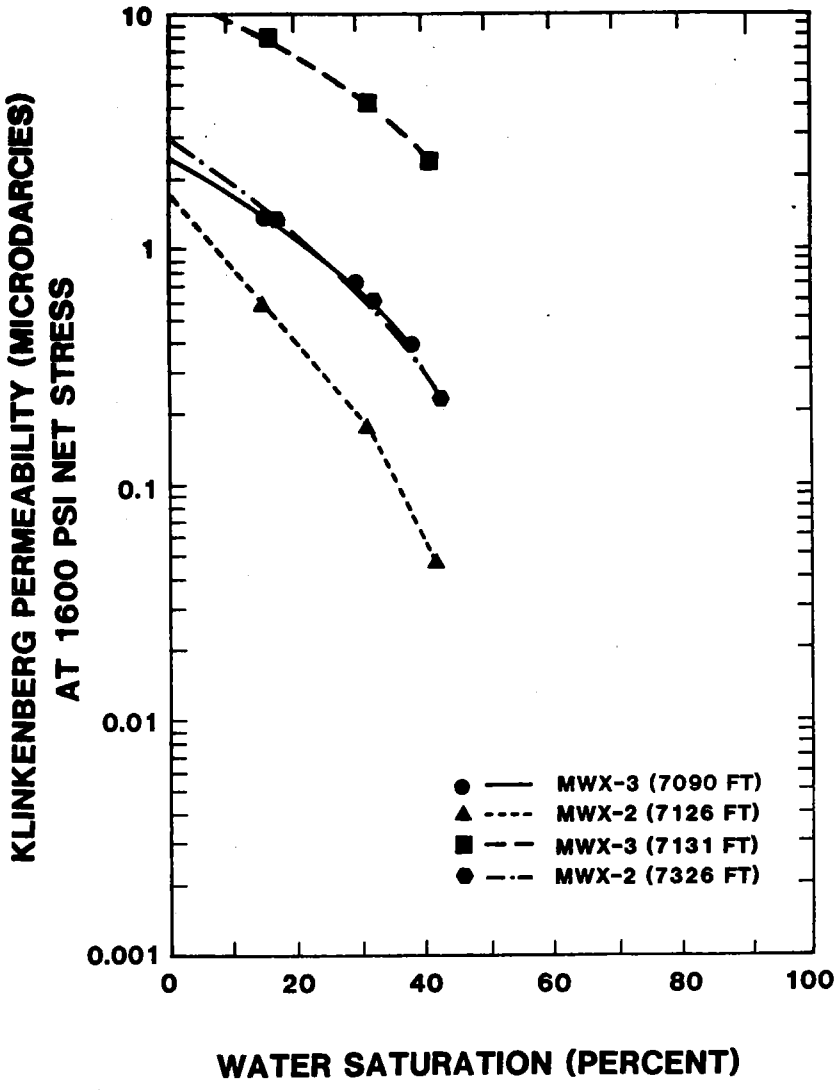

(a)

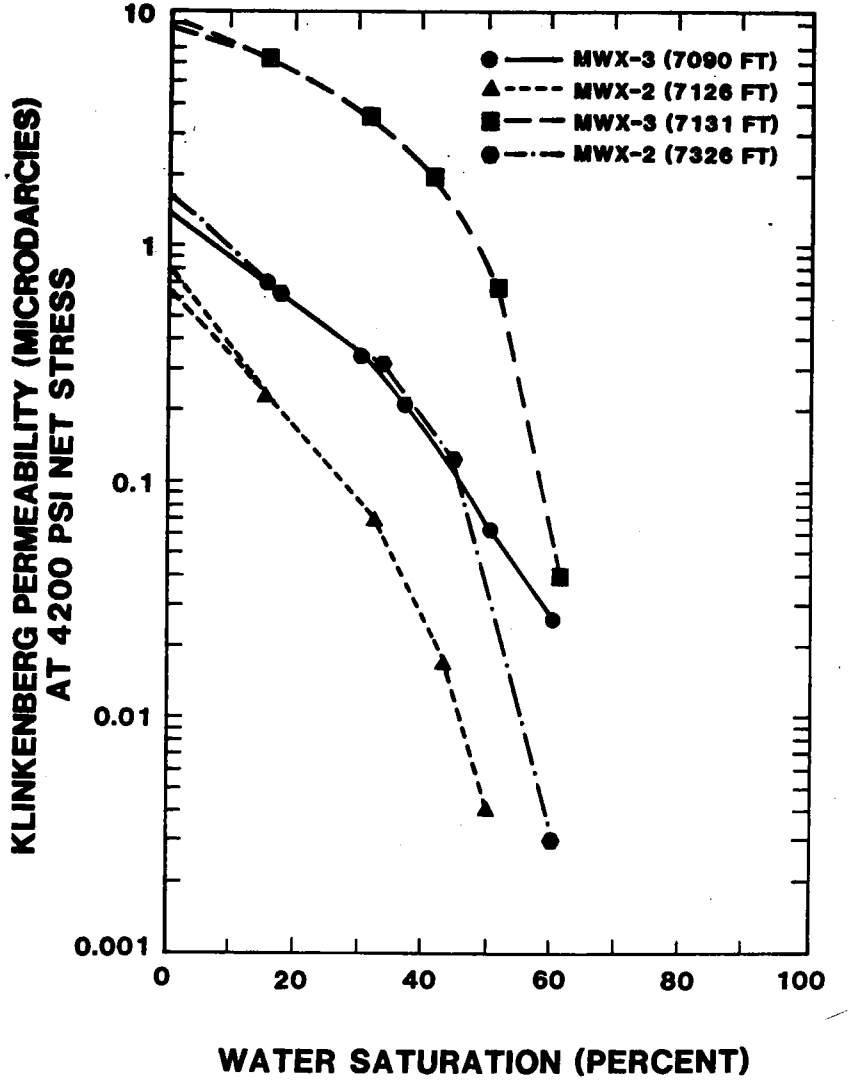

(b)

Figure 5.8 Permeability as a Function of Water Saturation and Net Stress: (a) 1600 psi (b) 4200 psi

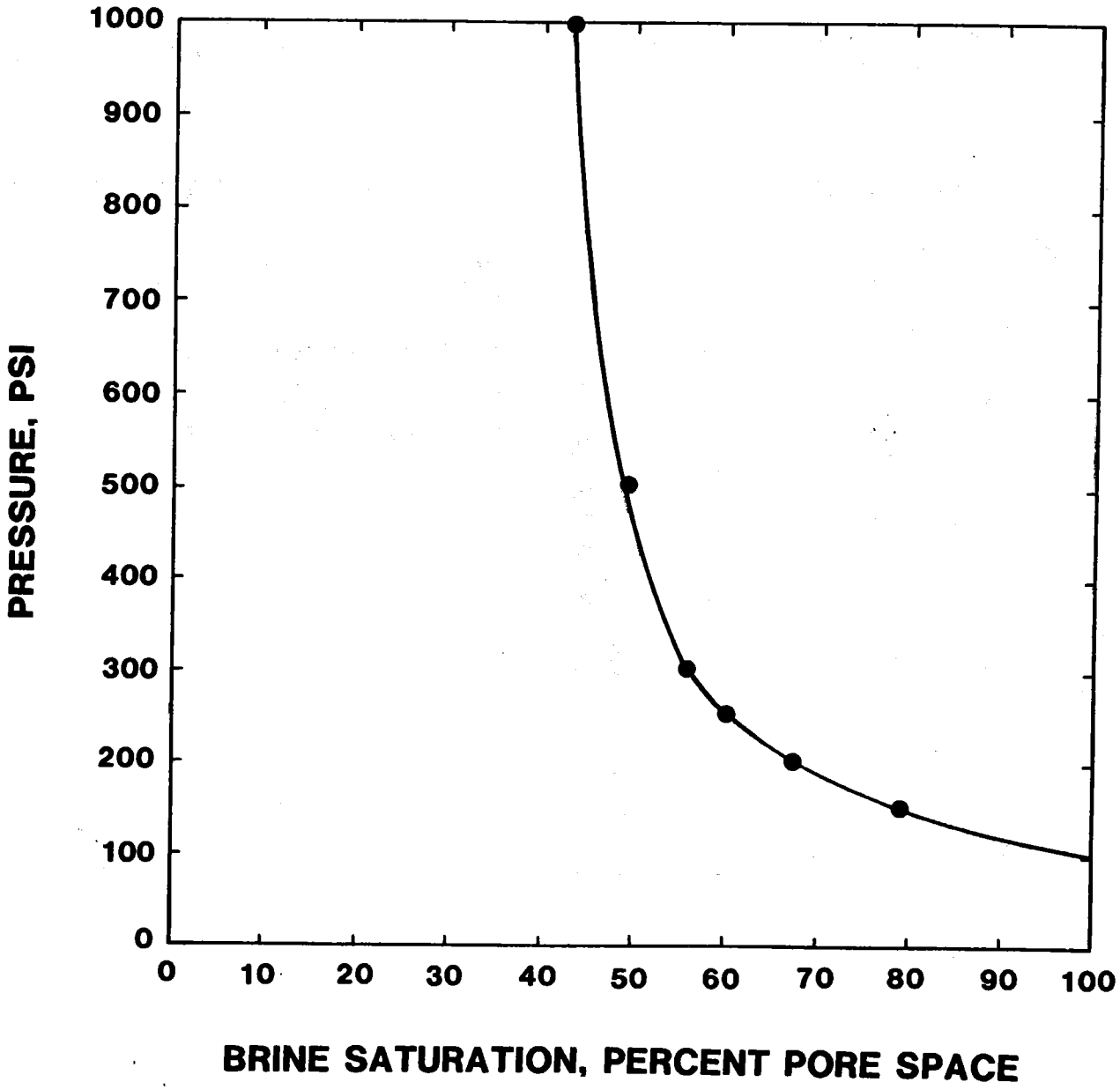

Figure 5.9 Example Capillary Pressure Curve (MWX-2, 7285.3 ft)

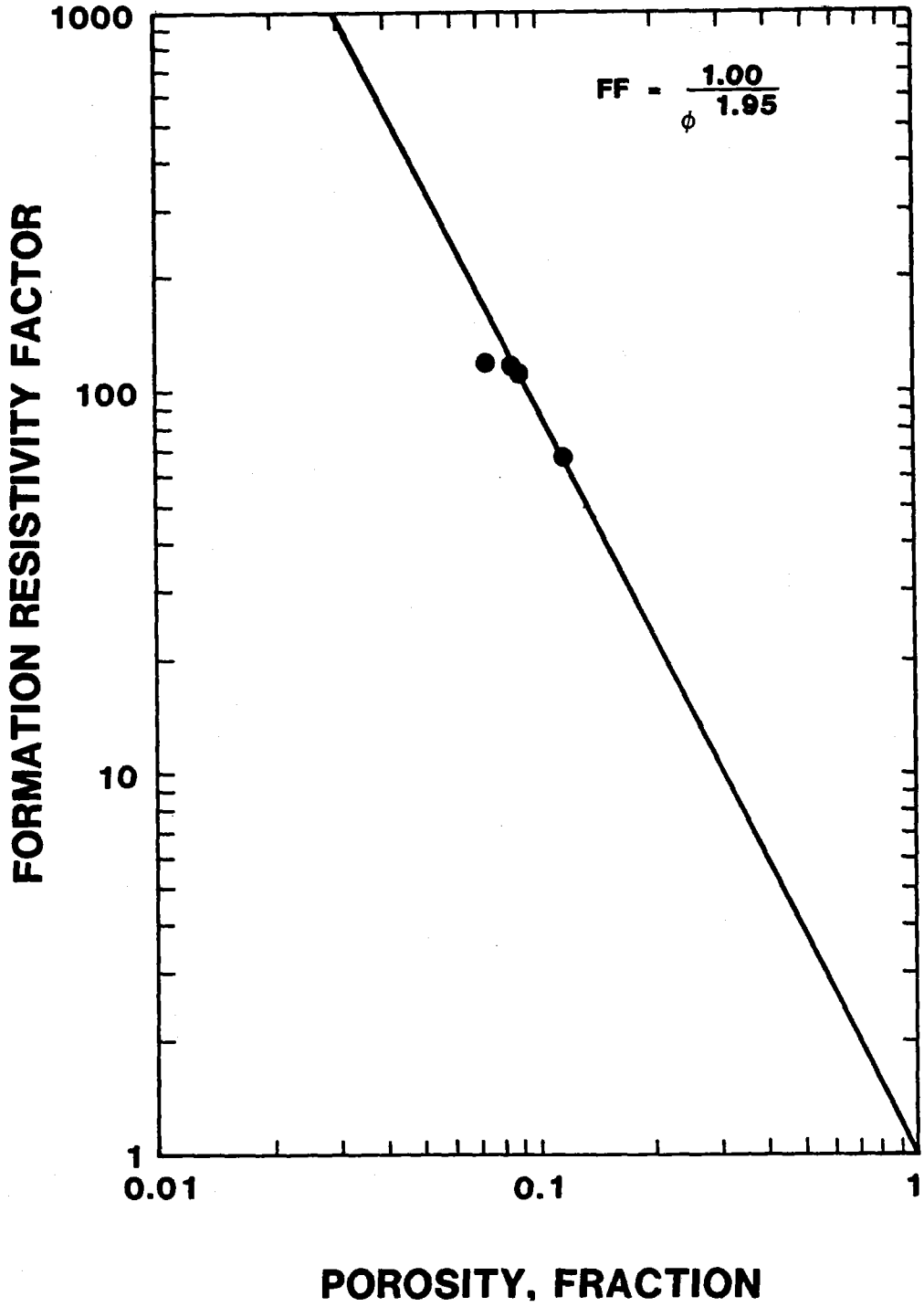

Figure 5.10 Formation Factor at 3600 psi Overburden Pressure

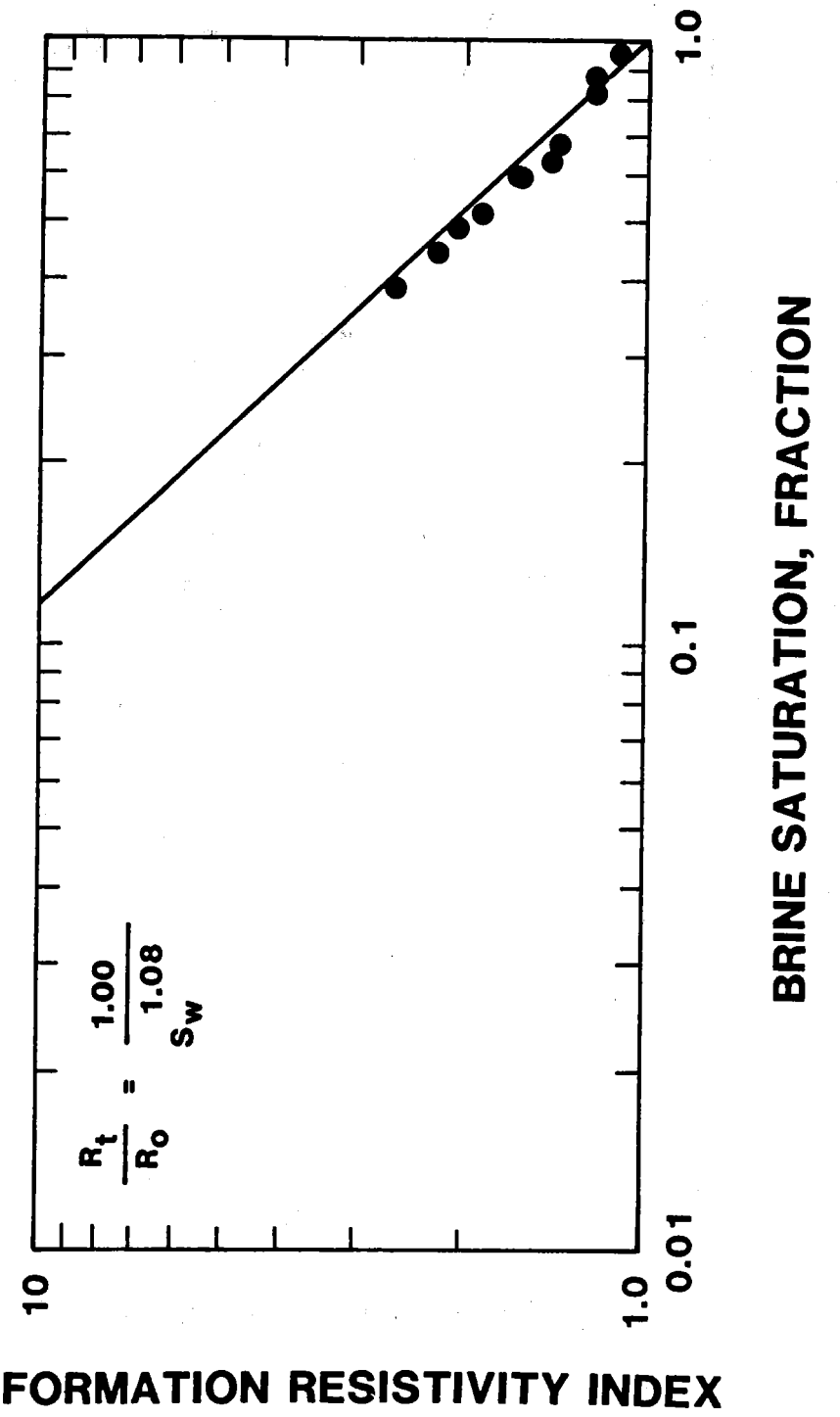

Figure 5.11 Resistivity Index at Ambient Pressure

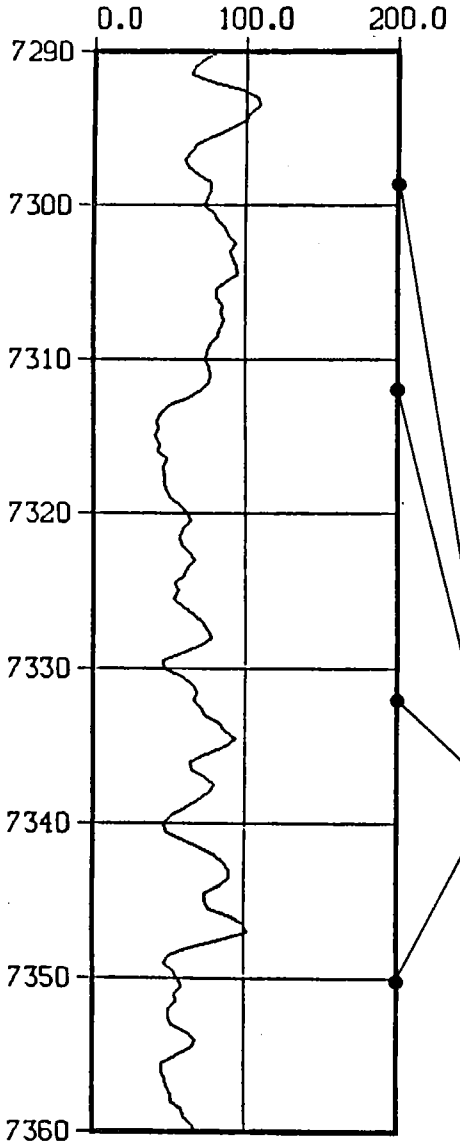

LITHOLOGY	INTERVAL (FT.) (LOG DEPTH)	BRAZILIAN TESTS	TRIAXIAL TESTS			
		TENSILE STRENGTH (MPa)	CONFINING PRESSURE (MPa)	COMPRESSIVE STRENGTH[a] (MPa)	E^b (GPa)	ν^b
Carb. Mudstone	(7298.1-7299.0) 7308.1-7309.0*	-8.38 ± 1.97	20 30	157.2 164.3	28.4 27.8	.20 .27
Silty Sandstone	(7312.1-7312.8) 7322.1-7322.8*	-6.25 ± 0.10	20 30	190.2 222.3	29.6 30.5	.23 .25
Carb. Mudstone	(7332.9-7333.9) 7342.9-7343.9*	-9.11 ± 0.88	20 30	178.5 272.8	30.1 41.2	.19 .25
Silty Sandstone	(7350.9-7352.0) 7360.9-7362.0*	-7.31 ± 0.22	0 10 20 30	93.3 122.2 92.8 245.0	23.1 25.0 18.9 30.0	.19 .16 .13 .25

*Sealed at well
[a] Ultimate Axial Stress Difference
[b] Calculated for Stresses Between 20 and 60 Percent of Ultimate Axial Stress Difference.

Figure 5.12 Mechanical Rock Properties of Zone 1 in MWX-2

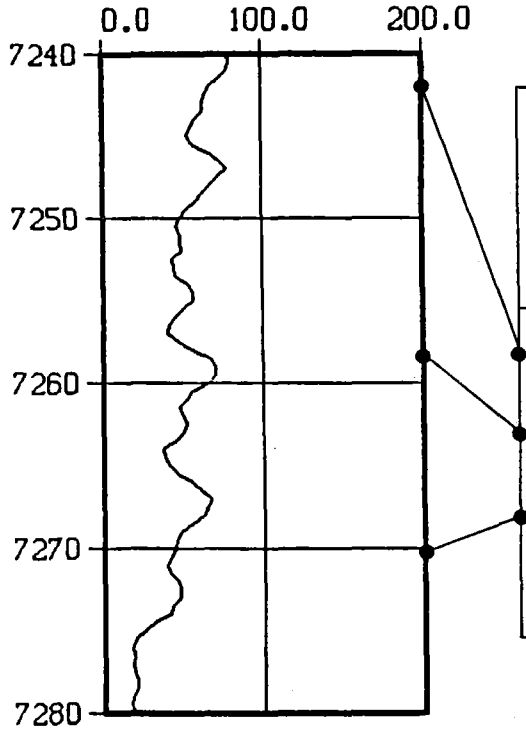

LITHOLOGY	INTERVAL (FT.) (LOG DEPTH)	BRAZILIAN TESTS	TRIAXIAL TESTS			
		TENSILE STRENGTH (MPa)	CONFINING PRESSURE (MPa)	COMPRESSIVE STRENGTH[a] (MPa)	E^b (GPa)	ν^b
Siltstone	(7243.0-7244.0)	-12.07 ± 4.80	20	190.3	29.2	.22
	7253.0-7254.0*		30	192.7	28.6	.25
Silty Sandstone	(7258.8-7259.5)	-5.60 ± 1.27	20	159.5	25.7	.21
	7268.8-7269.5*		30	172.6	26.4	.24
Sandstone	(7270.5-7271.5)	-8.19 ± 0.93	0	137.7	-	-
	7280.5-7281.5*		20	250.8	36.8	.23
			30	275.8	36.5	.23

* Sealed at well
[a] Ultimate Axial Stress Difference
[b] Calculated for Stresses Between 20 and 60 Percent of Ultimate Axial Stress Difference.

Figure 5.13 Mechanical Rock Properties of Zone 2 in MWX-2

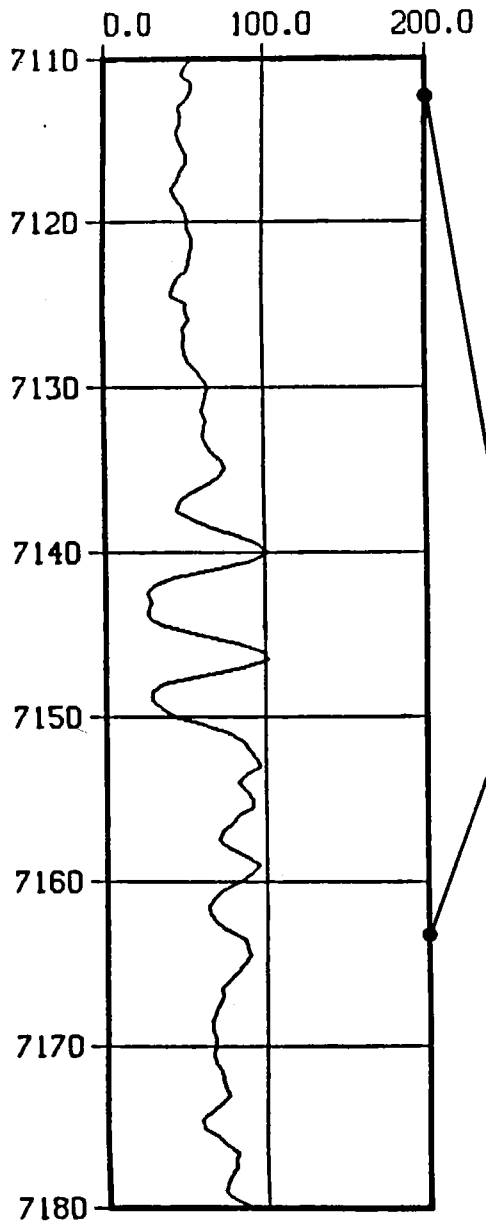

LITHOLOGY	INTERVAL (FT.) (LOG DEPTH)	BRAZILIAN TESTS	TRIAXIAL TESTS			
		TENSILE STRENGTH (MPa)	CONFINING PRESSURE (MPa)	COMPRESSIVE STRENGTH[a] (MPa)	E^b (GPa)	ν^b
Sandstone	(7113.0-7113.7)	-6.36 ± 0.84	20	171.1	25.5	.23
	7121.0-7121.7*		30	194.9	25.9	.25
Siltstone	(7152.0-7153.0)	-9.38 ± 2.16	0	103.8	34.3	.24
	7162.0-7163.0*(2)	(2 & 3)	10 (3)	252.8	43.8	.16
	(7164.0-7165.0*)		20 (3)	152.2	28.2	.22
	7171.1-7172.0*(3)		30 (3)	165.2	28.1	.23

* Sealed at well
[a] Ultimate Axial Stress Difference
[b] Calculated for Stresses Between 20 and 60 Percent of Ultimate Axial Stress Difference.

Figure 5.14 Mechanical Rock Properties of Zone 3 in MWX-2

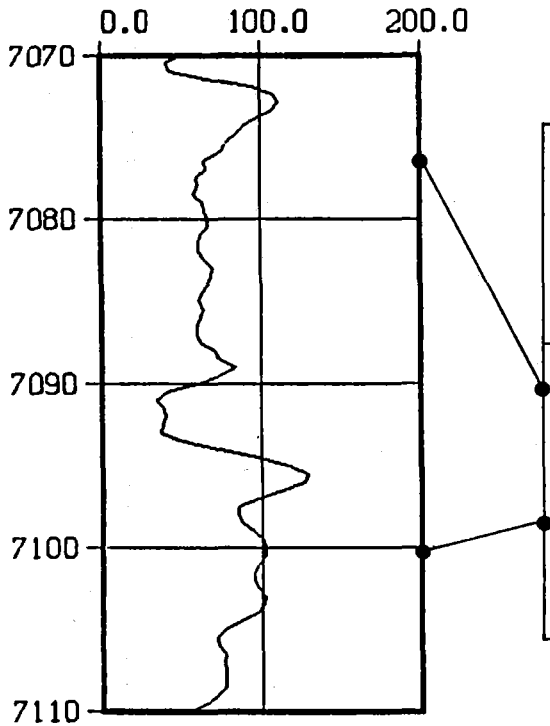

LITHOLOGY	INTERVAL (FT.) (LOG DEPTH)	BRAZILIAN TESTS	TRIAXIAL TESTS			
		TENSILE STRENGTH (MPa)	CONFINING PRESSURE (MPa)	COMPRESSIVE STRENGTH[a]	E^b (GPa)	ν^b
Sandstone	(7077.6-7079.0)	-9.77 ± 1.41	0	198.7	41.6	.18
	7085.6-7087.0*		10	259.0	40.9	.20
			20	294.4	40.3	.22
			30	221.4	29.5	.24
Siltstone	(7100.3-7100.9)	-9.81 ± 1.16	10 (1)	98.9	36.0	.26
	7108.6-7108.3*(1)		20 (2)	153.4	18.4	.13
	7107.6-7108.3*(2)		30 (1)	192.6	31.1	.20
	(7099.6-7100.3)		50 (1)	257.0	35.3	.22

* Sealed at Well
[a] Ultimate Axial Stress Difference
[b] Calculated for Stresses Between 20 and 60 Perent of Ultimate Axial Stress Difference

Figure 5.15 Mechanical Rock Properties of Zone 4 in MWX-2

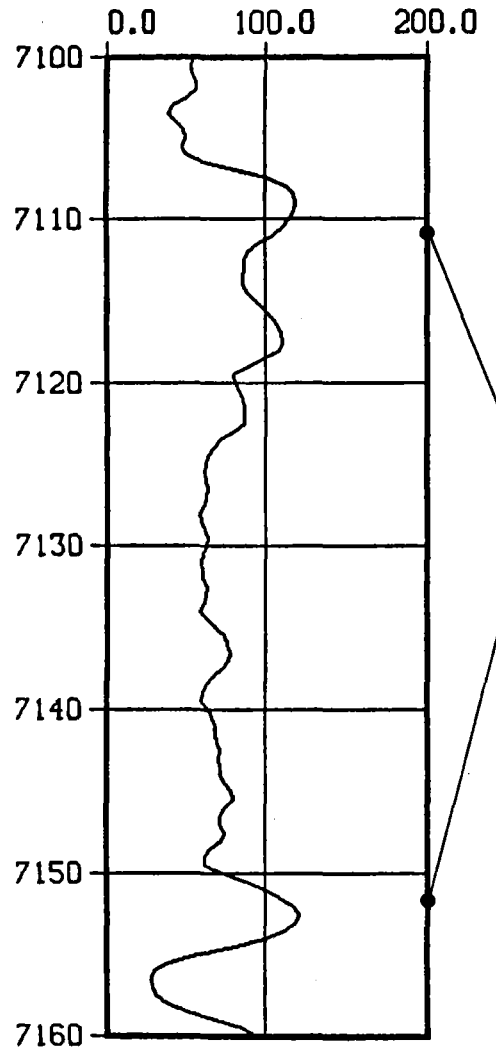

LITHOLOGY	INTERVAL (FT.) (LOG DEPTH)	BRAZILIAN TESTS	TRIAXIAL TESTS			
		TENSILE STRENGTH (MPa)	CONFINING PRESSURE (MPa)	COMPRESSIVE STRENGTH[a] (MPa)	E^b (GPa)	ν^b
Shale	(7111.1-7112.4) 7112.1-7113.4*	-7.5 ± 1.2	0	87.1	27.1	.26
			10	130.8	24.0	.24
			20	155.6	24.5	.23
			30	175.5	23.7	.23
Sandstone	(7151.7-7132.9) 7132.7-7133.9*	-7.9 ± 04	0	81.5	17.9	.24
			10	126.2	23.0	.22
			20	172.2	28.1	.22
			30	181.2	24.7	.18

* Sealed at the Well
a Ultimate Axial Stress Difference
b Calculated for Stresses Between 20 and 60 Percent of Ultimate Axial Stress Difference.

Figure 5.16 Mechanical Rock Properties of Zone 3 in MWX-3

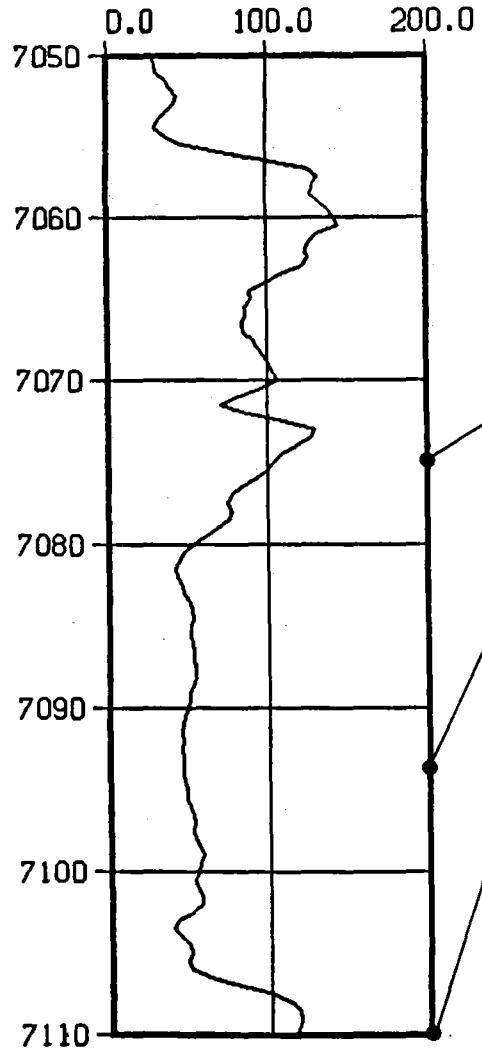

LITHOLOGY	INTERVAL (FT.) (LOG DEPTH)	BRAZILIAN TESTS	TRIAXIAL TESTS			
		TENSILE STRENGTH (MPa)	CONFINING PRESSURE (MPa)	COMPRESSIVE STRENGTH[a] (MPa)	E^b (GPa)	ν^b
Shale	(7075.2-7075.9)	-9.9 ± 4.4	20	164.1	22.8	.21
	7076.2-7076.9*		30	161.8	21.8	.26
			50			
Sandstone	(7094.75-7095.1)	-5.6 ± 1.3	0	84.1	17.8	.25
	7094.75-7096.1*		10	131.8	21.7	.19
			20	167.1	23.9	.19
			30	199.1	24.3	.19
			50	-	-	-
Shale	(7111.1-7112.4)	-7.5 ± 1.2	0	87.1	27.1	.26
	7112.1-7113.4*		10	130.8	24.0	.24
			20	155.6	24.5	.23
			30	175.5	23.7	.23
			50	-	-	-

* Sealed at Well
a Ultimate Axial Stress Difference
b Calculated for Stresses Between 20 and 60 Percent of Ultimate Axial Stress Difference

Figure 5.17 Mechanical Rock Properties of Zone 4 in MWX-3

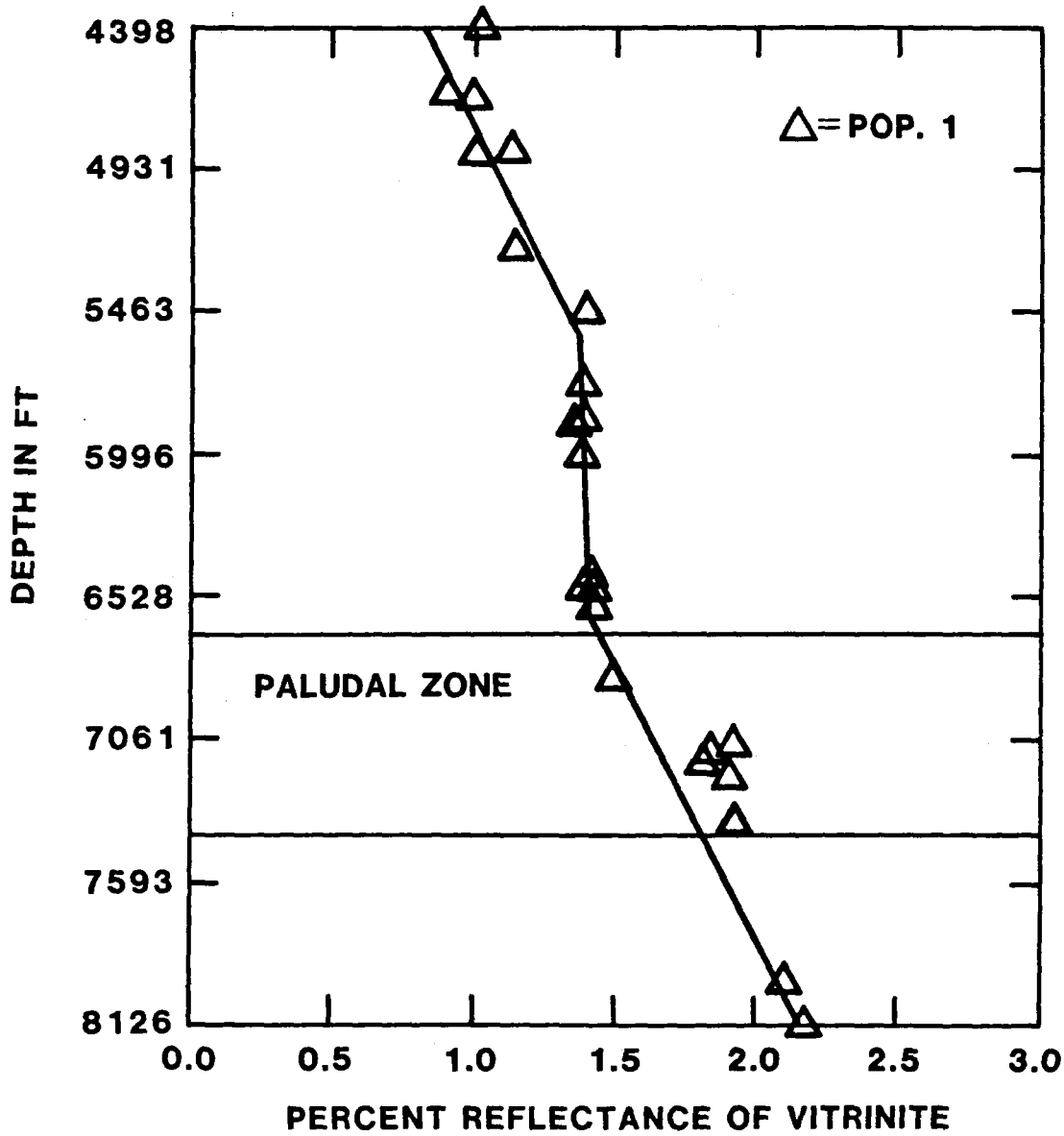

Figure 5.18 Vitrinite Reflectance of Carbonaceous Rocks at MWX Site

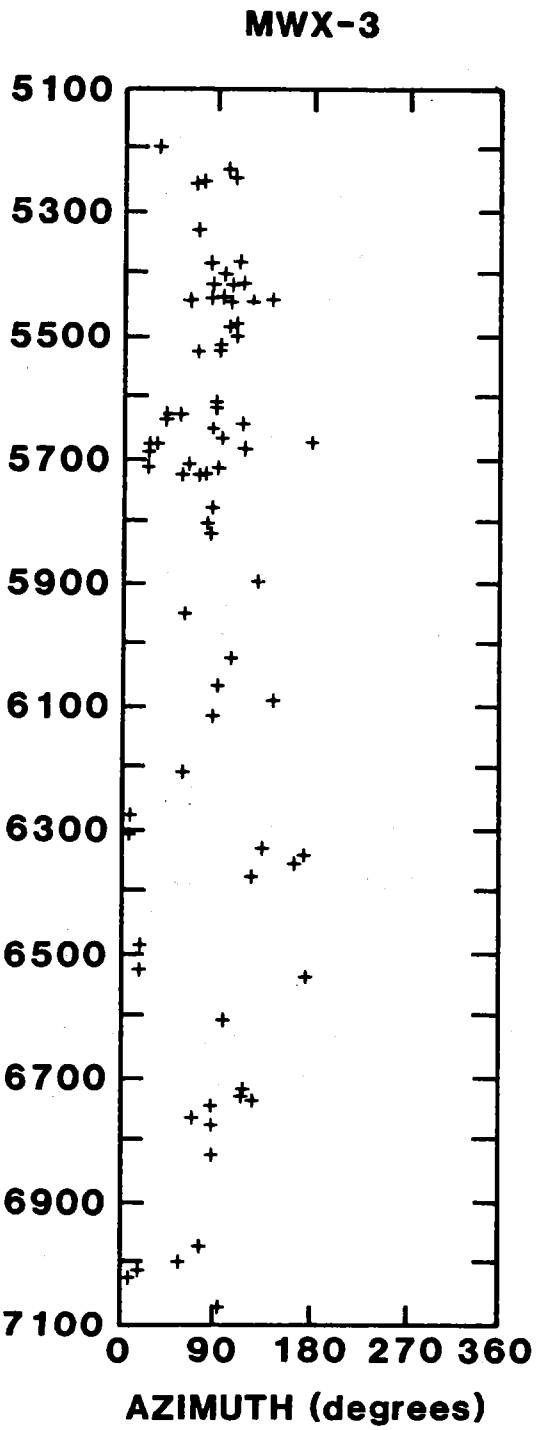

Figure 5.19 Depth Distribution of Natural Fractures From Televiewer Logs

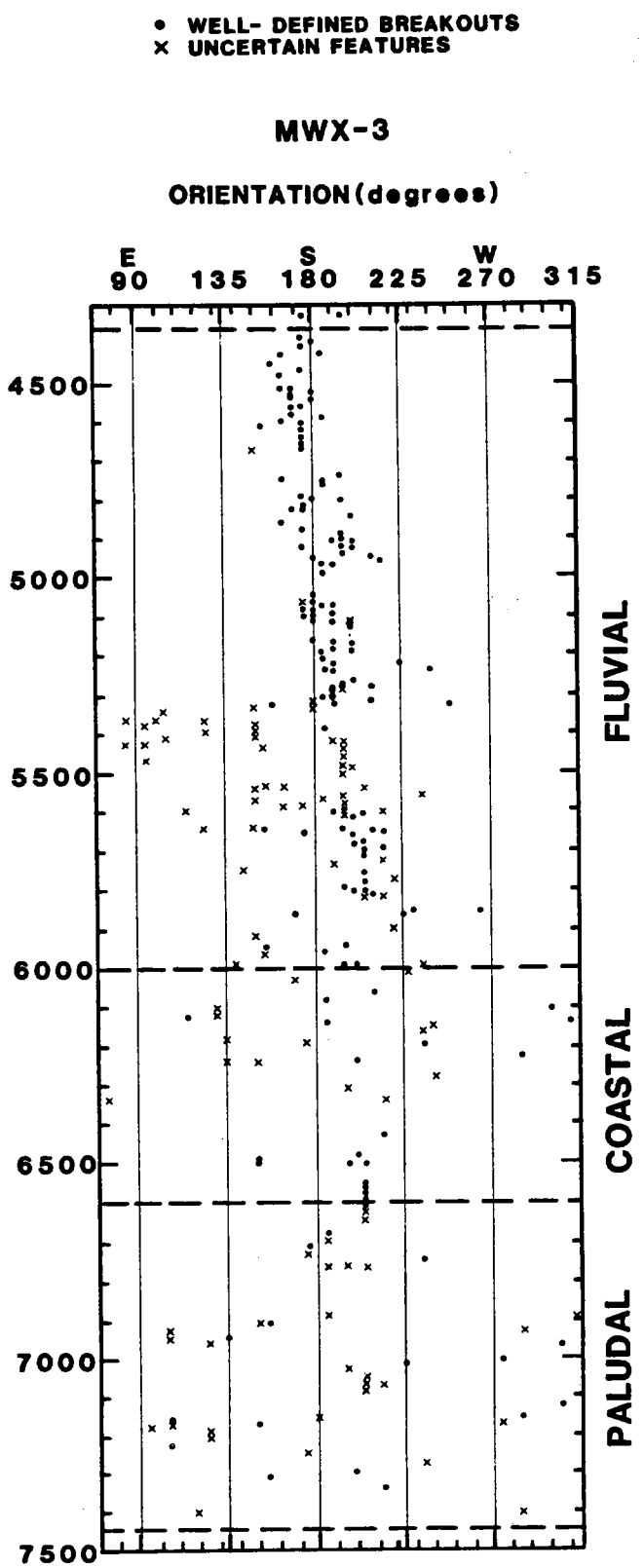

Figure 5.20 Directional Depth Distribution of Breakouts From Televiewer Logs

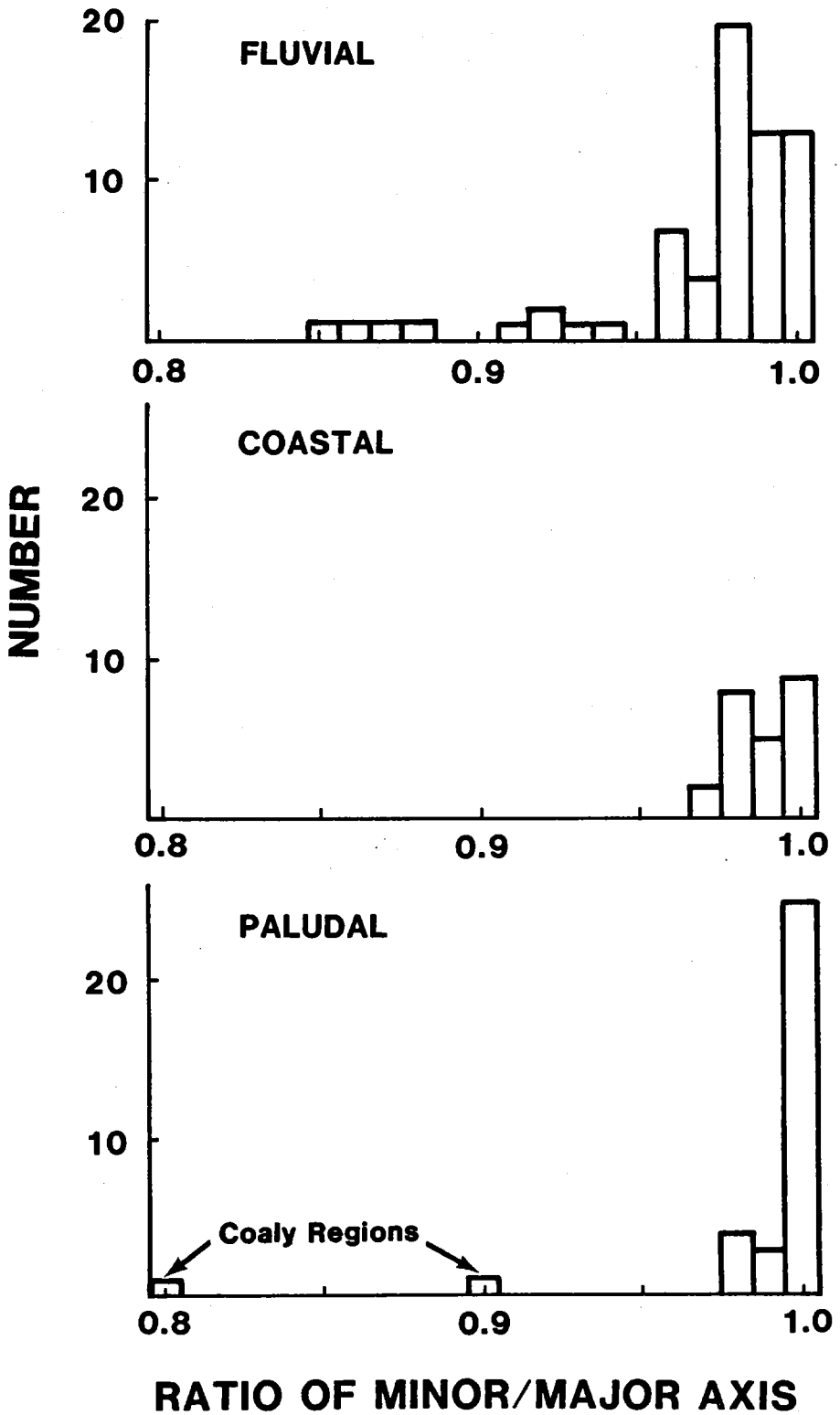

Figure 5.21 Borehole Eccentricity From Four-Arm Oriented Caliper Log

6.0 IN SITU STRESS

N. R. Warpinski
Sandia National Laboratories

6.1 OBJECTIVE

The objective of the in situ stress testing program is to determine the vertical distribution of the minimum, principal, horizontal in situ stress for the purpose of evaluating hydraulic fracture containment. In addition, these stress data are important for estimating net stresses on reservoir rocks (for property measurements), on prop packs, and on natural fracture systems. Anelastic strain recovery (ASR) measurements are made to provide the orientation of the stress field and information on the maximum, principal horizontal in situ stress.

6.2 IN SITU STRESS MEASUREMENTS

The vertical distribution of the minimum principal horizontal in situ stress (hereafter referred to as the minimum in situ stress, σ_{Hmin}) is now known to have a significant influence on hydraulic fracture geometry. Perkins and Kern[1] noted its importance with respect to fracture height and Simonson et al[2] demonstrated how to calculate fracture height in a nonuniform, but symmetric, stress field. Laboratory[3,4,5] and mineback[6] experiments have proven the effect of minimum in situ stress differences on fracture height, but, as yet, field experiments have not yielded conclusive results. This is primarily due to the lack of detailed in situ stress data and viable fracture height measurement techniques. In addition, few in situ stress measurements have been obtained in intervals where core is available so that stress/rock-property correlations can be attempted. In this study, we attempt to overcome these previous limitations by conducting a careful series of minifrac stress tests. Additionally, we have several ASR measurements[7] that were made on oriented core in this interval.

6.2.1 Hydraulic Fracturing Measurements

The stress testing technique and the instrumentation and equipment used are fully described in Ref. 8. Briefly, small volume hydraulic fractures (5-200 gal) are conducted through a 2-ft perforated interval. Pressures are measured accurately with a quartz crystal oscillator gage. A bottomhole closure tool is employed to provide fast shut-ins with no wave or storage effects. Typically, three to six repeat injections are performed for each zone. The instantaneous shut-in pressure (ISIP) is determined from the pressure record and the minimum, principal, horizontal, in situ stress, σ_{Hmin} is taken to be

$$\sigma_{Hmin} = \text{ISIP}. \qquad (1)$$

In these tests, no information can be obtained about the maximum, principal, horizontal, in situ stress.

6.2.2 Strain Recovery Measurements

The anelastic strain recovery (ASR) technique used in these experiments is described in references 9-11. Briefly, it consists of mounting clip-on displacement gages on a piece of sealed, oriented core and recording the time-dependent relaxation of that core. In vertical holes in flat-lying beds, as in these experiments, only four gages are used (one vertical, three horizontal). Determination of the orientation of the stress field has been shown to be straightforward.[12,13] for many sedimentary rocks and is readily calculated by determining the principal strain orientations. If there is no rock fabric to distort the results, the maximum strain direction is found to be coincident with the maximum stress direction as determined by an independent method.

The determination of the stress magnitudes is more complicated and requires a model for the ASR process. Blanton[14] and Warpinski and Teufel[15] have developed different types of viscoelastic models to explain the behavior. Both models will be used in the analyses of these data.

Blanton's[14] solution, referred to as the direct model, is the easiest to apply and yields a direct calculation of the stresses from the principal strains as

$$\sigma_1 = (\sigma_v - \alpha P) \frac{(1-\nu)\Delta\varepsilon_1 + \nu(\Delta\varepsilon_2 + \Delta\varepsilon_v)}{(1-\nu)\Delta\varepsilon_v + \nu(\Delta\varepsilon_1 + \Delta\varepsilon_2)} + \alpha P \qquad (2)$$

and

$$\sigma_2 = (\sigma_v - \sigma P) \frac{(1-\nu)\Delta\varepsilon_2 + \nu(\Delta\varepsilon_1 + \Delta\varepsilon_v)}{(1-\nu)\Delta\varepsilon_v + \nu(\Delta\varepsilon_2 + \Delta\varepsilon_1)} + aP \qquad (3)$$

where the $\Delta\varepsilon$ are the change in the principal strains between any two times, ν is Poisson's ratio, P is the pore pressure, α is a poroelastic constant (approximately unity for Mesaverde rocks at the MWX site) and the subscripts 1 and 2 refer to the maximum horizontal and minimum horizontal directions, respectively, while v refers to the overburden. Important assumptions for the direct model include (1) linearly viscoelastic behavior, (2) constant Poisson's ratio throughout the relaxation process, (3) step unloading of the in situ stresses at the moment of coring, (4) a constant a throughout the process, (5) a vertical overburden stress and wellbore, and (6) isotropic behavior.

Warpinski and Teufel's model,[15] referred to as the strain-history model (because it requires fitting a theoretical model to the measured strain history), requires a least-squares fit of the entire strain data set to an expected relaxation behavior of the form

$$\varepsilon_r(t) = (2\sigma_1 \cos^2\theta + 2\sigma_2 \sin^2\theta - \sigma_1 \sin^2\theta - \sigma_2 \cos\theta^2 - \sigma_v)\, J_1(1-e^{-t/t_1}) + (\sigma_1 + \sigma_2 + \sigma_v - 3P)\, J_2\,(1 - e^{-t/t_2}) \qquad (4)$$

and

$$\varepsilon_v(t) = (2\sigma_v - \sigma_1 - \sigma_2)\, J_1\, (1 - e^{-t/t_1}) + (\sigma_1 + \sigma_2 + \sigma_v - 3P)\, J_2\, (1 - e^{-t/t_2}) \quad (5)$$

where θ is the gage angle orientation with respect to the maximum stress, J_1 and J_2 are distortional and dilatational creep compliance arguments (i.e., equilibrium values of the creep compliance), t is the time, t_1 and t_2 are deviatoric and dilatational time constants, respectively, and the subscript r refers to radial direction in the horizontal plane. Important assumptions for this model are (1) the rock behaves as if it is linearly viscoelastic, (2) the behavior is exponential and can be described using standard models, (3) the overburden stress and wellbore are vertical, (4) the rock is isotropic, (5) the bulk modulus of the grain material is not a viscoelastic parameter (since the process appears to be a fracturing phenomenon), and (6) step unloading of the in situ stresses at the moment of coring.

Once the data are least-squares fitted, estimates of the stresses can be made if J_1 is known. Alternately, a minifrac in tandem with the ASR data (so σ_2 is known) allows J_1 to be determined. In this study, we are still acquiring data on J_1 and thus cannot use these data to determine σ_2. We currently use the minifrac data to calculate σ_2 and J_1.

The primary problems with ASR are (1) to ascertain that rock fabric is not distorting the results and (2) to obtain sufficient data to use either viscoelastic model to calculate stress magnitudes.

6.3 STRESS TEST RESULTS

Figure 6.1 and Table 6.1 show all of the in situ stress measurements which were performed in the depth interval 6800-7450 ft. These data

include the following:

- nine stress tests in MWX-2,
- three stress tests in MWX-3 (in MWX-3 because of the proximity to the fault at 7050-7080 ft),
- a breakdown of zone 2 in MWX-1 for well testing,
- a breakdown of zones 3 and 4 in MWX-3, and
- a step-rate flowback test in zones 3 and 4 in MWX-1.

These results show that the stimulation interval, between about 7060 and 7140 ft is a low stress region compared to the surrounding shales, mudstones, siltstones, and coals. However, the high stress region above the frac interval is fairly thin and will probably not act as a barrier for large treatments. Outside of this one case, no other large stress difference is apparent for other sandstone-shale pairs. Generally, there is no good correlation between stress and rock type or rock properties.

The confidence level and the accuracy of these measurements are not nearly as good as the stress test measurements in the marine section. We believe that the major reason for this is the difference in lithology between the two intervals. In the marine zone, nearly all of the tests were conducted in fairly massive sections--even in the shales. On the other hand, the paludal interval is characterized by a very complex lithologic environment where rock types vary dramatically over feet or even inches, as described in Section 3.0. The complexity of the rock variations is especially evident outside of the main channel sands. Since the most important stress tests are in the barrier zones, this is probably typical of the rocks in which we are attempting to measure the stress.

We suspect that each of these thin layers has somewhat different stresses and a hydraulic fracture stress test probably provides a weighted average of the individual stresses. As we increase the volume of the fracture, we then intersect new layers with different stresses or possibly containment barriers. Barriers would result in higher treatment pressures since the crack would need to grow under a more confined configuration. Obviously, interpretation of some of our tests could be difficult in these situations. Discussion and examples of some stress test pressure records are given in the next section.

6.3.1 Stress Test Data

This section shows example pressure records from each of the stress tests. In some cases, all of the injections are shown to demonstrate a feature of testing in this lithology. For most zones, only the best or a representative pressure curve from one of the injections is shown.

Starting with the deepest paludal interval, the third pump of the test in a coal at 7423-25 ft is shown in Figure 6.2. This is not a good pressure record for determining the ISIP and is typical of all of the tests in this zone. While there were indications of fracturing in the first injection, the possibility exists that a hydraulic fracture was never created and fluid was only injected into pre-existing cleats. In such a case, the minimum stress would be higher than 6900 psi.

A stress test for a silty sandstone was attempted at 7394-96 ft but some mechanical problems developed and we conducted a quick, surface-monitored breakdown pump to ascertain that all systems were functioning. When we tried to conduct a normal stress test with downhole instrumentation, we developed communication with an adjacent set of perforations. Thus the only data from this zone are the surface data from the breakdown pump, shown in Figure 6.3. Accuracy of this test is obviously poor, as is usually the case with surface-monitored tests.

The second injection of a test in a mudstone at 7303-05 ft is shown in Figure 6.4. This is a good test with a clear ISIP. The somewhat higher-than-expected leakoff for an impermeable mudstone may be due to some loss along the cement. Cement bond in this coaly region was often poor. This result is a case where a barrier material is low stress compared to nearby reservoir rocks.

Zone 2, a channel sandstone, was tested at 7263-65 ft in MWX-2. The pressure record from injection #4 is shown in Figure 6.5. In this test there was some concern about the large pressure drop at shut in (900 psi), but the ISIP appeared to be fairly clear. It is possible that the fracture initiated through a cement channel rather than directly out the perforation, resulting in large entrance pressure drops. The stress appears to be fairly high for a sandstone, but in MWX-2, paludal zone 2 is silted out and we are probably testing the channel margin.

The complete pressure records for a siltstone at 7206-7208 ft are shown in Figure 6.6. In the first three pumps there is a large pressure drop at shut-in; this 600-700 psi drop is much larger than we feel comfortable with. In the last two pumps we investigated the effect of rate on the treatment pressure and we found that it is very rate sensitive. Additionally, the pressure-rate behavior is nearly linear, as shown in Figure 6.7. This suggests that the restriction is the entrance to the fracture or a microannulus in the cement. Other common restrictions would be rate-squared dependent. However, even with this problem we still manage to get good ISIPs. The stress here is about 6900 psi.

The second pump of a test at 7169-71 ft in a mudstone is shown in Figure 6.8. These data are good, the ISIP is clear, and the character is typical of shales and mudstones. This high stress provides a good barrier below the paludal frac interval.

A mudstone above the paludal frac interval at 7068-70 ft was tested in MWX-3. The fifth pump is shown in Figure 6.9. The ISIP in all tests appeared to be quite low. While it seemed probable from earlier pressure records that some fracturing had been initiated, high flow rates (30-45 gpm) were required and the possibility exists that the fracture broke up along the cement into an overlying coal or down into the sand and these stress data are not correct. This is an unusually low stress for a mudstone or siltstone.

The results from a coal at 7048-7050 ft in MWX-3 are shown in Figure 6.10. The first pump at 13 gpm obviously did not fracture the rock; instead fluid was probably being injected into the cleats. In subsequent pumps we injected KCl water at 20-30 gpm and were able to propagate a fracture. In the third test we changed rate to make certain that we were propagating a fracture (a small pressure response). For the last three tests we did not get a clear ISIP, but this was also typical of the other coal tested. Whether this is due to material properties of the coal, the cleat system, or some other cause is unknown. In this test we believe that the minimum stress is about 7200 psi with an accuracy of $\pm$100 psi.

The third injection into a mudstone at 7032-34 ft in MWX-3 is shown in Figure 6.11. This is a good, typical mudstone test with a reasonably clear ISIP. Again, the high leakoff after shut-in may be due to the cement bond.

Figure 6.12 shows the complete pressure record for a mudstone in MWX-2 at 7010-12 ft. (The first pump is not shown because the bottomhole closure tool did not seat properly and no shut-in occurred.) This record is typical of shale, mudstone, and siltstone tests; that fracturing occurred is clear from only the first two or three pumps. ISIP's, however, continue to become more easily defined with successive pumps and are generally consistent.

The first pump for a sandstone at 6963-65 ft is shown in Figure 6.13. Some kind of initial breakdown occurred before a clear fracture began propagating. The ISIP is not completely clear, but is certainly definable within ±50 psi.

The complete pressure record for a test at 6928-30 ft in a mudstone is shown in Figure 6.14. This shows an example of another common problem: variable-treatment pressures. The first test is not shown because of a failure to seat the bottomhole closure tool. In pumps #2 and #3, we obtained a 6700 psi injection pressure and an ISIP of about 5850 psi. Since the pressure drop at shut-in was larger than desired, we tried pumping at 35 gpm and obtained much higher pressures. We subsequently reduced the rate to 8.5 gpm on the next test and still had high treatment pressures, indicating that for the most part there was not a rate effect. Believing it to be a volume (or size) effect, we bled down the tubing to atmospheric pressure (at the surface) and let the previously injected frac fluid bleed out of the fracture. After a sufficient bleed time, we reinjected at 10 gpm, obtaining much lower treatment pressures, and a good ISIP near 5800 psi. We took 5830 psi as an average stress in this zone.

Because of all these complexities and problems, the determination of the stress in this interval is more difficult and less accurate than similar measurements in the marine section. In addition, it may require both rate and volume tests to diagnose the stress condition. Nevertheless, useful and valid measurements can be made in this lithologic environment if care is taken and these measurements provide valuable data for hydraulic fracture design and analysis.

6.3.2 Additional Stress Data

Some additional stress data were obtained from breakdowns of sand intervals and a step-rate/flowback test in the paludal frac interval.

The step-rate/flowback test result is discussed in section 8.2, but the data are included in Table 6.1.

The initial breakdown of zone 2 in MWX-1 from 7256-7284 ft was started by conducting three small pumps at ~10 gpm. The first pump is shown in Figure 6.15. This test shows an ISIP of about 6300 psi with a very small pressure drop at shut-in.

The initial breakdown of the paludal frac interval in MWX-3 at 7080-7102 ft and 7126-7142 ft was conducted at 50 gpm and is shown in Figure 6.16. The ISIP is fairly clear at about 5800 psi.

6.4 ASR DATA AND RESULTS

Only ASR data taken from measurements on core from MWX-3 will be presented and discussed. The MWX-3 data were obtained with the improved ASR gages, and are more accurate and reliable than earlier data.[10] Additionally, we did not include any data where the rock had a pre-existing fabric.

Figure 6.17 shows example ASR data for a paludal sandstone at 7146 ft. We show the actual ASR data for the four gages taken at hour intervals and the calculated strain-history fits of the data using the strain-history model.[15] Using this model, we are able to estimate the total strain which the piece of core has undergone. (Note that the format for Figure 6.17 does not imply that the rock has experienced negative strains in early times. For convenience, we preserve the original form of the data, i.e., all strains start at zero at the time the core is first instrumented, and the early negative strains represent the anelastic strains that the core experienced before being instrumented.)

We can see that the data quality is excellent for these Mesaverde sandstones and the theoretical viscoelastic strain-history model[15] fits the measured response very well. In all of our tests the vertical strain relaxation is considerably greater than the horizontal strain relaxation, implying that the maximum principal stress is the overburden stress.

The orientation of the maximum horizontal strain, which is found to be coincident with the maximum horizontal stress if no rock fabric distorts the results, is -65.7° with respect to the zero degree gage (a minus sign indicates that the angle is between the 0° and 90° gages), which is N62°W. Calculated principal strain data and corresponding strain orientations for all paludal data are given in Table 6.2. (No error analysis of the strain orientation is given because the results are derived from the least-squares fit of the data. Error analyses of nonlinear regressions are nontrivial. The largest source of error is the orientation survey, which at best is accurate to 5°-10°.)

Calculated stresses using the direct model are 7238 and 6408 psi. Using the strain-history model with minifrac data to provide calibration points, we calculate a maximum stress of 7085 psi. Comparisons of these results with minifrac data and estimates of errors will be made later. Tabulated stress calculation results are given in Table 6.3.

Figure 6.18 shows ASR results for a paludal mudstone at 7154 ft. The most obvious feature of all of mudstone tests is the horizontally isotropic strain behavior. There is no preferred horizontal strain orientation, and by implication, no preferred horizontal stress orientation, in the mudstones. The overburden strain relief is generally somewhat greater, which may be due to transverse anisotropy or an overburden stress that is somewhat greater than the horizontal stresses.

Calculations of the horizontal stresses using the direct model yield values of 7177 and 7029 psi for the maximum and minimum horizontal

stresses. The strain-history model yields a value of 7162 psi for the maximum stress. Little difference is observed between the two horizontal stresses in the mudstones.

Additional ASR tests of sandstones at 6896, 6897, and 7147 ft are shown in Figures 6.19, 6.20, and 6.21, respectively. All these tests look similar to the sandstone at 7146 ft discussed previously. As seen in Table 6.2, we usually find closest agreement in the derived stress direction for samples close to one another; such closely spaced tests have the same orientation survey shot point. The largest source of error in the ASR technique is the accuracy of the orientation survey.[10]

The stress data obtained using the ASR technique are shown in Figure 6.22 and are compared to the minifrac stress data. The gamma log on the left is for the MWX-3 well and is shown to illustrate major lithological features and the locations of the major intervals. In addition, we have highlighted the sandstones in which we have stress data so that the effect of lithology on the stress state is clearer. All of the other tests are in clay-rich rocks which are predominantly mudstones. Minimum stresses are shown in the center graph and consists of minifrac stress test results, ASR results using the direct model and one DSCA (differential strain curve analysis) measurement provided by Dowell-Schlumberger. The straight line is the average overburden stress as determined by an integration of the density log; this integration yields 1.05±.1 psi/ft for an overburden stress gradient through this section. The right-side graph shows the maximum horizontal stress and consists of ASR results using both the direct and the strain-history models and the one DSCA result. The overburden stress calculation is also shown here.

The most important feature shown in Figure 6.22 is the effect of lithology on the minimum horizontal in situ stress. Minimum horizontal stress differences between sandstones and the abutting clay-rich rocks are generally greater than 1000 psi. This is an important factor in

designing stimulation treatments for these reservoirs. Some of the minifrac stress measurements were not made in the same well as the gamma log shown in Figure 6.1. Since significant changes in lithology can occur over short lateral distances, care must be taken when comparing lithology with stress in this interval. We also emphasize that these large stress contrasts occur over distances of a few feet.

The horizontal stresses in the mudstones are close in magnitude to the overburden stress, although on the average they are slightly below the overburden value. Using the ASR results, little horizontal stress difference is seen in any of the mudstones. In the sandstones, horizontal stress differences are about 600-800 psi, which is in agreement with the results of an open-hole stress test[11] conducted in the Rollins marine sandstone at 7560 ft. The stress difference measured in the Rollins was 800 psi.

The orientation of the maximum horizontal stress, as determined primarily from ASR data, is shown as a function of depth in Figure 6.23. Also included are the DSCA measurement, one result[11] from an open-hole hydraulic fracture impression packer in the marine Rollins sandstone at 7560 ft, one hydraulic fracture azimuth measurement using borehole seismic diagnostic (Section 10.0), and four ASR data points at 7560 ft from marine interval tests.[11] We see that the maximum horizontal stress direction is 10-30° south of east. Good agreement is seen for all techniques.

The scatter seen in Figure 6.23 is normal for most ASR measurements and is due to several factors. These include the accuracy of the orientation survey (largest source of error) and gage placement, thermal and dehydration effects, and heterogeneities of the core. Generally the DSCA agrees well with the ASR data. Only sandstone results are shown because the shales have no preferred orientation.

6.5 HYDRAULIC FRACTURE CONTAINMENT

The main purpose for the stress tests is to aid in the design and analysis of hydraulic fracturing treatments. Figure 6.24 shows the best estimate of the vertical stress distribution around zones 3 and 4. These zones were the fracture interval for the Phase I (Section 8.2) and Phase II (Section 8.4) stimulations. The accuracy of some of these measurements is only ± 100 psi and we may have missed some important stress features because of the complexity of the lithology. Nevertheless, the coal directly above the frac interval has the highest stress which we measured in the entire paludal interval and the shale or mudstone above it has a fairly high stress also.

Figure 6.25 shows the expected height growth out of the frac zone as a function of the treating pressure above the in situ stress. This calculation is based on an equilibrium solution of a pressurized crack in a layered stress medium. It requires 525 psi to break through the coal and 625 psi to break up through the zone above it. For higher treating pressures, unbounded growth is possible. Obviously, this is an oversimplification of the true situation because it neglects pressure drops in the vertical direction due to fluid flow through the crack as well as any modulus or fracture toughness effects.

6.6 CORRELATION WITH ROCK PROPERTIES

We would like to be able to correlate the stresses with rock properties, but as seen in Table 6.1, rock property data in this interval are limited. In addition, the long-spaced sonic log is marginally useful here because the ubiquitous coal seams will not allow clean propagation of the sound waves. Most of these data are not available or are questionable.

Even if good rock property data were available, the high pore pressures would limit the usefulness of such a correlation. When the

pore pressure is high, the effective overburden stress is small and the effective lateral stress is much smaller yet. The net result is that large changes in Poisson's ratio (say from 0.2 to 0.3) result in small calculated stress variations (100 to 200 psi). Pore pressure is the dominant component of stress.

Since we have measured stress differences in excess of 1000 psi, it is clear that, even if good rock property data were available, there would be no correlation. The stress state in this zone must be dominated by effects other than simple uniaxial strain. Thermal strains, locked-in stresses from past geologic events, and viscoelastic or fracture-induced relaxation are other possible causes of the measured differences.

6.7 SUMMARY

We have completed twelve stress tests, two breakdowns, and one step-rate/flowback tests in order to determine the vertical distribution of the minimum in situ stress. These results are generally not as accurate as results from marine tests,[8] but they still provide good guidance on stress characteristics of this region.

The frac interval around zones 3 and 4 has a thick, high-stress region below it that should be a good containment barrier. There is a fair containment feature above the frac interval, but it is quite thin and will not stop fracture growth, particularly for the high treatment pressures which we observed. However, these high stress zones will also tend to restrict fracture growth by reducing the width there. Fluid flow through these narrow passages will result in large pressure drops and thus decrease the rate of vertical propagation.

The orientation of the stress field is 100°-120°, as measured clockwise from North. The difference in horizontal stresses in the sandstones is about 600-800 psi. The difference in horizontal stresses in the mudstones is minimal.

6.8 REFERENCES

1. Perkins, T. K. and L. R. Kern, "Widths of Hydraulic Fractures," Journal of Petroleum Technology, Vol. 13, September 1961, p. 937.

2. Simonson, E. R., A. S. Abou-Sayed, and R. J. Clifton, "Containment of Massive Hydraulic Fractures," Society of Petroleum Engineers Journal, Vol. 18, February 1978, p. 27.

3. Warpinski, N. R., J. A. Clark, R. A. Schmidt, and C. W. Huddle, "Laboratory Investigation on the Effect of In Situ Stresses on Hydraulic Fracture Containment," Society of Petroleum Engineers Journal, Vol. 22, No. 3, June 1982, p. 333.

4. Teufel, L. W. and J. A. Clark, "Hydraulic Fracture Propagation in Layered Rock: Experimental Studies of Fracture Containment," SPE/DOE 9878, Proceedings, 1981 SPE/DOE Symposium on Low Permeability Gas Reservoirs, May 1981, Denver, Colorado, p. 449.

5. Hanson, M. E., G. D. Anderson, R. J. Shaffer, and L. D. Thorson, "Some Effects of Stress Friction, and Fluid Flow on Hydraulic Fracturing," Society of Petroleum Engineers Journal, Vol. 22, No. 3, June 1982, p. 321.

6. Warpinski, N. R., R. A. Schmidt, and D. A. Northrop, "In Situ Stresses: The Predominant Influence on Hydraulic Fracture Containment," Journal of Petroleum Technology, Vol. 34, March 1982, pp. 653-664.

7. Warpinski, N. R. and L. W. Teufel, "In Situ Stresses in Low-Permeability, Nonmarine Rocks," SPE 16402, Proceedings, 1987 SPE/DOE Joint Symposium on Low Permeability Reservoirs, Denver, CO, pp 125-138, May, 1987.

8. Warpinski, N. R., P. T. Branagan, R.and Wilmer, "In Situ Stress Measurements at U.S. DOE's Multiwell Experiment Site, Mesaverde Group, Rifle, Colorado," Journal of Petroleum Technology, Vol. 37, March 1985.

9. Teufel, L. W., "Prediction of Hydraulic Fracture Azimuth from Anelastic Strain Recovery Measurements of Oriented Core," in 23rd U.S. National Rock Mechanics Symposium, Berkeley, CA, ed. R. Goodman and F. Heuze, pp 238-246, 1982.

10. Teufel, L. W., "Determination of In Situ Stress from Anelastic Strain Recovery Measurement of Oriented Core," SPE 11649, Proceedings, SPE/DOE Symposium on Low Permeability, pp 421-430, Denver CO, March, 1983.

11. Teufel, L. W., and N. R. Warpinski, "Determination of In Situ Stress from Anelastic Strain Recovery Measurements of Oriented Core: Comparison to Hydraulic Fracture Stress Measurements," Proceedings, 25th U.S. Symposium on Rock Mechanics, Northwestern University, Evanston, IL, June, 1984, pp 176-185.

12. Teufel, L. W., C. Hart, A. R. Sattler, and J. A. Clark, "Determination of Hydraulic Fracture Azimuth by Geophysical, Geological and Oriented-Core Methods at the Multiwell Experiment Site, Rifle, CO," SPE 13226, presented at 59th Annual SPE Technical Conference, Houston, TX, Sept 16-19, 1984.

13. Lacy, L. L., "Comparison of Hydraulic Fracture Azimuth by Geophysical, Geological and Oriented-Core Methods at the Multiwell Experiment Site, Rifle, CO," SPE 13226, presented at 59th Annual SPE Technical Conference, Houston, TX, Sept 16-19, 1984.

14. Blanton, T. L., "The Relation between Recovery Deformation and In Situ Stress Magnitudes," SPE 11624, Proceedings, 1983 SPE/DOE Symposium on Low Permeability Gas Reservoirs, Denver, CO, March 14-16, 1983, pp 213-218.

15. Warpinski, N. R. and L. W. Teufel, "A Viscoelastic Constitutive Model for Determining In Situ Stress Magnitudes from Anelastic Strain Recovery of Core," SPE 15368, presented at 61st Annual SPE Technical Conference, New Orleans, LA, October 5-8, 1986.

Table 6.1 STRESS DATA AND ROCK PROPERTIES

MWX-2 Stress Tests

Depth (ft)	Lithology	σ_{min} (psi)	Estimated Error (± psi)	ν log	ν lab	E (10^6 psi)	Pi (psi)
7423-25	Coal	6865	75	-	-	-	5865*
7394-96	Siltstone	6720	150	.201	-	-	5815*
7303-05	Mudstone	6430	30	.237	0.20	4.1	5650*
7263-65	Sandstone	6755	50	.186	0.21	3.7	5600
7206-08	Siltstone	6900	30	.244	-	-	5455*
7169-71	Mudstone	7000	30	.224	-	-	5370*
7010-12	Mudstone	6325	50	-	0.23	3.7	5140*
6963-65	Sandstone	5745	50	-	-	-	5030*
6928-30	Mudstone	5830	100	-	-	-	4950*
			MWX-3 Stress Tests				
7068-70	Mudstone	5780	50	-	0.21	3.3	5280*
7048-50	Coal	7200	100	-	-	-	5230
7032-34	Mudstone	6800	100	-	-	-	5190
			Breakdown in MWX-1				
7256-84	Sandstone	6300	50	-	-	-	5600
			Breakdown in MWX-3				
7080-7102 7126-42	Sandstone	5805	50	-	0.21	3.8	5300
			Flowback Test in MWX-1				
7076-7100 7120-44	Sandstone	5900	-	-	-	-	5300

*Interpolated or Extrapolated from Nearby Zones

Table 6.2. ASR Strain and Orientation Data from MWX-3

Depth (ft)	Lithology	Core Age* (hrs)	ε_1	ε_2	ε_v	θ	Maximum Horizontal Stress Direction
6896	Sandstone	7-43	117	51	186	15.0	N80°W
6897	Sandstone	7-43	160	84	202	9.6	N75°W
7146	Sandstone	7-43	146	26	184	-65.7	N52°W
7147	Sandstone	7-43	158	45	222	-61.7	N56°W
7154	Mudstone	8-44	104	82	156	-	-

* Core age is the elapsed time interval (to the nearest hour) from when the core was cut (t=0), strain monitoring began (7 or 8), to when monitoring ended.

Table 6.3. ASR Stress Calculations

		Input Parameters			Direct Model		Strain-History Model	
Depth (ft)	Lithology	σ_v (psi)	σ_{2meas} (psi)	P (psi)	σ_1 (psi)	σ_2 (psi)	σ_1 (psi)	J_1 (10^6 psi^{-1})
6896	Sandstone	7240	5700*	5250*	6788	6356	6396	.054
6897	Sandstone	7240	5700*	5250*	7000	6572	6874	.049
7146	Sandstone	7505	5805	5400	7238	6408	7085	.085
7147	Sandstone	7505	5805	5400	7138	6483	6874	.103
7154	Mudstone	7510	7000	5400	7177	7029	7162	.106

*Interpolated from nearby zones of similar lithology.

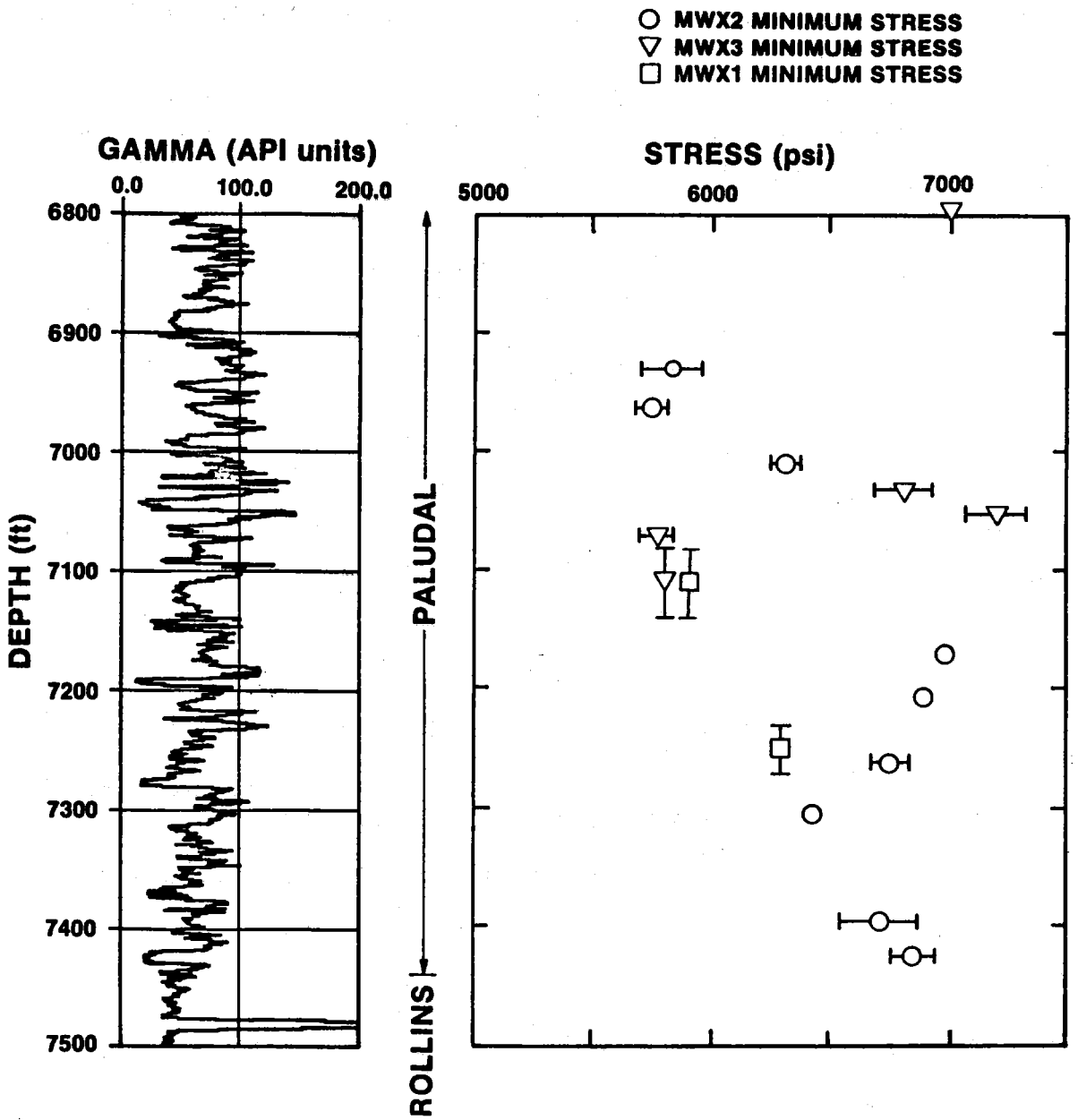

Figure 6.1 In Situ Stress Results

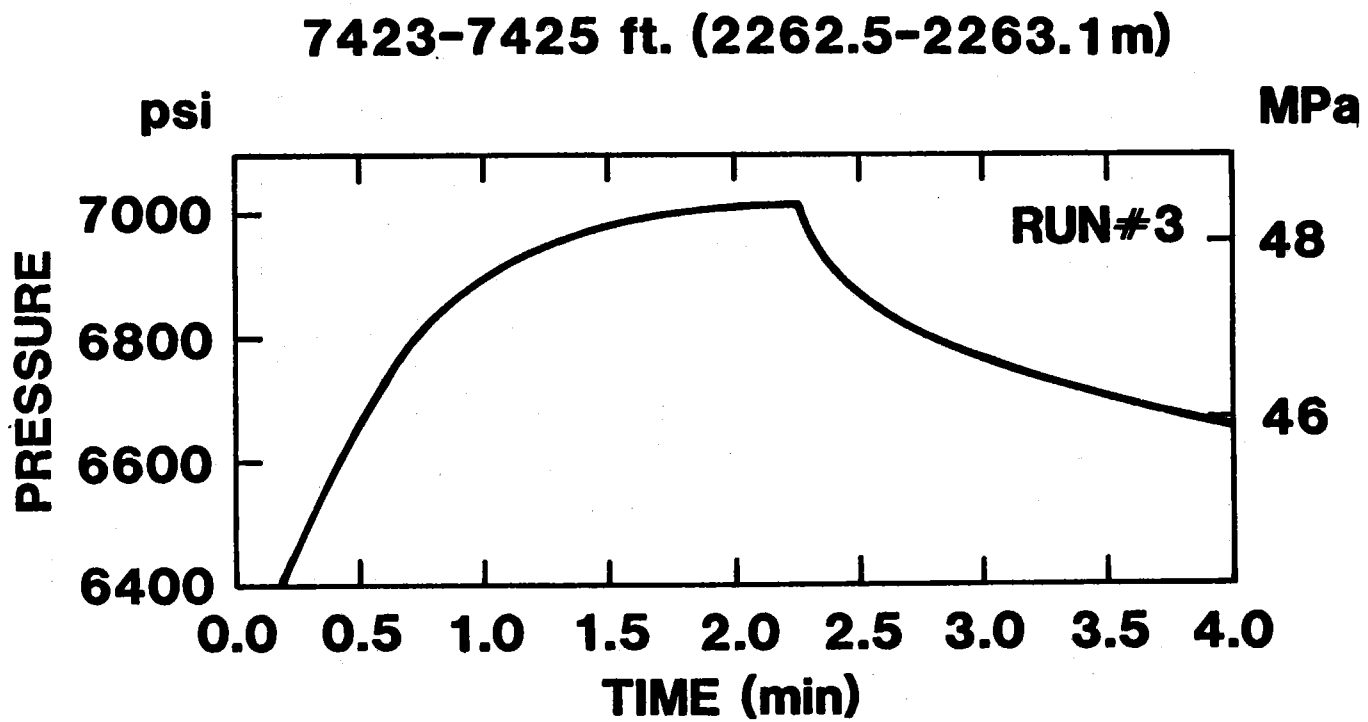

Figure 6.2 Stress test data from Coal at 7423-25 ft in MWX-2

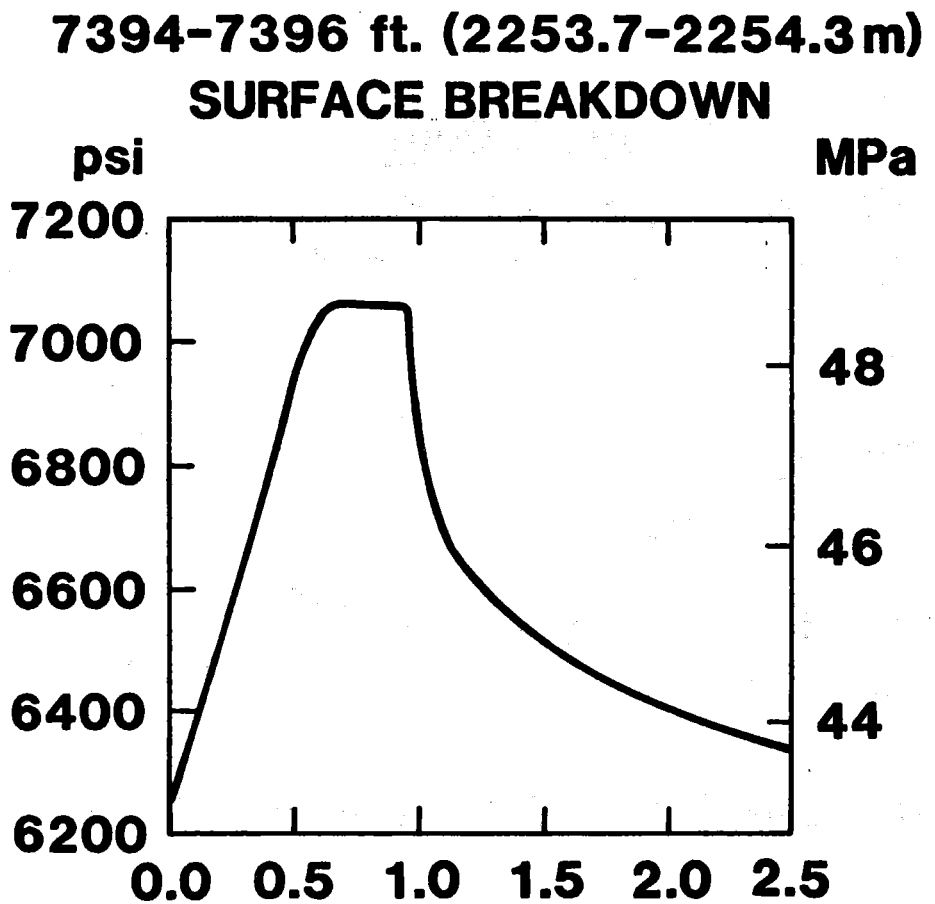

Figure 6.3 Stress test data from Siltstone at 7394-96 ft in MWX-2

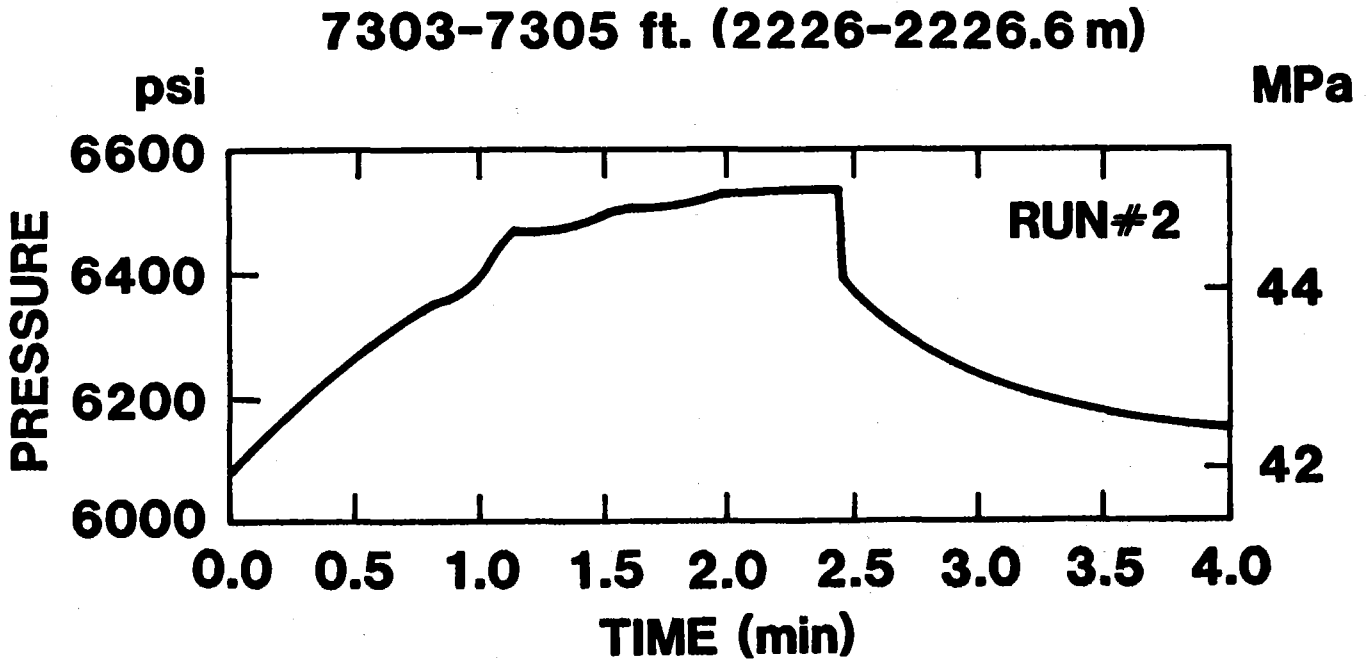

Figure 6.4 Stress test data from Mudstone at 7303-05 ft in MWX-2

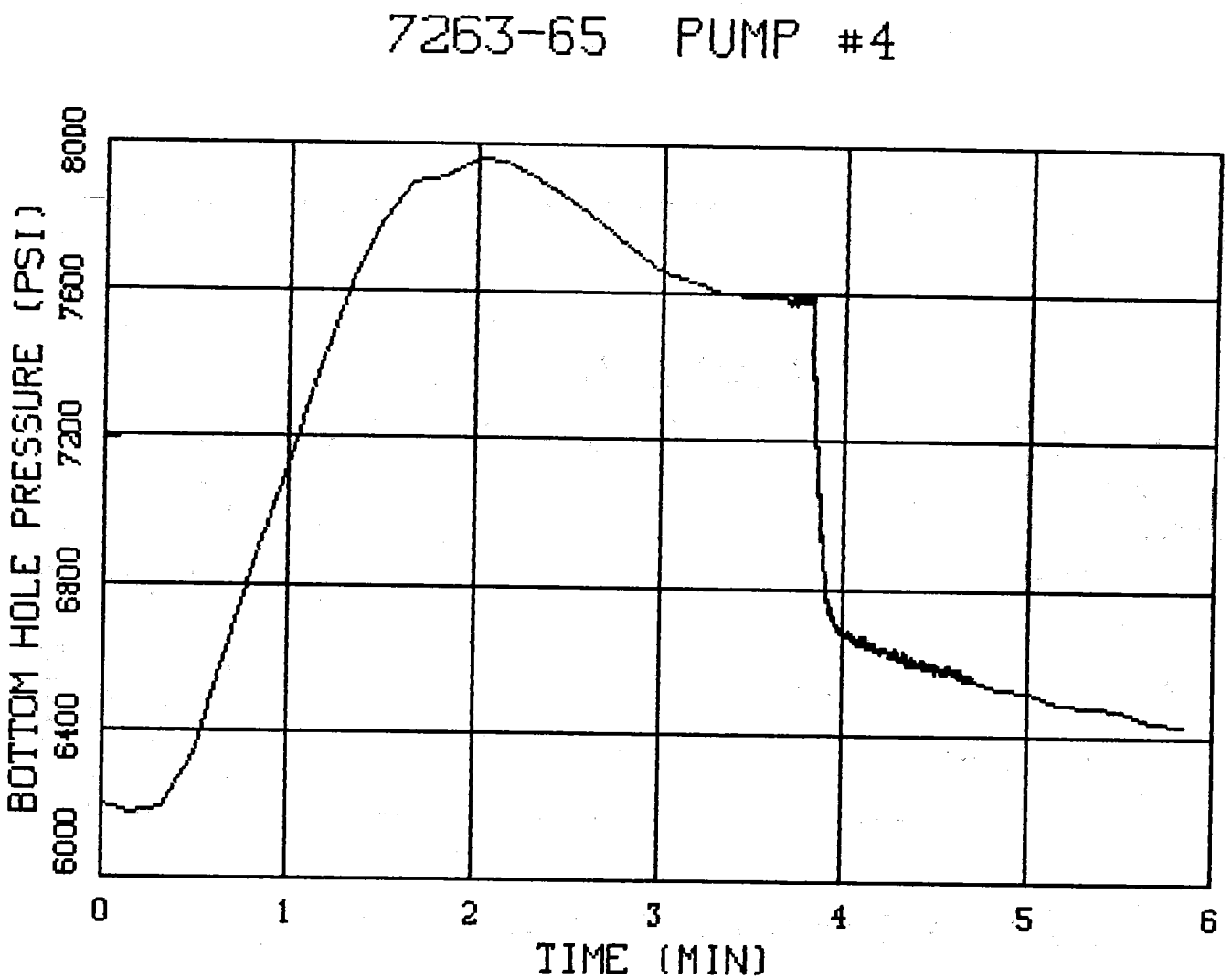

Figure 6.5 Stress test data from Sandstone at 7263-65 ft in MWX-2

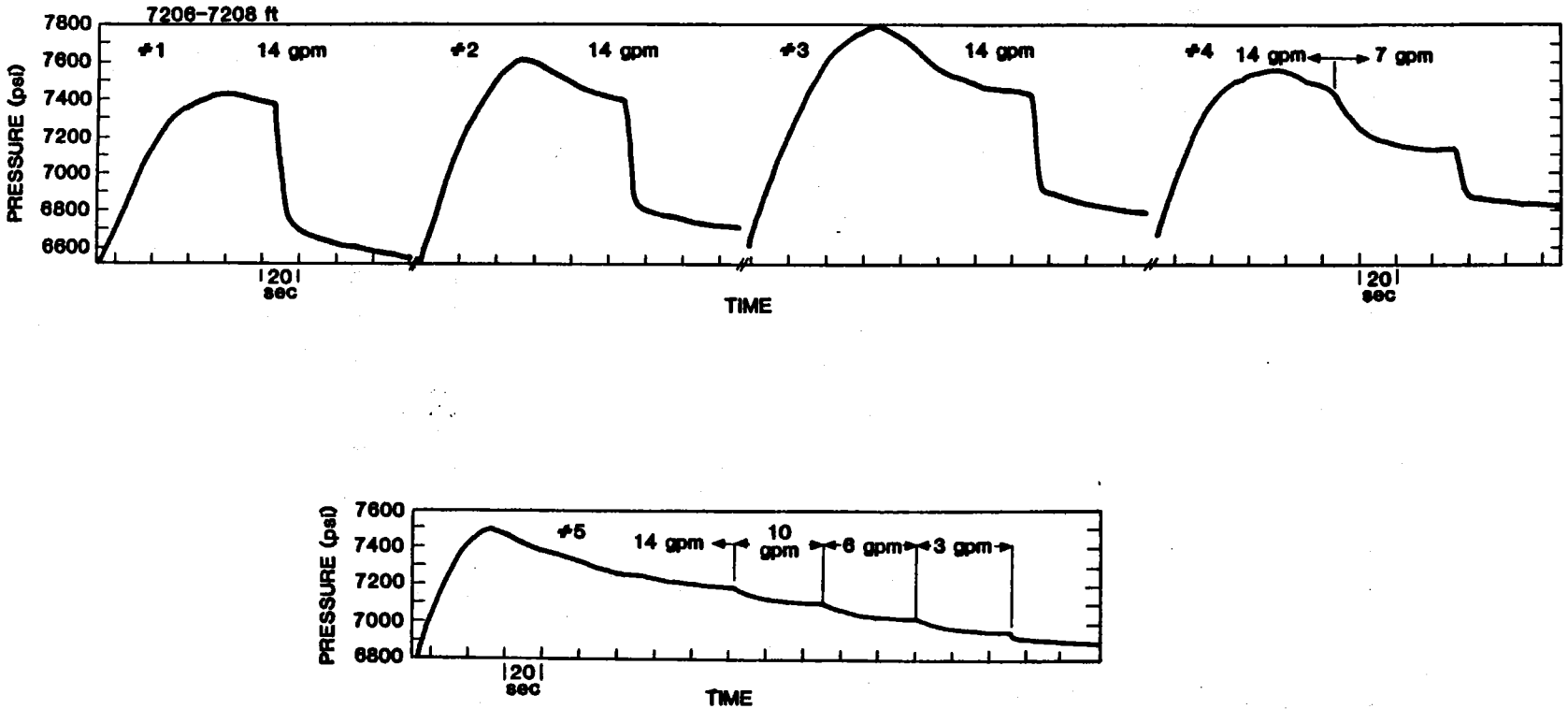

Figure 6.6 Stress test data from Siltstone at 7206-08 ft in MWX-2

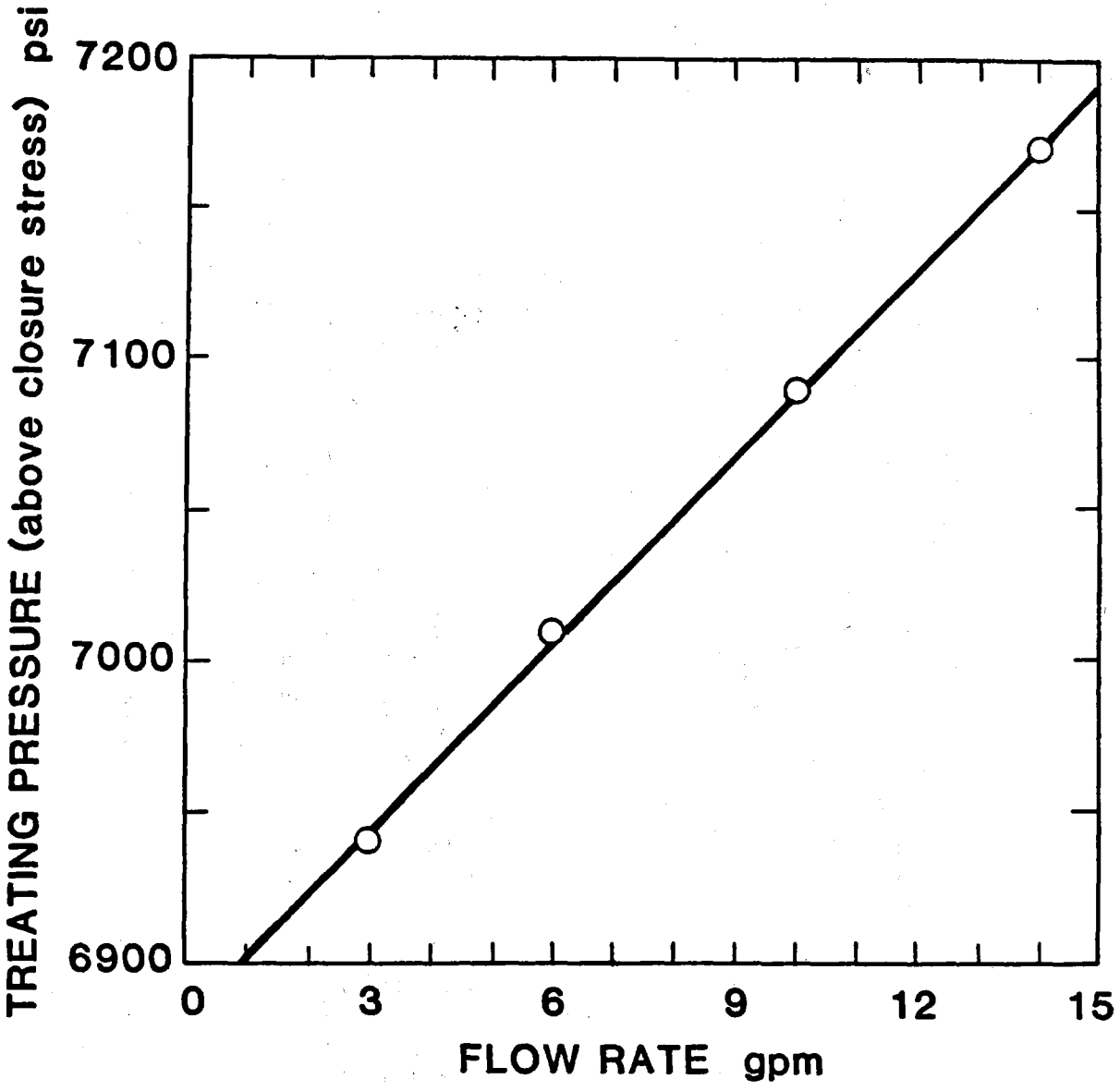

Figure 6.7 Linear pressure vs flow rate behavior

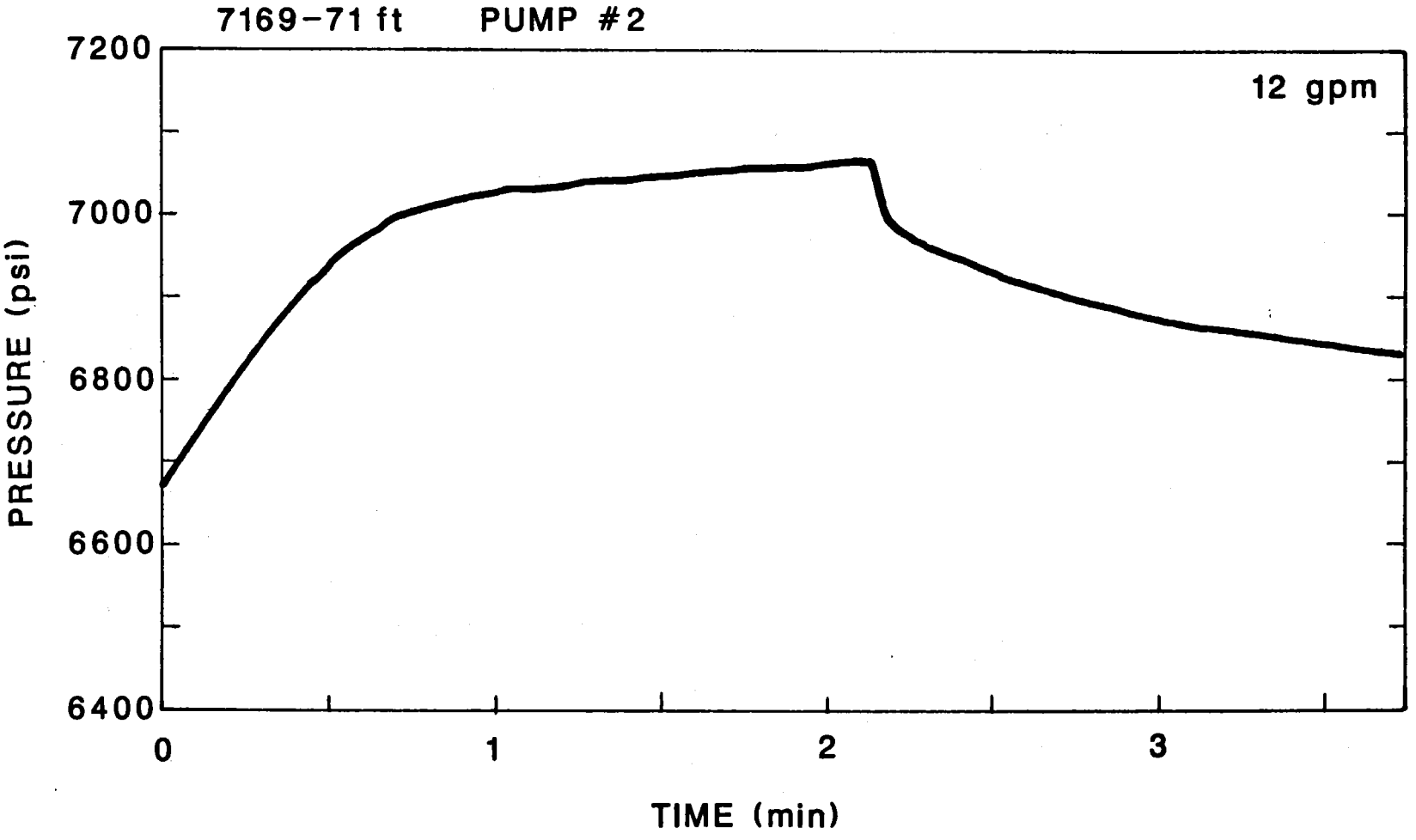

Figure 6.8 Stress test data from Mudstone at 7169-71 ft in MWX-2

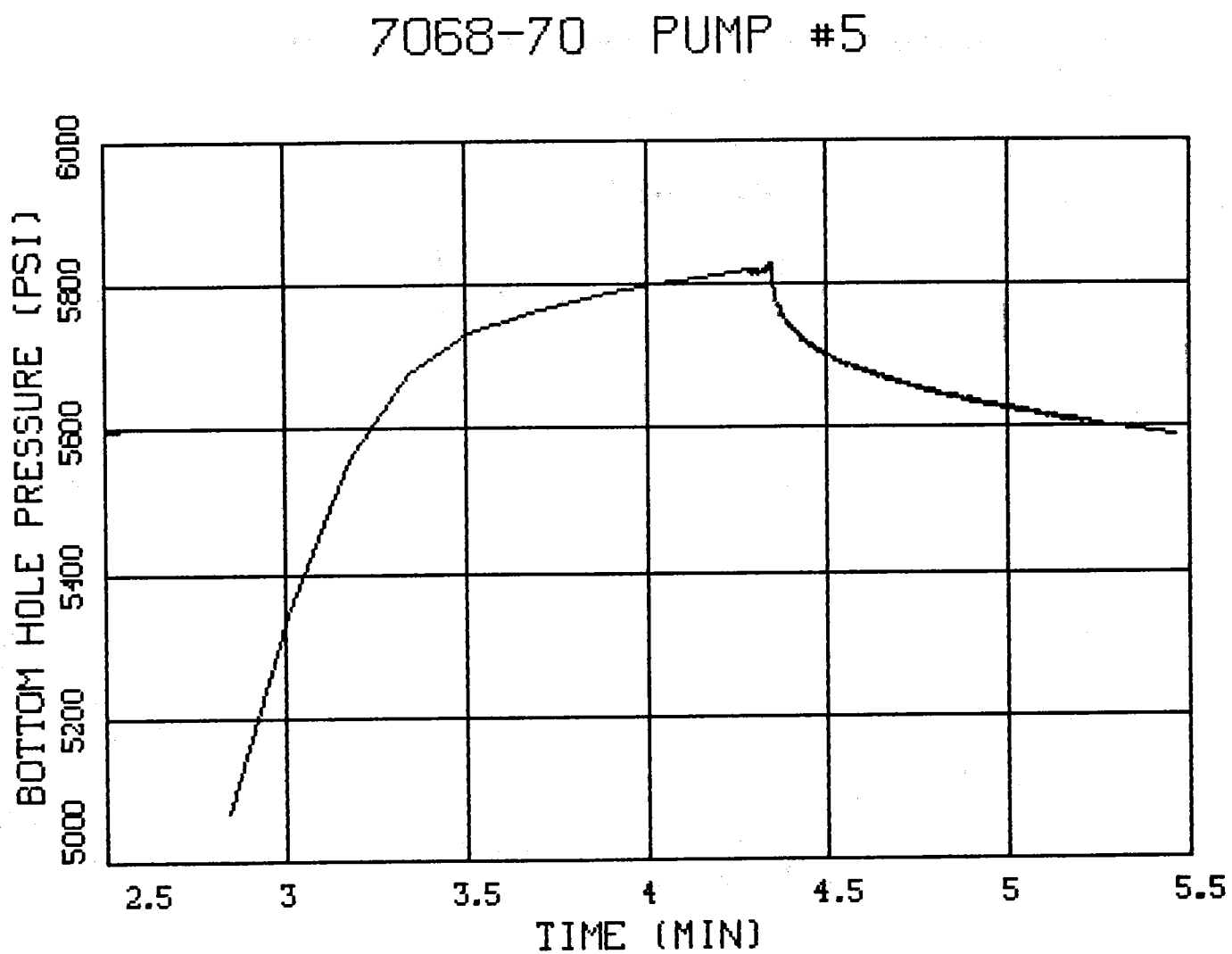

Figure 6.9 Stress test data from Mudstone at 7068-70 ft in MWX-3

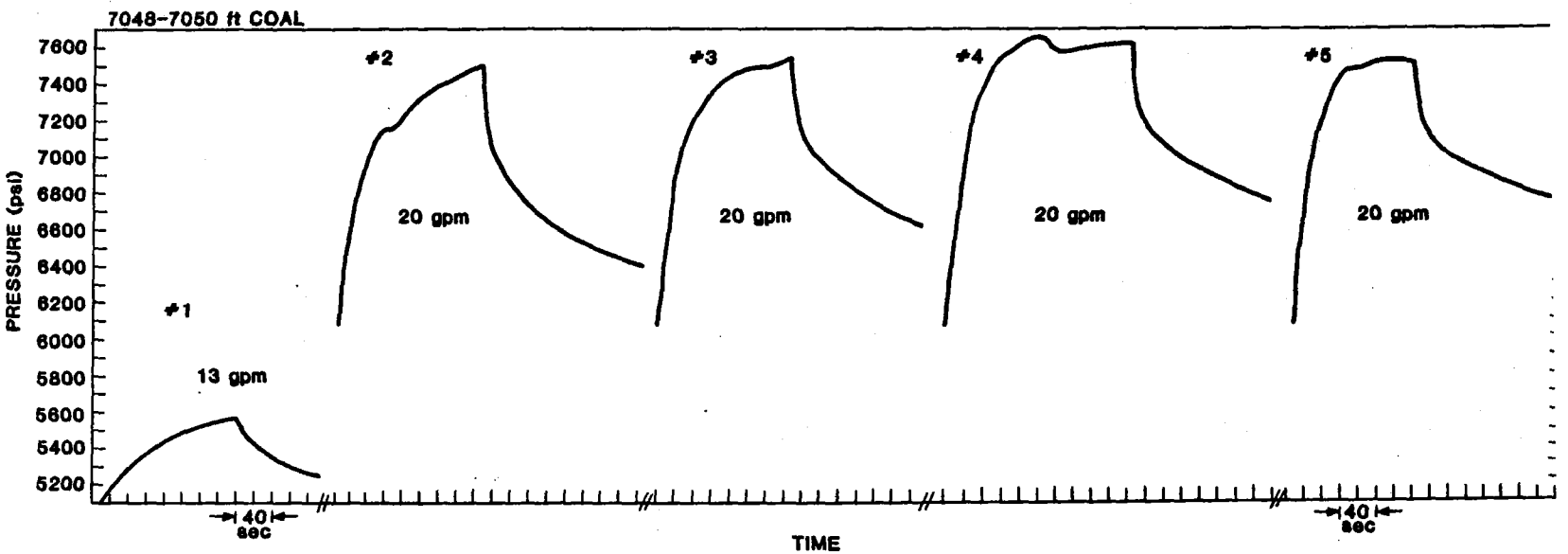

Figure 6.10 Stress test data from Coal at 7048-50 ft in MWX-3

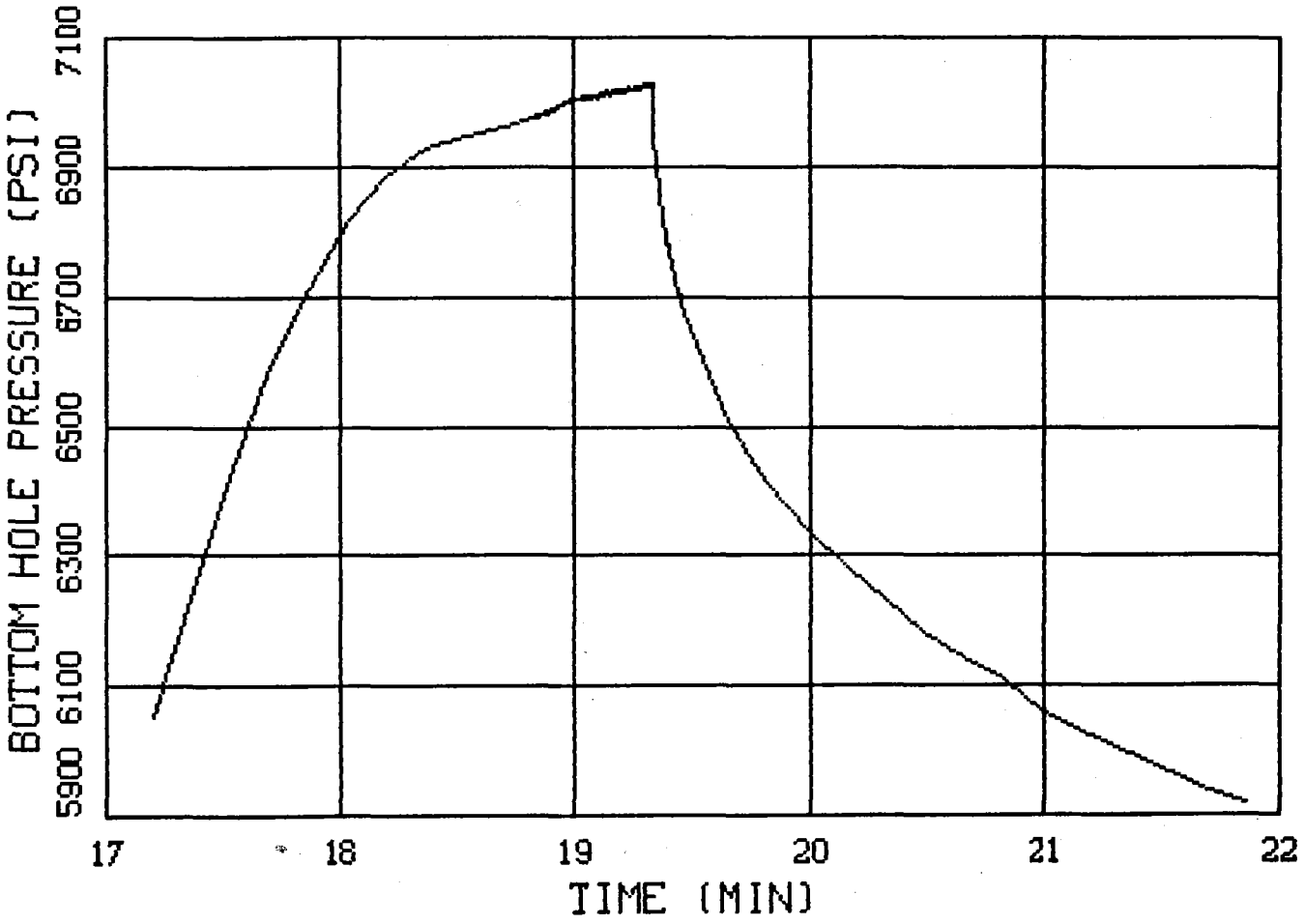

Figure 6.11 Stress test data from Mudstone at 7032-34 ft in MWX-3

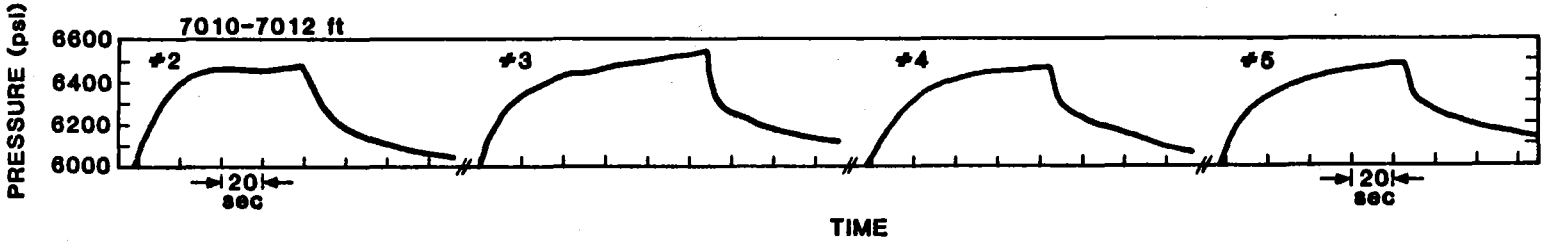

Figure 6.12 Stress test data from Mudstone at 7010-12 ft in MWX-2

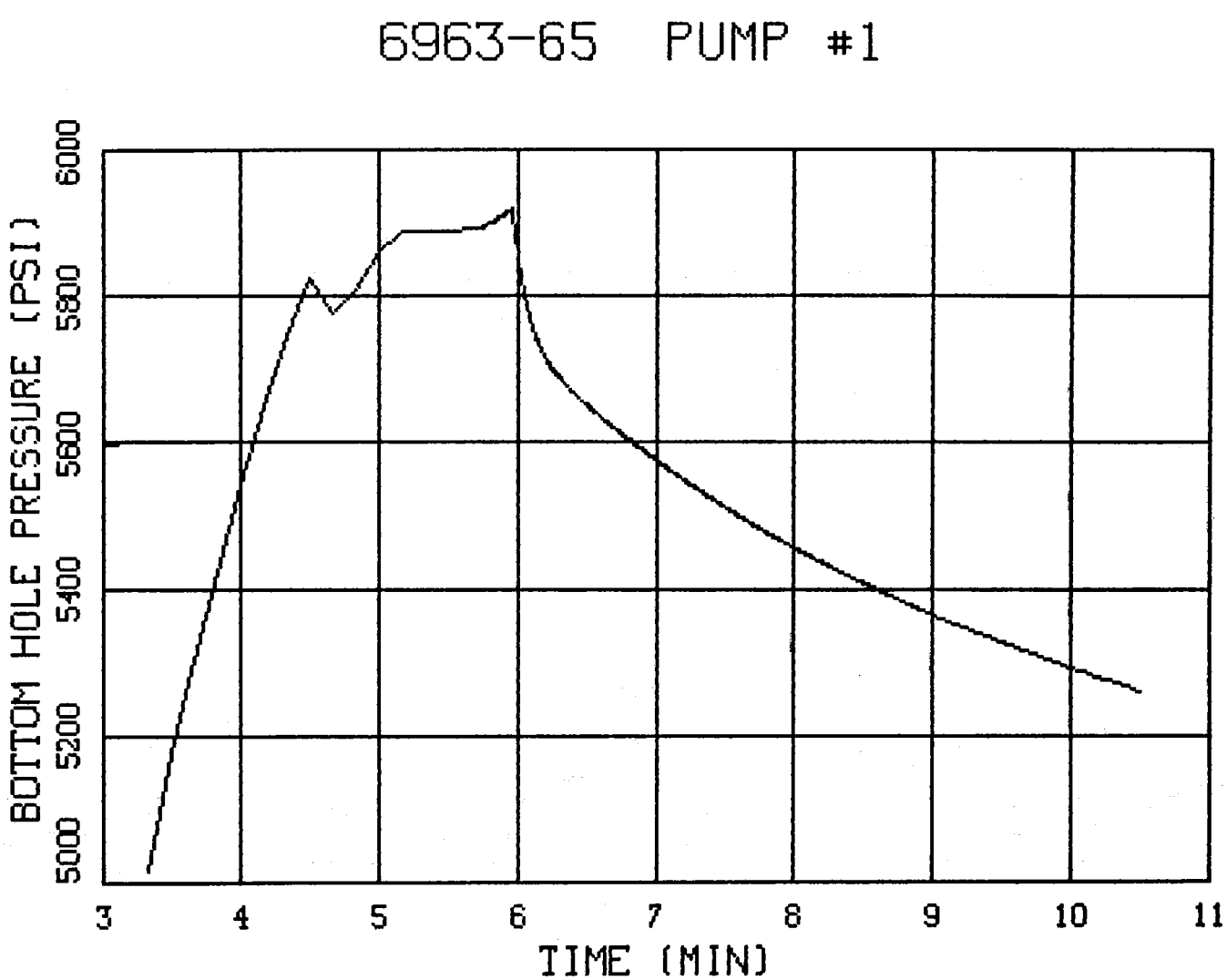

Figure 6.13 Stress test data from Sandstone at 6963-65 ft in MWX-2

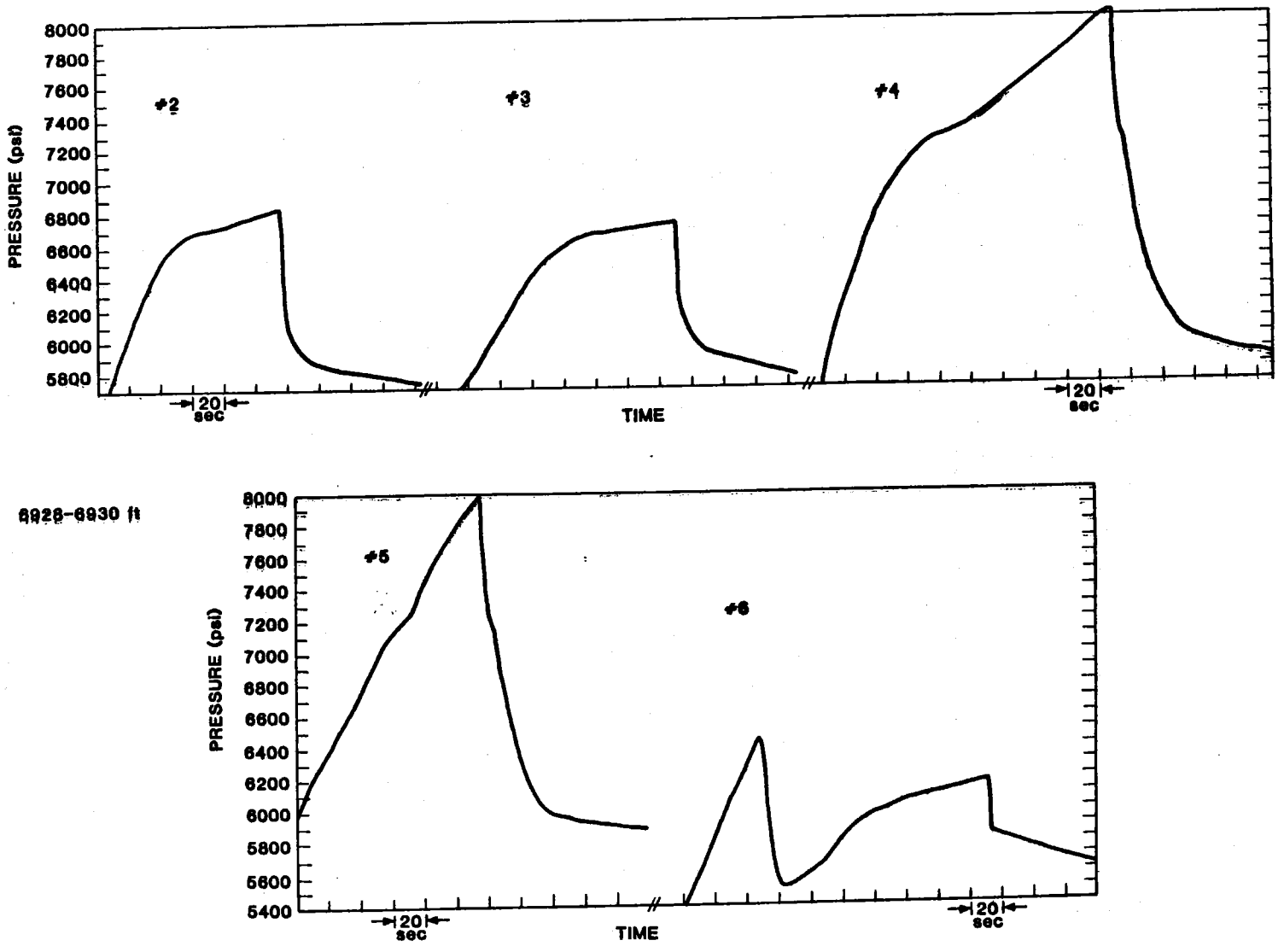

Figure 6.14 Stress test data from Mudstone at 6928-30 ft in MWX-2

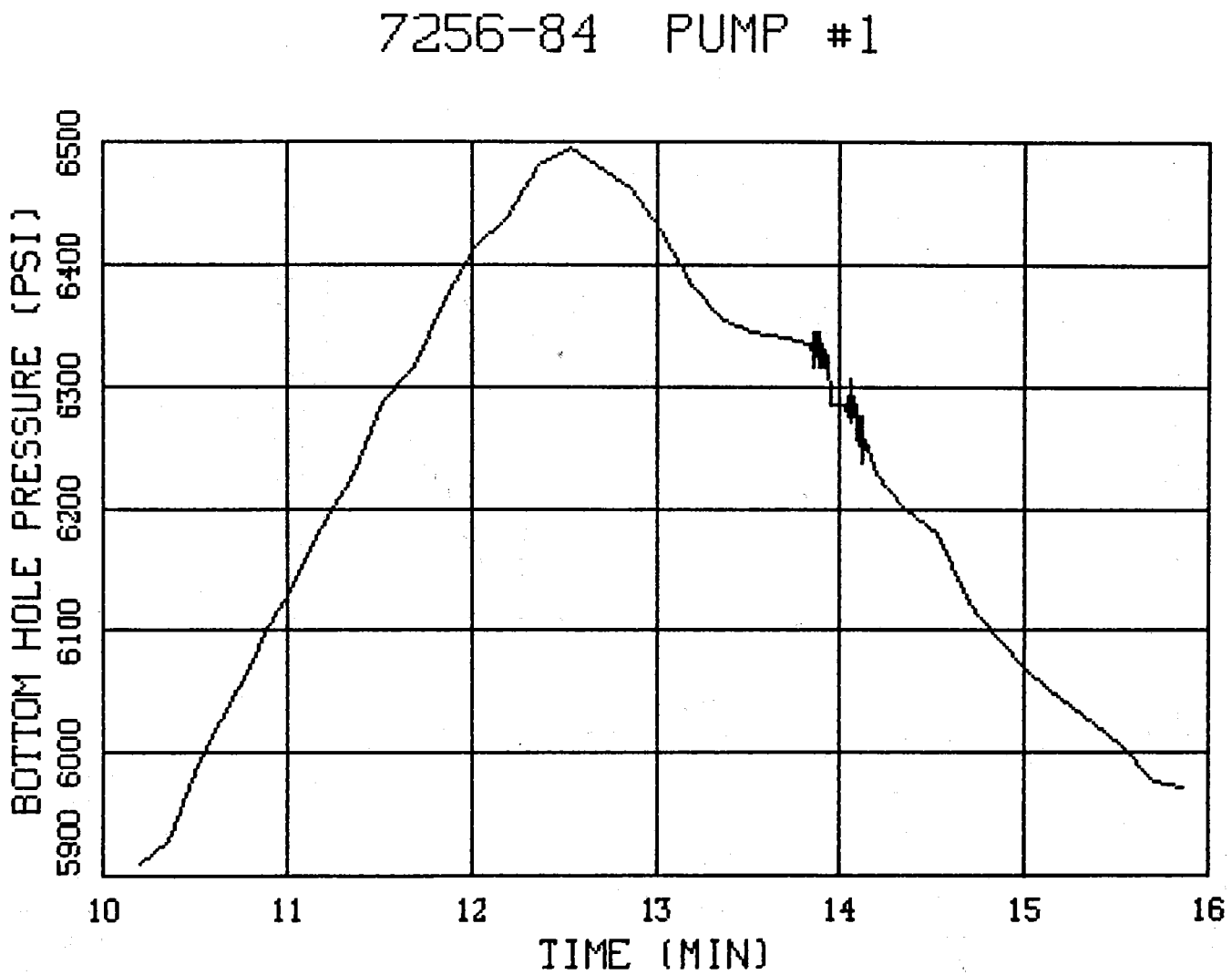

Figure 6.15 Breakdown data from Zone 2 7256-84 ft in MWX-1

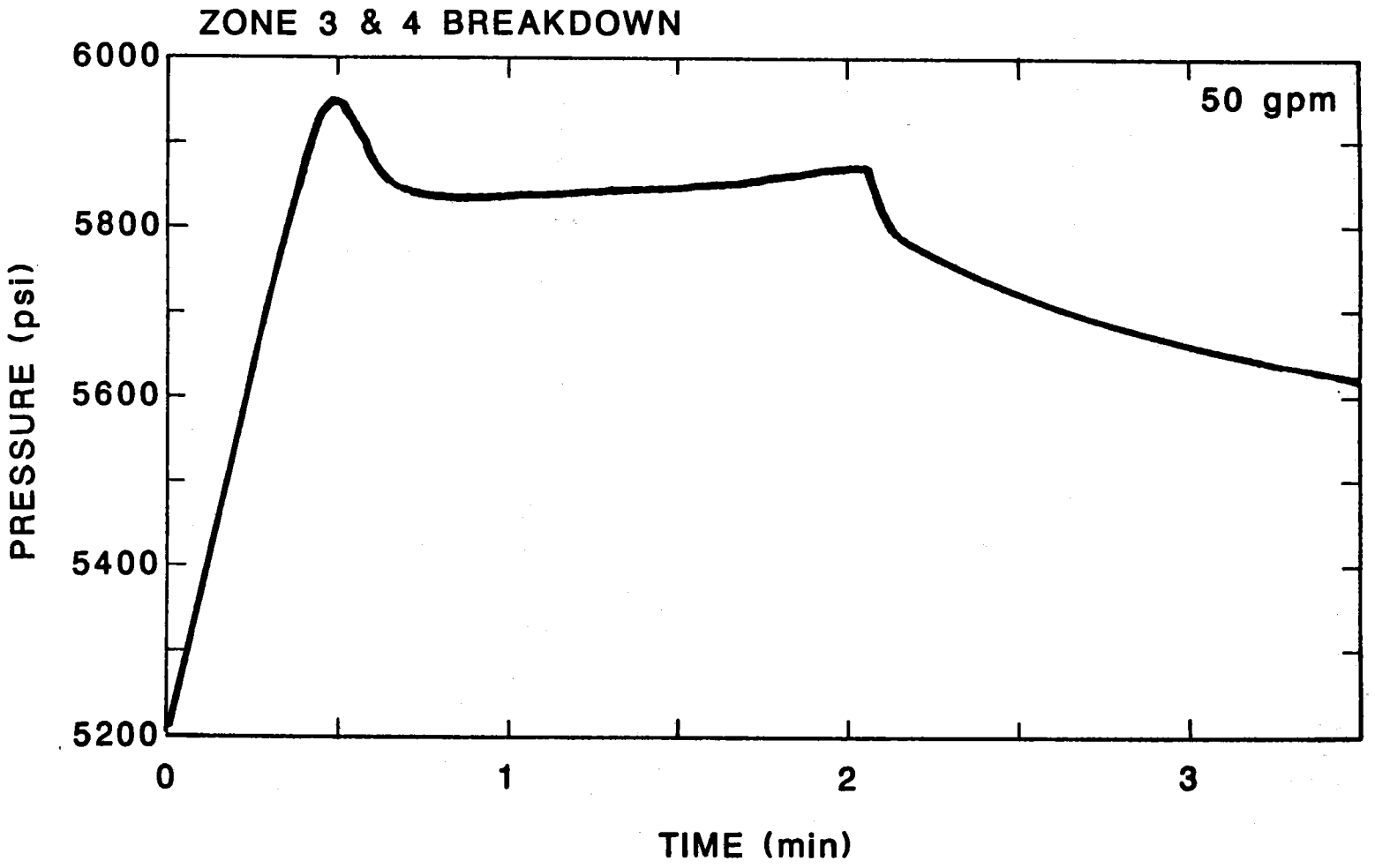

Figure 6.16 Breakdown data from Zones 3 and 4 at 7080-7102 and 7126-42 ft together in MWX-3

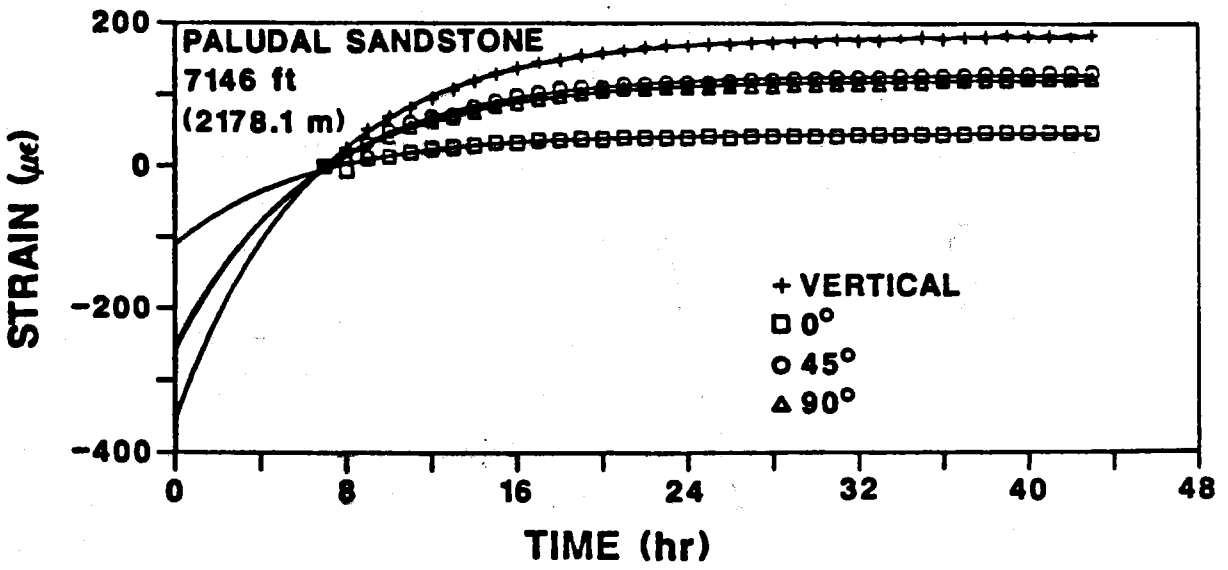

Figure 6.17 ASR data from Sandstone at 7146 ft in MWX-3

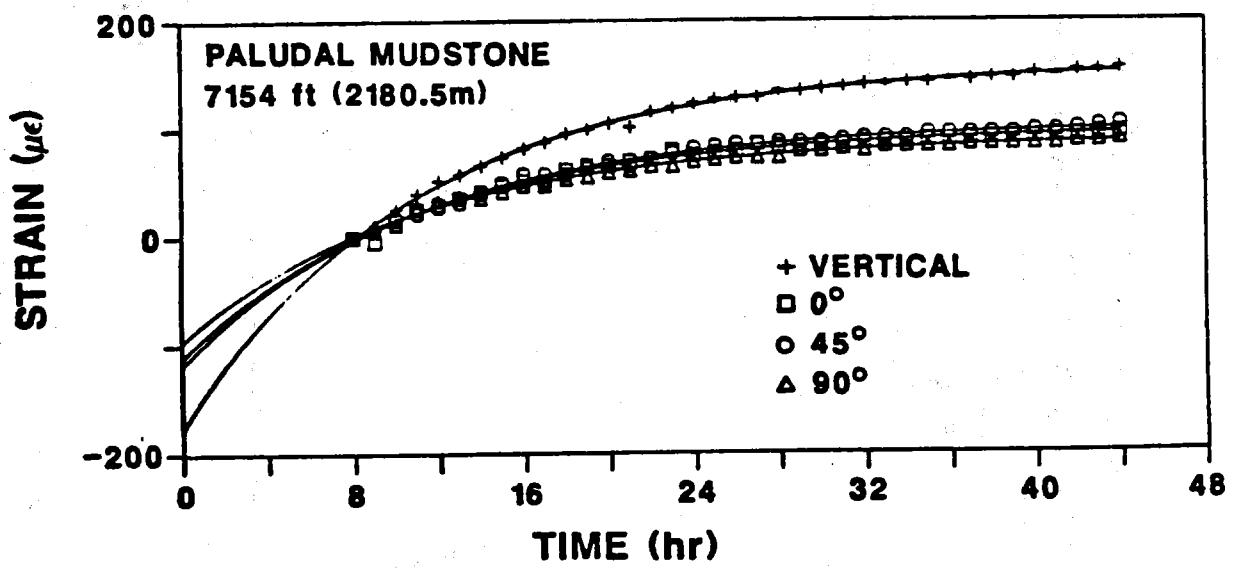

Figure 6.18 ASR data from Mudstone at 7154 ft in MWX-3

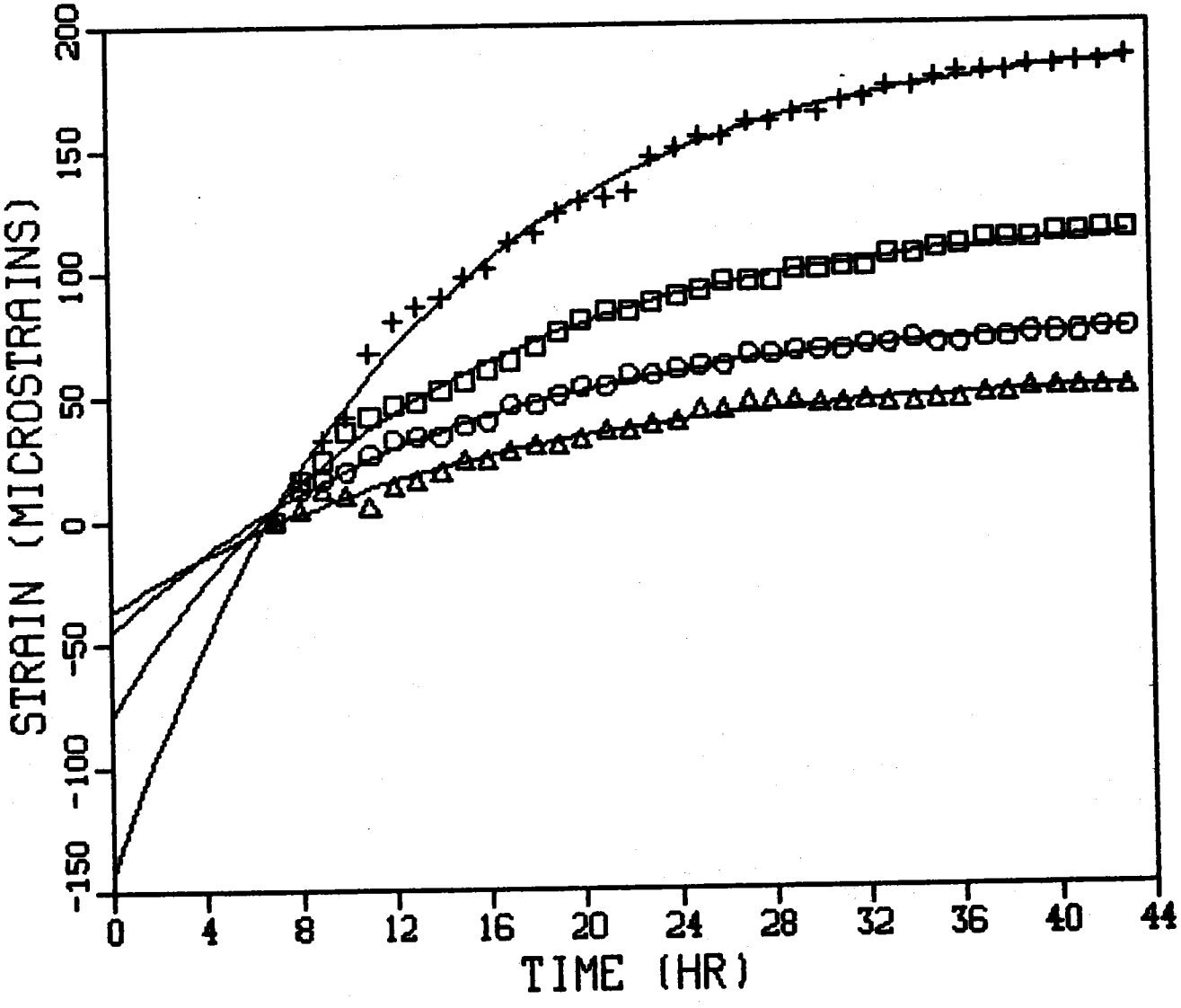

Figure 6.19 ASR data from Sandstone at 6896 ft in MWX-3

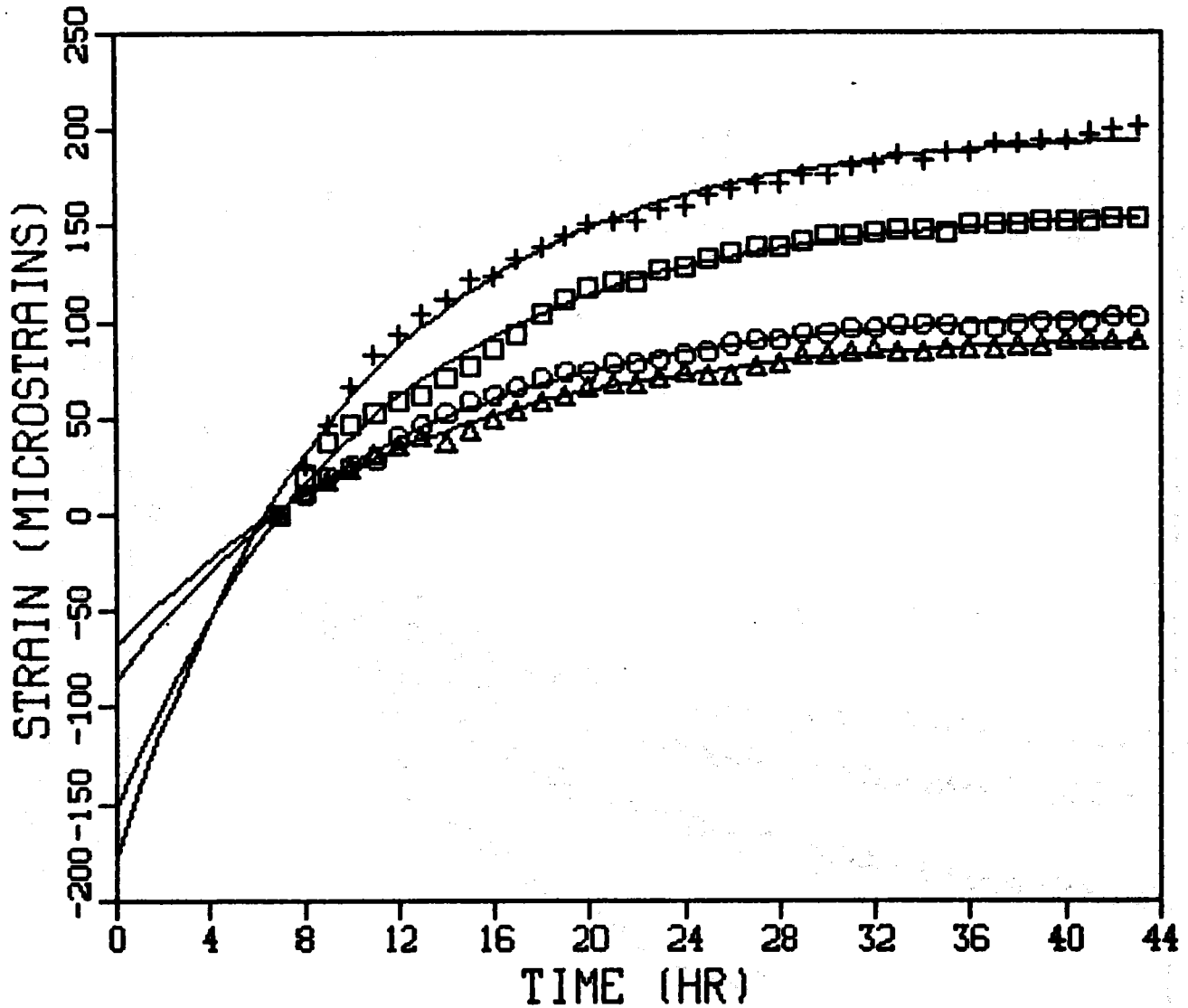

Figure 6.20 ASR data from Sandstone at 6897 ft in MWX-3

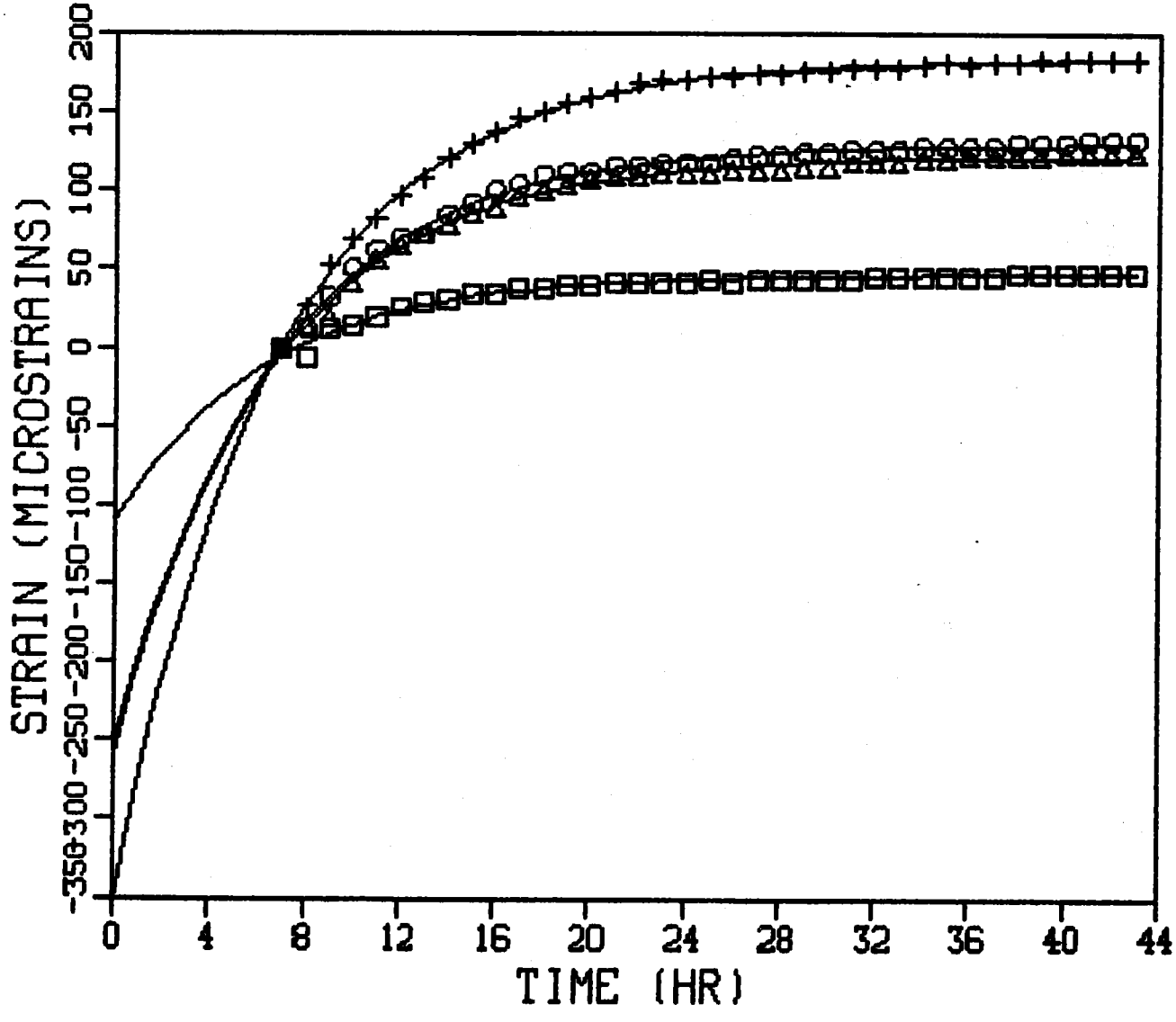

Figure 6.21 ASR data from Sandstone at 7146 ft in MWX-3

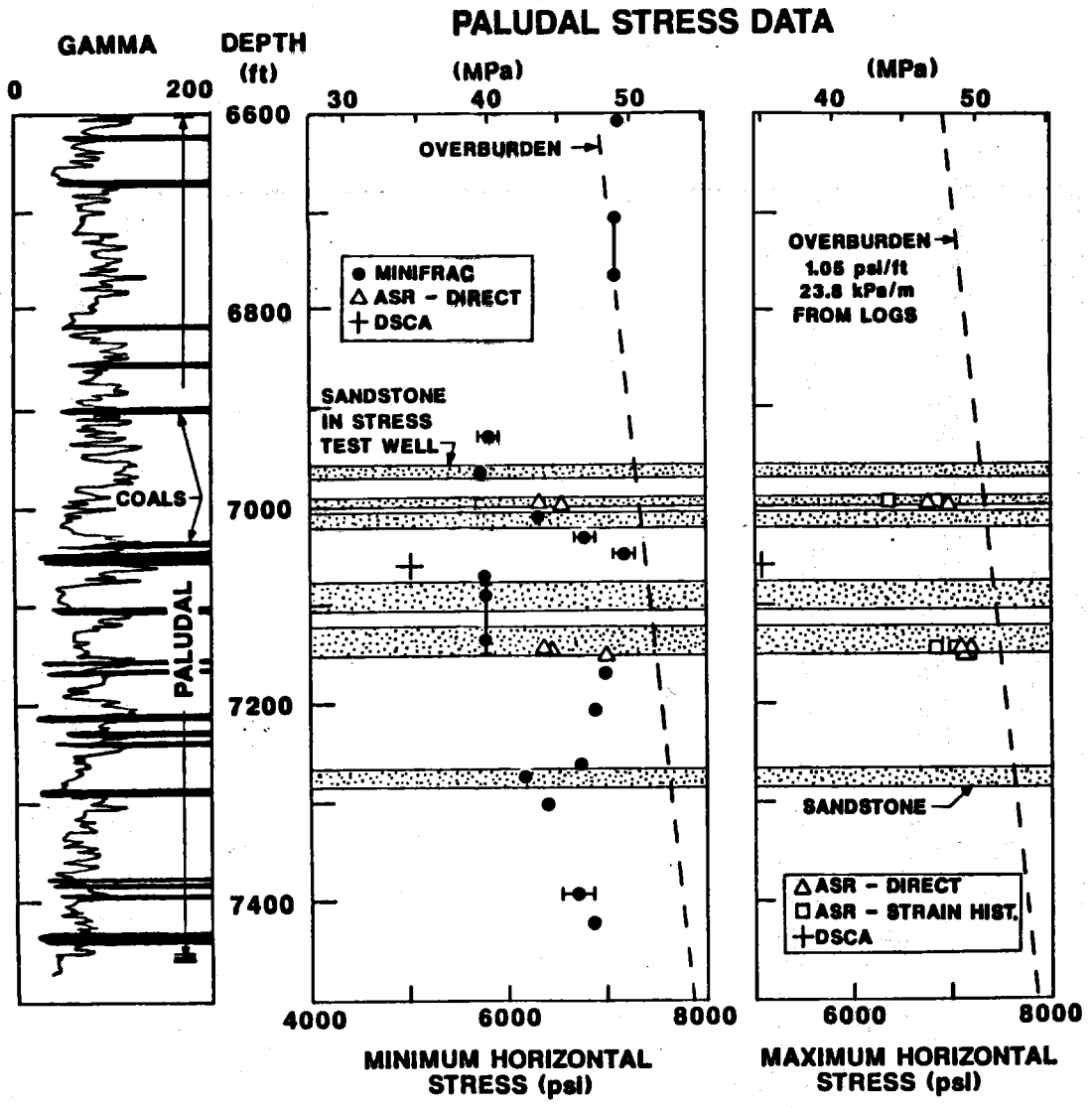

Figure 6.22 Combined paludal stress results

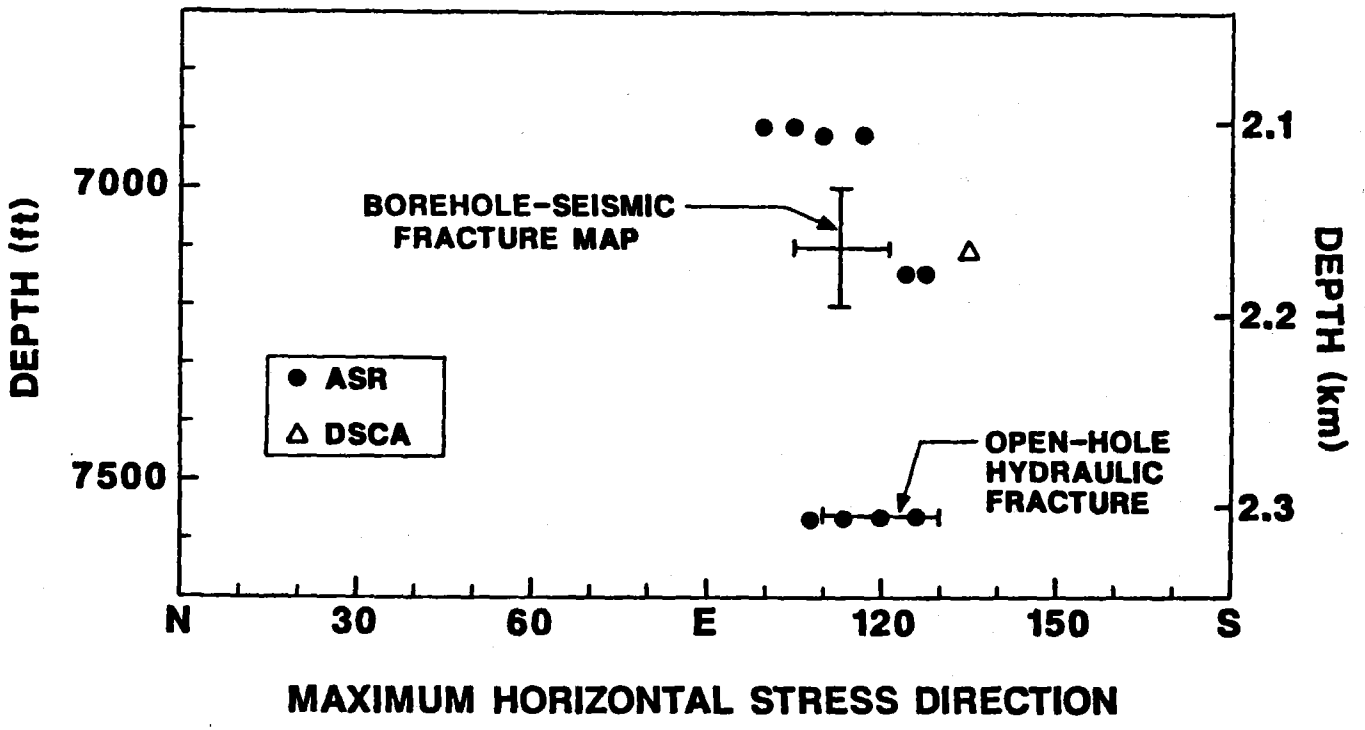

Figure 6.23 Paludal stress orientation results

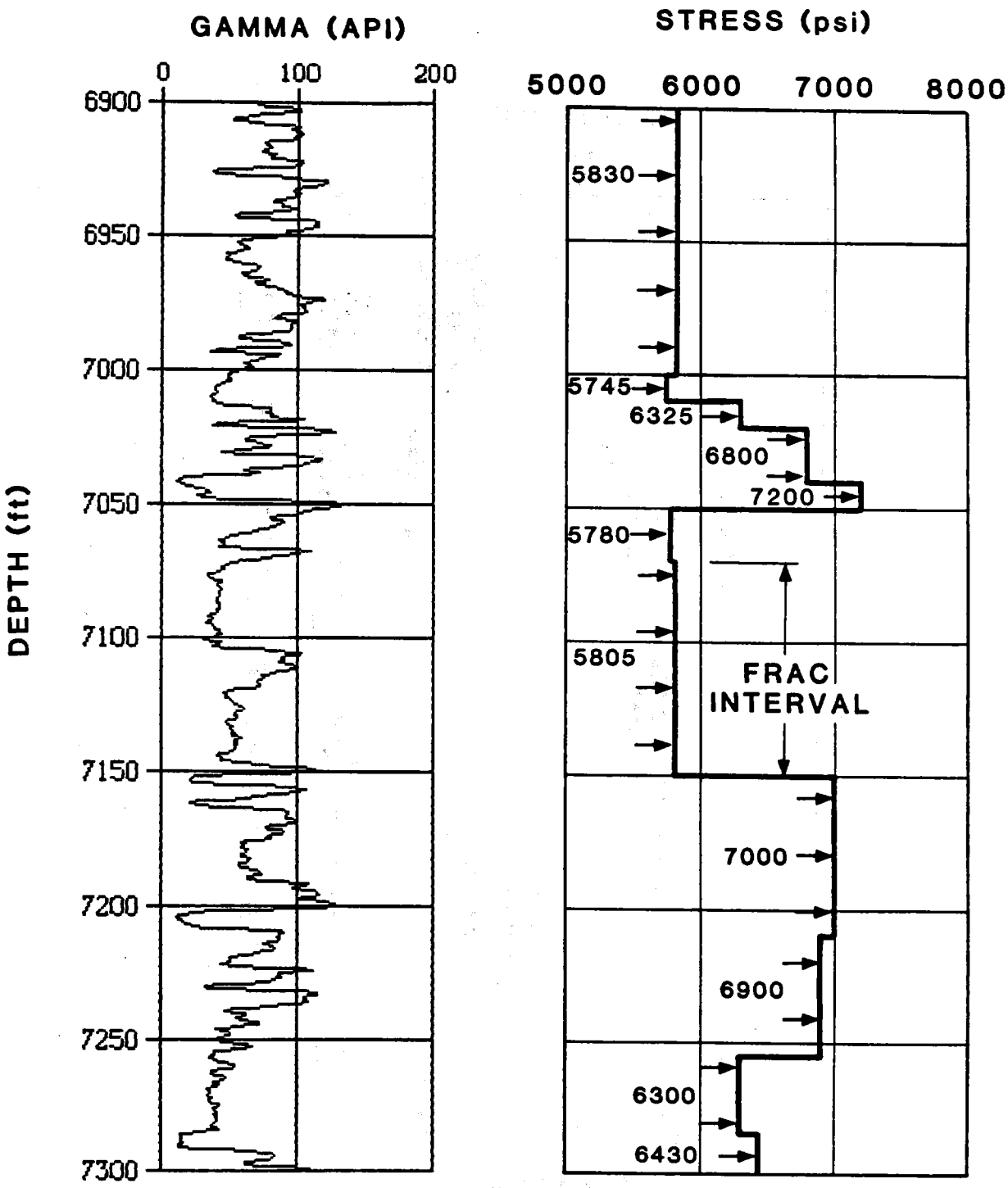

Figure 6.24 Estimated stress profile in MWX-1

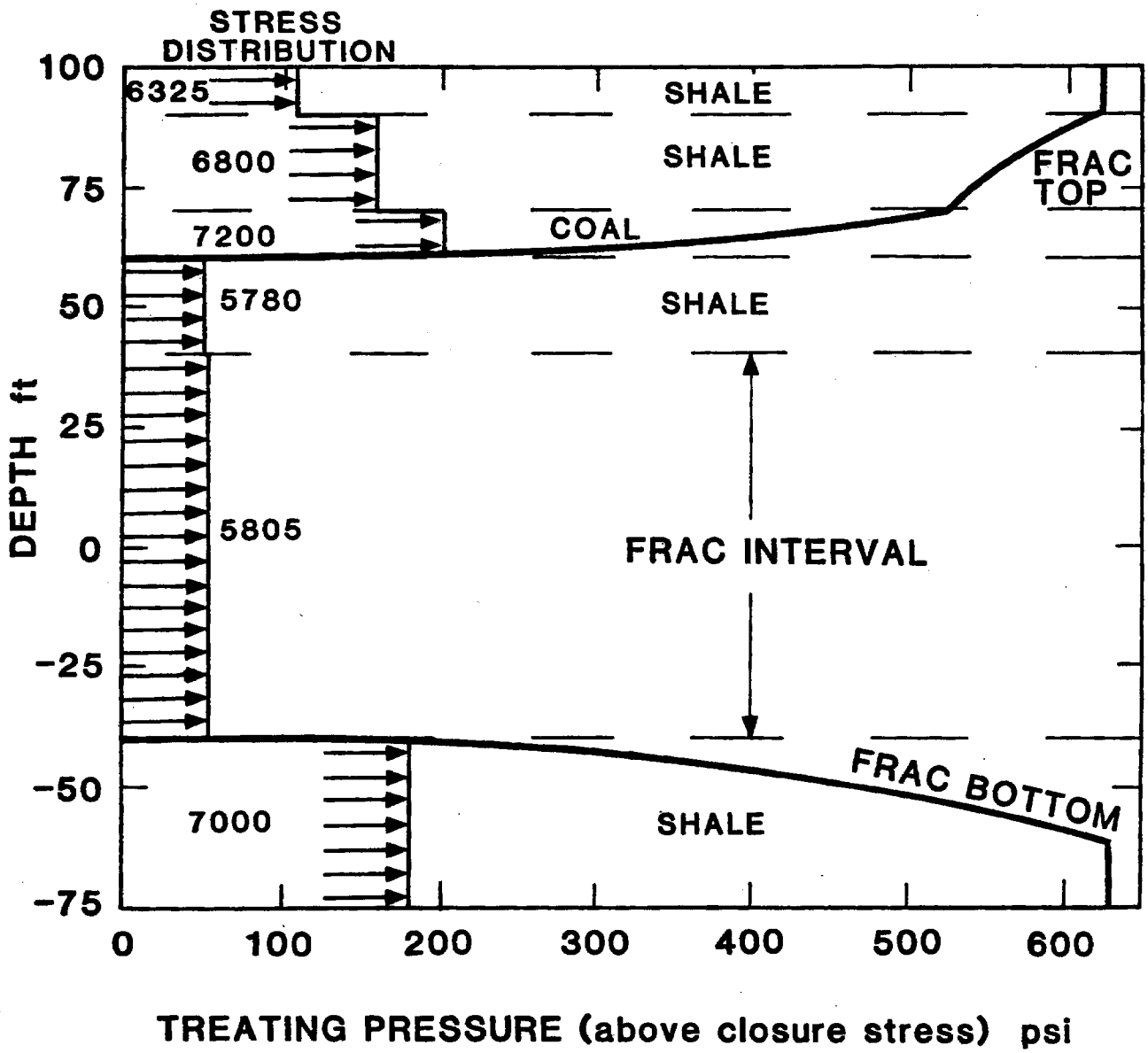

Figure 6.25 Fracture height vs stress distribution for the Zones 3 and 4 Frac Interval

7.0 WELL TESTING AND ANALYSIS, PALUDAL ZONE 2

P. T. Branagan
CER Corporation

7.1 TESTING

The objective of the MWX-1 paludal zone 2 well testing was to determine the natural reservoir characteristics of this potentially productive interval. Zone 2 is interpreted to be a distributary channel with a width of about 550 ft (Section 3.2.2). While zone 2 is well developed in MWX-1 with a gross sand thickness of 46 ft, it is marginal in both MWX-2 and MWX-3. Thus, zone 2 is not a contiguous productive gas reservoir over the areal extent of the three wells at the MWX site. Figure 7.1 is a graphic presentation from Lorenz[1,2] depicting his sedimentological interpretation of the possible location of this channel sandstone. Since the zone 2 reservoir production characteristics in MWX-2 and -3 were not favorable, a single well test in MWX-1 was considered adequate to assess the reservoir parameters.

No core was obtained from zone 2 in MWX-1, but core data from zone 2 in MWX-2 give a mean porosity and water saturation values of 8.1% and 31% respectively. The matrix permeability at restored stress (2000 psi effective stress) and water saturation conditions is 2.3 μd (section 5.3). Log analyses of zone 2 in MWX-1 (Section 4.3.1) yields an average porosity of 8.7% and a water saturation of 64%. The bottomhole temperature was about 215°F.

Figure 7.2 is a log showing the location of zone 2 in MWX-1. The sand was perforated between 7256 and 7284 ft, with two 14-gram jet shots per foot at 120° phasing. Due to the questionable cement bonding between the perforated interval and the coals above and below, production was expected to be enhanced. However, good cement bonding above the upper coal and below the lower coal should contain production between 7200 and

7294 ft; thus, the well testing should not be influenced by other potentially productive sandstones immediate to zone 2.

Previous testing and analysis of the lower marine Cozzette and Corcoran blanket sandstones indicated that a substantial natural fracture network existed within these submicrodarcy matrix reservoirs. In addition, a large number of natural fractures were found above 6200 ft. These results suggested that gas production from the paludal sands might be considerably greater than the production expected from a 1-2 μd sandstone.

Five weeks of well testing were scheduled to include approximately 25 days of production and 10 days of shut-in. A 65-bbl breakdown was performed through these perforations on July 12, 1983. Following breakdown, the well was unloaded and produced an unmeasured quantity of liquid, estimated to be less than 65 bbl. Unmeasured gas production which occurred during cleanup was estimated to be 300 MCF. Gas production through a test meter, measured at 275 MCFD, commenced at 1400 hrs, July 13, 1983. Production and shut-in alternated until July 18 in an attempt to dewater the near-wellbore formation in preparation for inserting the bottomhole HP pressure gauge. The maximum surface pressure measured during the buildups amounted to 4000 psi. The production rate was approximately 250 to 300 MCFD. On July 19, following a 24-hr buildup with a surface pressure of 4000 psi, the well was produced to the flare pit at approximately 500 MCFD for 6 hours. The HP gauge was lowered and positioned at 7100 ft. Flow rate was cut back to 300 MCFD. The well at that time produced approximately 2 bbl of water in slugs, which appeared to damage the HP gauge. The HP gauge was removed from the well and flaring operations halted due to hazardous conditions during the drilling and coring operations in MWX-3, just 200 ft away.

The well remained shut in until July 21, when the well was again produced to the pit, at a rate of about 700 MCFD. The HP gauge was

lowered in the well and the flow rate was reduced to 225 MCFD with a bottomhole flowing pressure of 780 psi. Production continued until July 25, when the well was shut in. At this time the final flowing pressure was 735 psi, the length of the production test was 123 hr (5.1 days) and the average flow rate was 140 MCFD. The buildup began July 25 and continued through July 31, with a final shut-in pressure of 4975 psi. This final pressure was still several hundred psi below the estimated reservoir pressure of 5390 psi.

A second drawdown began July 31, with an initial flow rate of 250 MCFD. Production continued for 108 hrs until August 4 at an average rate of 165 MCFD and a final flowing pressure of 750 psi. A second buildup was conducted from August 4-11; however, the late time pressure data were masked by intermittent surface leaks in the lubricator. The maximum bottomhole pressure was 4748 psi. The production data for all these tests are shown in Figure 7.3. A listing of relevant data is given in Appendix 12.7.1.

7.2 ANALYSIS

Figure 7.4 is a Horner plot that details the bottomhole pressure during the final buildup. Two straight lines have been added to the graph to emphasize the change in slope that occurred. Analytic solutions of these data, indicative of a no-flow boundary, suggested that the boundary was from 20 to 100 ft from MWX-1. Numerous attempts were made to simulate these data using the tight gas reservoir model. A range of permeabilities from 5 to 500 μd were used along with a single no-flow boundary at a distance between 12 and 80 ft from MWX-1. The results were not encouraging. The modeling attempts included parallel no-flow boundaries, which would fit the geologic model of "channel" sand lenses. However, the best fit required both boundaries to be within 50 ft of MWX-1.

Continued reservoir modeling of this and the initial buildup data required the inclusion of a no-flow boundary that was perpendicular to the anticipated channel boundaries shown in Figure 7.1. Evidence of a fault penetrating MWX-2 at 7055 ft was observed (Section 3.6). This fault, if extended through the location of Zone 2, would sever the test interval and might appear as a no-flow boundary when observed from MWX-1, assuming the same strike for the fault as for observed natural fractures in oriented core. Figure 7.5 is an areal view of the reservoir geometry applied to the model and includes the faulted boundary.

Figure 7.6 is an overlay of the simulated Horner plot and the field data. Figure 7.7 shows a comparison of the simulated second drawdown and the field data. In both cases the data fit is very good. The average reservoir permeability used in the model was 50 μd, more than 20 times the measured core matrix permeability.

The data derived from the well testing of zone 2 were significant in several respects, in that they

(1) clarified qualitatively that the paludal sandstone reservoirs were naturally fractured;
(2) confirmed the channel boundaries predicted from log, core, and sedimentological analysis;
(3) demonstrated that the existence of a nearby fault could be measured and modeled in a tight, naturally fractured reservoir; and
(4) yielded an estimate of the system permeability (50 μd) for this zone.

7.3 REFERENCES

1. Lorenz, J. C., "Sedimentology of the Mesaverde Formation at Rifle Gap, Colorado, and Implications for Gas-Bearing Intervals in the Subsurface," Sandia National Laboratories Report SAND82-0604, March 1982.

2. Lorenz, J. C., "Predictions of Size and Orientations of Lenticular Reservoir in the Mesaverde Group, Northwestern Colorado," SPE/DOE 13851, SPE/DOE Symposium on Low Permeability Reservoirs, Denver, Colorado, May 19-22, 1985.

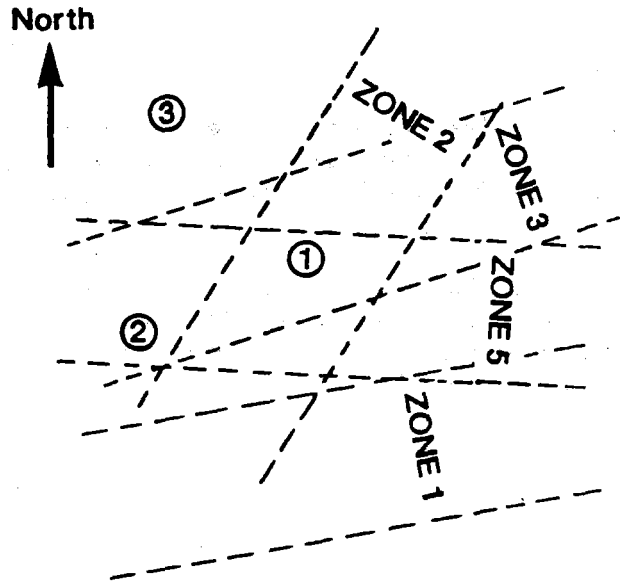

Figure 7.1 Sedimentological Interpretation of Paludal Sand 2's Location (From Lorenz, 1982)

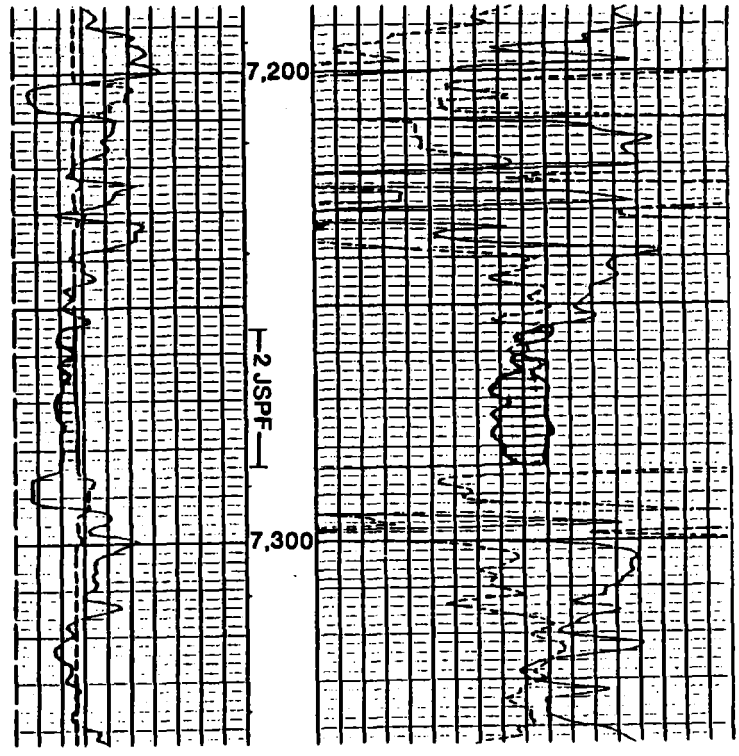

MWX-1
Paludal Zone No. 2
(7,238-7,284 ft)

Perfs. -7,256-84 ft (14gm, 2JSPF)
Res. Height $h = 28$ ft
Total Por. $\phi_t = 8.1\%$
Water Sat. $S_w = 31\%$
Core Perm.* $k_g = 2.3\mu d$

*MWX-2 core-derived average Klinkenberg permeability at 2,000 psi net stress.

Figure 7.2 Log Showing the Location of Paludal Sand 2 in MWX-1

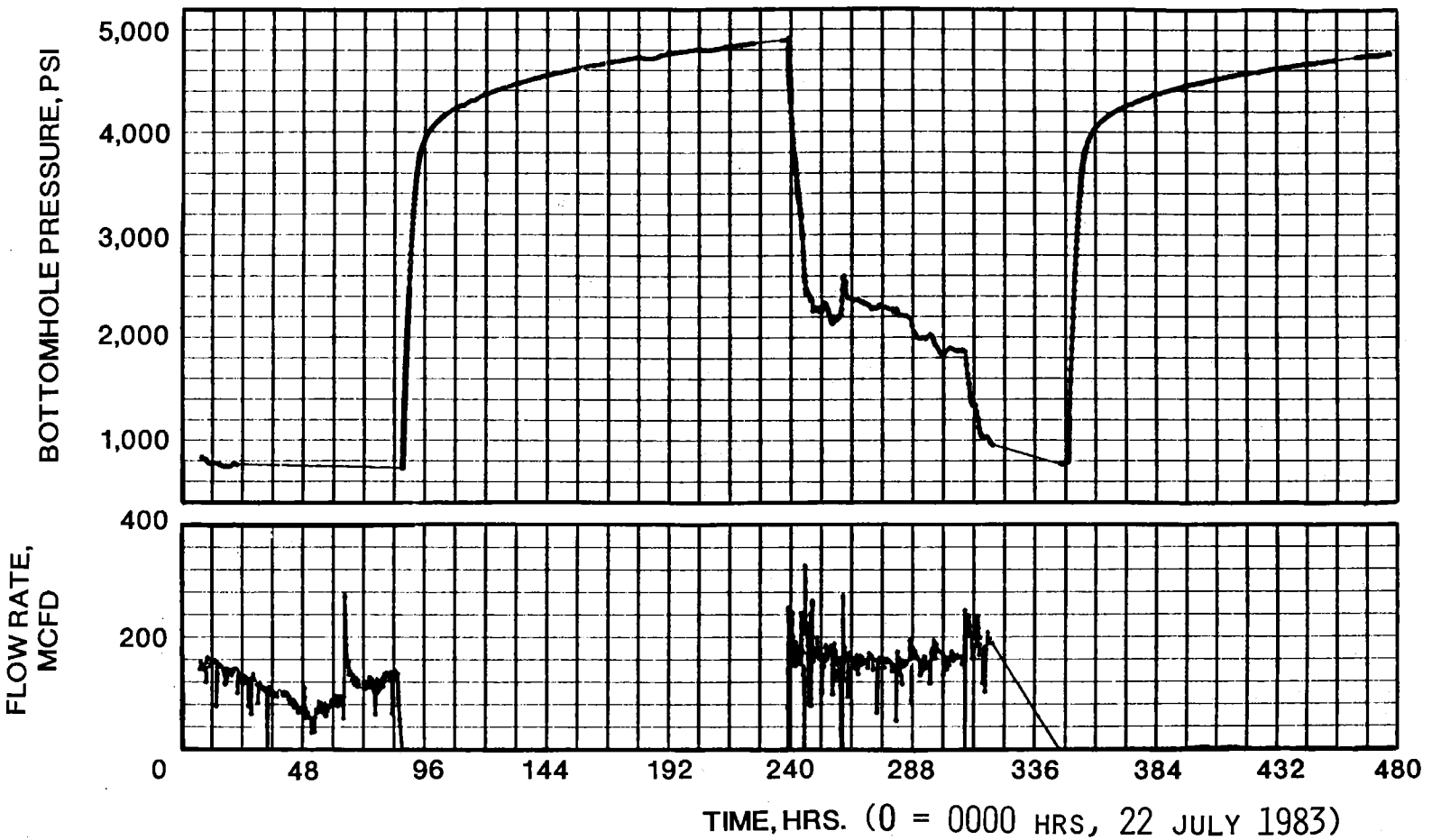

Figure 7.3 Production for the Zone 2 Test Period

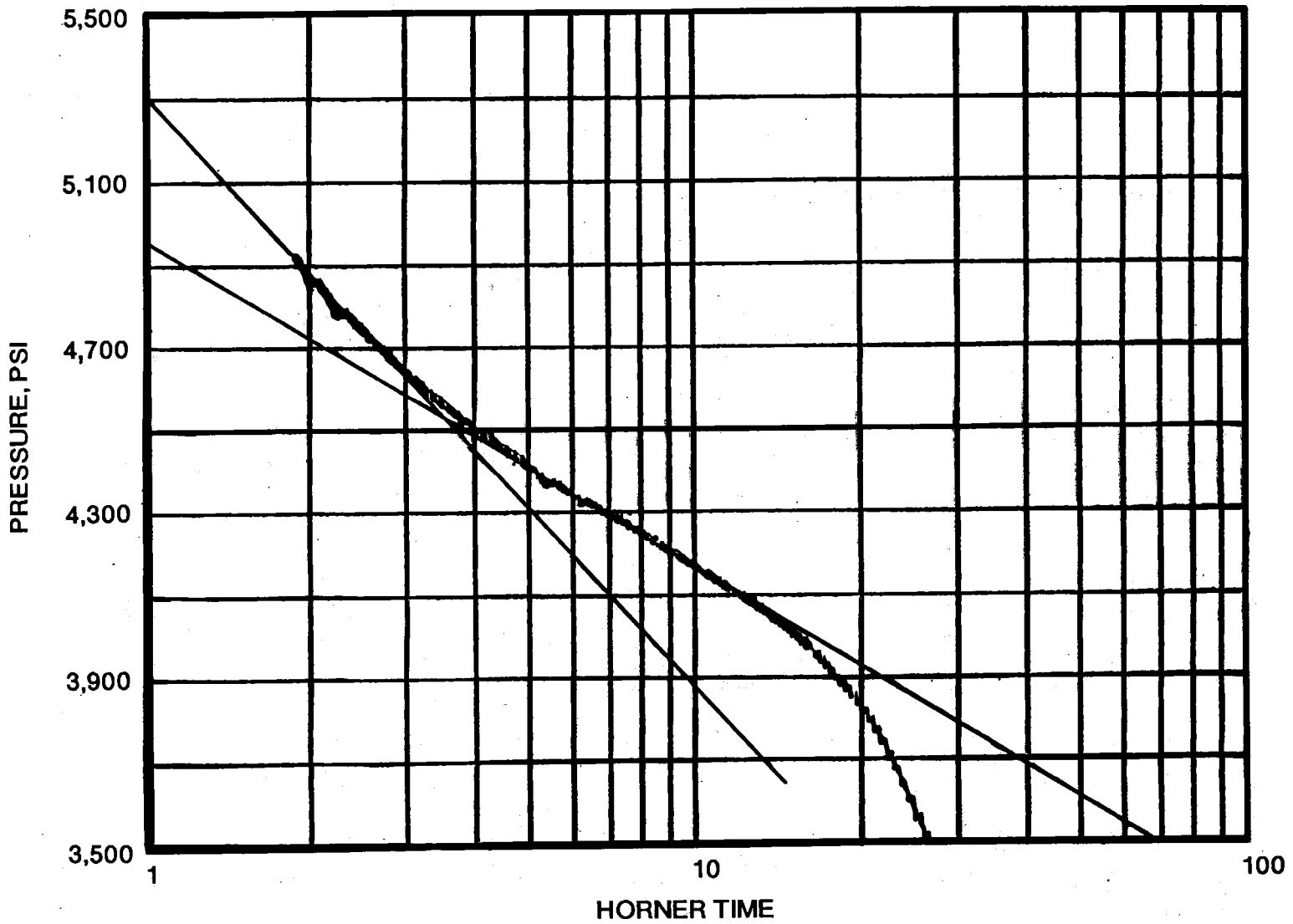

Figure 7.4 Horner Plot Detailing Bottomhole Pressure During the Final Buildup Test

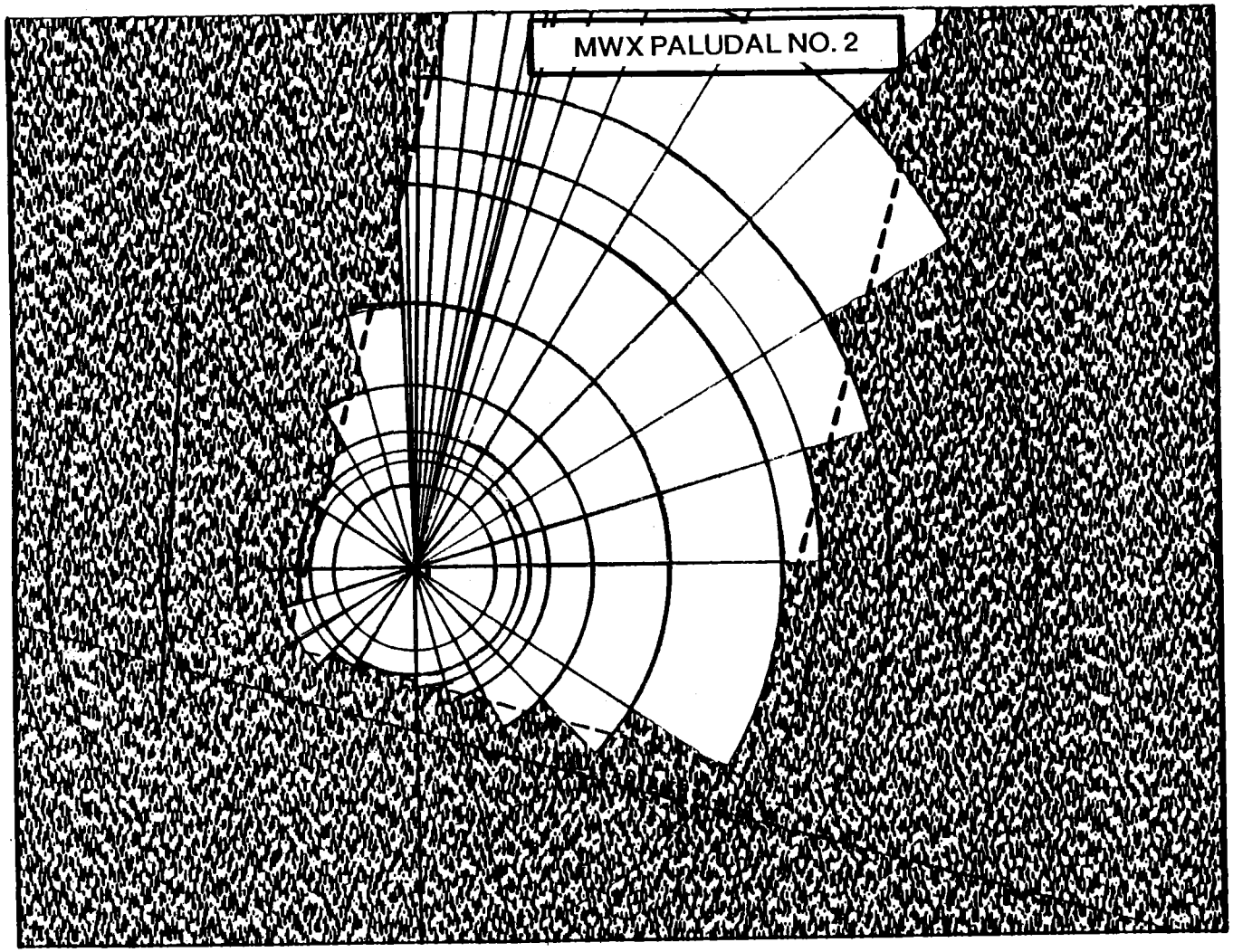

Figure 7.5 Areal View of the Paludal Sand 2 Reservoir Geometry with the Faulted Boundary

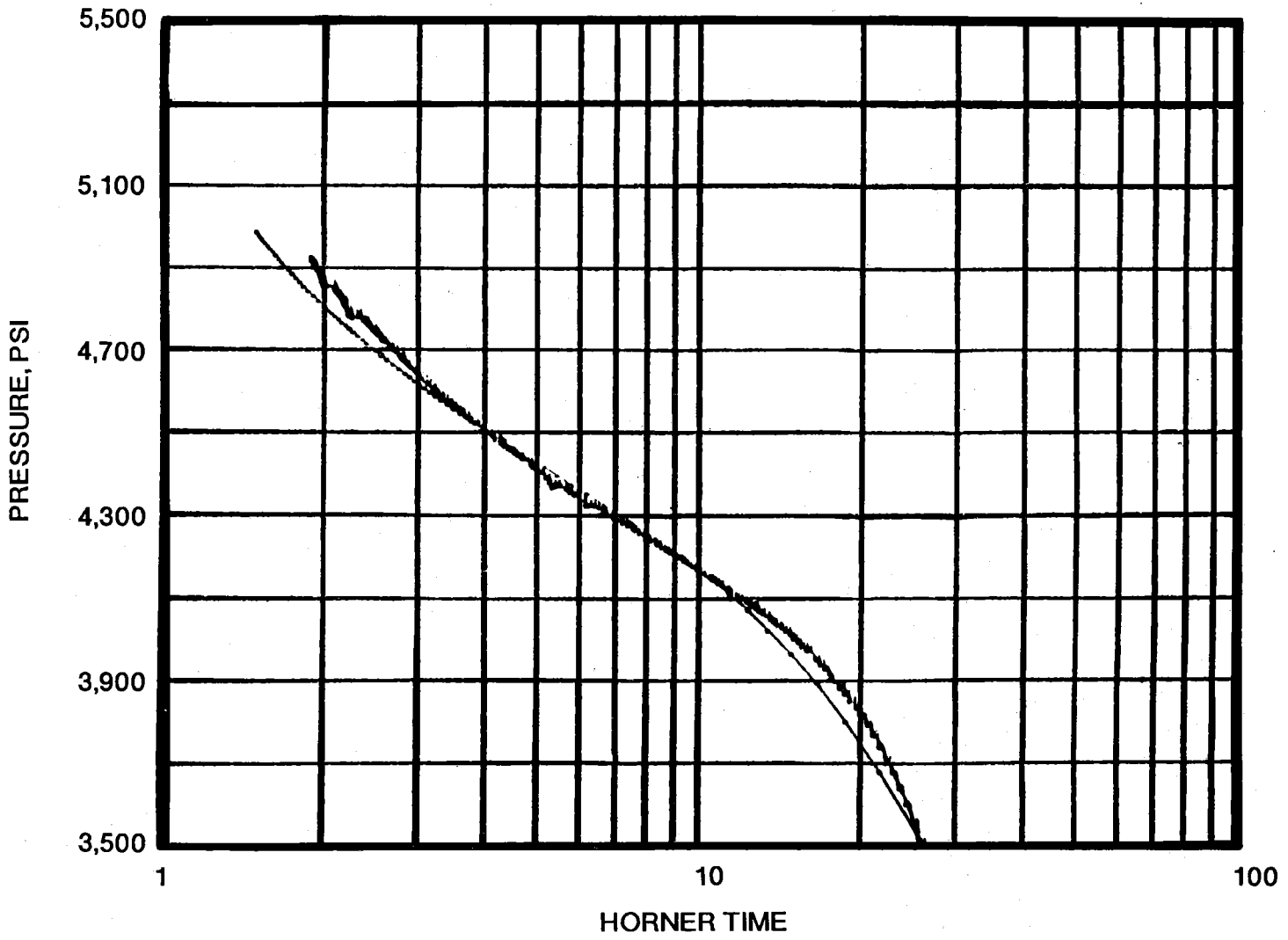

Figure 7.6 Data Fit Between Simulated and Field Data

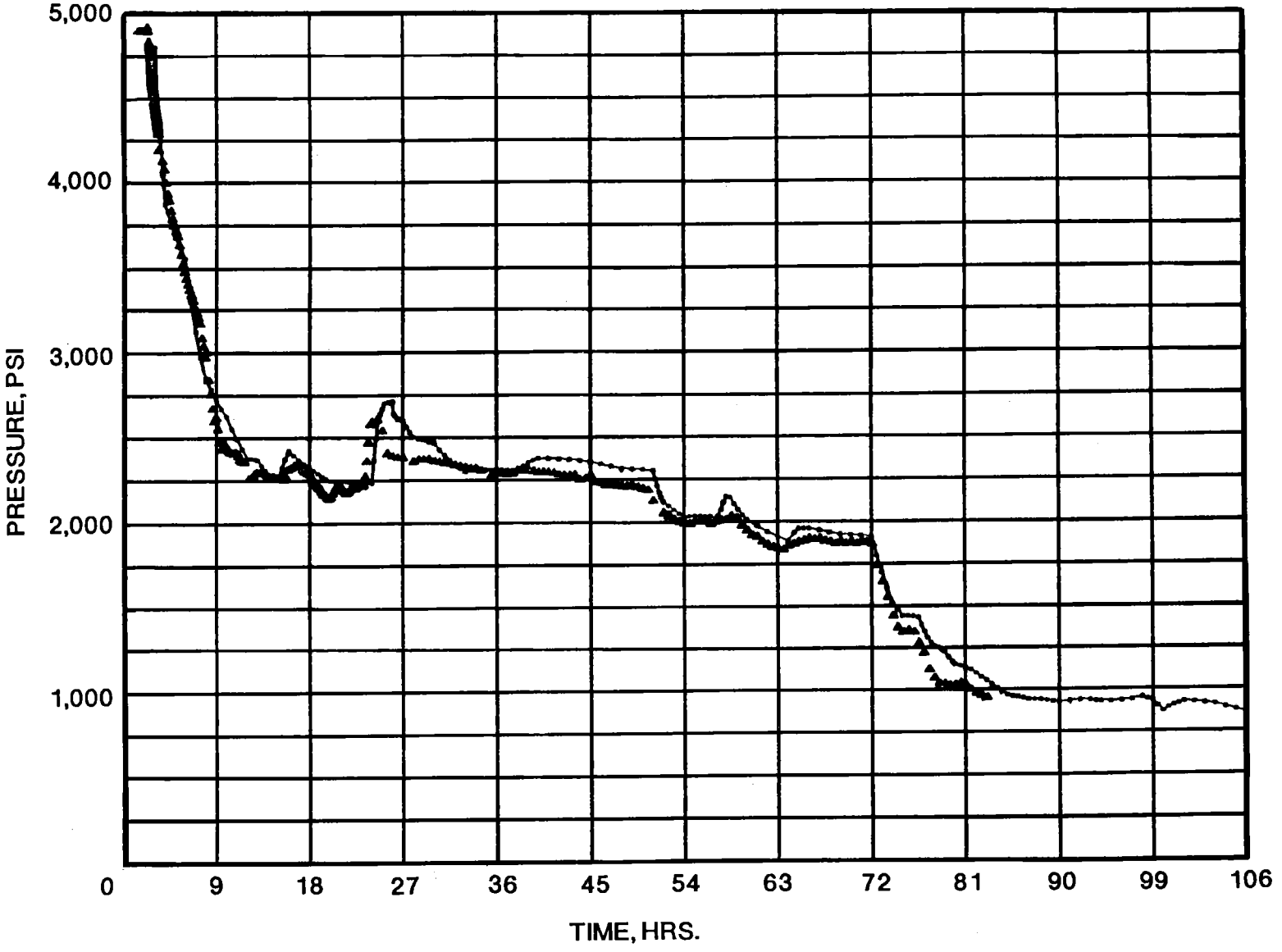

Figure 7.7 Model History Matching of the Paludal 2 Draw Down Test Data

8.0 STIMULATION EXPERIMENT--ZONES 3 and 4

8.1 PREFRAC WELL TESTING

P. T. Branagan
CER Corporation

8.1.1 DESCRIPTION

The paludal sandstones are interpreted[1,2] to be lenticular channel sandstones and splays deposited in a lower delta plain environment. The channels exhibit small width-to-length ratios, explaining the observed differences in sandstone thickness between the three closely space wells. Zones 3 and 4, shown on the logs in Figure 8.1.1, are located approximately in the middle of the paludal interval at about 7,100 ft.

An estimation of the areal extent of zones 3 and 4 was required. From outcrop studies and sedimentological analysis, channel widths were found to be approximately related to the gross sand thickness.[1,2] The channel widths for the paludal interval were found to be approximately 10 times the individual sand thickness. Therefore, zone 3 is taken to be a long channel sand, probably 300 to 400 ft wide, oriented approximately east-northeast. However, zone 4 is a splay deposit originating from the north-northwest and thinning toward the south-southwest. A fault was seen from log correlations intersecting MWX-2 above zone 4,[3] with a strike estimated to be perpendicular to the least principal stress[4] and a minimum dip of about 86 degrees northeast.

To accurately describe reservoir behavior requires integrating information from various independent data sets in to a most probable reservoir model. An extensive coring and logging program was carried out in the paludal interval to aid in this analysis (Sections 4.0 and 5.0). The core analyses included dry and restored state matrix permeability measurements. Figure 8.1.2 shows dry Klinkenberg permeability as a function of depth for cores taken from MWX-3. For zones 3 and 4 the dry

permeabilities are seen to range from 5 to 20 μd. Figure 8.1.3 illustrates the dramatic effect of net stress and water saturation on gas permeability. Depending on water saturation and net stress, in situ reservoir permeabilities may be 10 to 50 times less than dry Klinkenberg permeabilities. Based on core and log information, certain in situ reservoir parameters were estimated for each zone and are listed in Table 8.1.1.

Zones 3 and 4 were initially characterized by integrating a comprehensive set of core, log, geological, well testing and production data. The results indicated that the dominant production mechanism in zones 3 and 4 was a set of anisotropic natural fractures. The identification, quantification and incorporation of this anisotropic natural fracture system was critical to the subsequent postfrac production and well test analysis.

Prefrac well tests were performed to assess reservoir performance of zones 3 and 4. The proximity of the two observation wells allowed interference testing to be conducted in reasonable time periods. Interference data could be used in an assessment of areal reservoir continuity and to help describe the asymmetry of the natural fracture flow capacity. The data gathered from production/interference tests were interpreted using both standard analytical techniques and computer reservoir modeling. The fault intersecting MWX-2 perturbed normal test procedures but provided a unique opportunity for analysis.

The three wells were all completed by initially perforating zones 3 and 4 through 7-in. diameter casing with 14-gram charges at a shot density of 2 per foot. MWX-1 was perforated at 7076-7100 ft and 7120-7144 ft, MWX-2 was perforated at 7060-7088 ft and 7107-7131 ft and MWX-3 was perforated at 7080-7102 ft and 7126-7146 ft. A perforation breakdown/balloff was performed in MWX-1 with 3 percent KCl water through 2.875-in. production tubing. All subsequent well testing and stimulations were performed in the two commingled sands. Testing of the

individual sands was not conducted due to the proximity of the zones and testing time constraints.

8.1.2 WELL TESTING MWX-2 FAULT

A short pressure buildup test in MWX-2 was performed to assess the effects of the fault on reservoir behavior. No perforation breakdown was required and MWX-2 was produced for 24 hours at 150 MCFD and then shut in with a bottomhole shut-in tool. The results of the bottomhole pressure buildup data are shown in Figures 8.1.4 and 8.1.5, which are standard "square root of time" and Horner plots, respectively. Both plots exhibit a shape indicative of a linear vertical hydraulic fracture. Assuming an infinitely conductive vertical fracture,[5] an estimated fracture length, L_f, of 9 ft was calculated from the skin factor derived from the Horner plot. Analysis of the linear portion of the square root of time plot (Figure 8.1.4), shows a slope of about 470 psi/$\sqrt{\text{hr}}$. Assuming a uniform flux fracture[6] and a bulk matrix permeability of 3 md, a fracture length of 32 ft was calculated.

Although the above analytical methods have limitations, an estimate of the effective fault length can be made. The fault appears to behave as a highly conductive vertical fracture 10 to 35 ft in length. The slope of the Horner plot, as shown in Figure 8.1.5, increase sharply at about 48 hrs. If this slope change is assumed to be due to a nearby boundary, an approximate distance to the boundary is 50 ft.

8.1.3 MWX-1 PRODUCTION/INTERFERENCE TESTING

Drawdown, buildup, and interference tests were conducted in MWX-1 to determine certain reservoir parameters for eventual use in comparison with postfrac well testing. The drawdown and buildup tests provided "base-line" reservoir behavior, while the interference testing aided in describing areal reservoir continuity and asymmetry of the reservoir flow capacity.

Interference testing of paludal zones 3 and 4 began on October 20, utilizing MWX-2 and MWX-3 as observation wells and MWX-1 as the production well. Initial production began at 120 MCFD; however, it became apparent within several hours that production could not be maintained at that rate. The following day, MWX-1 was shut in for one day to rebuild pressure in order to lift liquids in the wellbore. The difference between surface and bottomhole pressures indicated a liquid height greater than 4000 ft. MWX-2 and 3 were previously shut in using bottomhole closure tools, and the bottomhole pressures in these well showed no indication of the small pressure perturbation generated by the first drawdown and shut-in of MWX-1.

On October 22, MWX-1 was put on production at a rate of 280 MCFD and within two hours was essentially dead. Surface pressures were at atmosphere and the well was producing only sporadically. When the bottomhole gauge in MWX-1 was removed, 10 bbl of water were produced. The well began to kick and some production began on October 24. The well was swabbed to within approximately 200 ft of the perforations and, following the swabbing, production increased rapidly to 270 MCFD and was choked back to 200 MCFD.

The production/interference testing of MWX-1 consisted of about 7 days of multiple flow rate drawdown testing (200 to 300 MCFD) and 7 days of bottomhole shut-in pressure buildup testing. Bottomhole pressures were recorded in all three wells. Figure 8.1.6 illustrates the flow rates and bottomhole pressures measured during the test. A listing of the relevant data is given in Appendix 12.7.2.

Although some small pressure changes appear in the observation wells, it can be seen in Figure 8.1.6 that no definite correlation of these small pressure fluctuations and the transient interference from the producing well, MWX-1, can be made. It is possible there is no areal sand continuity between the wells, but geologic and geophysical

information do not support this conclusion. Another possible explanation for the apparent absence of interference is that the test duration was insufficient to record the interference transient in the observation wells. However, analysis of buildup data from MWX-1, as shown in Figure 8.1.7, indicates a bulk reservoir permeability of about 36 μd (kh = 0.95 md-ft, skin = 0.59), which would indicate that pressure changes from MWX-1 should be seen 150 ft away in MWX-2 and probably 225 ft away in MWX-3 very early in the test. Several other phenomena, such as blockage at the observation wells caused by capillary pressure within the fractures, or a severely asymmetric fracture flow capacity within the reservoir, are probably acting either individually or in concert.

8.1.4 RESERVOIR MODELING--HOMOGENEOUS MODEL

Due to the complex nature of these two commingled sands, computer modeling was used to provide a more detailed analysis of the production/interference test results. The productivity and pressure data were initially studied using a single phase, single porosity, three-dimensional model. Figure 8.1.8 illustrates a plan view of the reservoir model representation. The productive portions of zone 3 are assumed to pinch out in the direction toward MWX-3, while zone 4 is a assumed to be continuous between all the wells. There were three major obstacles to developing an accurate reservoir model for zones 3 and 4:

- two commingled sands of differing sedimentological makeup, with somewhat ambiguous areal dimensions;

- no measurable pressure interference in the two observation wells; and

- a conductive fault passing near one of the zones in MWX-2.

Numerous reservoir simulations were performed in an attempt to evaluate and characterize the two sands and the observed fault. Variations were made to account for the fault spacing as a no flow boundary, or conversely as a constant pressure source. Zones 3 and 4 were assumed to be either similar or highly variable in permeability, and various size areas of reduced permeability around the observation wells were used to simulate near wellbore damage or blockage.

For most of the simulation runs, the main criterion was to maintain a match of flow rate and minimize the error in the bottomhole pressure in the production well, MWX- 1, while varying given reservoir parameters. Further, every effort was made to minimize the pressure transients at the observation wells. Table 8.1.2 gives example results for several simulation attempts. Input data are shown in the left-side columns and include the reservoir conditions at or behind the fault, the fault permeability and porosity, the reservoir porosity, and gas permeabilities for zones 3 and 4 independently. Calculated values are the flow rate after seven days of production and the interference pulses at wells MWX-2 and MWX-3. For almost all the cases that were analyzed, the simulation results indicate that interference pressures should have varied sufficiently to have been detected at the observation wells. This is not consistent with the well test data. The only case that exhibited marginally detectable interference pressures assumed that the fault in MWX-2 behaved as a constant pressure boundary, that the permeabilities in zones 3 and 4 were considerably different (75 md and 5 md, respectively), and that there was no areal continuity of zone 3 between MWX-1 and MWX-3.

8.1.5 RESERVOIR MODELING--NATURAL FRACTURE MODEL

To further investigate the characteristics of these sands, a naturally fractured reservoir simulator or dual porosity model was used to model reservoir testing behavior. This reservoir simulator provides the proper inclusion of transient pressure behavior in the matrix blocks

as well as the natural fracture system.[7] The formulation of the model allows accurate and efficient simulation of complex reservoirs, including an anisotropic, naturally fractured reservoir that contains a propped hydraulic fracture. In an attempt to simplify the model and reduce computation time, the two sands were considered as a single sand body.

A comprehensive naturally fractured reservoir simulation study was performed to obtain an acceptable model for zones 3 and 4. The prefrac, naturally fractured reservoir model consisted of a 350-ft wide channel sandstone, 40 ft thick, with an orthogonal natural fracture set spaced 5 ft apart.[8]

Initial simulations[9] used large anisotropy ratios (Kx/Ky) for natural fracture permeability. This was consistent with the pressure interference test results observed in the marine Cozzette sand and the lack of pressure interference in the two offset wells during paludal tests. In a two-well interference test in the Cozzette sandstone, an anisotropy ratio of about 100 was found to provide an acceptable match for both interference and production data. This rather large permeability anisotropy is also sufficient to model the lack of pressure interference in the paludal test. However, when the postfrac data are also considered, as will be discussed in later sections, the large anisotropy ratios cannot by themselves account for other features, such as damage caused by the hydraulic fracturing treatment.[11]

A good match of the prefrac data shown in Figures 8.1.6 and 8.1.7 was obtained using a matrix permeability of 0.001 md and a set of interconnected, anisotropic natural fractures with 5,000 md and 500 md permeabilities in the orthogonal directions. Figure 8.1.9 illustrates the naturally fractured reservoir simulation model used to history match the prefrac well test data. Table 8.1.3 lists the most significant reservoir parameters used to model the prefrac reservoir performance and well test data. These reservoir parameters were extracted from and

thought to be consistent with log, core, and geological data. The direction of maximum natural fracture permeability was taken to be in the direction of the maximum principal stress, N75°W.

The results of the naturally fractured reservoir simulation are compared with field data in the Horner plot in Figure 8.1.10 and the log-log/derivative plot in Figure 8.1.11. These plots show that the proposed naturally fractured reservoir simulation model accurately predicted the semi-log pressure, log-log pressure and log-log derivative behavior of the prefrac buildup. This also indicates that the naturally fractured reservoir model is sufficiently accurate to describe the different production mechanisms and reservoir properties of these paludal sandstones.

The prefrac reservoir modeling also indicated that a small area of reduced permeability probably extended about 2.5 ft from the wellbore. This damage zone was simulated by reducing the minimum natural fracture permeability from 500 to 100 md. This near wellbore damage was attributed to liquids and/or drilling fluids obstructing the flow of gas through the natural fractures.

This model predicts that observable pressure transients should have been present in the offset wells, whereas none were observed. However, each of the offset wells were broken down with KCl water and the tests were conducted with water in the wellbore. Capillarity and attendant water blockage effects in the small natural fractures may have significantly attenuated the pressure pulse. Secondly, and possibly more significant, these distributary channel reservoirs have many draping mudstone/carbonaceous features (Section 3.3) that may act as both permeability breaks and natural fracture breaks. Thus, these features may subdivide the channels into poorly connected segments and also attenuate any interference pulse.

This prefrac reservoir model forms the basis for all subsequent reservoir simulation analyses. The 10 to 1 permeability anisotropy of the natural fracture system is a key feature of these studies and controls many of the later postfrac results.

8.1.6 REFERENCES

1. Lorenz, J. C., "Sedimentology of the Mesaverde Formation at Rifle Gap, Colorado, and Implications for Gas-Bearing Intervals in the Subsurface," Sandia National Laboratories Report, SAND82-0604, March 1982.

2. Lorenz, J. C., "Predictions of Size and Orientations of Lenticular Reservoir in the Mesaverde Group, Northwestern Colorado," Proceedings, SPE/DOE 13851, Presented at SPE/DOE Symposium on Low Permeability Reservoirs, Denver, Colorado, May 19-22, 1985.

3. Kukal, G. C., "Well Log Analysis of the Paludal Interval," CER Report, October 1984 (given in Appendix 12.3).

4. Clark, J. A., "The Prediction of Hydraulic Fracture Azimuth through Geological, Core and Analytical Studies," SPE/DOE 11611, Presented at SPE/DOE Low Permeability Symposium, Denver, Colorado, March 14-16, 1983.

5. Matthews, C. S. and D. G. Russell, "Pressure Buildup and Flow Tests in Wells," Monograph Series, Vol. 1 Society of Petroleum Engineers of AIME, Dallas, TX, 1967.

6. Earlougher, R. C., Jr., "Advance in Well Test Analysis," Monograph Series, Vol 5, Society of Petroleum Engineers of AIME, Dallas, Texas, 1977.

7. Branagan, P. T., C. Cipolla, S. J. Lee, and J. Chen, "Designing and Evaluating Hydraulic Fracture Treatments in Naturally Fractured Reservoirs," SPE/DOE 16434, Proceedings, SPE/DOE Symposium on Low Permeability Reservoirs, Denver, Colorado, May 1987.

8. Lorenz, J. C. and S. J. Finley, "Differences in Fracture Characteristics and Related Production of Natural Gas in Different Zones of the Mesaverde Formation, Northwestern Colorado," SPE 16809, Presented at 62nd Annual Tech. Conf. of SPE, Dallas, TX September 27- 30, 1987.

9. Branagan, P. T., C. L. Cipolla, S. J. Lee, and R. H. Wilmer, "Comprehensive Well Testing and Modeling of Pre- and Post-Fracture Well Performance of the MWX Lenticular Tight Gas Sands," SPE 13867, Presented at SPE/DOE 1985 Low Permeability Gas Reservoirs Symposium, Denver, CO, May 19-21, 1985.

10. Northrop, D. A., ed., "Multiwell Experiment Final Report: I, The Marine Interval of the Mesaverde Formation," Sandia National Laboratories Report, SAND87-0327, April 1987.

11. Branagan, P. T., C. L. Cipolla, S. J. Lee, and L. Yan, "Case History of Hydraulic Fracture Performance in the Naturally Fractured Paludal Zone: The Transitory Effects of Damage," SPE 16397, Presented at 1987 SPE Low Permeability Reservoirs Symposium, Denver, CO, May 18-19, 1987.

Table 8.1.1 CORE AND LOG-DERIVED RESERVOIR CHARACTERISTICS OF PALUDAL ZONES 3 AND 4

Property		Zone 3	Zone 4
Total Matrix Porosity		10.3%	10.2%
Water Saturation		46.0%	46.0%
Matrix Gas Permeability at S_w = 45%		3.0 μd	<0.5 μd
Type of Deposit		channel	splay
Productive Thickness in:	MWX-1	8 ft	18 ft
	MWX-2	12 ft	2 ft*
	MWX-3	0 ft	14 ft
Gas Viscosity		0.02 cp	0.02 cp
Reservoir Temperature		210°F	210°F

*Fault masks true reservoir thickness in MWX.2

Table 8.1.2 Reservoir Modeling Paludal Zones 3 and 4

Reservoir Conditions at/or Behind Fault	Fault			Formation			Production Well MWX-1	Pressure Change at Interference Well	
	K_z	ϕ_g	K_{xy}	ϕ_g	K_g-3	K_g-4		MWX-2	MWX-3
No Flow Fault	0	0	0	0.036	60	60	300 MCFD 7 Days	0	127
	0	0	0	0.036	50	50	300 MCFD 7 Days	0	120.9
(Skin MWX-3 0.5μd)	0	0	0	0.036	50	50	300 MCFD 7 Days	0	107.6
(Skin MWX-3 5.0μd)	0	0	0	0.036	50	50	300 MCFD 7 Days	0	119.6
	0	0	0	0.036	80	20	300 MCFD 7 Days	0	31.4
Finite Reservoir Beyond a Highly Conductive Fault	∞	1	∞	0.036	75	5	250 MCFD 7 Days	77.5	0.8
	∞	.0036	∞	0.036	75	5	250 MCFD 7 Days	94.6	15.9
	0	.0036	∞	0.036	75	5	250 MCFD 7 Days	282.9	14.22
Constant Pressure Fault	∞	∞	∞	0.036 ∞	40 ∞	40 ∞	250 MCFD 7 Days	0.03	66.25
	∞	∞	∞	0.036 ∞	75 ∞	5 ∞	250 MCFD 7 Days	0.02	0.71

Table 8.1.3 Pre-Fracture Model Input Data

BASE RESERVOIR DATA	MATRIX PROPERTIES	NATURAL FRACTURE PROPERTIES
Channel width = 350 ft	k_m = 1.0 μd	k_x = 5,000 md
P_i = 5,400 psi	ϕ_g = 0.04	k_y = 500 md
Depth = 7,000 ft		ϕ_g = 1.0
T_{res} = 210° F		Spacing = 5 ft
h_{net} = 40 ft		w = 0.001 in.
SG = 0.626		skin, 2.5 ft in y-direction
		k_s = 100 md

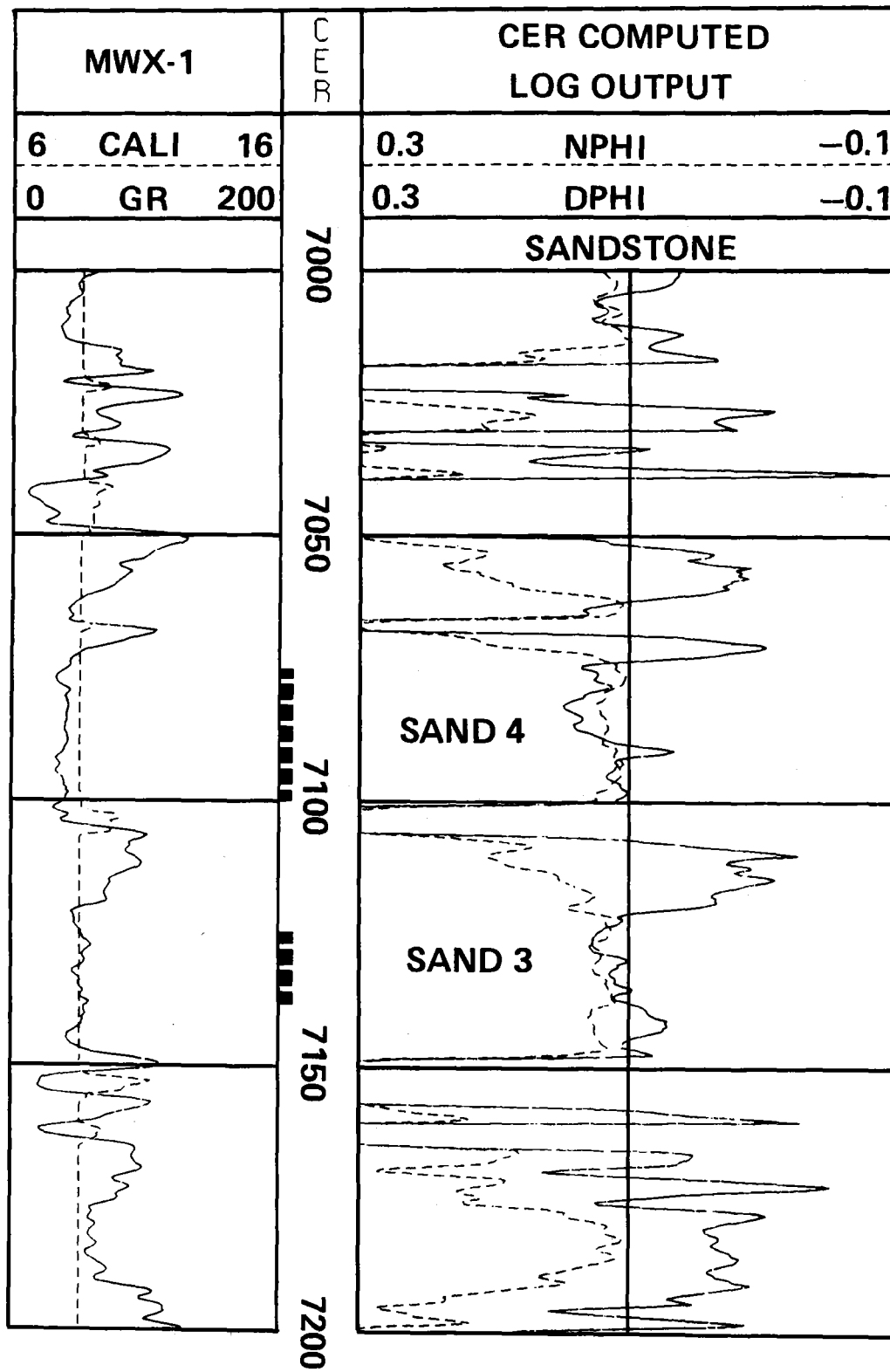

Figure 8.1.1 Gamma Ray and Density Logs for Paludal Interval, Illustrating Sands 3 and 4

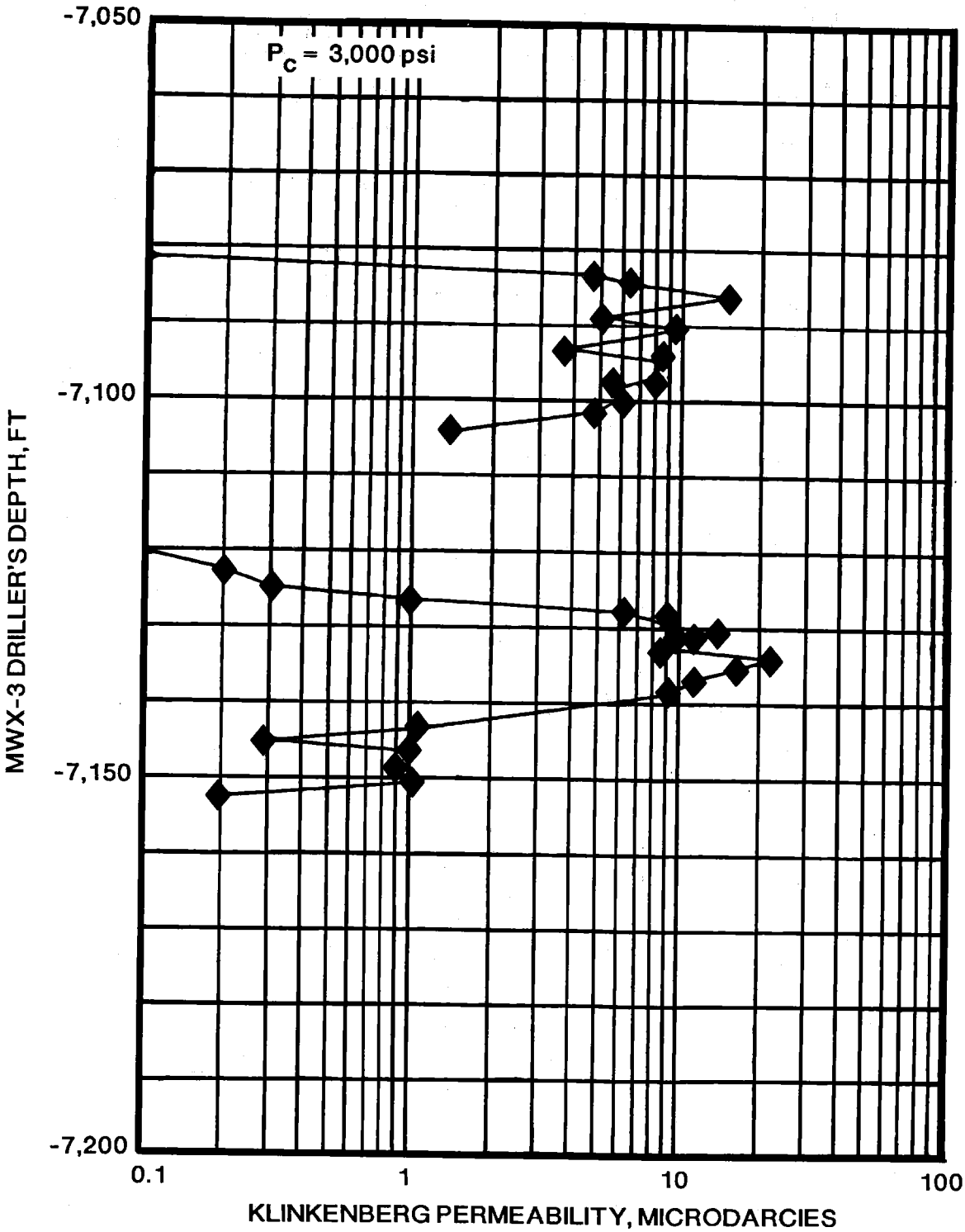

Figure 8.1.2 Dry Klinkenberg Permeability from MWX-3 Core, Paludal Sands 3 and 4

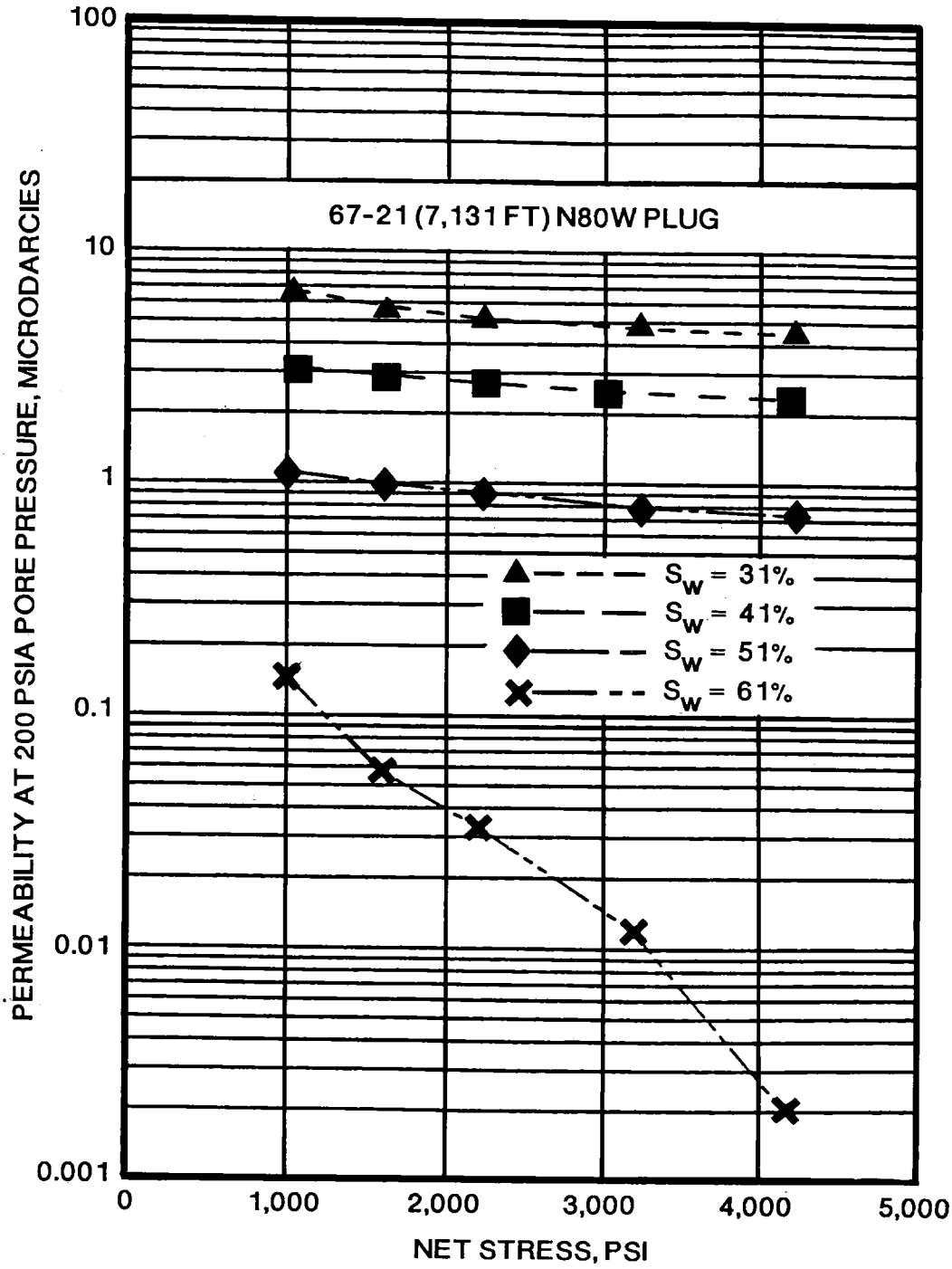

Figure 8.1.3 Effect of Net Stress and Water Saturation on Matrix Permeability of MWX-3, Paludal Sand 3 Core

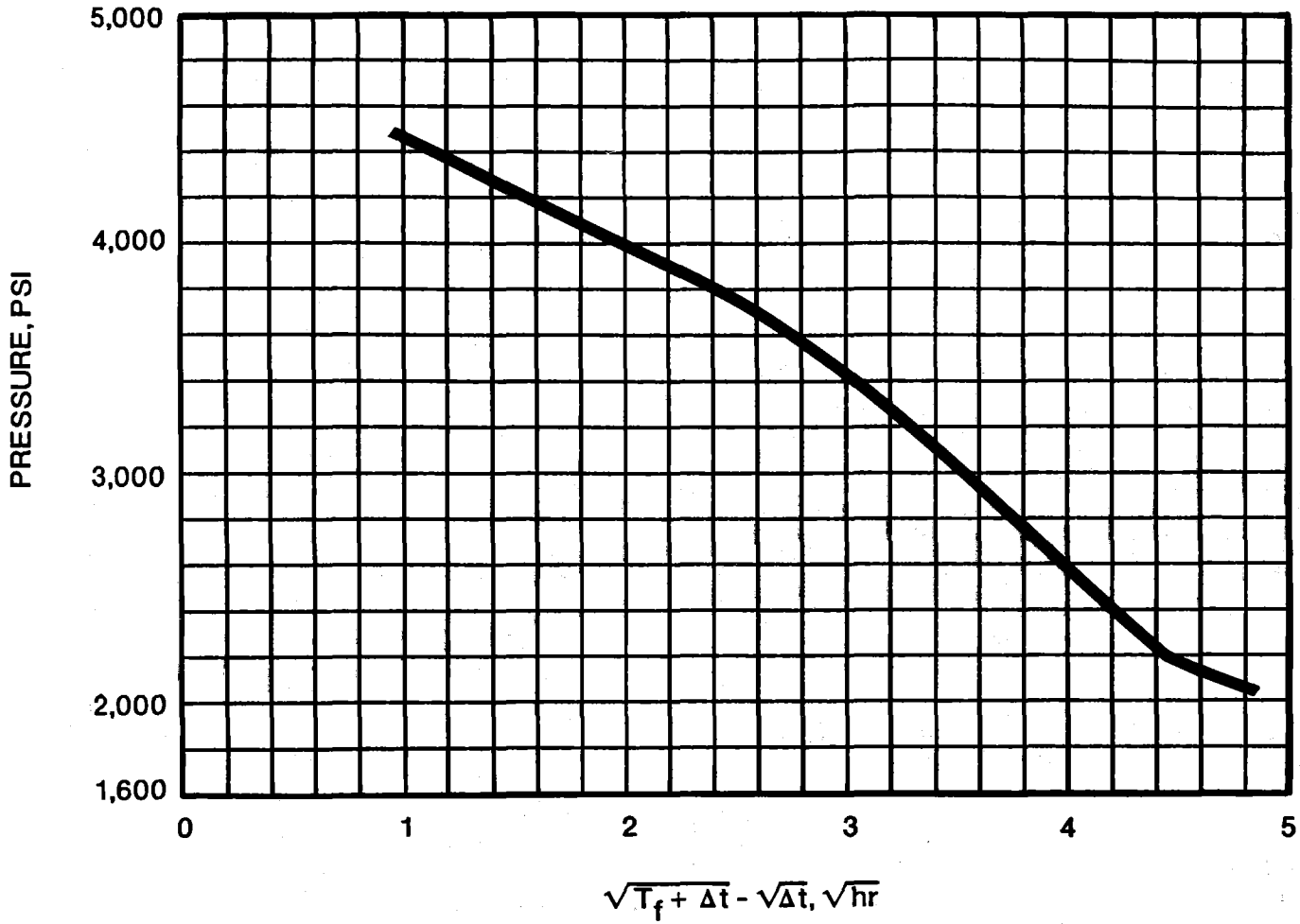

Figure 8.1.4 Pressure Vs. Square Root of Time from Buildup Data for the MWX-2 Fault

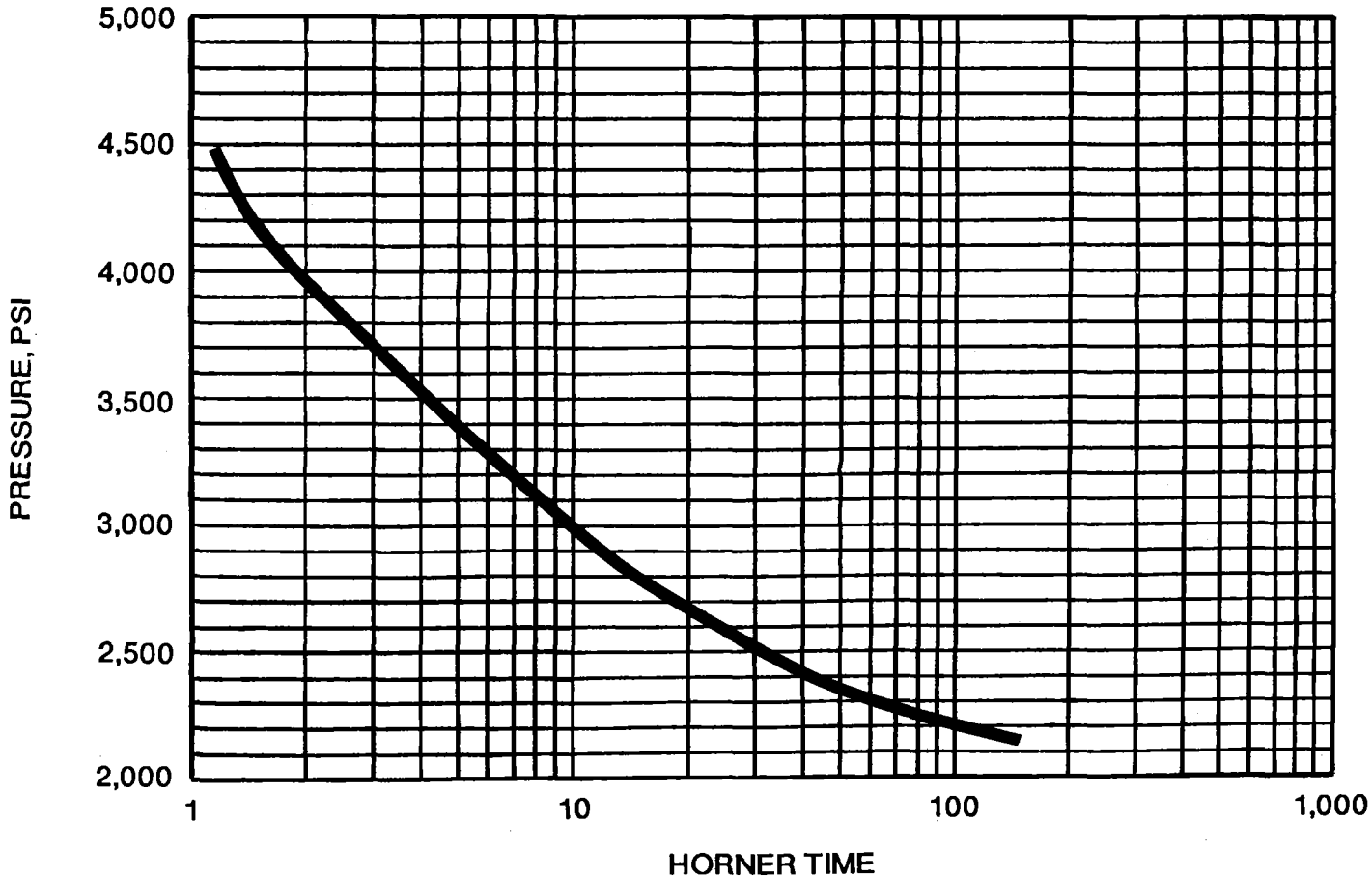

Figure 8.1.5 Horner Plot of Buildup Data for the MWX-2 Fault

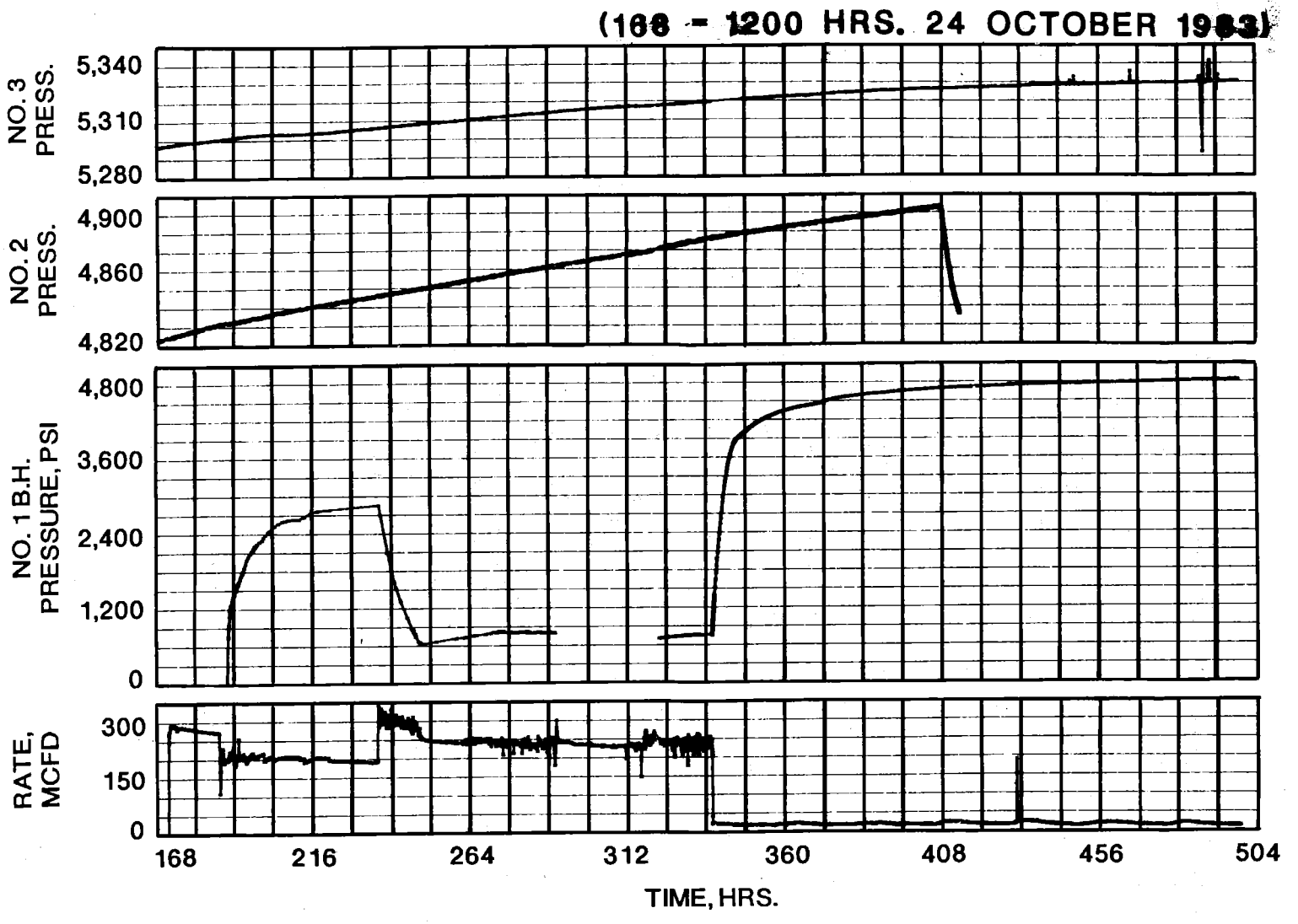

Figure 8.1.6 Pre-Frac Well Testing Flow Rate and Bottomhole Pressure Data for MWX-1 and Shut-In Bottomhole Pressure for Observation Wells MWX-2 and MWX-3

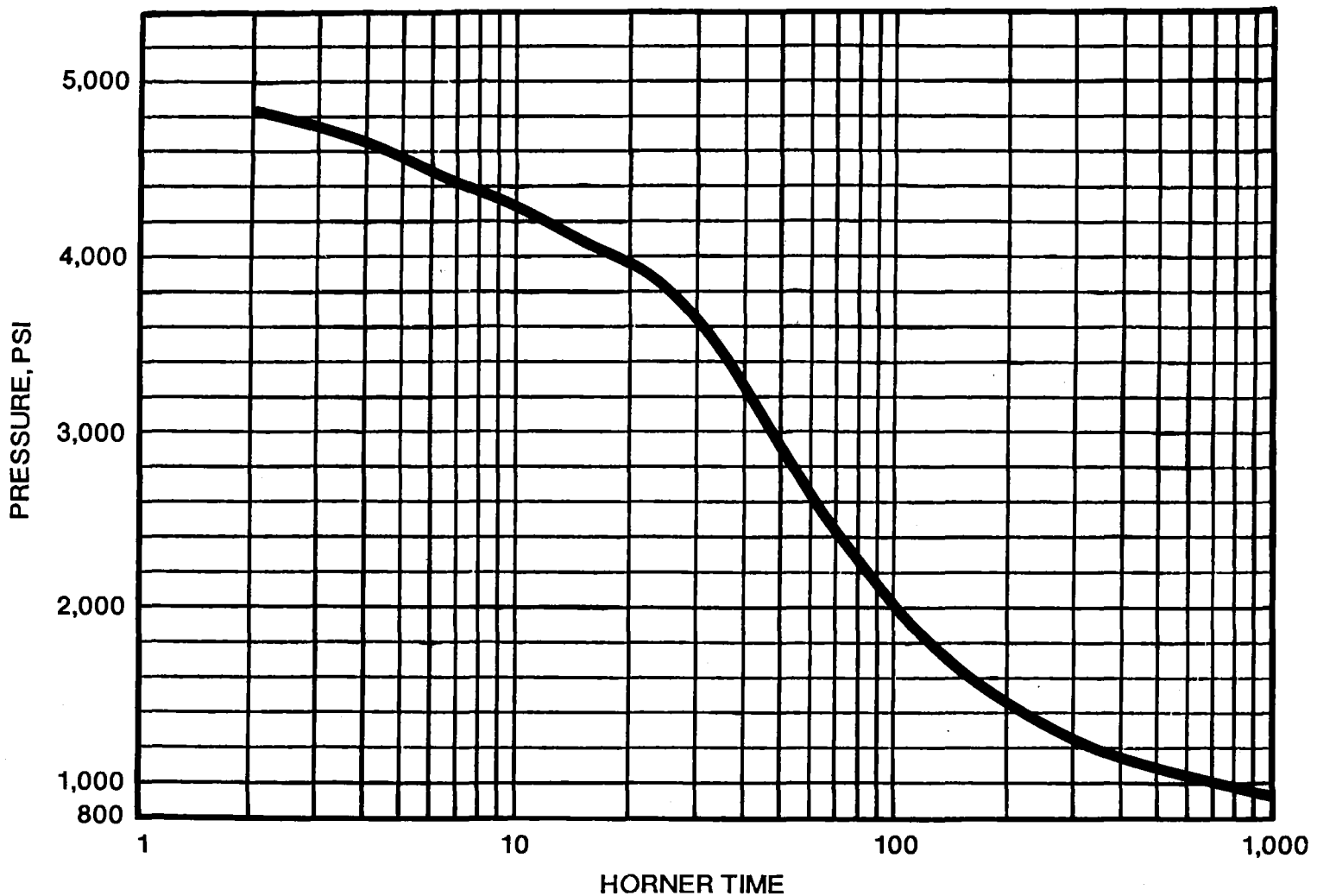

Figure 8.1.7 Horner Plot of Bottomhole Shut-In Pressure Data from Pre-Frac Well Testing, MWX-1

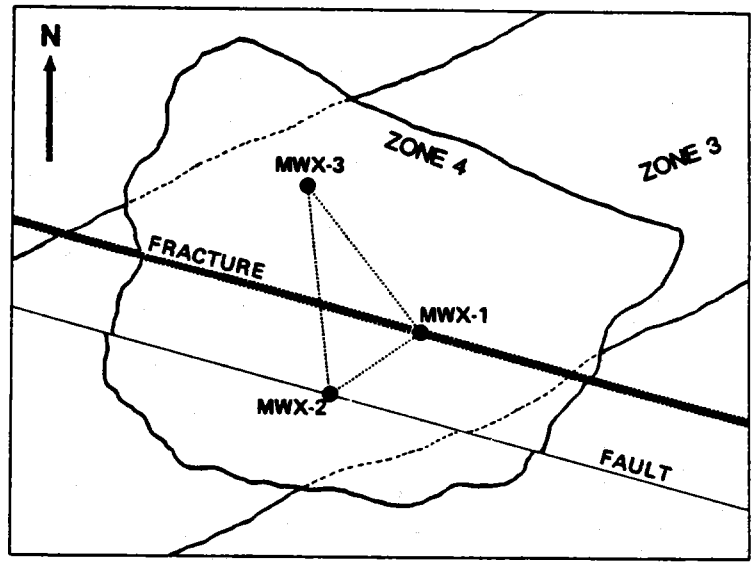

Figure 8.1.8 Estimated Areal Dimensions of Paludal Sands 3 and 4 Illustrating MWX Well Locations Along with Fracture and Fault Orientations

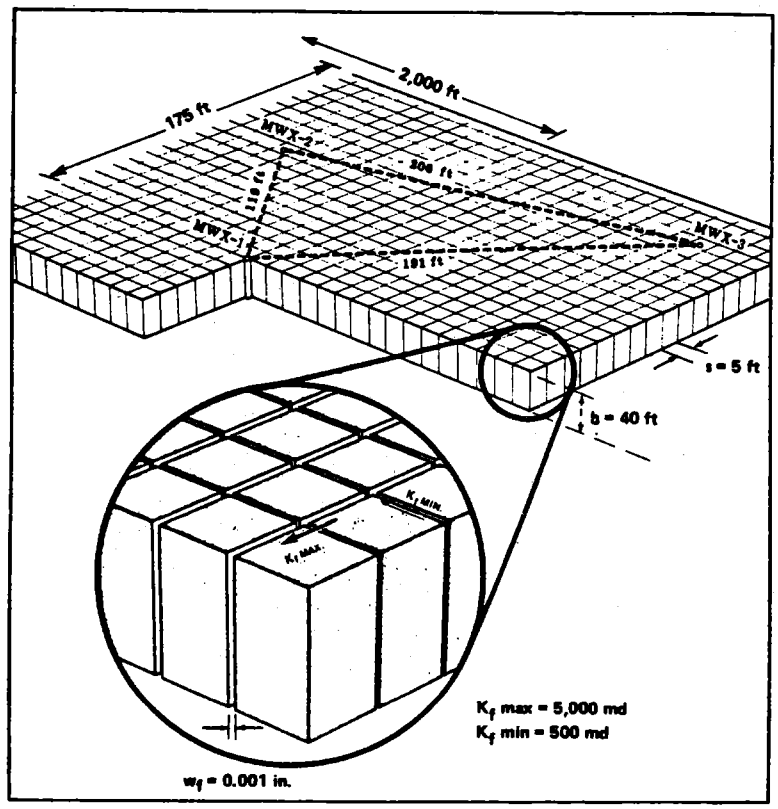

Figure 8.1.9 Naturally Fractured Reservoir Model for the Base Case Paludal Sands 3 and 4

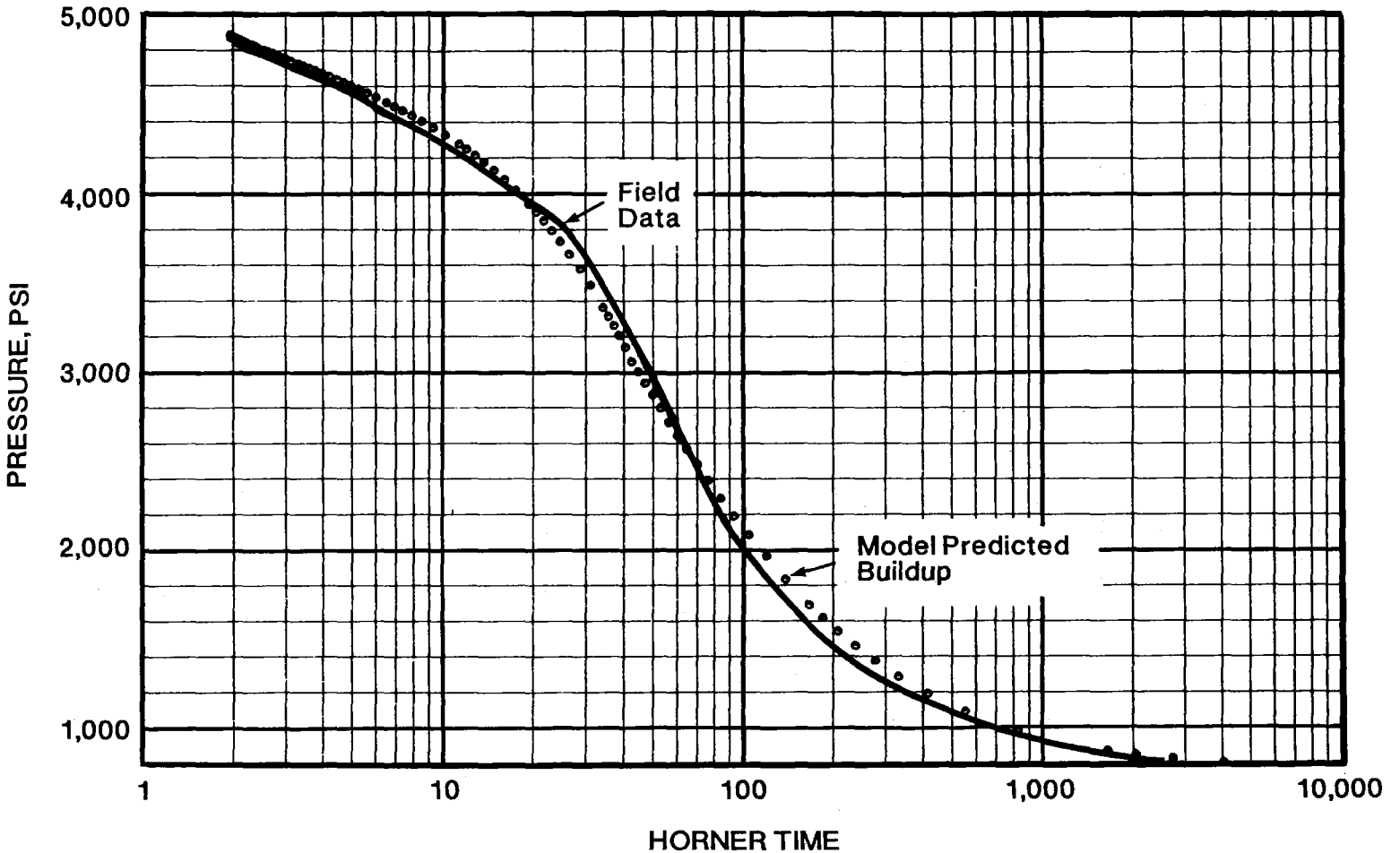

Figure 8.1.10 Pre-Fracture Horner Plot

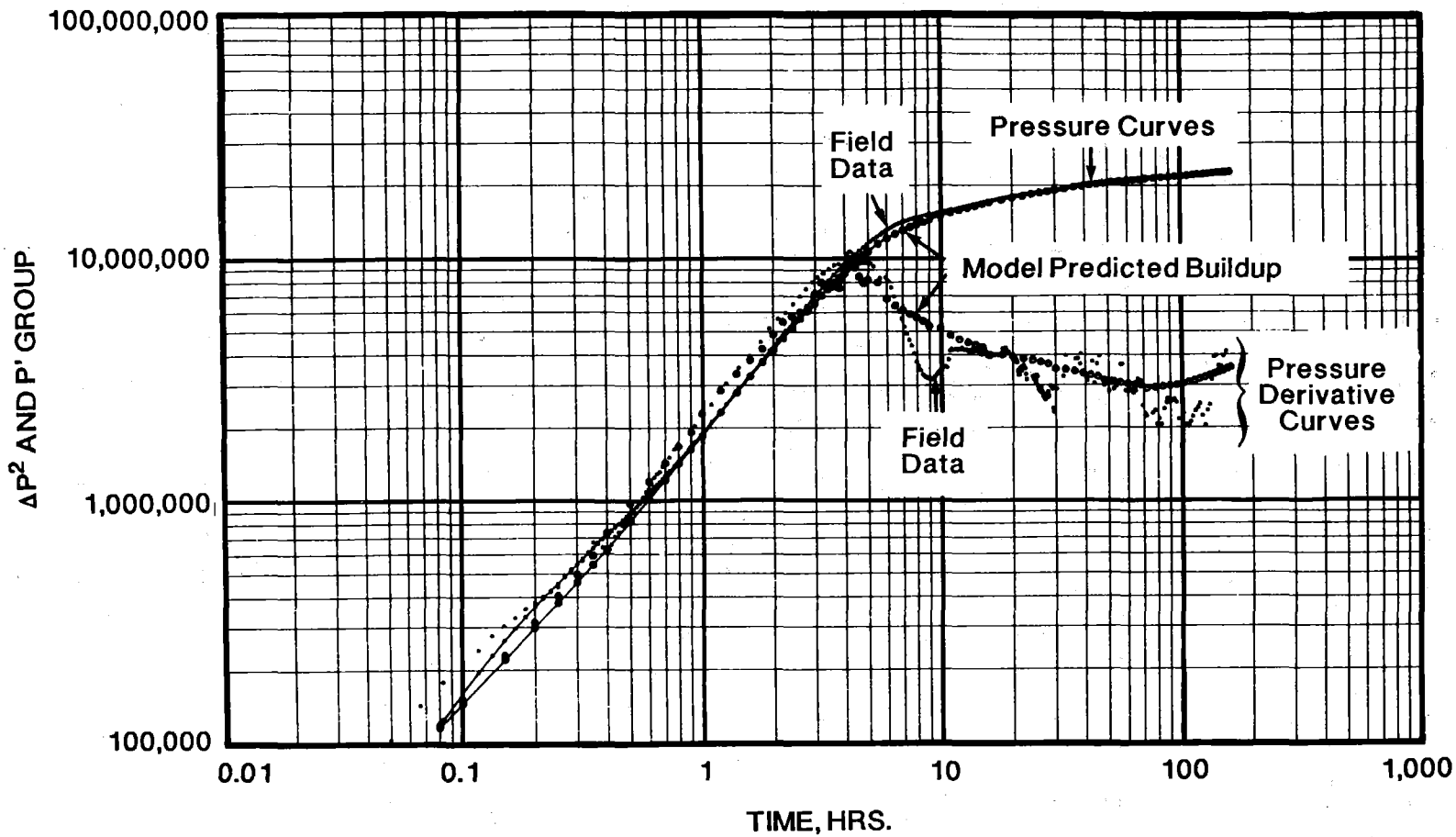

Figure 8.1.11 Pre-Fracture Log-Log Plot

8.2 STIMULATION--PHASE I

N. R. Warpinski
Sandia National Laboratories

8.2.1 OBJECTIVES

The objectives of the paludal stimulation were (1) to map and characterize hydraulic fracture behavior in a lens and (2) to test stimulation techniques and resulting production mechanism in this complex lithology. To achieve these objectives, the stimulation was divided into two phases. Phase I consisted of a series of step rate tests, pump-in/flowback tests and minifracs while Phase II was the primary stimulation. A summary of all of these tests can be found in Reference 1.

The purpose of the phase I minifracs was twofold: 1) to attempt to map fracture behavior in a lenticular reservoir; and 2) to obtain design information for the main treatment. The approach was to conduct one small, unpropped minifrac and try to determine its important characteristics, and then to conduct a second minifrac with twice the volume while determining any differences in fracture behavior or geometry that might be attributable to the lens morphology and associated stress and lithologic features. Since no proppant was used in these tests, we could maximize the information by obtaining careful pressure decline data after the treatment for a Nolte-type analysis.[2] Additionally, we conducted step-rate/flow-back and pump-in/flow-back tests prior to the minifracs to obtain additional closure stress data which was averaged over the commingled zones. This series of tests was conducted in MWX-1 in December 1983 by Smith Energy Services.

8.2.2 DESIGN

The treatment schedule for the two minifracs are given in Table 8.2.1. Both the fluid volume and the gel concentrations were doubled for

the second minifrac. Smith Energy Services performed the treatment and their chemically modified guar gum, WGA-2, was used for both treatments. The methanol spearhead was used in both tests to try to improve initial load recovery since the well would be shut in over the winter.

Based on stress tests in well MWX-2, we estimated that the stress distribution around MWX-1 would be as shown in Figure 8.2.1. We were fortunate to find a good stress barrier below the frac interval and a moderate one above. Such good barriers were not evident in some lower sands, nor in some upper sands. However, this paludal region is lithologically complex and generalizing one stress measurement over a large vertical region or over large lateral distances may not be very accurate. Assuming this distribution is correct, the upper barrier is at most ~55 ft thick and, thus, the fracture could easily penetrate it.

Based on this stress data, fracture design lengths were calculated[3,4,5] to be approximately 200 ft and 400 ft for the two minifracs, with heights from 90-130 ft. Pressures were calculated to be 250-400 psi above the closure stress and containment should have been satisfactory under these conditions. Initial zone height for these calculations were 77-120 ft, depending on the model used.

8.2.3 WELL CONFIGURATION AND INSTRUMENTATION

The frac interval was perforated from 7144-7120 ft and 7100-7076 ft in MWX-1 with a bridge plug set at 7200 ft. As shown in Figure 8.2.2, open-end tubing was run in the hole to 6811 ft--considerably above the frac interval to allow for postfrac temperature surveys--and a quartz crystal oscillator pressure transducer and temperature gauge were lowered on wireline to 6772 ft and 6769 ft, respectively, in the tubing. These data were recorded at the surface. Surface pressure, flow rate, and back flow rate were also recorded. Borehole seismic units were lowered in MWX-2 and MWX-3 to positions slightly above the frac zone.

8.2.4 SCHEDULE

The hydraulic fracturing activities associated with Phase I were conducted during the week of December 5, 1983, as follows:

a. a step rate and flow back test on December 6,
b. a pump-in and flow-back test on December 6,
c. the 5,000 gal minifrac on December 7, and
d. the 30,000 gal minifrac on December 9.

8.2.5 STEP RATE TEST

A step rate test[6] was conducted to determine the minimum fracturing pressure and the approximate minimum in situ stress. Two percent KCl water was pumped into the formation at low rates and this rate was increased in small increments at three minute intervals while the pressure at the end of each interval was recorded. Figure 8.2.3 shows the flow rates during the test and Figure 8.2.4 shows the pressure record. These data are plotted in Figure 8.2.5 and fit using linear regressions. The crossover is at about 5940 psi and should be a good estimate of the minimum fracturing pressure. The zero intercept (5790 psi), which might be interpreted as the injection pressure at zero flow rate, should be a fair estimate of the minimum stress. In fact, these two numbers probably bracket the closure stress. Figure 8.2.6 shows the bottomhole temperature during the test.

8.2.6 FIRST FLOW BACK TEST

The flow back test[6] is probably a better estimate of the closure stress. This test is performed by immediately flowing the well back at a constant, predetermined rate and monitoring the pressure decay. Figures 8.2.7-9 show the pressure, flow back rate and temperature, respectively, for this test. The inflection point in the pressure record (Figure 8.2.7) is a good estimate of the closure stress as it reflects a

change in the mode of pressure decline. Since the inflection point is very difficult to determine by eye, these data were fit with a least squares, variable order polynomial routine. The fit of the data is shown in Figure 8.2.10; the line fitting the data points can barely be distinguished. Table 8.2.2 gives the time and data near the inflection point and first derivatives and second derivatives from the polynomial fit, as well as the value of the fit at each point. The discrepancy between the fit and the actual data is normally less than 1 psi. The inflection point is at ~5900 psi where the second derivative is zero. This is in good agreement with the step rate results, but is slightly higher than the stress measured in MWX-3.

8.2.7 PUMP-IN/FLOWBACK TEST

A second flowback test was conducted by repumping 2% KCl water into the fracture at ~8 bpm (120 bbl total) and then flowing back at a constant rate again. The pressure behavior for the overall test is shown in Figure 8.2.11. Shut-in occurs at about 27 min on this scale; the shutdown at about 19 min was a look at the water hammer response of the system. Figures 8.2.12-14 show the bottomhole pressure, flow rate and bottomhole temperature, respectively, during the pump-in phase. No surface pressure was obtained on the computer for this test.

The flowback rate is shown in Figure 8.2.15 and the resultant pressure behavior is given in Figure 8.2.16. Again, it was necessary to fit the data with a least squares polynomial routine to determine the inflection point (Table 8.2.3). The second derivative data show the inflection at 6100 psi. This is somewhat greater than the previous value, possibly due to additional induced stresses caused by fluid leakoff and the fracture. The bottomhole temperature during the flowback is shown in Figure 8.2.17.

8.2.8 TEMPERATURE SURVEY #1

A postfrac temperature survey was run about three hours after completion of the step rate and flow back tests. The results are shown in Figure 8.2.18. The frac height is estimated to be about 90 ft. Determination of the frac top is complicated by a large coal seam at 7140-7150 ft which has significantly different thermal properties than the silts and sands. No circulation test was run to observe the effect.

8.2.9 MINIFRAC #1

The first minifrac consisted of 15,000 gal of 30 lb/1000 gal WGA-2 and a 2100 gal spearhead of methanol injected into the formation at 10 bpm. Subsequently, the well was shut in for almost twice the pumping time to record the pressure decline. Figure 8.2.19 shows the full pressure record for this entire test, with shut-in occurring at ~43 min. The pressure drop at ~38 min was a one-minute stop in pumping to determine if the water hammer response provided any information regarding fracture geometry.

Figures 8.2.20-23 show the bottomhole pressure, flow rate, bottomhole temperature and surface pressure during the pumping. Based on a closure stress of 5900 psi, the treatment pressure above the closure stress is given in Figure 8.2.24. The pressure reaches nearly 900 psi, about three times the design prediction. This is also shown on a log-log plot in Figure 8.2.25; this is a useful representation because it can be viewed in terms of the analysis of Nolte and Smith.[2] There is a constant slope of 0.28 which indicates that there is nearly confined fracture length growth. The slope is actually a little high for these fluid properties ($n' = 0.76$, $k' = 0.00072$ lb-sec$^{n'}$/ft^2), but this may be due to including the methanol spearhead in the pumping time.

The difference between the bottomhole pressure and the surface pressure is shown in Figure 8.2.26. The first seven minutes show

increasing pressure due to pumping methanol into the formation and out of the casing. After seven minutes, the pressure increase should be due to viscosity effects alone.

Figures 8.2.27 and 8.2.28 show the bottomhole pressure and temperature, respectively, during the shut-in period following the minifrac. A Nolte[2] analysis was performed using the pressure decline data and is given in a later section.

8.2.10 TEMPERATURE SURVEY #2

Another temperature survey was run after minifrac #1. Figure 8.2.29 shows these results compared to a prefrac survey. We estimate fracture height to be ~135 ft, but the presence of the coal at 7040 ft makes interpretation of the upper portion of the survey difficult due to thermal conductivity differences. This survey was run rather late (22 hrs) because of icing of the lubricator.

8.2.11 NOLTE ANALYSIS OF MINIFRAC #1

The data from the pressure decline curve of minifrac #1 were used in a Nolte-type analysis[1] to determine fracture parameters. The results of the type curve fit are shown in Figure 8.2.30. The best estimate of P* is 180 psi. The basic equation for this analysis is:

$$P^* = \frac{C H_p E' \sqrt{to}}{H^2 \beta s} \qquad (1)$$

where

C is the leakoff coefficient,

H is the fracture height (135 ft from temp survey),

H_p is leakoff height (55 ft from logs),

E′ is an appropriate Young's modulus as given below,

to is the pumping time (43 min)

βs is an average pressure ratio, given later.

The appropriate Young's modulus, E′, is given by

$$E' = \frac{E}{1 - \nu^2} \tag{2}$$

where ν is Poisson's ratio. However, the correct E′ is some kind of weighted average over the various layers in the interval. For this analysis, $E' = 4.51 \times 10^6$ psi is used. The parameter βs is given by

$$\beta s = \frac{2n' + 2}{2n' + 3 + a} \tag{3}$$

where n′ is the fluid consistency index and a is a parameter that describes the amount of viscosity degradation in the fracture. For this fluid, medium degradation (a = 1) is expected. This yields $\beta s = 0.638$ ($n' = 0.76$, $a = 1$).

Equation (1) can now be solved for the leakoff coefficient by

$$C = \frac{P^{*2} H \beta s}{H_p E' \sqrt{to}} \tag{4}$$

which results in C = 0.00129 ft/$\sqrt{}$min. The pressure decline ratio, ρ, can be calculated as

$$\rho = G(\delta, \delta o) \frac{1}{2} \frac{\beta p}{\beta s} \frac{P}{\Delta P(\delta o, \delta)} \tag{5}$$

where

P is 770 psi, the ISIP pressure above the closure stress (6670 psi - 5900 psi),

$\Delta P(\delta,\delta o)$ is the difference in decline pressure between normalized times δo and $\delta(\delta = \Delta t/to)$

$G(\delta,\delta o)$ is a pressure decline function, and

the ratio $\beta p/\beta s$ is given by

$$\frac{\beta p}{\beta s} = 1 - \frac{n'}{3n' + 3 + a} = 0.86 \qquad (6)$$

where n' and a are the same as above.

Since the value of ρ changes depending upon the times involved, a weighted value of $\rho = 1.85$ was used for the analysis. The fluid efficiency is found by

$$\text{eff} = \frac{\rho}{1 + \rho} \qquad (7)$$

Using $\rho = 1.85$, this gives a fluid efficiency of 65%.

The fracture length can be estimated from

$$L = \frac{Q\sqrt{to}}{\pi\, CH_p(1 + p)} \qquad (8)$$

where Q is the flow rate (10 bpm) and L is the <u>total</u> frac length. Using the previously obtained values, L = 485 ft, which corresponds to a wing length of 242 ft.

In addition, Nolte's analysis can be used to estimate the average width (0.28 in) and the width at the wellbore (0.54 in). Time to fracture closure (from shut-in) is about three hours.

All of these results are summarized in Table 8.2.4 and are quite close to the design values. The calculated fracture length is longer than the design, but this is probably due to neglecting the methanol prepad in the design calculations and calculating a lower gross leakoff coefficient than used in the original design.

Additionally, two shut-ins during the treatment were analyzed following Nierode[8] and resulted in a leakoff coefficient less than 0.001 ft/$\sqrt{}$min. Results from the borehole geophones will be given in a later section.

8.2.12 MINIFRAC #2

The second minifrac consisted of 30,000 gal of 60 lb/1000 gal WGA-2, with a 4500 gal spearhead of methanol, injected into the formation at 10 bpm. Subsequently, the well was shut-in for over twice the pumping time to record the pressure decline. Figure 8.2.31 shows the full pressure record for the entire test. In this record, pumping starts at about 10 min and shut-in occurs at about 100 min.

The bottomhole pressure, flow rate, bottomhole temperature and surface pressure are given in Figures 8.2.32-35, respectively, for the pumping phase. In Figure 8.2.32, the gel is seen to hit the perfs at about 22 min., when the pressure suddenly increases. The bottomhole temperature stabilizes in this test at about 108°F as seen in Figure 8.2.34.

Figure 8.2.36 shows the treatment pressure above the closure stress and Figure 8.2.37 is a log-log plot of these same data. Again, these data indicate that the upper stress barrier is probably much greater than

measured. The initial slope of the log-log plot is 0.33 which is higher than expected for this fluid[7] ($n' \simeq .46$, $k' \simeq 0.02$ lb•sec$^{n'}$/ft^2), but it then drops to a slope of ~0.16 which is near the lower limit. This indicates that there is not extensive height growth, although some limited growth may be occurring near the end of the treatment.

The difference between the bottomhole and surface pressure is shown in Figure 8.2.38. The pressure increases steadily for about 40 min of pumping (400 bbl) and may reflect the effect of the changing temperature conditions on the gel. For example, initially, the methanol was spotted with the gel to the depth of the bottom of the tubing. The gel then sat in the casing for over an hour while the instruments were lowered downhole. During this time, the viscosity undoubtedly degraded somewhat.

After shut-in, the decline pressure and temperature are shown in Figures 8.2.39 and 8.2.40. The pressure data are analyzed in a later section.

8.2.13 TEMPERATURE SURVEY #3

After completion of the second minifrac, temperature surveys were run at four hours and five hours after shut-in (shown in Figure 8.2.41). Estimated fracture height is 150 ft. Again, the coals may cause interpretation problems with respect to the fracture top.

8.2.14 ANALYSIS OF MINIFRAC #2

The same equations given in the previous section are used for this analysis. The results of this type curve fit are shown in Figure 8.2.42. P* is about 120 psi. Additionally, H = 150 ft, to is 88 min. and βs = 0.594 for this fluid ($n' = 0.46$, $k' = 0.02$ lb•sec$^{n'}$/ft^2, $a = 1$). This gives a leakoff coefficient of 0.0007 ft/$\sqrt{}$min, about half of the previous test.

The pressure decline ratio, ρ, is 3.56 and the fluid efficiency is 78%. The total fracture length is 880 ft (440 ft wing) and the average and wellbore widths are, respectively, 0.39 in. and 0.75 in. Time to closure is about 18 hours. These results are shown in Table 8.2.4.

An analysis of two shut-ins during this test gave an estimated leakoff coefficient of less than 0.001 ft/$\sqrt{}$min. The low leakoff coefficient suggests that the nearby coals were not thieving excessive frac fluid.

8.2.15 ANALYSIS USING PRESSURE HISTORY MATCHES

The high treatment pressures, measured stress contrasts, and observed fracture geometry need to be reconciled to provide a reason for the observed fracture behavior. The borehole geophones (see Section 10) gave fracture heights of about 120 ft for minifrac #1 and 150 ft for minifrac #2. The measured lengths are more uncertain, but appear to be about 250-350 ft for minifrac #1 and 375-500 ft for minifrac #2. These results agree with the temperature logs and the Nolte analysis, but are not compatible with our understanding of the stresses and properties around the zone.

The major problem is the high pressures during the treatments. If a constant height simulator is used and the fracture height is assumed to be 80 ft, then treatment pressures of about 300 and 600 psi would be expected for the two minifracs. If height growth is allowed, then the treatment pressures will be slightly lower because of the extra fracture area. Shlyapobersky[8] suggested that the high pressures in these tests can be explained by fracture toughnesses that are 1-2 orders of magnitude greater than measured in the lab because of some process zone effect. Palmer[9] modeled such an effect and was able to match the final treatment pressures, but then he also obtained heights which were much smaller than measured.

We have attempted to assemble a more realistic analysis of fracture growth that does not depend upon a postulated, unproven increase in the fracture toughness, but rather uncertainties in the other data. The first piece of uncertain data is the stress distribution. While we believe that most of the measured stresses are correct, we also believe that the complex lithology of this paludal interval has resulted in a complicated stress state where each individual layer may have widely different stress values. As discussed in the stress testing section, these layers are from inches to at most a few feet thick. There is a limited amount of stress data and we may have missed many of the important high stress layers. The most glaring omission is the shale interval between the two paludal sands, which we were unable to stress test because of communication problems. As a result we have only one stress data point for both sands and the middle shale. Rather than use the stress distribution shown in Figure 8.2.1, we might more logically assume that the 15 ft shale has a high stress value. If we assume that it has the same gradient as the shales below, then its stress will be about 6950 psi.

A second location where the stress may have been misinterpreted is the shale/siltstone directly above the frac interval. While a stress test seemed to indicate low stress in this region, this low value may have been a result of communication and we may have actually retested the sand because of a channel in the cement. The path of least resistance would have been down the channel and into the low stress sand, rather than into the high stress shale. If this shale also had the same gradient as the shales below, then its stress would be about 6900 psi.

A "revised" stress distribution is now shown in Figure 8.2.43. Even this new stress distribution is not sufficient to explain the high treatment pressures if we allow only a single hydraulic fracture. However, if we assume that each sand has its own separate fracture and that each fracture remains separate even after propagating into the other sand, then most of the high pressure can be explained.

In another approach and using such a postulated stress distribution, we have attempted to history match the pressure behavior of the minifracs in a way that is consistent with the measured fracture geometry. The history matches were obtained using a Perkins & Kern type simulator with height growth. All equations are finite-differenced independently, which allows for any type of pressure-drop relation (laminar or turbulent, Newtonian or non-Newtonian), any type of leakoff relation, multiple stages with different properties, different rates (including shut-in) and screen outs. In these minifracs, only two stages were required. Both treatments had initial methanol spearheads followed by the gels.

Figure 8.2.44 shows the history match for minifrac #1. In order to achieve this match, we also needed to assume that the pressure drop relationship underestimates the true pressure drop in the fracture.[10] In this example the friction factor for flow through the fracture is increased by a factor of six. Such an increase can easily be the result of multiple-fracture stranding, tortuosity, offsets at joints and other factors. The actual value has little meaning in this case because we have already made so many assumptions about the stresses. The main discrepancy between the model and the measured data is the fast rise in pressure in the calculations compared to the gradual increase in the measured data. This could also be due to a stress state that is much more complex than we have modeled. The length growth is shown in Figure 8.2.45 and indicates a slightly longer fracture than measured, although the measured value is quite uncertain. The height growth is shown in Figure 8.2.46 and yields a maximum height of about 115 ft, in good agreement with the measured 120 ft height.

The data for the history match are shown in Table 8.2.5. Stage 1 is the methanol prepad for which the flow is turbulent. The relative roughness used was 0.05, which is quite large. In addition, the friction factor for the methanol was increased by a factor of 2 (fff). The high relative roughness increases the friction factor considerably, so the large difference in fff between the two stages is not significant.

The second minifrac is more of a problem. In the second minifrac the pressures were sufficiently high that the fracture would have eventually broken entirely through the upper barrier, with treatment pressures leveling at about 850-900 psi above closure. To circumvent this problem we have artificially limited the upper growth of the fracture by restricting growth past 200 ft of total height. The mechanism for this restriction may not be a high stress layer per se, but may be the effects of flow restriction due to known high-stress layers, inefficient fracture propagation across bedding or coals, or any of many other possibilities. For whatever reason, the temperature logs and the borehole geophones show that fracture height was restricted, and a reasonable history match must have such a restriction.

The pressure history match for minifrac #2 is shown in Figure 8.2.47. With the two separate fractures and the restricted height growth above 200 ft, the pressure can be easily made to fit the measured values. Data for this history match are also shown in Table 8.2.5. Where appropriate (e.g., fff, relative roughness), parameters for the two minifracs were kept constant. Length growth is shown in Figure 8.2.48 and is probably somewhat misleading. This second minifrac was conducted two days after the first one and little of the load water from the first treatment was recovered. We assume that the leakoff of methanol spearhead for this second treatment is reduced because it must force the gel from the previous treatment to move ahead of it. Because of this, the efficiency of the methanol stage is good and a fairly long fracture (but small width and height) can develop before stage 2 takes over. The change in slope of the length growth at the end of the job is due to the fracture contacting new rock, yielding higher leakoff. The wing length of about 400 ft agrees well with measured data. Finally, the height growth is shown in Figure 8.2.49. The artificial restriction is important throughout much of stage 2, yielding a maximum height of about 200 ft, somewhat greater than measured.

8.2.16 DISCUSSION OF MINIFRACS

After the minifracs we were pleased at the similarity of the results of the borehole geophones, the temperature log and the Nolte analysis. This agreement in independent diagnostic techniques gave us confidence in their accuracy. Additionally, the fracture azimuth determined during the treatment agreed with prefrac predictions obtained from core, log, and surface stress orientation measurements.

We apparently had acceptable containment even though the treatment pressures were so much higher than any barrier stress that any barrier (particularly the top one) should have been penetrated. We attribute this to these high stress layers acting as restrictions rather than absolute barriers. Because of the high stresses, fracture widths are much smaller in these layers and thus pressure drops become very large when fluid is forced through them at any fast rates. Thus, vertical growth occurs quite slowly. Another possible mechanism for fracture restriction is complex fracturing, such as bifurcations, offsets or multiple strands, as the fracture propagates across the varied and complex bedding planes in this zone.[10] The high treatment pressures are a problem for any analyses of these tests.

The step-rate/flowback tests in MWX-1 provided minimum stress data that agreed well with a stress test in MWX-3. However, the stress appeared to be increasing fairly rapidly with additional pumping. This may be a result of back stresses or the larger treatment volume intersecting higher stress layers.

8.2.17 REFERENCES

1. Warpinski, N. R., Branagan, P. T., Sattler, A. R., Lorenz, J. C., Northrop, D. A., Mann, R. L. and Frohne, K-H., "Fracturing and Testing Case Study of Paludal, Tight Lenticular Gas Sands," SPE 13876, presented at SPE/DOE 1985 Low Permeability Gas Reservoirs Symposium, Denver, CO, p 267-275, 1985.

2. Nolte, K. G., "Determination of Fracture Parameters from Fracturing Pressure Decline," SPE 8341, 54th Annual SPE Meeting, Las Vegas, NV, September, 1979.

3. Warpinski, N. R., memo on "Preliminary Design Calculations for Phase I Frac," November 19, 1983.

4. Palmer, I. D., Craig, H. R. and Luiskutty, C. T., "Prediction of Fracture Height for Paludal Zone Stimulation at 7100 ft in MWX," private communications, November 1983.

5. Curry, T., "Stimulation Proposal for Sandia Laboratories, MWX-1," Smith Energy Services Stimulation Proposal, November 21, 1983.

6. Nolte, K. G., "Fracture Design Considerations Based on Pressure Analysis," SPE 10911, SPE Cotton Valley Symposium, Tyler, Texas, May, 1982.

7. Nolte, K. G. and Smith, M. B., "Interpretation of Fracturing Pressures," JPT, Vol. 33, September, 1981, p. 1767.

8. Shlyapobersky, J., "Energy Analysis of Hydraulic Fracturing," 26th U.S. Symposium on Rock Mechanics, Rapid City, June, 1985.

9. Palmer, I., "Stimulation Models for Lenticular Sands," Proceedings of the Unconventional Gas Recovery Contractors Meeting, DOE/METC 86/6034, p 174, November 1985.

10. Warpinski, N. R. and Teufel, L. W., "Influence of Geologic Discontinuities on Hydraulic Fracture Propagation," SPE 13224, presented at 59th Annual SPE Conference, Houston, TX, September 1984.

Table 8.2.1 Minifrac Treatment Schedules

		Minifrac #1	Minifrac #2
Fluid:	Volume (gal)	15,000	30,000
	Base Fluid	2% KCl	2% KCl
	Gel Type *	HPG	HPG
	Gel Concentration (lb/1000 gal)	30	60
	Bactericide (gal/1000 gal)	0.25	0.25
	Clay Stabilizer (gal/1000 gal)	1.0	1.0
	Chemical Breaker (lb/1000 gal)	1.0	2.0
	Buffer (to pH 7.0)	yes	yes
	Surfactant (gal/1000 gal)	1.0	1.0
Prepad:	Volume (gal)	2100	4500
	Type	methanol	methanol
	Surfactant (gal/1000 gal)	1.0	1.0
	Low pH Additive (gal/1000 gal)	7.0	7.0
Sand Proppant		0	0
Average Pumping Rate (bpm)		10	10

*Smith Energy Services Water Gelling Agent #2 (WGA-2) without crosslinker.

Table 8.2.2. Least squares polynomial fit of flowback #1 pressure data
Polynomial order = 9; Significance = 0.735 psi)

J	TIME	DATA	DRV1	DRV2	YFIT
25	40.00680	6084.1800	-58.4990	1.8319	6080.4746
26	40.10820	6074.4500	-58.3177	1.7471	6074.5520
27	40.27500	6064.7100	-58.0357	1.6407	6064.8484
28	40.44180	6055.0100	-57.7687	1.5647	6055.1905
29	40.60860	6045.4500	-57.5126	1.5084	6045.5761
30	40.77480	6035.9100	-57.2658	1.4635	6036.0382
31	40.94160	6026.4400	-57.0251	1.4224	6026.5064
32	41.10840	6017.0000	-56.7914	1.3796	6017.0142
33	41.27520	6007.5900	-56.5652	1.3310	6007.5604
34	41.44140	5998.0300	-56.3486	1.2734	5998.1774
35	41.60820	5988.7400	-56.1418	1.2042	5988.7958
36	41.77500	5979.4700	-55.9476	1.1222	5979.4478
37	41.94180	5970.1300	-55.7682	1.0268	5970.1309
38	42.10860	5960.8600	-55.6058	.9178	5960.8425
39	42.27480	5951.6000	-55.4632	.7962	5951.6130
40	42.44160	5942.3600	-55.3415	.6619	5942.3722
41	42.60840	5933.2500	-55.2430	.5163	5933.1498
42	42.77520	5924.1600	-55.1698	.3609	5923.9417
43	42.94140	5914.9400	55.1232	.1977	5914.7767
44	43.10820	5905.7100	-55.1044	.0272	5905.5841
45	43.26480	5896.4500	-55.1130	-.1375	5896.9545
46	43.44180	5887.2300	-55.1541	-.3274	5887.1963
47	43.60860	5878.0400	-55.2238	-.5083	5877.9912
48	43.77480	5868.7700	-55.3233	-.6889	5868.8052
49	43.94160	5859.4700	-55.4532	-.8691	5859.5668
50	44.10840	5850.1500	-55.6131	-1.0470	5850.3043
51	44.27520	5840.8000	-55.8023	-1.2214	5841.0127
52	44.44140	5831.4200	-56.0195	-1.3908	5831.7207
53	44.60820	5822.0800	-56.2653	-1.5555	5822.3565
54	44.77500	5812.6300	-56.5380	-1.7142	5812.9491
55	44.94180	5803.2400	-56.8368	-1.8666	5803.4940

Table 8.2.3 Least squares polynomial fit of flowback #2 pressure data
(Polynomial order = 11; Significance = 0.32 psi)

J	TIME	DATA	DRV1	DRV2	YFIT
20	30.16500	6260.8600	-41.0841	1.2353	6261.0208
21	30.33360	6253.9800	-40.8876	1.1021	6254.1109
22	30.49860	6247.1800	-40.7142	1.0051	6247.3789
23	30.66480	6240.3900	-40.5532	.9370	6240.6258
24	30.83520	6233.6600	-40.3975	.8941	6233.7289
25	30.99840	6226.9400	-40.2534	.8748	6227.1478
26	31.16520	6220.2800	-40.1079	.8734	6220.4457
27	31.33140	6213.6300	-39.9618	.8864	6213.7919
28	31.50000	6207.0600	-39.8105	.9103	6207.0670
29	31.66500	6200.4000	-39.6578	.9405	6200.5108
30	31.83180	6193.9300	-39.4982	.9739	6193.9091
31	31.99860	6187.5000	-39.3330	1.0065	6187.3345
32	32.16660	6181.0100	-39.1614	1.0351	6180.7409
33	32.33160	6174.5500	-38.9888	1.0556	6174.2935
34	32.49840	6168.0400	-38.8117	1.0657	6167.8049
35	32.66520	6161.6500	-38.6340	1.0624	6161.3459
36	32.83140	6155.2000	-38.4588	1.0434	6154.9395
37	32.99820	6148.8400	-38.2876	1.0066	6148.5390
38	33.16500	6142.5000	-38.1241	.9503	6142.1664
39	33.33180	6136.1100	-37.9717	.8735	6135.8201
40	33.49980	6129.6400	-37.8329	.7747	6129.4528
41	33.66480	6123.3200	-37.7[illegible]6	.6566	6123.2204
42	33.83340	6116.9600	-37.6156	.5144	6116.8704
43	33.99840	6110.5700	-37.5435	.3552	6110.6701
44	34.16640	6104.2200	-37.4988	.1738	6104.3670
45	34.33140	6097.8400	-37.4861	-.0216	6098.1812
46	34.49820	6091.0300	-37.5072	-.2344	6091.9272
47	34.66500	6084.9300	-37.5650	-.4602	6085.6667
48	34.83360	6078.7600	-37.6626	-.6986	6079.3256
49	34.99980	6072.5700	-37.7987	-.9406	6073.0553
50	35.16480	6066.4200	-37.9740	-1.1843	6066.8047
51	35.33340	6060.2500	-38.1947	-1.4334	6060.3842
52	35.49840	6054.0300	-38.4511	-1.6735	6054.0615
53	35.66520	6047.6300	-38.7500	-1.9088	6047.6235
54	35.83140	6041.3300	-39.0859	-2.1322	6041.1558
55	35.99820	6034.9200	-39.4593	-2.3415	6034.6056
56	36.16500	6028.3600	-39.8660	-2.5324	6027.9904
57	36.33180	6021.8000	-40.3029	-2.7014	6021.3047
58	36.49860	6015.1100	-40.7658	-2.8455	6014.5439
59	36.66480	6008.3300	-41.2488	-2.9614	6007.7287
60	36.83160	6001.1700	-41.7504	-3.0476	6000.8068

Table 8.2.4 Results of Minifrac Pressure Decline Analysis

	Minifrac #1	Minifrac #2
P* (psi)	180	120
Leakoff Coefficient (ft/$\sqrt{}$min)	0.00129	0.0007
Pressure Decline Ratio, ρ	1.85	3.56
Fluid Efficiency (percent)	65	78
Wing Length (ft)	242	440
Average Width (in)	0.28	0.39
Width at Wellbore (in)	0.54	0.75
Time to Closure (hr)	3	18

Table 8.2.5 Data for Pressure History Match of Minifracs

	Gel Stage	Methanol Stage
Minifrac #1		
Leakoff Coefficient (ft/$\sqrt{}$min)	0.002	0.004
Spurt (gal/ft^2)	0.01	0.00
K' (lb-sec$^{n'}$/ft^2)	0.00072	-
n'	0.76	-
Viscosity (cp)	-	0.43
Relative Roughness	-	0.05
Friction Factor Factor, fff	6	2
Minifrac #2		
Leakoff Coefficient (ft/$\sqrt{}$min)	0.001	0.001
Spurt (gal/ft^2)	0.00	0.00
K' (lb-sec$^{n'}$/ft^2)	0.02	-
n'	0.46	
Viscosity (cp)	-	0.3
Relative Roughness	-	0.05
Friction Factor Factor, fff	2	2

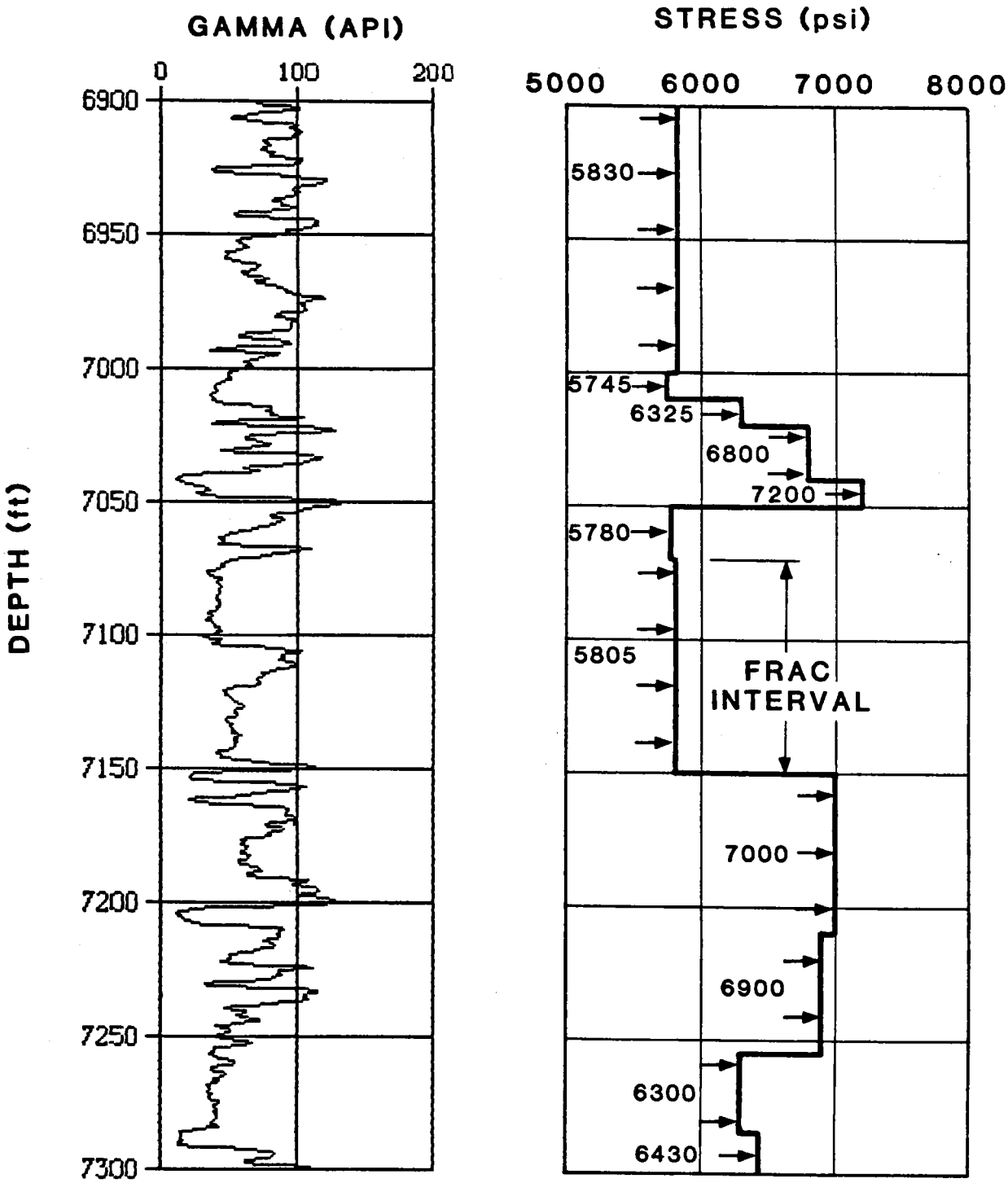

Figure 8.2.1 Estimated Stress Profile in the Paludal Frac Interval

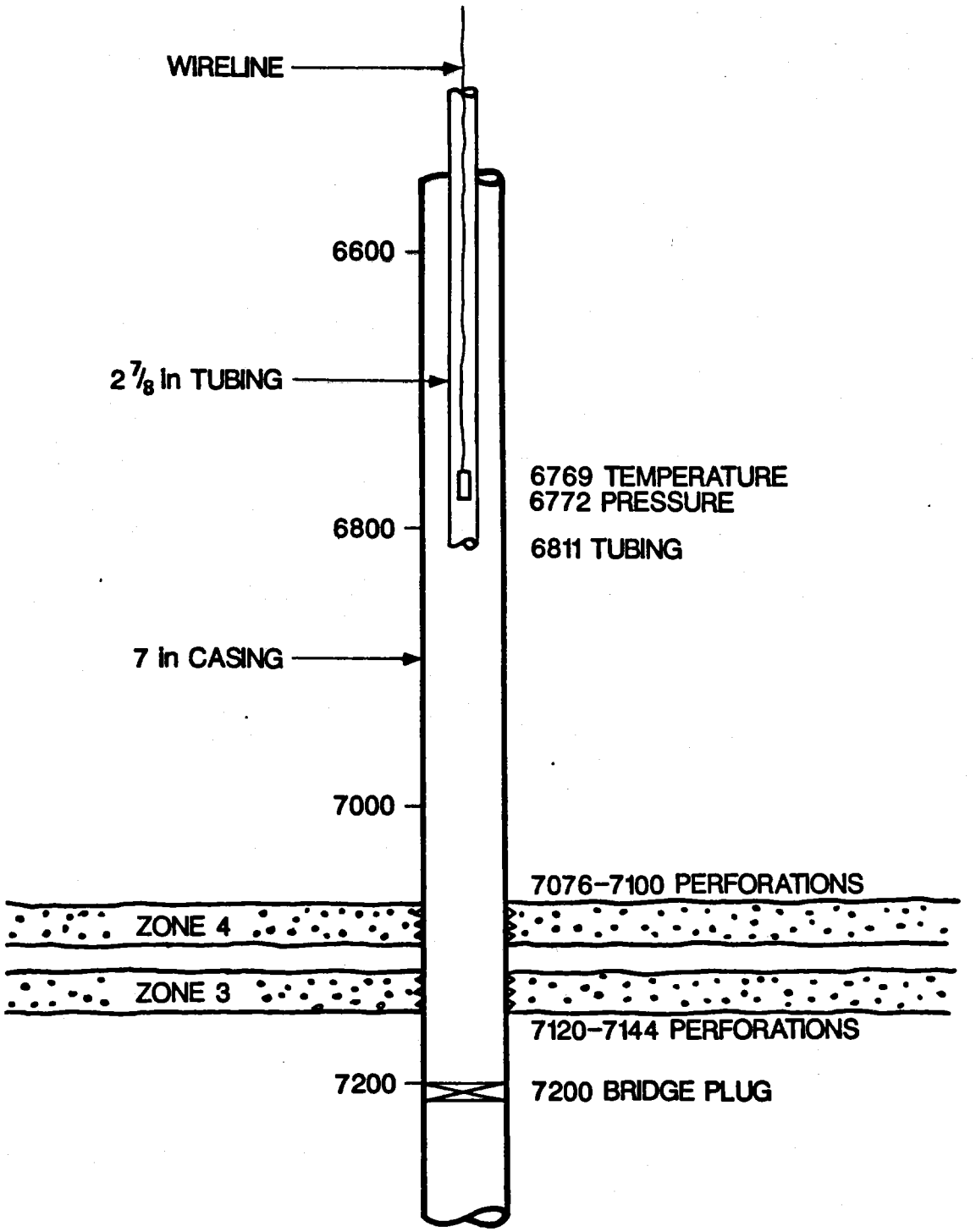

Figure 8.2.2 Well Configuration During Phase I

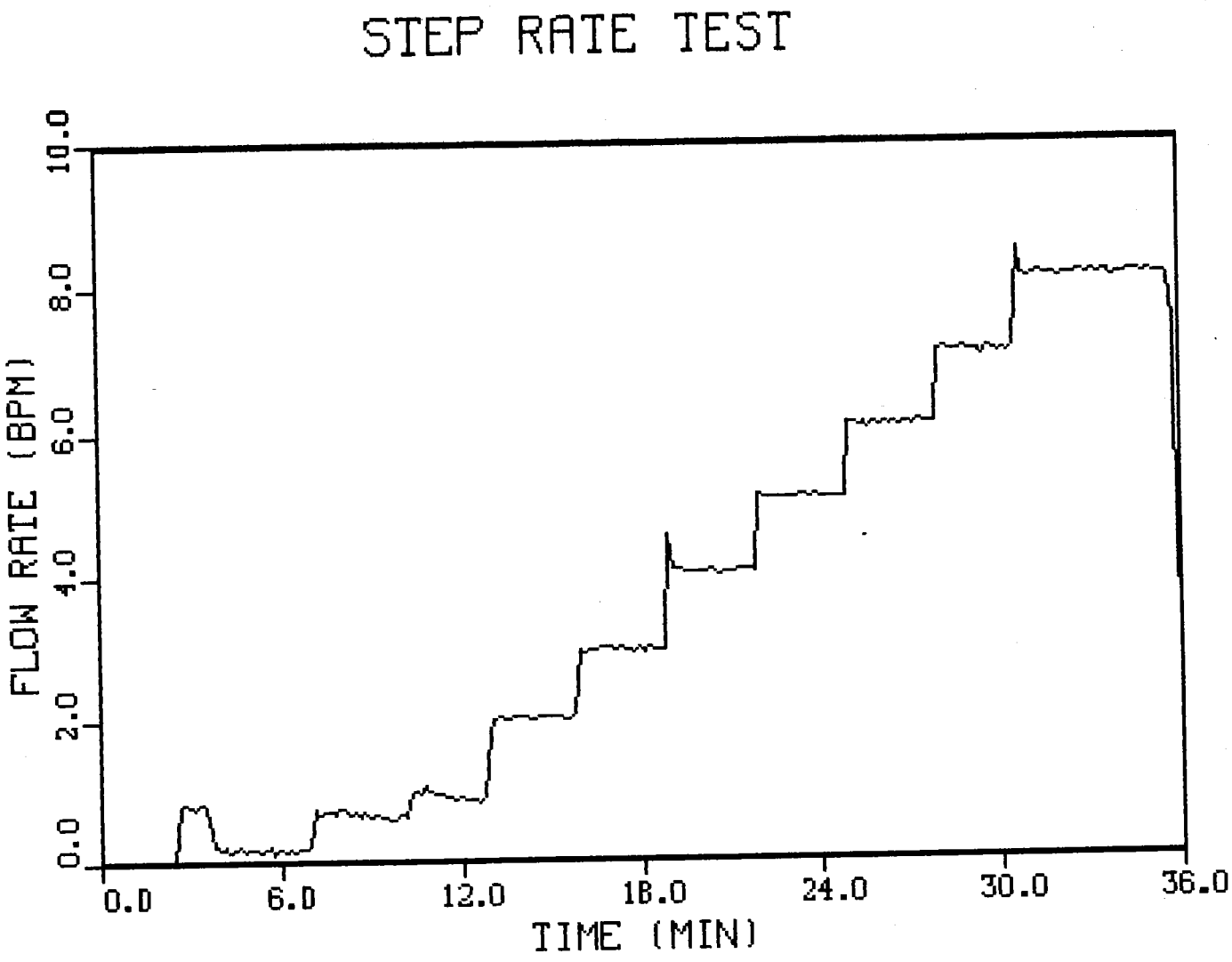

Figure 8.2.3 Step Rate Flow Data

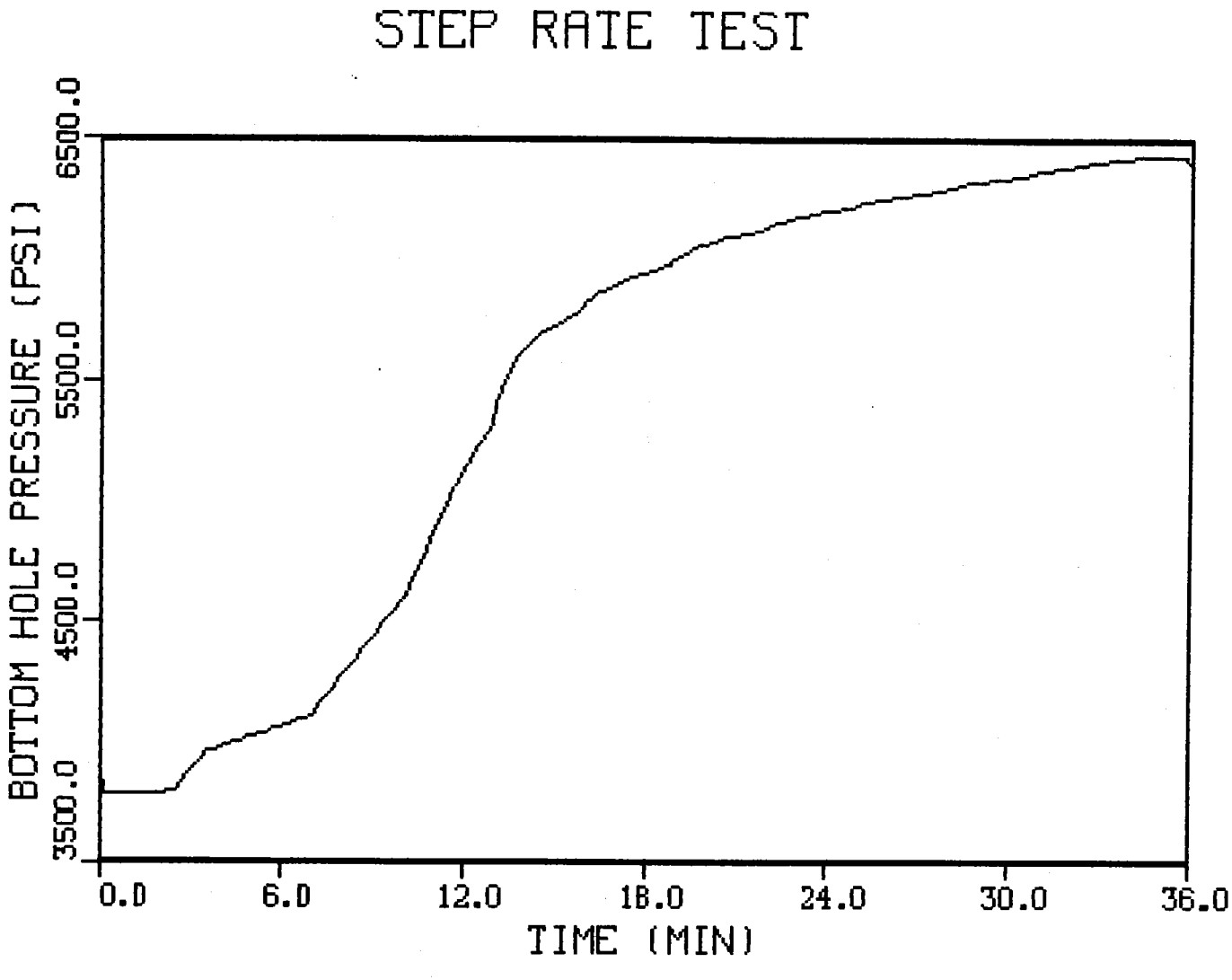

Figure 8.2.4 Step Rate Pressure Data

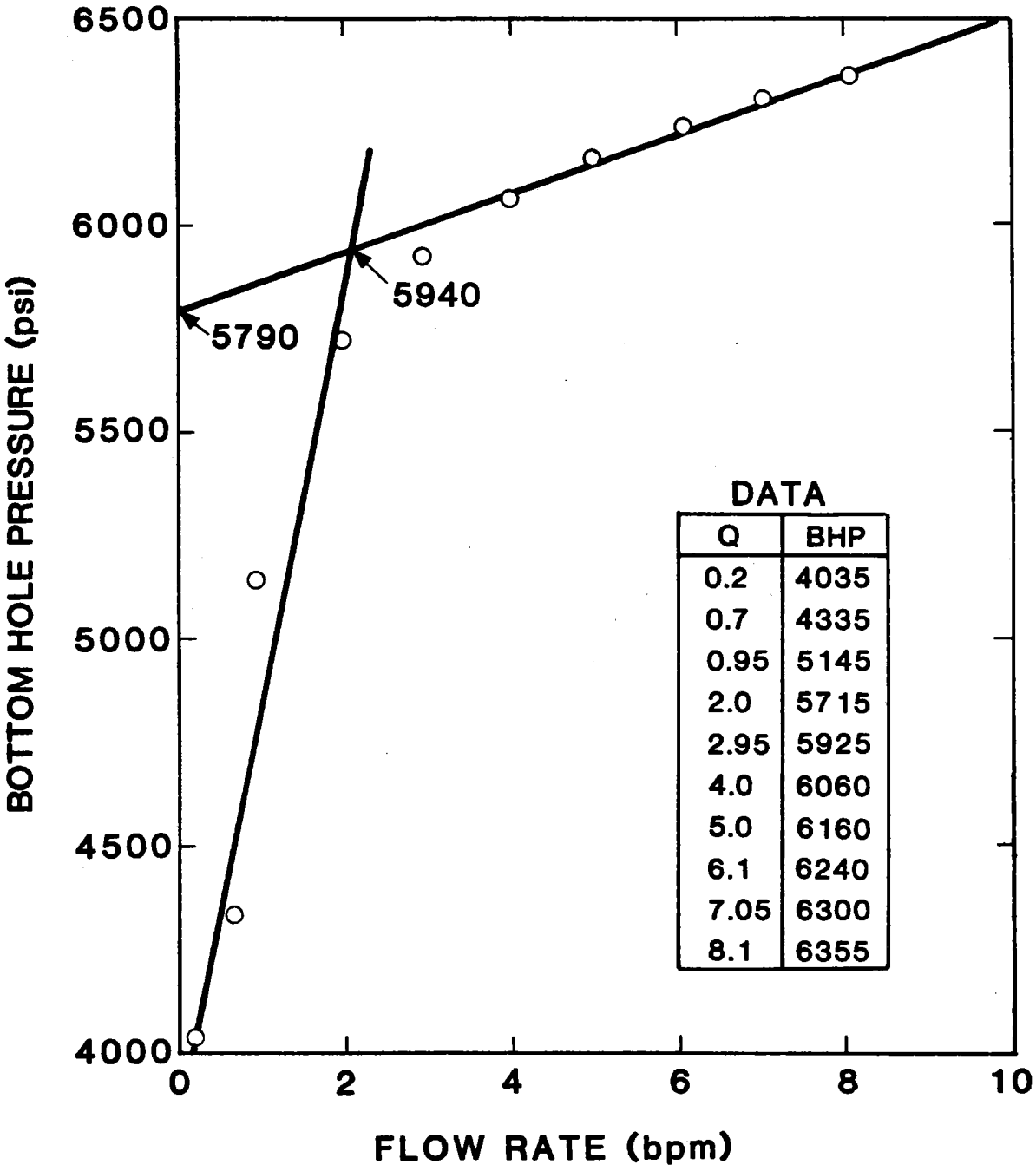

Figure 8.2.5 Step Rate Results

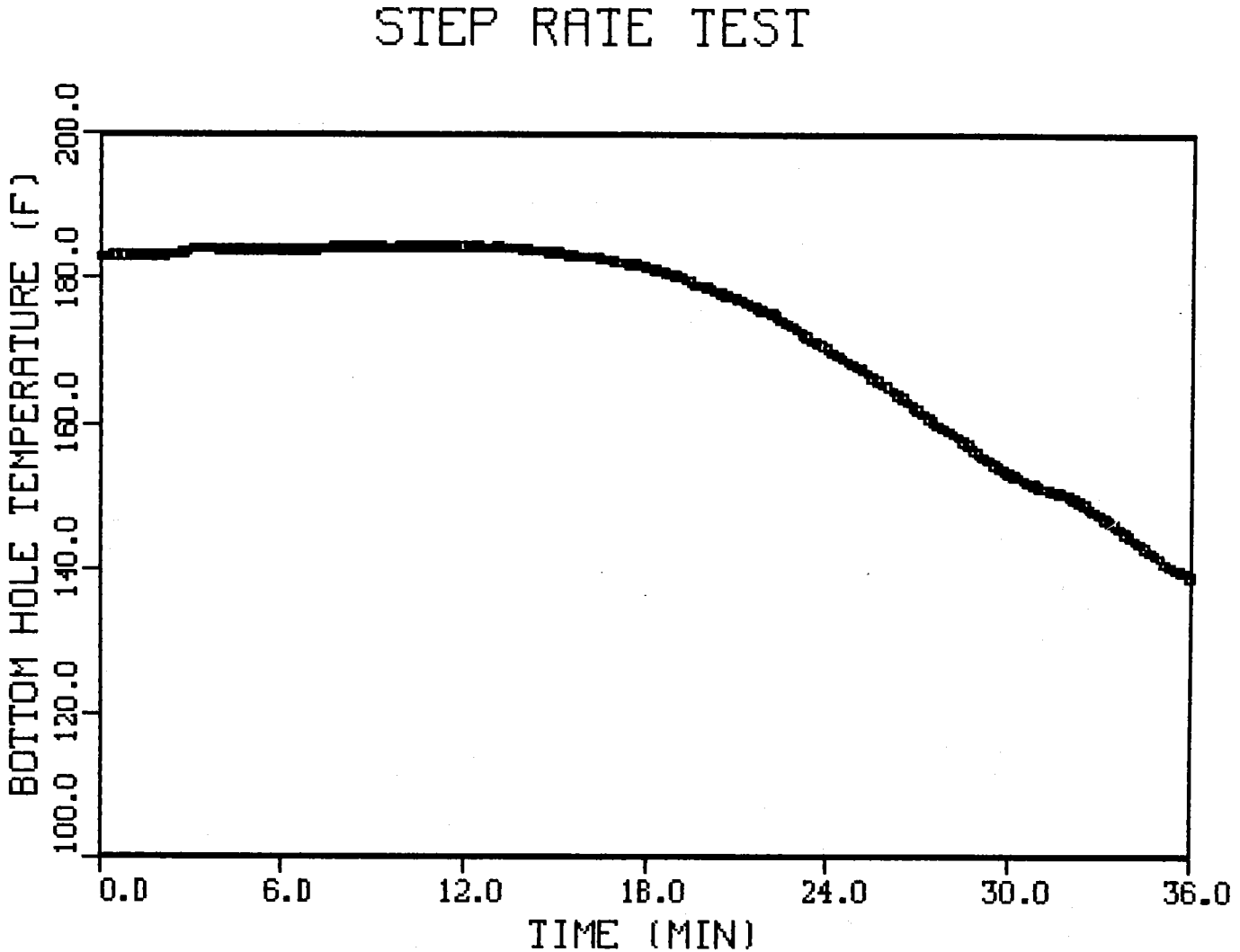

Figure 8.2.6 Step Rate Temperature Data

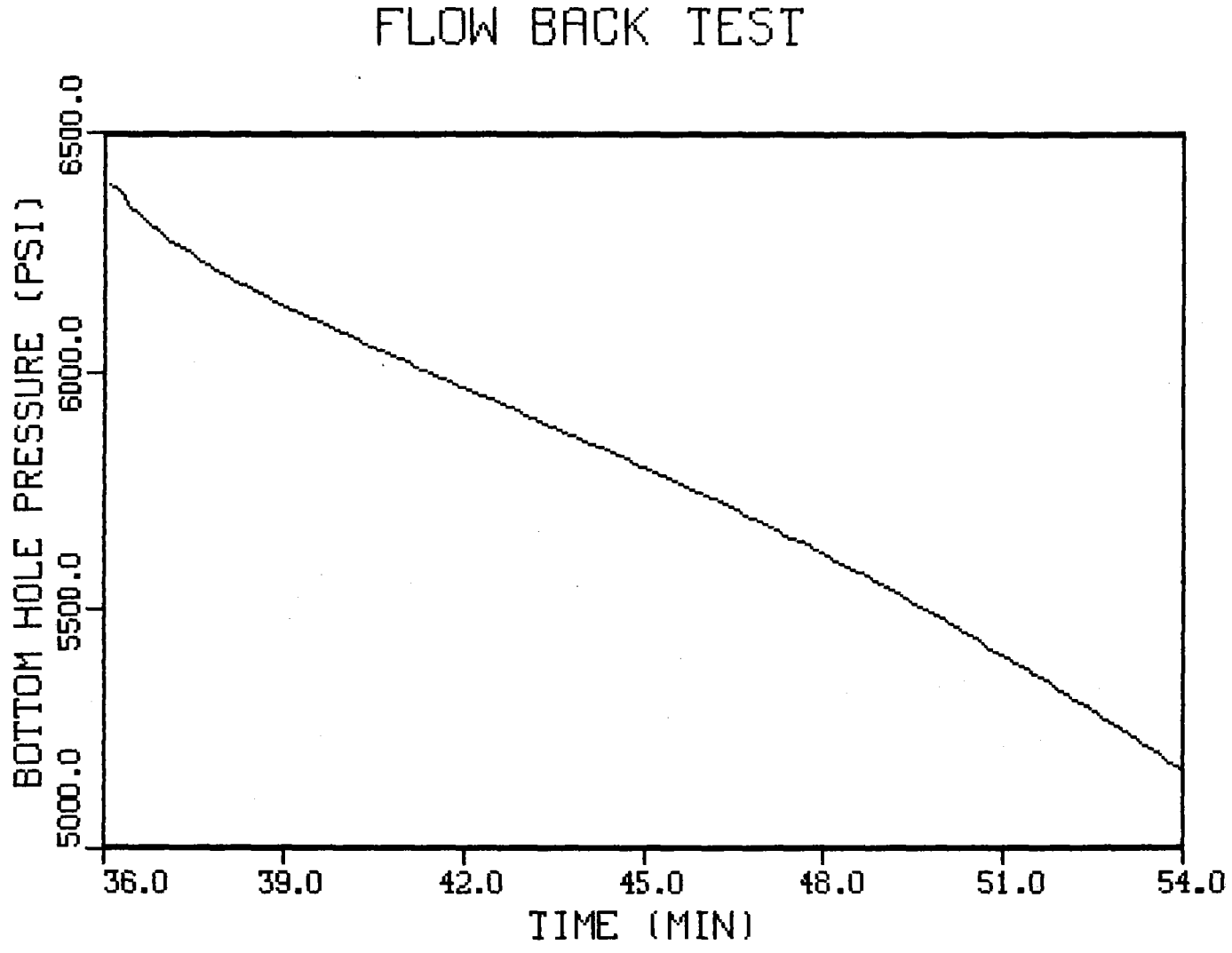

Figure 8.2.7 Flow Back Pressure Data

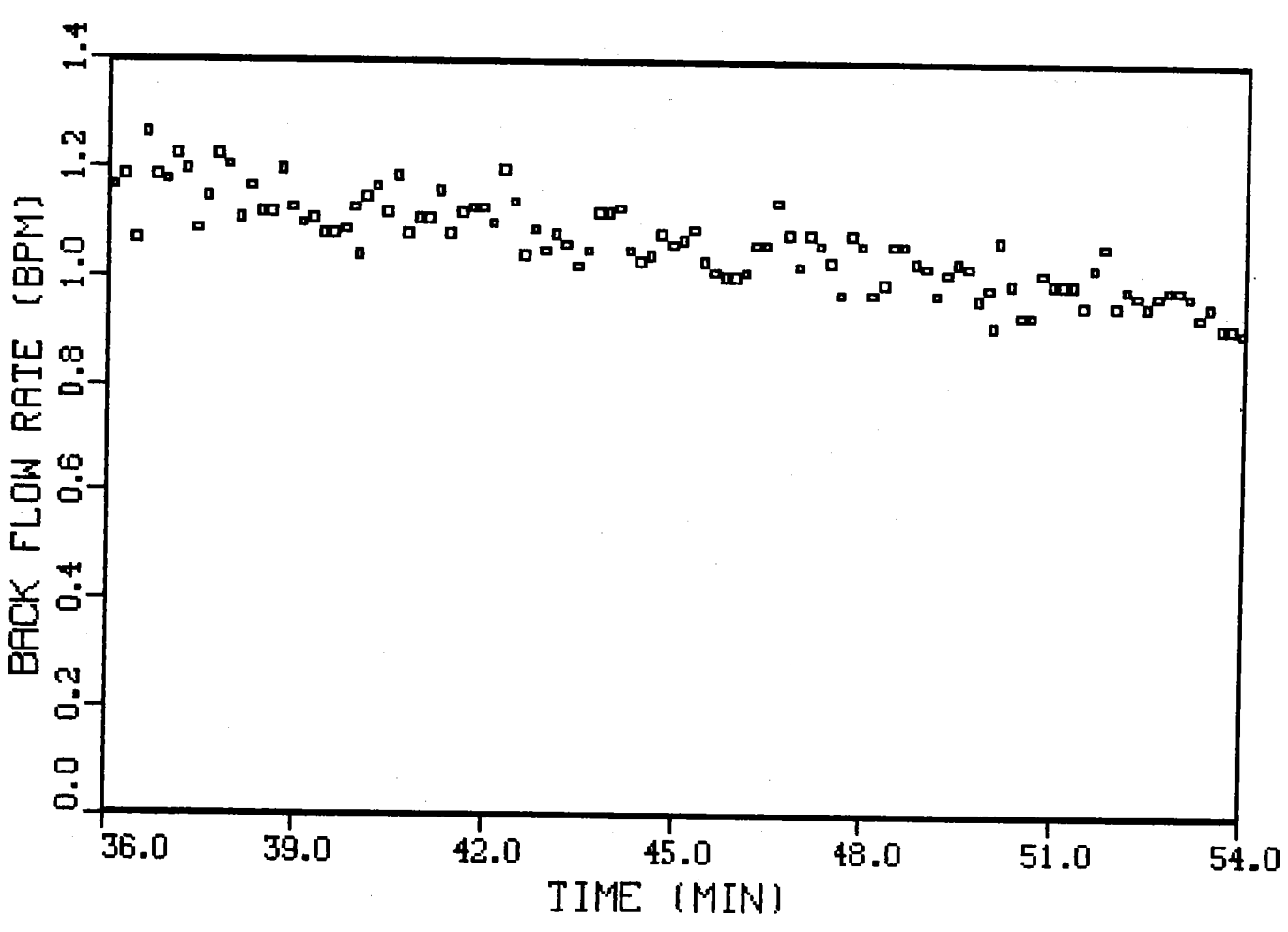

Figure 8.2.8 Flow Back Rate Data

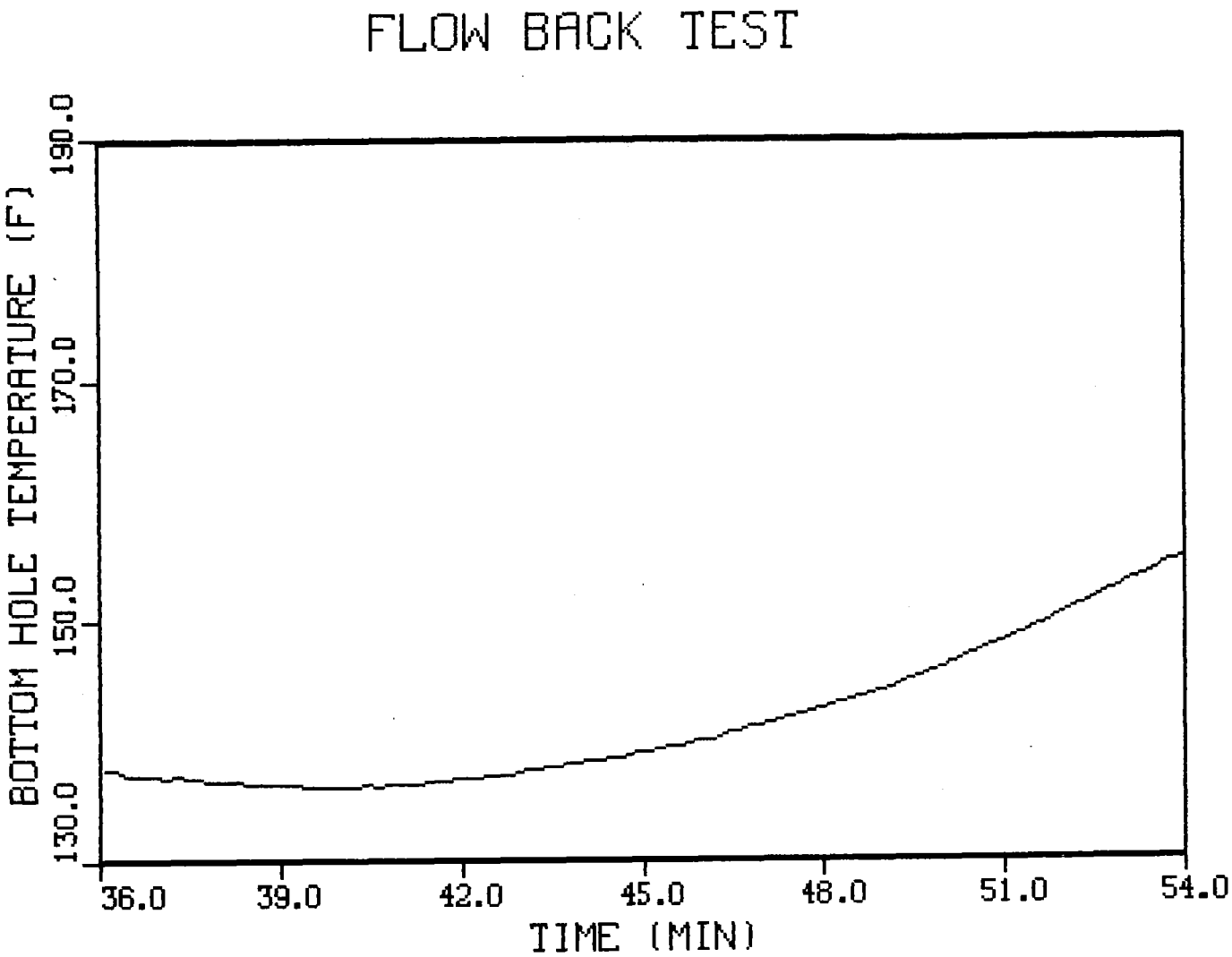

Figure 8.2.9 Flow Back Temperature Data

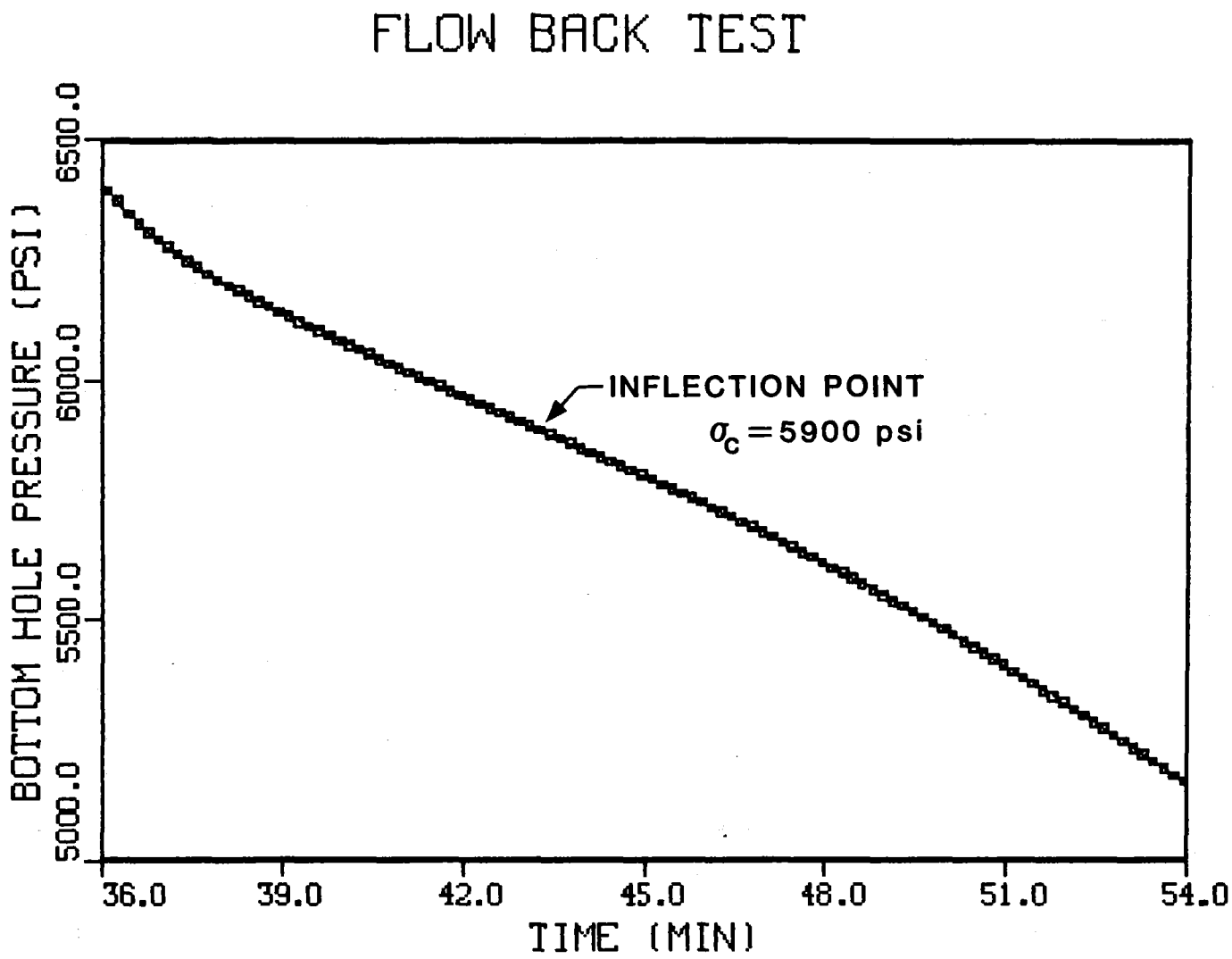

Figure 8.2.10 Least Squares Polynomial Fit of Flow Back

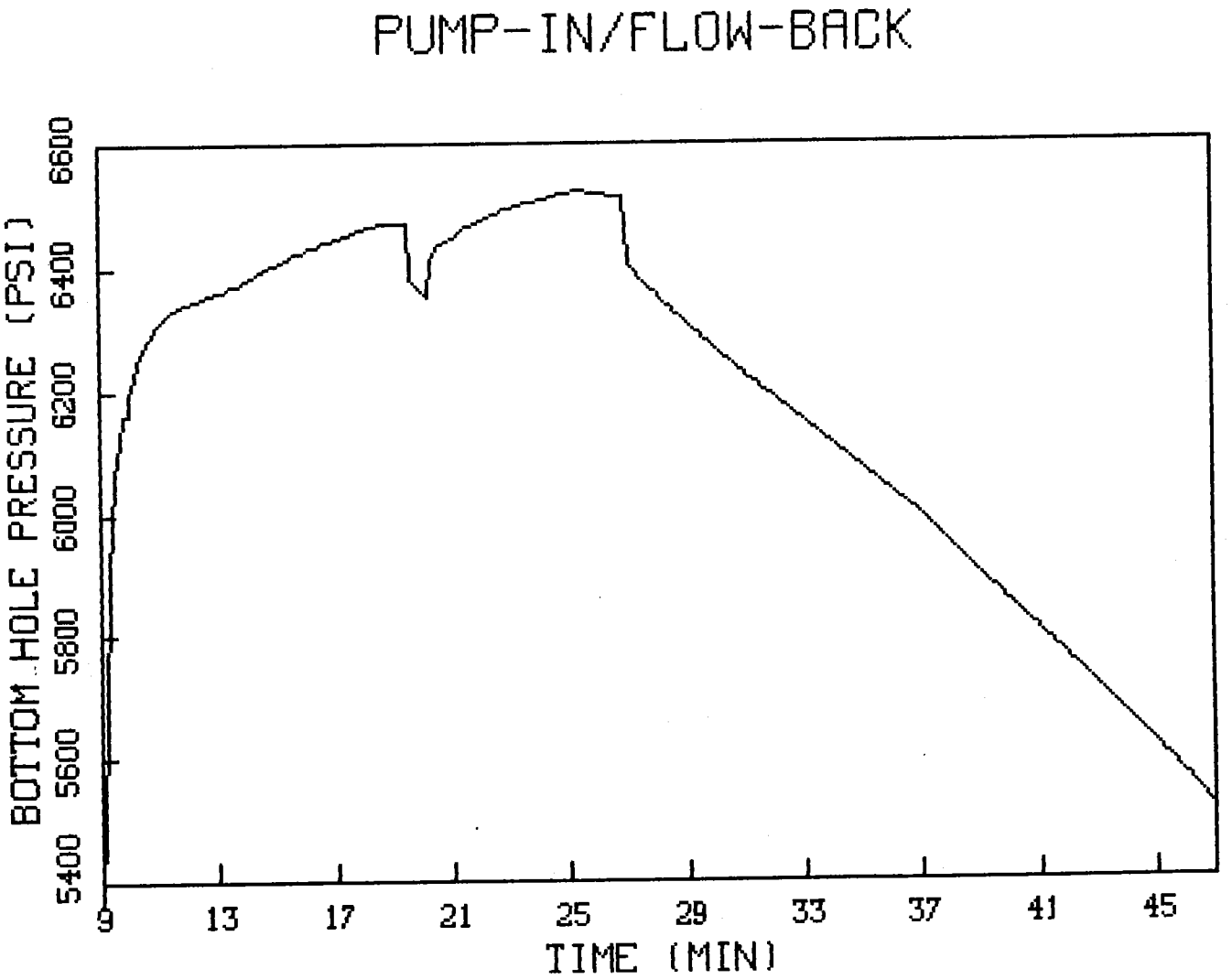

Figure 8.2.11 Pump-In/Flow-Back Pressure Data

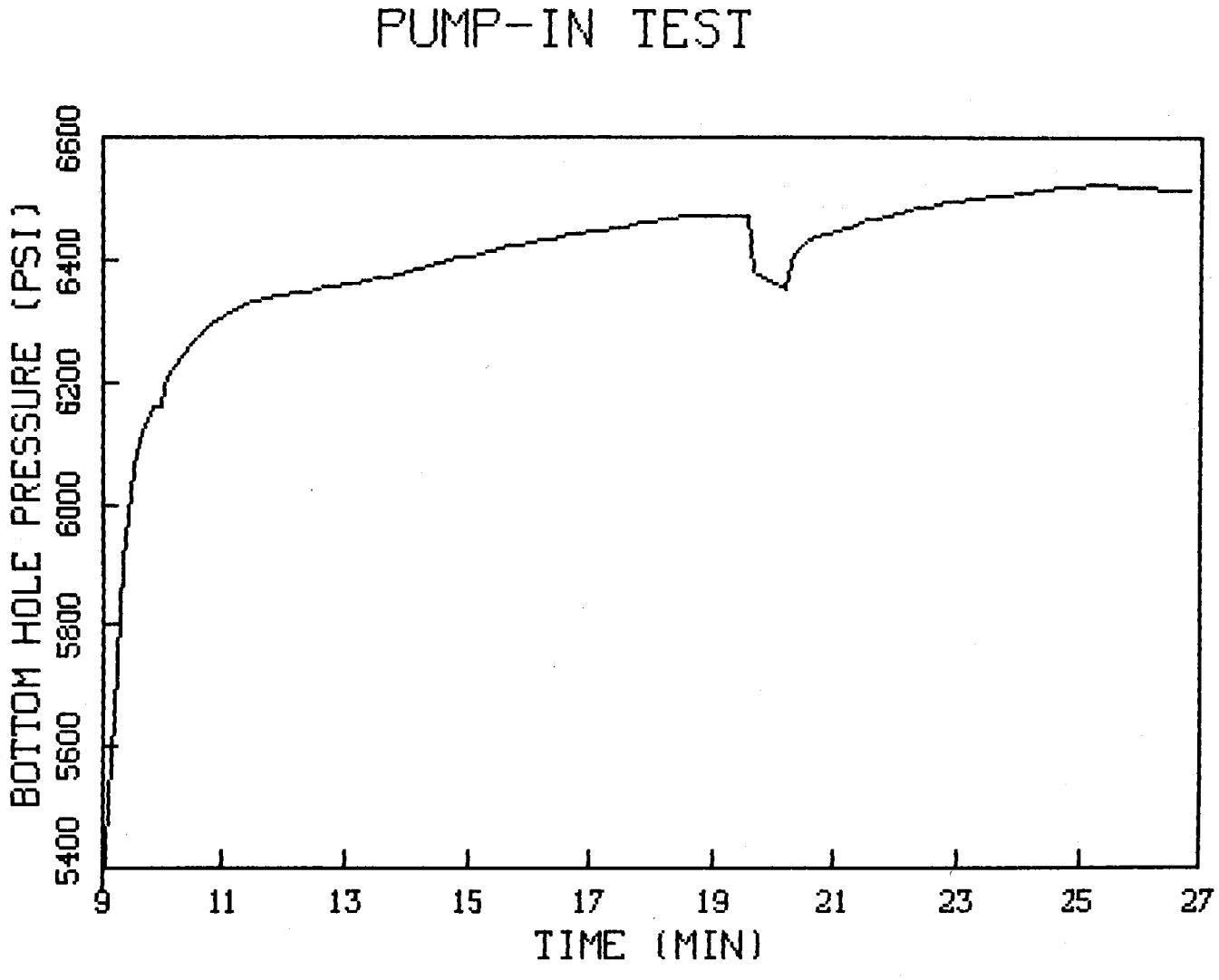

Figure 8.2.12 Pump-In Pressure Data

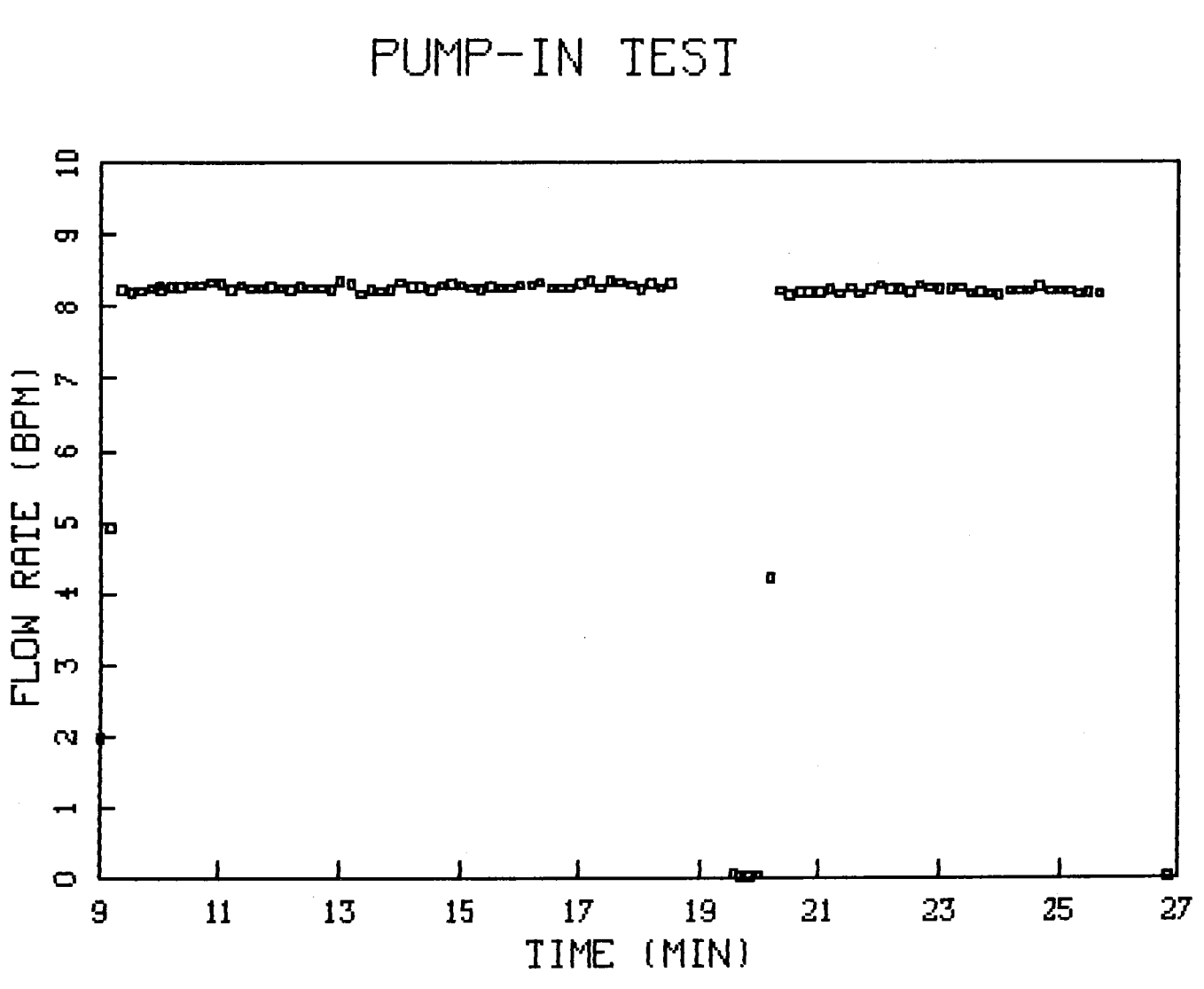

Figure 8.2.13 Pump-In Flow Rate Data

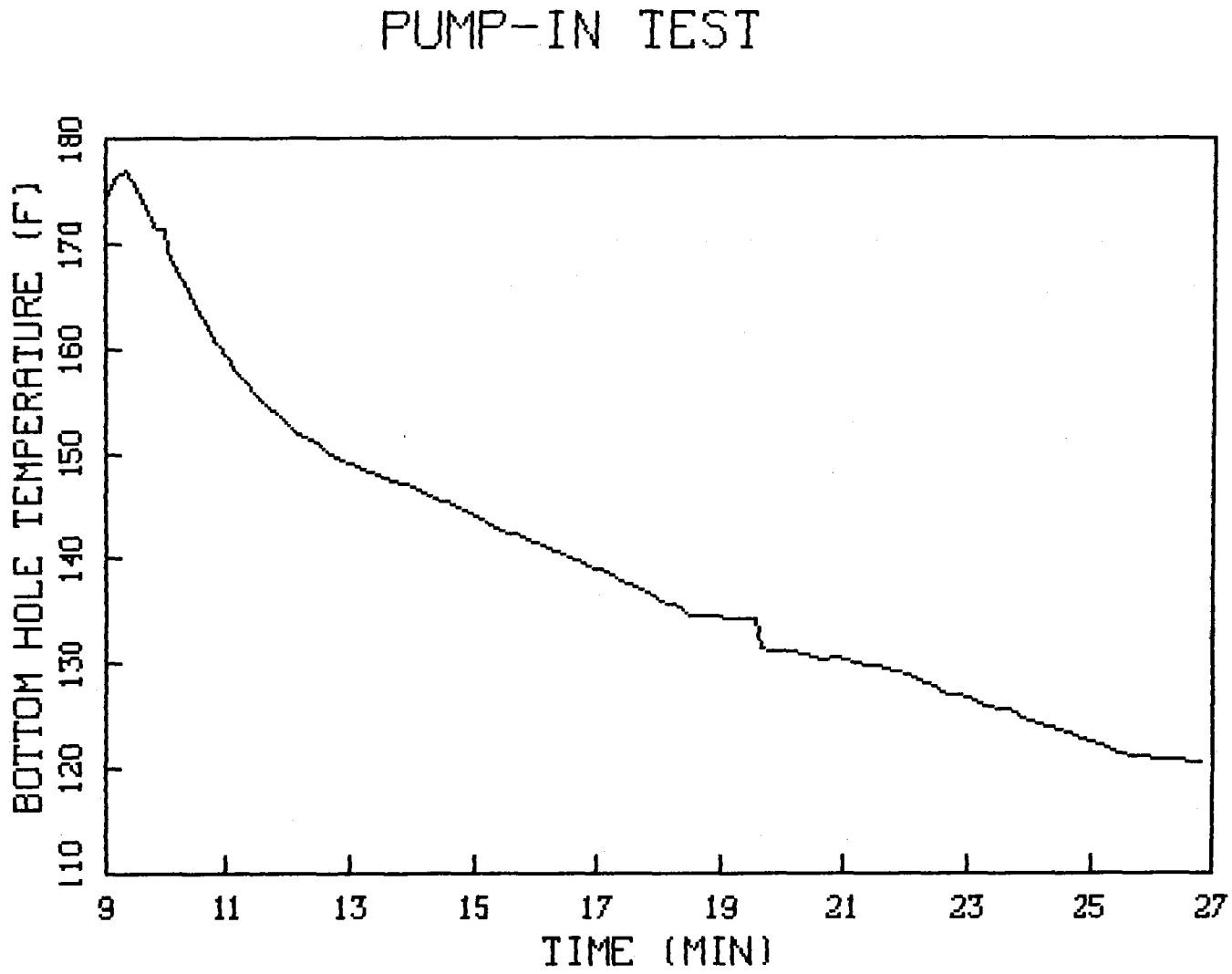

Figure 8.2.14 Pump-In Temperature Data

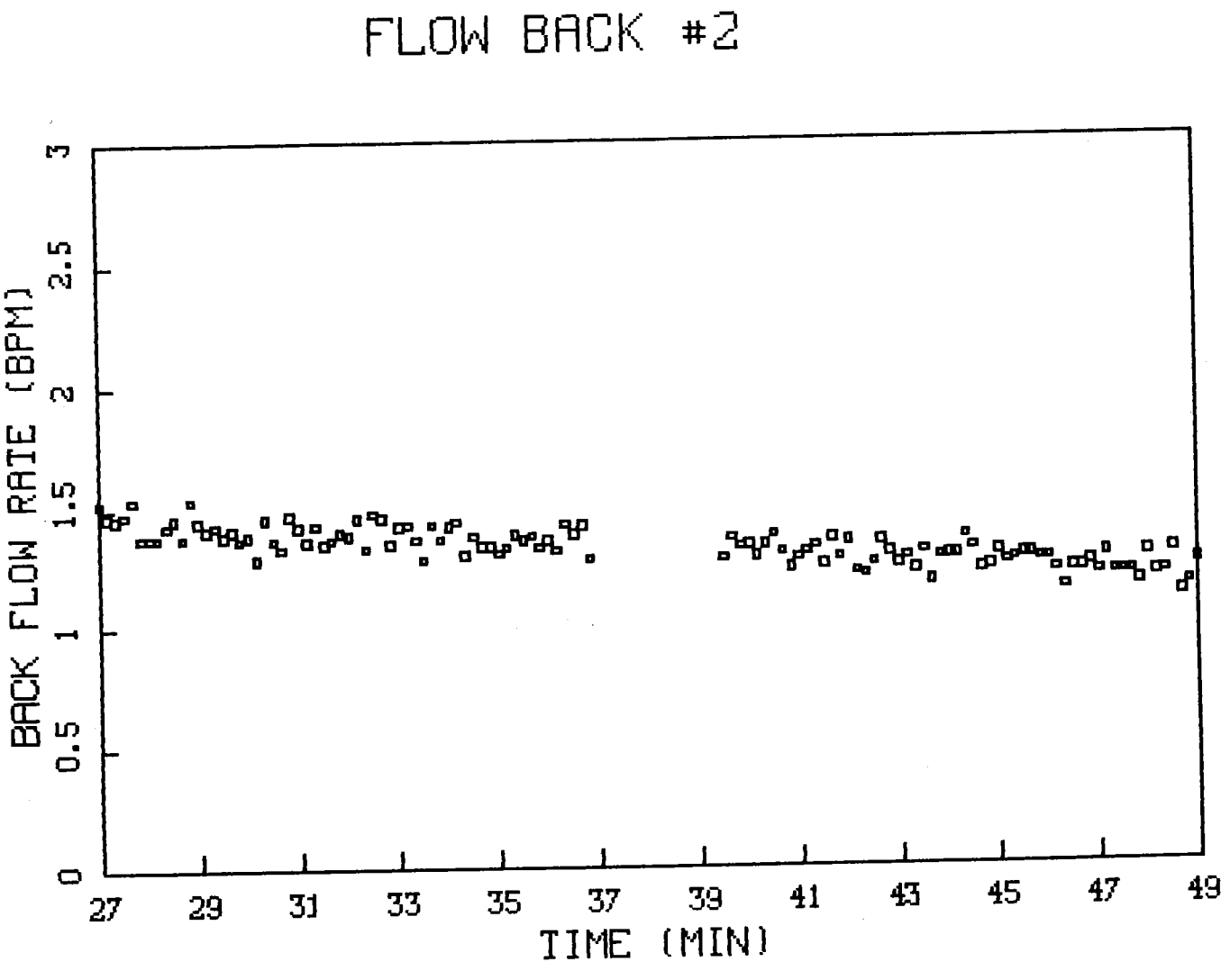

Figure 8.2.15 Flow Back Rate Data

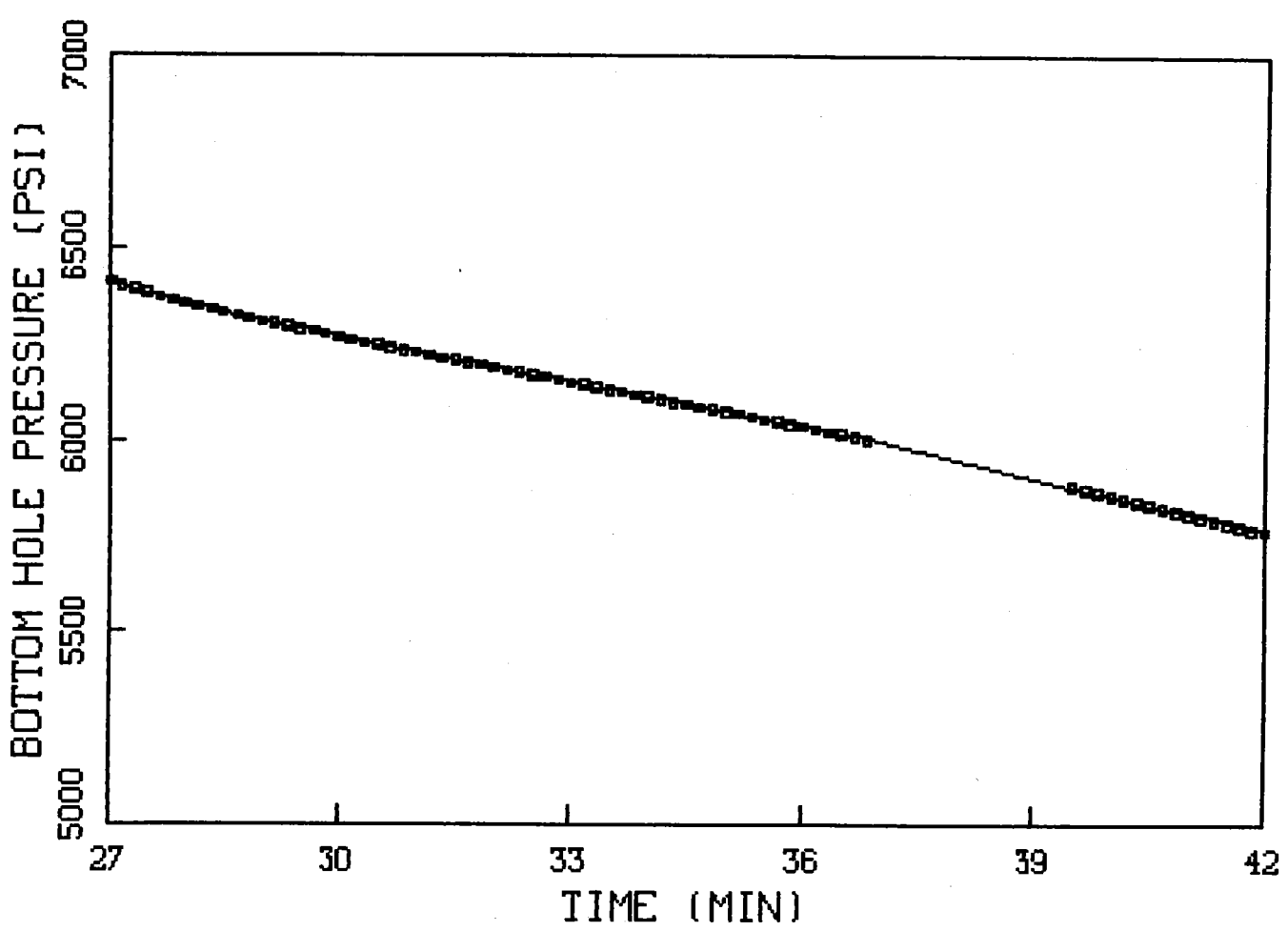

Figure 8.2.16 Flow Back Pressure Data

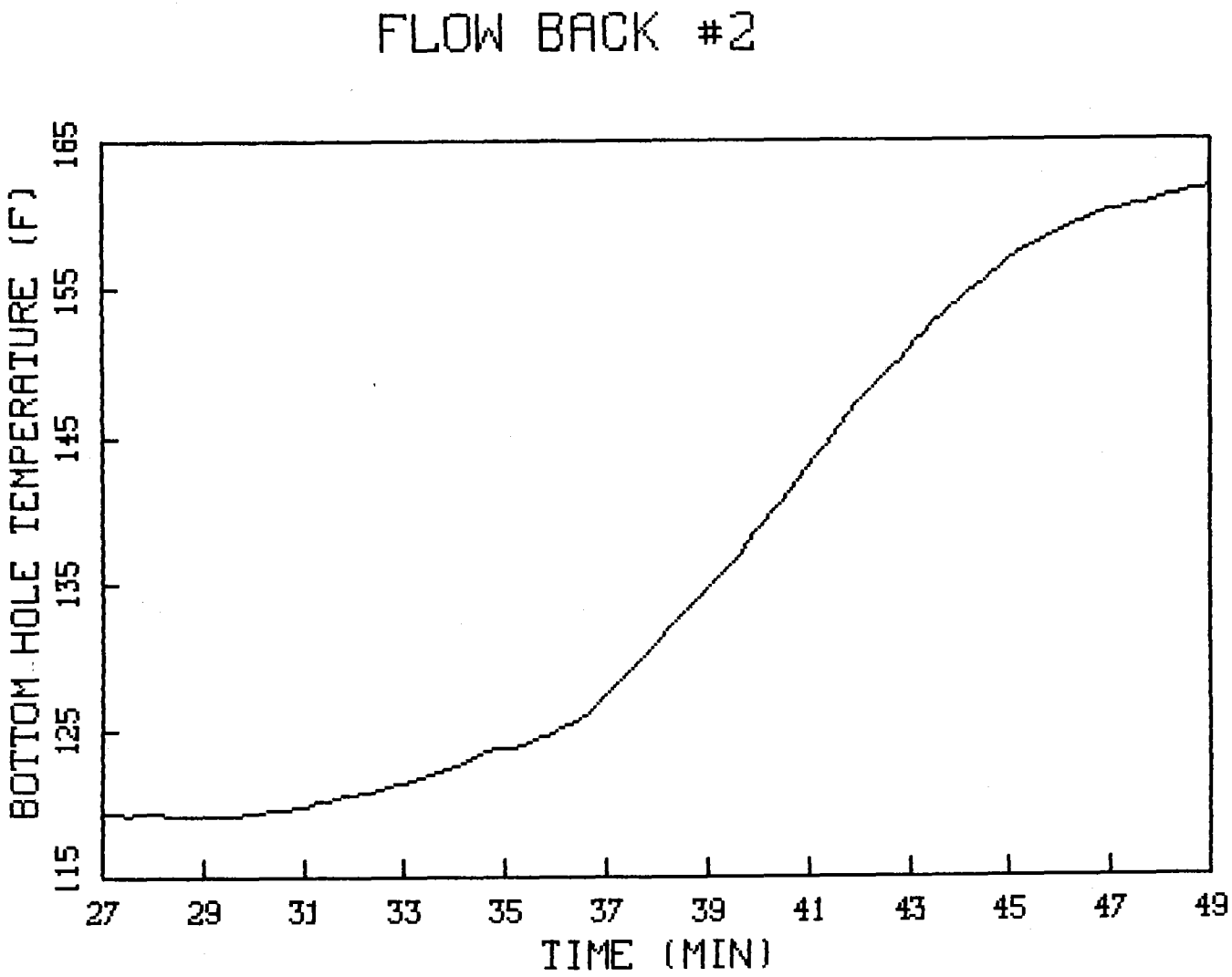

Figure 8.2.17 Flow Back Temperature Data

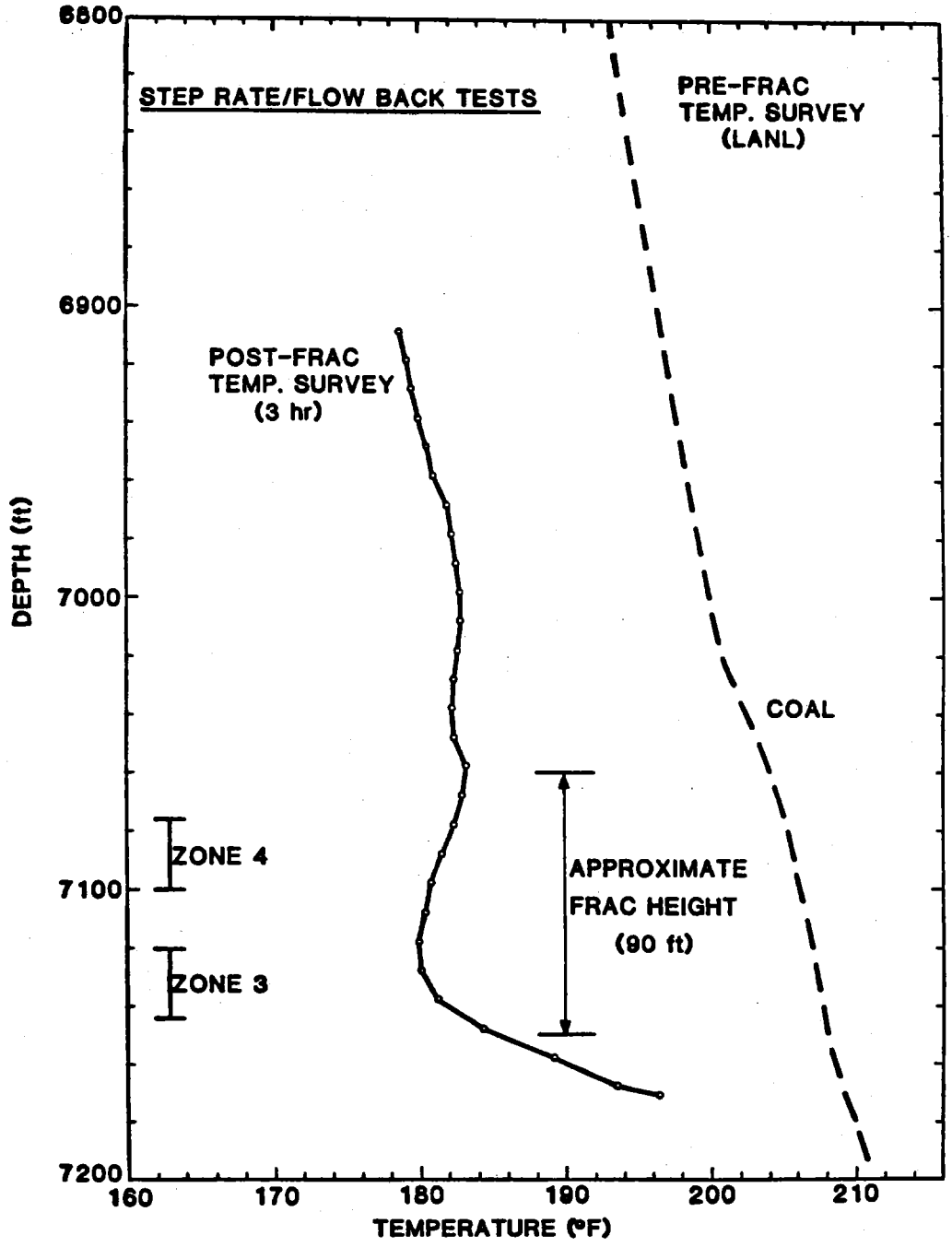

Figure 8.2.18 Step-Rate/Flow-Back Temperature Log

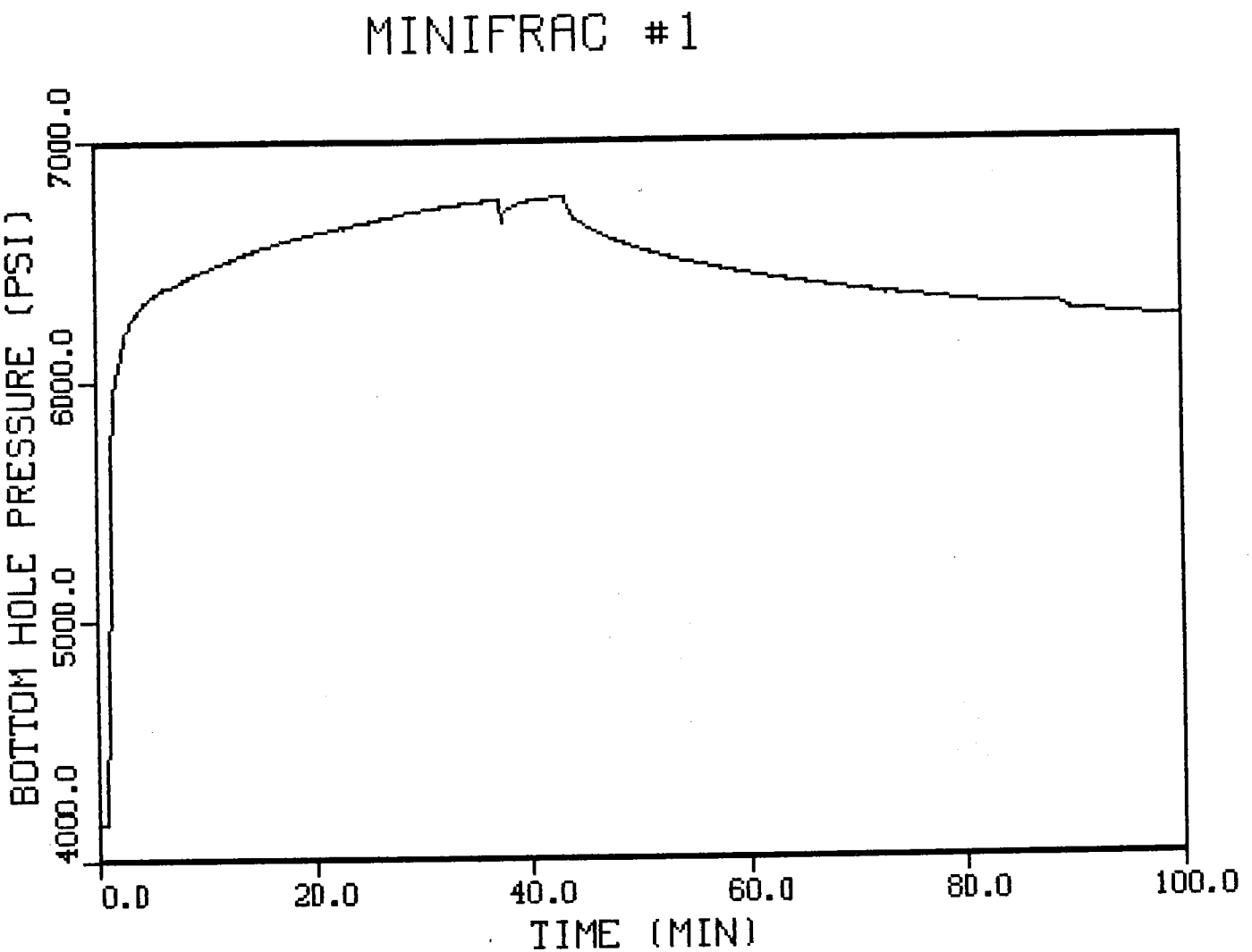

Figure 8.2.19 Minifrac #1 Pressure Data

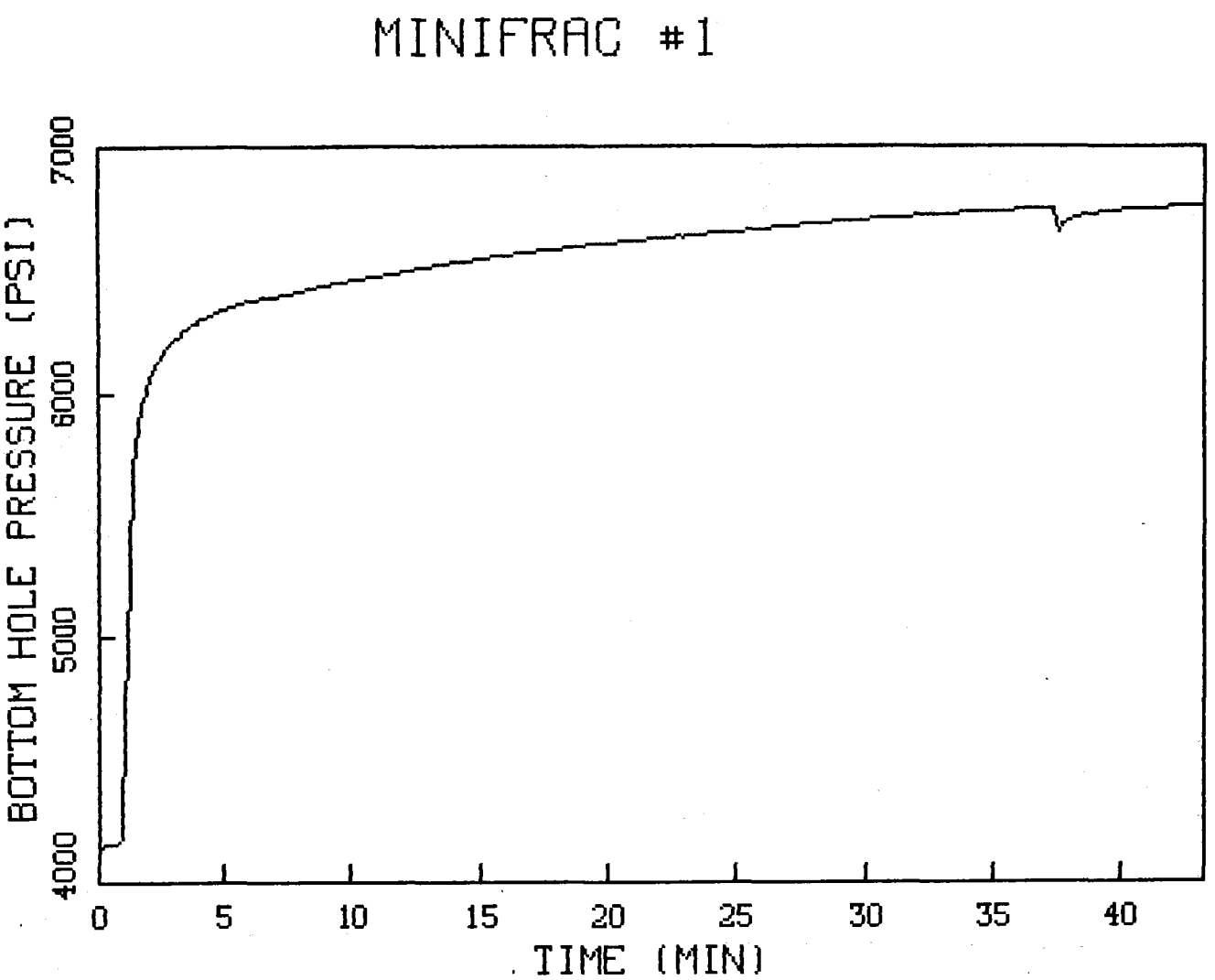

Figure 8.2.20 Minifrac #1 Injection Pressure Data

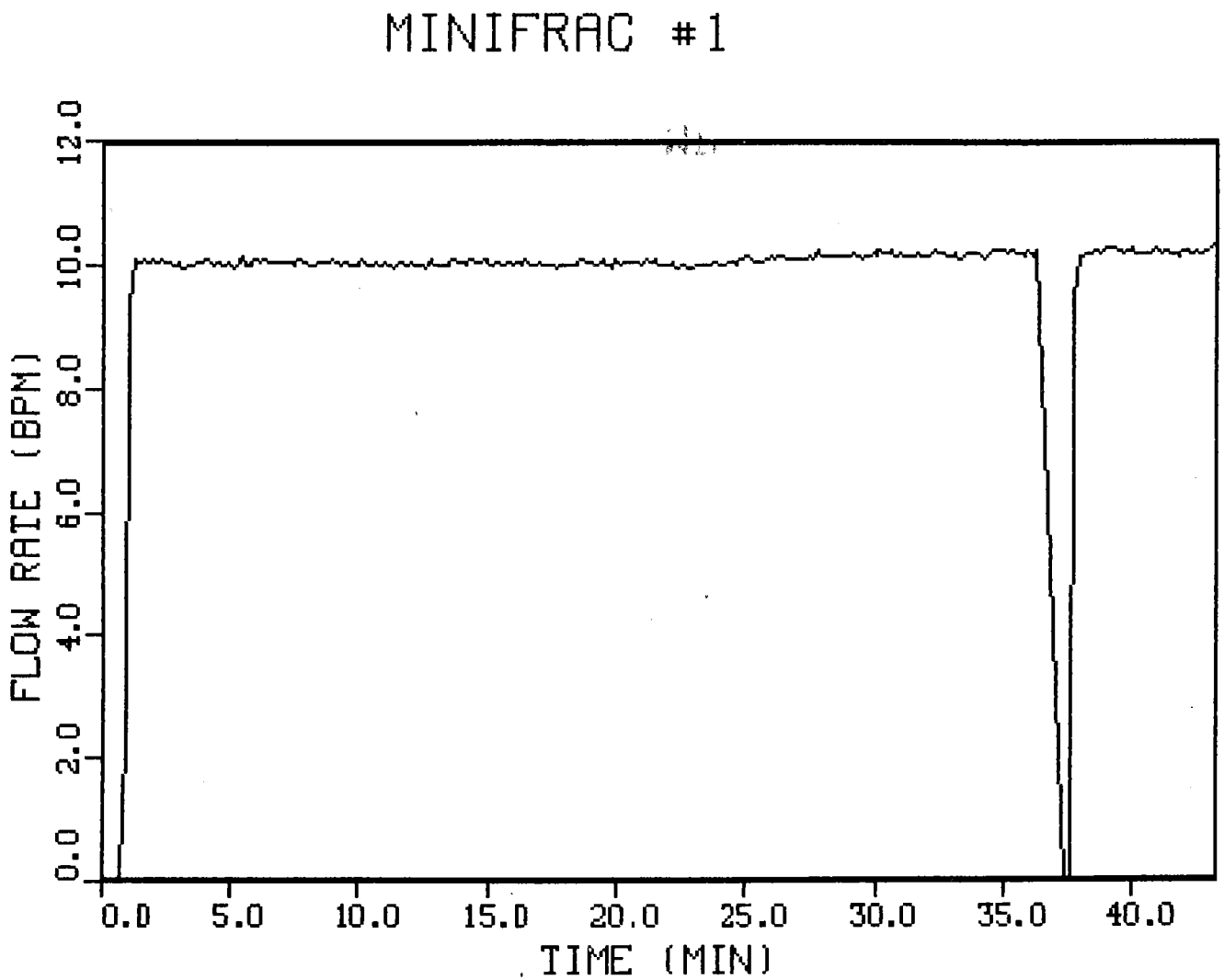

Figure 8.2.21 Minifrac #1 Flow Data

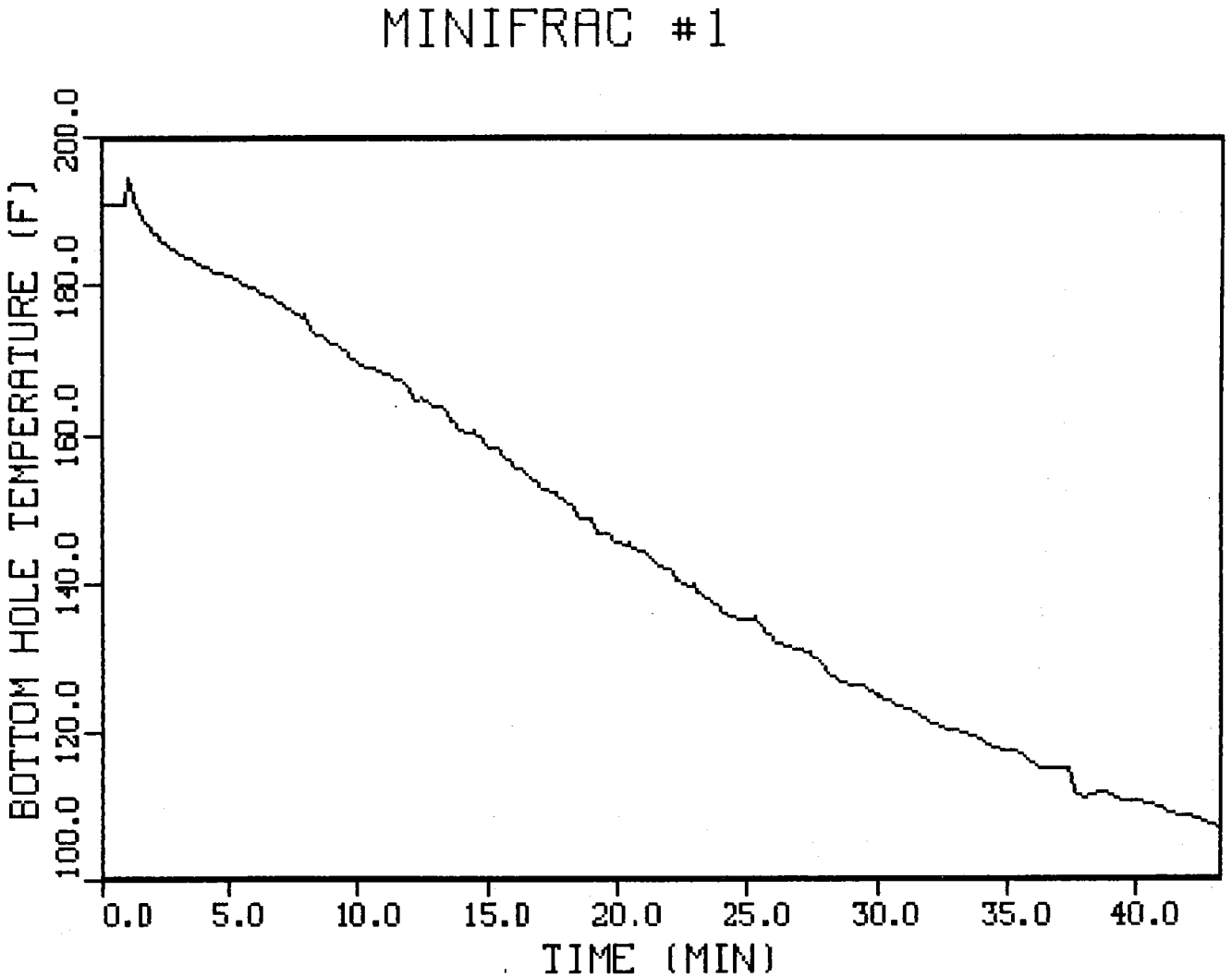

Figure 8.2.22 Minifrac #1 Temperature Data

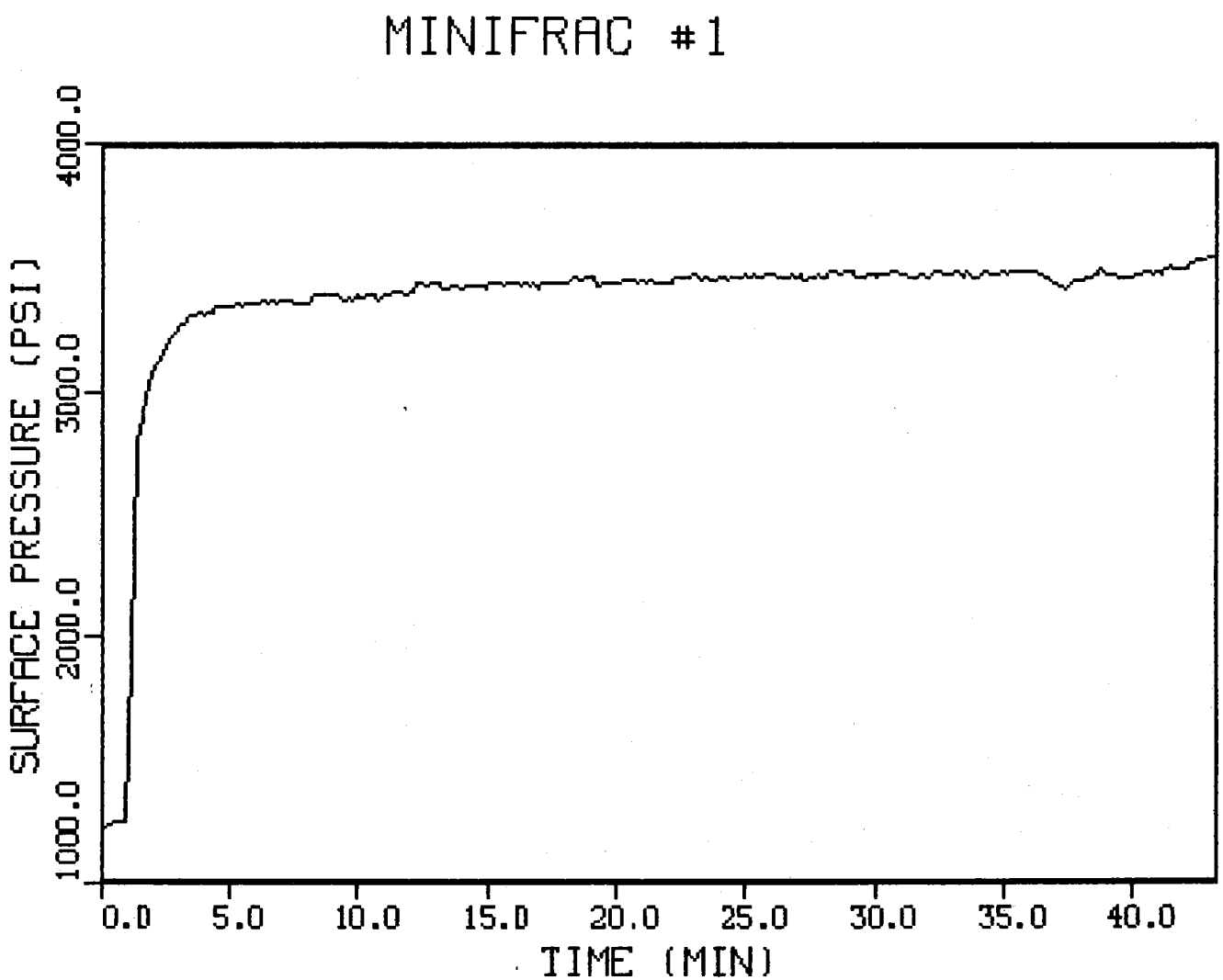

Figure 8.2.23 Minifrac #1 Surface Pressure Data

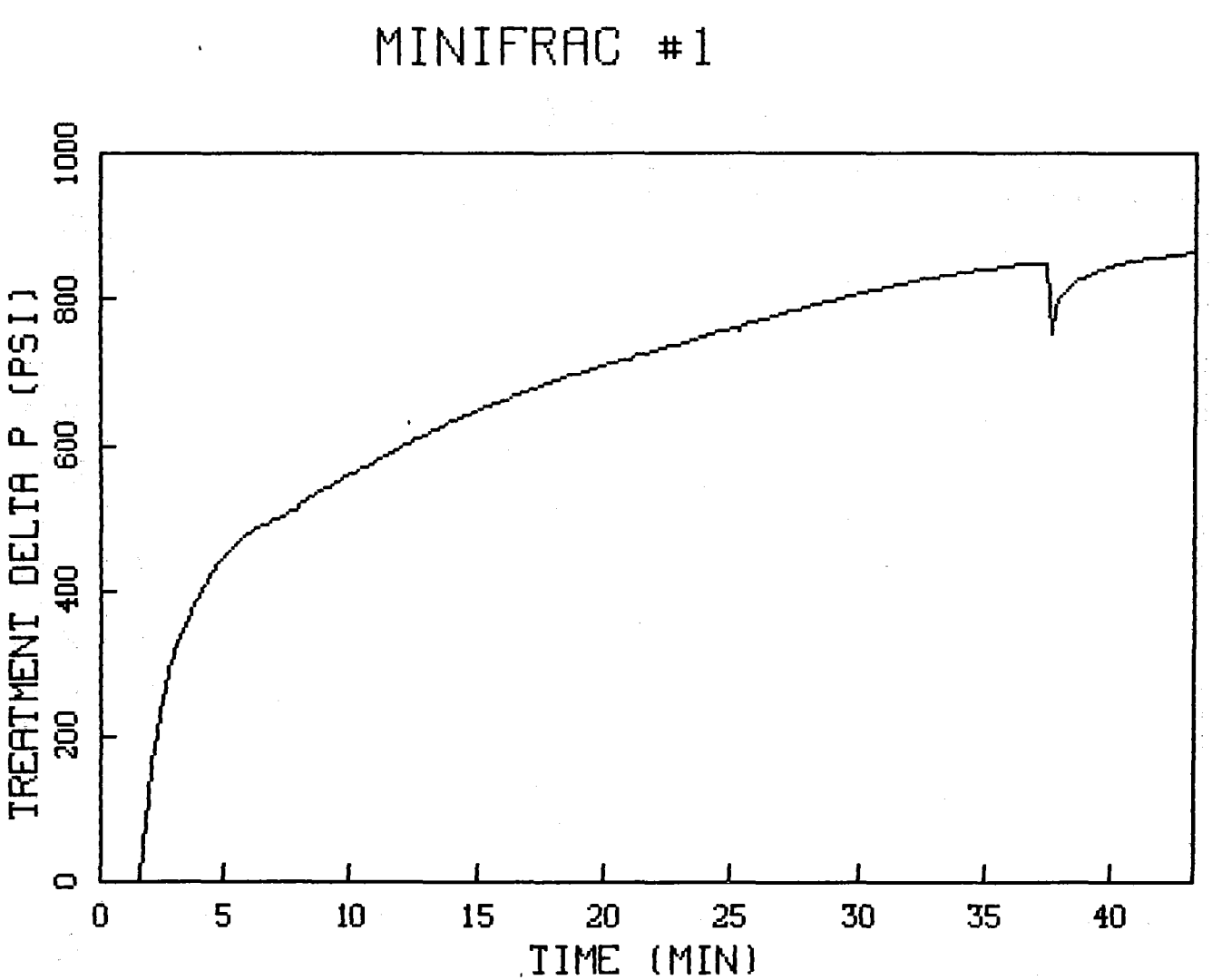

Figure 8.2.24 Minifrac #1 Treatment Delta Pressure

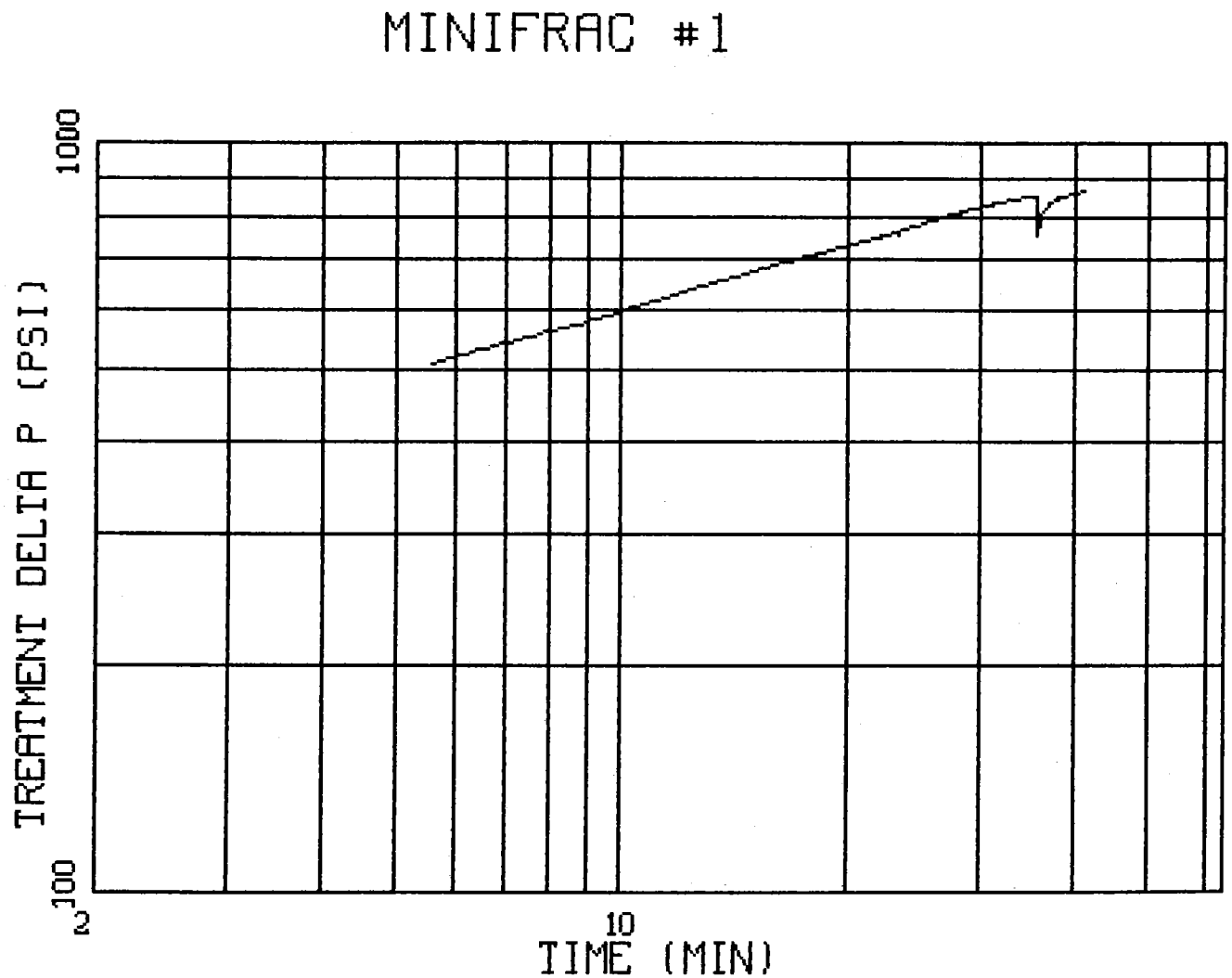

Figure 8.2.25 Minifrac #1 Nolte Smith Plot

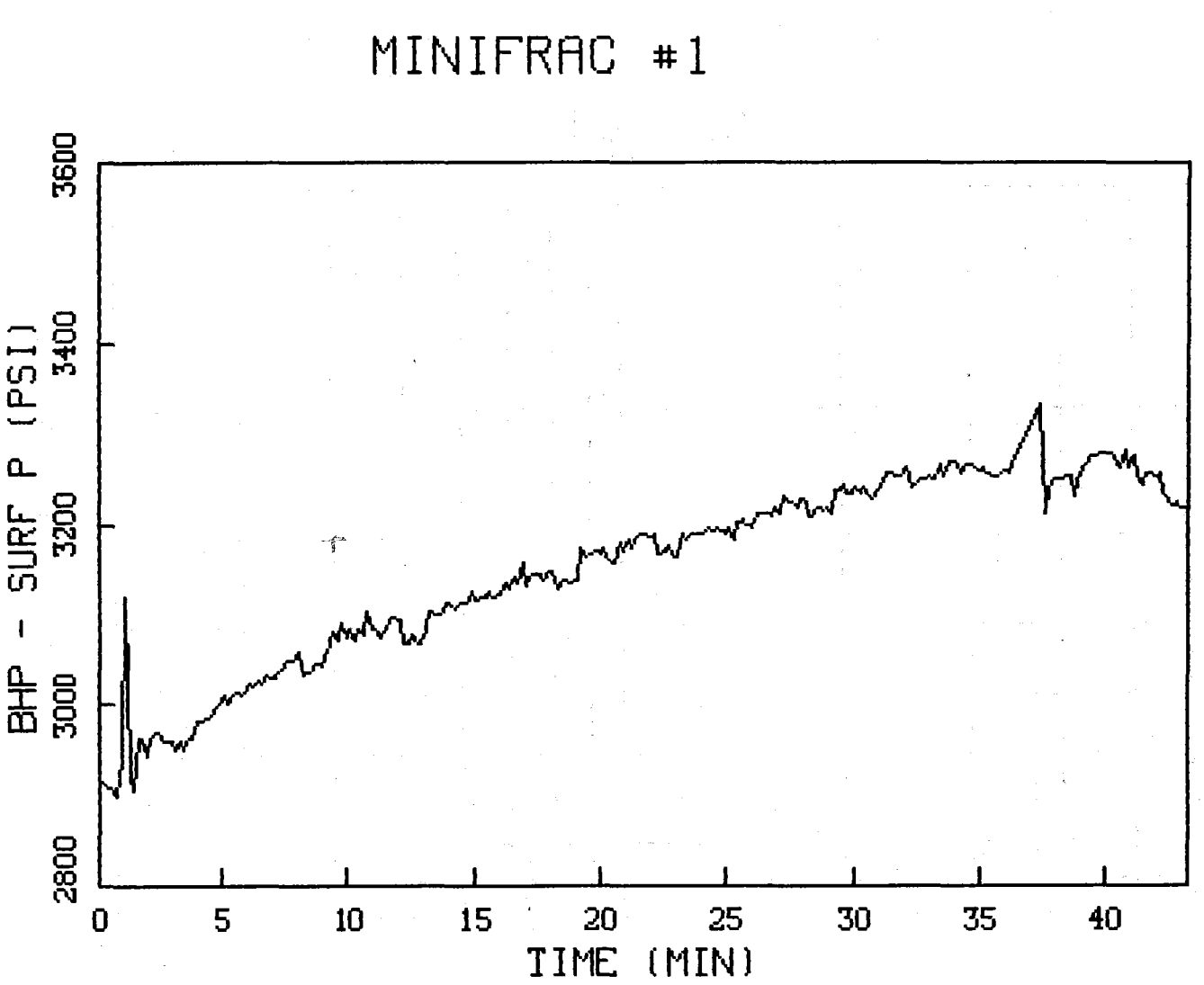

Figure 8.2.26 Minifrac #1 Pressure Differential Between Surface and Bottom Hole

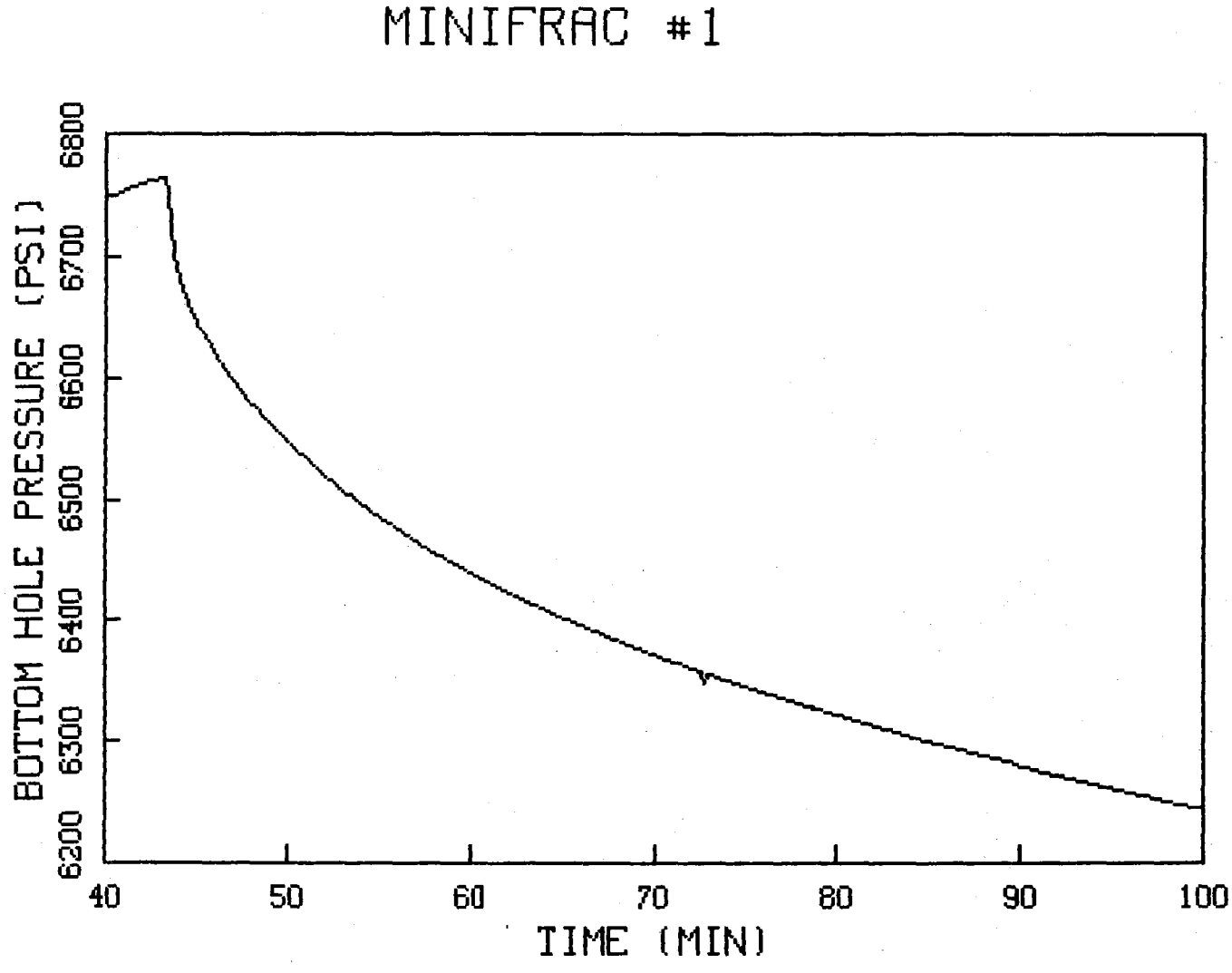

Figure 8.2.27 Minifrac #1 Pressure Decline Data

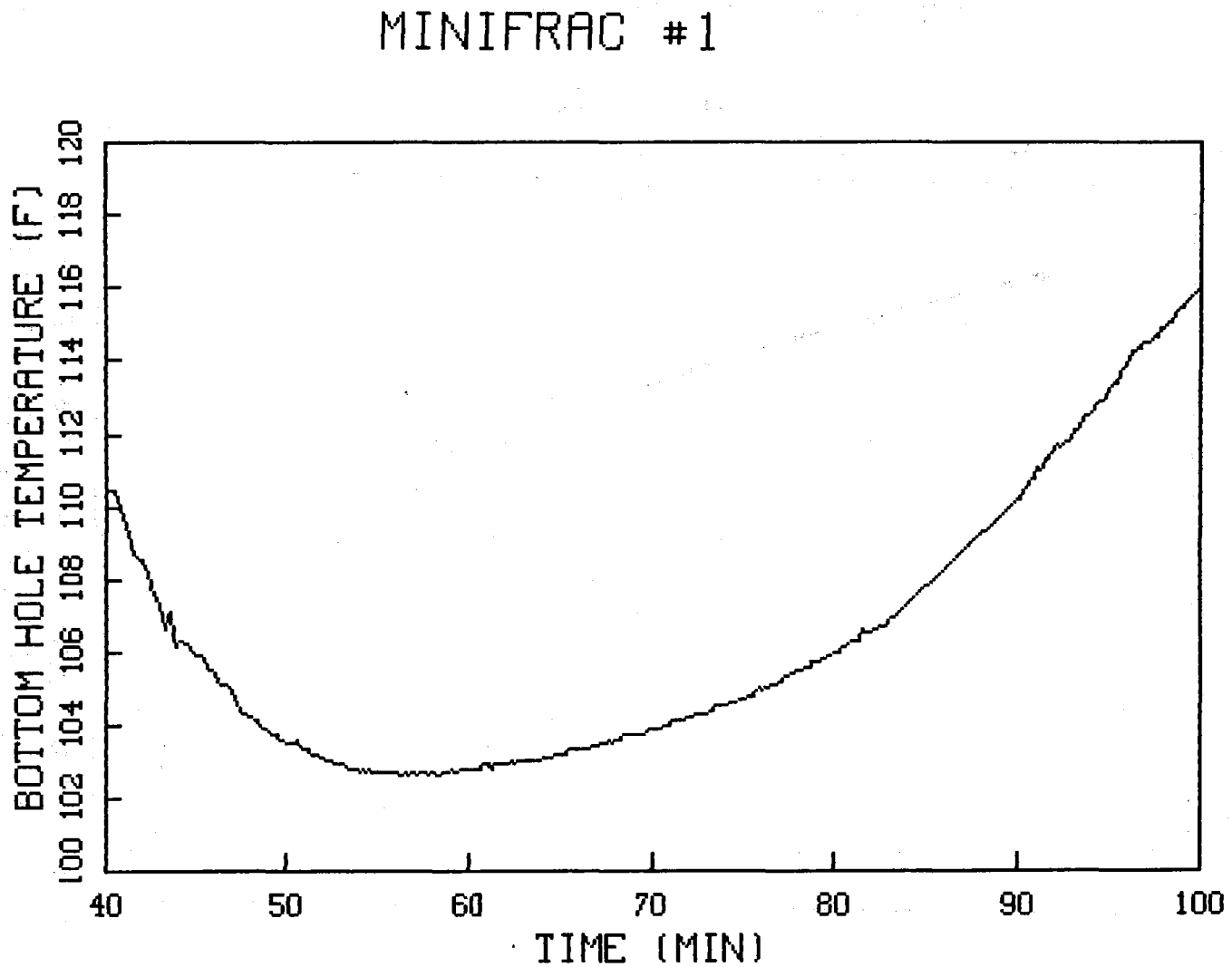

Figure 8.2.28 Minifrac #1 Temperature Data During Pressure Decline

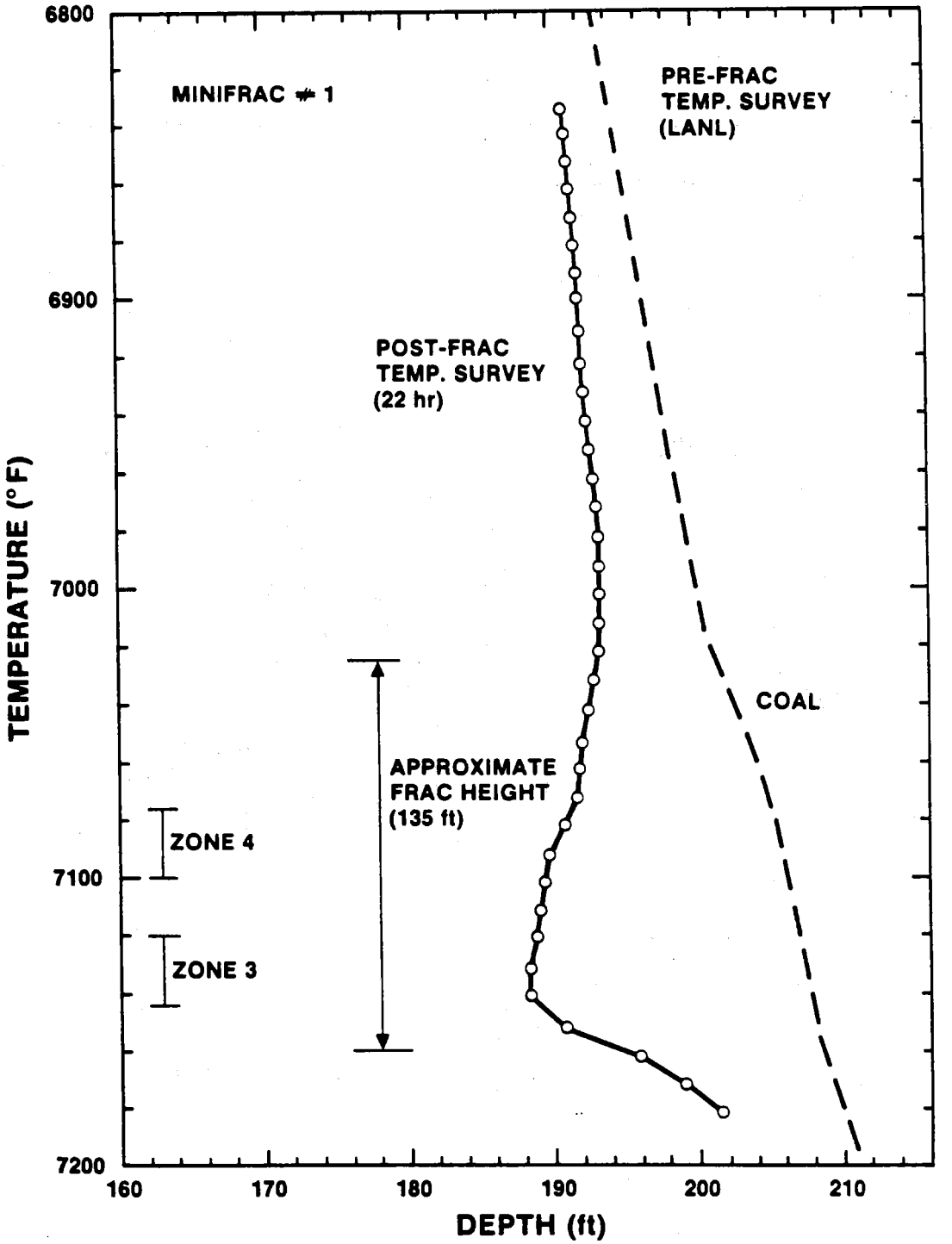

Figure 8.2.29 Temperature Log After Minifrac #1

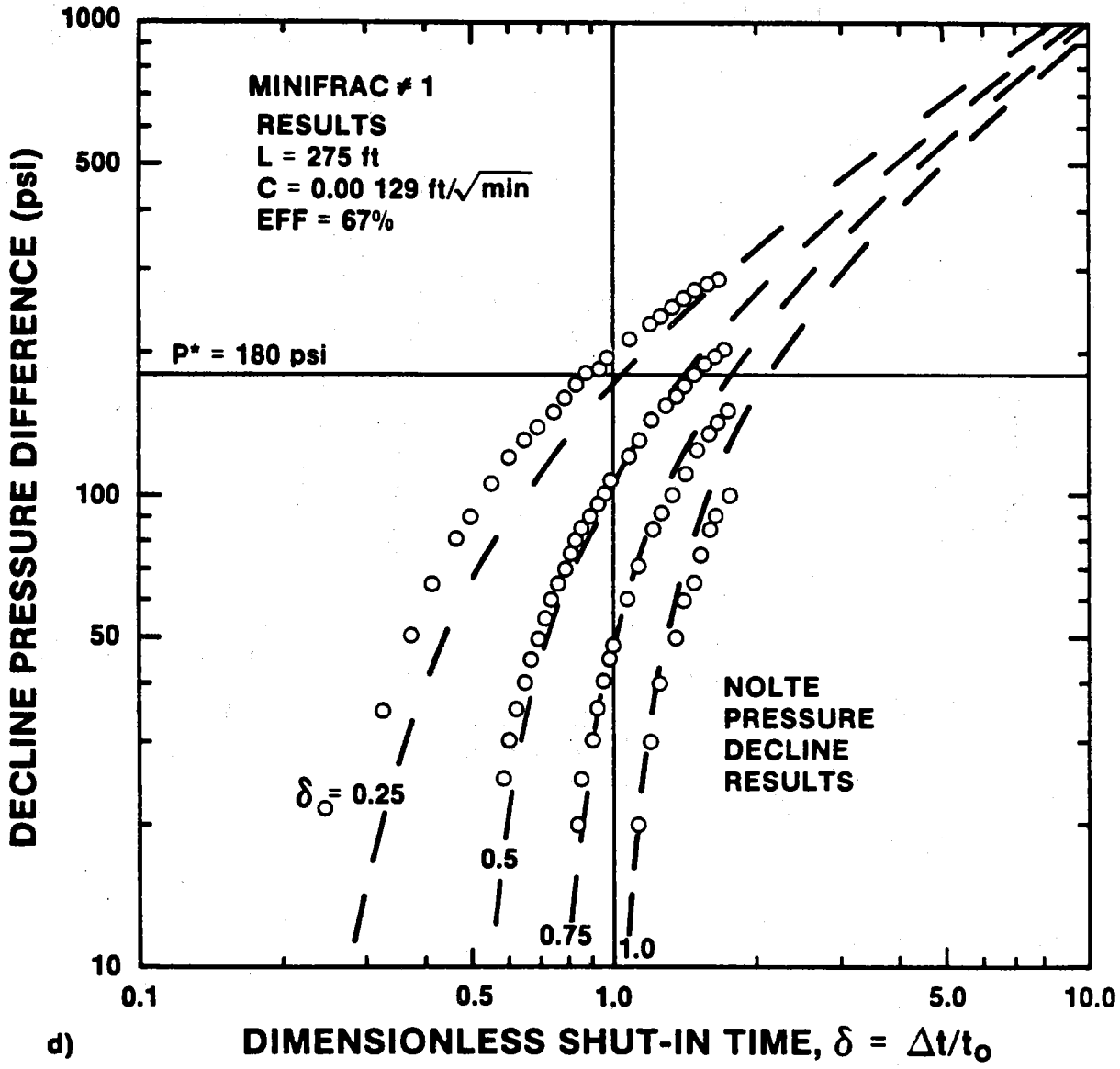

Figure 8.2.30 Minifrac #1 Nolte Analysis

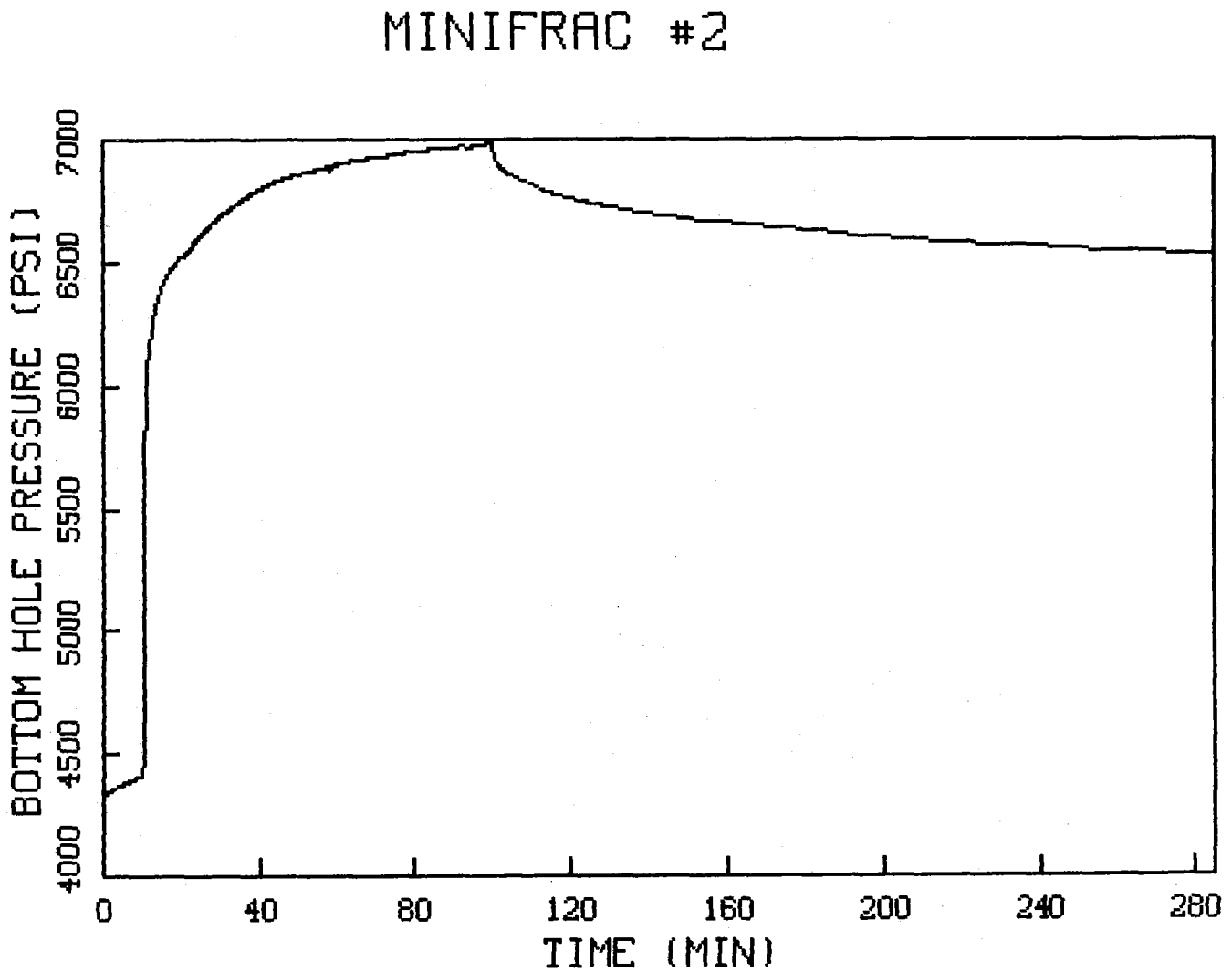

Figure 8.2.31 Minifrac #2 Pressure Data

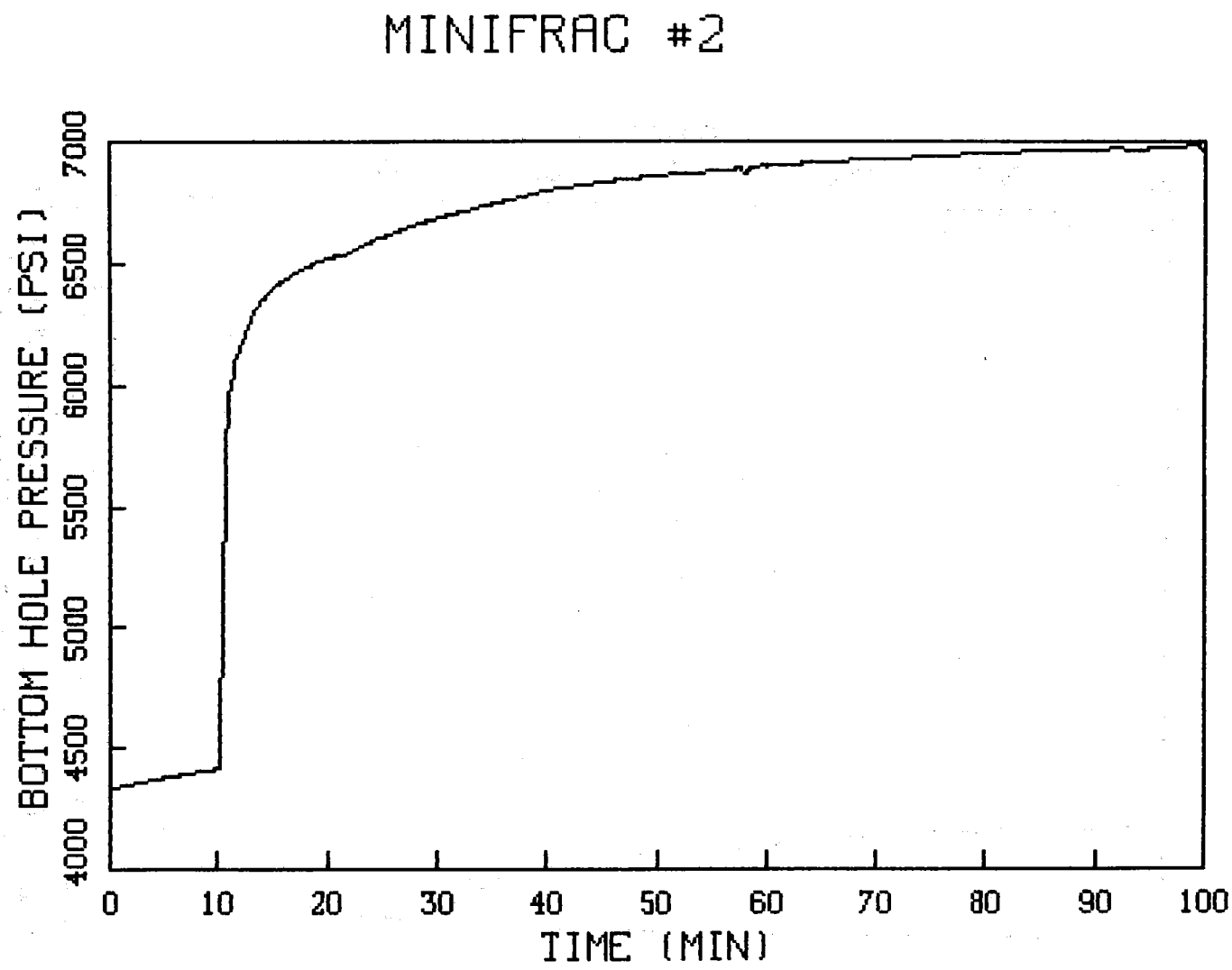

Figure 8.2.32 Minifrac #2 Injection Pressure Data

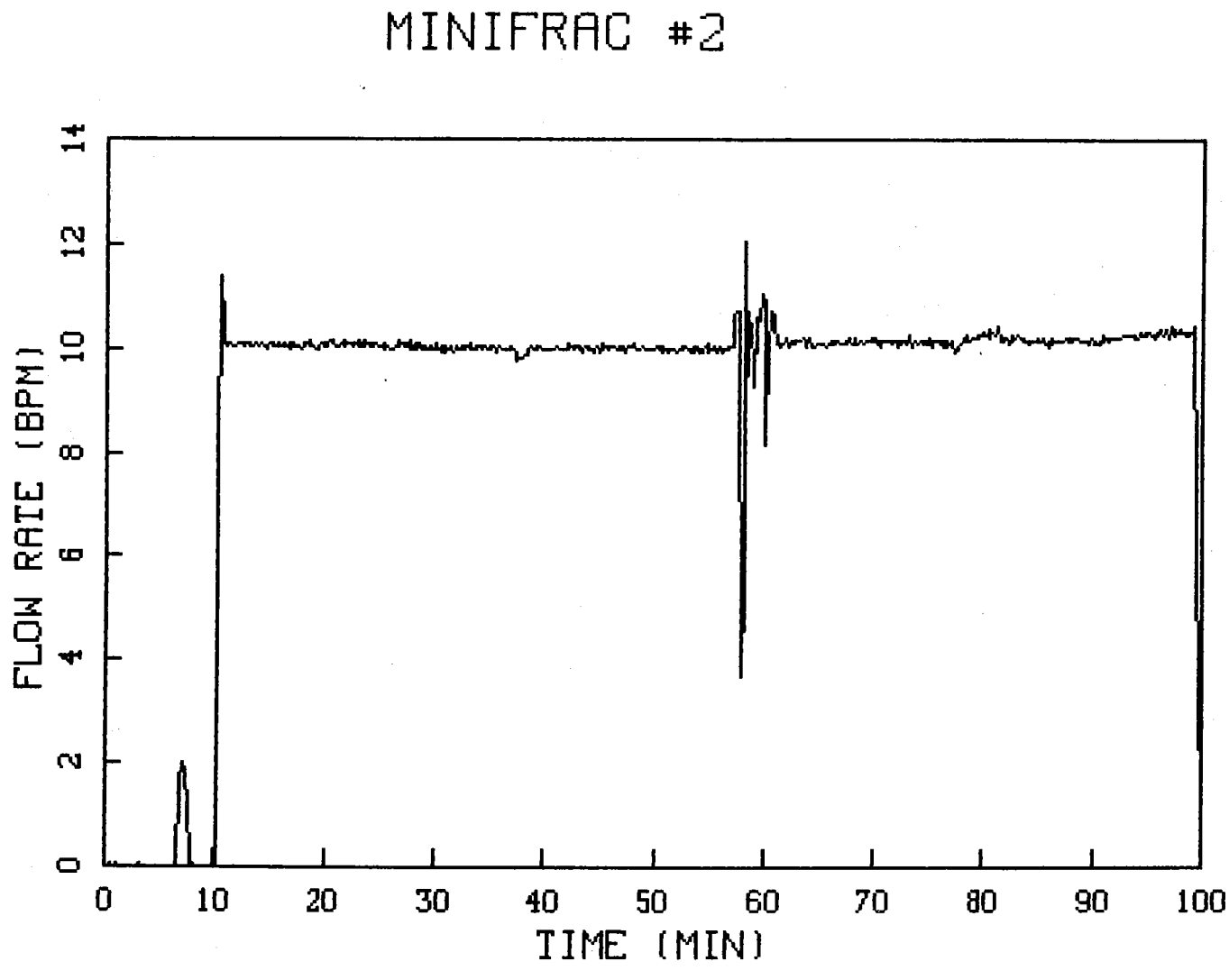

Figure 8.2.33 Minifrac #2 Flow Rate Data

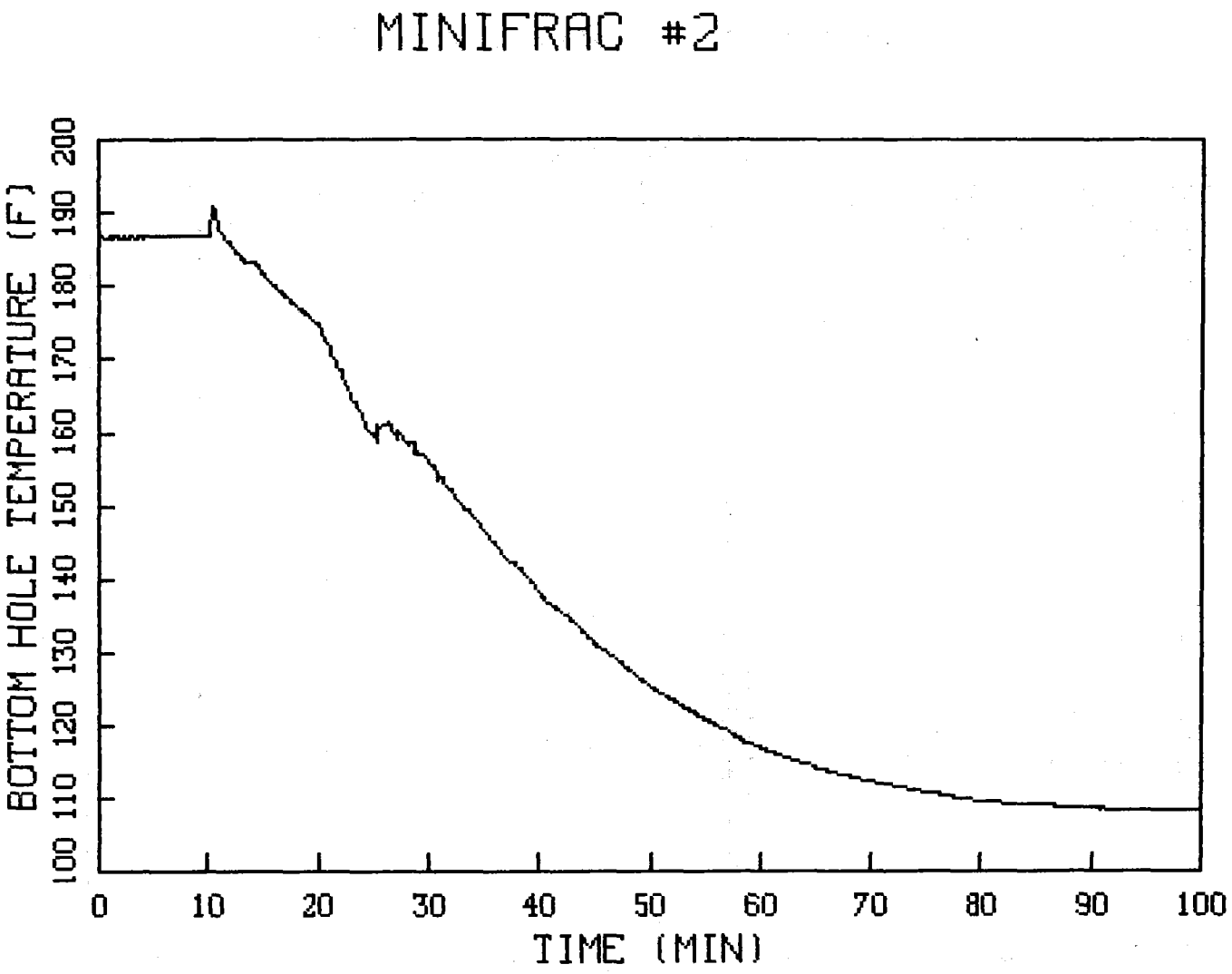

Figure 8.2.34 Minifrac #2 Temperature Data

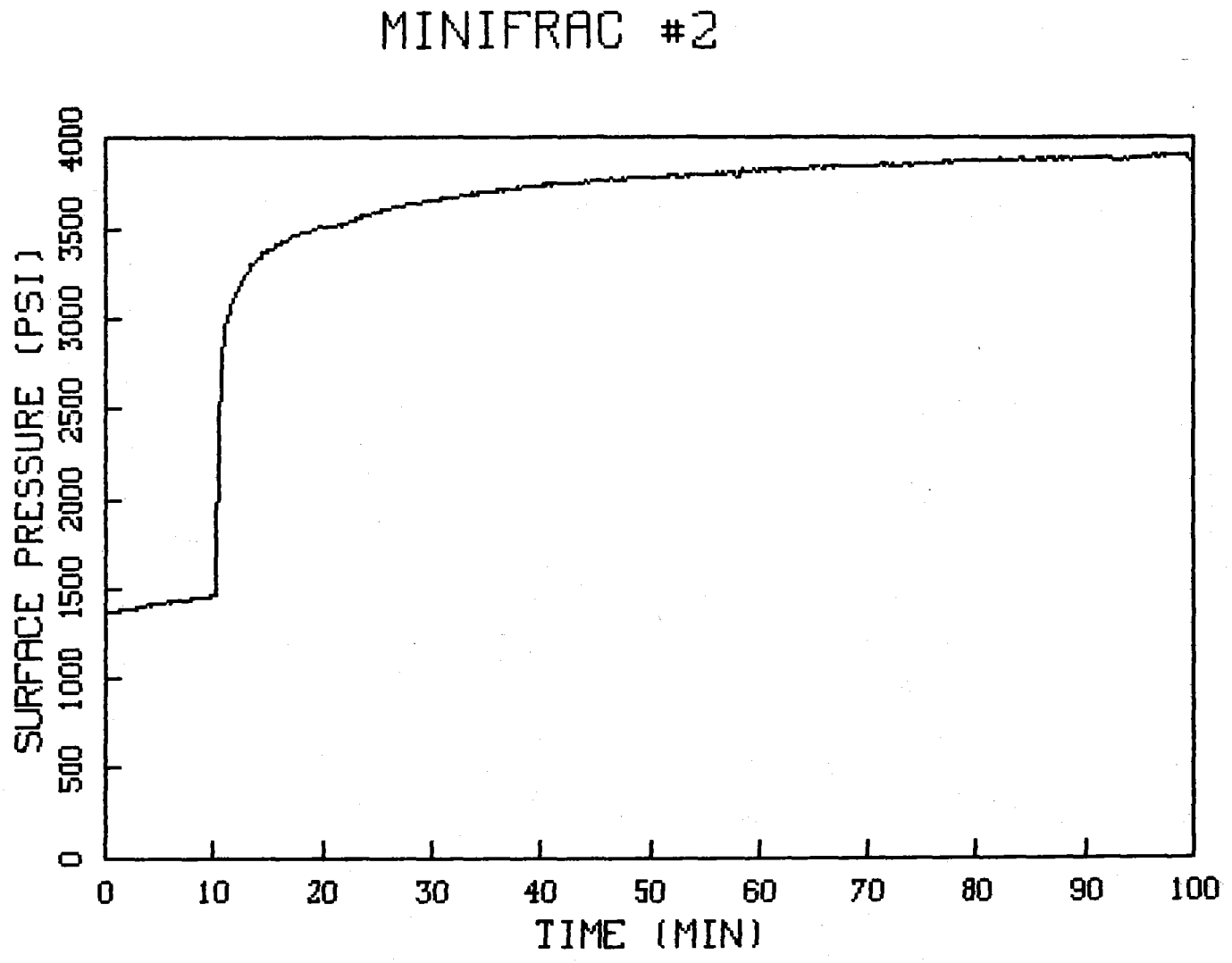

Figure 8.2.35 Minifrac #2 Surface Pressure Data

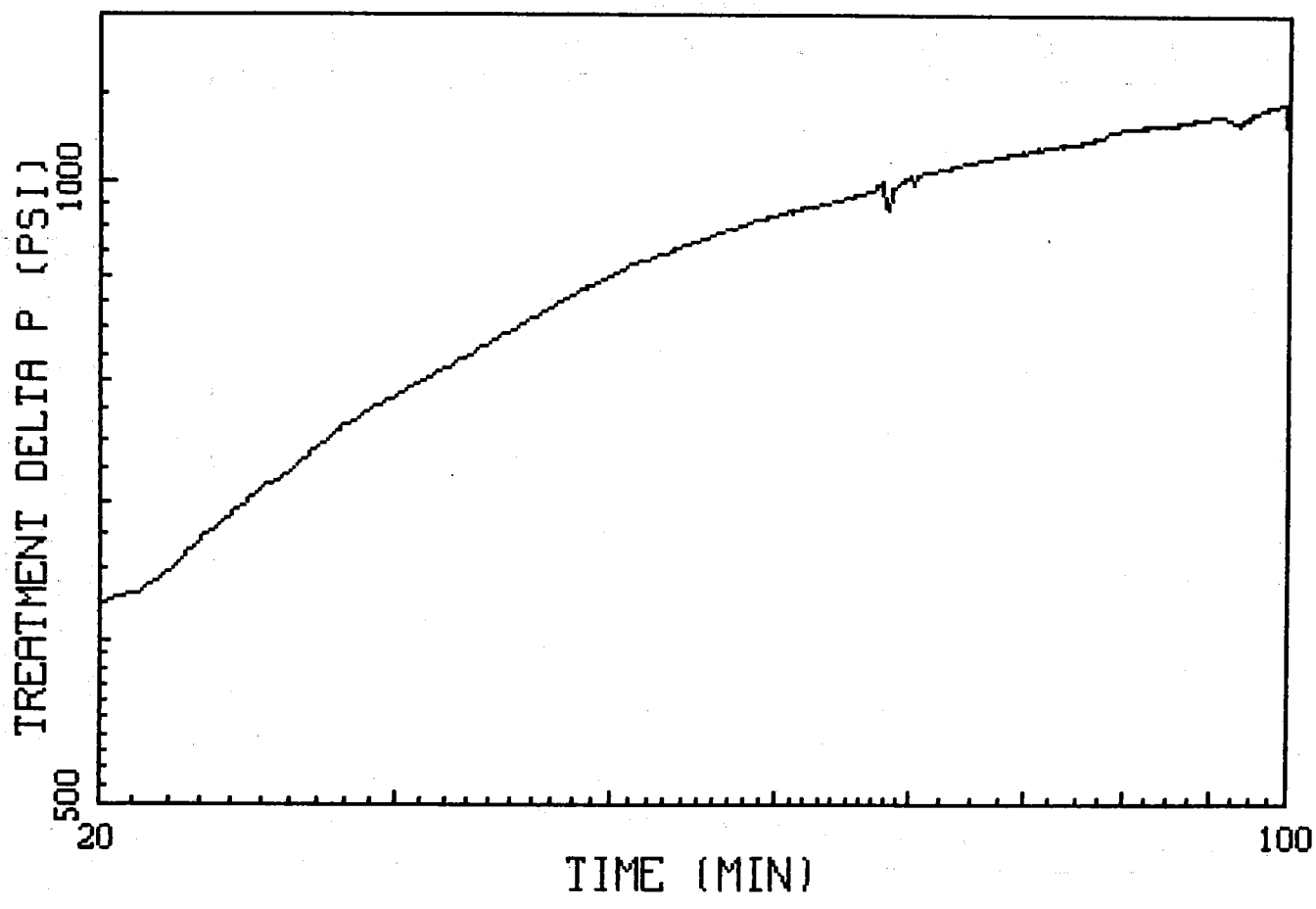

Figure 8.2.36 Minifrac #2 Treatment Delta Pressure

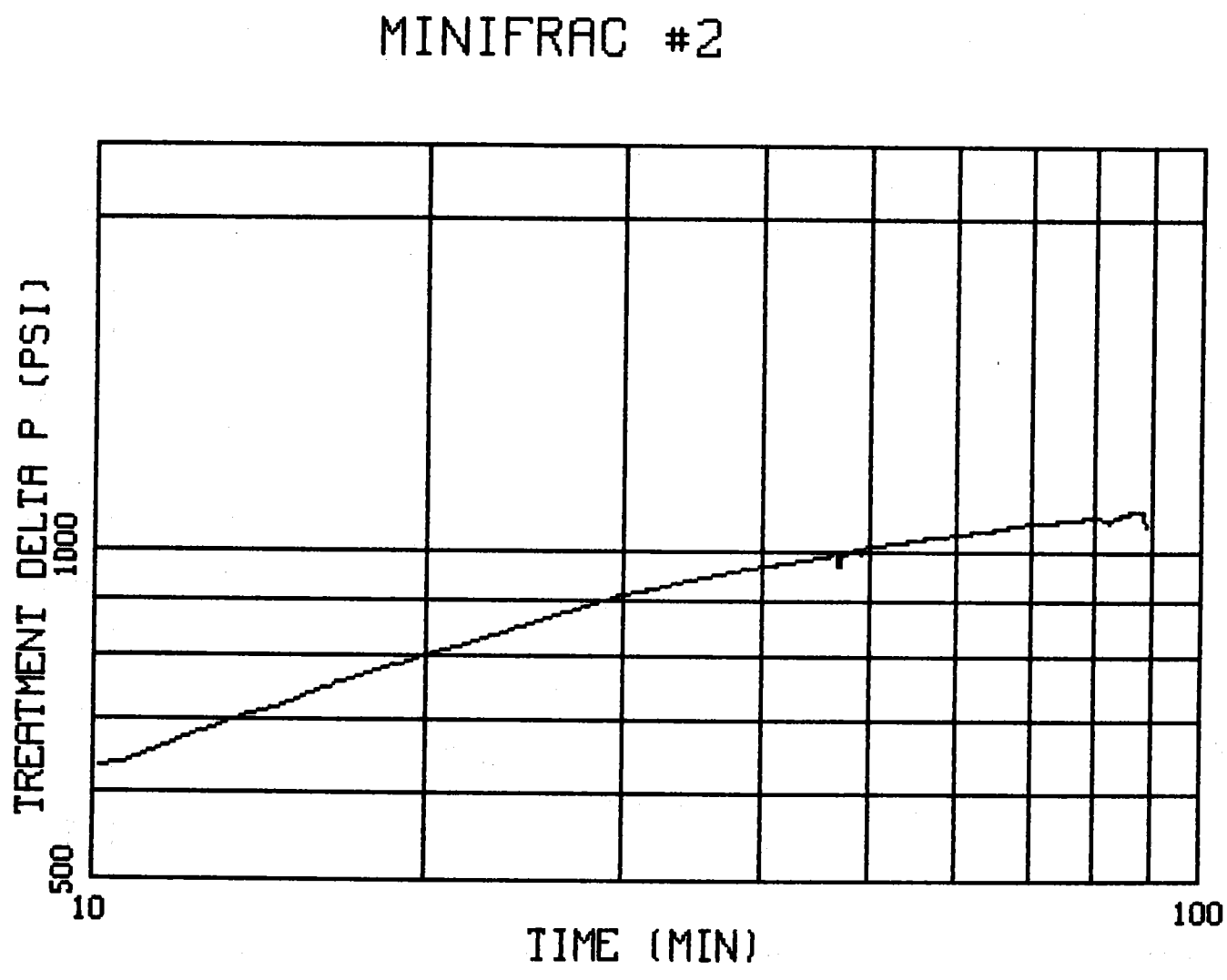

Figure 8.2.37 Minifrac #2 Nolte-Smith Plot

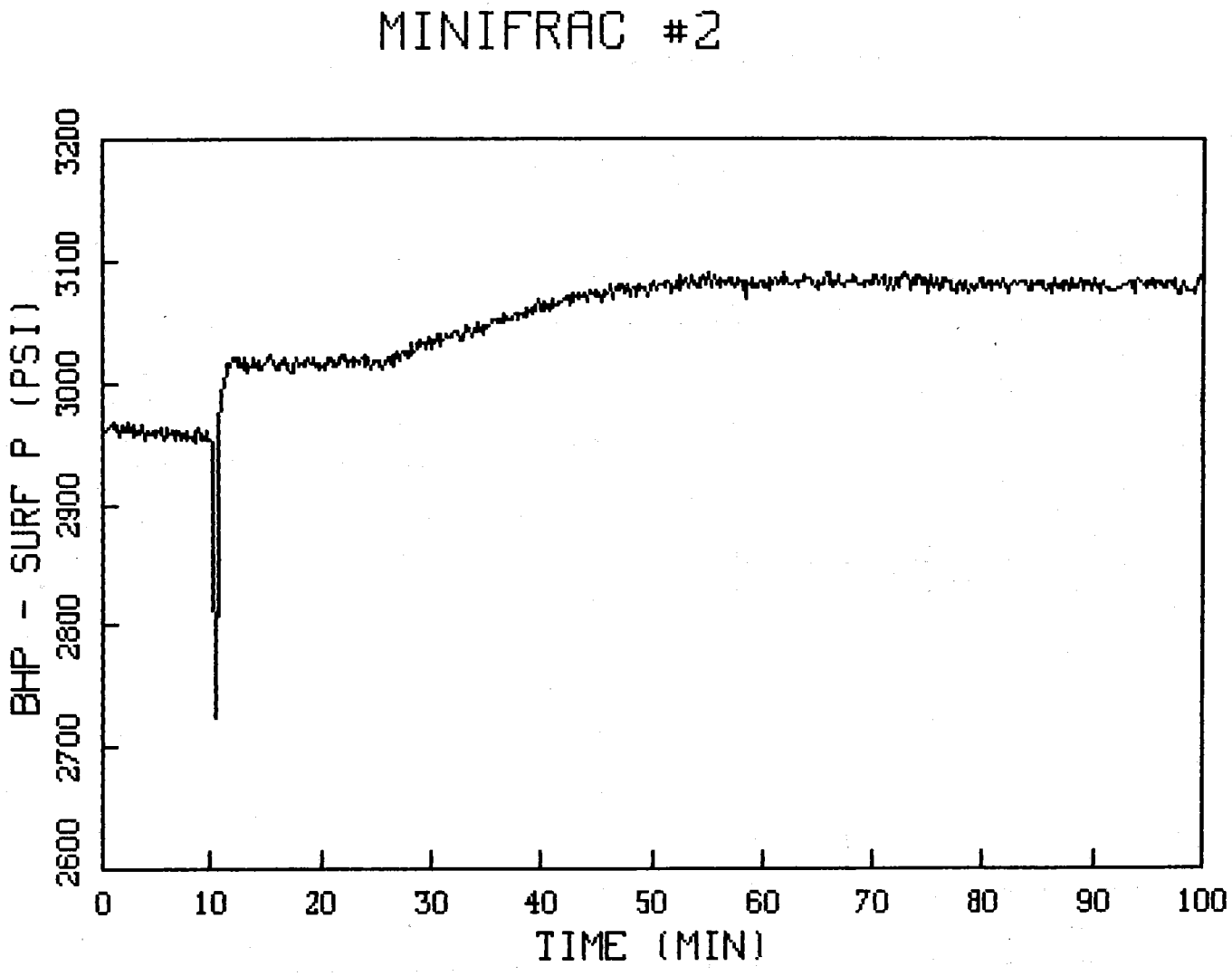

Figure 8.2.38 Minifrac #2 Pressure Differential Between Surface and Bottom Hole

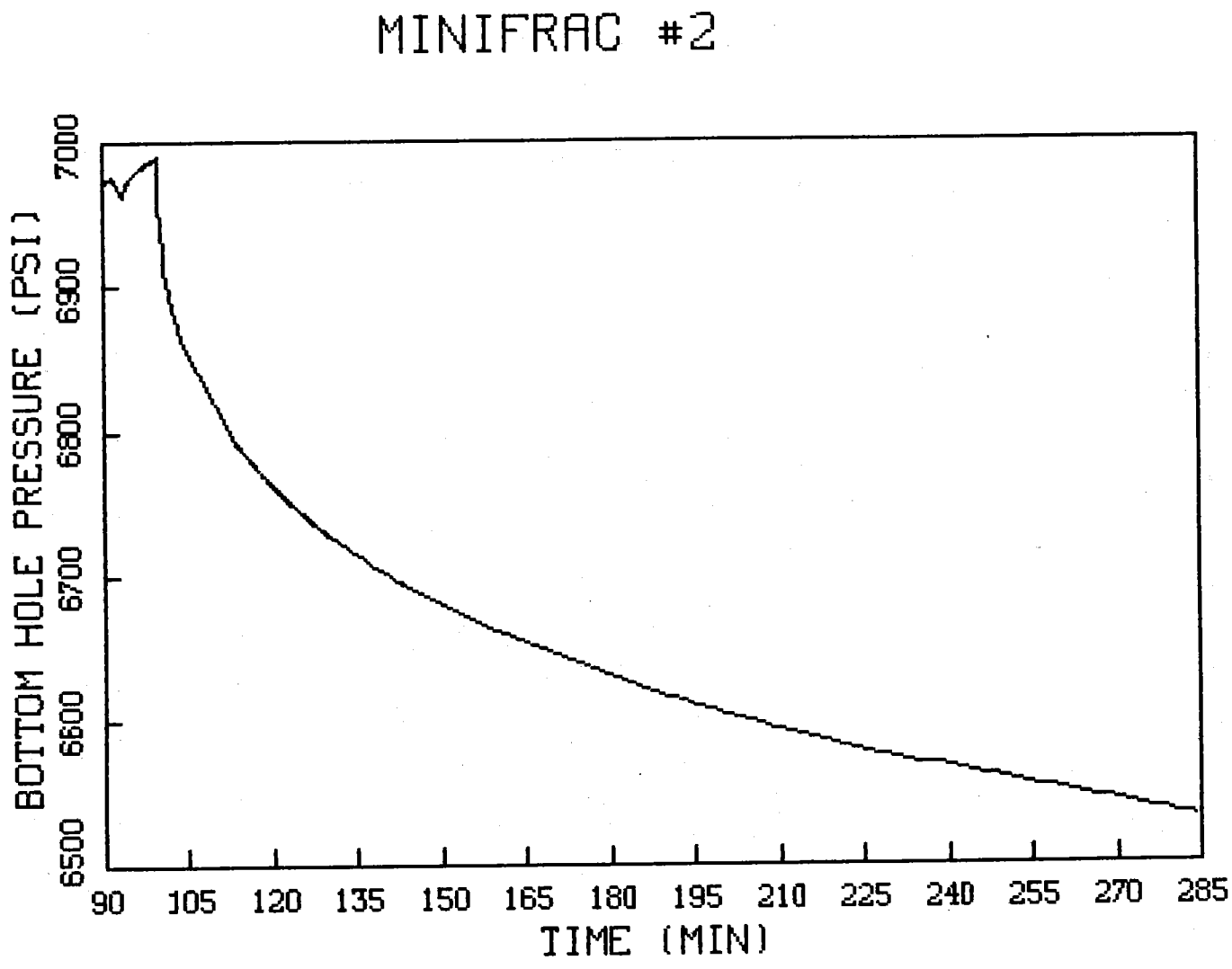

Figure 8.2.39 Minifrac #2 Pressure Decline Data

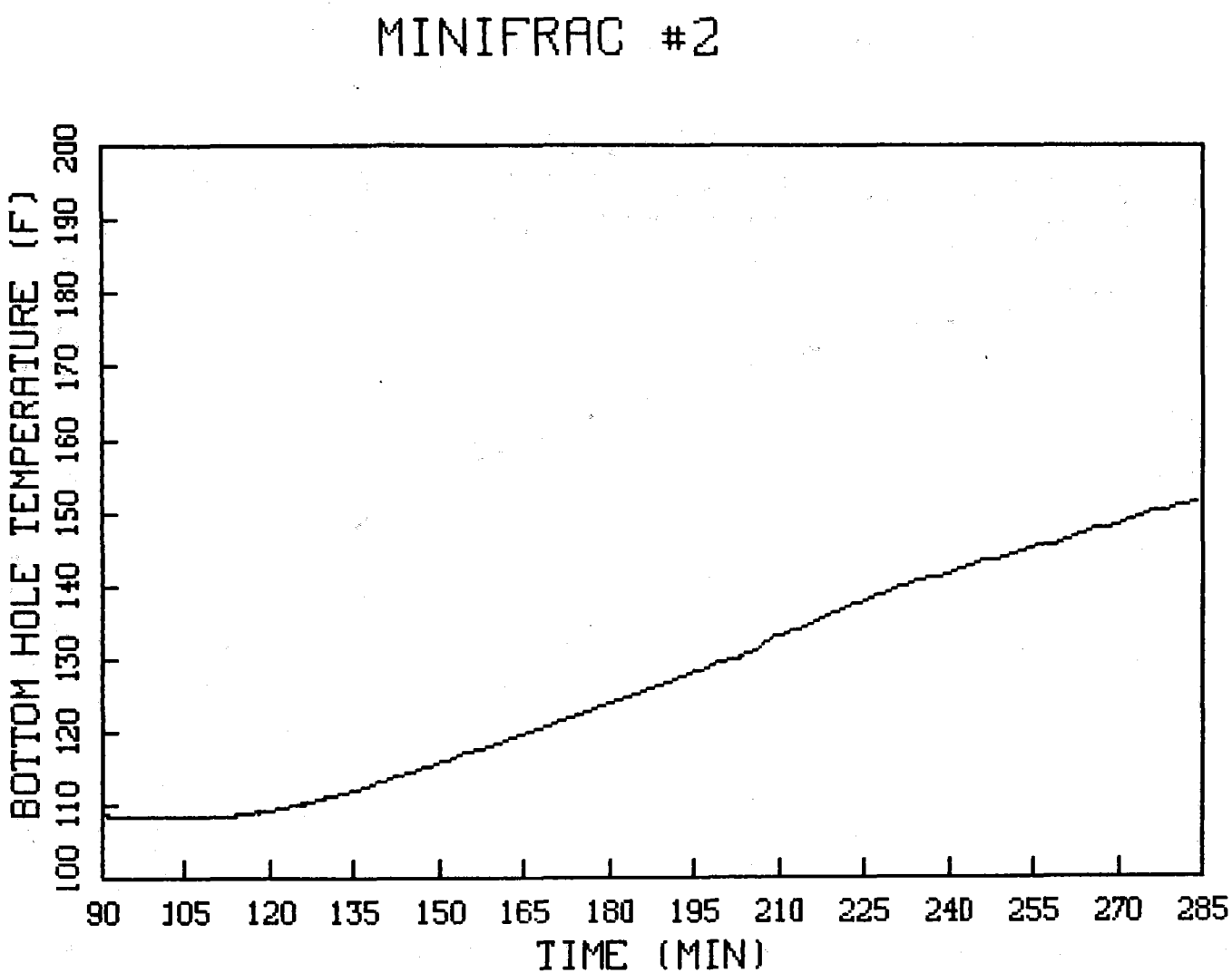

Figure 8.2.40 Minifrac #2 Temperature Data During Pressure Decline

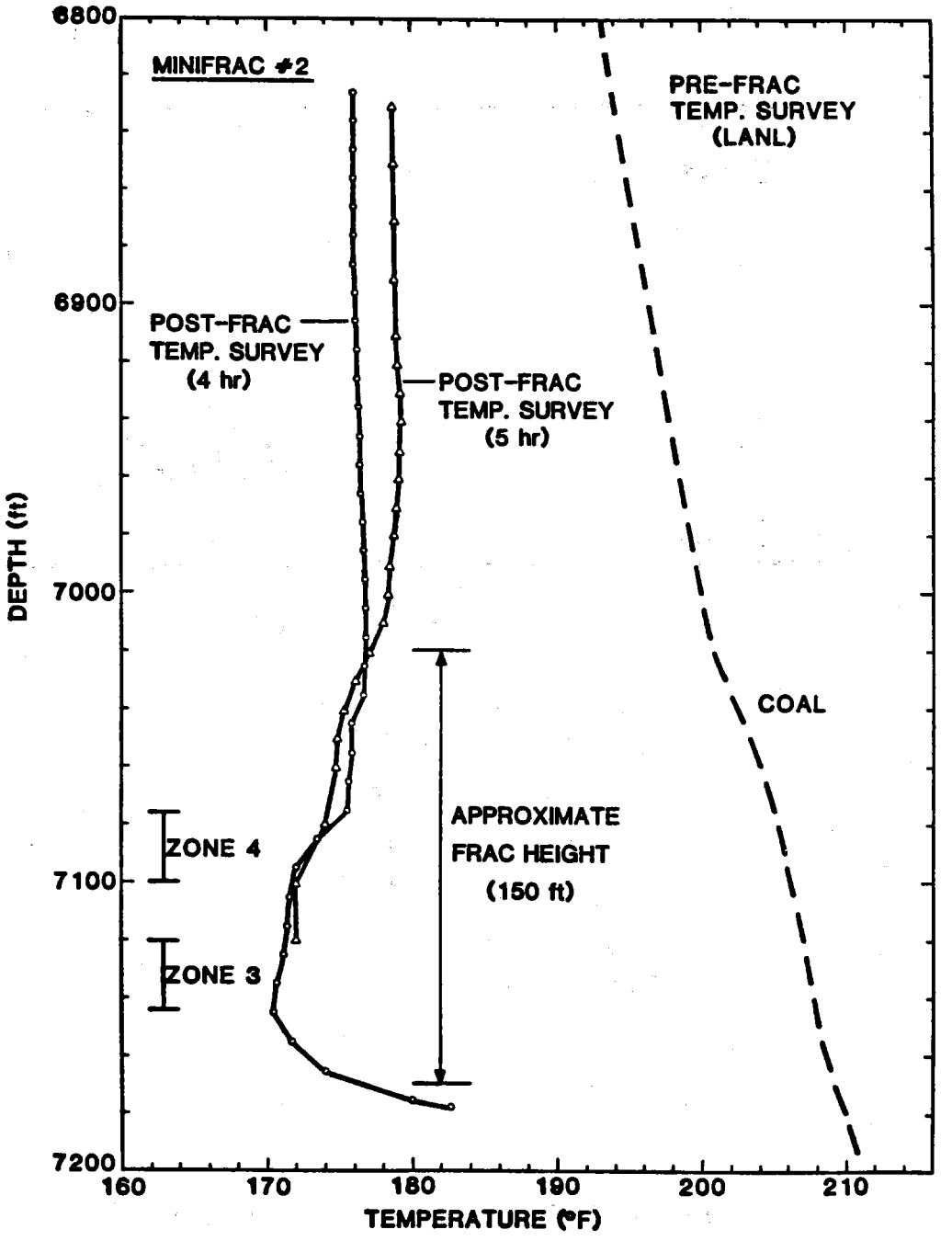

Figure 8.2.41 Minifrac #2 Temperature Log

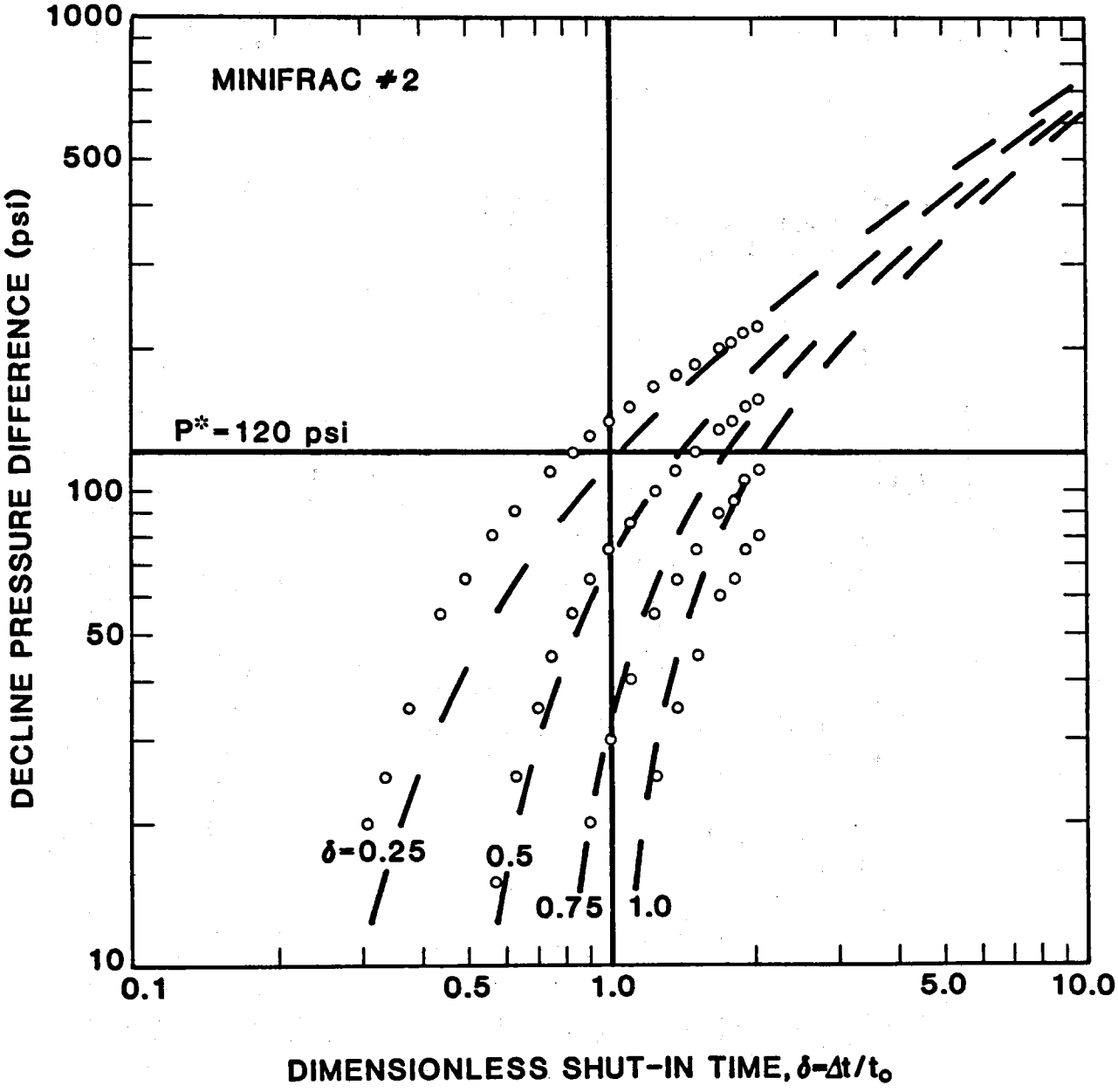

Figure 8.2.42 Minifrac #2 Nolte Analysis

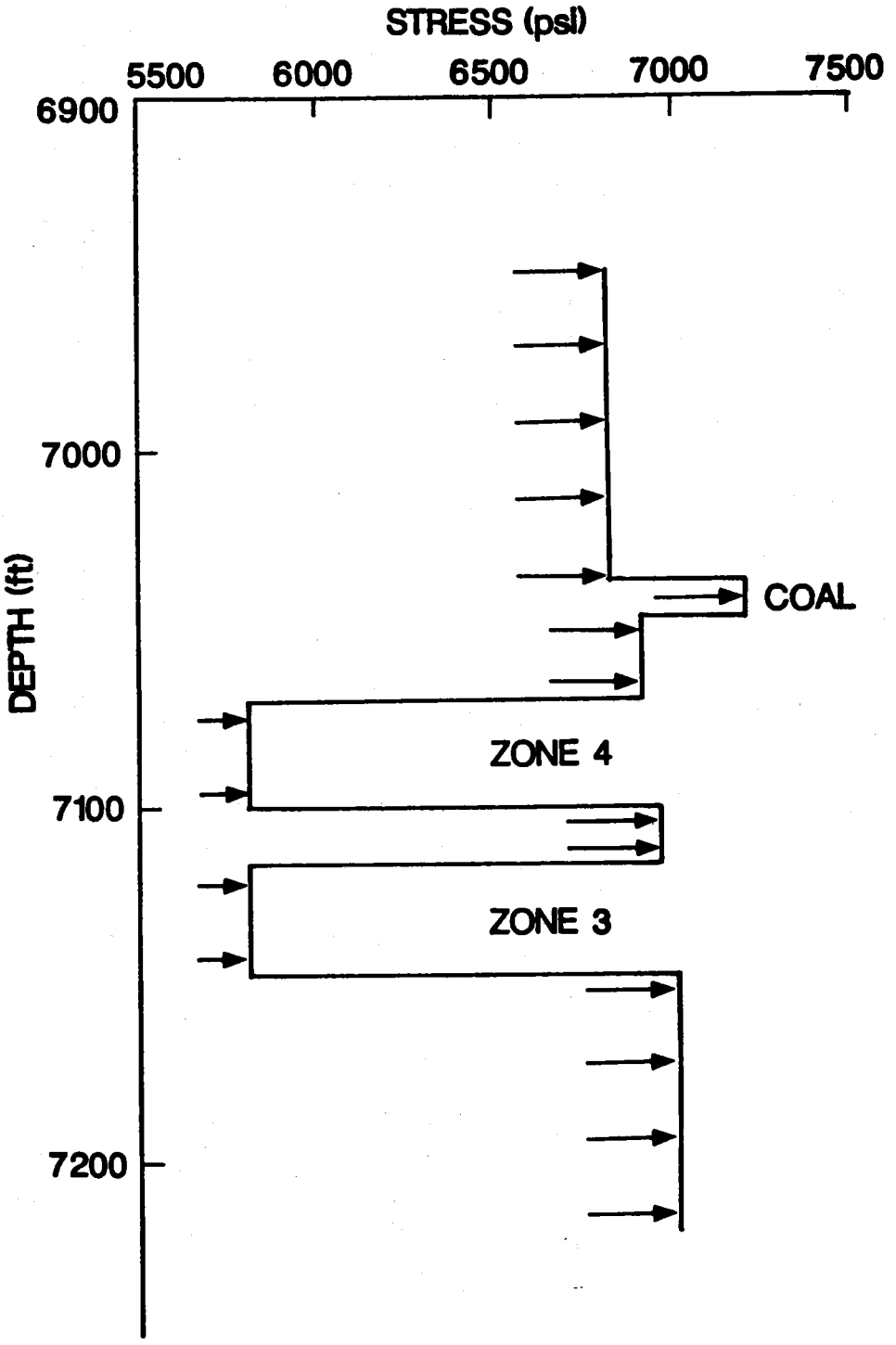

Figure 8.2.43 "Revised" Stress Profile

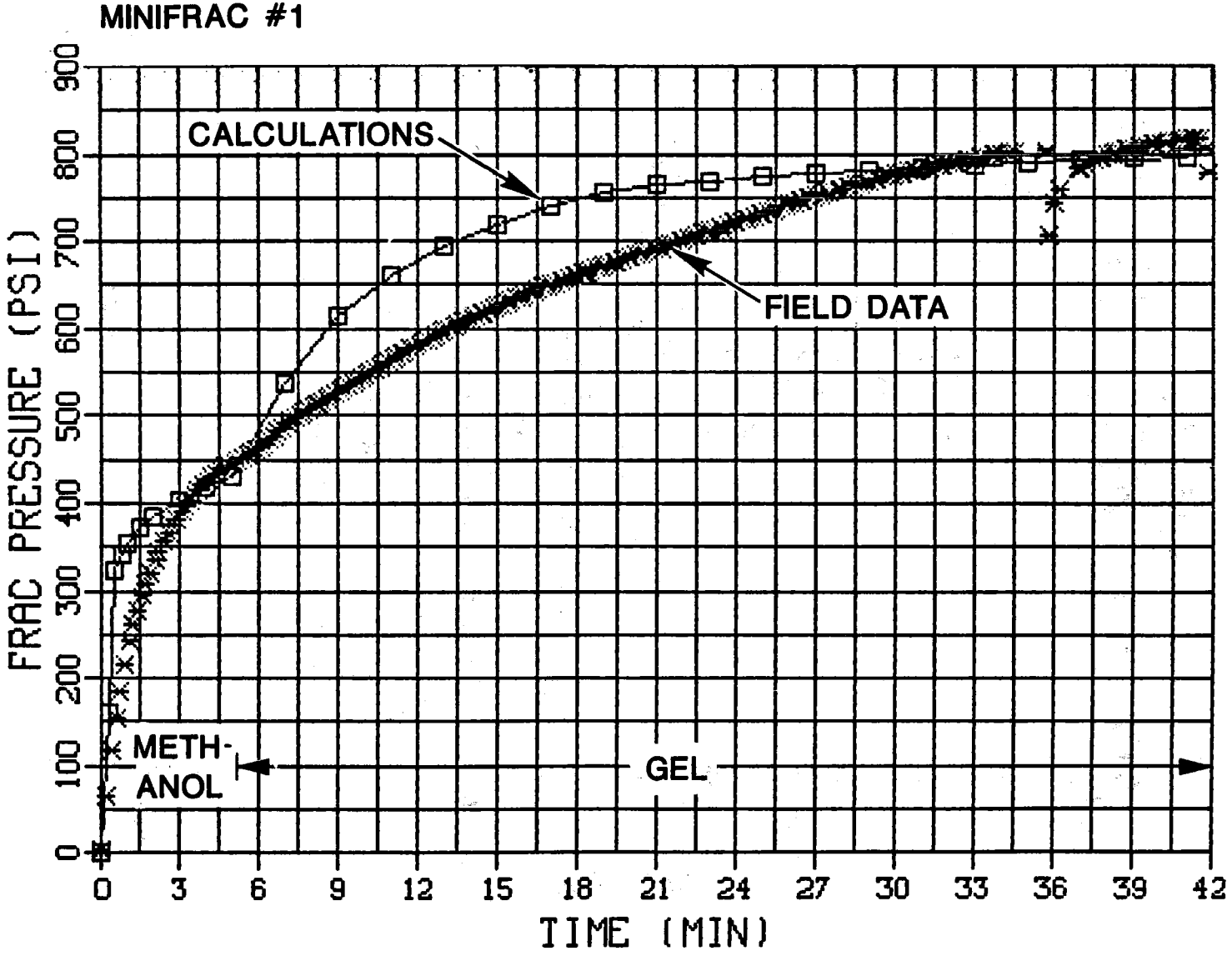

Figure 8.2.44 Minifrac #1 Pressure History Match

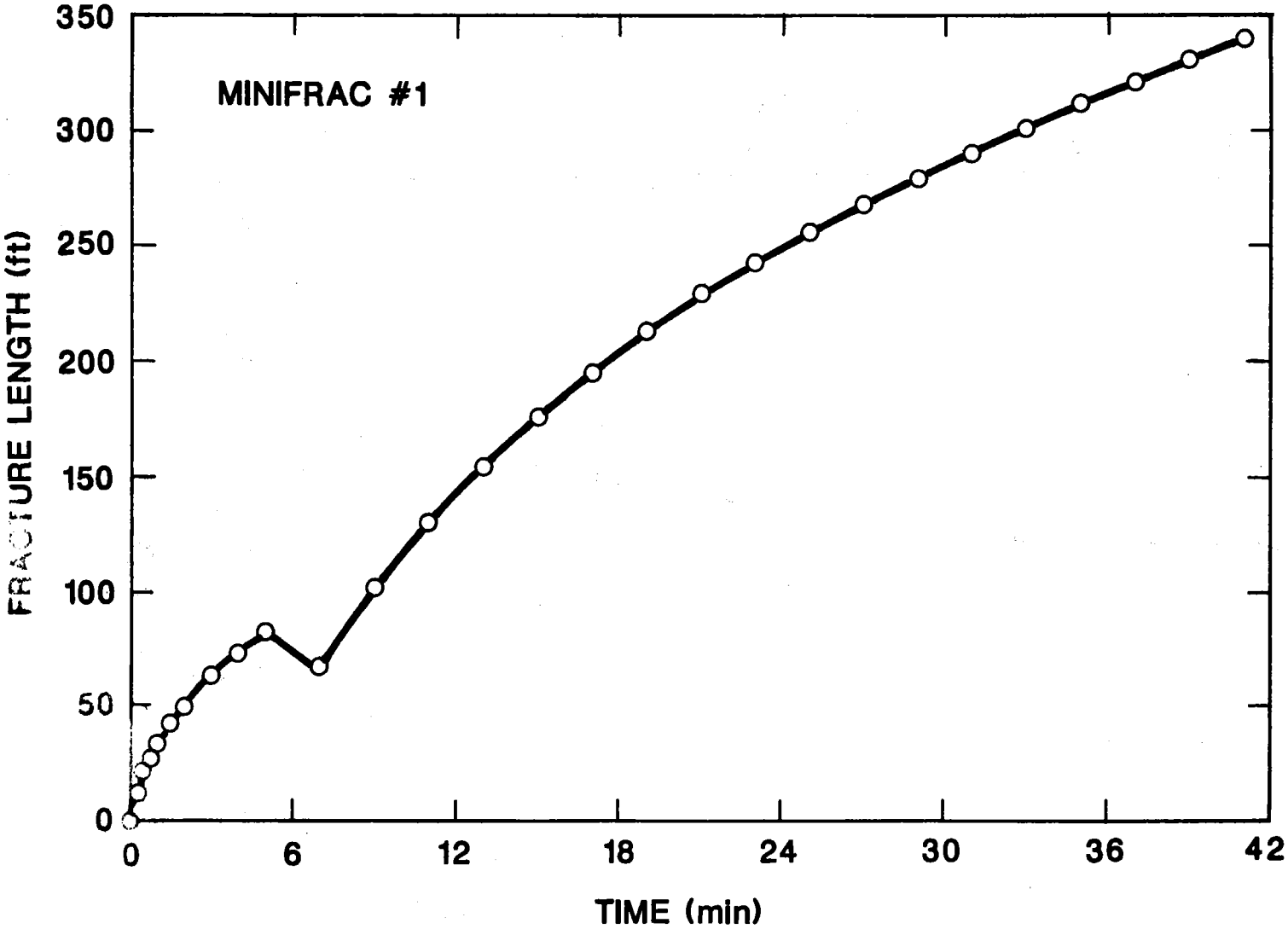

Figure 8.2.45 Minifrac #1 Pressure History Match Length

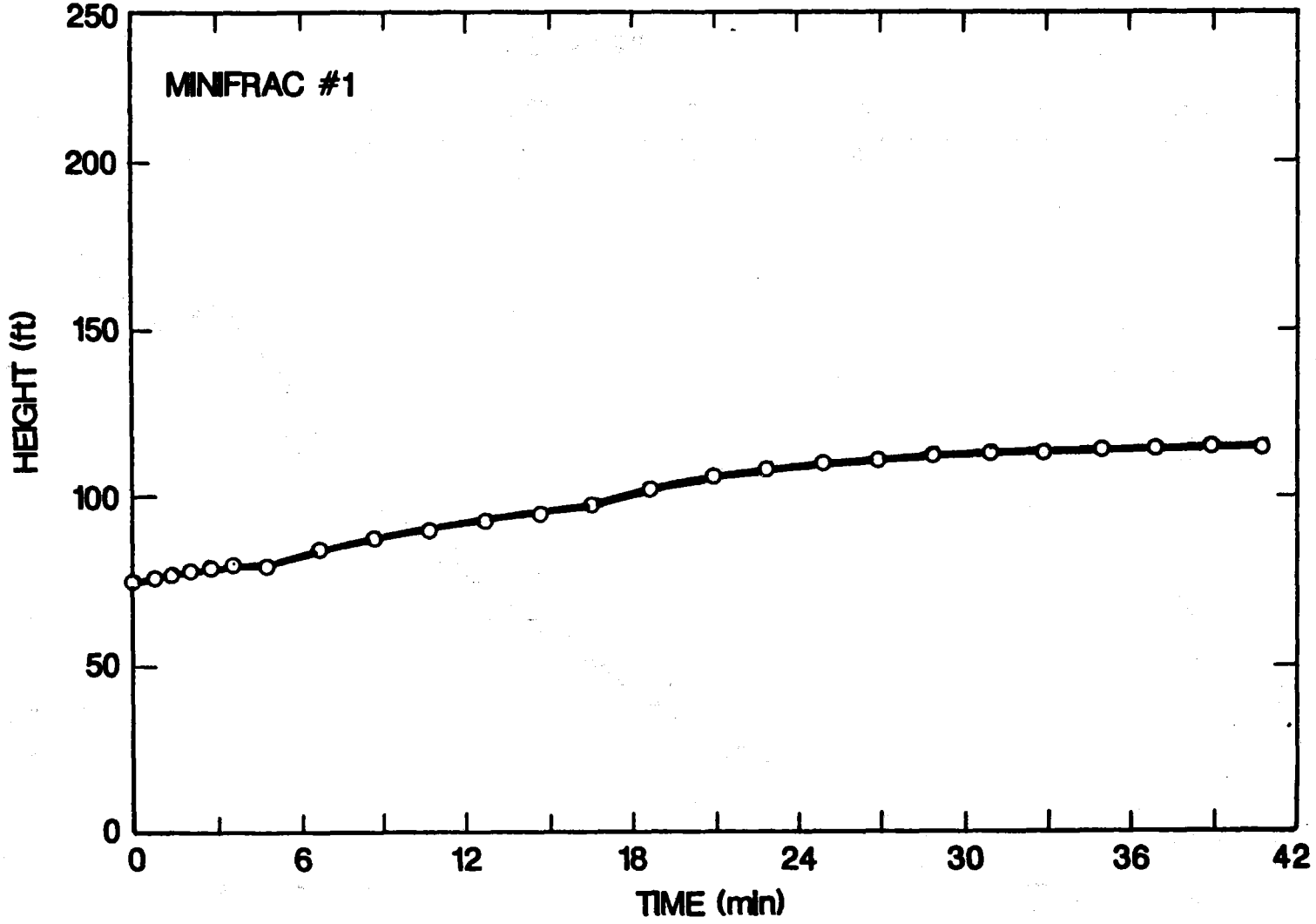

Figure 8.2.46 Minifrac #1 Pressure History Match Height

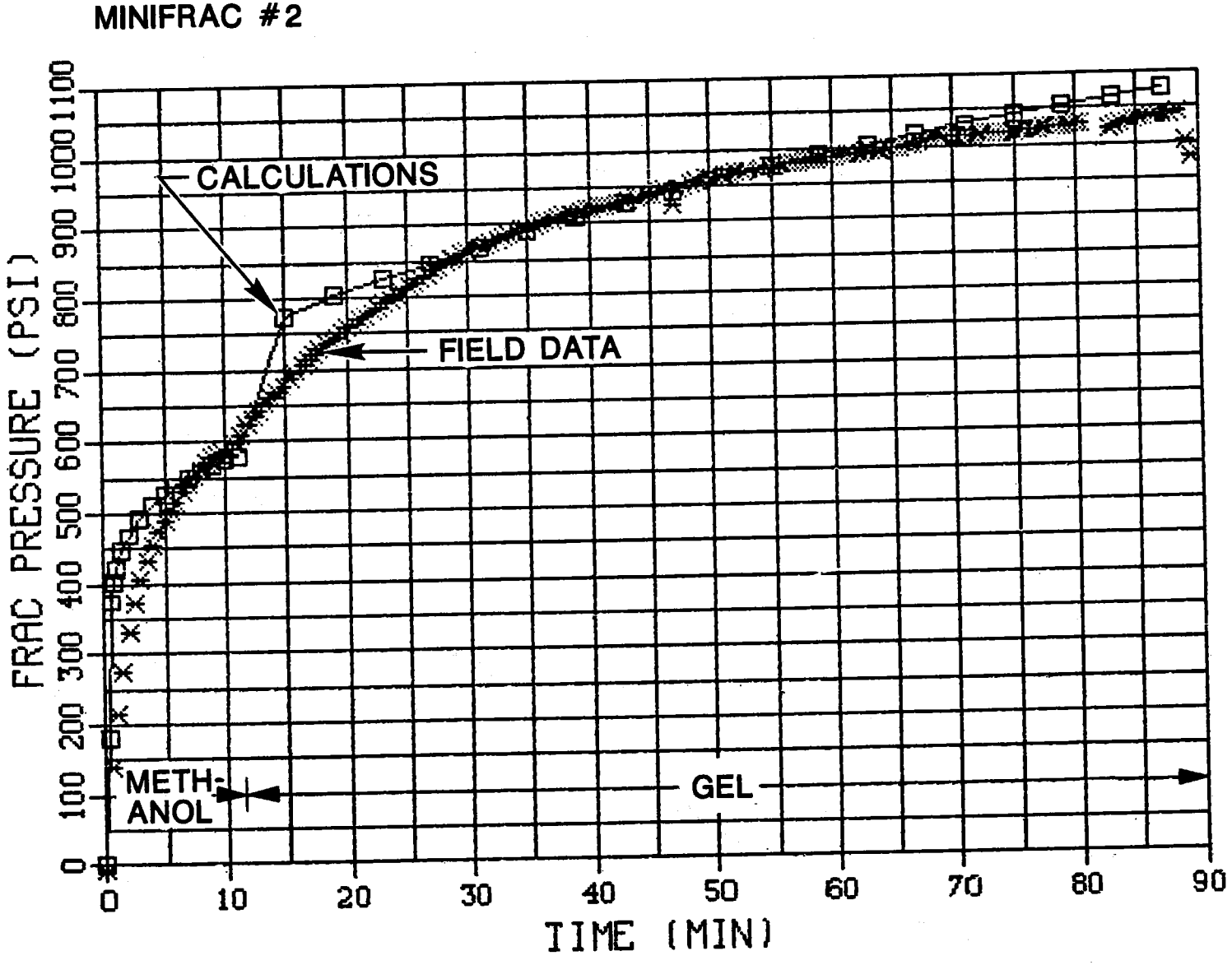

Figure 8.2.47 Minifrac #2 Pressure History Match

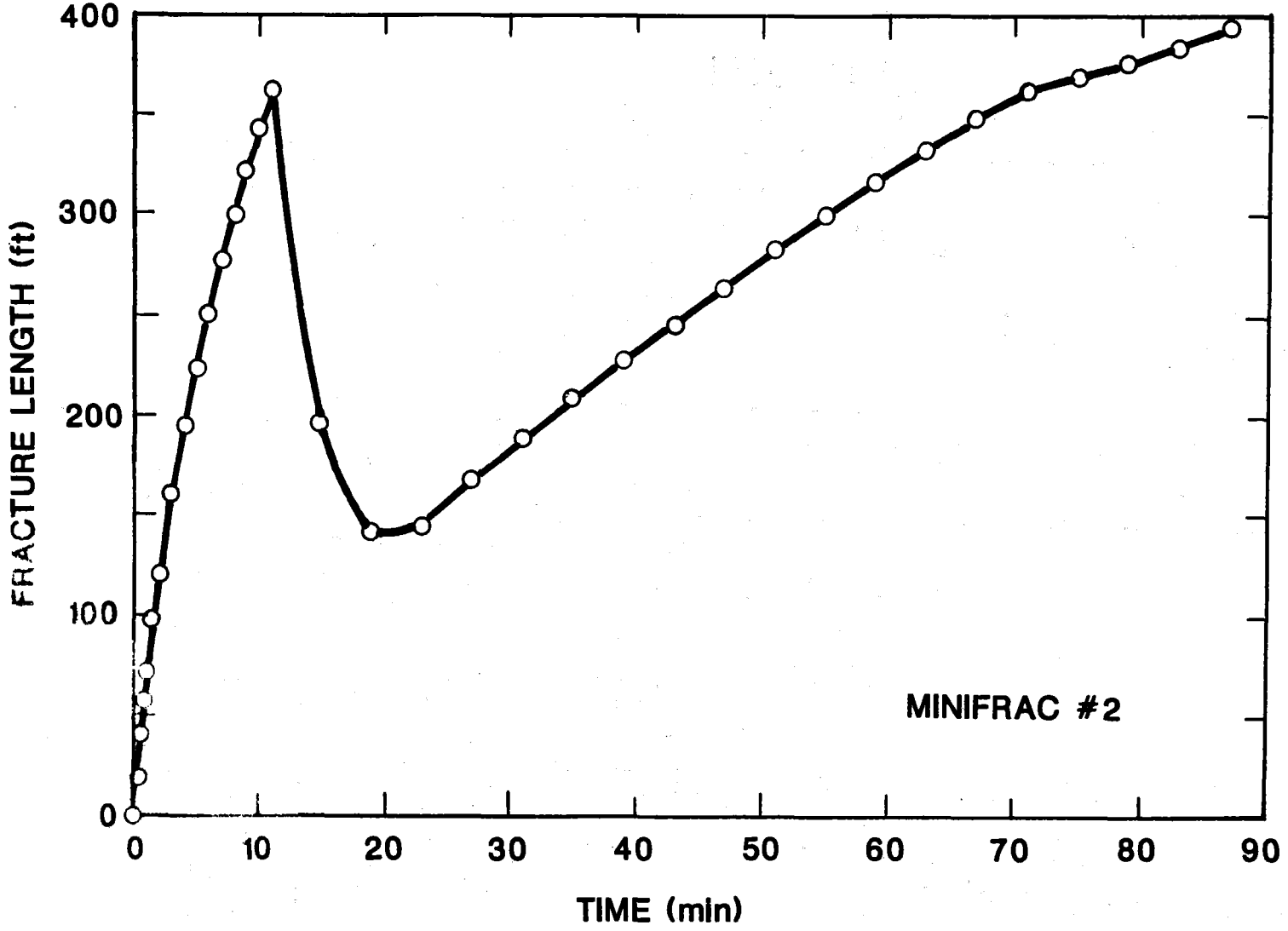

Figure 8.2.48 Minifrac #2 Pressure History Match Length

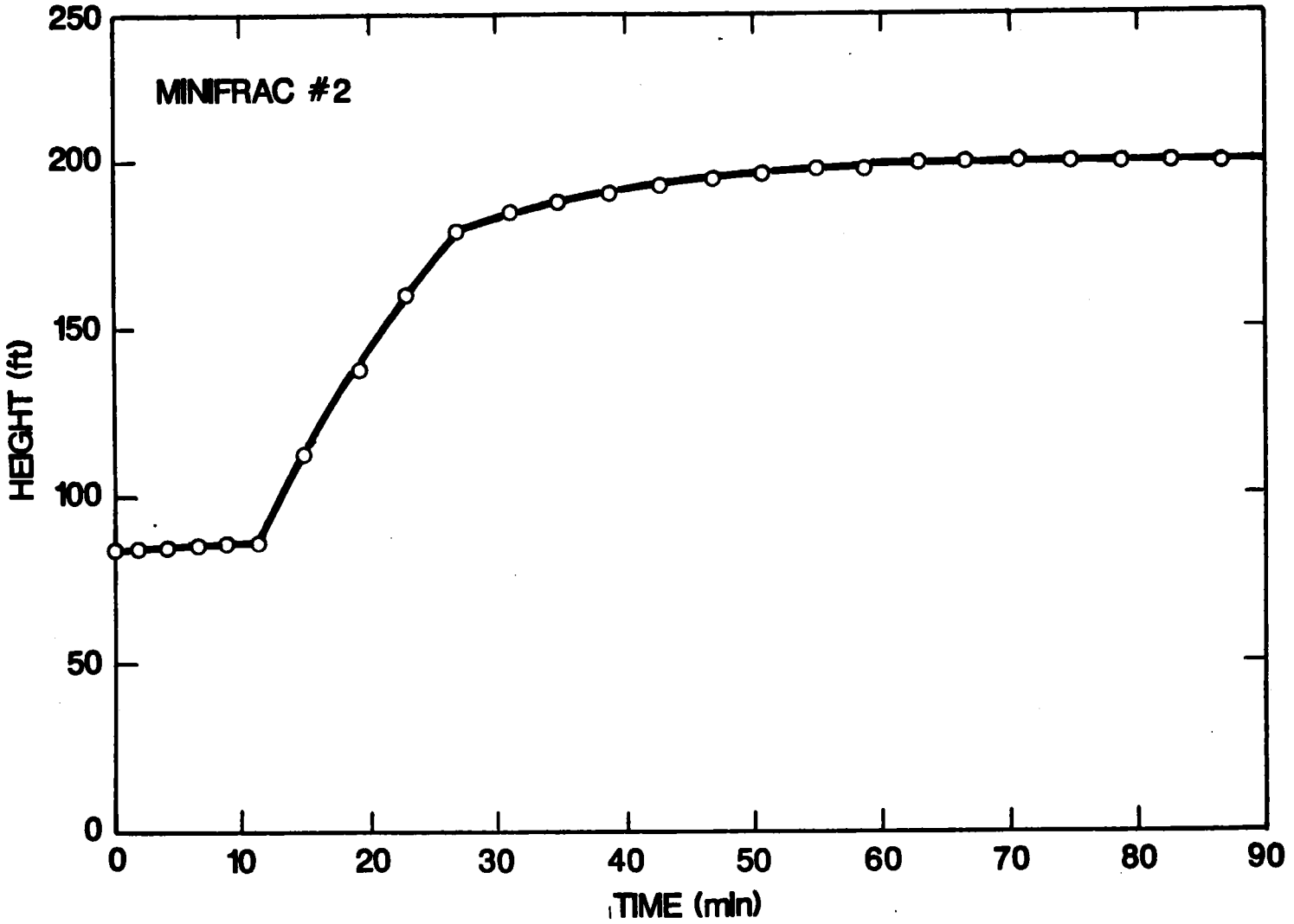

Figure 8.2.49 Minifrac #2 Pressure History Match Height

8.3 INTERIM WELL TESTING

P. T. Branagan
CER Corporation

8.3.1 WELL TESTING

The Phase I hydraulic fracturing treatments consisted of performing two unpropped minifracs in MWX-1. The objective of the well testing that followed the Phase I treatment was to observe changes in the reservoir resulting from the minifracs, to characterize the postfrac reservoir production behavior and to determine criteria for future interference tests. A variety of independent measurements (discussed in Section 8.2), including postfrac temperature logs and borehole seismic data, provided estimates of fracture height and length that were subsequently incorporated into the overall analysis.

The post-Phase I testing in MWX-1 consisted of three consecutive drawdown periods, a shut-in period and a final drawdown. The bottomhole pressure and flow rate data for these tests are shown in Figure 8.3.1 and a listing of the data is given in Appendix 12.7.3. From borehole seismic and postfrac temperature logs, fracture height and length were estimated to be about 150 ft and 450 ft, respectively. The orientation of the fracture found to be N73W, was assumed perpendicular to the minimum in situ stress. Figure 8.1.8 illustrates the two reservoirs, the fault and the hydraulic fracture.

The Horner plot of the Phase I buildup data is shown in Figure 8.3.2. The results indicate a formation capacity, kh = 0.64 md-ft and a skin of -3.8. As previously discussed, prefrac well testing indicated a formation capacity, kh = 0.95 md-ft, with a small positive skin of 0.59.

8.3.2 ANALYSIS

To analyze the behavior of this unpropped fracture, a square root of time plot was made from the buildup data as shown in Figure 8.3.3. The fracture capacity was derived from the early portion of the test when the reservoir was assumed to be producing primarily in a linear flow regime. Analytical type curve techniques from Agarwal[1] were also used to analyze the data. The calculated dimensionless fracture capacity was 2.5, resulting in a fracture conductivity of 7.14 md-ft. The square root of time analysis resulted in a calculated 80- to 100-ft fracture length.

It should be noted that the drawdown period included about 16 days of primarily dry gas production along with some sporadic water production. The water production occurred mainly during the first 100 hours of the test when a major portion, 335 bbl, of the residual fracturing fluid was recovered.

The Phase I well testing results shows that a fairly conductive fracture was created as a result of these unpropped fracture treatments. However, the estimated average formation capacity was reduced by approximately 20 percent from prefracture conditions, indicating that some degradation to matrix and/or the natural fractures occurred. Qualitatively, this is evident by comparing pre- and postfrac flow rates and pressure. Therefore, the creation of this unpropped, yet conductive, fracture seems to have compensated, in part, for the degrading effect of the treatment, as seen from the slightly negative skin. Due to the short testing period, more detailed analysis of unpropped fracture characteristics was not possible. However, it appeared that the fracture length in contact with a productive reservoir was about 100 ft and is considerably shorter than frac design and borehole seismic data.

8.3.3 LOAD WATER RECOVERY

A total of 1490 bbl of KCl water and linear gels were pumped into the wellbore and formation. Sixty percent of this volume was recovered during short cleanup periods conducted during a winter site shutdown. During the postfrac testing, 335 bbl of additional water were produced for a final recovery of 92%. Some of this recovered water was probably formation water, rather than load water.

8.3.4 REFERENCE

1. Agarwal, R. G., et al., "Evaluation and Prediction of Performance of Low Permeability Gas Wells Stimulated by Massive Hydraulic Fracturing," SPE 6838, presented at the SPE-AIME 52nd Annual Meeting, Denver, Colorado, October 9-12, 1985.

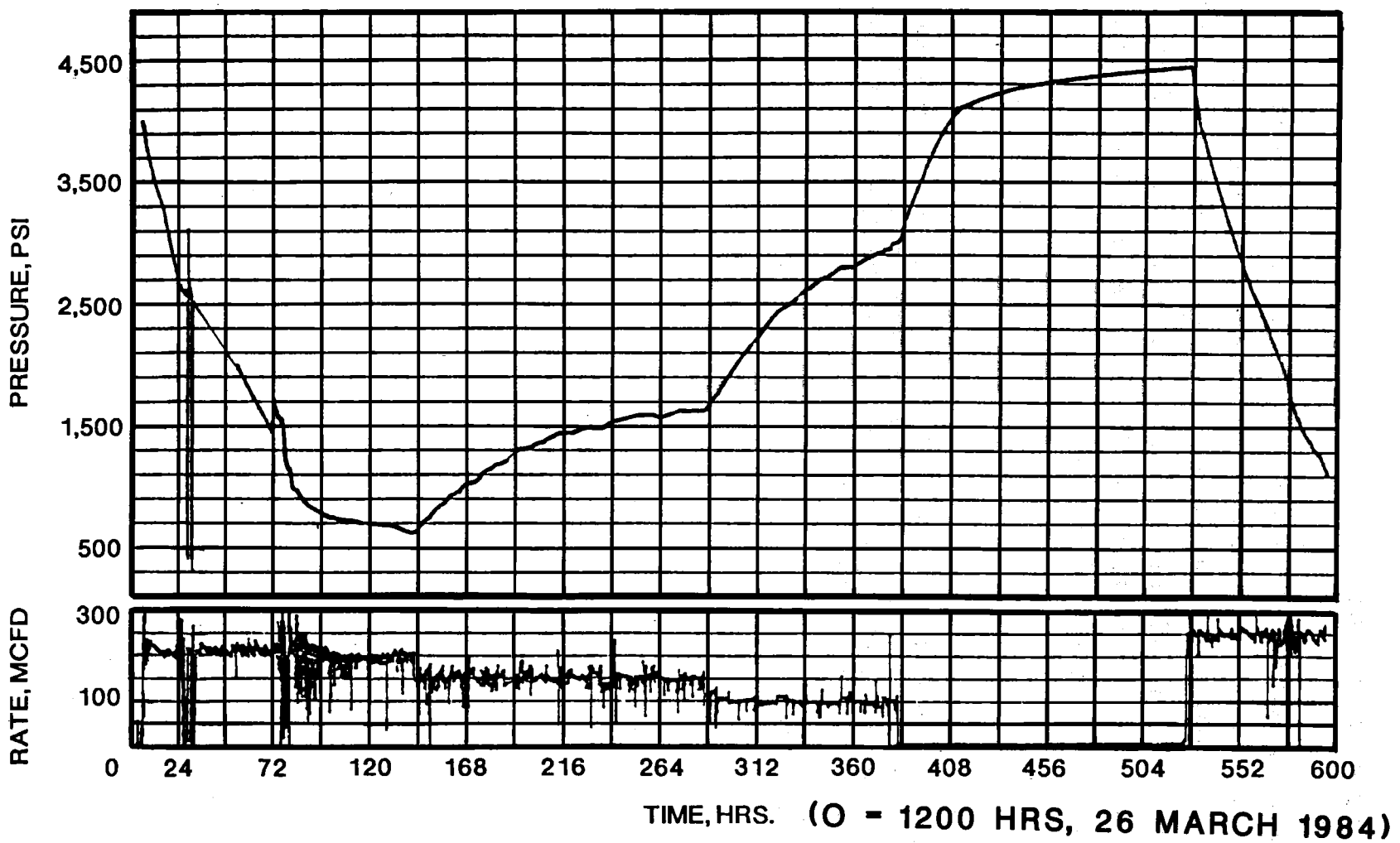

Figure 8.3.1 MWX-1 Post Phase I Well Testing, Flow Rate and Bottomhole Pressures

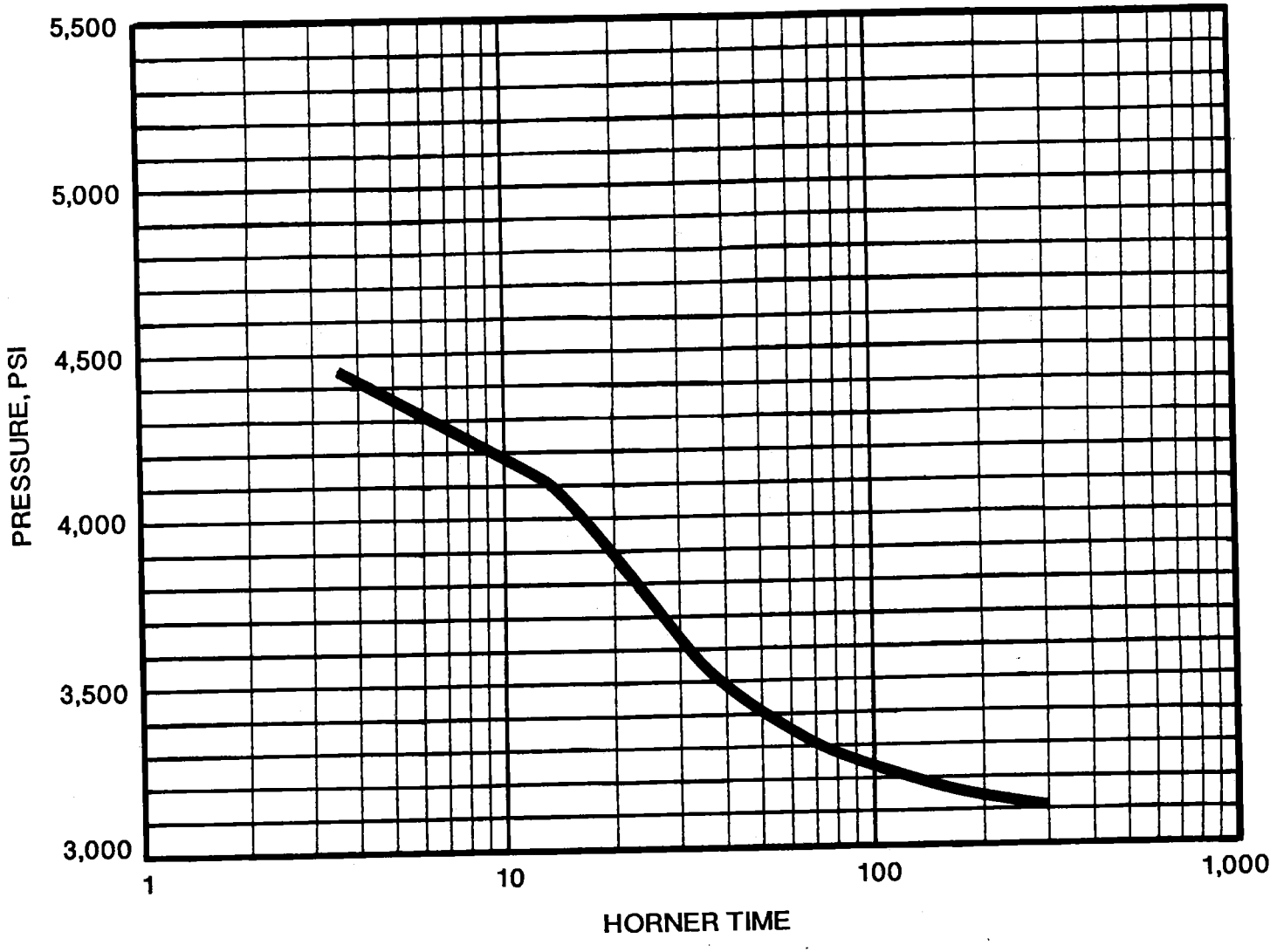

Figure 8.3.2 Horner Plot of Post Phase I Buildup Data

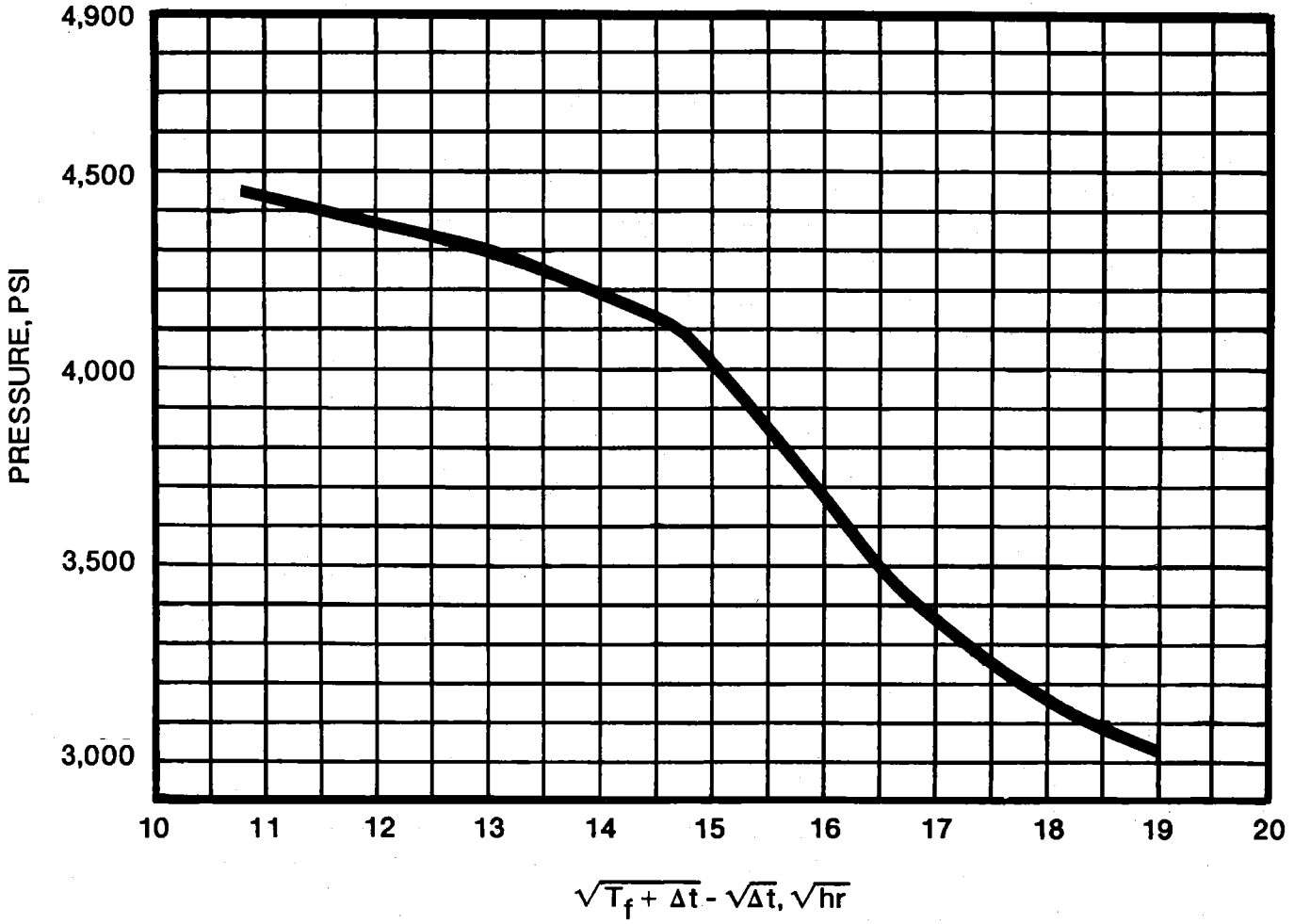

Figure 8.3.3 Square Root of Time Plot of Post Phase I Buildup Data

8.4 STIMULATION--PHASE II

N. R. Warpinski
Sandia National Laboratories

8.4.1 OBJECTIVES

The objectives of the Phase II Stimulation were (1) to continue to investigate and map fracture behavior in lenticular formations, (2) to determine production mechanisms in this complex lithology and (3) to characterize the productive potential of the paludal zone. To meet these objectives, a single, propped fracture treatment with various fracture diagnostics was performed.

8.4.2 DESIGN

The full-scale hydraulic fracture stimulation of the paludal zone in MWX-1 was conducted on Wednesday, May 2, 1984. This treatment was performed by Western Company of North America and designed using information gained from the two minifracs which were performed in December 1983.

The design of phase II stimulation--the main hydraulic fracture treatment--was influenced by several considerations. First, we wanted to optimize propped fracture length with respect to sand reservoir size. As the extent of zone 3 was probably 200-500 ft and the extent of zone 4 was unknown (Figure 8.4.1), there were no reasons for creating a fracture with a propped length greater than 500 ft. Second, we were concerned with the high treatment pressures and preferred keeping the viscosities, flow rates, and volumes low to minimize the pressure. Third, we had no information on remote lenses (those not intersected by the wells) and we were concerned with the effects of the coals on the treatment and production. Fourth, the borehole geophones could only "see" about

400 ft, so a much longer fracture would be beyond the range of detection. All these factors favored a relatively small fracture.

Western Co. designed the fracture treatment using a Perkins and Kern type model. Fracture height for the design models was uncertain because we had broken through the known upper barrier, yet there had been no excessive out-of-zone growth. This is probably because the upper barrier significantly reduced fracture width there and acted as an efficient flow restriction. Because of these complications we assumed a constant fracture height of 200 ft for design purposes. A gross leakoff coefficient of 0.00065 ft/$\sqrt{}$min for a full 200 ft height was based on the minifrac results. Rock and reservoir properties are shown in Table 8.4.1.

Western's Apollo gel system was used. This cross-linked, HPG-based gel system was used in a 3% KCl water base with gel concentrations ranging from 40 lb/1000 gal in the pad to 25 lb/1000 gal in the final proppant stage. For analyses requiring rheological data, the 35-lb gel at a residence time of one hour and temperature of 193°F was considered average. These fluid properties are $n' = 0.78$, $k' = 0.0061$ lb-sec$^{n'}$/ft^2, $C_{III} = 0.00465$, and $S_p = 0.0$. The overall treatment is shown in Table 8.4.2.

Because of the high temperatures, breaker was added only in stages 7 and 8 in concentrations of 0.25-0.5 lb/1000 gal; the addition of breaker in the earlier stages would have reduced viscosity sufficiently that sand fall-out would have been expected before the slurry reached the fracture extremities. Because of the success with fluid recovery in the minifracs, a methanol prepad was again used. Flow rate for the treatment was nominally 20 bpm.

Sand concentrations were staged up to 5.5 lb/gal, the maximum that we felt confident of being able to inject at rates of 20 bpm. This results

in an average design sand concentration in the fracture of about 1 lb/ft^2. 20/40 mesh sand was used for all stages except the final one (number 8) in which 12/20 mesh was used for a tail-in. A radioactive-sand tag was used in the entire job; iridium 192 was used in the first half and iodine 131 in the last half of the treatment. Sufficient sand concentrations were used so that if the fluid broke before final closure, the resultant sand bank would fill both channel sands. Ammonium thiocyanate in a concentration of about 100 ppm was used as a fluid tag.

8.4.3 WELL CONFIGURATION AND INSTRUMENTATION

The well configuration is shown in Figure 8.4.2. The well has 7-in./29# casing with a bridge plug at 7200 ft and 2-7/8-in. tubing landed open ended at 6750 ft. The perforated interval is 7076-7100 for zone 4 and 7120-7144 for zone 3.

During the treatment an HP pressure transducer and a GO temperature tool were hung in the tubing at 6700 ft while the fluid was pumped down the annulus. Surface data included casing treatment pressure, static-tubing pressure, flow rate, sand concentration, base gel viscosity, and temperature of the frac fluid.

Borehole geophones were located in MWX-2 and MWX-3 to monitor any signals created by the hydraulic fractures. These were located between 6950 and 7000 ft and oriented with a surface thumper.

Western Co. provided a Treatment Monitoring Vehicle where they recorded and displayed all pertinent data. In addition, we also recorded all data on our well-test-facility computer.

8.4.4 TREATMENT PROCEDURE

First, 3% KCl water was circulated down the annulus and out the tubing, followed by 7700 gal of methanol. Then, 300 gal of methanol were

pumped down the tubing to inhibit freezing of the lubricator and the temperature and pressure tools were lowered on a wireline to 6700 ft in the tubing.

During the pumping of the pad, we planned to conduct 3 shutdowns to measure the ISIP and perform Nierode's[1] leakoff analysis. These shutdowns occurred after 8000, 12,000 and 17,000 gal of pad were pumped into the formation. During the treatment we monitored the log of the treatment-pressure-minus-closure-stress vs the log of time (Nolte-Smith[2] analysis). Finally, we planned to shut in for several hours after the treatment to perform a Nolte[3] pressure decline analysis.

Only one problem occurred during the treatment and this was due to trouble with the bottomhole pressure processer. When pumping started, we began to get misleading BHP data and we shut in after pumping 104 bbls of pad, which put only methanol in the formation. We attempted to remedy the problem, resumed pumping, but were forced by continued problems to shut down again, this time with 163 bbls pumped. After 40 minutes of repair, the instrumentation was functioning properly and we completed the remainder of the treatment with no further problems.

8.4.5 DATA

Western's plots during the treatment are shown in Figures 8.4.3-5, starting after the second unscheduled shutdown. The curve labeled actual pressure in Figure 8.4.4 is the static tubing pressure with a pressure offset (so it can be seen), while the tool pressure is the bottomhole pressure gage. (In Figure 8.4.5, the downhole temperature between 0 and 10 min should have 100° added to it.) Figure 8.4.6 shows Western's plot of the treatment plus the following pressure decline.

Figure 8.4.7 is a plot of the bottomhole pressure (BHP) during the entire test. Initially, there are three shutdowns to measure the ISIP

for Nierode's analysis, followed by steadily increasing pressure during the treatment. The shut-in portion shows a relatively rapid initial pressure decline followed by a much slower decrease after 250 min. The pressure disturbance at N 360 min is real and probably reflects some internal shifting of the fluid and sand in the fracture as the fracture closes. The bottomhole temperature (BHT) for the entire test is shown in Figure 8.4.8 and the surface pressure in Figure 8.4.9. The BHP minus the surface pressure is shown in Figure 8.4.10. In all these plots we have corrected the BHP for the difference in depth between the gage and the perforations by adding 150 psi. This is not correct for the first few minutes of the treatment because there is still some methanol in the casing, but should be a good correction for the pressure decline when there was a fresh water flush in the casing. The hydrostatic load of ~3100 psi at the end of the test is close to the calculated value of 3150 psi.

The static tubing data is shown in Figure 8.4.11 and a strange behavior is noted. Figure 8.4.11 is plotted on the same pressure scale as the BHP in Figure 8.4.7 and when the two are overlain, the pressures begin to diverge at ~ 145 min. With a static correction of ~ 3030 psi (accounting for 300 gals of methanol, compressibility, and a BHP depth of 7076 ft), the initial treatment data seem to be correct and the later data diverge by ~ 150 psi. This 150 psi is approximately the difference between the static column in the tubing (with the methanol) compared to the static column in the casing (again accounting for compressibility and a BHP depth of 7076 ft). Possibly we developed a near-surface leak between casing and tubing at 145 min. This may have occurred when the pressure differential between the two was at its greatest, about 600 psi. Qualitatively, there is a shift in pressure differential between surface casing and tubing pressure from early times to late times, but this is obscured somewhat because there appears to be a 50-70 psi error difference between the two gages.

Figures 8.4.12-16 show the BHP, BHT, surface pressure, static tubing pressure, and flow rate, respectively, during the treatment. The three initial ISIP's are clearer here and will be discussed in more detail later (Section 8.4.6). Note that the BHT leveled off at ~ 85° with the injection of 70° gel. The flush was 20° cooler and its effect can easily be seen at the end of the treatment. Figure 8.4.17 shows the difference between the BHP and surface pressure during the treatment and shows a hydrostatic correction of about 3200-3250 psi and the expected increasing hydrostatic load with increasing sand concentration.

In Figure 8.4.18, the treatment BHP minus the closure stress is plotted vs time on a log-log graph. This is the well-known Nolte-Smith[5] analysis which is a qualitative look at the manner in which the treatment is progressing. The three shut-ins complicate the graph, but they don't affect the late time results which are of most interest. For a pseudoplastic fluid with $n' = 0.78$, we would expect a slope of 0.14-0.22 for constant-height fracture extension. During the last 40 min of the treatment we actually observe a half slope which doesn't fit comfortably into any of the four categories described by Nolte and Smith. While the increasing slope is often indicative of an impending screenout, here it may be indicative of complex fracture behavior resulting in abnormal treating pressures, as described by Medlin and Fitch.[4]

The treatment data for the pressure decline after shut-in are shown in Figures 8.4.19-22. The bottomhole pressure data are used for the Nolte[6] pressure decline analysis which is described later. A closer look at the ISIP is shown in Figure 8.4.23. The value is apparently between 7300 and 7500 psi but it is difficult to pick.

8.4.6 NIERODE ANALYSIS

Three short shutdowns were incorporated into the design of the treatment in order to perform Nierode's[1] analysis for determination of

the leakoff coefficient. Figures 8.4.24-26 show the data for the three shut ins, including BHP, flow rate, and surface casing pressure. The large number of data points at shut-in are due to switching to a "burst" mode where data are taken at a rate greater than one per second. However, the shutdown of the pumps was generally so slow that the burst mode was over before the complete shut in had occurred. Additionally, the burst-mode data is noisier so that clear ISIP's are sometimes difficult to determine. We chose ISIP values of 6740, 6720, and 6795 psi, respectively, for the three tests.

Nierode developed a semiempirical theory to explain the increasing ISIP values during a treatment. He suggested that in many cases the increase in ISIP is due to an increase in the closure stress as a result of fluid leakoff and the concomitant pressurization of the pore space surrounding the frac. Using empirical data and a logical form for the change in closure stress, Nierode arrived at

$$FG(t_2) = FG\ (t_1)\ [1 + A\ (C\sqrt{t_2 - t_1})^B] \qquad (1)$$

where

FG is the frac gradient (ISIP/depth),
C is the leakoff coefficient,
t is time, and
A and B are empirical constants.

For a Perkins and Kern geometry crack, Nierode's fit of his data gave A = 0.20233 and B = 0.47850. Using these values, type curves can be developed and data from new wells fit to them.

Such data for the paludal stimulation are shown in Figure 8.4.27. The three shut-ins during the pad and the final shut-in were used. The initial data showed a low fluid loss coefficient (the accuracy of these

low points is questionable), but the final shut-in indicates a much greater fluid loss. Whether this is real in the sense that much greater fluid loss occurred at late times (possibly into the natural fractures) or whether there is some other explanation is uncertain.

8.4.7 NOLTE PRESSURE DECLINE ANALYSIS

The Nolte[3] analysis provided the most informative look at fracture behavior as seen in Figure 8.4.28. Attempts to fit the pressure decline data to the type curve were unsuccessful until we realized that something unusual occurred at a dimensionless time of 0.7 (70 min after shut-in). The pre-0.7 data can be fit nicely, while the post-0.7 data flattens significantly. We interpret this as initial frac closure on the proppant, at least near the wellbore. The only way this could occur so early was if the gel broke, the sand fell to the bottom of the frac, and then any additional incremental leakoff would result in immediate closure of the bottom of the frac on the proppant.

P* for the pre-0.7 data was 225 psi. The fracture parameters were calculated following the Nolte analyses and equations given in Section 8.2.11. Results are shown in Table 8.4.3 for two different fracture heights. We should remember that this model is based on an ideal Perkins-and-Kern type fracture. If we actually have complex fracture behavior, these estimates may be meaningless.

8.4.8 POST-FRAC SURVEYS

About 6 hrs after shut-in, a temperature survey was attempted but we could only lower the tool to a depth of 6950 ft before it tagged bottom, apparently on sand in the wellbore. No obvious temperature anomaly was observed. The following day, after having flowed back the well to begin recovering the load, we ran a series of surveys.

The temperature log shown in Figure 8.4.29 is a composite of three logging runs taken over a one-hour period at 28 hours after the frac. No change in temperature was evident among the three log runs. The first log was the deepest but the scale was such that it was difficult to distinguish "breaks" in the temperature gradient. Afterwards, additional log runs at an expanded temperature scale and reduced depth scale could only reach within 30 ft of the depth of the first log. We believe that some additional sand was slugged back into the wellbore. Frac top is around 7000 ft, but the fracture appears to be mostly closed to about 7050 ft. Below this depth, a more significant temperature anomaly exists.

A post-frac gamma survey was run several days later after sand was circulated out of the wellbore. The results do not show much radioactive sand near the wellbore. As shown in Figure 8.4.30, only a few gamma spikes can be observed and all of these are in the perforated intervals.

The borehole geophones were plagued by high noise levels during this treatment and only a few analyzable seismic signals were obtained (Section 10.2). These limited seismic data showed that fracture azimuth was approximately the same as the minifracs and the few signals that were obtained all fell within a 200 ft height window.

8.4.9 PRESSURE HISTORY MATCH ANALYSIS

As with the minifracs, we performed pressure history match analyses to try to understand fracture behavior. We used the same stress profile as used for the minifracs (Figure 8.2.43). We also used the same basic data for the methanol prepad (stage 1) as used in the minifracs and simply divided the main treatment into two primary stages, the pad (stage 2) and the sand (stage 3). We did not bother to subdivide the sand stage further because of (1) a lack of good data to use for many of the parameters and (2) little change in the properties.

Figure 8.4.31 shows the pressure history match for this treatment, including the methanol prepad, the shut-ins and rate changes. The data for this match are shown in Table 8.4.5. Note that the friction factor was increased from 6 to 8 during the sand stage to account for additional pressure losses caused by sand bridging and other processes. Length growth is shown in Figure 8.4.32, yielding a total length of about 600 ft. Height growth is shown in Figure 8.4.33, with a maximum height of about 250 ft.

8.4.10 DISCUSSION OF STIMULATION EXPERIMENTS

During all fracturing tests in this zone, we observed very high treatment pressures. Several possible reasons exist for such high pressures. The first is complex fracturing, as discussed by Medlin and Fitch[4] for other wells in the Mesaverde in the Piceance basin and expanded on by Warpinski and Teufel[5] for the effect of natural fractures. The second possibility is that the fracture reached the boundaries of the lens so that treatment pressures would need to increase substantially for major fracturing to occur in the higher stress shales. The short effective fracture lengths measured in well tests support this. The third possibility is back stresses due to fluid leakoff, but this is typically a much smaller effect. The fourth possibility is the presence of high stress stringers, such as between the zones 3 and 4, which would reduce fracture widths and increase pressures somewhat. All of these factors may have contributed to the high pressure levels. Whatever is the cause, high pressures can result in many deleterious effects; the most obvious ones being wider and shorter fractures and higher leakoff.

We had been concerned about the effect of the coals in the treatment and gas production, but no obvious deleterious effects seemed to occur. One positive effect was the high stress in the coal above zone 4 (the highest stress in the paludal interval) which probably was a significant

factor limiting height growth. No obvious loss of frac fluid occurred because of the coals, as deduced from the low leakoff coefficients.

Finally, we have successfully completed a series of hydraulic fracturing experiments in tight lenticular sands. While there are still many aspects of fracture behavior that are not clear, we have made positive steps to diagnose the geometry of the fracture.

8.4.11 REFERENCES

1. Nierode, D. E., "Comparison of Hydraulic Fracture Design Methods to Observed Field Results," JPT, Vol. 37, N. 11, Oct 1985.

2. Nolte, K.G. and M. B. Smith, "Interpretation of Fracturing Pressures," JPT, Vol 33, Sept 1981, p 1767.

3. Nolte, K. G., "Fracture Design Considerations Based on Pressure Analysis," SPE 10911, SPE Cotton Valley Symposium, Tyler, TX, May 1982.

4. Medlin, W. L., and J. L. Fitch, "Abnormal Treating Pressures in MHF Treatments," SPE 12108, presented at 58th Annual SPE Meeting, San Francisco, CA, Oct. 1983.

5. Warpinski, N. R. and L. W. Teufel, "Influence of Geologic Discontinuities on Hydraulic Fracture Propagation," SPE 13224, presented at 59th Annual SPE Tech. Conf., Houston, TX, Sept. 1984.

Table 8.4.1. Frac Data

Frac height	200 ft
Closure stress	5900 psi
Young's Modulus (avg)	4.51×10^6 psi
Poisson's ratio	0.22
Reservoir pressure	5300 psi
Porosity	9.2 %
Permeability (bulk)	20 μd
Water saturation	35%
Gross leakoff coefficient.	0.00065 ft/$\sqrt{}$min

Table 8.4.2. Treatment Schedule

	Fluid				Sand	
Stage	Type	Volume (gal)	Gel Conc. (lb/1000 gal)	Breaker (lb/1000 gal)	Concentration (lb/gal)	Size (mesh)
1 prepad	methanol	7,700	-	-	-	-
2 pad	Apollo	18,000	40	0	-	-
3	Apollo	3,000	35	0	1.5	20/40
4	Apollo	5,000	35	0	2.0	20/40
5	Apollo	6,000	35	0	3.0	20/40
6	Apollo	14,000	35	0	4.0	20/40
7	Apollo	18,000	25	0.25-0.5	5.5	20/40
8	Apollo	1,000	25	0.5	5.5	12/20
9 flush	water	8,764	-	-	-	-

Total Volume: 81,464 gal of which 65,000 gal was gel

Total Sand: 193,000 lbs.

Table 8.4.3. Results of Fracture Pressure Decline Analysis*

	Case 1	Case 2
Assumed Fracture Height (ft)	180	200
P* (psi)	225	225
Leakoff Coefficient (ft/$\sqrt{min}$)	0.00123	0.00152
Pressure Decline Ratio, ρ	2.85	2.85
Fluid Efficiency (percent)	74	74
Wing Length (ft)	520	420
Average Width (in)	0.59	0.65

* Leakoff height of sands and coals: 80 ft
Appropriate Young's modulus: 4.75×10^6 psi
Pump Time: 100 min
Flow behavior index: $n' = 0.78$
Degradation index: $a = 1.0$

Table 8.4.4. Data for the Pressure History Match of the Main Fracture

	Stage 1	Stage 2	Stage 3
Flow rate (bpm)	20	15,20	20
Fluid	Methanol	Pad	35# Gel + Sand
Density (gm/cc)	0.8	1.05	1.1
Leakoff coefficient (ft/$\sqrt{min}$)	0.002	0.001	0.001
Spurt (gal/ft^2)	0	0	0.01
Viscosity (cp)	0.3	-	-
n'	-	0.78	0.78
k'	-	0.0061	0.0061
fff	2	6	8
relative roughness	0.05	0	0

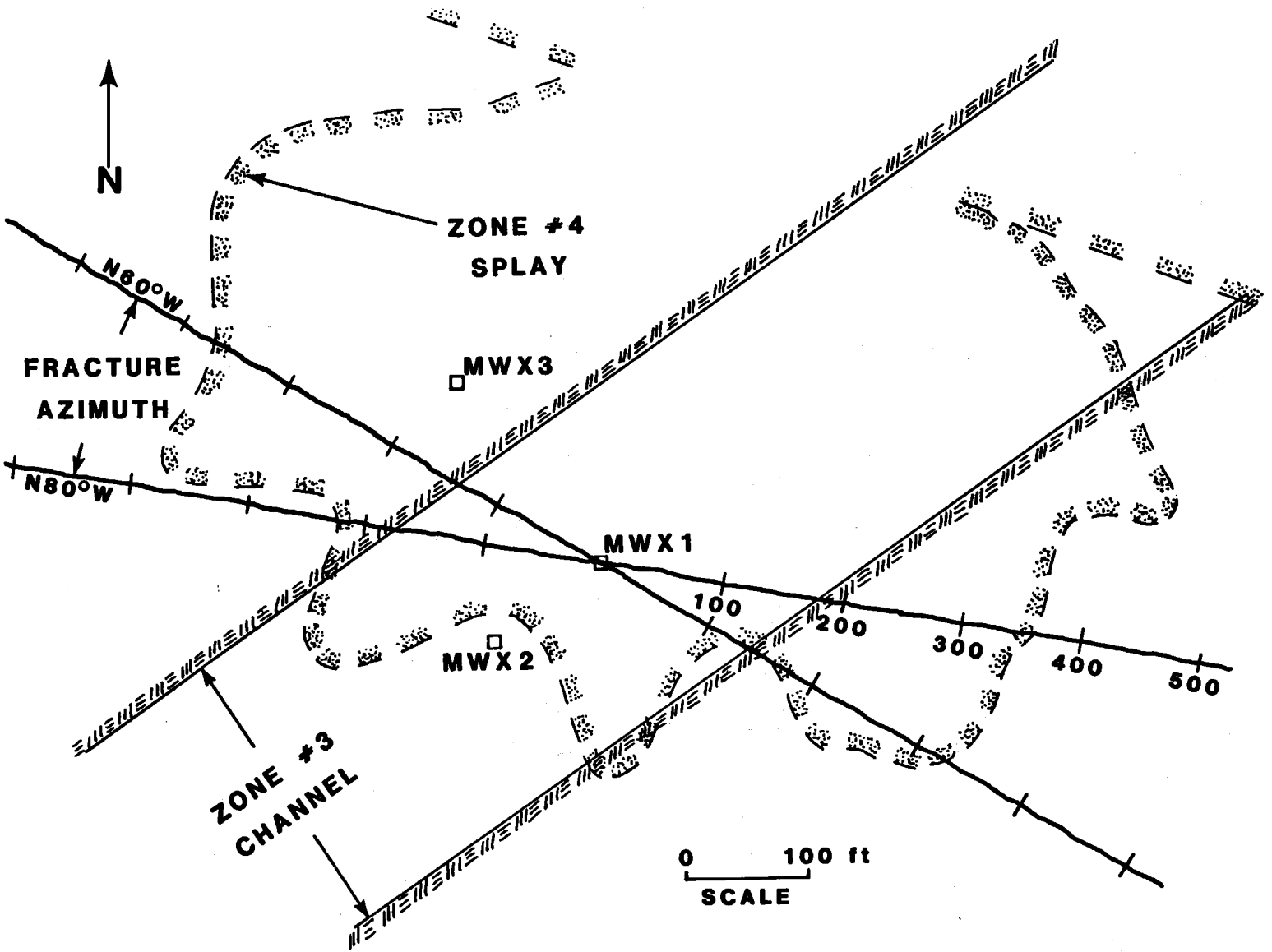

Figure 8.4.1 Estimated Sand Geometry

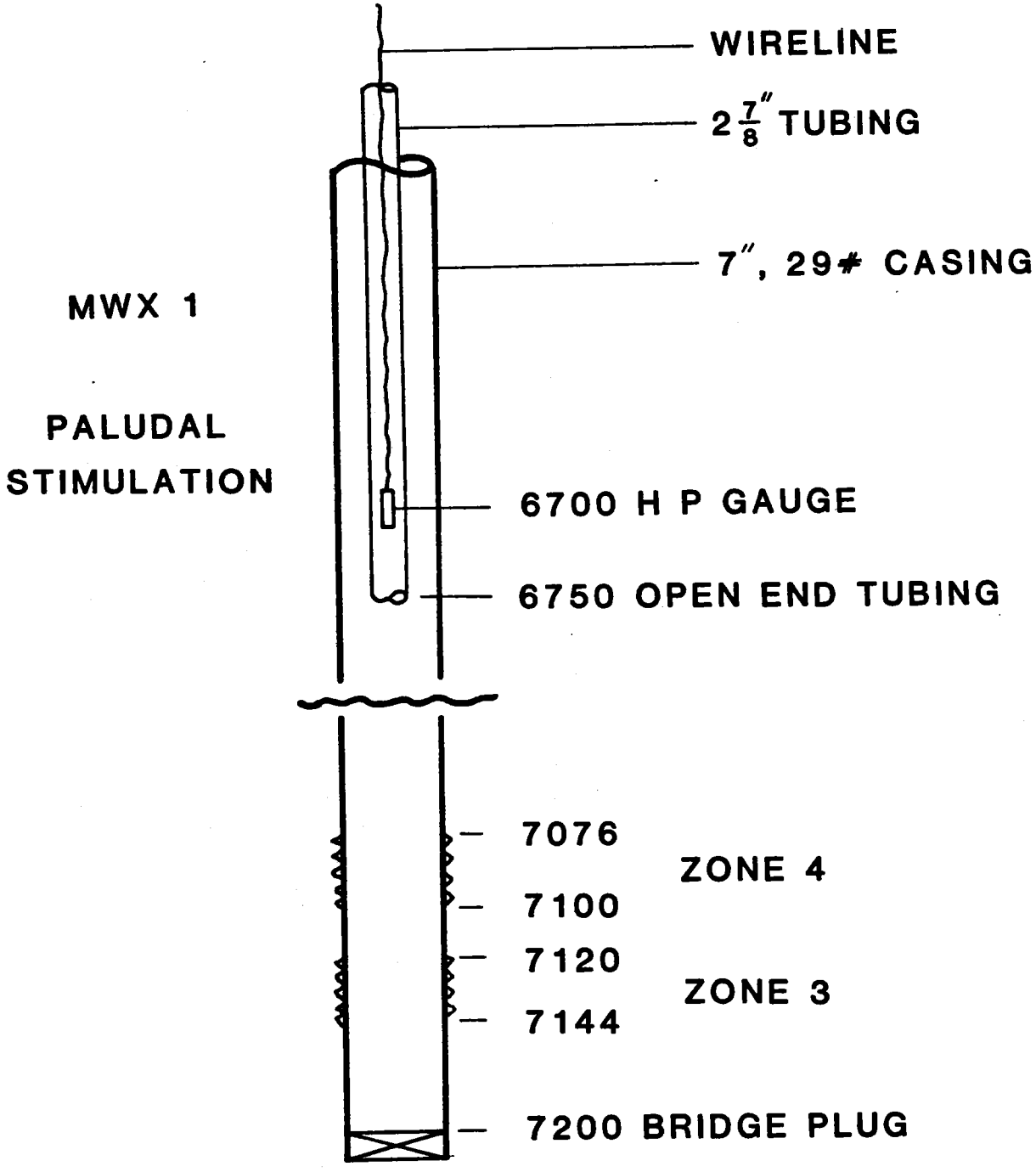

Figure 8.4.2 Well Configuration

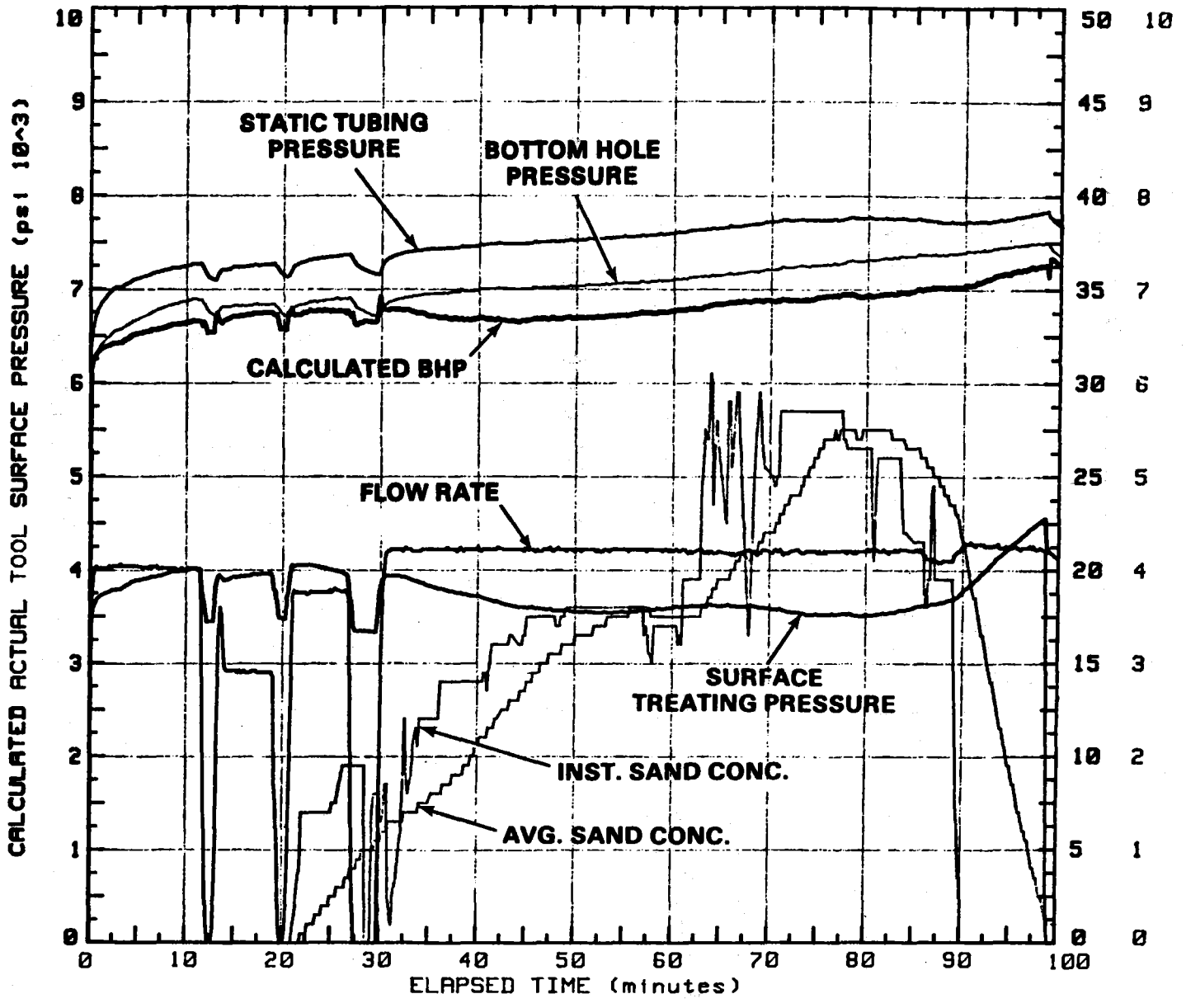

Figure 8.4.3 Treatment Data

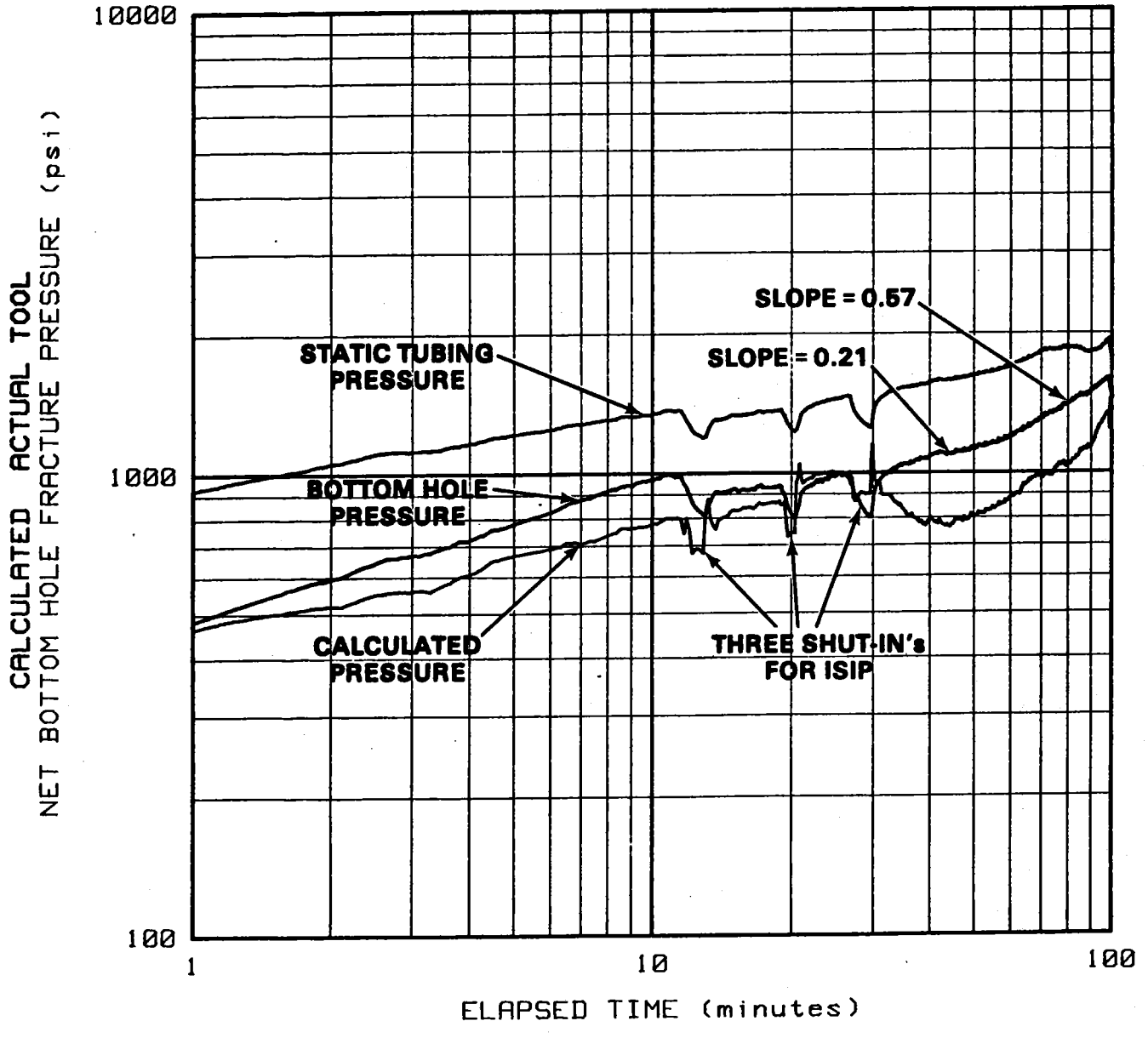

Figure 8.4.4 Nolte-Smith Plot

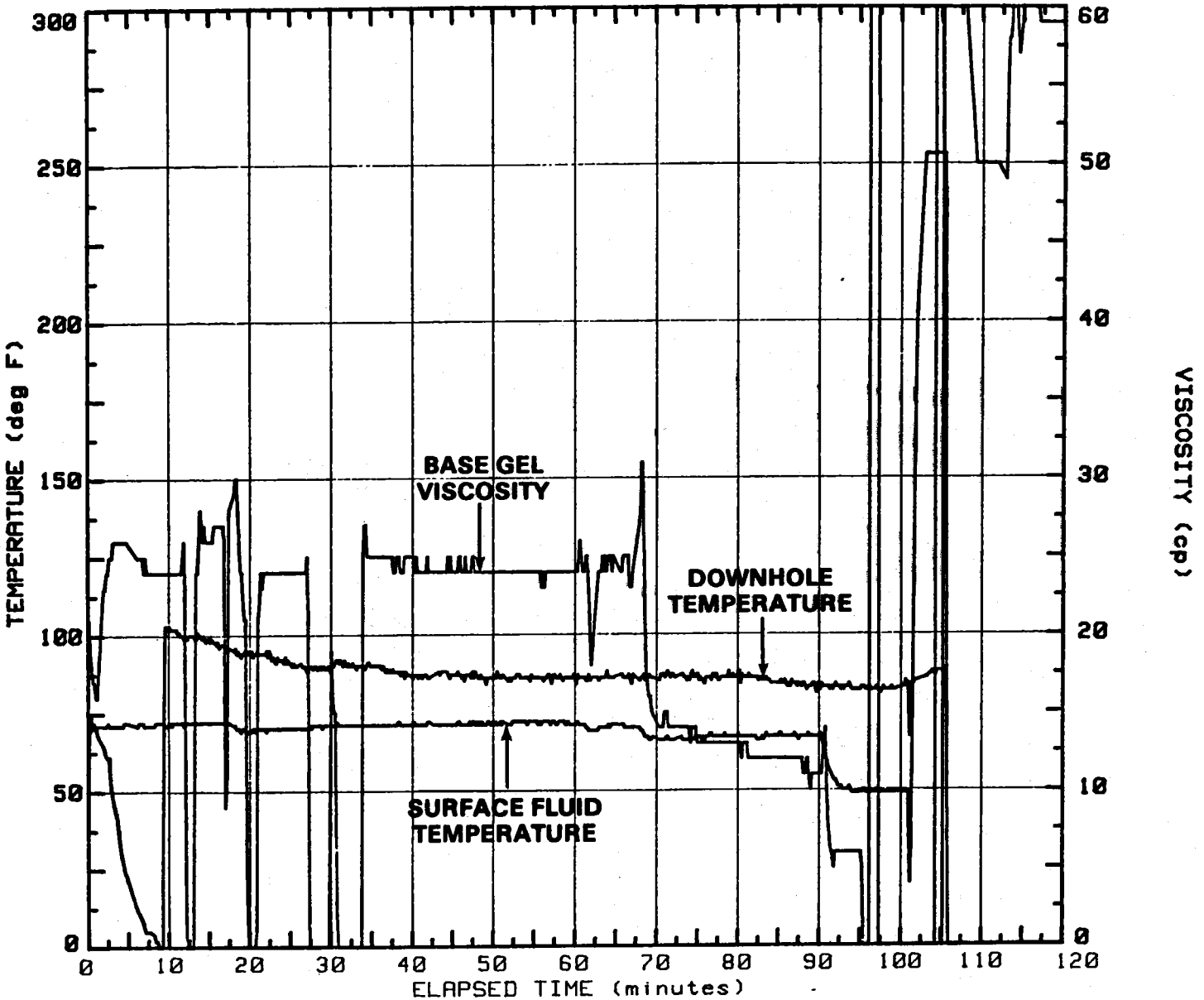

Figure 8.4.5 Treatment Data

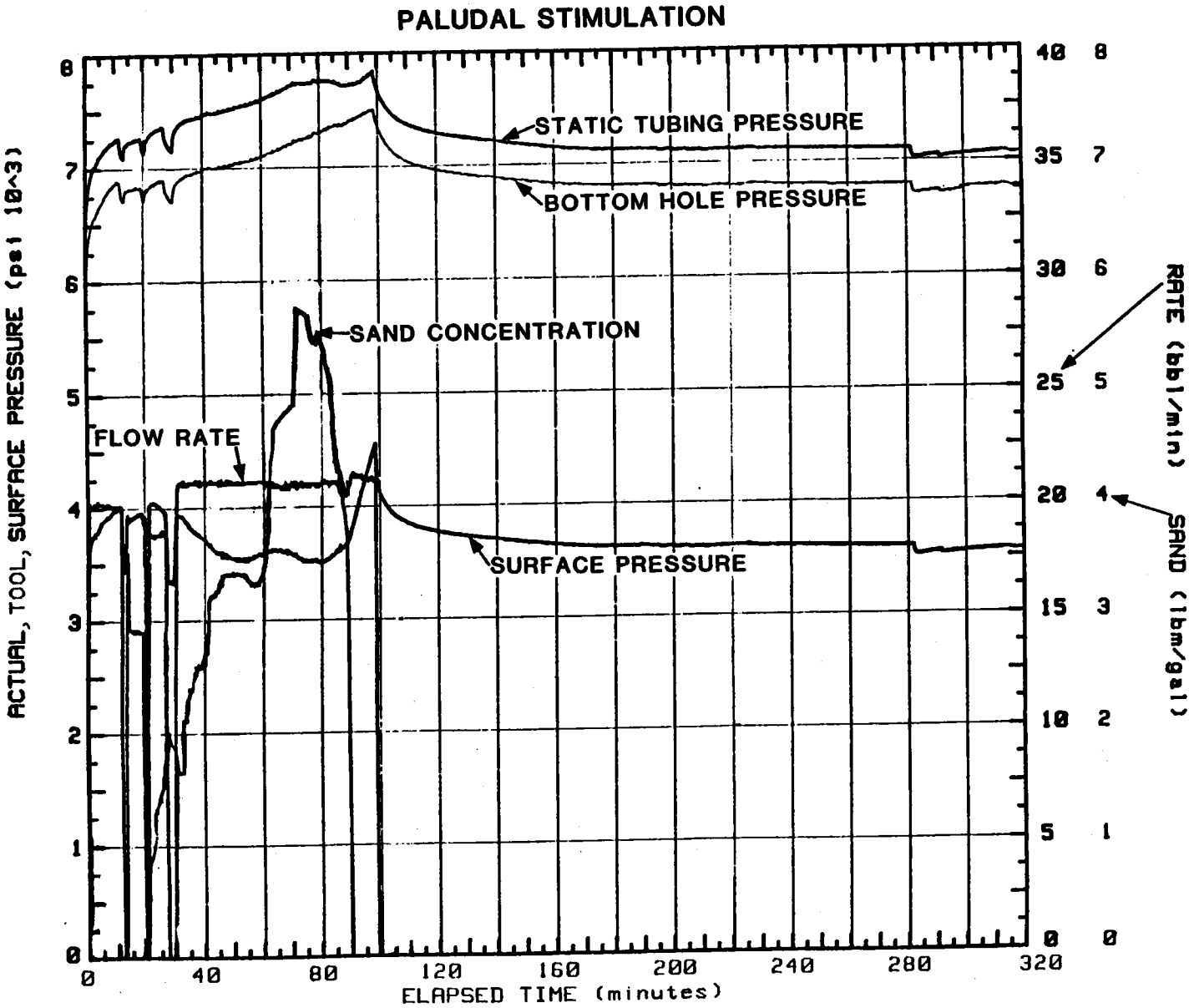

Figure 8.4.6 Treatment Data

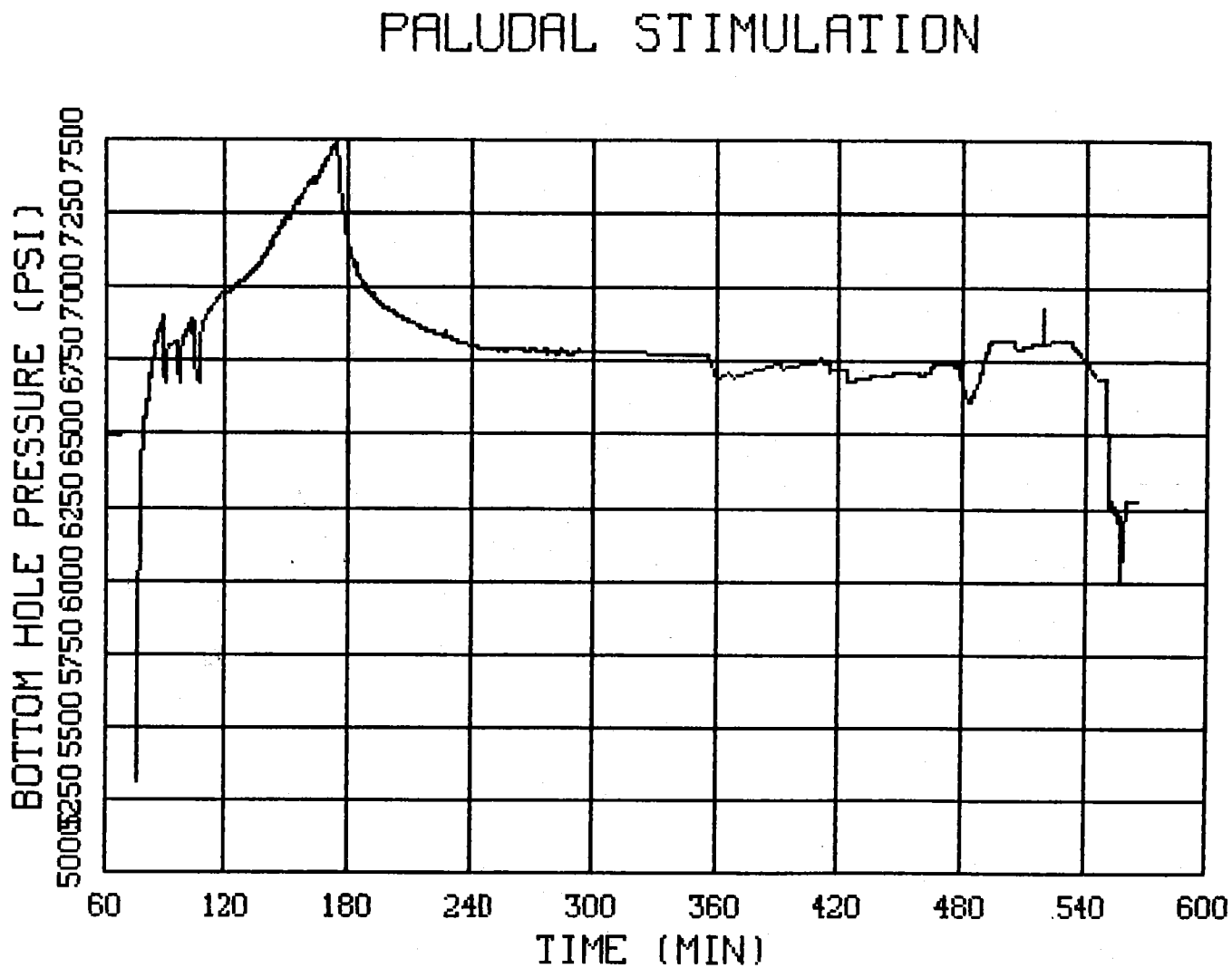

Figure 8.4.7 Bottom Hole Pressure Data

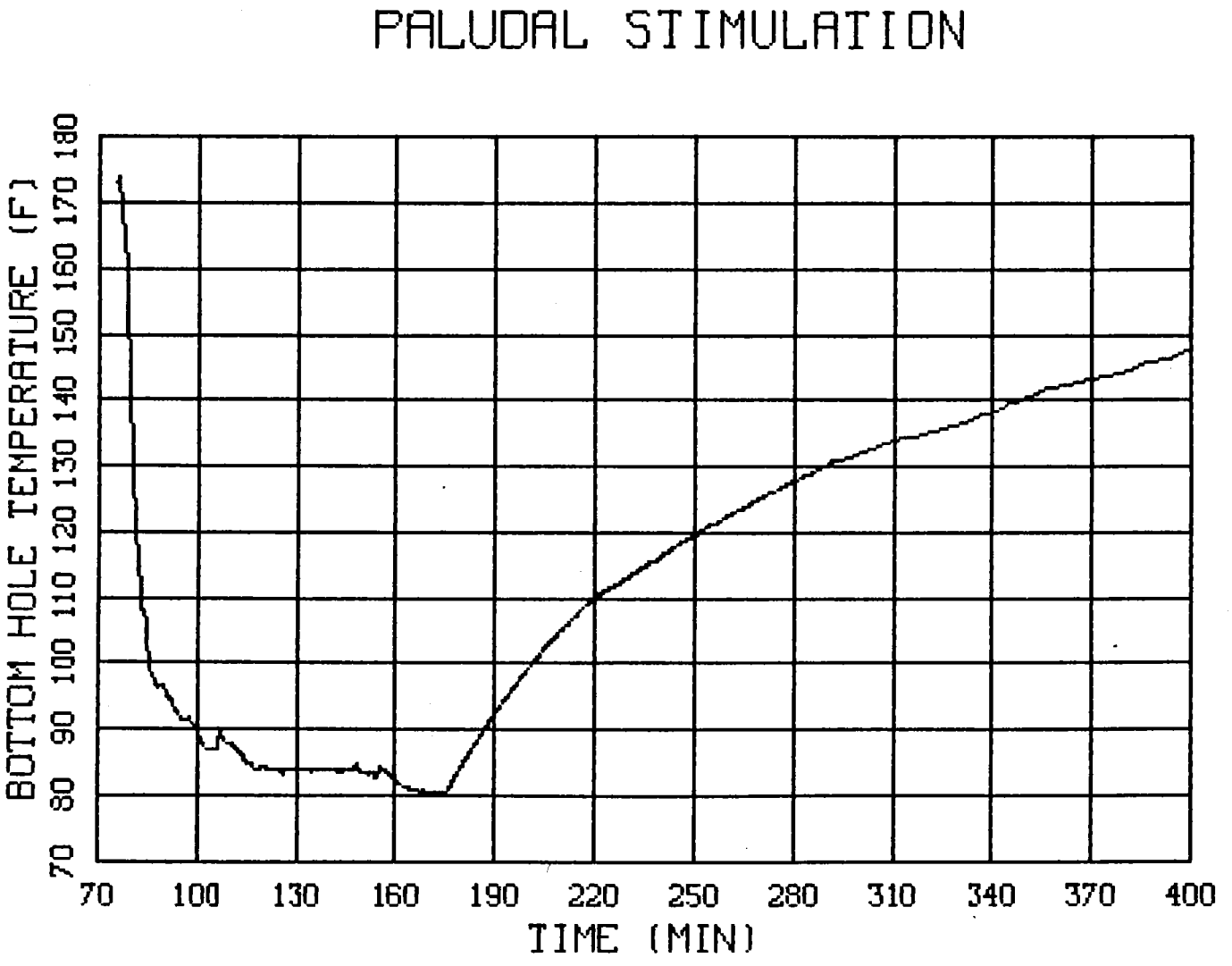

Figure 8.4.8 Bottom Hole Temperature Data

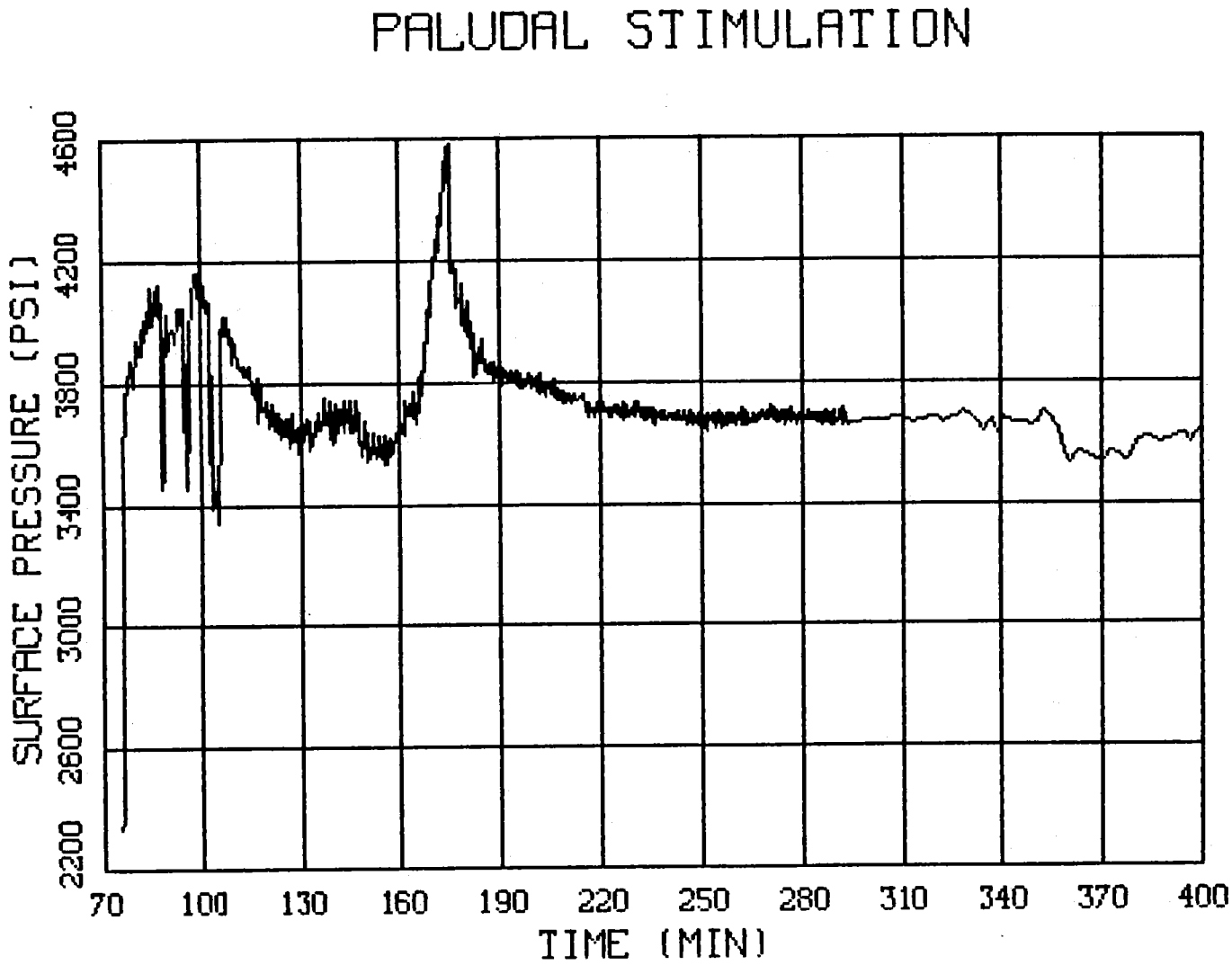

Figure 8.4.9 Surface Pressure Data

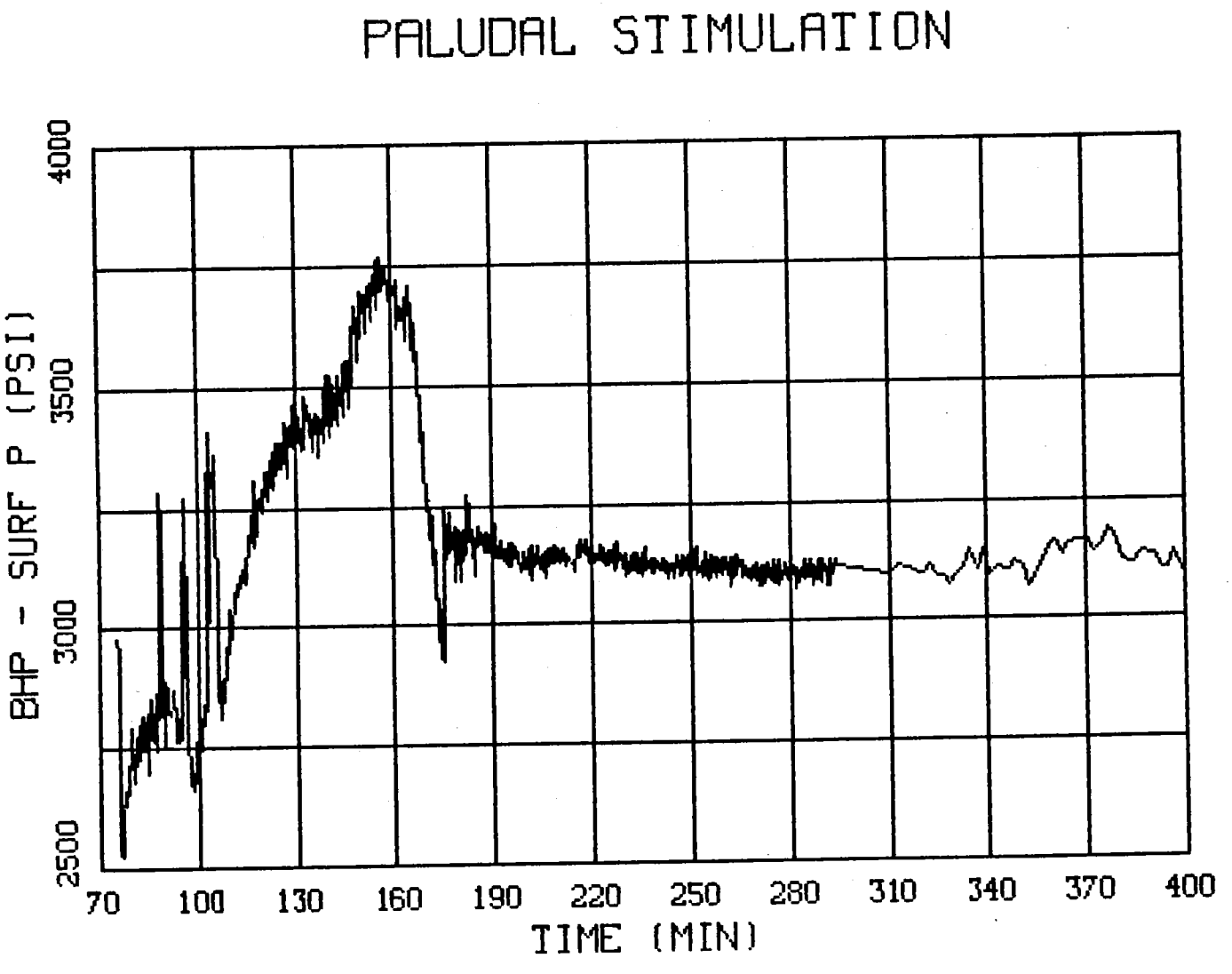

Figure 8.4.10 Bottom Hole Minus Surface Pressure Differential

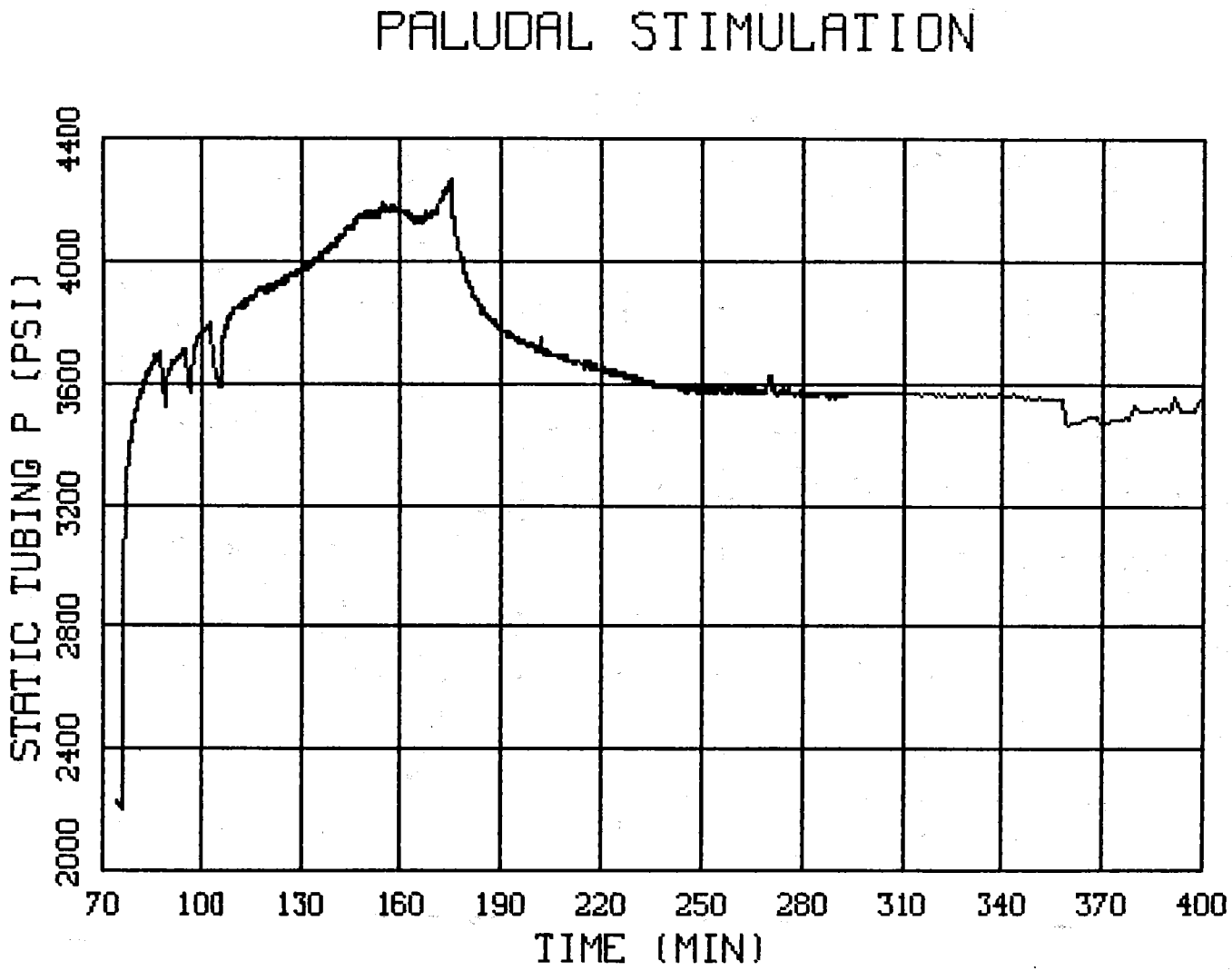

Figure 8.4.11 Static Tubing Pressure

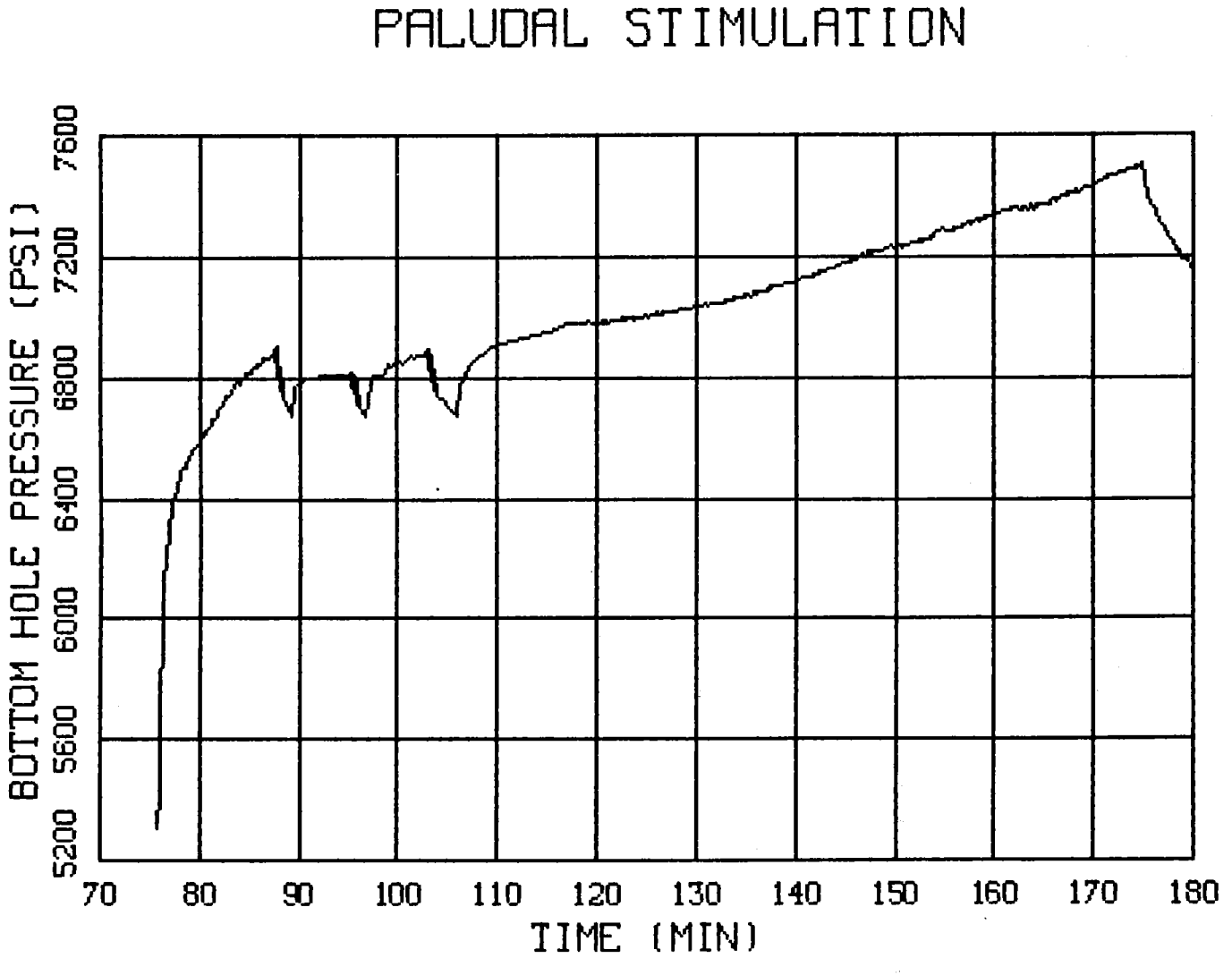

Figure 8.4.12 Injection Bottom Hole Pressure

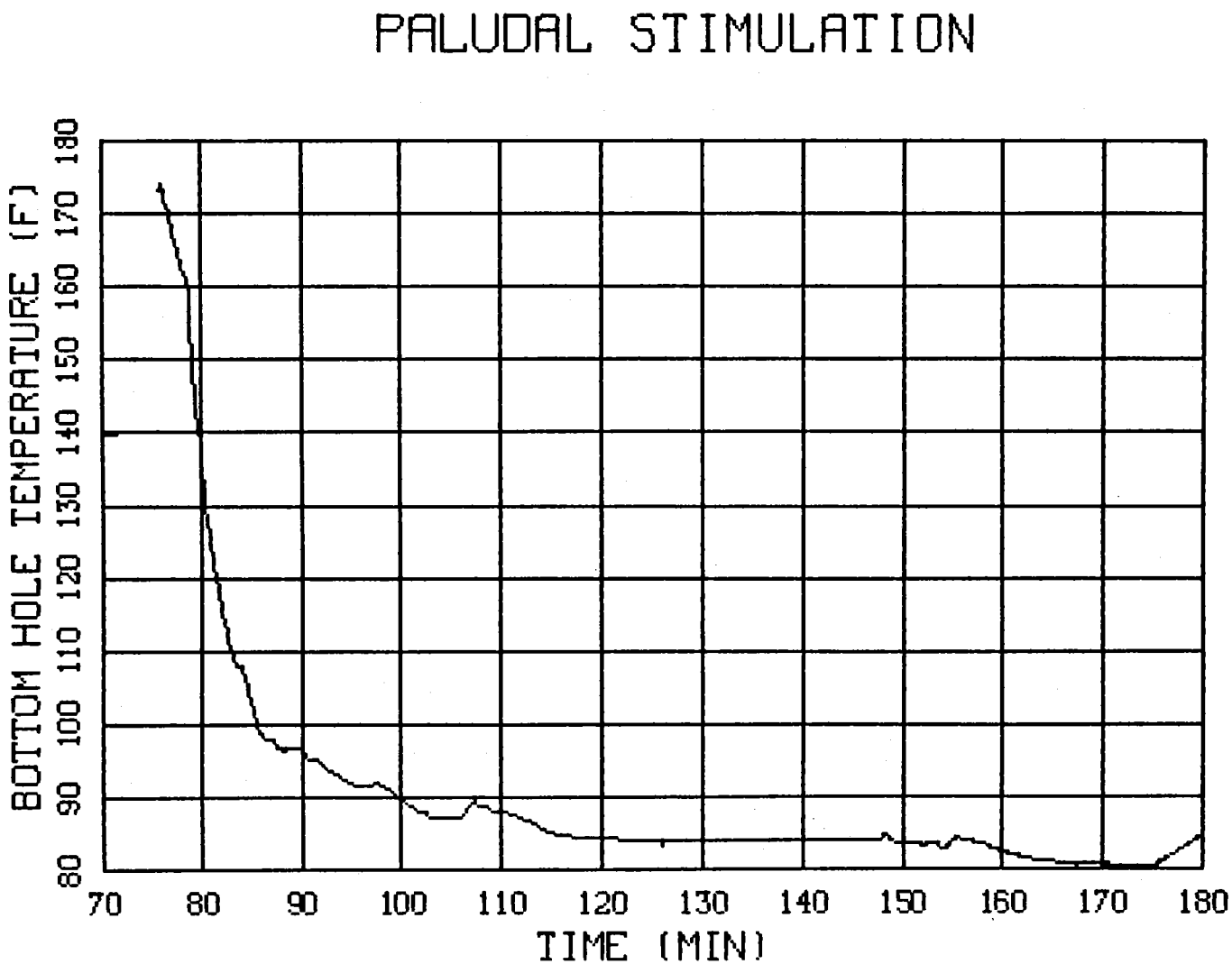

Figure 8.4.13 Injection Bottom Hole Temperature

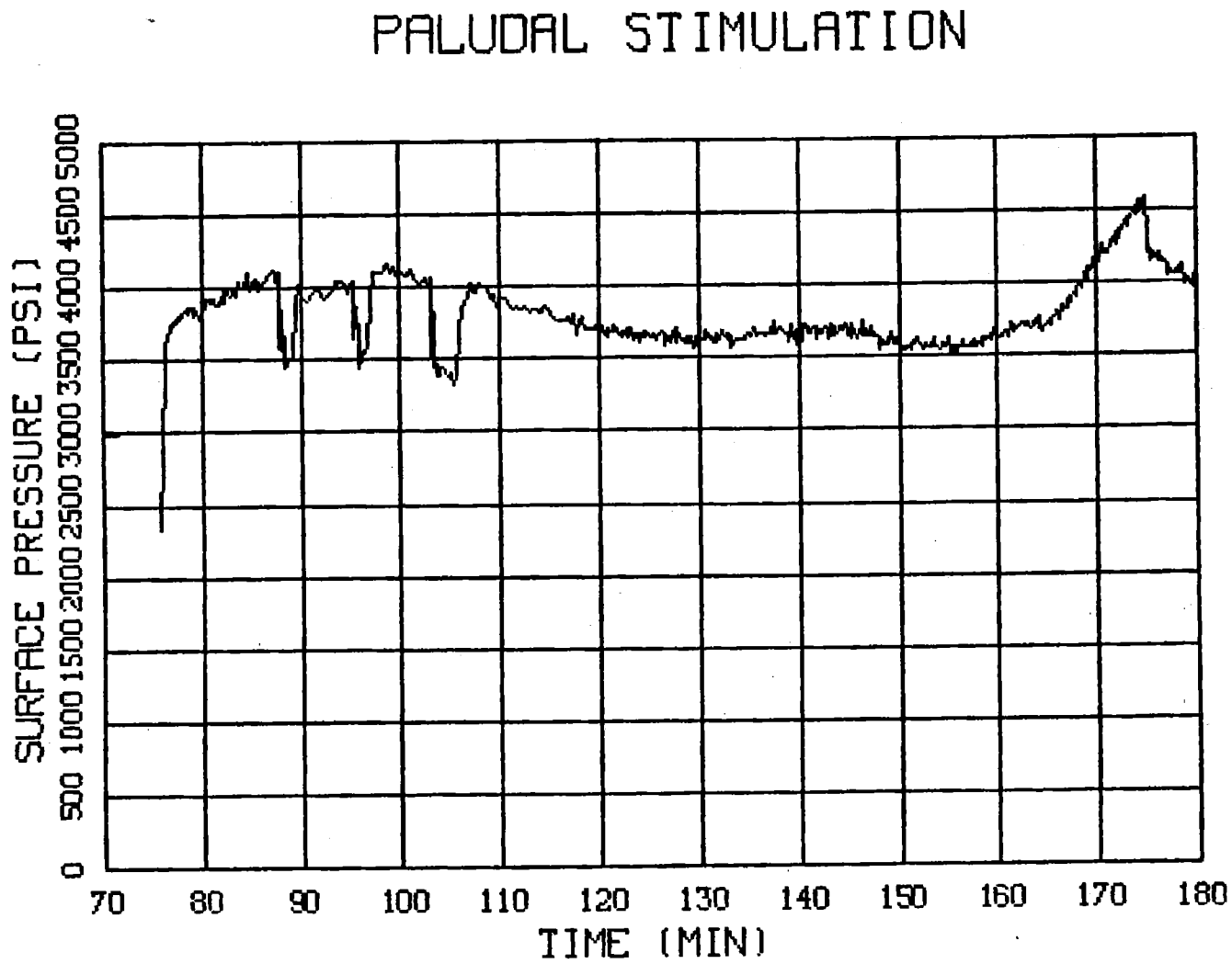

Figure 8.4.14 Injection Surface Pressure

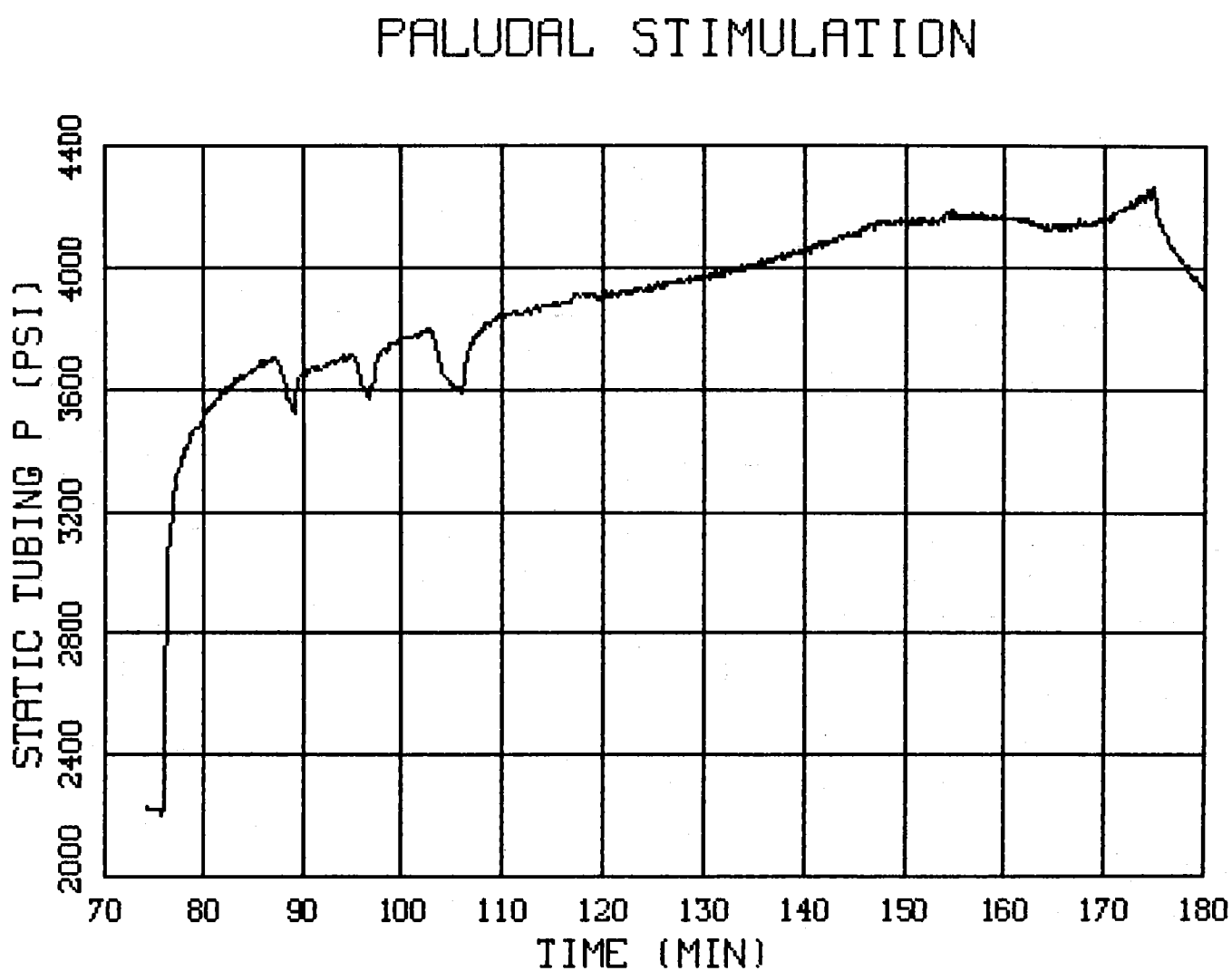

Figure 8.4.15 Injection Static Tubing Pressure

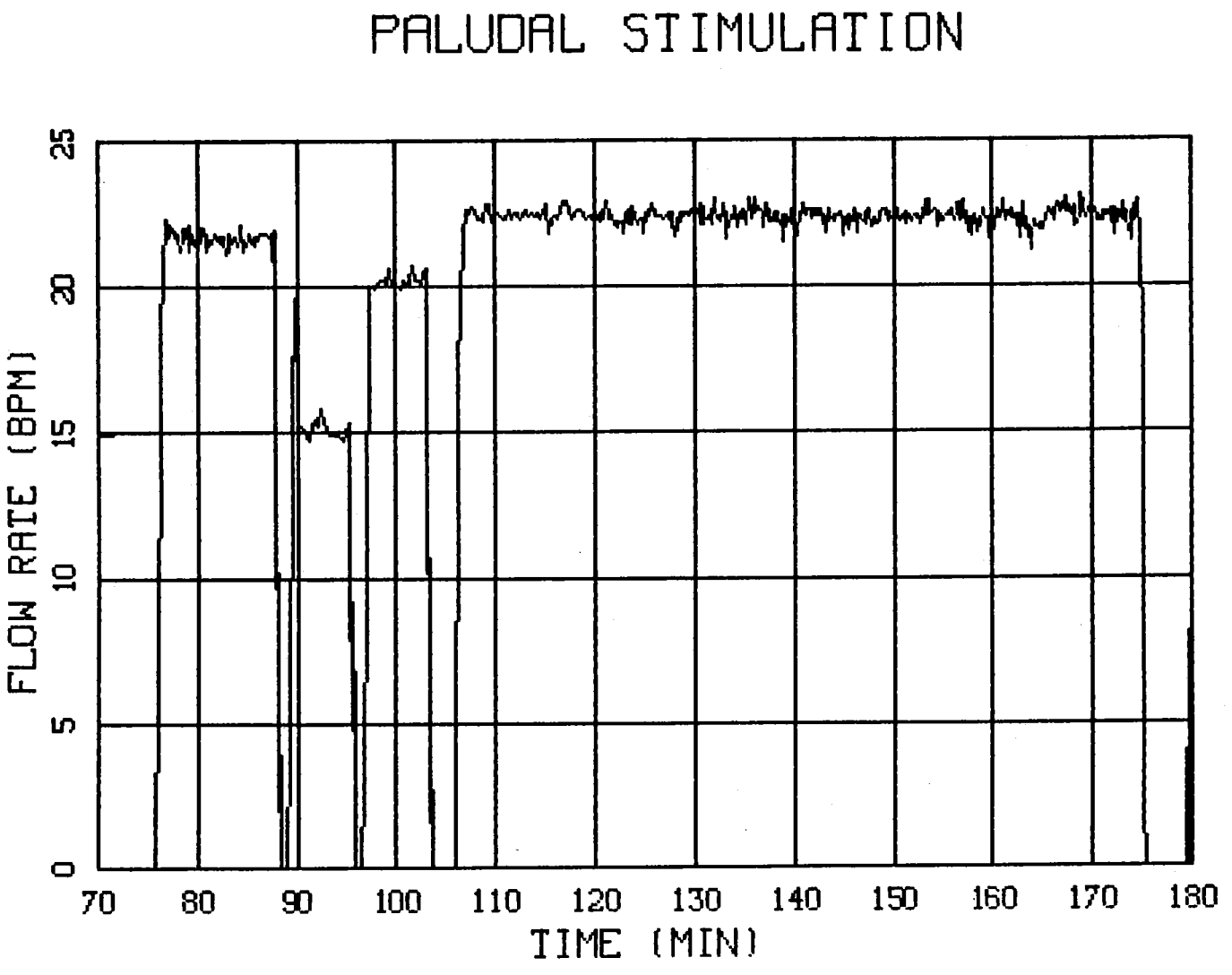

Figure 8.4.16 Injection Flow Rate Data

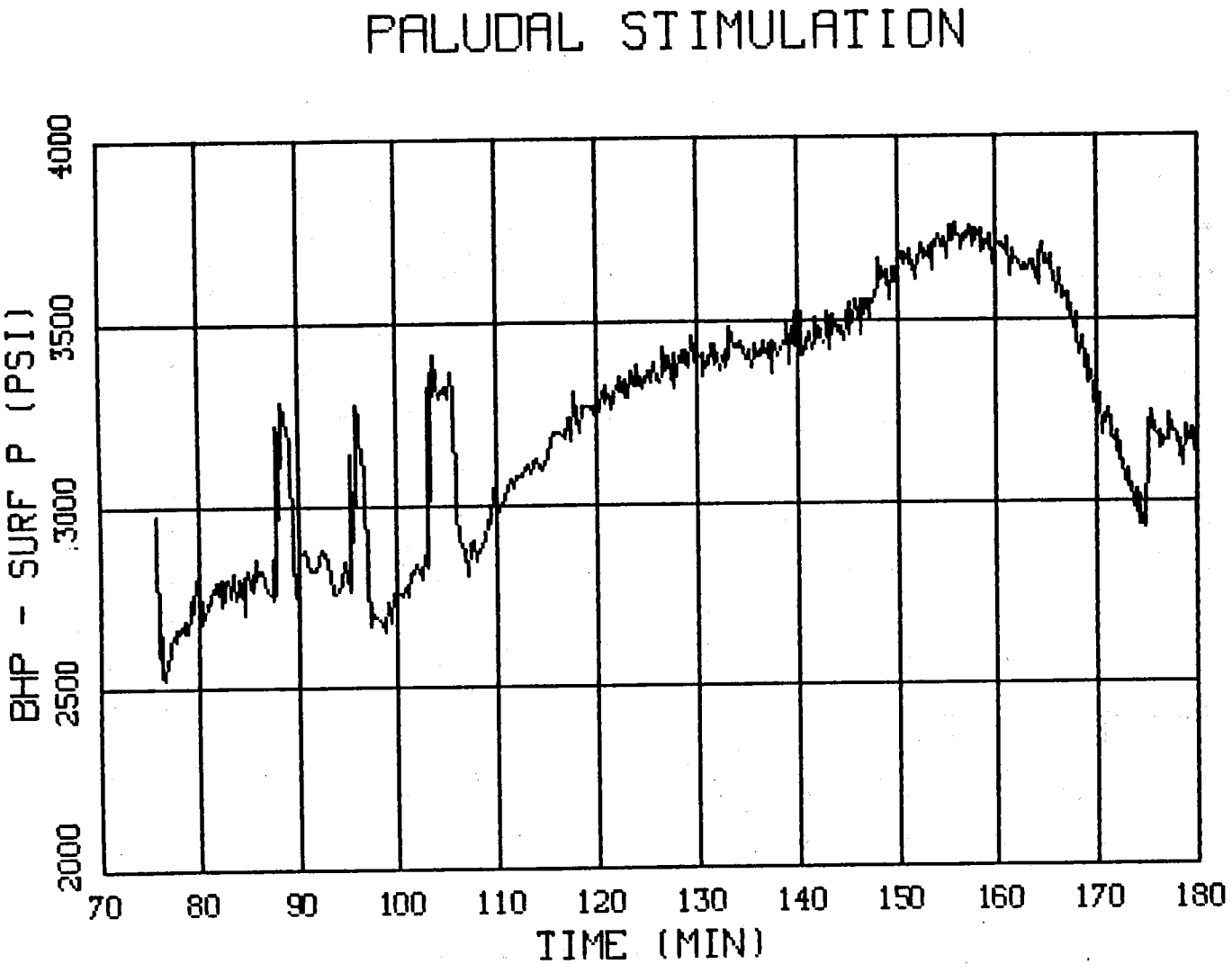

Figure 8.4.17 Injection Pressure Differential, Bottom Hole Minus Surface

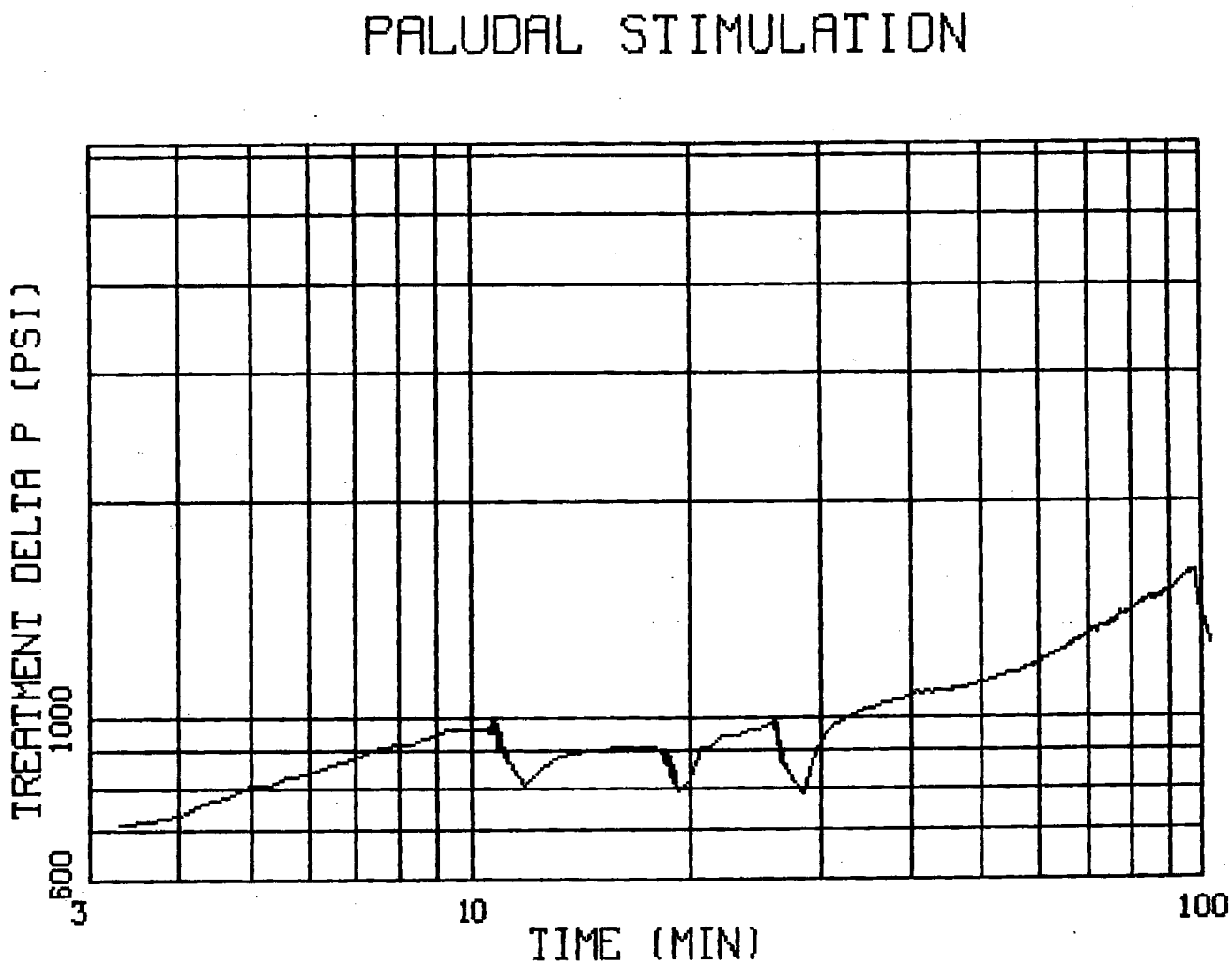

Figure 8.4.18 Nolte-Smith Plot

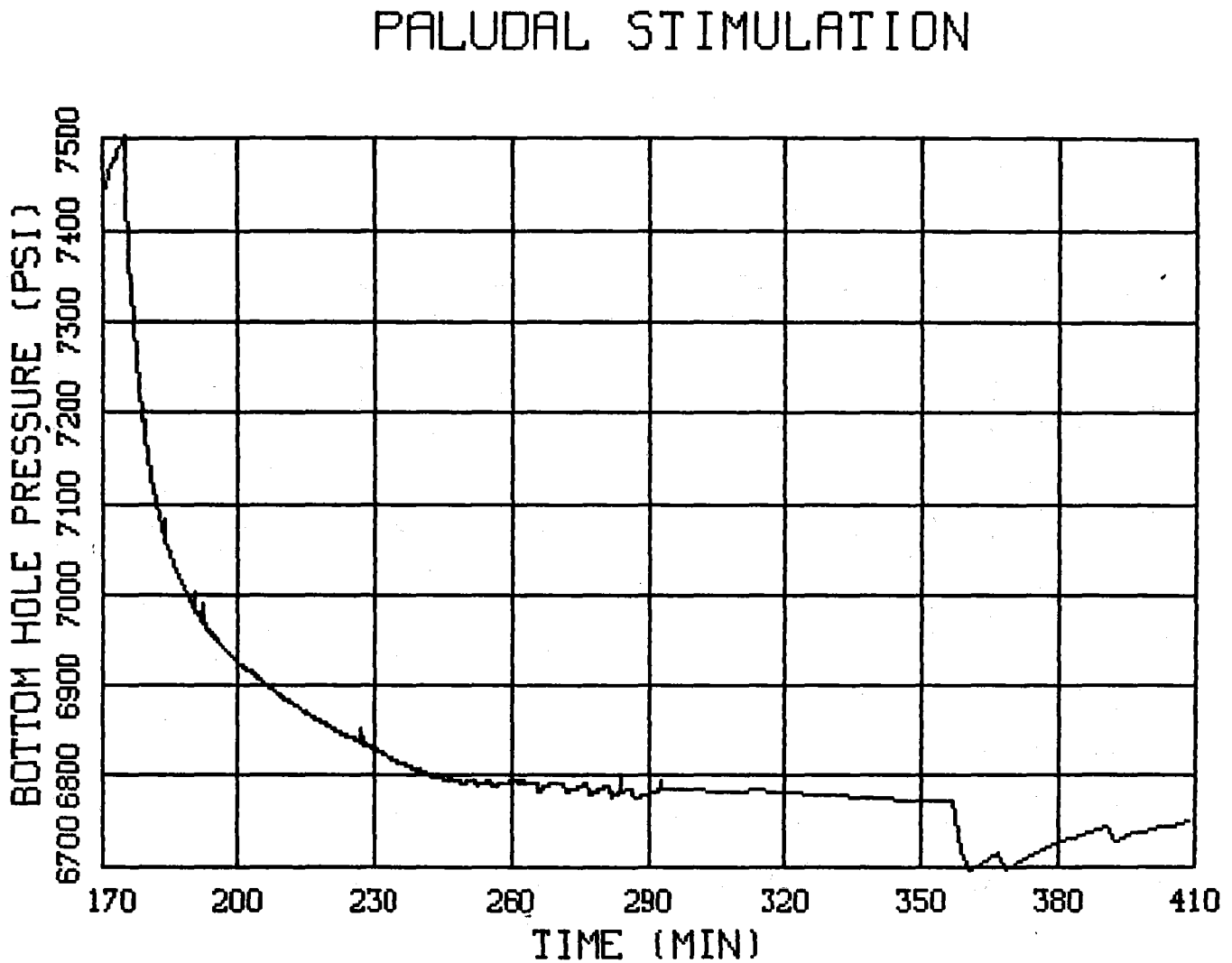

Figure 8.4.19 Pressure Decline Data

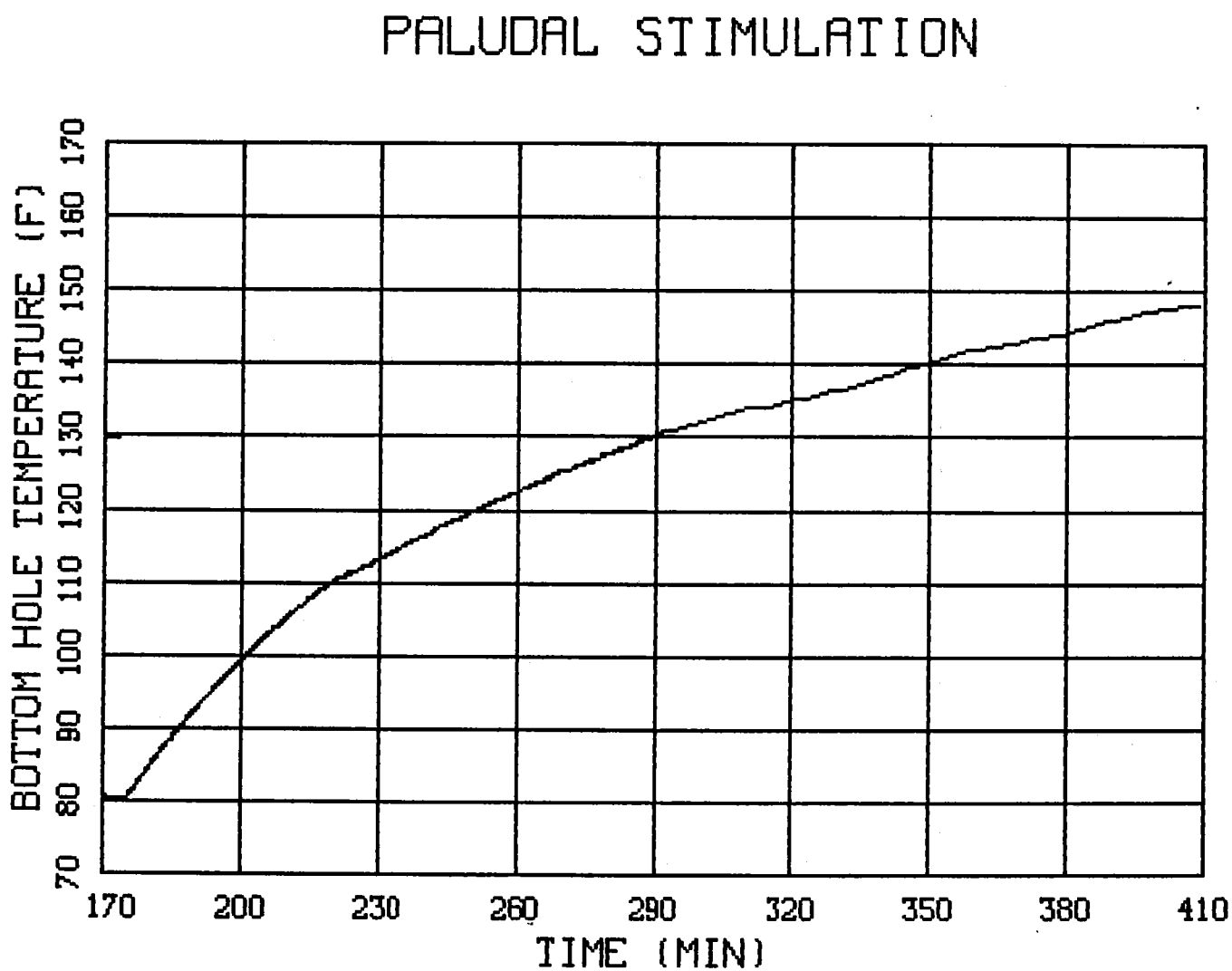

Figure 8.4.20 Bottom Hole Temperature During Pressure Decline

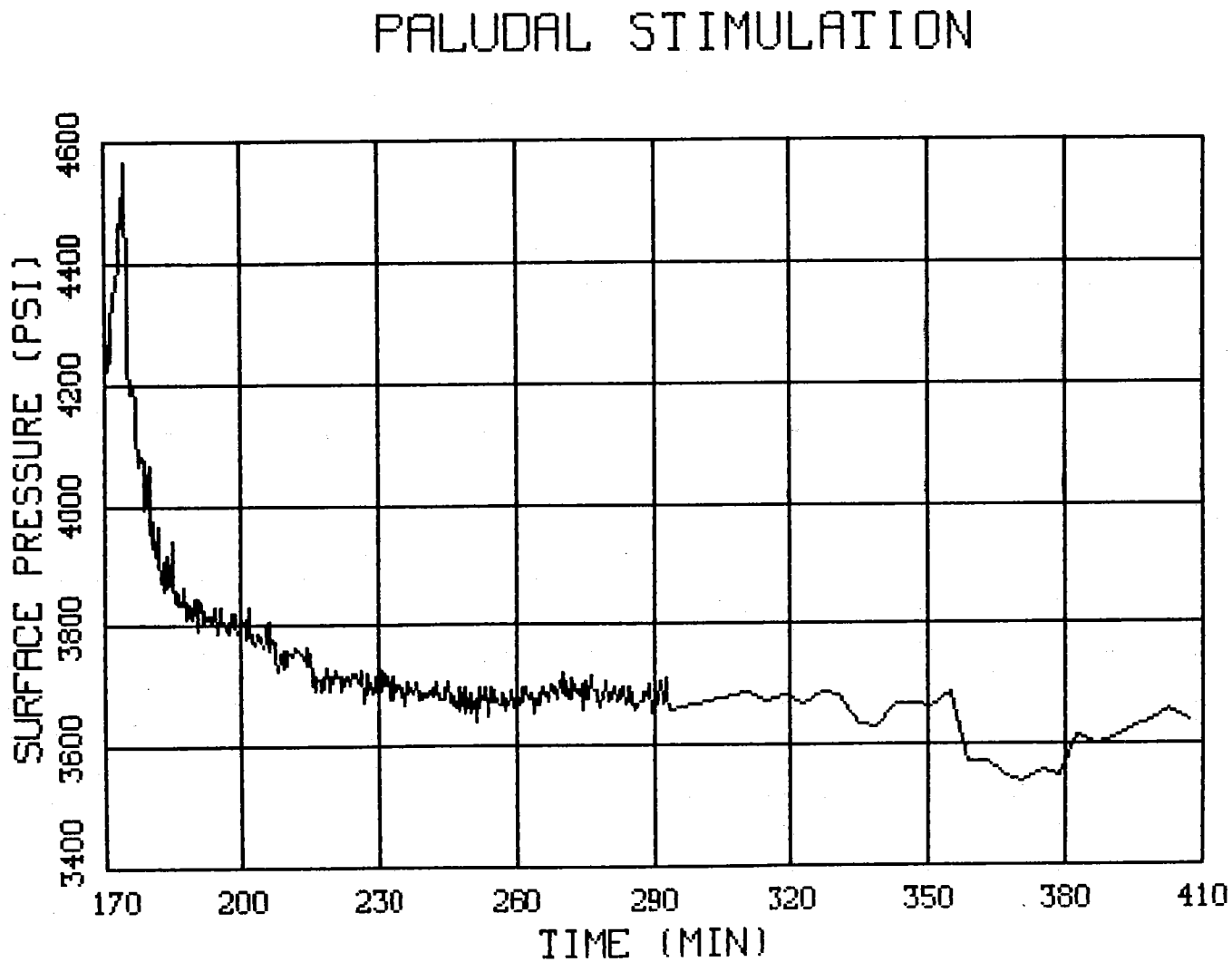

Figure 8.4.21 Surface Pressure During Pressure Decline

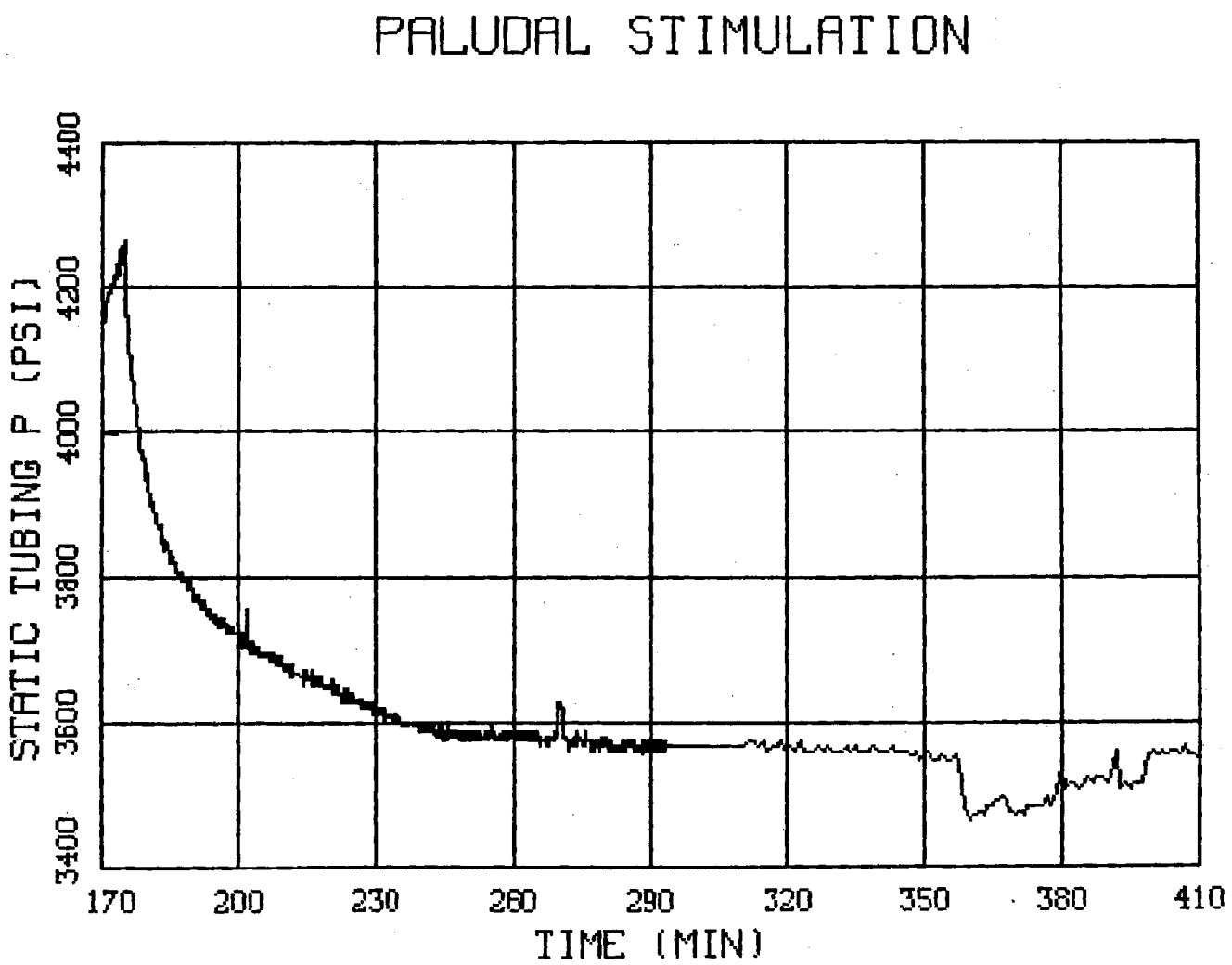

Figure 8.4.22 Static Tubing Pressure During Pressure Decline

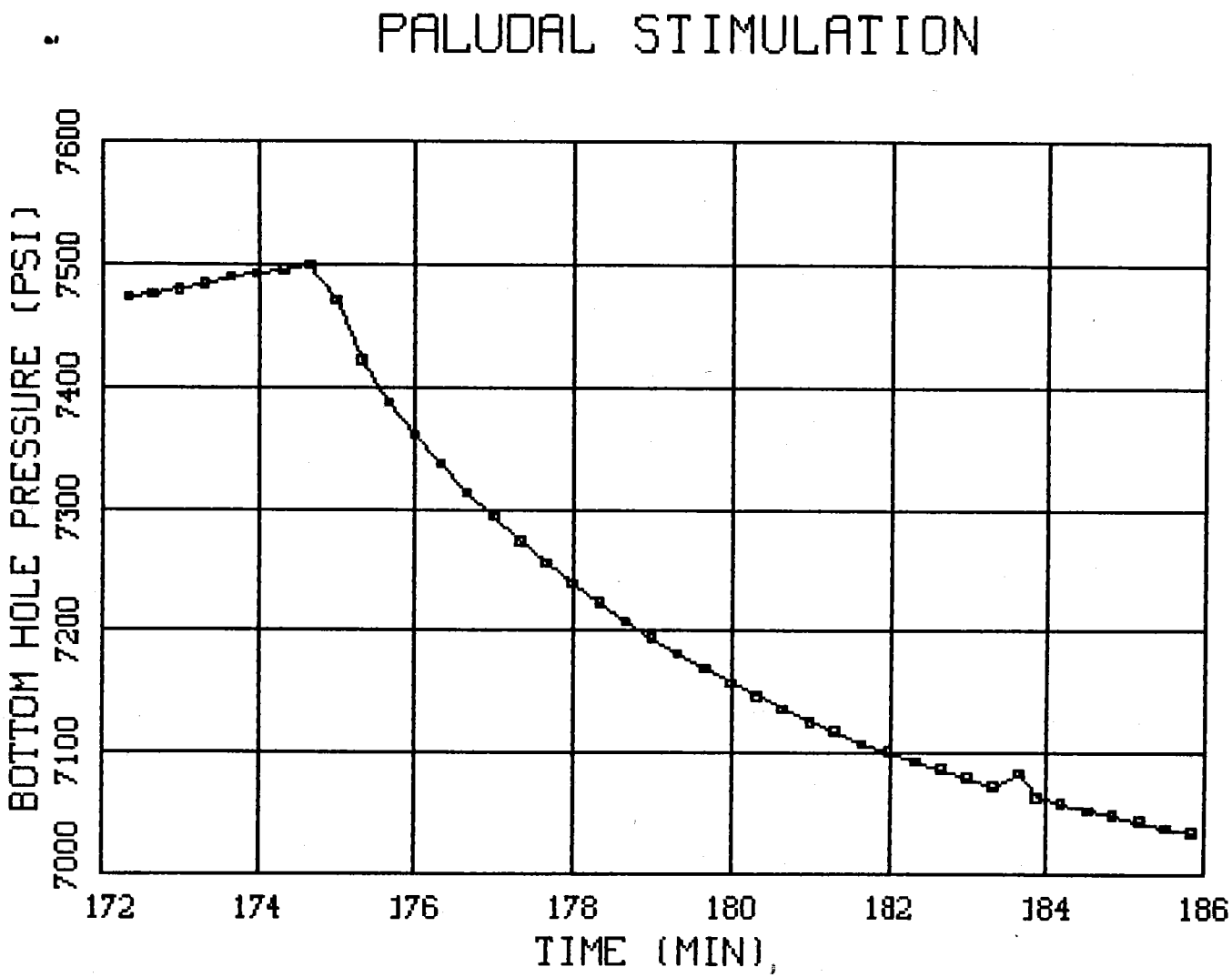

Figure 8.4.23 Bottom Hole Pressure Data At Shut In

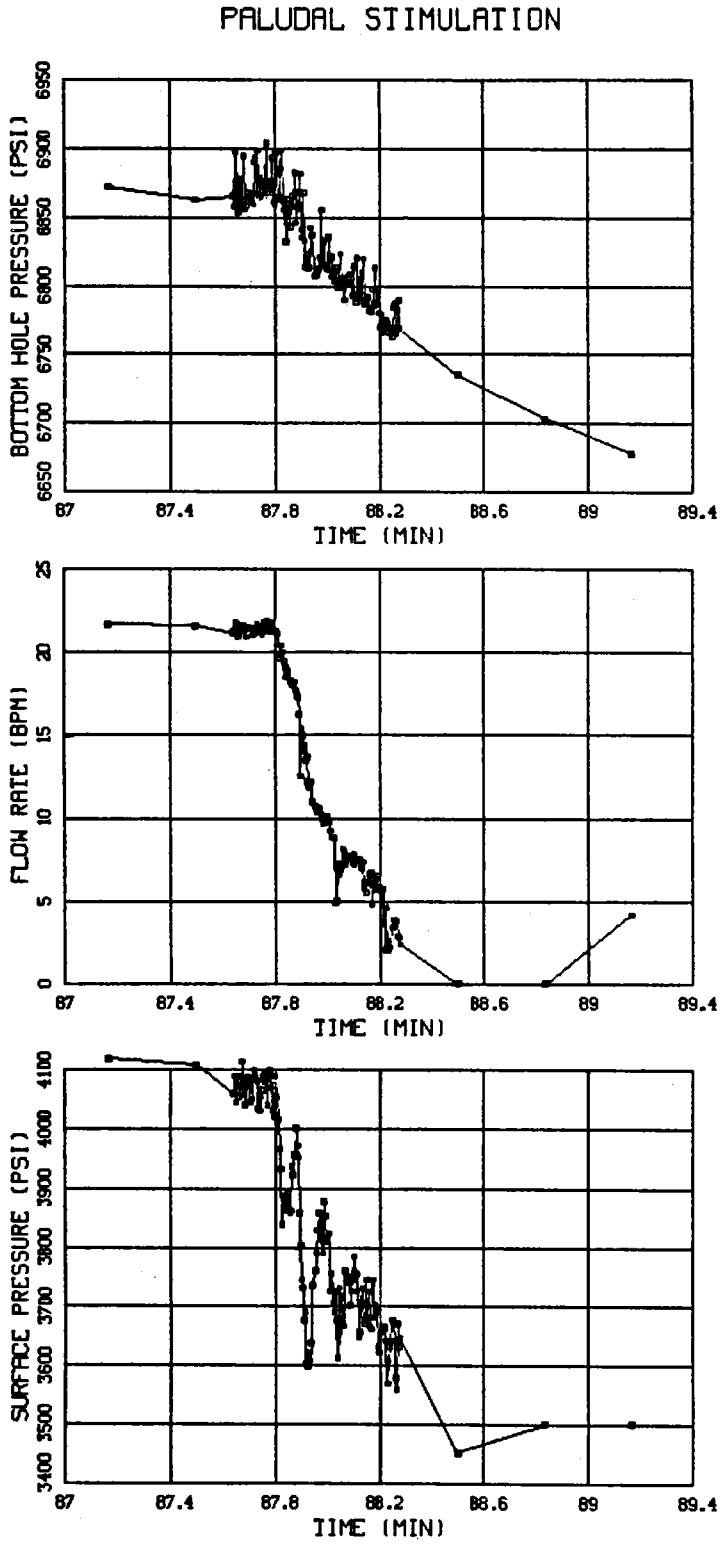

Figure 8.4.24 Shut-In #1 Data

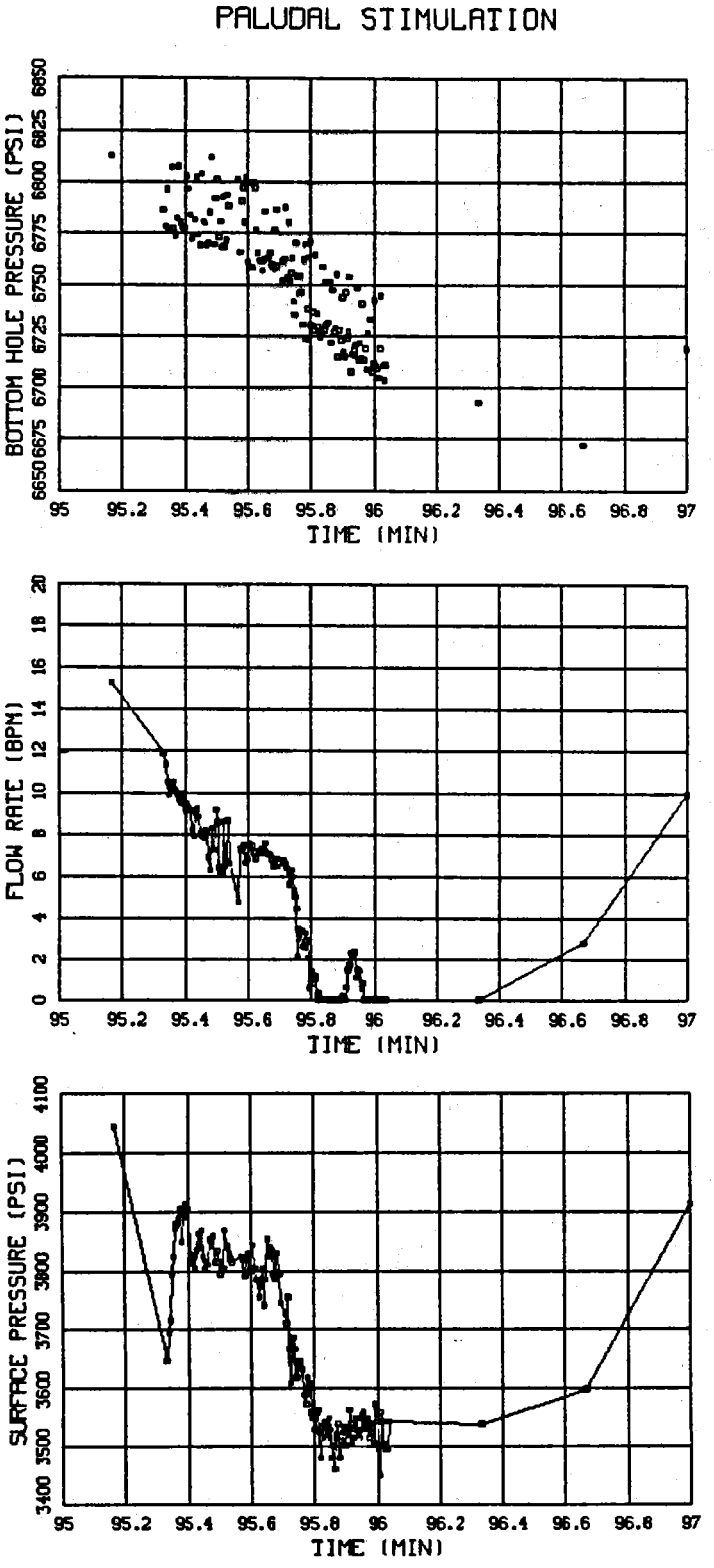

Figure 8.4.25 Shut-In #2 Data

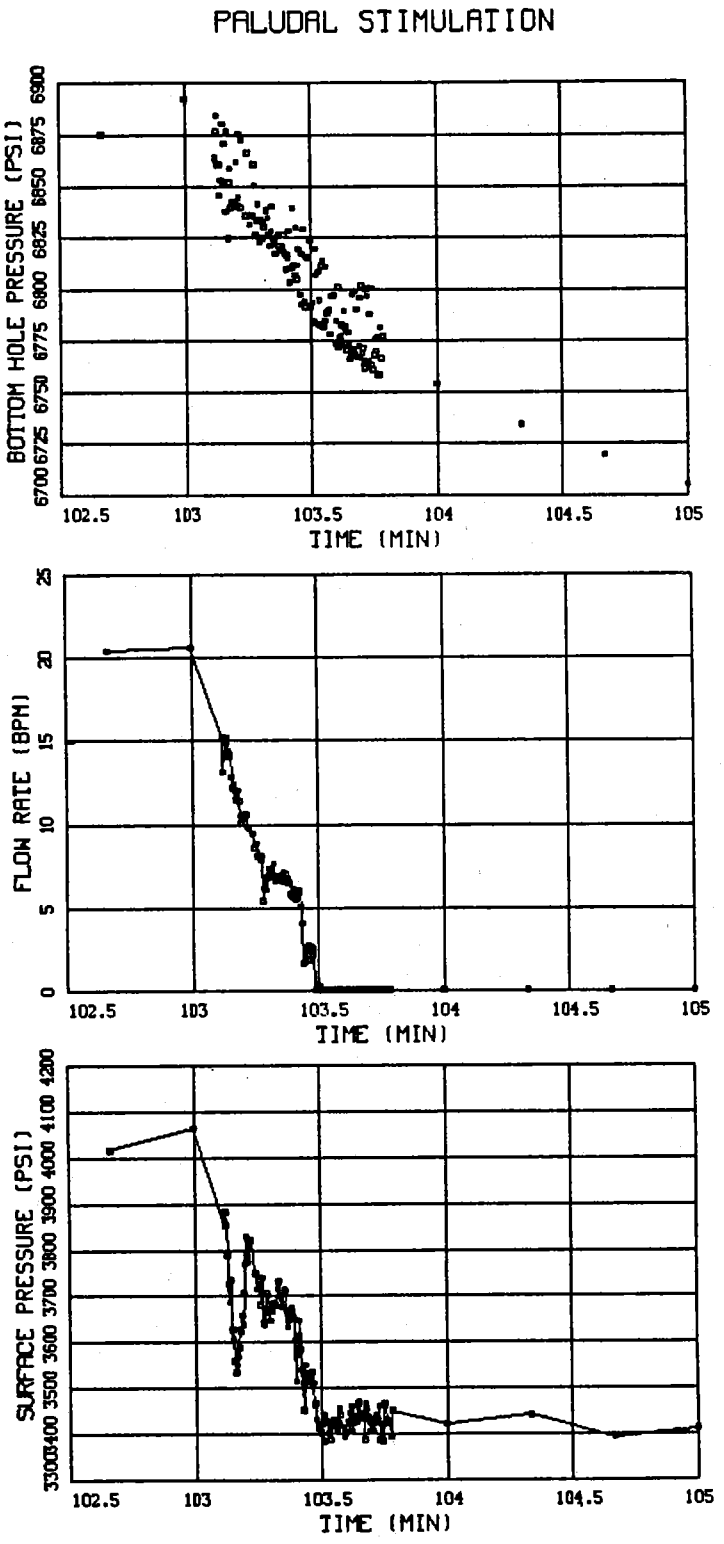

Figure 8.4.26 Shut-In #3 Data

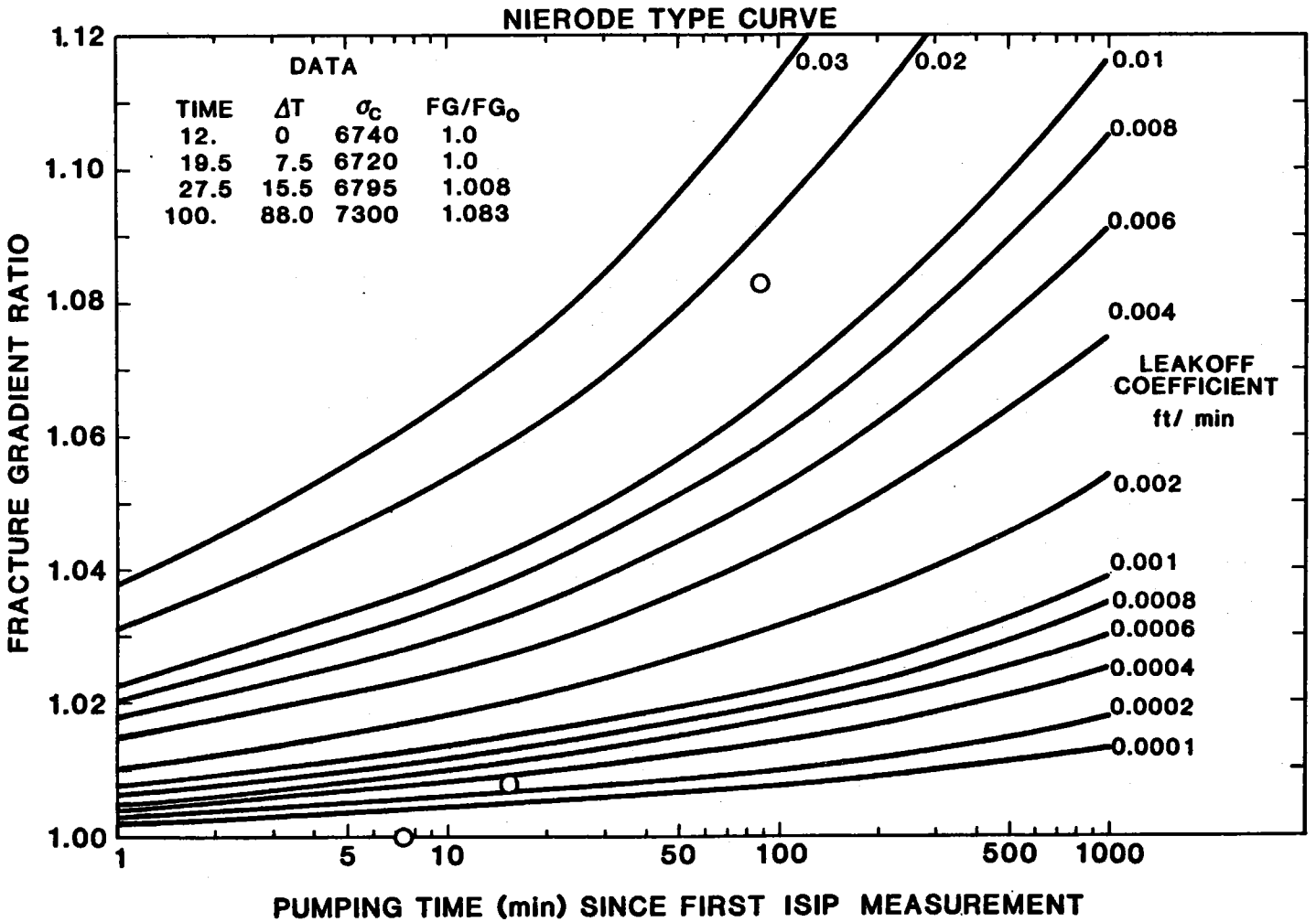

Figure 8.4.27 Nierode Analysis

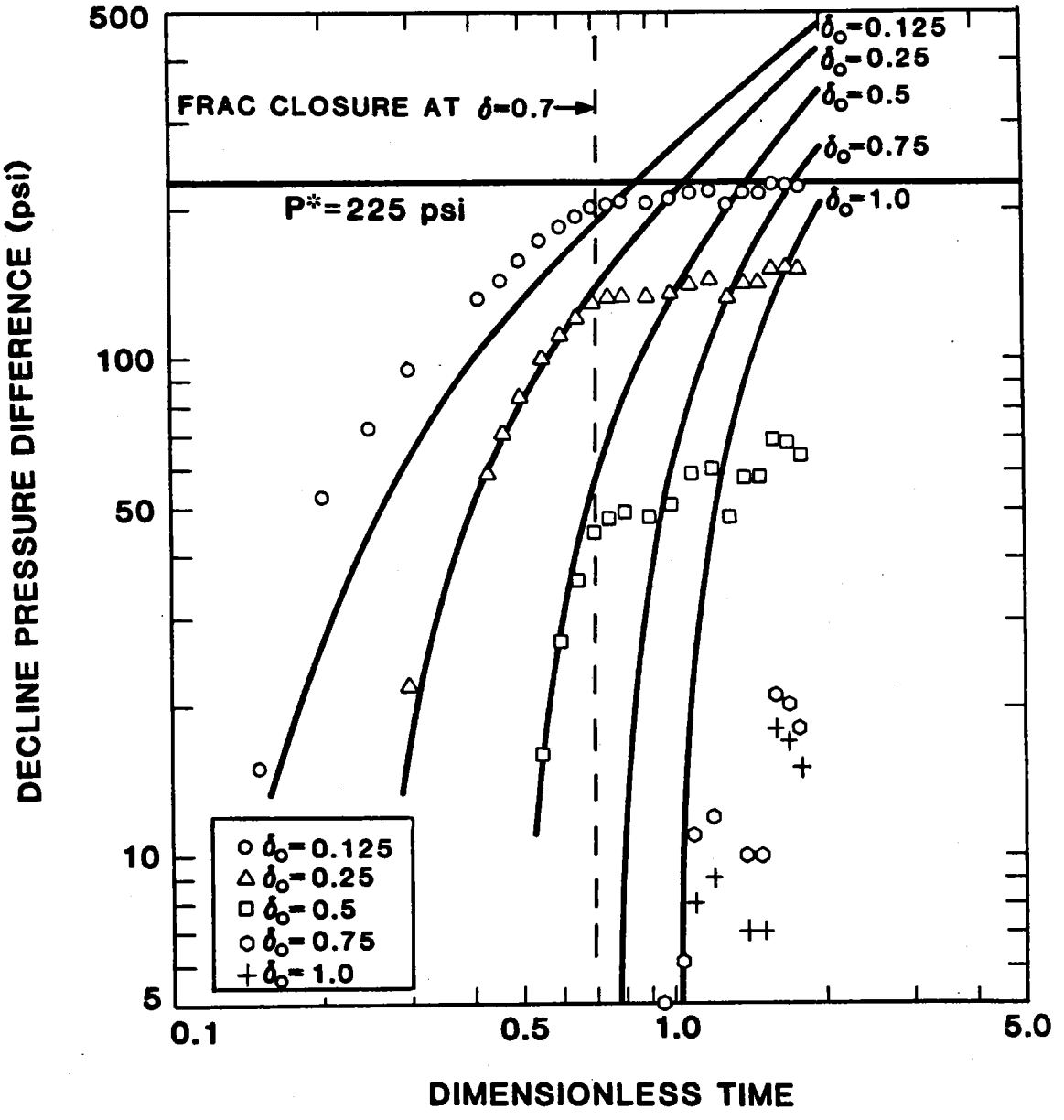

Figure 8.4.28 Nolte Plot

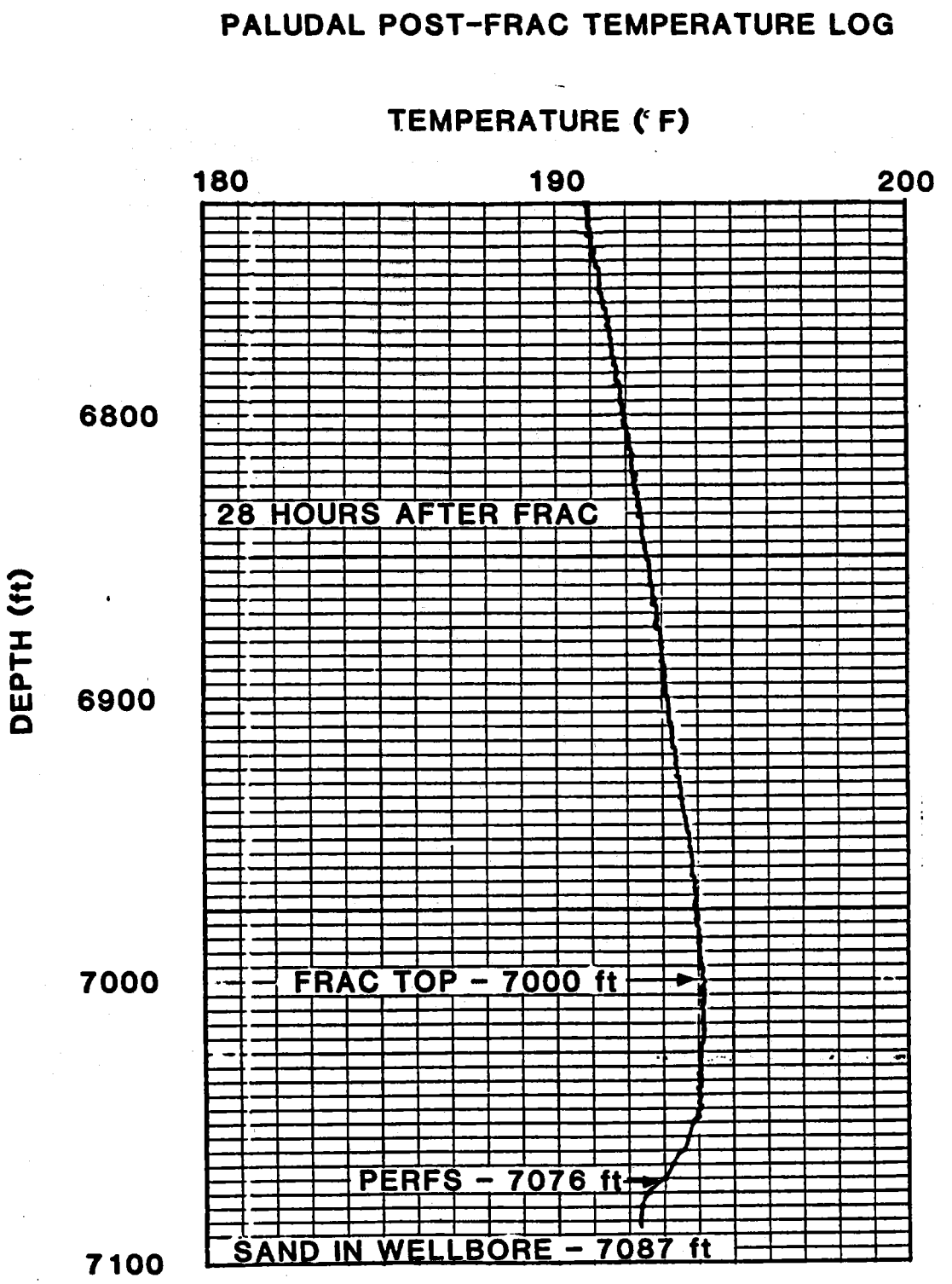

Figure 8.4.29 Post-Frac Temperature Log

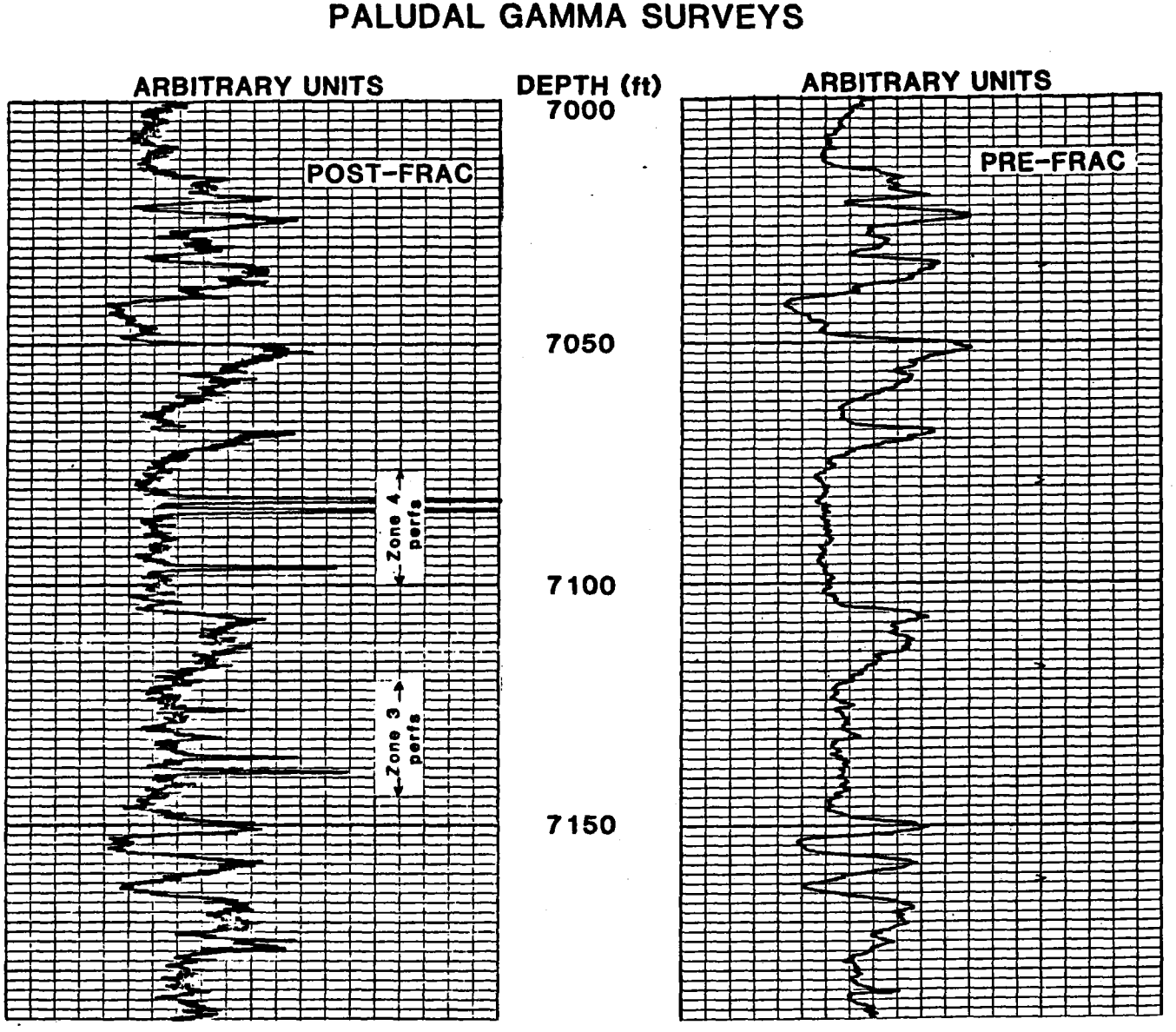

Figure 8.4.30 Gamma Surveys

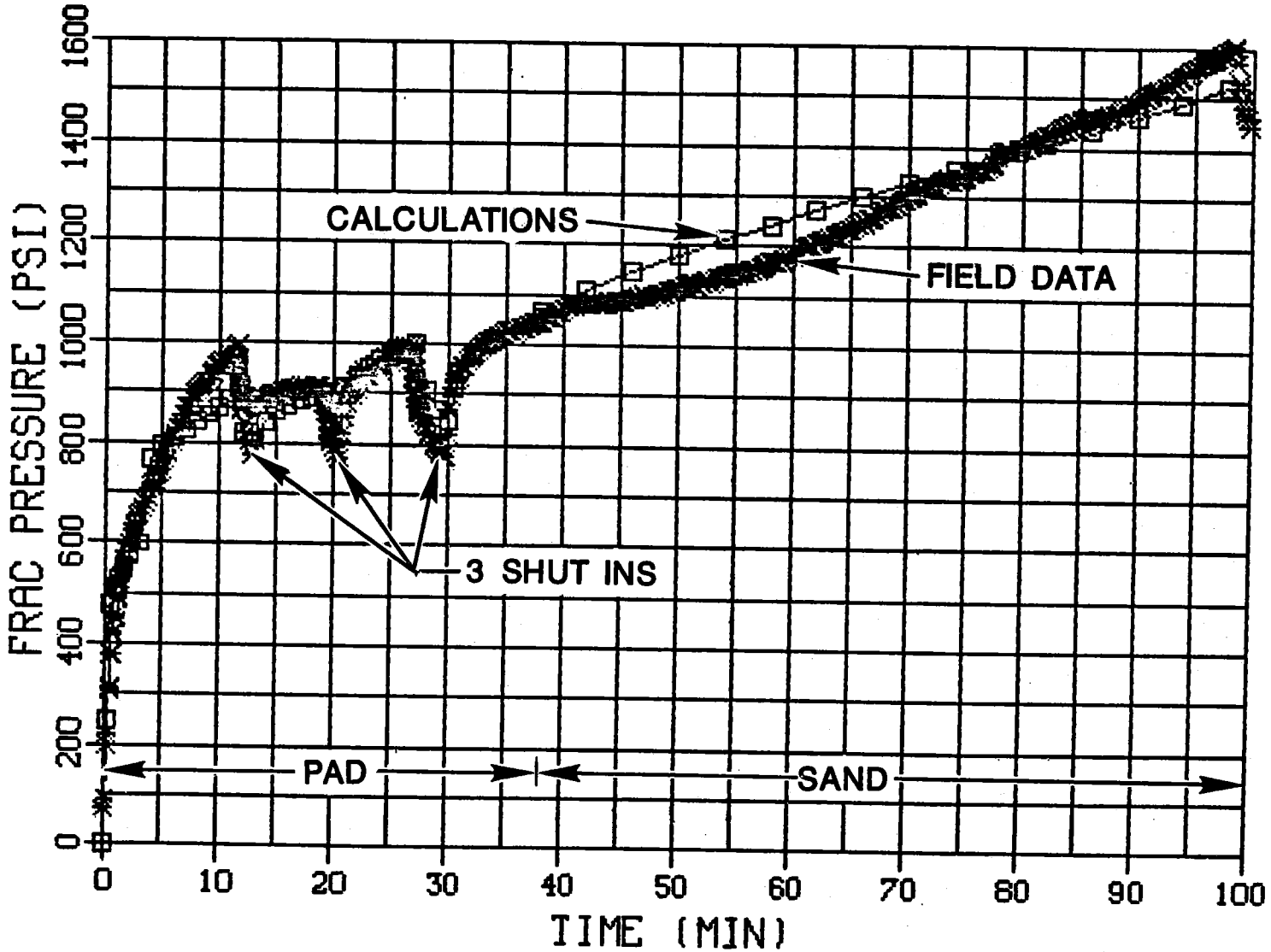

Figure 8.4.31 Pressure History Match

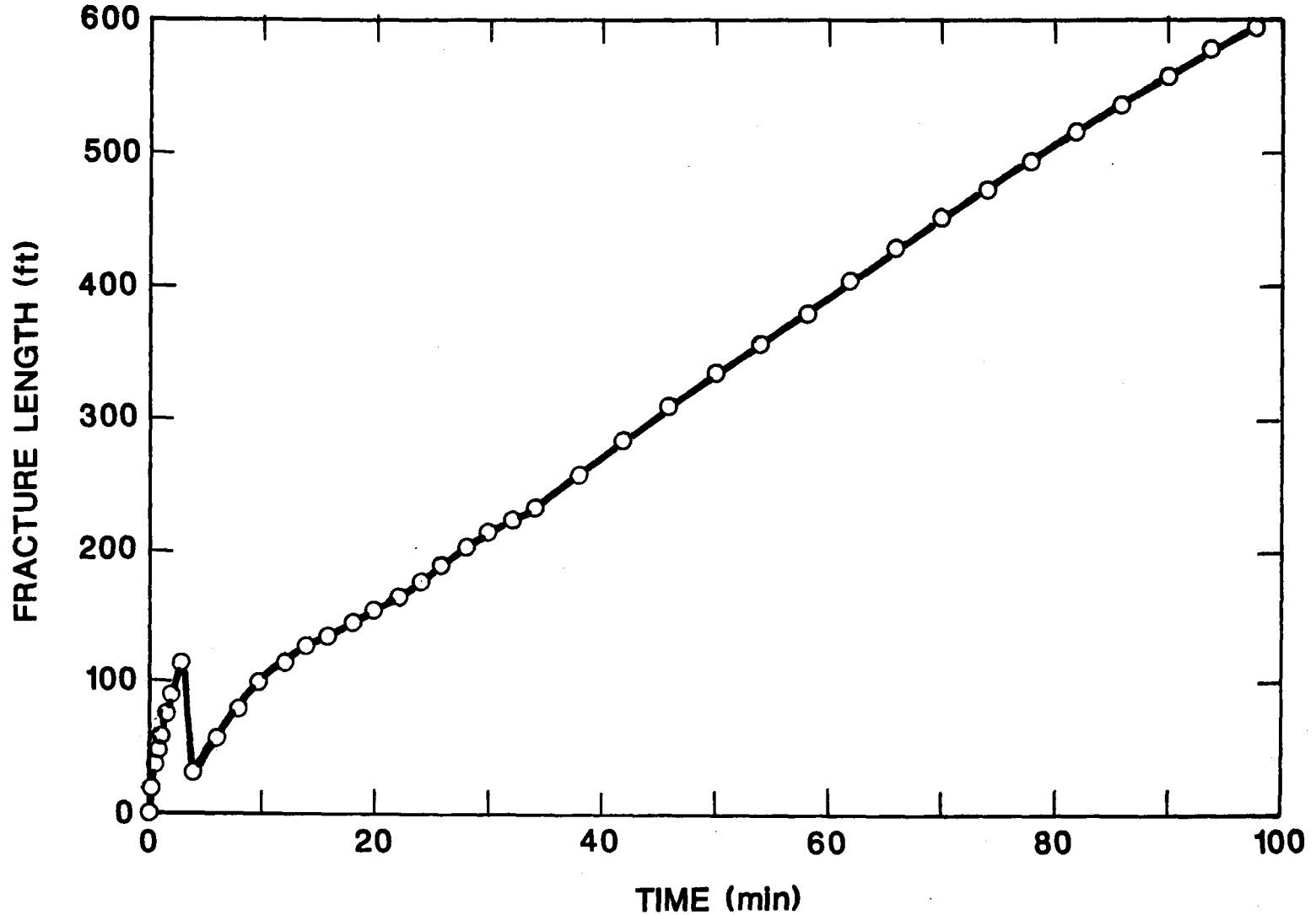

Figure 8.4.32 Pressure History Match Length

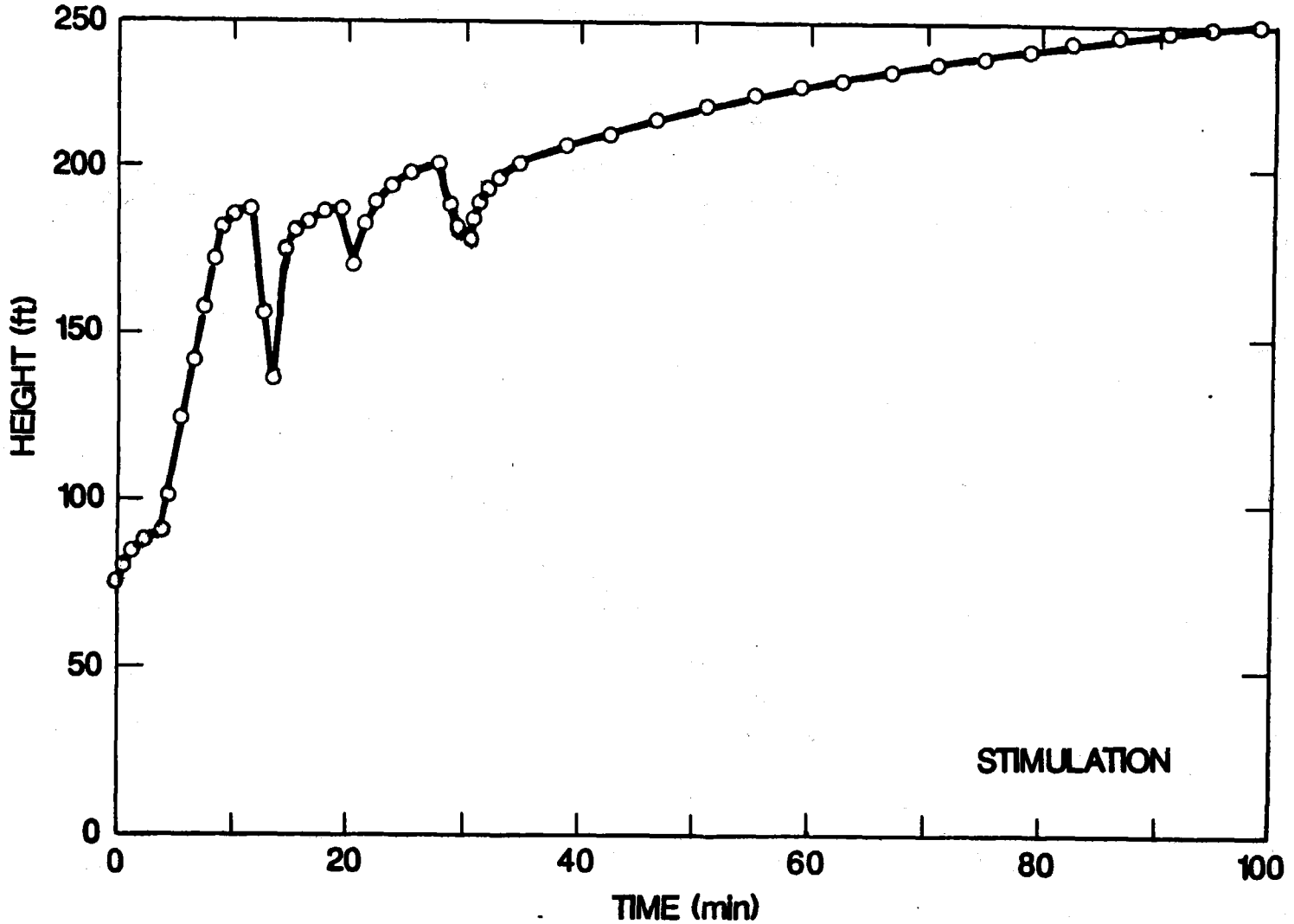

Figure 8.4.33 Pressure History Match Height

8.5 REMEDIAL TREATMENT

P. T. Branagan
CER Corporation

8.5.1 TREATMENT

Upon completion of the Phase I well testing, the Phase II propped fracture treatment was performed. The Phase II treatment consisted of injecting almost 80,000 gal of 3% KCl water with crosslinked hydroxypropylguar (HPG) and 193,000 lbs of 20/40 mesh sand as given in Table 8.4.2. The treatment was performed as designed, with no major operational problems. Early postfracture production was low and cleanup was slow. Frac liquid recovery was relatively good, as shown in Table 8.5.1, although there were still more than 750 bbl remaining in the formation after two weeks. Recovery rates were down to 3-6 bbl/day at the beginning of June. Problems with sand proppant in the wellbore and other operational requirements resulted in several shut-in periods and the need to circulate water on several occasions. These operations hampered the cleanup process and increased the amount of residual liquid to be recovered.

Several short buildups during these cleanup periods indicated that the fracture was very short (~10 ft), as if it was clogged or bridged. Periodic fluid samples were taken and analysis of the organics indicated molecular weights on the order of 2×10^6. It seemed likely that minimizing the amount of breaker in order to assure good proppant transport may have resulted in inadequate breaking of the gel (at least over this few-week period). This may have created a gel plug in the near wellbore region. Since schedule concerns would not allow an indefinite wait for the gel to break thermally, a remedial breaker treatment was designed and conducted. Until the stimulated reservoir could be made to produce, other possible damage mechanisms, such as degrading the matrix rock or crushed proppant plugging fractures, could not be addressed.

The remedial treatment was conducted June 6, 1984, and consisted of 6500 gals of 3% KCl water with 135 lb/1000 gal of ammonium persulfate breaker plus 1000 gal of 3% hydrogen peroxide. This 7500 gal total volume was sufficient to more than fill the entire propped pore volume. The treatment was injected at sufficiently low rates (1-2 bpm) to keep the bottomhole pressure below 6000-6200 psi and thus not reopen the fracture. The maximum surface treating pressure during the pump was 3150 psi. Table 8.5.2 contains data for the remedial treatment.

8.5.2 INJECTION INTERFERENCE TESTING

Bottomhole pressure measurements were acquired from both observation wells, MWX-2 and MWX-3, prior to, during, and after the pumping of the breaker into MWX-1. Downhole shutoff tools were used to isolate the bottomhole HP pressure transducers from the almost 7000 ft of tubing. Figure 8.5.1 is a selected portion of the BHP data acquired from MWX-2. The lower portion of the figure shows the surface pumping pressure in MWX-1 and can be used as a reference for pressure response that was observed in MWX- 2. Note that a small pressure pulse is superimposed on what appears to be the normal pressure recovery of the reservoir and is seen to be concurrent with the pressurization of MWX-1. The response time of this pressure observation is on the order of minutes and thus is most probably the result of a direct fractured connection between MWX-1 and MWX-2.

The BHP acquired from MWX-3 did not show any apparent signs of pressure interference as a result of the injection occurring in MWX-1. This was in part due to sporadic noise that resulted in pressure variations of 2 to 3 psi, which appeared to be in the HP gauge itself. Since the amplitude of the interference pressure pulse observed in MWX-2 was on the order of the noise in MWX-3 and considering the geometry of the wells, this noise is probably well in excess of the amplitude of the

interference pulse at MWX-3 and couldn't have been observed. Nevertheless, it is the authors' opinion that if an interference pulse was present at MWX-3, its amplitude was less than 1 psi and would have been difficult to observe no matter what the disposition of the HP gauge.

As previously discussed, interference pressures were not observed in either MWX-2 or MWX-3 during prefracture testing. However, Figure 8.5.1 clearly shows interference during the remedial treatment. The exact nature of the communication between the two wells is not entirely clear. However, direct flow paths could exist through a combination of the MWX-1 hydraulic fracture, reservoir natural fractures, and/or the MWX-2 fault. It is also possible that the observed interference may be from poroelastic communication where the reopening of the fracture in MWX-1 was transmitted poroelastically through the reservoir to MWX-2. Theory exists to explain this phenomenon, but exact analysis is difficult due to many unknown parameters. Another possible explanation for the injection interference is the stress sensitive permeability of the natural fracture system. Under injection conditions, fracture permeability could be increased considerably.

8.5.3 TREATMENT RESULTS

Following the remedial treatment on June 6, the fracture well, MWX-1, was shut in overnight to give sufficient time for the breakers to act upon the remaining high molecular weight gels. At 0815 hrs, June 7, MWX -1 began production on a 20/64-in. choke. Wellhead pressure was 1,030 psi, which, for a full column of liquid in the tubing, would correspond to about 4,000 psi bottomhole. Returned liquid and sediments were flowed to a 400 bbl tank, and samples were taken approximately every half-hour from the flow line. Table 8.5.3 lists the data for the first five days of flowback, and as of June 11, the well had returned almost 380 bbl of liquids. Liquid production toward the end of June was about double that prior to the remedial treatment. Gas production remained

poor. In fact, gas from the observation well, MWX-2, was injected into the annulus of MWX-1 to enhance its ability to lift liquids. However, this procedure was discontinued due to the lack of further liquid production.

Analyses of returned fluid samples by NIPER indicated the molecular weight of the gels had decreased to well below 100,000. Thus the addition of the chemical breakers did result in breakage of the large molecular chains. The breakers, however, were found to leave a salt precipitate on the cores that were used for the flow tests, and this may have had some impact on the ability of the formation and/or fractures to produce.

As a quality control measure, the remedial treatment fluid was sampled and tested. Field test results given in Table 8.5.4 show the treating fluid contained the proposed concentrations of B-5 breaker and KCl. (Concentration of peroxide was not measured because an adequate field test was not available.) Further analyses were made on samples taken after 40, 80, 120 and 160 bbl of treating fluid were pumped and the results are given in Table 8.5.5. Two samples were taken from each fluid transport. The B-5 breaker (ammonium persulfate) concentration was measured before and after heating the treating fluid. At temperatures above 150°F, ammonium persulfate produces hydrogen peroxide and sulfate anion. Therefore, the increase in sulfate concentration after heating should be a direct indication of the amount of ammonium persulfate present.

Cycling between buildup and production was continued in an attempt to increase liquid recovery. Throughout the cleanup phase, the well configuration consisted of open-ended tubing landed just above the perforations. Gas flow rates were too low to lift or unload the tubing. After a month of gradual cleanup, the well configuration was changed and a packer was set above the perfs with tubing extending below the

perfs. The packer provided better control of bottomhole pressure (at least 800 psi bottomhole pressure is required in the paludal to maintain flow). The extended tubing provided a method to remove liquids from the perforations. About 50 bbl of liquid were recovered immediately and gas flow rates in excess of 100 MCFD were maintained. At this point, the total recovery of all load fluids was over 80%.

Table 8.5.1 Phase II Propped Frac Liquid Recovery

Date	Total Liquids Injected (bbl)	Total Liquids Recovered (bbl)	Percent Recovered (%)	Ammonium Thiocyanate, SCN (ppm)	Remarks
5-2-84	2253	0	0	100	Phase II Frac
5-3-84	2253	480	21	100	Begin Flowback; Sand at 7,050 ft in Wellbore
5-4-84	2253	1120	50	72	
5-5-84	2253	1208	54	50	
5-6-84	2253	1208	54	50	
5-7-84	2617	1296	50	54	364 bbl Added During Wellbore Sand Cleanup
5-8-84	2617	1296	50	54	Temp/Gamma Ray Survey
5-9-84	2617	1490	57	58	
5-10-84	2617	1490	57	58	
5-11-84	2617	1490	57	58	
5-12-84	2617	1523	58	40	
5-15-84	2617	1523	58	40	
5-21-84	2617	1571	60	41	
5-24-84	Workover Rig on MWX-1 through 5-31-84 to Remove Packer; 620 bbl Added During Workover				
5-31-84	3257	2461	75	23	
6-1-84	3257	2476	75	24	
6-2-84	3257	2481	76	20	
6-3-84	3257	2485	76	20	
6-4-84	3257	2488	76	24	
6-5-84	3257	2492	77	29	
6-6-84	Remedial Chemical Breaker Injection				

Table 8.5.2 Remedial Treatment Data from Phase II

Post-Fracture Breaker Injection

Treatment Fluids/Ingredients:

3% KCl Water	6,500 gals
5% Hydrogen Peroxide	1,000 gals
B-5 Breaker	975 lbs

Total Liquids to Recover:

Treatment	7,500 gals (179 bbl)
Tubulars/Flush	10,248 gals (244 bbl)
Total Liquids	17,748 gals (423 bbl)

Treatment Parameters:

Date	June 6, 1984
Time	10:20 to 12:23 (2.05 hrs)
Average Rate	1.45 bpm
Maximum Surface Pressure	3,150 psi

Table 8.5.3 Liquid Recovery from Remedial Breaker Injection

Date	Daily Liquid Prod. (bbl)	Cumulative Prod. (bbl)
June 7	220	220
June 8	125	345
June 9	-	-
June 10	32	337
June 11	5	382

Table 8.5.4 Remedial Treatment Quality Control

	Design Fluid	Field Results
KCl water	3% (2.6% w/dilution)	2.8% (2.4% w/dilution)
Hydrogen Peroxide	5%	Not Tested
Breaker B-5	150 lbs/1,000 gals (130 lbs/1,000 gals w/dilution)	140 lbs/1000 gals (120 lbs/1000 gals w/dilution)

Table 8.5.5 Remedial Treatment Fluid Analysis

	Room Temperature				Elevated Temperature			
Sample (bbl)	40	80	120	160	40	80	120	160
Sulfates (mg/ℓ)	1100	1700	1000	1250	15,000	15,000	12,500	10,000
Temperature (°F)					150°	180°	190°	160°
Chlorides (mg/ℓ)-								
Sample 1	11,000	10,500	11,250	13,000				
Sample 2	11,800	-	-	11,000				
Average	11,400	10,500	11,250	12,000				
pH	2	2	2	2.5	3.5-4.0		3.5-4.0	

Note: Chlorides from site KCl water = 12,500 mg/ℓ

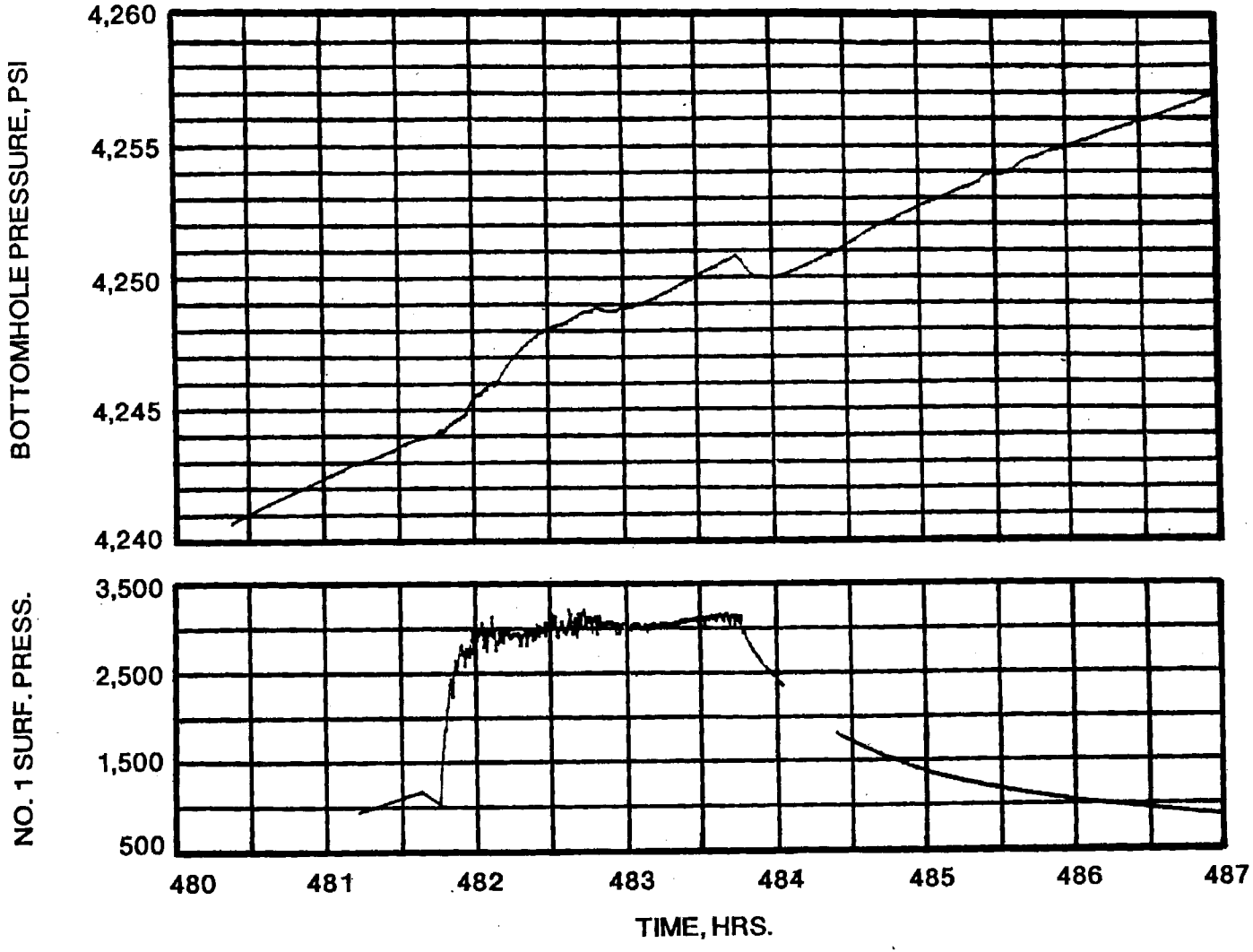

Figure 8.5.1 MWX-1 Surface Pressure and MWX-2 Bottomhole Shut-In Pressure During MWX-1 Breaker Injection

8.6 POSTFRAC WELL TESTING

P. T. Branagan
CER Corporation

8.6.1 MWX-1 PRODUCTION/INTERFERENCE TESTING

The objective of the post-Phase II well testing was to determine the changes in production due to the inclusion of the propped fracture and to characterize the fracture. Borehole seismic data indicated the orientation of the propped fracture to be essentially the same as that of the unpropped Phase I fracture, as was seen in Figure 8.1.8. As with prefrac testing data, analysis was conducted using both analytical techniques and computer reservoir modeling.

Following the remedial breaker injection and the cleanup period, the post-Phase II well testing commenced. As before, bottomhole pressure gauges were positioned in the offset wells, MWX-2 and MWX-3, to record any possible interference pressures. A third bottomhole pressure transducer was lowered in MWX-1 to record bottomhole flowing and shut-in pressures.

The postfrac production/interference test consisted of 33 days of well testing. As shown in Figure 8.6.1, the initial 2-3 days of production was still dominated by cleanup and liquid production, but the rate was soon stabilized at about 150 MCFD. Six days of production were followed by a 2-day buildup, a 5-day drawdown, a second 2-day buildup, a 7-day drawdown and a final 11-day buildup. The flow rate during all drawdowns was about 150 MCFD at bottomhole pressures of 1200-1900 psi. A listing of relevant data is given in Appendix 12.7.4.

Figure 8.6.2 shows the bottomhole pressures in the offset wells correlated with the MWX-1 production data. Some pressure disturbances occur in MWX-2 and MWX-3; however, these disturbances are very irregular.

They do not appear to correspond to the induced pressure behavior in MWX-1 in any time-related manner; that is, the time between a change in rate and pressure in MWX-1 and the interference response in MWX-2 or MWX-3 should be constant, but no constant differences are seen. Qualitatively, the observed pressure interference responses support the possibility of communication between the wells, but no analysis is tractable for irregular behavior. Some possible causes of this behavior include stress-sensitive, natural-fracture flow capacity, poorly interconnected reservoir segments, near-wellbore liquids effects at the offset wells, the thinning of zone 3 towards MWX-3, and the fault near MWX-2.

The maximum sustainable post-Phase II gas production was found to be about 150 MCFD, substantially below the 250 MCFD prefrac production test data. This production decline indicates that some additional formation and/or natural fracture degradation had probably occurred. A Horner plot of the last post-Phase II buildup data, shown in Figure 8.6.3, exhibited a shape characteristic of a hydraulically fractured well, indicating that a fairly conductive fracture was created.

Square-root-of-time analysis, as previously described, was also applied to the data from the last buildup. Figure 8.6.4 shows the three buildups on a square-root-of-time plot. Assuming infinite fracture conductivity, fracture half-lengths from 65 to 100 ft were calculated and were considerably shorter than the 400- to 500-ft design lengths. These analyses indicate that a shorter conductive fracture was created or the projected channel width was only 130-200 ft.

As mentioned previously, prefrac production from zones 3 and 4 was primarily a function of the natural fracture flow capacity and a 65-100 ft fracture should have provided some measurable increase in productivity. The postfrac well testing data, with the reduced flow rate, suggest that the natural fracture system was somehow altered and

diminished in its ability to contribute to productivity as a result of the treatment.

An examination of Figures 8.1.7, 8.3.2 and 8.6.3 indicates a steady decline in projected reservoir pressure from initial prefrac testing to final post-Phase II well tests. The decline in projected reservoir pressure could indicate a limited reservoir or a complex drainage pattern and is most certainly influenced by the existence of a natural fracture system.

8.6.2 RESERVOIR MODELING AND HISTORY MATCHING

To simulate this hydraulically fractured reservoir, with the possibilities of narrow channels, short fracture lengths, and damage adjacent to the hydraulic fracture, a numerical model was designed with the areal dimensions shown in Figure 8.1.9. Because of the reservoir and hydraulic fracture complexity, initial analyses were performed with a single-layer, single- phase, single-porosity reservoir simulator.

While analytical methods indicated the existence of a conductive fracture, the average gas production had decreased from previous tests, so it was assumed that the flow capacity of the natural fracture system adjacent to the hydraulic fracture was probably diminished. The objectives of the modeling were to estimate the depth and value of reduced permeability in this diminished zone as well as provide an estimate of the length and conductivity of the hydraulic fracture.

Initially, the simulator assumed that the undamaged average reservoir permeability was 36 μd, a value based on the prefrac well tests and modeling. Propped fracture half-lengths between 75 and 400 ft with varying permeabilities were then introduced, along with a small damaged zone that surrounded this fracture geometry. The depth of this damaged zone was varied from 0 to 40 ft, and the permeability from 0.6 to

3.0 μd. To simulate the effects of earlier production on the testing transients, initial reservoir pressure was taken to be 5300 psi and then diminished by varying cumulative production in a range from 3 to 10 MMCF over the long periods of testing and production. In order to show the sensitivity of the model to certain reservoir parameters, several simulations are presented. Some show reasonable matches with the data, while others show significant disparity and are not possible solutions.

Figure 8.6.5 shows example simulations for a 250-ft hydraulic-fracture wing length with several different damage cases overlaid on the field data. The data at the top describe the three simulations shown. Total Q is the volume of gas produced prior to the start of the simulation, K_{damage} is the value of the reduced permeability zone adjacent to the hydraulic fracture and X_{damage} is the depth of the damaged zone. Note that no reasonable simulations can be made with wing lengths of 250 ft or larger.

Figure 8.6.6 shows similar data for a 150-ft fracture length. The drawdown pressures are closer to the field data, but the final buildup is still not accurately represented.

Figure 8.6.7 shows a much closer simulation with a hydraulic-fracture wing length of 80 ft. These results also show the importance of including in the model all production prior to the flow test. Note the difference in the drawdown pressures for 6 MMSCF of previously produced gas compared to 9 MMSCF of previously produced gas. The initial conditions are critical for this type of analysis.

Figure 8.6.8 shows the simulation runs for the best-match fracture wing length, 75 ft. These modeling runs were found to provide very adequate pressure history matches for MWX-1, when the fracture half length was taken to be 75 ft, initial reservoir pressure was 5300 psi, and undamaged bulk formation permeability was 36 μd. Further, cumulative

gas production prior to the post-Phase II test was about 8 MMCF and the zone of diminished permeability was characterized as 2.4 μd, extending 9 ft into the formation adjacent to the propped fracture.

The areal extent or the boundary effects of zones 3 and 4 and the propped fracture were also studied. Computer model runs were performed varying channel width and propped fracture half-lengths with all other parameters being the same as above. Figure 8.6.9 shows simulation runs for a 75-ft channel that contains a 75-ft or a 400-ft hydraulic fracture length. The results indicate that only 75 ft of conductive fracture length (one wing) was observed in the testing and that channels of wider dimensions were indistinguishable from a 75-ft channel. Further, longer propped fractures that might extend beyond the channel and into nonproductive zone, such as a shale, would yield results similar to the fixed productive channel width.

The final aspect of the modeling consisted of analyzing the effects of propped fracture conductivity on the pressure history at MWX-1. It was found that increasing fracture conductivity from 16 to 160 md-ft (1 to 10 darcies) would have little effect on pressures measured at MWX-1. These simulations are shown in Figure 8.6.10. The final best-match for the single-phase, single layer, single-porosity simulation is shown in Figure 8.6.11.

The postfrac reservoir modeling allowed an in-depth characterization of reservoir and propped fracture parameters. The modeling indicated that the natural fractures system adjacent to the propped hydraulic fracture was probably no longer capable of enhancing formation matrix production, and that the reservoir permeability near the hydraulic fracture had been diminished to approximately the matrix values, 1 to 3 μd. The extent of this damaged zone was extensive enough to eliminate any production increase from the propped fracture, with overall production capacity actually being impaired. The conductive half-length

of the propped fracture was estimated at 75 ft with a minimum conductivity of 16 md-ft (1 darcy). The total width of the paludal channel could be as small as 150 ft, but test results cannot clearly distinguish between larger widths and a fixed 75-ft conductive fracture.

The previous simulation results provided input and guidance for the two-porosity simulations. The importance of the 10 to 1 anisotropy ratio becomes clear when modeling of the damage is attempted. Larger anisotropy ratios are difficult to damage because of the small cross fracture transmissibility relative to the matrix transmissibility. Smaller anisotropy ratios are possible, but they will result in even larger pressure responses in the offset wells, responses that were not observed. The 10 to 1 ratio is the largest anisotropy ratio that could provide a suitable match of the prefrac field data and also result in the productivity reduction to 150 MCFD due to some damaged zone of limited depth. Of course, larger anisotropy ratios are possible if the damaged zone is allowed to extend more than a few tens of feet into the reservoir. Figure 8.6.12 shows the simulated production for a damaged natural fracture.

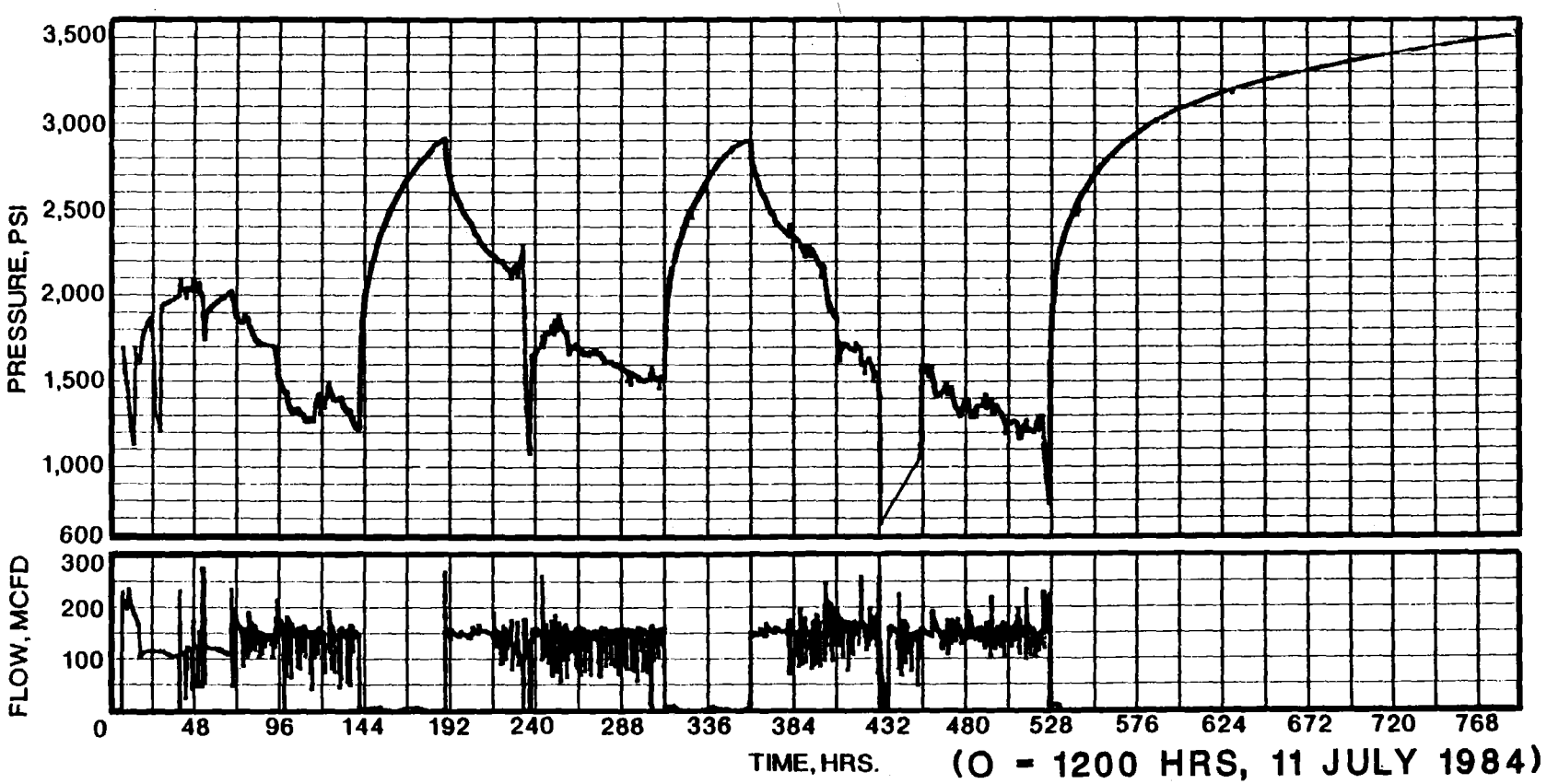

Figure 8.6.1 Post Phase II Well Testing Surface Flow Rate and Bottomhole Pressure

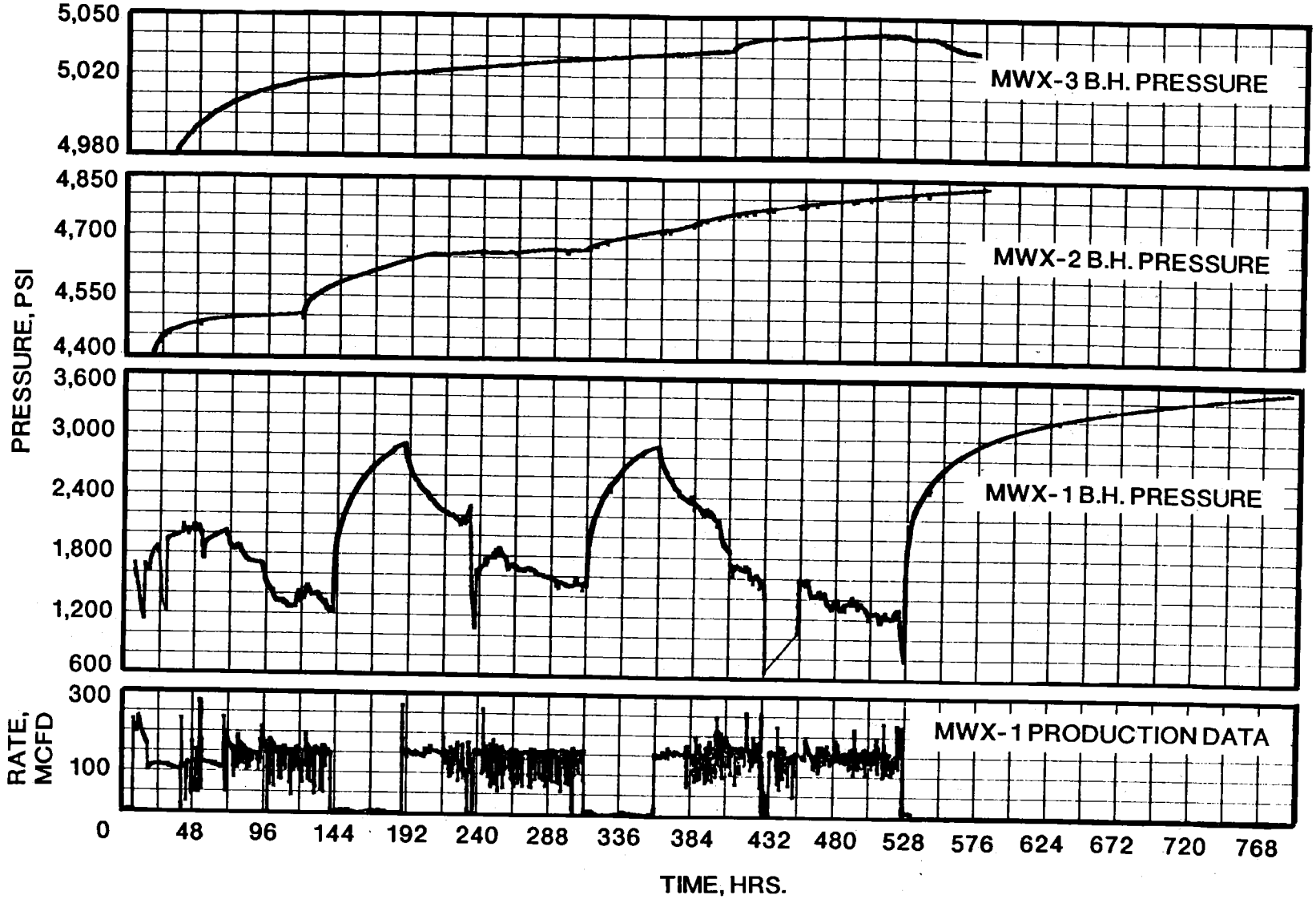

Figure 8.6.2 Post Phase II Well Testing Surface Flow Rate and Bottomhole Pressure Data for MWX-1 and Shut-In Bottomhole Pressure Data for Observation Wells MWX-2 and MWX-3

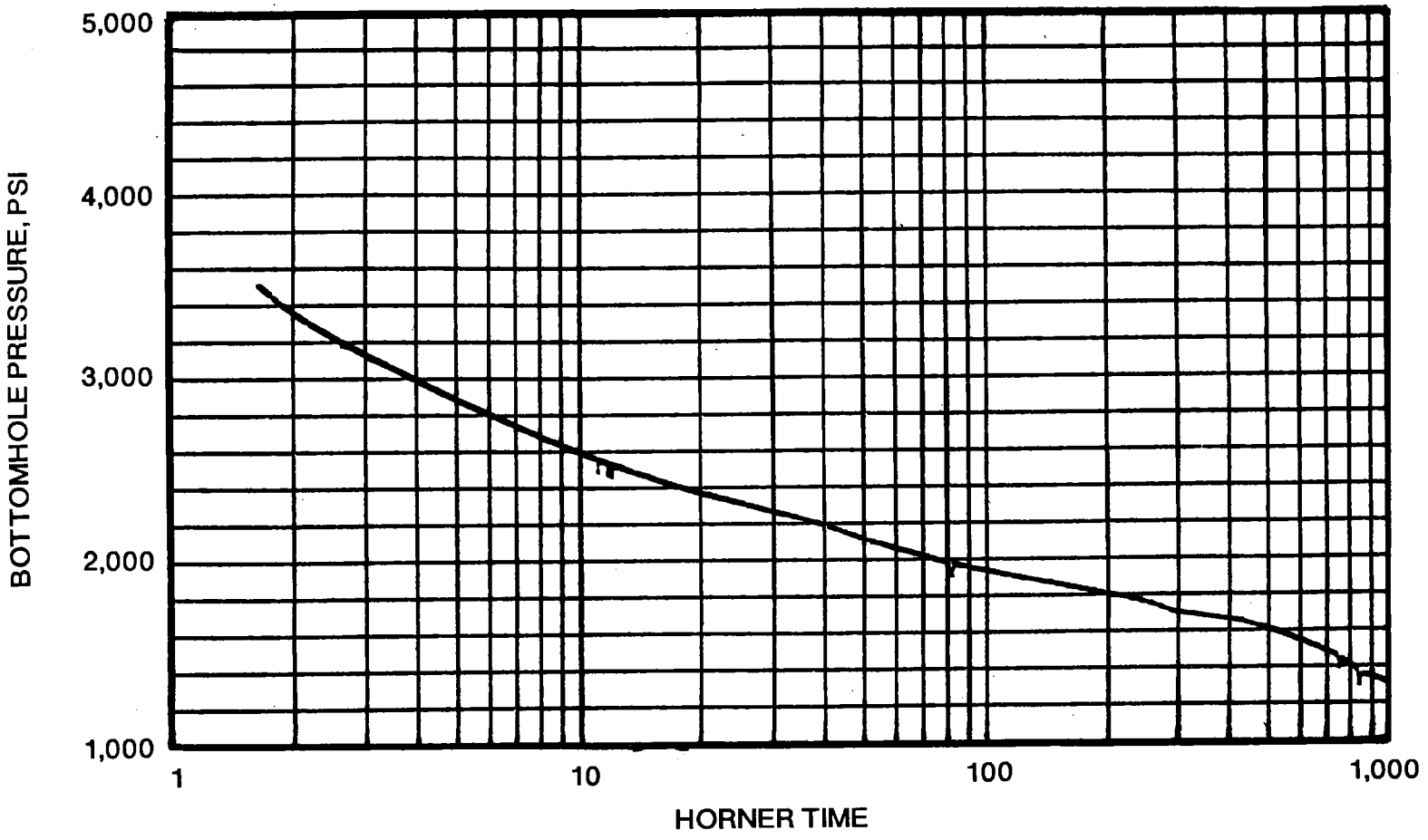

Figure 8.6.3 Horner Plot of Post Phase II Pressure Buildup Data

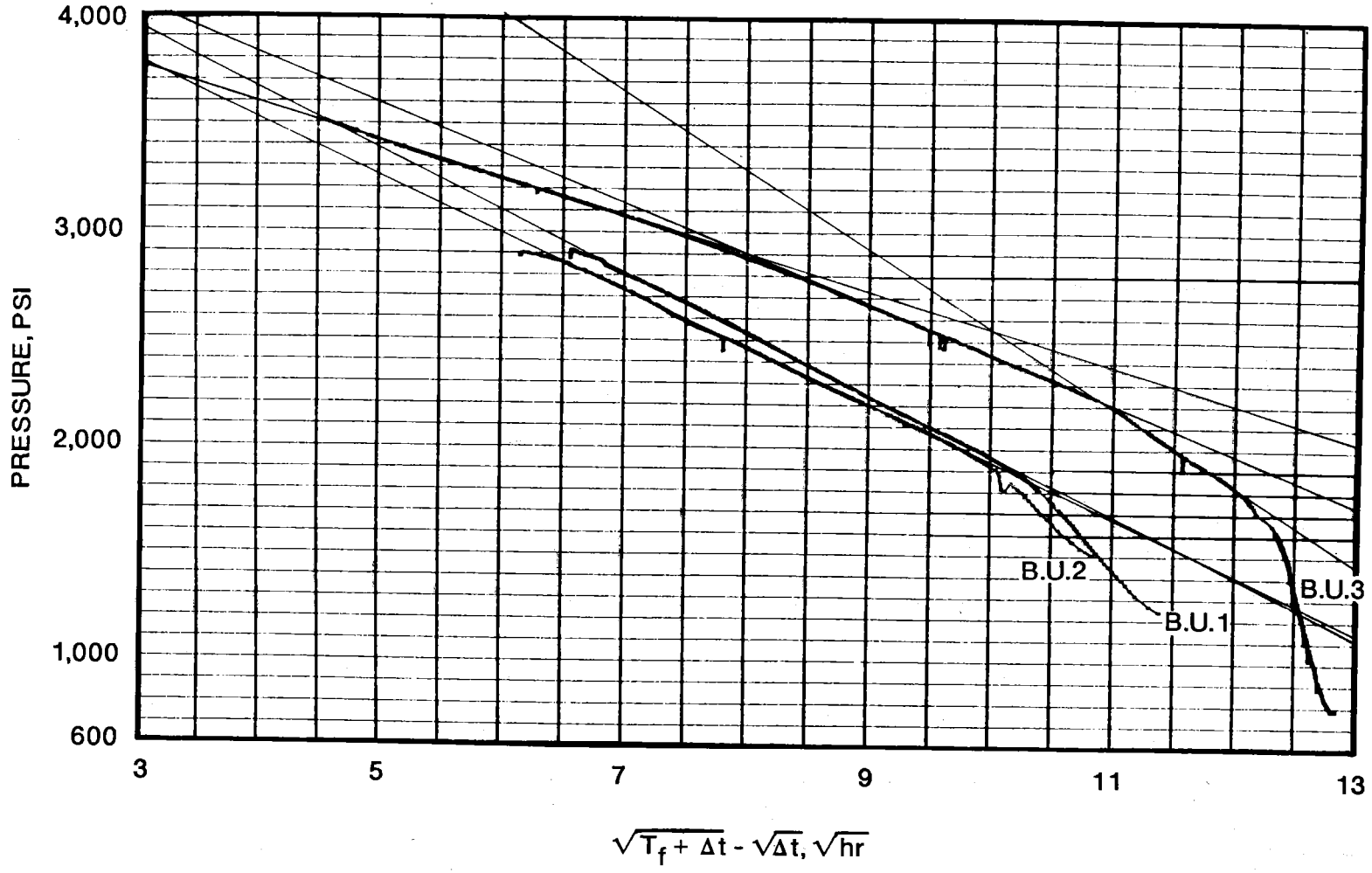

Figure 8.6.4 Square Root of Time Plots for the Three Buildup Periods in the Post Fracture II Well Tests

Run No.	k_{res}	P_i	Total Q	x_f	k_{damage}	x_{damage}
A-952	36 μd	4500	10 MMCF	250	0.6μd	11 ft
B-951	36 μd	4500	7.9 MMCF	250	1.2 μd	25 ft
C-950	36 μd	4500	5.6 MMCF	250	1.0 μd	23 ft

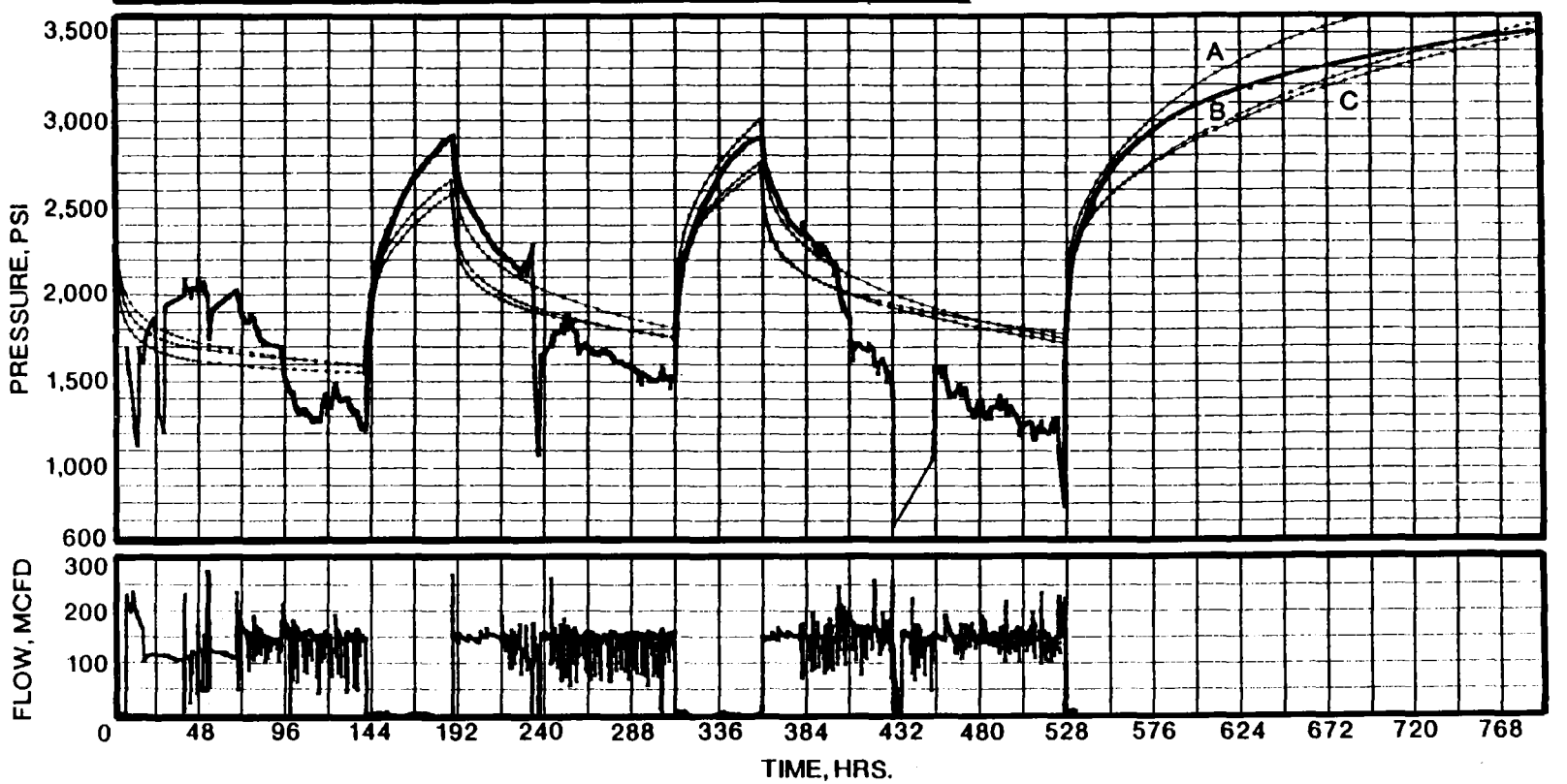

Figure 8.6.5 Model History Matching of the Test Data, Where the Model Fracture Length of 250-ft was Fixed While Pre-Test Production and Fracture Damage Parameters were Varied

Run No.	k_{res}	P_i	Total Q	x_f	k_{damage}	x_{damage}
A-932	36 μd	5300	9.6 MMCF	150	0.9 μd	13 ft
B-933	36 μd	5300	9.2 MMCF	150	1.2 μd	20 ft
C-934	36 μd	5300	7.7 MMCF	150	1.8 μd	40 ft
D-931	36 μd	4500	3.0 MMCF	150	0.9 μd	15 ft

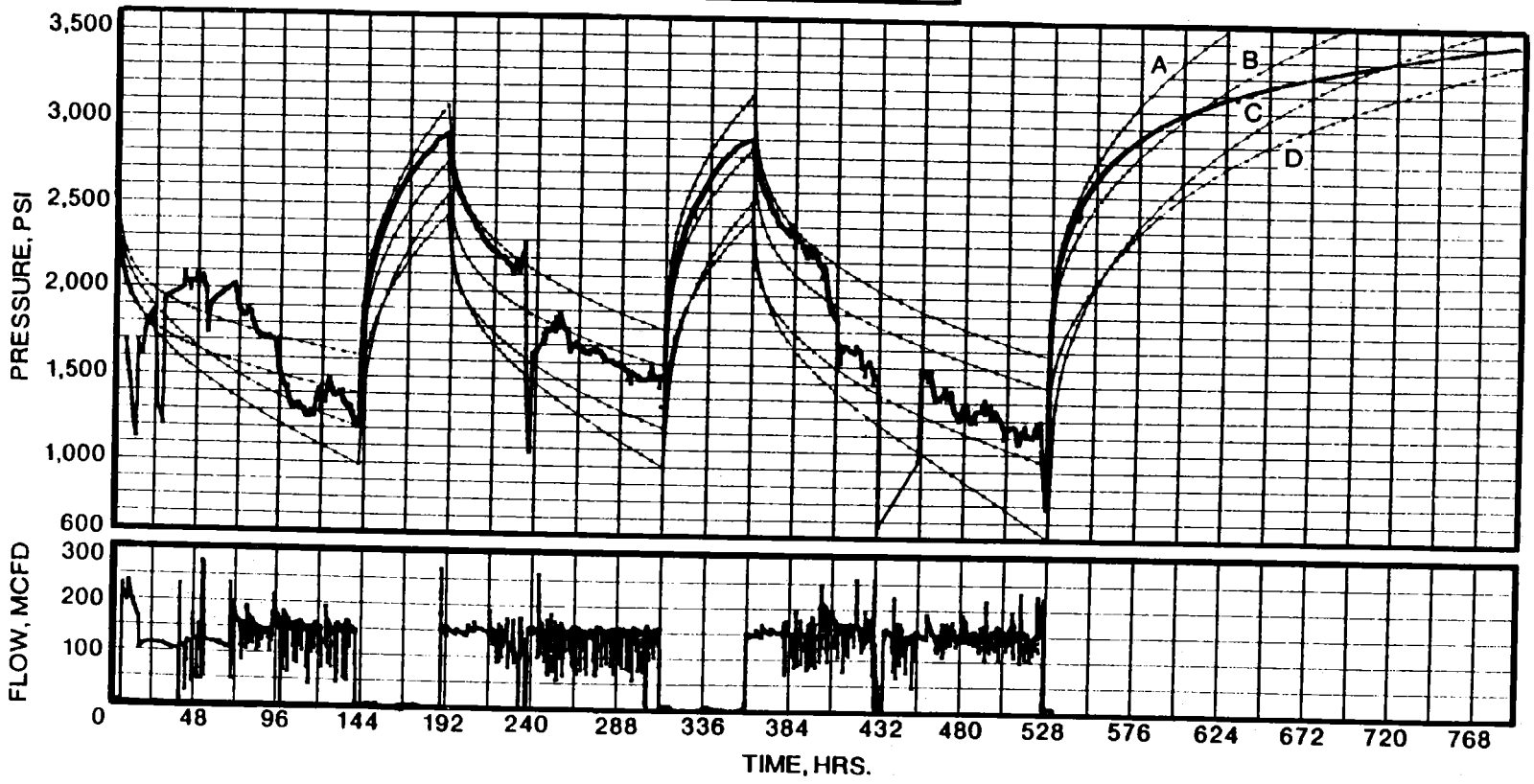

Figure 8.6.6 Model History Matching of the Test Data, Where the Model Fracture Length of 150-ft was Fixed While Pre-Test Production and Fracture Damage Parameters were Varied

Run No.	k_{res}	P_i	Total Q	x_f	k_{damage}	x_{damage}
A-983	36 μd	5300	9.0 MMCF	80	3 μd	10 ft
B-982	36 μd	5300	8.0 MMCF	80	3 μd	15 ft
C-981	36 μd	5300	9.6 MMCF	80	2 μd	8 ft
D-984	36 μd	5300	9.5 MMCF	80	1.5 μd	6 ft
E-980	36 μd	5300	6 MMCF	80	2 μd	15 ft

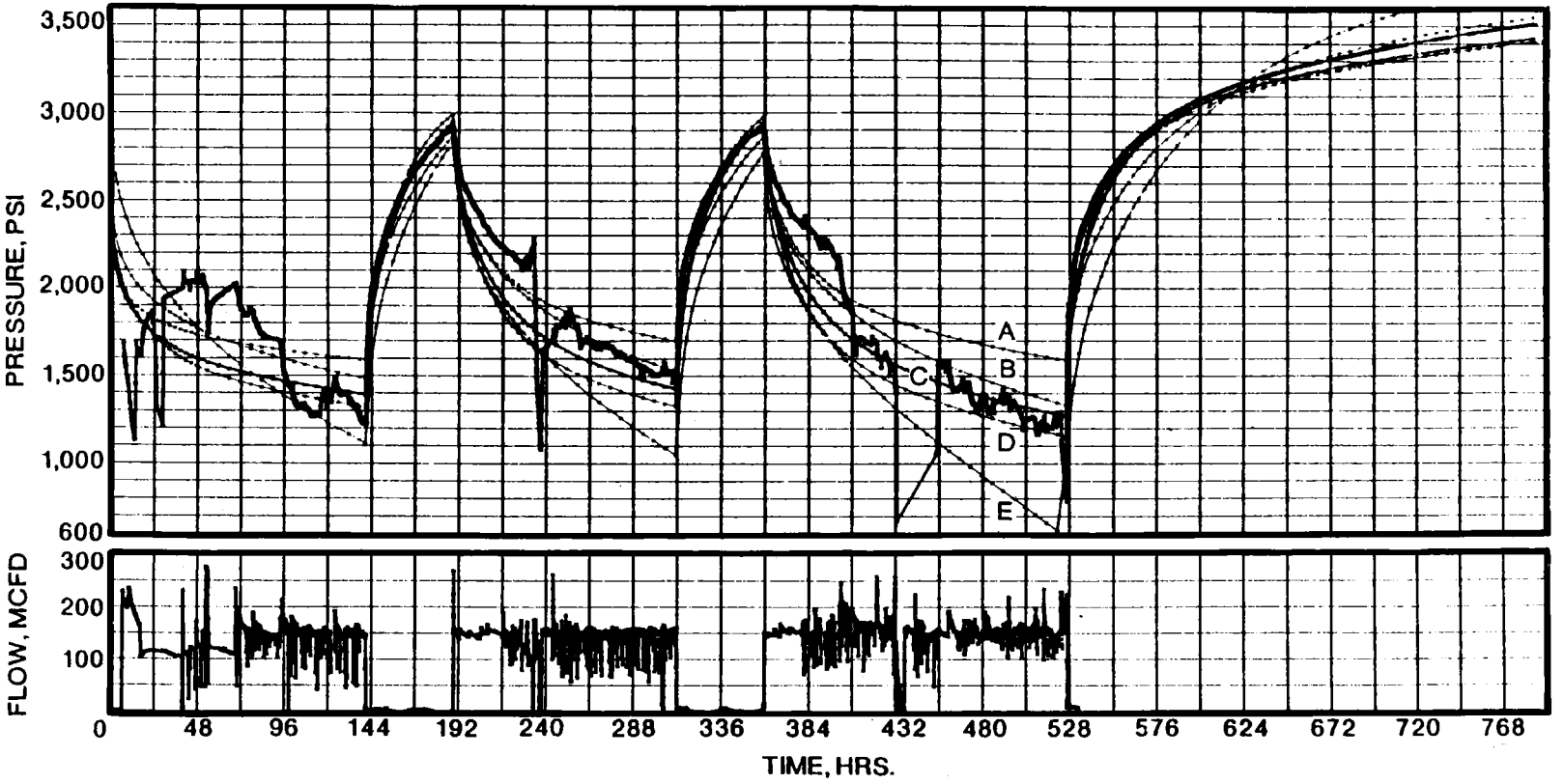

Figure 8.6.7 Model History Matching of the Test Data, Where the Model Fracture Length of 80-ft was Fixed While Pre-Test Production and Fracture Damage Parameters were Varied

Run No.	k_{res}	P_i	Total Q	x_f	k_{damage}	x_{damage}
A-985.2	36 μd	5300	7 MMCF	75	3 μd	12 ft
B-990	36 μd	5300	8.0 MMCF	75	2.4 μd	9 ft
C-986.2	36 μd	5300	8.25 MMCF	75	2 μd	7 ft
D-987	36 μd	5300	8.0 MMCF	75	1.8 μd	7 ft

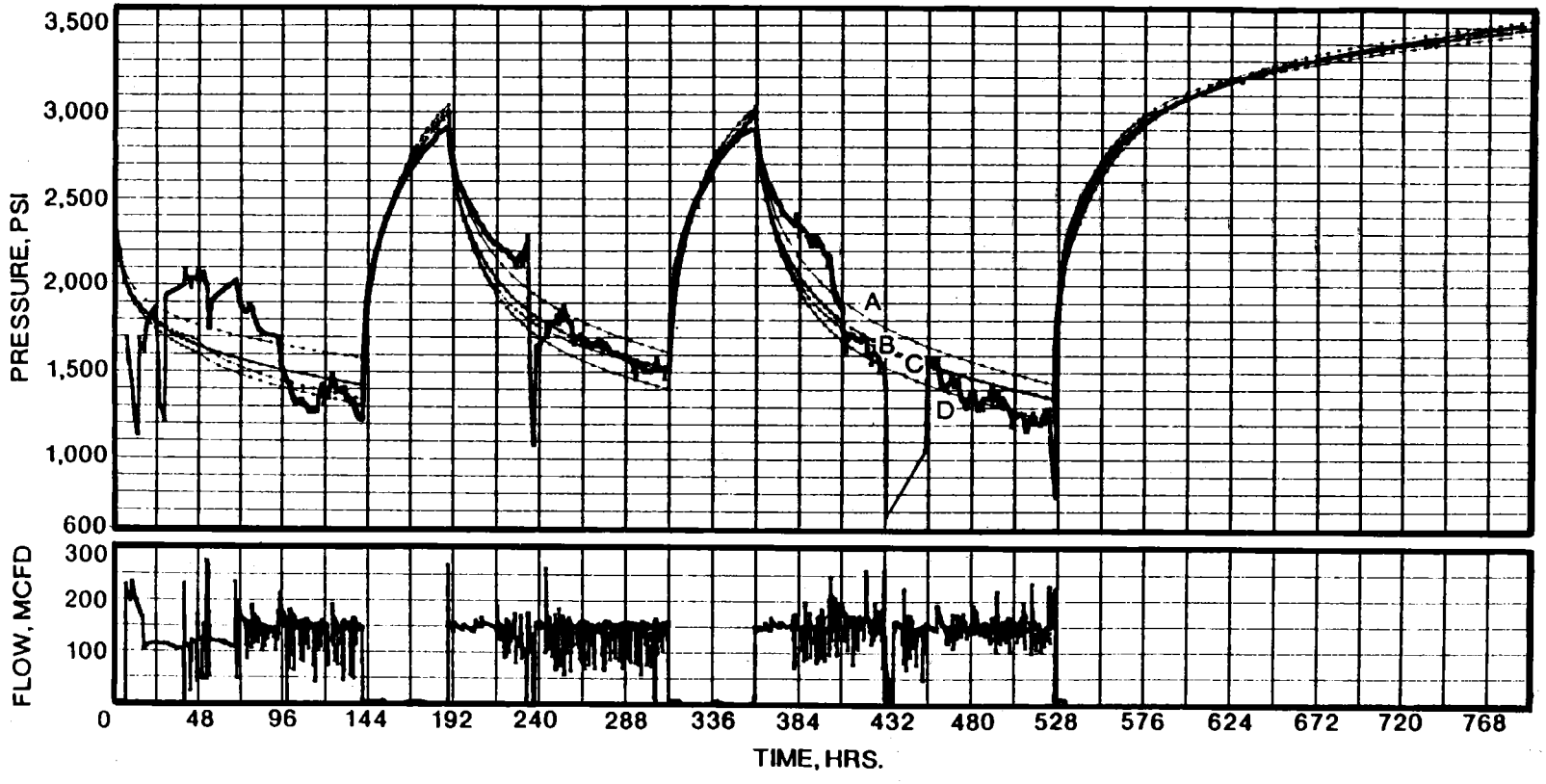

Figure 8.6.8 Model History Matching of the Test Data, Where the Model Fracture Length of 75-ft was Fixed While Pre-Test Production and Fracture Damage Parameters were Varied

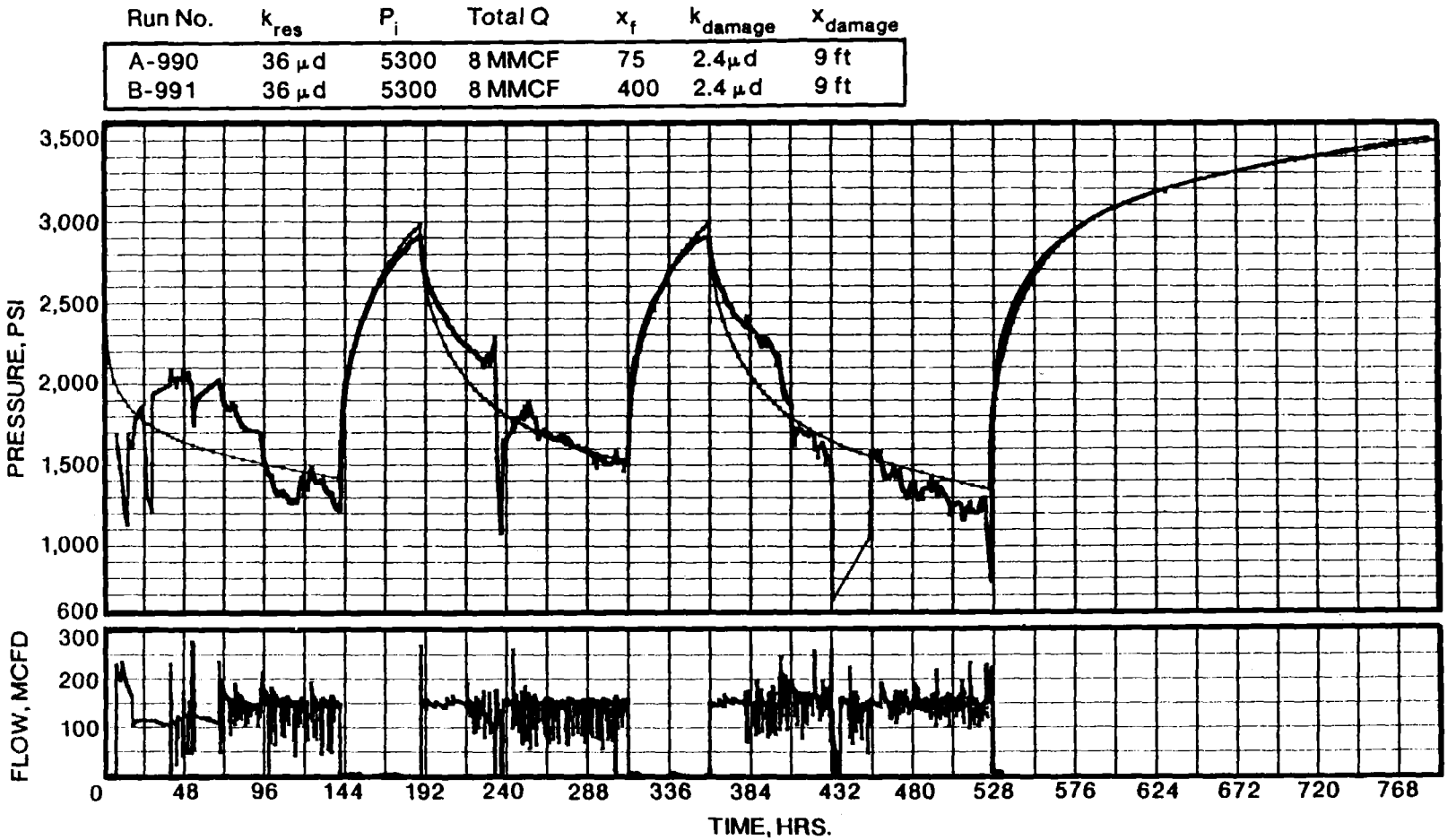

Figure 8.6.9 Model History Matching of Test Data Showing the Almost Negligible Effect Fracture Length Would Have if it Exceeds the Channel or Productive Interval of 75-ft

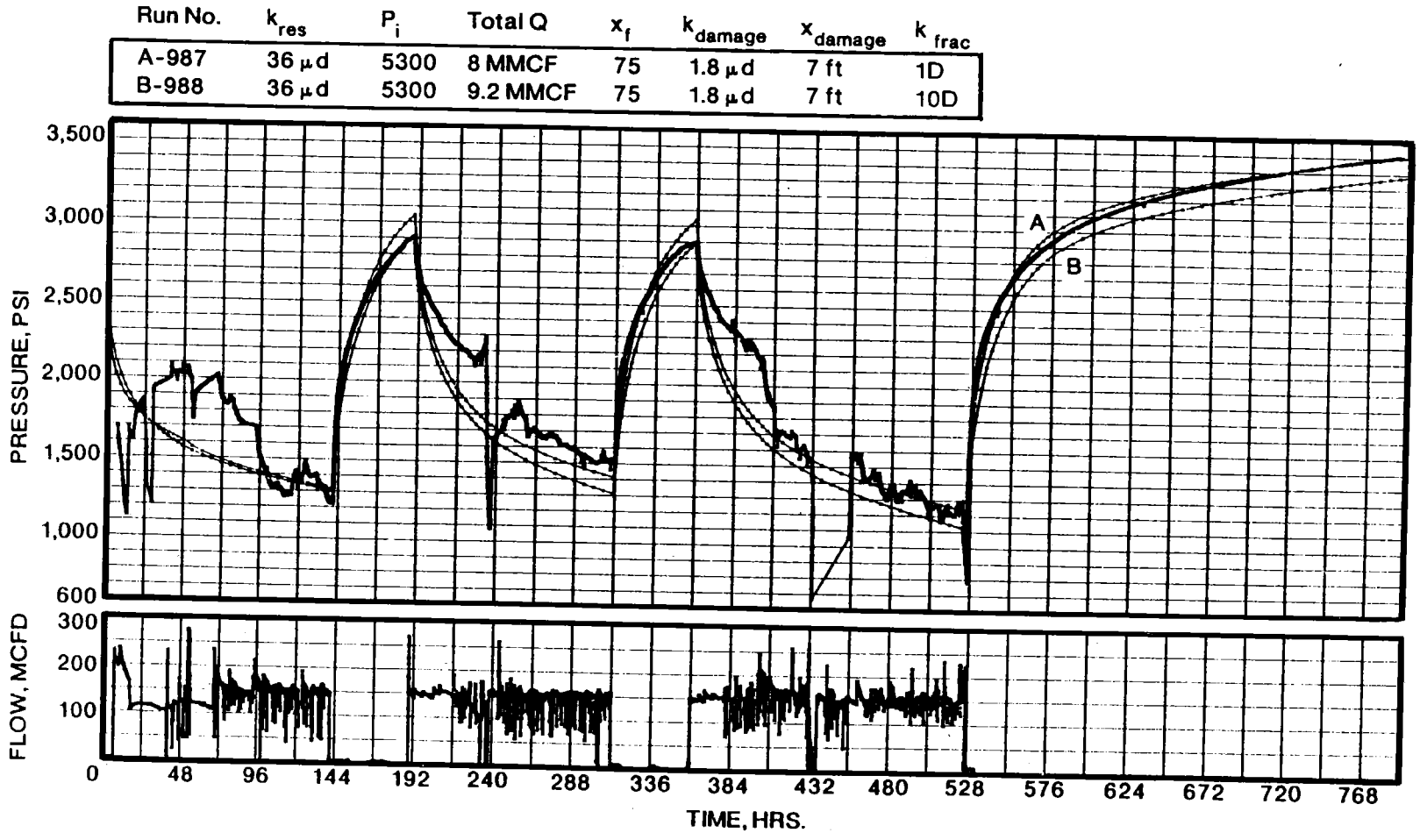

Figure 8.6.10 Model History Matching of the Test Data Showing the Small Effects of Varying Fracture Conductivity

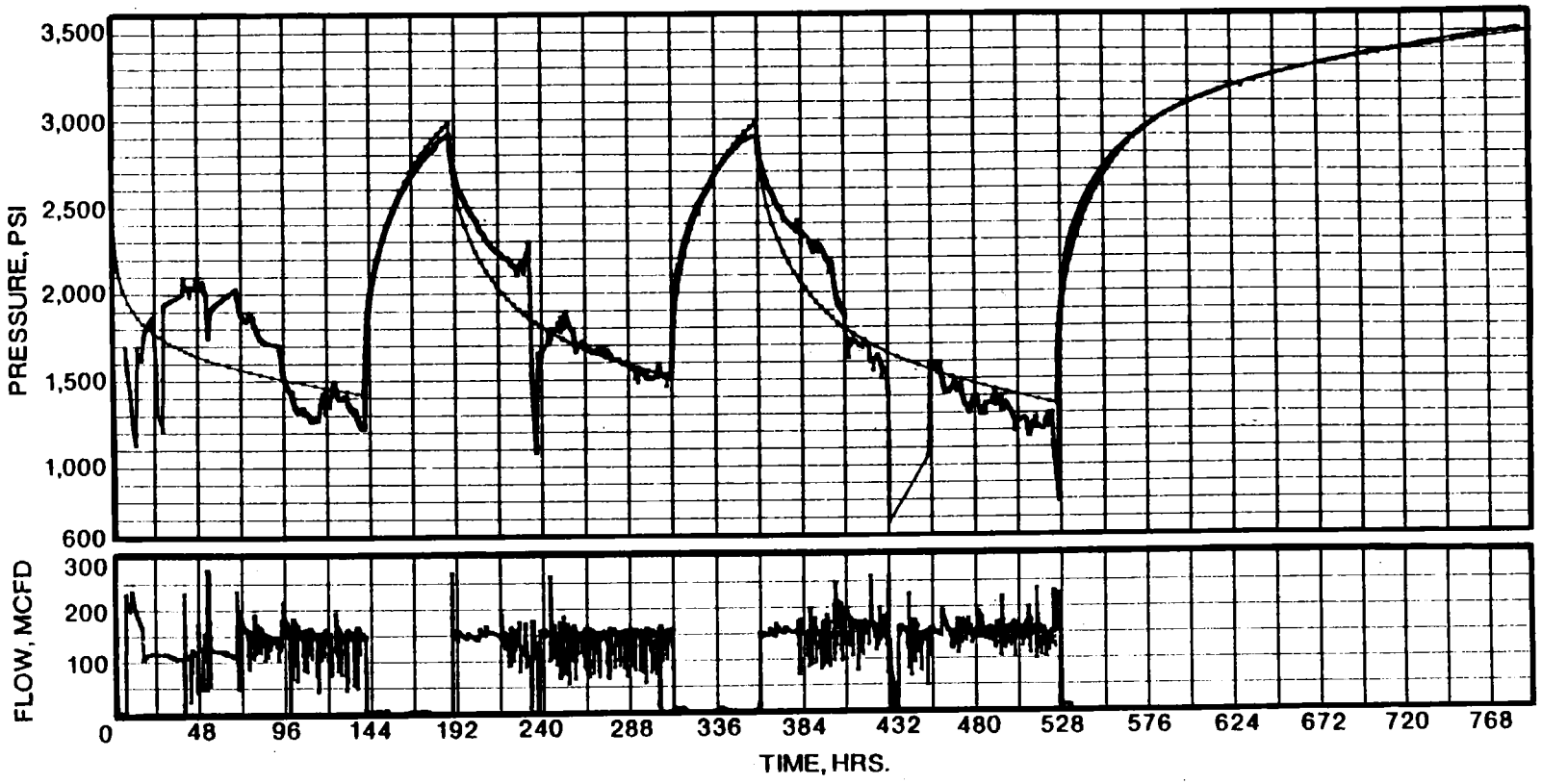

Figure 8.6.11 Reservoir Model History Match of Post Phase II Well Test Data

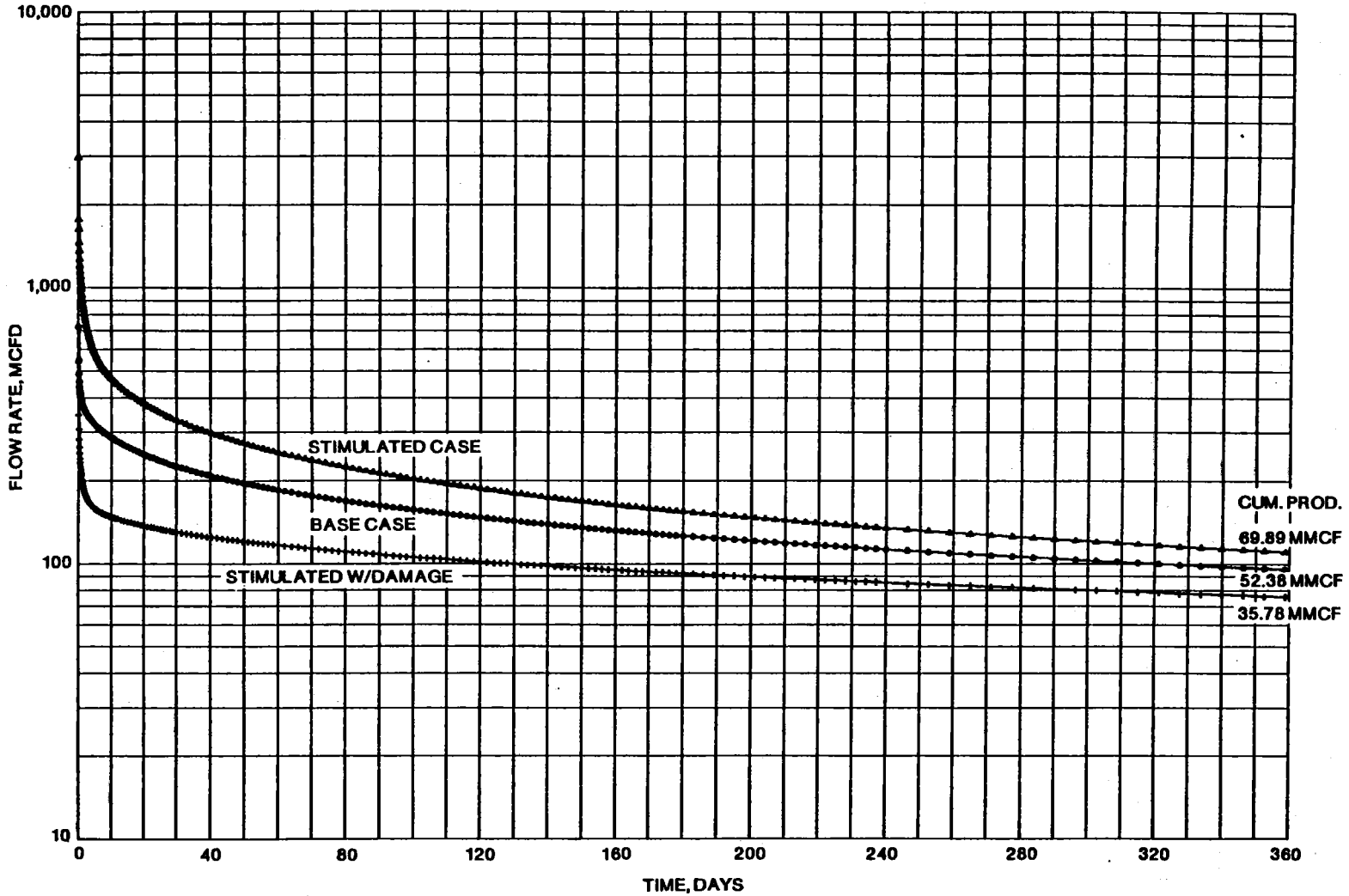

Figure 8.6.12 Simulated 1-Year Production History for the Paludal Base Reservoir, a Stimulated Case and Stimulated Case with a Small Damage Zone Surrounding the Propped Fracture

8.7 REENTRY WELL TESTING

P. T. Branagan
CER Corporation

8.7.1 TESTING

Testing of these paludal zones was suspended in mid-August, 1984 in order to test other zones uphole. Schedule and budget constraints would not allow an indefinite cleanup period in which to attempt to correct reservoir damage. However, in late March, 1986 (20 months later), an opportunity arose to retest these zones to evaluate any time dependence of the suspected damage.

Bottomhole pressure bombs were set in MWX-1 at 7000 ft on March 21, 1986. These two pressure bombs, a Kuster with a 5500 psi max pressure and a Squire Whitehouse with a 10,000 psi max pressure, were set to monitor bottomhole pressure before and during the early portion of the flow test period. Once the surface tubing pressure decreased to about 2500 psi, an HP pressure gauge replaced these bombs in the bottom of MWX-1. Unfortunately, there was no opportunity to place pressure gauges in the offset wells at these depths to try and measure interference.

Preparations were made to flow MWX-1 into the Western Slope pipeline through the MWX/CER separator and flow meter. Real time surface pressure measurements were made using both a high resolution HP pressure gauge and a standard surface pressure gauge. Flow rates were monitored using the MWX/CER flow metering system and then were compared with Western Slope's circular chart.

Production from zones 3 and 4 began on March 24, 1986 and flow continued for seven weeks. Figure 8.7.1 shows the gas and water production rate and the bottomhole pressure. Initial gas production rate during the first 10 days was in excess of 400 MCFD, while the latter 30

days exhibited gas production rates of about 325 MCFD. These gas production rates can be compared to the initial prefrac rate of 250 MCFD (see Figure 8.1.6) and the postfrac production rate of 150 MCFD (see Figure 8.6.1). The improvement in gas production after the 18-month shut-in appears to confirm the transitory nature of the damage mechanisms. After 40 days, the well was shut in through a series of steps in the flow rate to evaluate water productivity as a function of gas flow rate. At the end of the buildup, the well was flowed briefly to determine if the remaining liquids in the wellbore, hydraulic fracture, and natural fracture would cause problems restarting gas production. However, normal production was easily resumed. A listing of all relevant data is given in Appendix 12.7.5.

It is interesting to note that the water production rate during the reentry testing period ranged from 20 to 40 BWPD, while there was little appreciable water production during previous testing. The fracturing fluid had been tagged with a thiocyanate tracer at a concentration of 100 ppm. Thiocyanate was found to be present in the produced reentry water at an almost constant concentration of 8 ppm. Volumetric accounting of injected and recovered liquids showed that produced liquids were well in excess of the injected fracturing liquids, thus indicating that formation water was being produced. Figure 8.7.2 shows the thiocyanate results correlated with cumulative produced water.

The cumulative gas volume produced during the reentry test was 15.8 MMSCF and the cumulative water production was 842 bbls. No water was produced in the first five days of the test.

Following 48.5 days of production, a pressure buildup test was conducted. These results will be discussed in the next section.

Qualitatively, these production results suggest that the damage resulting from a stimulation treatment may be reversible and is probably

due to water and gel blockage of the natural fractures. Over the long shut-in, the gel would have degraded further and imbibition of the water into the matrix rock probably cleared the natural fractures of most water and dehydrated any remaining gel. When production was resumed, gas production through the natural fractures was no longer hindered by water and gel, and flow rates were much closer to the expected values. Only after five or six days of production, when pressures dropped considerably, did water production begin, probably from the matrix rocks.

8.7.2 MODELING AND ANALYSIS

To assess the effects of the extended shut-in period, a reservoir simulation study of the reentry production and well test data was conducted. This portion of the study utilized the reservoir model developed during the prefrac well test analysis. Again, the base reservoir model is a naturally fractured channel sand, 350 ft wide. Previous results have indicated that a hydraulic fracture in the paludal sands would be oriented approximately 85 degrees west-northwest, and would be roughly perpendicular to the channel banks that define the nearest reservoir boundaries (see Figure 8.1.8). Figure 8.7.3 illustrates the reservoir simulation model used for the reentry study. The orientation of the hydraulic fracture was confirmed by seismic data taken during the fracturing experiments in the two observation wells.

The best match of the reentry production and well test data was obtained using a fracture half-length of 100 ft and a fracture conductivity of 104 md-ft. Table 8.7.1 lists the modeling parameters used to match the reentry data. The reentry modeling showed that no significant natural fracture impairment was present after the extended 20-month shut-in. The model-generated Horner and log-log pressure buildup behavior are compared to the actual data in Figures 8.7.4 and 8.7.5, respectively.

It should be emphasized that the direction of the propped fracture is perpendicular to, and thus intersects, the low permeability natural fractures. Thus, the high permeability natural fractures are not intersected by the hydraulic fracture but are parallel to each other (see Figure 8.7.3). The hydraulic fracture direction is primarily determined by the in situ stress field. Therefore, the production enhancement from this hydraulic fracture is limited because of the natural anisotropy of the reservoir.

The ability to rigorously model the complex nature and interaction of the anisotropic natural fracture system and the propped fracture allowed a much better understanding of the production and damage mechanisms present in these paludal reservoirs.[1] The reentry modeling has shown that the damage mechanism(s) in the paludal sands were transitory in nature and that an extended shut-in period did significantly reduce the effects of the damage.

8.7.3 REFERENCE

1. Branagan, P. T., C. Cipolla, S. J. Lee, and L. Yan, "Case History of Hydraulic Fracture Performance in the Naturally Fractured Paludal Zone: The Transitory Effects of Damage," SPE/DOE 16397, SPE/DOE Symposium on Low Permeability Reservoirs, Denver, CO, May 1987.

Table 8.7.1 Re-Entry Model Input Data

BASE RESERVOIR DATA	MATRIX PROPERTIES	NATURAL FRACTURE PROPERTIES	HYDRAULIC FRACTURE PROPERTIES
Channel width = 350 ft	k_m = 1.0 μd	k_x = 5,000 md	k_f = 5 Darcy
P_i = 5,400 psi	ϕ_g = 0.04 (4%)	k_y = 500 md	w_f = 0.25 in.
Depth = 7,000 ft		ϕ_g = 1.0	L_f = 100 ft
T_{res} = 210° F		Spacing = 5 ft	
h_{net} = 40 ft		w = 0.001 in.	
SG = 0.626			

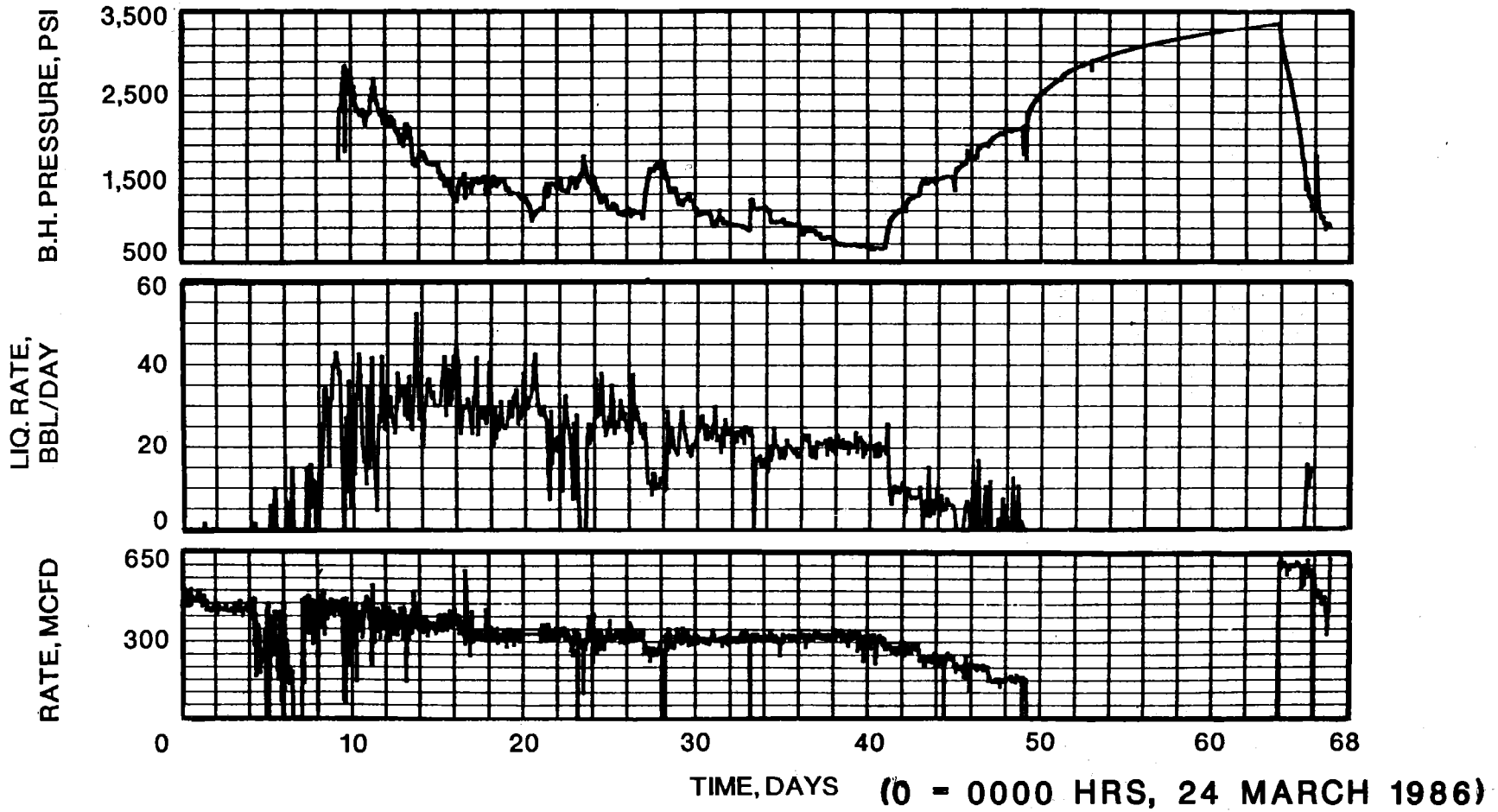

Figure 8.7.1 Re-Entry Well Test Data from Paludal Sands 3 and 4

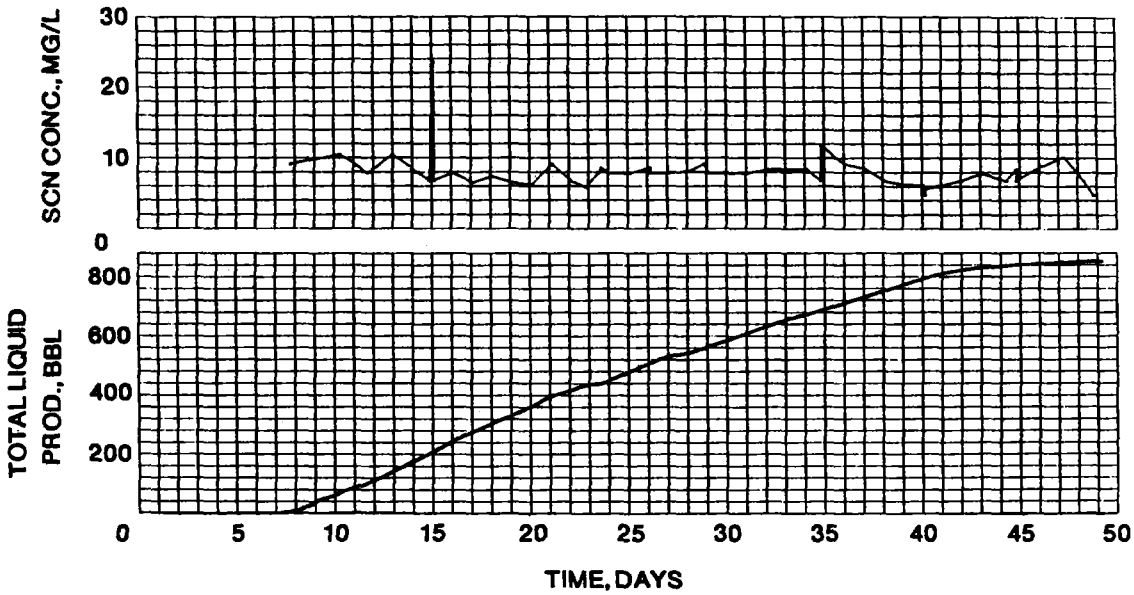

Figure 8.7.2 Cumulative Liquid Production and Tracer Concentration Returned During Re-Entry Well Testing

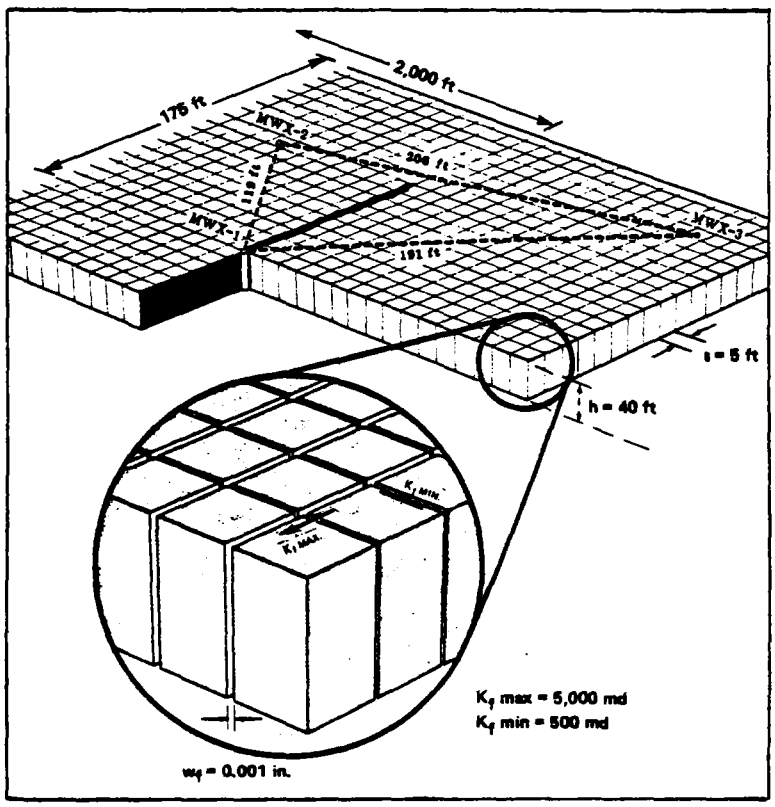

Figure 8.7.3 Naturally Fractured Reservoir Model for the Paludal Sands 3 and 4 with 100-ft Propped Fracture

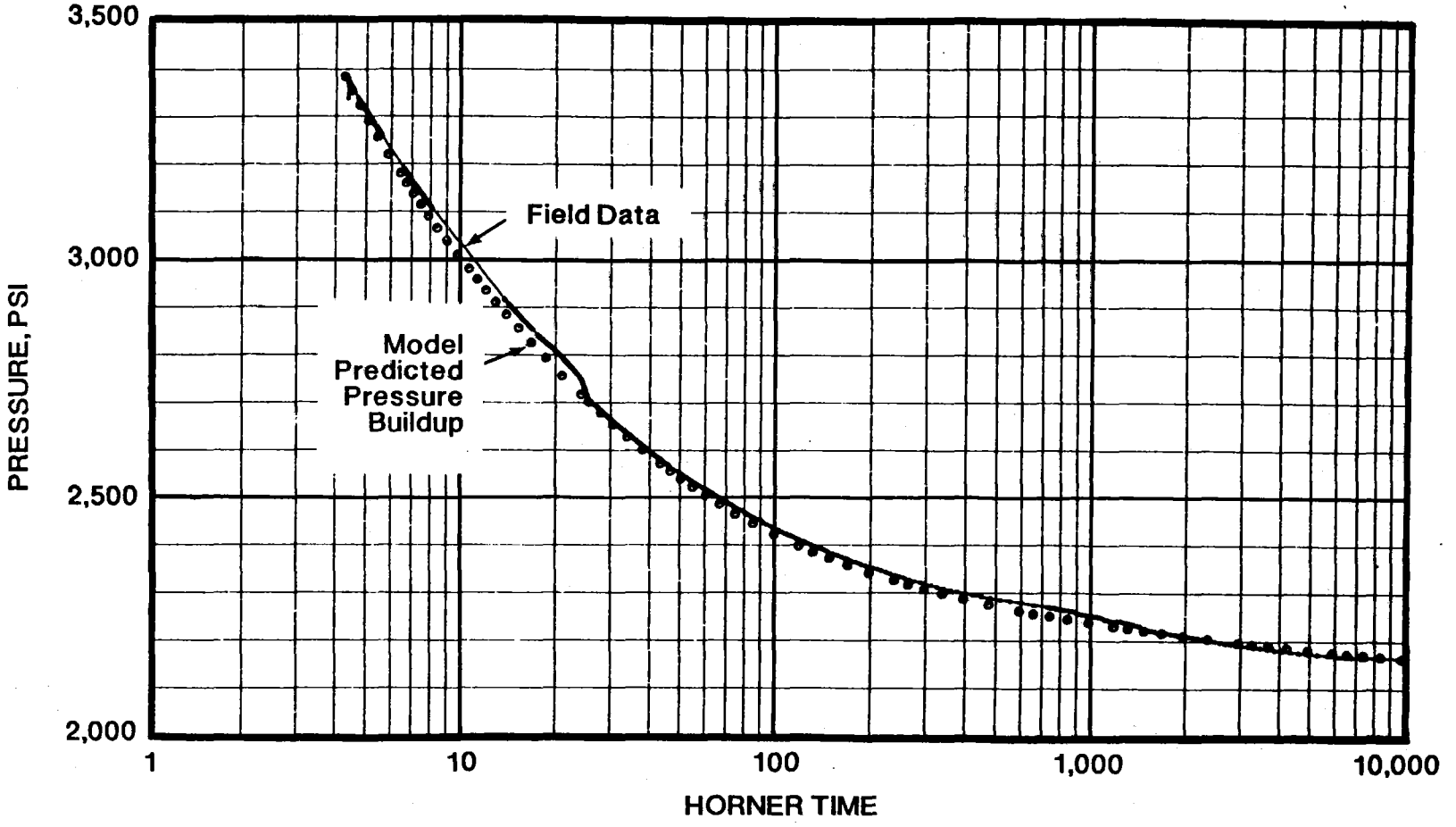

Figure 8.7.4 Post-Fracture Horner Plot

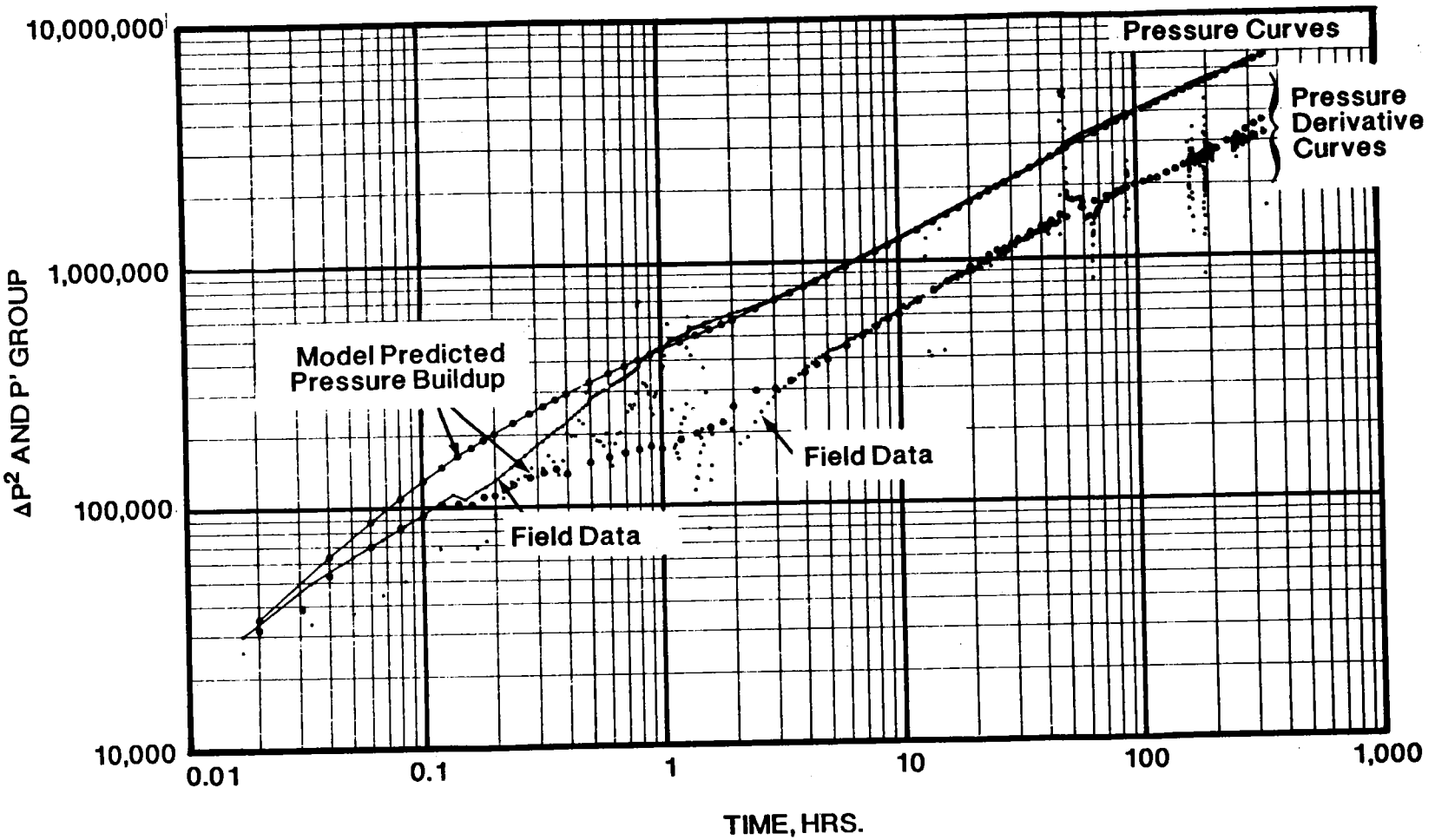

Figure 8.7.5 Post-Fracture Log-Log Plot

8.8 SUMMARY AND CONCLUSIONS

An extensive set of geological, log, core, production, and well test data have been integrated into an accurate reservoir model of a set of paludal sandstones present in the Mesaverde Group at the MWX site. The reservoir simulation study of the pre- and postfrac well test and production data has shown that two damage mechanisms are probably related to stimulation fluids:

- liquids which reduce the relative gas permeability of the natural fractures that were intersected by the hydraulic fracture, and

- fracturing fluid polymers that impair gas flow from the intersected natural fractures.

Both of these damage mechanisms should be time-dependent. The high capillary pressures in the low permeability matrix rock should result in the imbibition of the liquids in the natural fractures, thus reducing natural fracture liquid saturation and increasing gas permeability. The nature of the fracturing fluid polymers should result in a decrease in molecular weight with time and temperature, again increasing gas permeability.

The observed decrease in production from 250 to 150 MCFD after the propped fracture treatment, coupled with the pre- and postfrac reservoir modeling, indicated that these stimulation treatments damaged the natural fractures system. The reentry production of 400 MCFD and the subsequent well testing and reservoir modeling indicated that after the 20-month shut-in the damage was no longer present.

The data and modeling presented illustrate the difficulties associated with stimulating anisotropic, naturally fractured reservoirs. The study supports the following conclusions.

- The preservation of the gas permeability of the natural fractures intersected by a hydraulic fracture is critical to production enhancement.

- Damage to the natural fracture system can be due to liquid and/or fracturing fluid polymers, and if these damage mechanisms are predominant, their effects may decrease with time.

- The anisotropic nature of the natural fracture system in the paludal sandstones and the direction of the hydraulic fracture, parallel to the maximum permeability natural fractures, magnified the effects of damage and minimized the production enhancement possible due to a hydraulic fracture.

9.0 LABORATORY STUDIES

A. R. Sattler
Sandia National Laboratories

9.1 INTRODUCTION

This section describes the laboratory work supporting the Phase I and II stimulation operations of paludal zones 3 and 4 in MWX-1. The original goals of the laboratory program were mainly to support the stimulation designs and that work is described in sections 9.2 and 9.3.

However, serious production problems were encountered following the Phase II frac when the well was incapable of sustained production flow (Section 8.5).[1,2] The remedial treatment a month later did not seem to improve the situation. In fact, sustained gas flow was not realized for over a month until the tubing string was extended below the perforations. This change improved fluid recovery and 50 bbl of water were recovered the first day and gas production resumed. Even then, rates of 170 MSCFD could not be sustained, as compared with production rates of 250 MSCFD for pre-Phase I production and 200 MSCFD for post-Phase I/pre-Phase II production.

Because of these problems, the scope of these laboratory studies was broadened considerably for the paludal and in subsequent intervals. These studies became part of a synergistic approach to stimulation design and analysis. Specifically, the purpose of the laboratory studies became (1) to examine all core analysis data relevant to the stimulation,[3] (2) to undertake laboratory studies supporting stimulation design and postfrac investigations, and then (3) to integrate these studies with field data from both the Phase I and II stimulations, particularly with respect to possible damage mechanisms.

Prior to the paludal zone reentry, a number of damage mechanisms were postulated to explain the production performance of MWX-1. These were based on field and laboratory work centered about the Phase I and II operations. The resulting paludal zone reentry production rate of 350 MSCFD obtained after a 20 month shut-in[4] were generally consistent with, and in fact confirmed, many of our earlier interpretations of damage mechanisms. The reentry tests showed that certain forms of formation damage were in part reversible. Reports have been published which describe the material presented in this section in greater detail.[5,6]

9.2 LABORATORY STUDIES BEFORE THE PHASE I STIMULATION

Limited prefrac laboratory experiments were conducted to prepare for the Phase I paludal stimulation. These were felt to be adequate, since the Phase I stimulation was not propped, and oriented only toward fracture diagnostics and containment verification and fracture parameters. Smith Energy Services, the service company for Phase I, performed mineralogy-petrology studies and permeability damage studies.[7] The National Institute of Petroleum and Energy Research (NIPER) performed permeability damage studies.[8] Capillary pressure measurements were also made by the Petroleum Recovery Research Center (PRRC) at New Mexico Institute of Mining and Technology.[9]

9.2.1 Mineralogy and Petrology

Smith studied core from zones 3 and 4 petrographically and by scanning electron microscopy/energy dispersive spectroscopy (SEM/EDS). This was done primarily to determine frac fluid/reservoir rock compatibility. The studies were in general agreement with the Bendix and USGS results which are discussed in section 3.2.3. The work indicated that no adverse reaction would take place between the formation rock and the frac fluid uses in Phase I.

9.2.2 Formation Damage

NIPER and Smith performed formation damage measurements on paludal core to prepare for the Phase I stimulation. The fluids used were brine solutions with hydroxypropyl guar (HPG) at 30 to 50 lb/1000 gal concentrations. These studies focused on finding the permanent damage (permeability reduction) resulting from both unbroken gels (NIPER, Table 9.1) and broken gels (Smith, Table 9.2) being pumped against the core.

Smith's results for broken gel are different from NIPER's results with the unbroken gel; there is larger damage with the broken gel. Allowed "cleanup" times by Smith were one hour vs three or more hours by NIPER. NIPER also performed one run with broken gel using longer cleanup times (overnight). They found damage of the broken and unbroken gel about the same, and much less than the damage reported by Smith. Allowed cleanup times and differences in permeability of the samples, rather than the state of the gel, probably account for the difference in results.

Notable in Smith's studies was the use of a methanol-based prepad injected in the core. This totally averted any damage due to broken gel--at least in the laboratory. At the time methanol was thought to enhance permeability by removing much of the pore water in these tight sands. These results led to the decision to use a methanol prepad in the minifracs. The effects of methanol were further investigated by NIPER and the Western Company in their laboratory work preparatory to the Phase II frac.

NIPER also showed that permeability degradation increases with exposure to the gel as seen in Figure 9.1. This shows the importance of prompt flowback of the fracture fluid.

9.2.3 Fluid Leakoff

NIPER results showed that leakoff is quite small, with a rather small (~20%) reduction of gas permeability. However, the degradation of the brine permeability from treatment with gel is much larger, $\geq$ 50%.

9.2.4 Capillary Pressure

The use of methanol is advocated by many service companies to improve fracture fluid recovery. Methanol is supposed to mix with pore water and lower both the surface tension and the capillary pressure in the matrix rock. PRRC[9] performed capillary pressure curves of brine water alone and brine water with a 4% methanol-surfactant mixture. The methanol added to the brine did not change the capillary pressure curve significantly. PRRC did not investigate the effect of the other Smith prepad additives with the methanol.

9.3 LABORATORY STUDIES BEFORE THE PHASE II STIMULATION

A more comprehensive group of laboratory experiments was conducted to prepare for the Phase II stimulation. The Western Company of North America, the service company for Phase II, conducted mineralogy-petrology studies, formation damage studies, proppant embedment and crush studies, and rheology studies of Apollo gel.[10,11] NIPER studied formation damage, proppant embedment and crush studies, and leakoff studies.[8]

9.3.1 Mineralogy/Petrology

The Western Company conducted mineralogy/petrology analyses on zone 3 and 4 samples via X-ray diffraction (XRD) and microscopic methods. Their results were in general agreement with Smith,[7] Bendix, and the USGS (Section 3.2.3). These studies showed that there would be no adverse reaction between the formation rock and the frac fluid used in Phase II.

9.3.2 Permeability Damage

Western showed permeability degradations of 35% for the Apollo gel with additives (Table 9.3). The damage to the matrix rock was somewhat higher than expected but the result was considered satisfactory. The laboratory fluids containing methanol/surfactant flowed back at a much faster rate.

NIPER performed additional permeability damage studies. Gas permeability, after exposure to 2% or 3% KCl brine, was only slightly greater than that measured after exposure to cross-linked HPG gel. The gel residue would form a "filtercake" which retarded flow of fluid through the core. Further reductions in already low brine permeabilities would result (Figure 9.2). (The very tightest rock did not show much effect, since the "filtercake" from gel residue was large compared to the pore size and thus was not effective in lowering the already low permeabilities.)

Figure 9.3 shows the cleanup time vs gas permeability. Since the dry permeabilities of dry paludal core range from 0.03 to 27 md, averaging about 7 md, long cleanup times can be expected.

9.3.3 Fluid Leakoff

Fluid loss curves from NIPER are shown in Figure 9.4 for cross-linked and noncross-linked HPG. Fluid loss coefficients calculated from the slopes of these curves differ by a factor of 1.7. The values were 0.003 and 0.0018 $ft/min^{1/2}$, respectively, with the higher coefficient associated with the cross-linked gel used on Phase II. The coefficients were dependent on the type of fluid and were independent of core permeability if it was greater than 10 md. Core with permeabilities less than 10 md had lower fluid loss characteristics. Field derived fluid loss coefficients (0.0007-0.0015 $ft/min^{1/2}$) were lower than lab values.

Leakoff would allow the gel to be injected at high pressure into the narrow, natural fractures and leak into, or form a filter cake on, the matrix rock.

9.3.4 Proppant Embedment

These tests were conducted by Western to measure the embedment strength of the formation and the resulting loss of conductivity due to embedment of a sand pack into the formation. Embedment strengths of the sand and carbonaceous shales are rather high. Conductivity loss in the sands and shales is minimal at 6000 psi. Even for the coal sample, the loss of conductivity approaches only 20% at 6000 psi. NIPER performed additional proppant related measurements which were in general agreement with the Western results. They performed some embedment experiments on paludal sands at the crush strength (13,000 psi) of the Ottawa sand used in the frac. Even at that crush strength, the reduction in laboratory fracture width was under 15%. Proppant embedment does not appear to be a problem in either the paludal zones 3 and 4 or in the materials abutting them.

9.3.5 Proppant Crushing

Western performed proppant crush tests on the 20/40 and 10/20 sands used in the paludal stimulation. Both Western and NIPER simulated production/shut-in cycling of 20/40 sand at realistic pressures. They found for six cycles that about 9% fines were generated and the proppant pack width was reduced about 5%. Proppant crushing does not appear to be a problem for the number of cycles tested.

9.3.6 Fluid Rheology

Western studied the rheology and cross link of Apollo gel to note any effect of the addition of ammonium thiocyanate tracer on the Apollo

system. No changes were noted by the addition of 100 ppm tracer concentration. Also, no changes in rheology were noted for a 5% vs 3% KCl solution. The more conductive 5% KCl solution was investigated for a possible fracture diagnostics application.

9.4 LABORATORY STUDIES AFTER THE PHASE II STIMULATION AND THE REMEDIAL TREATMENT

We reexamined all aspects of the Phase II stimulation when MWX-1 failed to sustain gas production. This reexamination included: breaker schedule, effect of formation temperature on gel with and without breaker, viscosity and molecular weight degradation of frac fluid, molecular weights of returned fluids, effect of postfrac workover operations, effect of methanol, leakoff, skin effect/imbibition, and effects on natural fracture system.

The main focus was upon the frac fluid system, particularly on breaker performance. No breaker was used in this treatment except in the final two stages and even in those last two stages the breaker concentration was low: 0.25-0.50 lb/1000 gal. The 200°F temperatures encountered in the well were considered sufficient to break the gel. The Nolte analysis of the Phase II stimulation indicated that the formation closed on the proppant only 70 minutes after pump shutdown.[1,12]

For the formation to close on the proppant one of two things had to happen. There was either a large amount of leakoff or the fracture fluid lost its proppant carrying ability. If there was a large amount of leakoff, the fracture would have closed with the sand in suspension. This probably was not the case, since the Phase II closure projection, based on the unpropped Phase I stimulation, was 30 hours without viscosity loss. Further, laboratory and in situ estimates of leakoff were very small, and pressures were too high for appreciable leakoff to have occurred. Therefore, there was probably degradation of the

proppant-carrying ability of the fracture fluid and the sand must have begun falling to the bottom. At that time we did not know if the fracture fluid had undergone either a viscosity degradation or a significant decrease in the molecular weight. The words "gel break" may have been used to describe either or both of these phenomena, but the laboratory data were to point out that there is an important difference between viscosity degradation and breakdown of the basic gel.[13]

9.4.1 Before the Remedial Treatment

NIPER performed additional laboratory work to address the poor performance of MWX-1.[8] They measured the degradation of the Western Apollo gel used, with and without breaker at formation temperatures (Figure 9.5), as well as the viscosity degradation of the gel (Figure 9.6). These show that at 200°F the breaking of the basic gel occurs slowly without breaker, but that the viscosity decreases very rapidly at these temperatures. This viscosity decrease must be due to the breaking of the cross-linking. Thus, the fracture closure after 70 minutes must have resulted from a gel viscosity break. NIPER also determined the molecular weights of the polymer from successive samples of returned fluid (Figure 9.7). About three weeks after the Phase II stimulation, the average molecular weight of the polymer in the returned fluid was down only a factor of seven.

The original treatment and subsequent postfrac operations may have resulted in a 10-15°F suppression of the temperature for a couple of weeks. This would have retarded the decomposition of the gel further and would have rehydrated any gel remaining in the formation. Also, Western's postfrac fluid analysis indicated the presence of 5%-8% methanol which was used in the prepad. Later, NIPER studied the effects of breaker and methanol on the viscosity degradation of HPG gels.[13] Results for four combinations of these two additives are shown in

Table 9.4. Their findings showed:

- Gel with no breaker plus methanol is the most stable combination; the gel will degrade slowly.

- Gel with breaker and no methanol is the least stable combination.

- The effect of methanol is to retard degradation of the gel and to cancel the effect of breaker.

The Phase II frac configuration resembled the most stable combination above since methanol was about 8% of the total frac fluid and little breaker was used.

We encountered very high pumping pressures, up to 7000 psi, which were a few hundred psi higher than barriers predicted from stress testing.[1] It is possible that fluid was being pumped at very high pressures (unpropped and with little or no breaker) into a natural fracture system composed of very narrow fractures. This fluid leakoff would concentrate polymer, deplete breaker concentration, and inhibit production from these natural fractures as well as from matrix rock.

9.4.2 After the Remedial Treatment

We felt that one possible cause of our production problems was a gel block in the sand pack as the polymer had not decomposed as expected and limited buildup data indicated a short fracture. Therefore, we did a remedial treatment on MWX-1 with a highly acidic (1.3 pH) oxidizing solution containing 150 lb/1000 gal Western B5 breaker in a 5% hydrogen peroxide (H_2O_2) solution in an attempt to break down any residual gel or polymer in the formation (Section 8.5).

Both Western and NIPER conducted additional damage studies on core with the remedial treatment fluid. Western showed about a 30%-35% permeability degradation to gas. The work of NIPER suggested that with the B5 breaker alone, no H_2O_2, the degradation would be around 10%. However, with the combination of the breaker and peroxide, permeability degradation would approach 50% (Table 9.5)[8] and cleanup times would increase considerably.

Most of the fluid injected in this remedial treatment came back within a few days. The gel in the returned fluid samples was broken, molecular weights were less than 200,000, down from ~1,000,000 prior to the treatment (Figure 9.7). However, the returned fluids contained abundant red to tan to brown precipitate. Analyses showed that the precipitate was iron oxide/hydroxide.[14]

From these data we concluded that this reactive remedial treatment solution had reacted with the tubing and casing. When the tubing string was pulled after the Phase II well testing many sections were pitted, especially those next to the zone being treated and those at the top of the string (Figure 9.8). Presumably the casing was involved also as all paludal treatments had been conducted down the annulus between the tubing and casing.

NIPER duplicated the reaction in the laboratory with iron pipe obtaining the same precipitate that was obtained with returned fluid. They showed that if breaker alone was used, and no H_2O_2, there would have been little reaction with this iron pipe and loss of permeability (Table 9.5). Laboratory and field results appeared consistent.

The effects of this remedial treatment were duplicated further by NIPER.[8] They flowed 40 lb/gal HPG gel through a piece of artificially fractured paludal zone core. There was an initial 90% permeability

degradation which improved to about a 40% degradation during a simulated cleanup. The fluid similar to that used in the remedial treatment was flowed through the core after mixing the solution with iron. Thus, both the original gel and the highly reactive breaker fluid were pumped into this artificial fracture. The gas permeability degradation exceeded 90%. Cleanup times of this artificially fractured core increased over one hundredfold. (A similar treatment was given to a piece of matrix rock at the remedial treatment pressures.) Thus, iron fines from the tubing and casing generated by this very reactive remedial treatment may have been carried into the formation causing some damage. This treatment may actually have retarded actual fluid recovery and subsequent gas production even though the gel in the returned fluid samples was mostly broken after the treatment. All in all, it appeared that we had exchanged one set of problems for another.

Western analyzed samples of returned fluid for their organic content. An analysis of that data is shown in Figure 9.9. These results indicate:

- Most of the organic material (about 3/4 of that injected during Phase II) came back before the remedial treatment.

- Some additional organic material (<15%) was brought back by the remedial treatment. The increase in the amount of total organic material recovered just after the remedial treatment implies that some additional organic residue was recovered that would not have been otherwise.

- The remedial treatment also could have brought organic material from the Phase I treatment or from the organic rich formation itself. A good estimate of the organic material remaining in the formation was impossible.

- It is unlikely that a gel block existed in the proppant pack because (1) there was no immediate improvement in production as a result of the remedial treatment and (2) the amount of organic material brought up as a result of the remedial treatment was relatively small.

9.5 WATER ANALYSIS

Numerous water analyses were made on samples collected during various stages of activities in the paludal zone: from testing of zone 2, before and after the Phase II stimulation, and from the reentry testing of zones 3 and 4. There was a continuing question of production of formation water and whether the coals are contributing to the returned fluids.

9.5.1 Zone 2 Analyses

The USGS analyzed data from water samples from production testing of paludal zone 2 at 7238-7284 ft, just below zones 3 and 4.[15] The lithology is similar to zones 3 and 4: coals and organic siltstones and mudstones abut the sands. Prior to production testing, the perforations of zone 2 were broken down with a very small amount of 3% KCl solution to make a better communication between the wellbore and the formation. The USGS performed analysis of the Na, K, and Cl ions in the zone 2 samples collected during subsequent production testing, and concluded (with a 95% correlation) that there was an influx of formation waters which probably emanated from coals. The USGS estimated that the samples collected contained about 30% formation water by the end of the zone 2 production testing. The trends in the Na, K, and Cl concentrations in zone 2 are very similar to those observed in zones 3 and 4 after the Phase II stimulation, and the USGS later concluded that formation waters were also being produced in zones 3 and 4.[16]

9.5.2 After the Phase II Stimulation

Fluid samples and their analyses following the Phase II stimulation were complicated by the various operations and treatments used during this period as summarized in Figure 9.10.[17] Nevertheless, fluid samples were obtained routinely over a four-month period and the analyses by the Western Company are given in Table 9.6 and analyses from J. C. Kephart's Grand Junction Laboratory[18] are given in Appendix 12.8. Ammonium thiocyanate was used as a tracer in the Phase II stimulation fluid and CER Corporation's thiocyanate analyses are also presented in Appendix 12.8. The thiocyanate in the returned fluid showed almost a continuous decrease from 100 ppm in the stimulation fluid to less than 10 ppm in the last samples. This dilution is indicative of the production of formation water--an effect that would exacerbate the cleanup problem.

9.5.3 After Reentry

The paludal zone was reentered in December 1985 and an extensive final production test commenced in March 1986, 20 months after the zone was shut in (Section 8.7).[4] The reentry production data are shown in Figure 9.11. The initial rate was 420 MSCFD and the average sustainable rate was about 320 MSCFD. (This post-reentry rate can be compared with 250, 200, and 170 MSCFD for precompletion, post-Phase I/pre-Phase II, and post-Phase II production, respectively.) Initially, no liquids were produced, but after five days the surface tubing pressure dropped about 1000 psi and water production started. The water production increased rapidly to about 35 bbl/d, and totaled about 850 bbl.

Table 9.6 contains the water chemistry analyses of the returned fluid samples that were analyzed by the Western Company, both before[11] and after reentry.[19] Additional post-reentry analyses were performed by

both Core Laboratories, Midland[20] and the J. C. Kephart's Grand Junction Laboratory.[18] The results from the three laboratories are in general agreement with each other. Western's data in Table 9.6 were the only data from the three laboratories to span the post-Phase II and post-reentry testing periods.

There is little additional change in the sodium and chloride concentrations in returned fluid samples from those taken a the end of Phase II water sampling to those taken during the reentry production operation. The presence of > 3,000 ppm Na implied that there was a fair amount of formation water in the returned fluids[20] and it remained constant during the testing periods. This interpretation is an agreement with some special USGS water analyses.[16]

The potassium and sulfate concentrations in the returned fluid samples started decreasing after the Phase II frac, but became very high after the remedial treatment. The sulfate concentration was so high it could not be measured in the returned fluid samples until about four days after the remedial treatment when it was around 5000 ppm. After that, both potassium and sulfate ions were seen in decreasing quantities as long as returned fluid analyses continued. The large perturbations in the concentration of these ions caused by both the remedial treatment and the original frac itself became smaller as post-Phase II water analyses continued and were even less noticeable after the long shut-in. The concentrations of these ions continued to decrease throughout the post-reentry test period.

The bicarbonate concentration in returned fluid samples started increasing after the Phase II frac. This concentration was perturbed and greatly reduced by the remedial treatment. The bicarbonate concentration resumed it increase in returned fluid samples through the post-Phase II testing period. After that it appeared to increase during the long shut-

in after the Phase II testing and stayed nearly constant during the reentry production. This increasing bicarbonate concentration is suggestive of some influx of water from the coals.

Thiocyanate concentration was measured in the returned fluids from the reentry operation and was found to be relatively constant at 8-10 ppm. This is about the same value as just prior to shut-in and considerably less than the 100 ppm in the Phase II frac fluid. This relatively low, constant thiocyanate concentration suggests that the frac fluid had mixed well with a large volume of formation water. This conclusion is supported by the presence of methanol in the fluid samples.[22] Its concentration leveled off to a constant value during the reentry test. (Methanol was also used in Phases I and II in the frac fluid system. However, methanol was used to keep flow lines from freezing during the early part of the reentry operation.)

9.6 INTEGRATION OF RESULTS AND DISCUSSION OF DAMAGE MECHANISMS

When the paludal zone was shut in in August, 1984, there were still numerous unanswered questions about the production performance of MWX-1 and these centered mainly on the nature of the formation damage. Laboratory work did provide some direct evidence in the following areas:

- The conditions when either the viscosity or the molecular weight of a gel might degrade.

- Knowledge of the difference between viscosity break and molecular weight degradation.

- Downhole reaction kinetics of gel solution with and without breaker and/or methanol.

- Returned fluid analyses on (1) the state and amount of the organic material polymer downhole at a given time, and (2) the chemistry of the fluids in the vicinity of the borehole.

- Permeability degradation of the matrix and artificial fractures due to exposure to frac fluids.

- Consequences of the remedial treatment.

- Elimination of possible problems such as massive leakoff of frac fluid into matrix rock, long-term permeability degradation of matrix rock, gel block in the sand pack, and proppant effects.

In spite of this body of information, a unique explanation could not be given for the failure of MWX-1 to produce following the Phase II stimulation nor could an explanation be given for the overall production declines following both the Phase I and II stimulations. Thus, a decision was made to reenter the paludal zone once more for additional production testing. It was hoped that this additional production data might provide additional information on the damage mechanisms involved.

A unique explanation of all the production problems of MWX-1 following the Phase I and II fracs is still not possible even after the reentry data became available. However, from the reentry operation we do know:

- Formation damage incurred in Phase I and II must be reversible, at least in part.

- Fluids were not produced until the downhole pressure fell to around 1000 psi, a value in the neighborhood of the capillary pressures of paludal core.

Moreover, certain damage mechanisms postulated earlier seem consistent with this new body of data and, as a result, seem much more plausible. It appears that the formation damage involved the natural fracture system and was due to a reversible fluids effect, at least in part. Factors involving the natural fractures and fluids effects include:

- Fracturing pressures were 800, and 1100 psi higher in the two Phase I minifracs than were predicted from stress data. Further, they were 1500 psi higher in the Phase II stimulation than expected (Sections 6, 8.2 and 8.4).

- The natural fractures may have opened up and gel may have been pumped into them at high pressures. After the stimulation the fractures may have closed on the gel making it very difficult to recover that gel.

- The low breaker/high methanol combination of additives stabilized the gel and retarded its decomposition. The observed Phase II hydraulic frac closure was due to viscosity reduction of the fluid; the basic gel/polymer molecular weight decreased much more slowly.

- Postfrac workover operations may have suppressed formation temperatures, further stabilizing the gel.

- During the long post Phase II shut-in, gel not affected by the remedial treatment may have decomposed further. Pressure gradients within the reservoir (between the fairly unperturbed matrix and the matrix and fractures near the wellbore) became small, and the ~1000-psi capillary pressures once more dominated. Water may have been moved (imbibed) from the natural fractures into the matrix

rock. It is interesting to note that water production from the final production test began only after downhole pressures dropped to ~1000 psi. which perhaps allowed the pressure gradient to once more overcome pore capillary pressures.

- Some forms of mechanical damage to the natural fractures (asperity shearing, proppant induced stresses and fines) may also have been involved.[22] However, these would be difficult to quantify on the basis of the data available.

The matrix rock also could have been affected to some extent by fluids. Mechanisms involving the matrix rock and fluids include:

- Any leakoff into the matrix could have made low water permeabilities even lower, and would have slowed down the cleanup process.

- Capillary pressures are high, permeabilities to gas and water are low, and cleanup times are long.

- Pre- and post-Phase II operations involved large amounts of water in the wellbore perhaps causing an initial skin effect.

- Some water production from nearby coals was likely.

- The improved water recovery resulting from the extra section of tubing to extend below the perforations in the post-Phase II operations could have spurred both matrix and natural fracture production.

The remedial treatment was designed to remove a possible gel block in the sand pack. In retrospect, we don't think one existed. The remedial treatment solution was very reactive and it may have done as much harm as good.

In conclusion, it is felt that the primary damage to the formation was due to fluids in the natural fracture system and that a portion of that damage was reversible--at least as observed after 20 months of shut-in. Problems with matrix rock may have added to or compounded the production difficulties with MWX-1. However, the laboratory work shows that most of the permeability degradation of the matrix due to frac fluids is eventually regained.

9.7 REFERENCES

1. Warpinski, N. R. et al., "Fracturing and Testing Case Study of Paludal, Tight, Lenticular Gas Sands," SPE 13876, Proceedings of the 1985 SPE/DOE Symposium on Low Permeability Reservoirs, Denver, CO, May 19-22, 1985.

2. Branagan, P., C. Cipolla, S. J. Lee, and R. Wilmer, "Comprehensive Well Testing and Modeling of Pre and Post Frac Well Performance of the MWX Lenticular Tight Gas Sands," SPE 13867, Proceedings of 1985 SPE/DOE Symposium on Low Permeability Reservoirs, Denver, CO May 1985.

3. Sattler, A. R., "The Multi-Well Experiment Core Program," SPE 11763, Proceedings of the 1984 SPE/DOE Unconventional Gas Recovery Symposium, Pittsburgh, PA, May 16-18, 1984.

4. Branagan, P. T., C. L. Cipolla, S. J. Lee and L. Yan, "Case History of Hydraulic Fracture Performance in the Naturally Fractured Paludal Zone: The Transitory Effect of Damage," SPE/DOE 16397, Proceedings of the 1987 SPE/DOE Symposium on Low Permeability Reservoirs, Denver, CO, May 18-19, 1987.

5. Sattler, A. R. et al., "Integration of Laboratory and Field Data for Insight on the Multiwell Paludal Stimulation," SPE 13891, Proceedings of the 1985 SPE/DOE Symposium on Low Permeability Reservoirs, Denver, CO, May, 1985.

6. Sattler, A. R., "Integration of Laboratory and Field Data for Insight on the Multiwell Experiment Paludal Stimulation," Sandia National Laboratories Report, SAND86-0087, June 1986.

7. Smith Energy Services "CER MWX Study," Reports 1645, 1703, December 1983.

8. Raible, C. J., and B. L. Gall, National Institute of Petroleum Research Annual Report, 1984.

9. Ward, J. S., and N. R. Morrow, "Multiwell Special Core Analysis" PRRC (New Mexico Tech) Report 84-25, October 1984.

10. The Western Company, Permeability Study 3496, May 1984.

11. Fulkerson, R., and R. Clarke, Series of Letter Reports from the Western Company to A. R. Sattler, May-August 1984.

12. Nolte, K. G., "Determination of Fracture Parameters from Fracturing Pressure Decline," SPE 8341, 54th Annual Fall SPE Technical Conference and Exhibition, Las Vegas, NV, September 23-26, 1979.

13. Gall, B. L. and C. J. Raible, "Molecular Size of Degraded Fracturing Fluid Polymers," SPE 13566, 1985 International Symposium on Oilfield and Geothermal Energy, Phoenix, AZ, April 1985.

14. Spencer, C. W., Memo to K-H. Frohne, "Report of Sediment Recovered on Flowback after MWX-1 Remedial Breaker Treatment of June 6, 1984," July 1984.

15. Spencer, C. W., memo to A. R. Sattler, "Report on MWX-1 Paludal Zone Water Analyses," July 1984.

16. Kimball, B., Internal USGS memo to C. W. Spencer, May, 1985.

17. CER Corporation, "Phase II Propped Liquid Recovery," computer tabulation, September 1984. (Presented as Appendix 12.8.)

18. Series of reports from John C. Kephart and Company, Grand Junction Laboratories, to CER Corporation, 1983-84.

19. Walker, D., Series of Western Company Letter Reports to A. R. Sattler, April, 1986.

20. Core Laboratories, Midland, Series of Water Analysis Reports, January-June, 1986.

21. NIPER, Quarterly Report performed under Contract 95-4340, July, 1986.

22. Lorenz, J. C., et al., "Fracture Characteristics and Reservoir Behavior of Stress Sensitive Fracture Systems in Flat Lying Lenticular Formations," SPE 15245, Proceedings of the SPE Unconventional Gas Technology Symposium, Louisville, KY, May, 1986.

Table 9.1 Conditions and Results on Permeability Studies (NIPER)*

	MWX-2	MWX-3
Depth (ft)	7138.3	7138.3
Core and fluid temp.(°C)	100	100
Core length (cm)	1.87	2.13
Porosity (%)	7.1	7.1
Regained permeability at irreducible S_w		
undamaged core (μd)	4.3	13
gel-damaged core (μd)	4.0	11
percent reduction	7	15
Brine permeability		
undamaged core (μd)	0.40	2.3
through filter cake and core (μd)	0.24	0.43
Fluid leakoff coefficient ($ft/min^{1/2}$)	0.0005	0.0020
Fluid penetration rate after filter cake buildup (cm/hr)	1.1	4.7
t_{80}--time required to reach 80 percent of final regained permeability (min)	465	195

*All tests performed with 40 lb/1000 gal unbroken gel.

Table 9.2 Permeability Damage Studies
Damage Studies (Smith Energy Services)

Depth	Initial Permeability	Treatment	Final Permeability	Percentage of Damage or Improvement
7135.5'-7135.3'	0.071 md	A	0.015 md	-78.9%
7135.5'-7135.3'	0.070 md	B	0.026 md	-62.8%
7135.5'-7135.3'	0.050 md	C	0.023 md	-54.0%
7135.5'-7135.3'	0.053 md	D	0.054 md	+ 1.9%
7138.75'-7139.6'	0.078 md	B	0.450 md	-41.9%
7138.75'-7139.6'	0.047 md	C	0.018 md	-61.7%
7138.75'-7139.6'	0.060 md	D	0.059 md	- 1.7%
7081.5'-7082.4'	0.090 md	D	0.093 md	+ 3.4%

CONDITIONS

Temperature - 210°F
Confining Pressure (around the core plug) - 500 psi

The systems tested were:

A. 50 lb/1000 gal broken gel
B. 30 lb/1000 gal broken gel
C. 30 lb/1000 gal broken gel containing 1 gallon FRS-1 (fluid recovery surfactant) per 1000 gallons broken gel.
D. A prepad system called LPM-1 (low pH methanol) which consists of 100% methanol containing 7 gallons LPA-91 (low pH additive) per 1000 gallons methanol. This prepad system was followed by the 30 lb/1000 gal broken gel frac fluid containing 1 gallon FRS-1/1000 gallons broken gel.

Contents of 30# and 50# Gels

2% KCl
30 lb/1000 gal or 50 lb/1000 gal WGA-2 (gelling material)
0.25 gallons BCS-2 (bactericide)/1000 gallons H_2O
1 gallon CSP-3 (clay stabilizer)/1000 gallons H_2O
4 lb/1000 gal WCB-1 (chemical breaker)/1000 gallons H_2O
BW-4 (buffer) amount needed to attain pH 7.0

Table 9.3 Permeability Degradation Studies
Prior to Phase II Stimulation (Western)

Depth (ft)	Well	Treatment Fluid	Permeability (md) Prior to Treatment	Following Treatment	Permeability Recovery (%)	Time (min)
7084	3	A	No measurable flow			
		B	No measurable flow			
		C	No measurable flow			
7120	2	A	No measurable flow			
		B	No measurable flow			
		C	No measurable flow			
7131	3	A	.0108	.0024	22	480
		B	.0145	.0101	70	476
		C	.0136	.0084	62	475
		D	.0151	.0107	71	420
7136	2	B	.0101	.0087	60	512
		C	.0096	.0063	66	465
		D	.0212	.0142	67	435
6753	3	B	.002	.001	50	>1240

Fluids:

A Apollo 35 Gel + 2% KCl
B Apollo 35 Gel + 3% KCl
C Apollo 35 Gel + 3% KCl + 1/2 gal Clay Master-3/1000 gal
D Apollo 35 Gel + 3% KCl + 10% methanol + 2 gal Flow-Back 10/1000 gal

Conditions:

Temperature - 200°F
Closure - 1500 psi

Table 9.4 Viscosity (cp) at 65°F and 27.7 sec^{-1} of Cross-Linked HPG Reacted at 190°F

Time (hrs)	No Breaker		0.006 w/o Breaker	
	5% Methanol	No Methanol	5% Methanol	No Methanol
6	153	107.7	29.1	3.2
24	79.9	32.2	15.2	3.0
48	62.6	22.5	13.1	2.4
168	21.4	7.6	7.0	<1.8

Table 9.5 Regained Permeability in Paludal Matrix Rock After Various Breaker Treatments (NIPER)

Core Depth	Fluid Treatment	Gas Permeability,* md Before Treatment	Gas Permeability,* md After Treatment	Recovered Perm. (%)	Increased Cleanup Time (%)
MWX-3 7135.1	A	.0326	.0300	92	6
Same Core Damaged by Treatment A	B	.0300	.0168	56	128
MWX-3 7135.1	B	.0320	.0170	53	194

* Measured at irreducible S_w

Treatment A 2% KCl; 0.5% B5 Breaker
Treatment B 3% KCl; 3% H_2O_2; 1.8% B5 Breaker

Table 9.6 Water Analysis of Returned Fluid from Phase II Stimulation (Western)

Date Sampled	Fluid (bbl)	Concentration (ppm) K	Na	Cl	HCO_3	SO_4	pH
5/2/84	Frac Fluid	11,064	416	12,225	456	1,478	7.4
5/2	250	13,801	1,578	12,347	607	249	7.5
5/2	410	9,771	3,920	12,347	910	50	7.5
5/3	530	11,005	3,592	12,347	796	25	7.6
5/4	856	11,030	4,706	12,347	1,275	75	7.6
5/4	1,050	7,214	4,338	12,347	1,396	50	7.9
5/7	1,250	5,050	5,234	13,294	1,596	50	7.8
6/2 Remedial Treatment							
6/2	Fluid	21,709	309	12,047	0	-	1.3
6/7	2,497	22,699	527	15,719	457	-	7.4
6/7	2,515	22,971	790	17,379	670	-	7.3
6/7	2,545	23,039	1,290	13,903	825	-	7.2
6/7	2,775	20,569	1,164	15,641	1,017	-	7.9
6/10	2,893	3,232	384	12,225	801	4,296	7.8
6/12	2,915	3,433	3,344	7,055	708	4,926	7.7
6/14	2,947	3,751	3,636	7,054	1,366	4,478	7.8
6/15-6/27 Corrosion Inhibitor + KCl Water Added							
6/29	3,050	2,551	3,621	8,689	1,631	2,696	7.6
7/3	3,081	7,272	4,350	8,605	1,453	1,948	8.1
7/6	3,097	8,138	5,822	6,986	1,571	1,478	8.1
7/9	3,105	1,814	3,155	5,672	1,366	1,000	8.1
7/13	3,158	2,122	3,875	9,842	1,687	995	7.6
7/16	3,171	2,258	3,779	7,091	1,903	1,250	8.2
7/19	3,172	2,258	3,986	6,726	1,940	2,500	8.1
7/24	3,183	1,894	3,905	7,091	2,111	1,250	7.8
7/27	3,183	1,917	4,174	7,091	2,159	1,000	7.4
7/31	3,221	1,502	3,773	5,672	2,318	500	7.3
8/2	3,235	1,630	3,714	5,672	2,208	500	7.3
			Upon Reentry				
4/1/86	3,245	1,361	3,877	5,971	2,864	200	7.5
4/2	3,205	1,077	3,648	5,971	3,059	325	7.6
4/3	3,295	1,094	4,154	5,959	3,345	125	7.4
4/4	3,325	754	2,815	5,959	3,333	195	7.4
4/5	3,355	1,140	3,794	5,959	3,321	125	7.7
4/6	3,375	1,253	3,799	5,959	1,618	174	7.6
4/7	3,415	1,326	3,872	5,959	1,679	125	7.6
4/8	3,445	795	3,873	5,977	3,367	150	7.5
4/9	3,485	977	3,708	5,977	3,212	125	7.5
4/10	3,5055	608	3,456	5,959	3,418	150	7.5
4/11	3,545	949	3,792	5,959	3,176	150	7.3
4/17	3,685	636	3,682	5,959	3,442	100	7.3
4/18	3,715	591	3,611	5,959	3,235	112	7.4

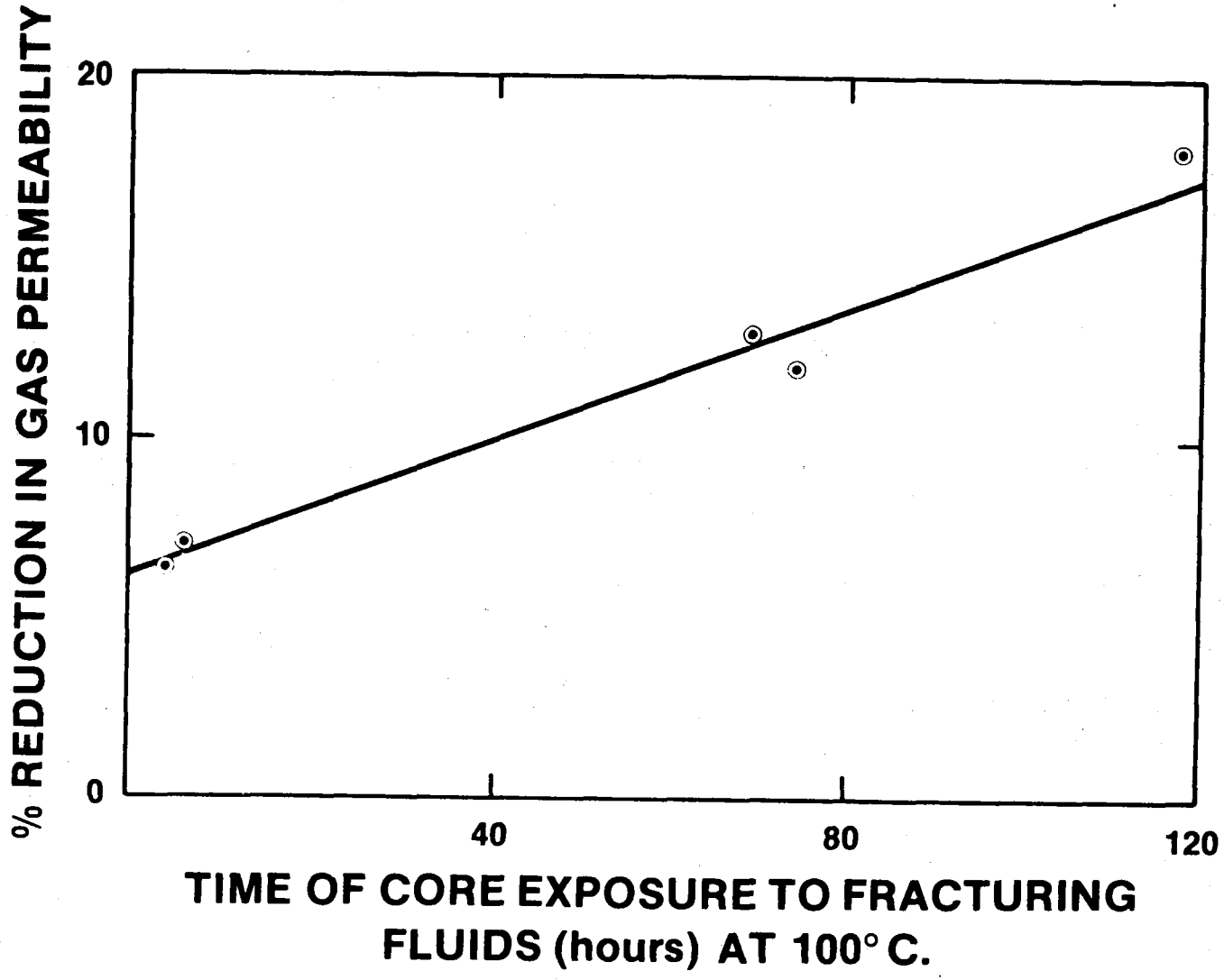

Figure 9.1 Percent Damage to Gas Permeability of MWX Core with Increasing Time of Exposure to Fracturing Fluids (40 lb HPG) at 100°C (NIPER)

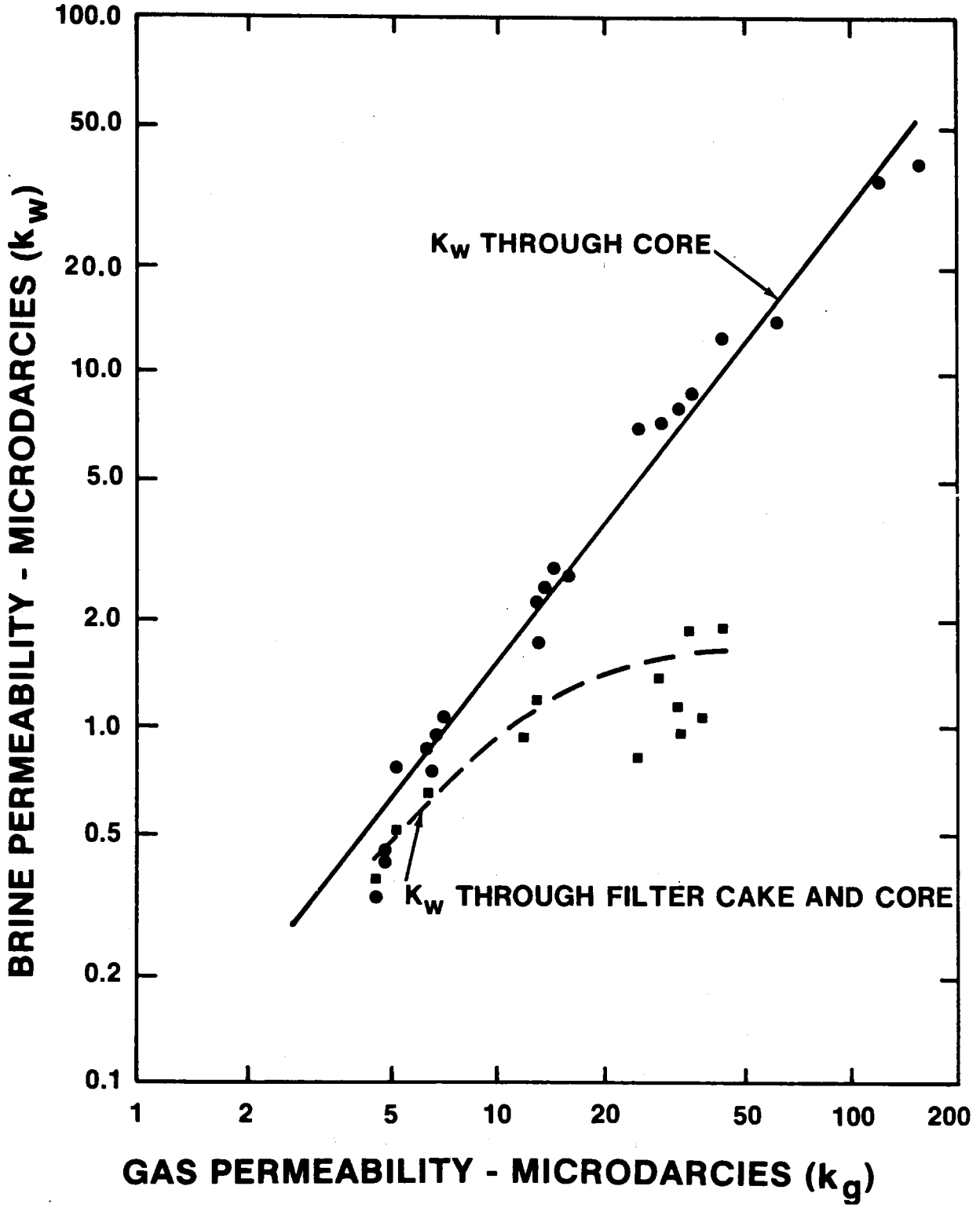

Figure 9.2 Brine Permeability for MWX Core (NIPER)

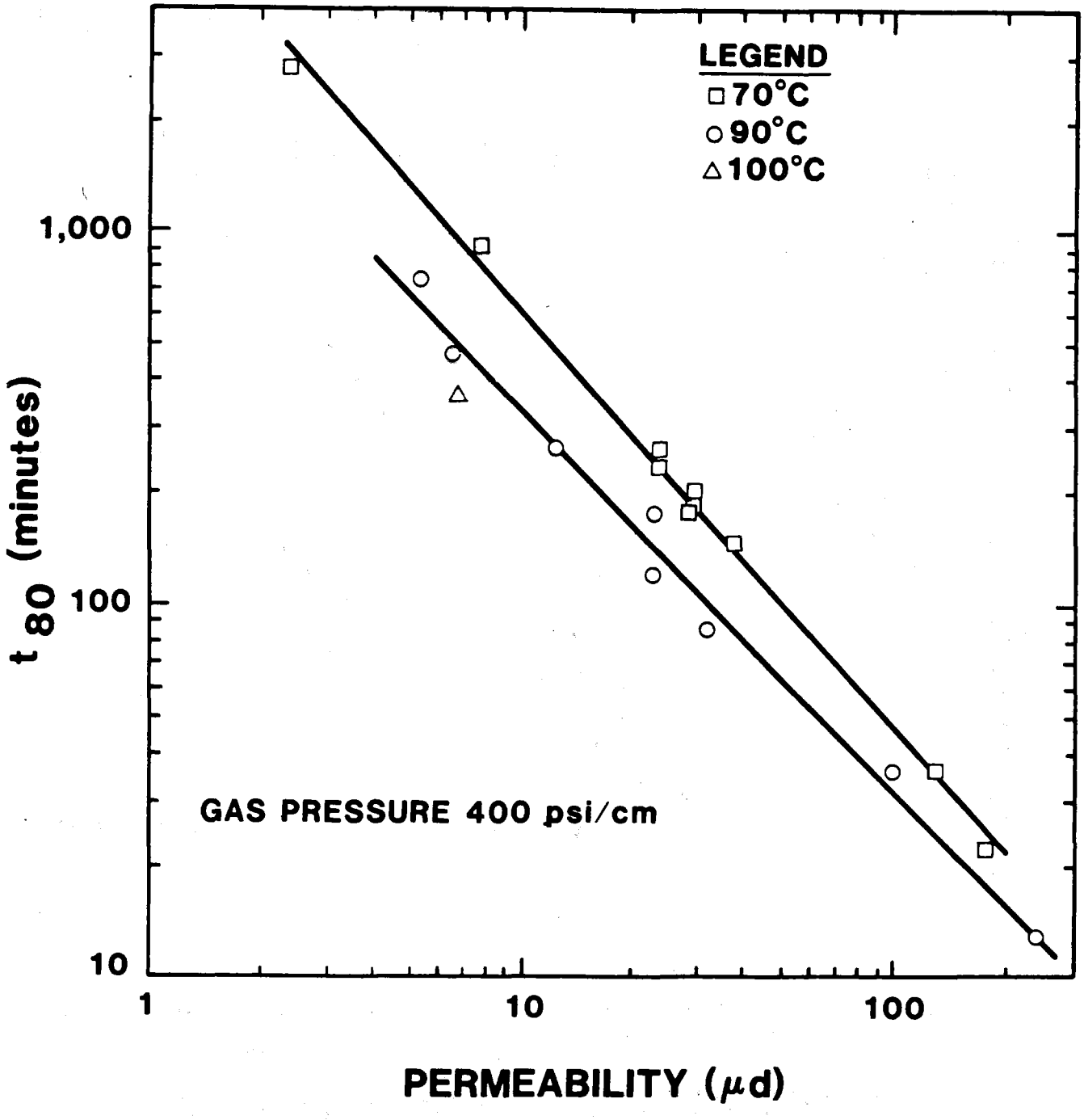

Figure 9.3 Cleanup Time (t_{80}) versus Core Gas Permeability (NIPER)

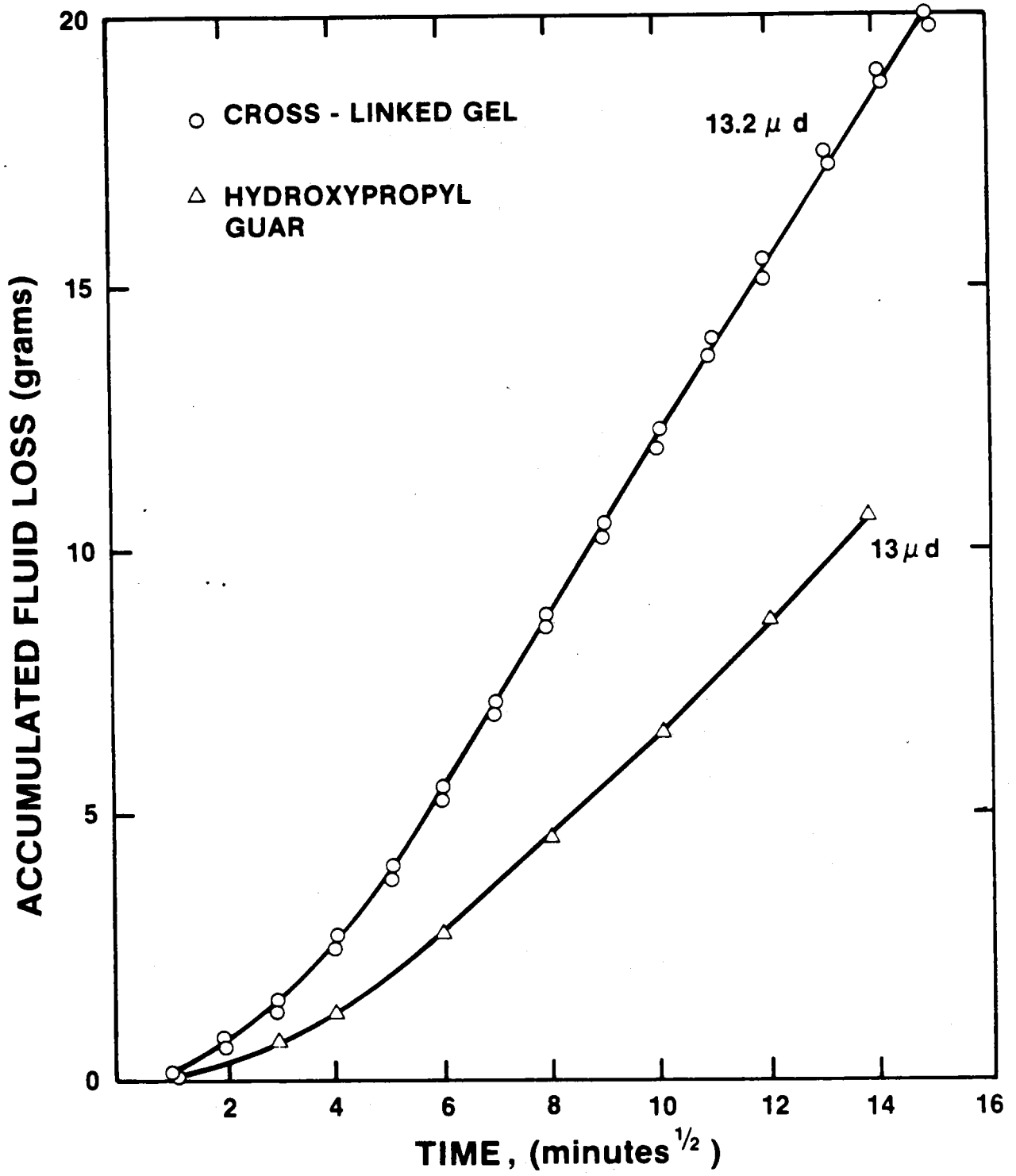

Figure 9.4 Fluid Leakoff in MWX Paludal Core (NIPER)

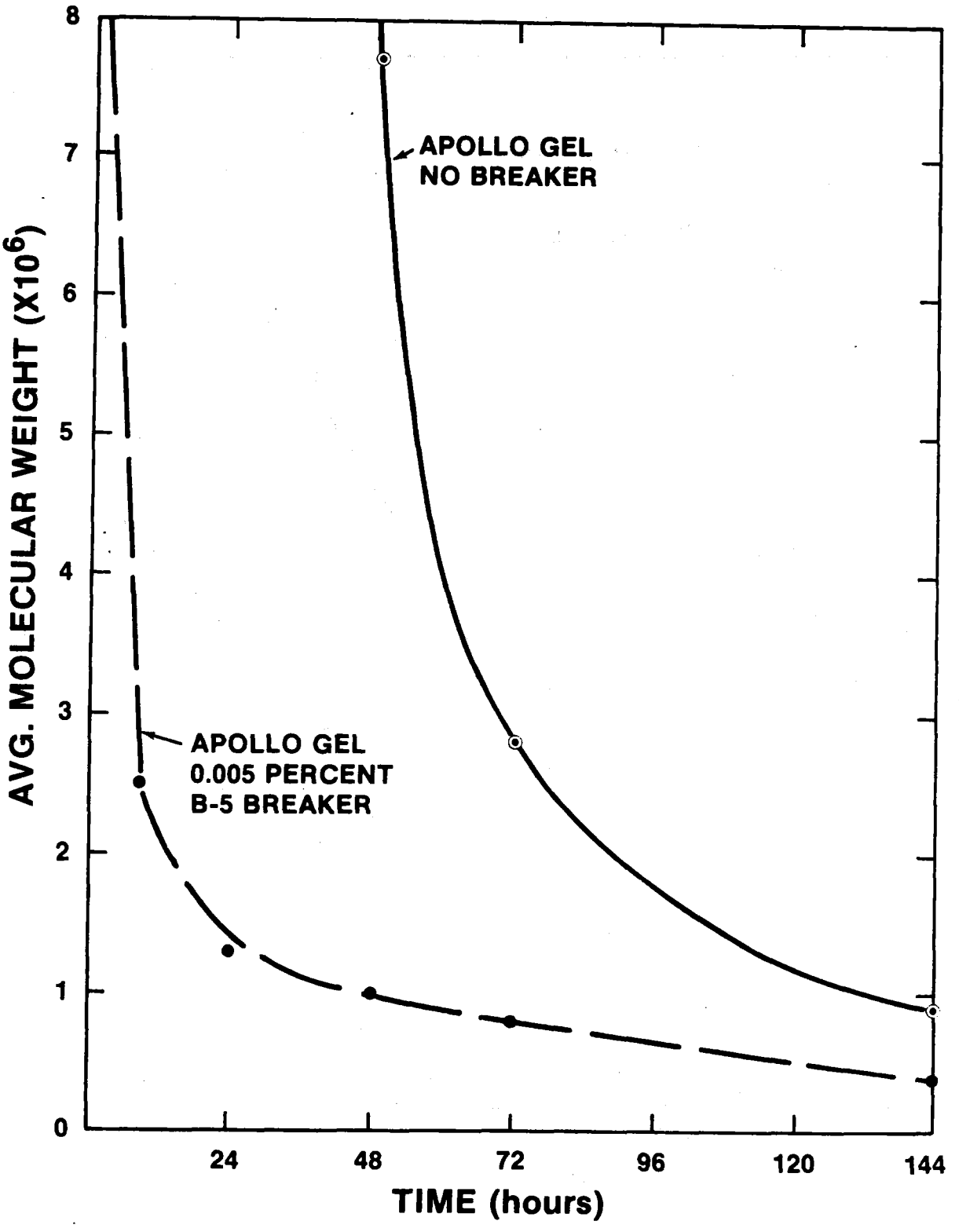

Figure 9.5 Degradation Times for Crosslinked Apollo Gel with and without Breaker (NIPER)

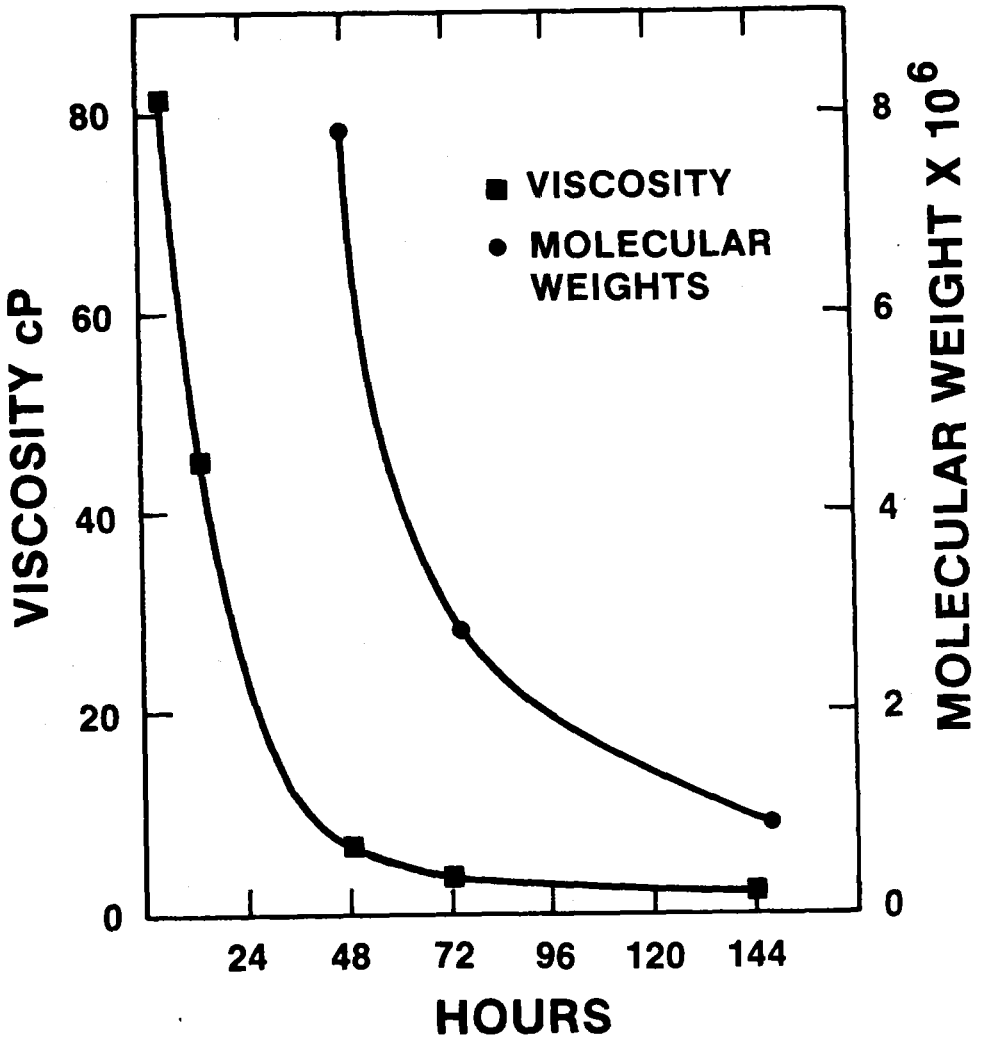

Figure 9.6 Degradation of Viscosity and Molecular Weights in Crosslinked Apollo Gel (NIPER)

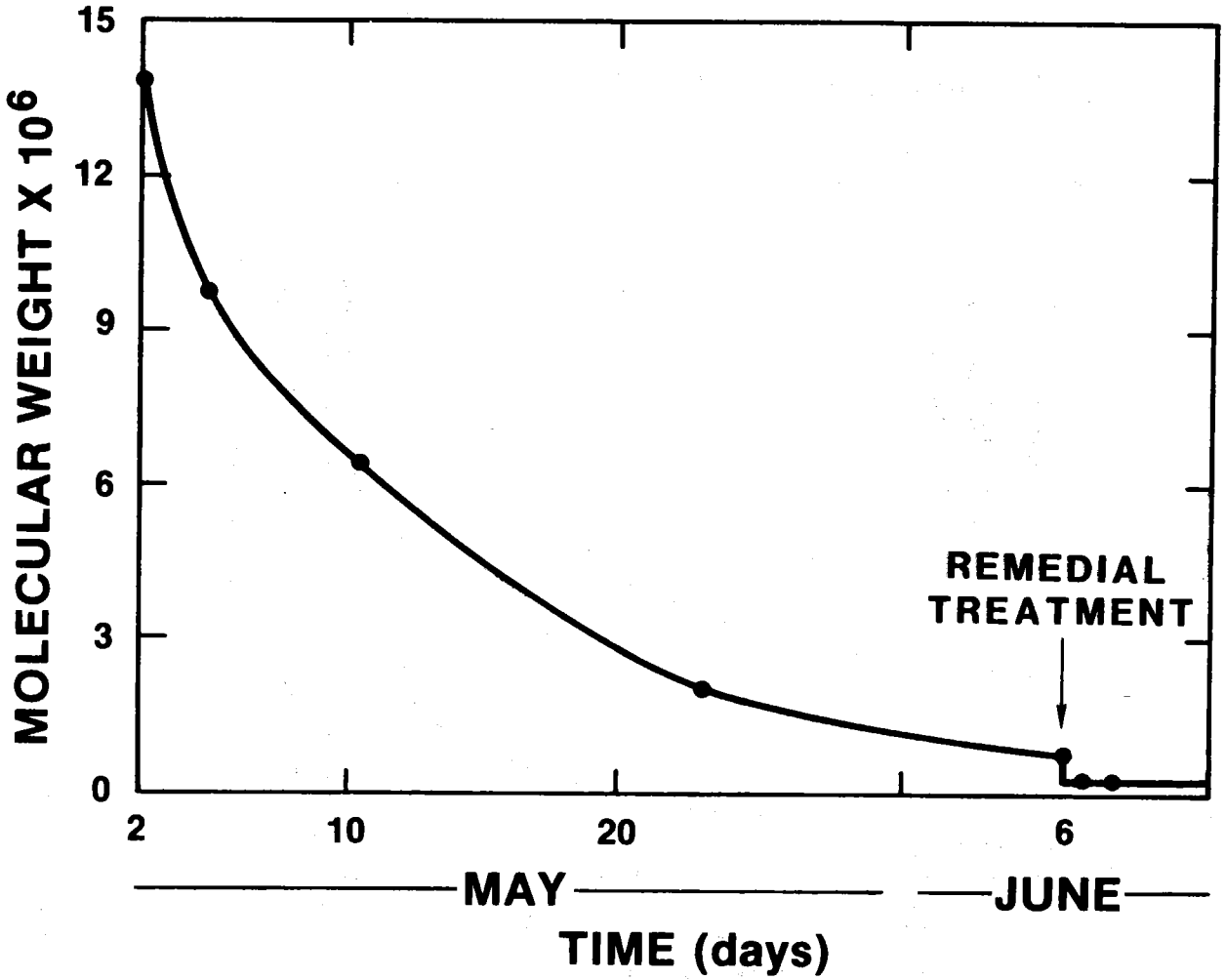

Figure 9.7 Molecular Weight in Returned Fluid vs Time (NIPER)

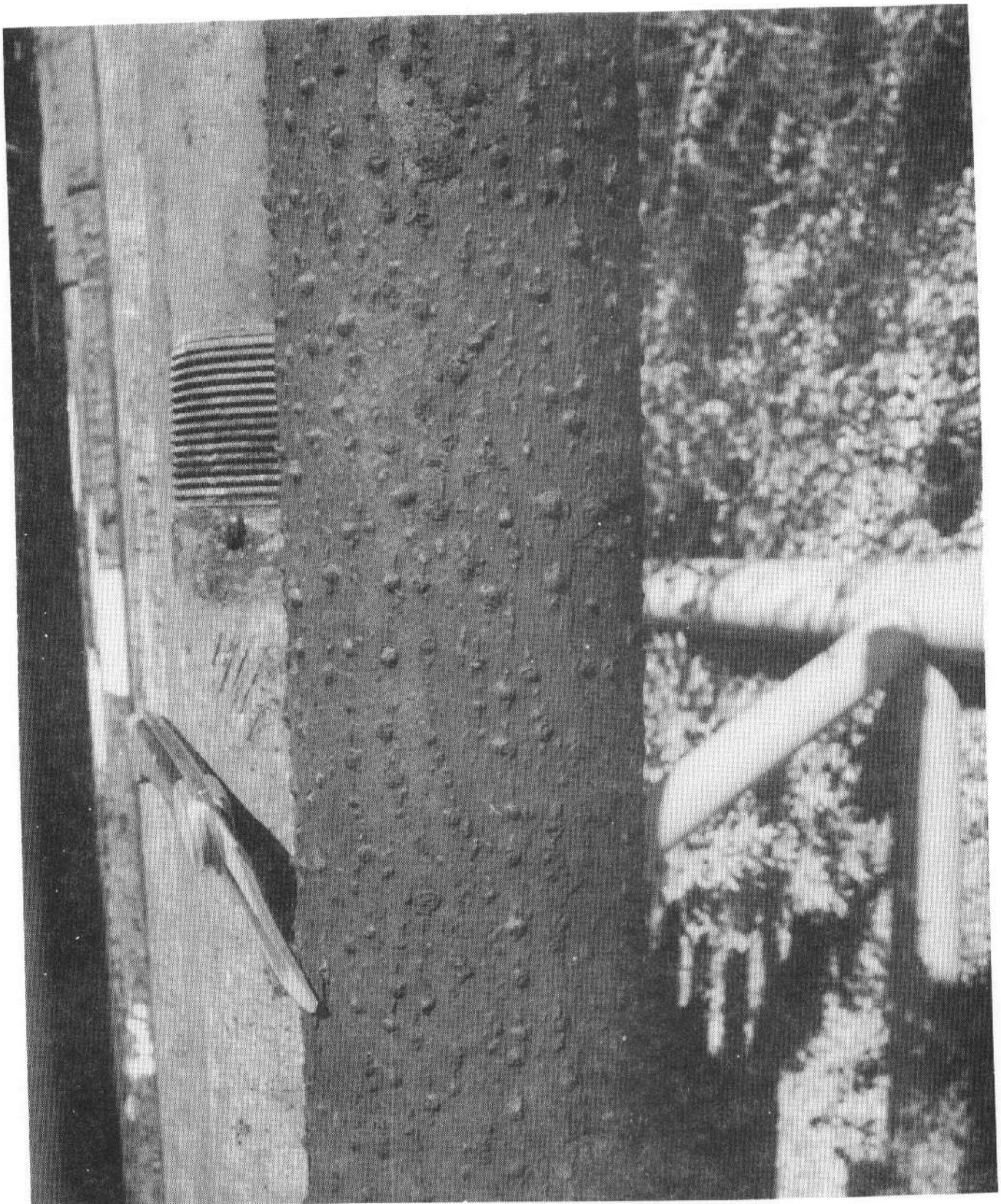

Figure 9.8 Corrosion of Section of Tubing Near Bottom of String from Remedial Treatment

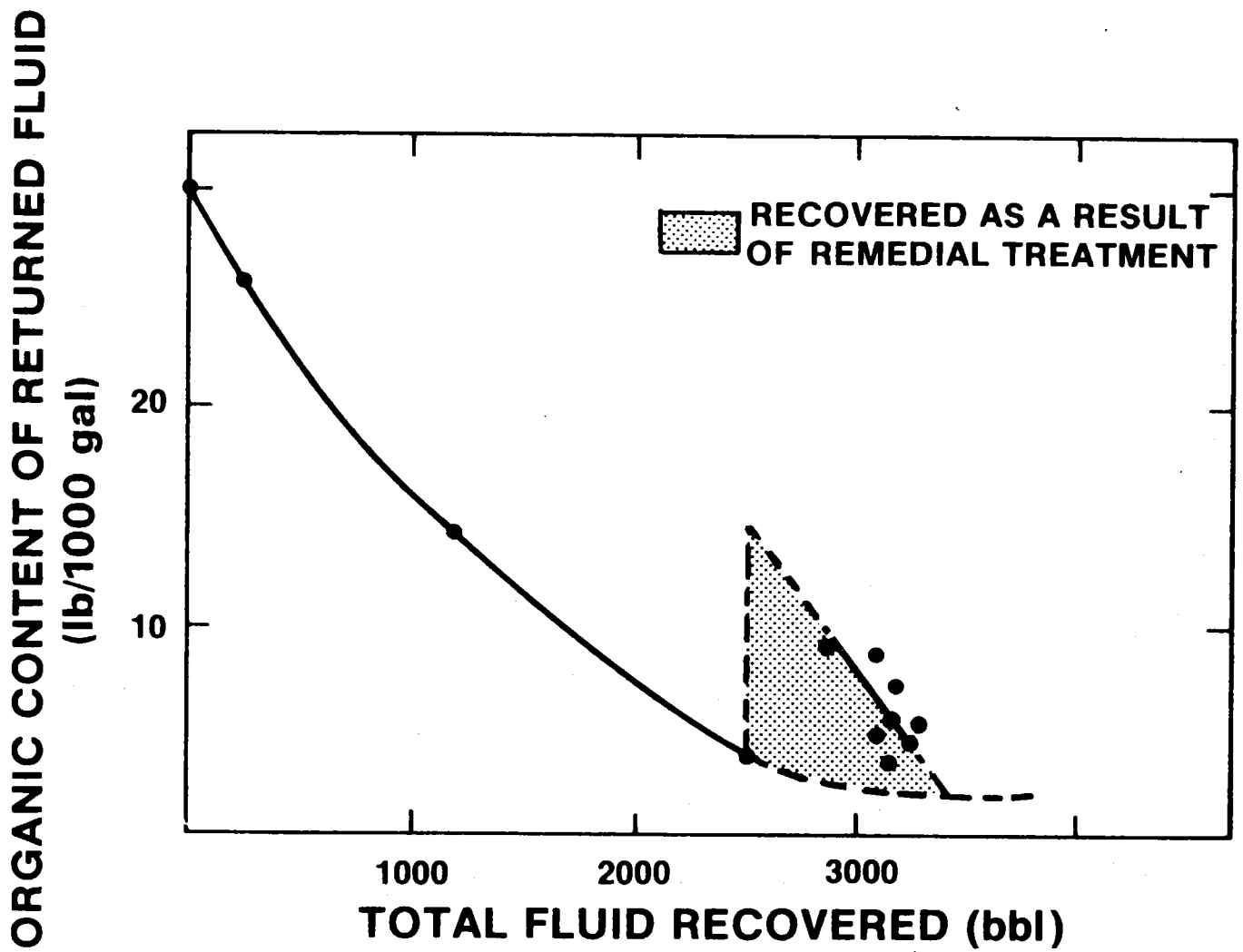

Figure 9.9 Amount of Organic Material in Returned Fluid (Western)

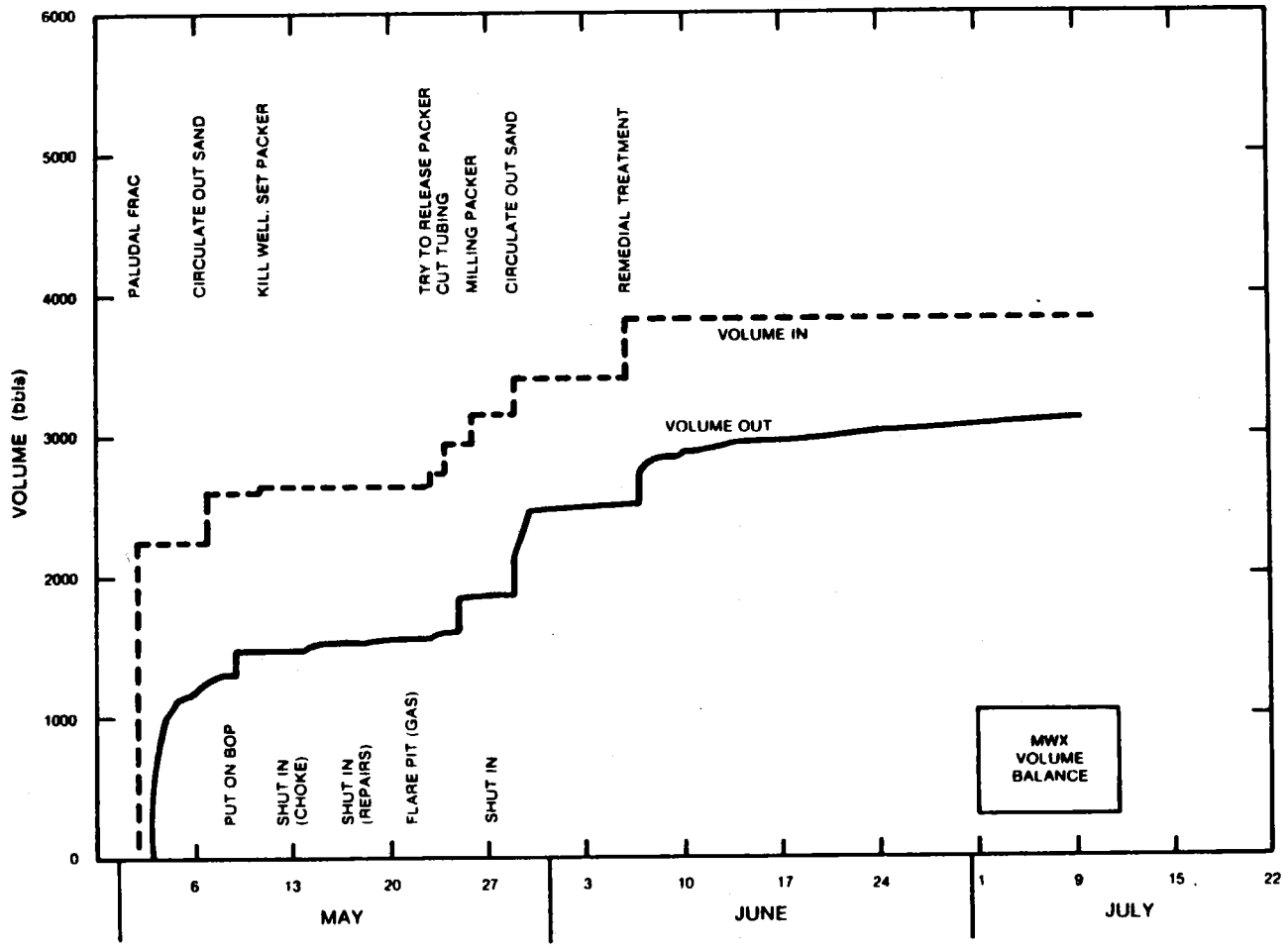

Figure 9.10 Volume Balance of Fluids from Phase II Stimulation

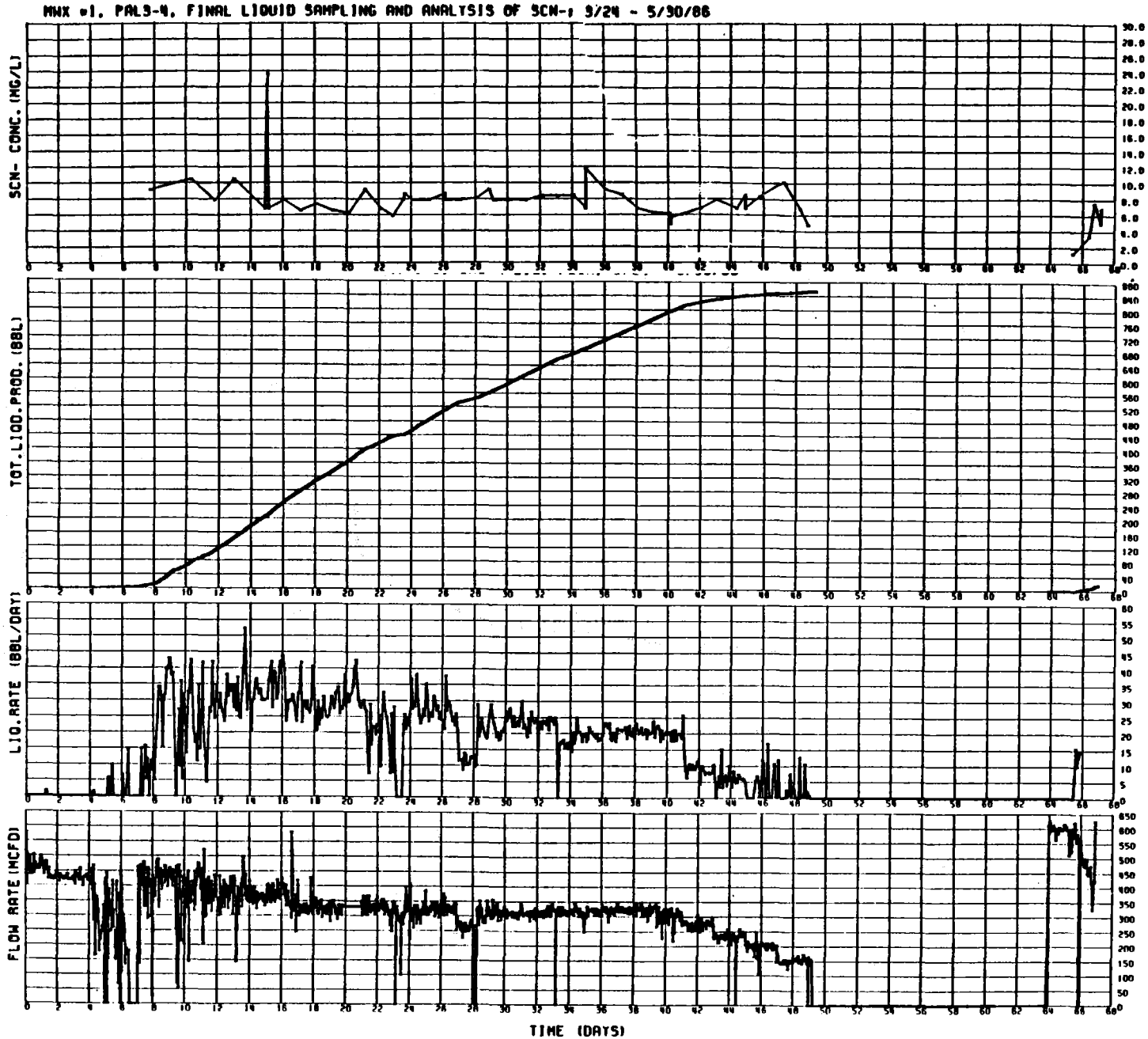

Figure 9.11 Reentry Production Data

10.0 BOREHOLE SEISMIC ANALYSIS OF PALUDAL STIMULATIONS

Billy J. Thorne
Sandia National Laboratories

Borehole seismic data acquisition and analysis of Phase I and Phase II of the paludal stimulation were carried out by two separate teams using different methods. The Phase I effort was documented in SPE/DOE/GRI 12852 by C. M. Hart, D. Engi, R. P. Fleming and H. E. Morris.[1] The Phase II effort was documented in a draft report by E. P. Chael and T. Cabe.[2] This section is extracted from those two reports.

10.1 PHASE I

10.1.1 Instrumentation

Microseismic activity was monitored prior to, during, and subsequent to the December 6, 7, and 9 treatments using two three-component geophone packages designed to operate downhole.[3] A schematic of the geophone tool is shown in Figure 10.1. The unit is 3-5/8 in. in diameter and 9 ft in length and is operated on a single conductor wireline which provides power to the electronics, control to a clamping arm, and the return path for the multiplexed output from the geophones.

For this experiment, borehole seismic units were lowered on wirelines in MWX-2 and MWX-3 to depths of 6990 ft and 7035 ft, respectively, and locked against the wellbores by extending the retractable arms. Bridge plugs had been set at 7050 ft in MWX-2 and 7060 ft in MWX-3 (to prevent gas flow from the perforated zones) creating a lower boundary for tool depth. A squeeze job was performed in MWX-2 to shut off perforations above the bridge plug at 7054 ft.

After the triaxial tools were clamped against their respective wellbores, downhole orientation of the triaxial geophone package, with

respect to North, was determined by firing 6-gram perforation shots at known locations in Zone 4 of MWX-1.

10.1.2 Microseismic Events

Acoustic emissions detected by the downhole tools during and following stimulation treatments were used to map the fracture plane. The seismic events examined are thought to be caused by shear failure induced by the open, pressurized fracture, the localized high pore pressure zone surrounding the fracture, and the presence of inhomogeneities (thus, planes of weaknesses) existing in the rock surrounding the hydraulic fracture.[4] Although these events are not thought to be caused by tensile failure at the hydraulic fracture's expanding edge, their location can still be used to infer fracture azimuth and growth because the shear events are believed to cluster in a tight band near the hydraulic face.[5]

Stressed suddenly at a point, two elastic pulses travel outward from the source with approximately spherical wavefronts at different speeds, as illustrated in Figure 10.2. The faster P-wave (primary, compressional, longitudinal, dilatational) directions of particle motion are in the direction of advance of the wave, while the slower S-wave (secondary, shear) directions of particle motion are orthogonal to the direction of advance of the wave. Both waves intersect the wellbore where a real-time event detector, which triggers on signal amplitude, detects the particle motion. An example of a shear failure detected in MWX-3 during these experiments is shown in Figure 10.3. These events, 300-350 Hz in frequency, usually had clear P and S arrivals. Several other signal types were observed that did not have these characteristics. These are not fully understood and were not used in the analyses.

P-wave polarization of the microseismic events was used to determine the direction to the seismic source by inspecting velocity hodograms constructed from the two horizontal (H^1 and H^2) and one vertical (V) geophone responses. Velocity hodograms are plots displaying the

polarization of time series signals. The strike of the propagating signal relative to the geophone axis can be found from a hodogram of the outputs from the two horizontal geophones, while the apparent dip can be calculated from a hodogram in which the vertical geophone axis is plotted versus the resultant horizontal vector. Figure 10.4 exemplifies hodograms of the three axis recordings of a typical microseism. The event is characterized by a clear polarization of the P-wave and the nearly 90 phase shift with respect to the P-wave polarization when the S-wave arrives. This figure indicates a source azimuth of 44 or 224 and an inclination of 50 or 230.

Although the strike of a line containing the raypath is easily inferred from the events recorded by a single geophone package, the direction from which the signal is approaching, a, is ambiguous within 180 (i.e., a or a + 180). It was hoped that this ambiguity would be overcome by fielding borehole seismic units in both MWX-2 and MWX-3. Since the well-spacing at depth and tool depths were known, and horizontal and vertical angles of incidence for the two tools could be obtained from velocity hodograms, the source locations could be estimated using a triangulation process. The validity of this concept was tested by using three of ten perforation shots to orient the tools and attempting to locate the remaining seven shots by triangulation. All of the shots were located within a few feet of their known locations, so the technique located the perforation shots with a reasonable degree of accuracy. However, gas bubbling, from the bridgeplug or squeezed perforations, in MWX-2, prevented the detection of events during and after stimulation treatments in MWX-2 because the frequent "bubbling" signals masked the desired shear events. During the later stages of minifrac #2, MWX-2 was pressurized and the seismic activity, thought to be unrelated to the fracturing, subsided significantly, further substantiating the gas flow hypothesis.

Since triangulation was not possible, an attempt was made to locate the seismic sources using the data from the single triaxial geophone package in MWX-3. From knowledge of the compressional and shear wave

arrival times and wave velocities, the distance (D) to a seismic source can be calculated from a single package by

$$D = \frac{V_p V_s}{V_p - V_s} (t_s - t_p) \qquad (10.1)$$

where

V_p = P-wave velocity,
V_s = S-wave velocity,
t_s = time at which the P-wave arrives, and
t_s = time at which the S-wave arrives.

The time difference between P- and S-wave arrivals could be determined from the geophone output. The MWX site velocity data had been determined from previous seismic surveys.[6] However, the paludal zone is so lithologically complex that the seismic velocities of the medium were extremely variable with depth. Extrapolating these data over the region of interest could have potentially resulted in large inaccuracies. However, since the perforation shots used for orientation exhibited similar frequencies to the detected events, their exact locations (thus, distances) were known and the S-P delay times were available from the orientation data set. The quantity

$$k = \frac{V_p V_s}{V_p - V_s} \qquad (10.2)$$

was determined between MWX-1 and MWX-3. This empirical valve for k was substituted into Equation 10.1 to compute the distance to the source. The validity of this approach was demonstrated by again using several perforation shots to orient the MWX-3 tool and determine k, and locating the remaining shots with Equation 10.1. The use of the empirical valve for k was further substantiated when the initial shear failures were located at the MWX-1 wellbore.

10.1.3 Step Rate/Flowback Tests

During these preliminary tests, approximately 120 bbls of 2% KCl water were injected into the formation at a maximum rate of 8 bpm. Because of the small injected volume and low injection rates, only four shear-type events having clear P- and S-wave arrivals and amplitude above the trigger level of 0.05 V at the computer interface were detected. The interpreted azimuth from these four events, however, show a tight grouping around N67°W from MWX-1 indicating a vertical fracture plane. The four events spanned a height of 105 ft (7120-7015 ft).

10.1.4 Minifrac #1

Of approximately 100 acoustic events that occurred during and after the first minifrac, 15 had amplitude of 0.05 V or greater with clear compressional (P) and shear (S) arrivals on all three components and could be located using the data from the single three-component package in MWX-3. These events fell on a N63°W azimuth from MWX-1 with an 11° standard deviation. There was a clear temporal progression of the microseisms with the earlier events clustering near MWX-1 and the later occurring near the perimeter of the fracture zone. Wing length of minifrac #1, as indicated by microseismic activity, was approximately 250 ft and the fracture extended vertically from 7140 ft to 7010 ft, giving a fracture height of approximately 150 ft.

10.1.5 Minifrac #2

Both the volume and the concentration of gel injected into the formation were doubled for minifrac #2, resulting in a substantial increase in seismic activity. Of over 700 acoustic events detected during and after this minifrac, 56 had amplitude greater than 0.05 V and were interpretable. Again, a temporal progression in the location of the microseisms was notable. The events clustered around a N67°W azimuth from MWX-1 with a 6° standard deviation. Fracture height, approximated

only from minifrac #2 microseismic activity, was 130 ft (7165 to 7035 ft). Past experience has indicated a range sensitivity for the borehole seismic tools in typical oil and gas producing reservoir rock from 20 to 500 ft.[5] The technique has not been effective beyond 500 ft because the signal from shear failure events is so attenuated that it is unobservable. During the later stages of minifrac #2, the received P-waves were attenuated such that they were no longer distinguishable from background noise. Although the fracture likely extended more than 375 ft from MWX-1, the seismic package in MWX-3 could not map the fracture beyond that distance.

Figure 10.5 shows the composite locations (from step rate/flow back tests, minifrac #1 and minifrac #2) of rock failures that could be determined from the single triaxial tool in MWX-3. These event locations, projected onto the horizontal plane at the depth of fluid injection, imply a vertical fracture plane oriented N67°W from MWX-1. The standard deviation of the points about the plane is 8°. This result is consistent with prefracture estimates of fracture azimuth at this depth. A number of independent geologic, core, and analytical predictions produced a mean orientation at this depth of N65°W±12°.[7]

A side view of the composite source locations is shown in Figure 10.6. This cross section shows vertical fracture growth from 7165 to 7005 ft, a 160 ft fracture height, and a minimum wing length of 375 ft.

10.1.6 Summary

The Phase I stimulation was completed December 6-9, 1983. One step rate test, two flowback tests, and two minifracs were conducted in MWX-1 while a borehole geophone package in MWX-3 monitored fracture growth.

Pressure and temperature data analyses approximate a composite fracture height of 150 ft, an average fracture width of 0.32 in., and a

total wing length of 440 ft (Section 8.2). Not only did these data closely match the design predictions which were based on analytical modeling, but they also agreed well with the empirical results obtained with the borehole seismic system.

At least in this case, downhole seismic monitoring in a single offset well provided an effective method of mapping the propagating fracture. Microseisms attributed to shear failures in the reservoir rock defined a composite N67°W±8° fracture plane, 160 ft in height, with a minimum wing length of 375 ft. Seismic signal attenuation prevented the detection of events beyond this distance. These results are also consistent with independent prefracture azimuth predictions of N65°W±12°.

10.2 PHASE II

10.2.1 System Tests

Prior to the Phase II hydrofracture, we fielded the seismic system at the MWX site in order to develop methods of orienting the borehole seismic units (BSUs) and to test system behavior. We oriented the BSUs by observing the P waves from controlled sources in known locations. P-waves in a homogeneous, isotropic medium are linearly polarized along the direction of propagation, so measuring their polarization (azimuth and inclination) gives the direction back to the source. Two source types were tested, perforation shots and a surface air gun.

To test air gun orientation, we clamped BSUs in MWX-2 and MWX-3 at 7037 and 7052 ft, respectively. An air gun was fired at a location 7800 ft north-northeast of the wells. The large offset from the wells insured that the arrivals were not traveling too near the vertical as they approached the BSUs. When recording the air gun shots we filtered the signals for 10-100 Hz and sampled them at 1 kHz per channel. We fired two series of shots, with 12 shots stacked in each series. The stacked signals for one of the series are shown in Figure 10.7. The P-

wave arrivals were very clean and well polarized in both wells. Figure 10.8 shows horizontal and vertical projections (hodograms) of the motion of the receiver velocity vector, made by combining the X, Y, and Z signals. A least squares fit to the horizontal hodogram gives the azimuth to the source from the +X geophone axis. The vertical hodogram resolves the 180° ambiguity in the azimuth, since the source lies above the receiver. Combining this azimuth with the known direction of the source from the well gives the orientation of the +X axis relative to north. In another test orientations were obtained using two different air gun locations which were about 77° apart from the wellheads. Only the BSU in MWX-3 successfully recorded the shots from both locations; the tool in MWX-2 had suffered an electrical failure. The orientation estimates in this case differed by 8°. It is unclear whether this discrepancy is due to propagation effects between the sources and receiver or to a nonuniform tool response. When orienting the BSUs with a surface air gun, it would be preferable to average the results from several locations distributed around the wellhead.

As an alternative orientation method, we fired 6 gm perforation charges into the casing in MWX-1 at depths below the receivers. The BSUs remained clamped in MWX-2 and MWX-3 where they had recorded an earlier series of air gun shots. This permitted a comparison between the two methods. The perf shots were fired within 200 ft of the seismometers, a distance similar to that expected for the hydrofracture events. The high frequencies in the perf signals attenuate rapidly and are readily scattered by the paludal zone's complex velocity structure. The P arrivals were much stronger at the BSU in MWX-3, situated near the bottom of a prominent coal seam, than at the BSU in MWX-2, above the same seam. Three shots fired in zone 3 near 7133 ft in MWX-1 gave signals too weak to analyze. Usable signals were obtained from nine shots fired in sand zone 4 at depths between 7086 and 7094 ft Sample data for one of the shots are shown in Figure 10.9. The signals were filtered for 100-500 Hz and sampled at 2.5 kHz. The shots were not repeatable enough to stack.

Only five of the nine shots in zone 4 were usefully recorded in MWX-3 because of sporadic electrical noise, while all nine shots were captured in MWX-2.

As with the air gun records, the first arrivals on the X, Y, and Z traces were combined to give vertical and horizontal hodograms. Examples are given in Figure 10.10. The five shots recorded in MWX-3 gave a standard deviation in azimuth of 1.6°, which reflects the quality of the observed P phases on the X and Y components. The apparent inclination showed much greater deviation about a nearly horizontal mean. The source and receiver locations give a predicted inclination of 79° from +Z (down). There may have been trouble with the vertical geophone in MWX-3 during the perf sequence because its signal is weak throughout the event coda (Figure 10.9). As a result, the inclination does not reliably resolve the 180° ambiguity in orientation in this case. The P-waves seen in MWX-2 had low signal-to-noise ratios on all components which led to a 16 standard deviation in azimuth.

The mean perf shot orientation for MWX-2 was rotated 13 clockwise from that obtained from air gun data. The perf result in MWX-3 was rotated 8° clockwise. The relative source distances argue in favor of the perf gun results, but the BSUs are more likely to suffer from a nonuniform response at the frequencies of the perf data. Further testing and development of both techniques is certainly warranted.

The perf shots also provided information about the average seismic velocities in the stimulation interval. We could not control the firing time of the shots with sufficient accuracy to permit direct measurement of the P- or S-wave travel times between source and receiver. Instead, the difference between the P and S arrival times at each receiver gave an estimate of the velocity coefficient, k (Eq. 10.2).

The perf shot records generally had high signal to noise, enabling reliable timing of arrivals. Because the distances involved were small, the S-wave arrived during the P-wave coda. The MWX-2 and MWX-3 data gave $k = 27.1 \pm 3.7$ ft/ms and 31.6 ± 2.8 ft/ms, respectively. The error bounds on the two estimates overlap, so we felt it reasonable to combine the data from both wells and determine a single representative value for k. This value, used in the subsequent analysis of hydrofracture events, was 29.3 ± 3.9 ft/ms.

We used the difference in arrival times of the P-wave at the two observation wells, together with the difference in propagation distance, to obtain an estimate of the P-wave velocity, $V_p = 12.1 \pm 1.1$ ft/ms. This is somewhat faster than the compressional wave velocity determined from an earlier vertical seismic profile of MWX-1[6] and close to the mean velocity indicated by the sonic logs. Using the S arrivals at the two wells, we obtained $V_s = 9.5 \pm 0.7$ ft/ms. These compressional and shear velocity estimates are consistent with the average value of the coefficient k within the measurement errors. The velocity estimates here represent only the two paths connecting the perf gun in MWX-1 with the BSUs in MWX-2 and MWX-3. As a result, the stated uncertainties do not indicate possible ranges in the values for other paths in the immediate vicinity. We have assumed that the interval of interest is homogeneous. The sonic logs demonstrate that this is not the case but incorporating the effects of velocity variations will require further study.

10.2.2 Hydrofracture Monitoring

To monitor seismic activity induced by the hydrofracturing, we clamped BSUs at 7037 ft in MWX-2 and 7052 ft in MWX-3. Before pumping began, we used the surface air gun to orient the geophone axes. This indicated that the +X axes in MWX-2 and MWX-3 were oriented along N224°E and N252°E, respectively. The high-gain X, Y, and Z geophone signals from both BSUs were filtered to pass 100-500 Hz, then sampled at 2.5 kHz per channel. The event detector scanned one horizontal channel from each

BSU. We initially set the trigger level at about five times the background noise level which had been observed with the pumps off. Unfortunately, the pumping added substantially to the noise in the 100-500 Hz band. With the pumps on, the background noise level roughly doubled in MWX-2 and more than tripled in MWX-3. This resulted in almost continuous triggering of the even detector, so the trigger level was increased during pumping to accommodate the greater noise level. Following shut-in, the trigger level was reduced to the value originally chosen.

The event detector triggered a total of 340 times in ten hours of hydrofracture monitoring. Only 12 events were judged to be both seismic in nature (originating away from the observation wells), and of sufficient quality to attempt to locate. Five of these 12 events occurred when the pumps were off, so the analysis of them is not degraded by the pumping noise discussed earlier. All 12 of the events which could be analyzed had coda durations of over 100 ms.

To locate an event, we picked P- and S-arrival times and measured the P-wave polarization for the data from both BSUs. The P- and S-arrivals were identified and timed by examining the original geophone signals, envelopes of the traces and hodograms. Identification of the phases was generally not definitive even for the 12 events deemed suitable for analysis. Timing was uncertain because of the typically emergent character of the P-waves and because S-waves usually arrived during the P-wave coda. The preferred picks were chosen to be both reasonable for the waveforms from a given BSU, and consistent between the two BSUs. The latter criterion in this case meant that the BSU with the earlier P-arrival should also have the shorter S-P time. A sample event and its preferred P and S picks are shown in Figure 10.11.

The single-station technique was applied separately to data from each BSU, yielding different location estimates for an event. The polarization of the P-wave gave the direction from the receiver back to

the source. A homogeneous, isotropic medium was assumed; no attempt was made to correct the measured directions for propagation effects. The distance to the source in the indicated direction was obtained from the S-P time, using Equation 10.1 and the velocity coefficient, k, determined from the perf shots. The single station method results in a two-fold ambiguity in location, since the source could lie along either half-line of the P polarization trend. Applying this method to two receivers thus produced four potential locations, and we retained the two which were in best agreement (one from each BSU). Alternative estimates of the epicenter were obtained by triangulating the polarization lines from the two BSUs, and by intersecting arcs drawn around each BSU with radii determined by the S-P times. In the latter case, the arcs were drawn on a horizontal plane and their radii were corrected for the inclinations of the P polarizations. Figure 10.12 shows the various epicentral estimates for the event of Figure 10.11.

The different locating schemes are not fully independent, but we feel that the discrepancies between them give an indication of the uncertainties involved. The average coordinates of the separate estimates were taken as the preferred location for each event. A circle with a radius equal to the root mean square distance between the mean location and the separate locations were used as an error estimate. The preferred locations with error circles for the 12 events analyzed are shown in Figure 10.13. Estimated depths for these events varied from 6969 ft to 7223 ft, a range of 254 ft.

The locations show a northwest-southeast trend through MWX-1, but the error circles allow a large range in angle for this trend. Ten of the 12 epicenters lie within 110 ft of MWX-1. Because the errors are on the order of 50 ft, substantially larger offsets of the events from the frac well would be required in order to tightly constrain the fracture azimuth. The errors similarly result in large uncertainties in wing length estimates.

Event 123 gave a location to the northwest of MWX-3, well away from all the other events. It would be incautious to conclude that the hydrofracture extended out into this region on the basis of this single datum.

10.2.3 Discussion

The major factor limiting the resolution and hence the usefulness of seismic fracture diagnostics at MWX is the low signal-to-noise ratio of the events. The microseismic events generated by the fracture treatment were too weak to produce signals at the BSUs which could be interpreted with any confidence. The fracture event shown in Figure 10.11, one of the cleanest detected, illustrates the problem. Accurate identification and timing of the P and S phases are essential if the events are to be located using only two stations, yet the data for the fracture events are very ambiguous. An error of 1 ms in the measured S-P time results in a location error of approximately 30 ft. At 300 Hz, 1 ms corresponds to less than 1/3 of a cycle. Because the P phase typically emerges slowly from the background nose and S phase arrives during the P coda, such timing accuracy is unattainable for the events we have observed. This is so even if identifications of P and S arrivals are unambiguous, which is not the case. The polarization directions of the P arrivals are also needed for two-station locations. The weak P signals relative to noise in Figure 10.11 clearly result in large uncertainties in such measurements, even if the tool response is assumed known. During the pumping of the frac fluid, the quality of the events was further degraded because of the increased background noise level.

Ideally, we would like to see frac event signals comparable in quality to the perf shot records (Figure 10.9). These records have acceptable signal-to-noise (especially in MWX-3), which results in some confidence in their analysis. The P arrival is generally well polarized and there is a definite break in polarization when S arrives. Timing and polarization show excellent repeatability between shots. However, the

consistency in this case represents the resolution in the measurements, not their absolute accuracy. Because the source and receiver locations were virtually the same for all of the perf shots, the measurements may contain systematic errors. Of great concern are errors in the polarization measurements caused by a nonuniform tool response. The complex stratigraphy of the paludal zone introduces another source of error. Sonic logs of this interval show significant velocity contrasts, especially at the many coal seams present. These interfaces scatter the seismic energy and induce complexities in the observed signal. Even if the identified first arrivals are the direct rays, and these are isolated from multiple and converted phases, the ray paths are still distorted by the structure. This results in errors both in the direction and distance to an event, which are inferred from the polarization and arrival time information.

Observations of the hydrofracture activity and from the prior background monitoring demonstrate the importance of using multiple stations. Many signals were recorded which had large amplitudes at one BSU and nothing above noise at the other. Such signals could not have originated away from the wellbore where they were observed. Discriminating these noises from events which are seismic in origin (and potentially associated with the hydrofracturing) is best accomplished by comparing signals from different receivers. Using more than one BSU also lead to better locations estimates. Since the stations are constrained to two offset wells at MWX, improvement on the configuration we used would require multiple BSUs in each well.

10.3 REFERENCES

1. Hart, C. M., D. Engi, R. P. Fleming, and H. E. Morris, "Fracture Diagnostics Results for the Multiwell Experiments Paludal Zone Stimulation," SPE/ DOE/GRI 12852, Unconventional Gas Recovery Symposium, Pittsburgh, PA, May 1984.

2. Chael, E. P. and T. Cabe, "Seismic Analysis of a Hydrofracture Treatment at the Multiwell Site," Draft Report, Sandia National Laboratories, February 1985.

3. Seavey, R. W., "Borehole Seismic Unit," Sandia National Laboratories Report, SAND 82-0373, May 1982.

4. Dobecki, T. L., "Hydraulic Fracture Orientation Using Passive Borehole Seismics," SPE 12110, 58th Annual SPE Meeting, San Francisco, CA, October 1983.

5. Albright, J. N. and C. F. Pearson, "Location of Hydraulic Fractures Using Microseismic Techniques," SPE 9599, 55th Annual SPE Meeting, Dallas, TX, September 1980.

6. Searls, C. A., M. W. Lee, J. J. Miller, J. N. Albright, J. Fried, and J. K. Applegate, "A Coordinated Seismic Study of the Multiwell Experiment Site," SPE 11613, SPE/DOE Symposium on Low Permeability Reservoirs, Denver, CO, March 1983.

7. Teufel, L. W., C. M. Hart, and A. R. Sattler and J. A. Clark, "Determination of Hydraulic Fracture Azimuth by Geophysical, Geological, and Oriented Core Methods at the Multi-Well Experiment Site, Rifle, Colorado," SPE 13226, 59th Annual SPE Meeting, Houston, TX, September 1984.

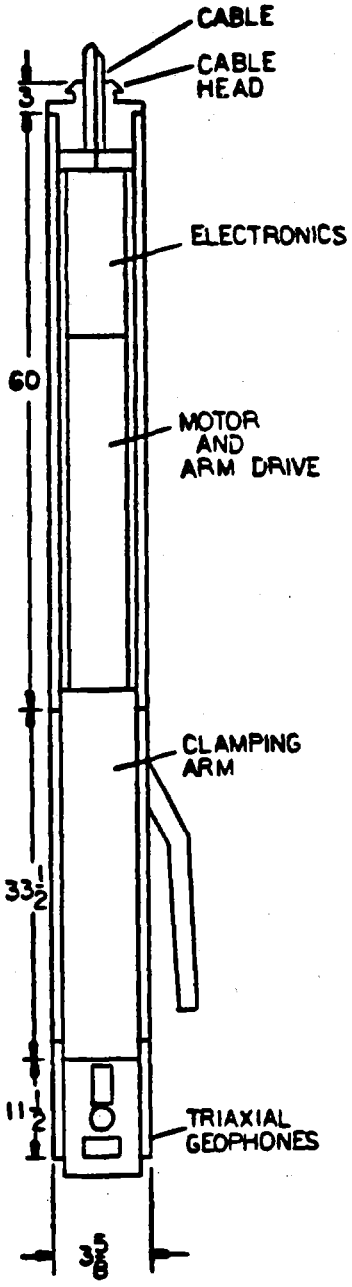

Figure 10.1. Schematic of the Borehole Seismic Units used in this test. Dimensions are in inches.

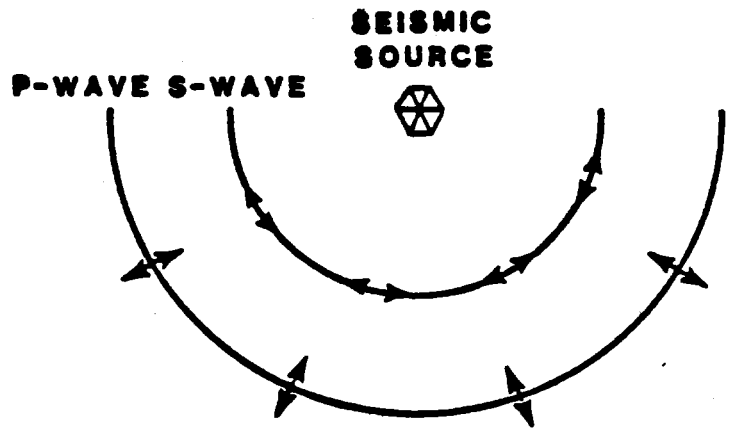

Figure 10.2. Seismic wave types.

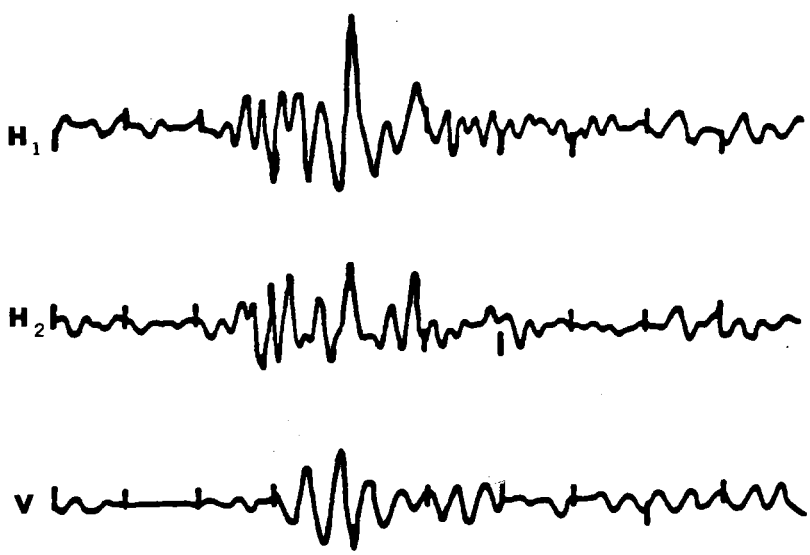

Figure 10.3. Sample event.

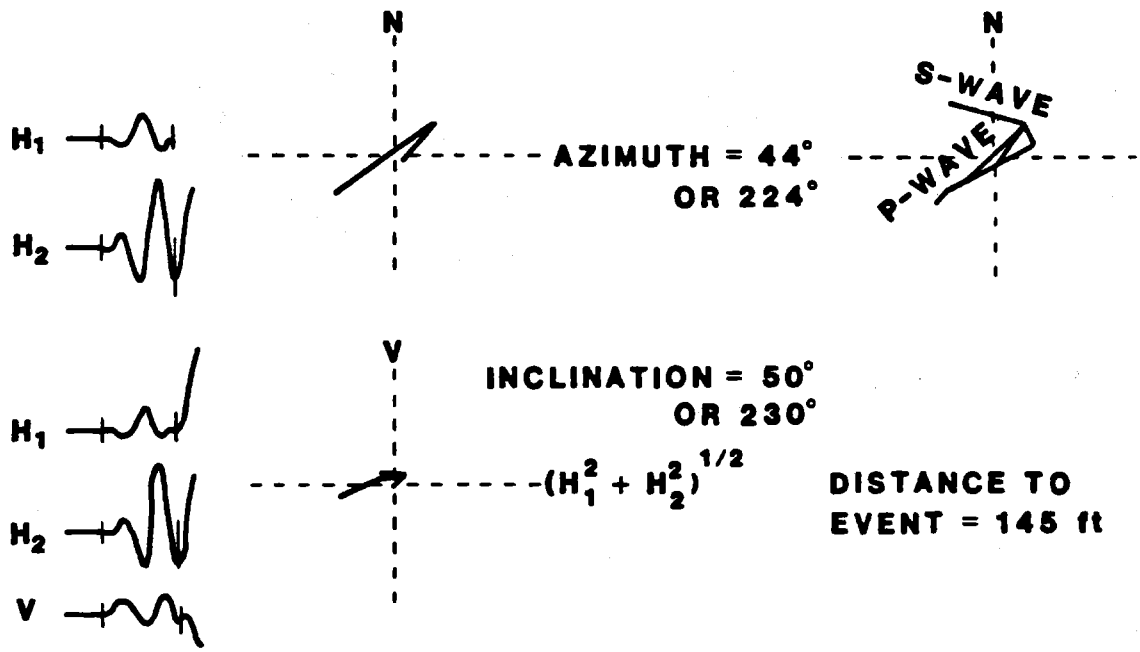

Figure 10.4. MWX/SX-1 event hodograms.

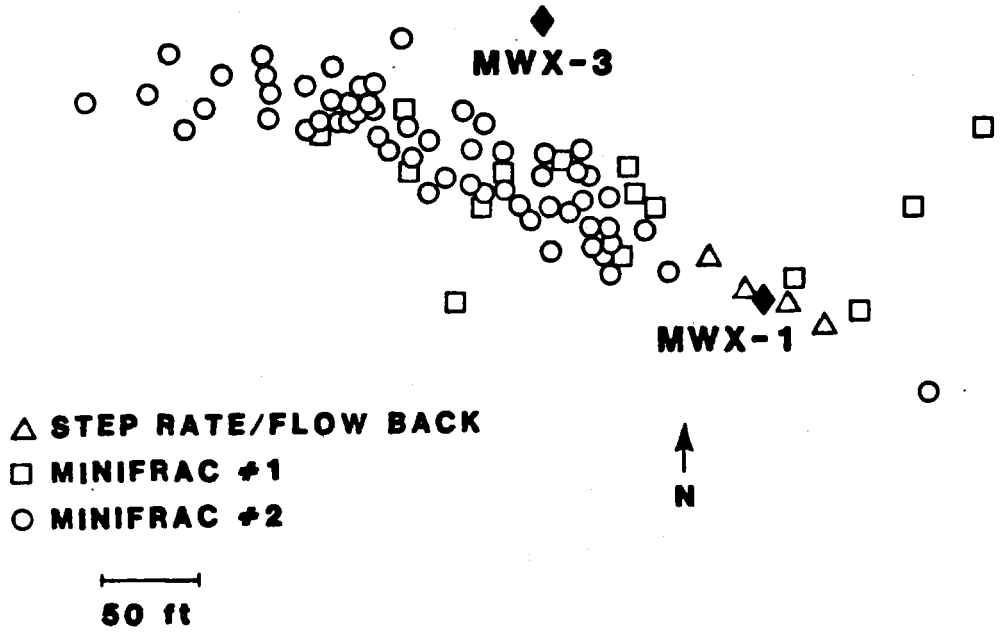

Figure 10.5. MWX-SX-1 event locations projected on horizontal plane.

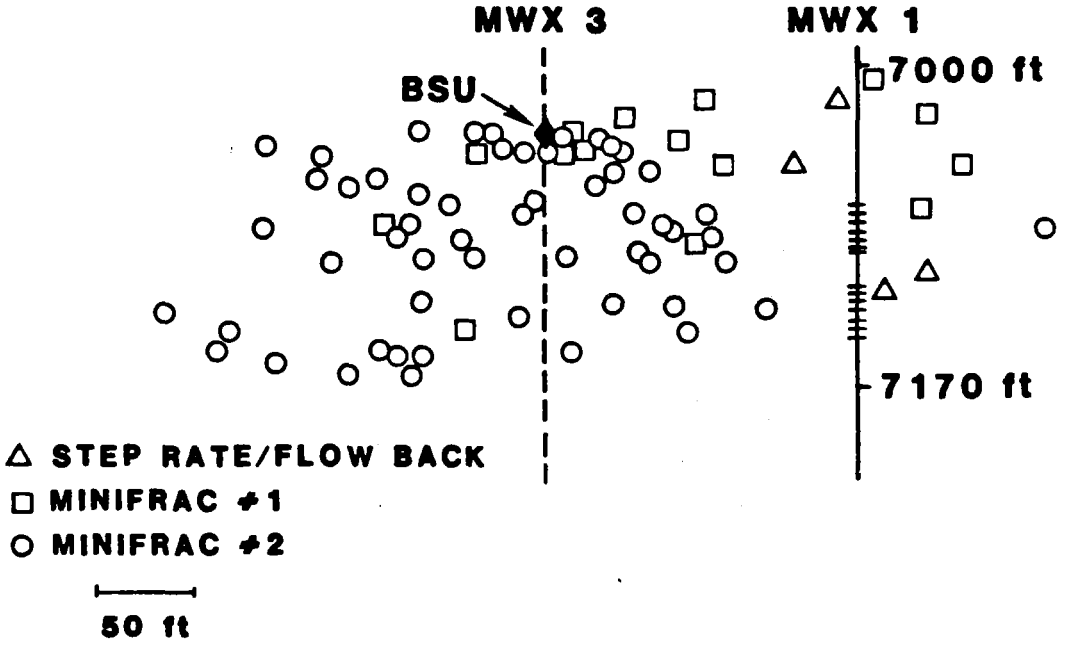

Figure 10.6. Event locations projected onto N67°W plane.

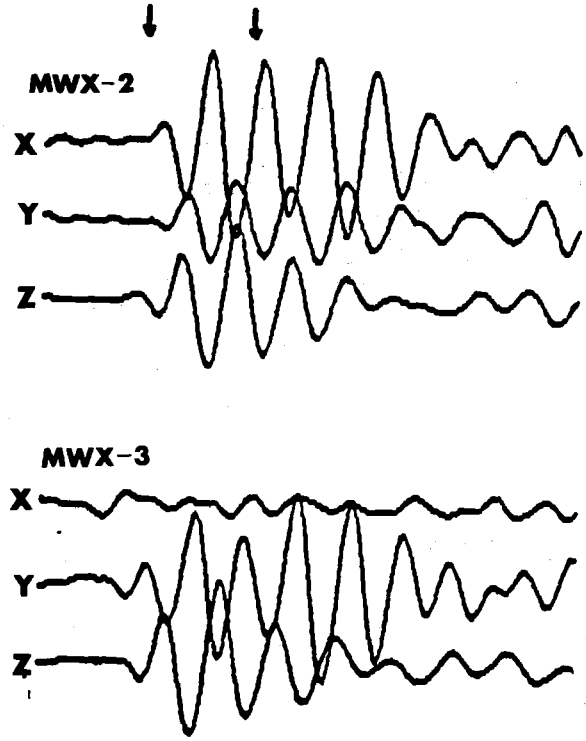

Figure 10.7. Seismograms obtained by stacking 12 shots from an air gun on the surface. Arrows bound interval of MWX-2 data used in the hodograms of Figure 10.8. The quiet X trace in MWX-3 indicates that the arrival was polarized along the Y-axis of that BSU.

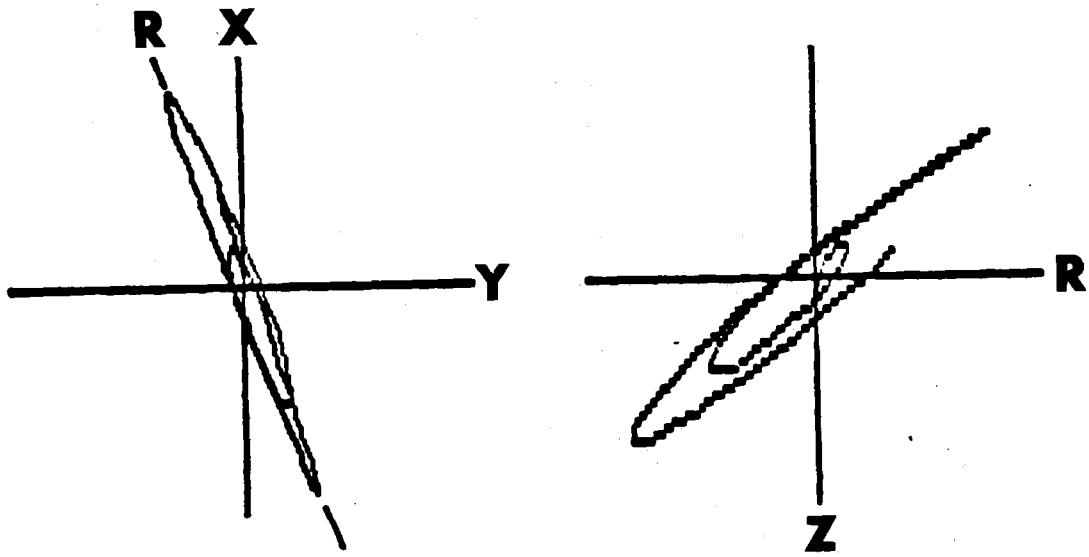

Figure 10.8. Polarization plots of the first arrival of the air gun pulse at MWX-2, obtained from the seismograms in Figure 10.7. The plot on the left shows the horizontal projection of the particle velocity vector. The plot on the right gives the vertical projection through R.

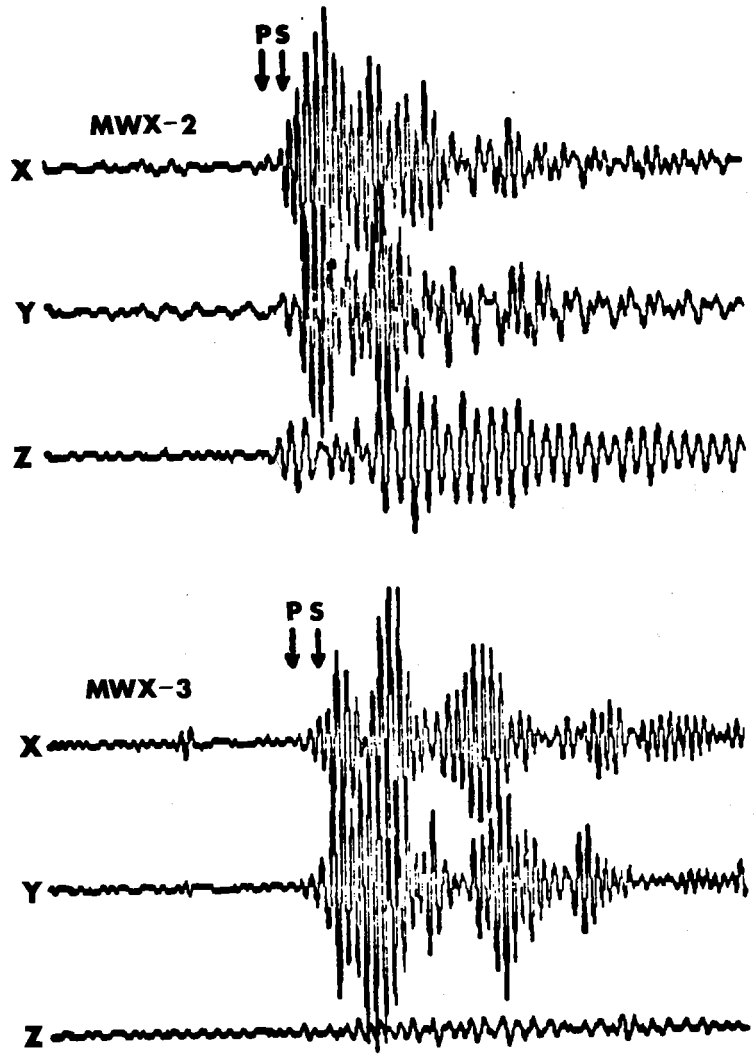

Figure 10.9. Seismograms from a perforation shot in MWX-1. Arrows show P and S phase picks.

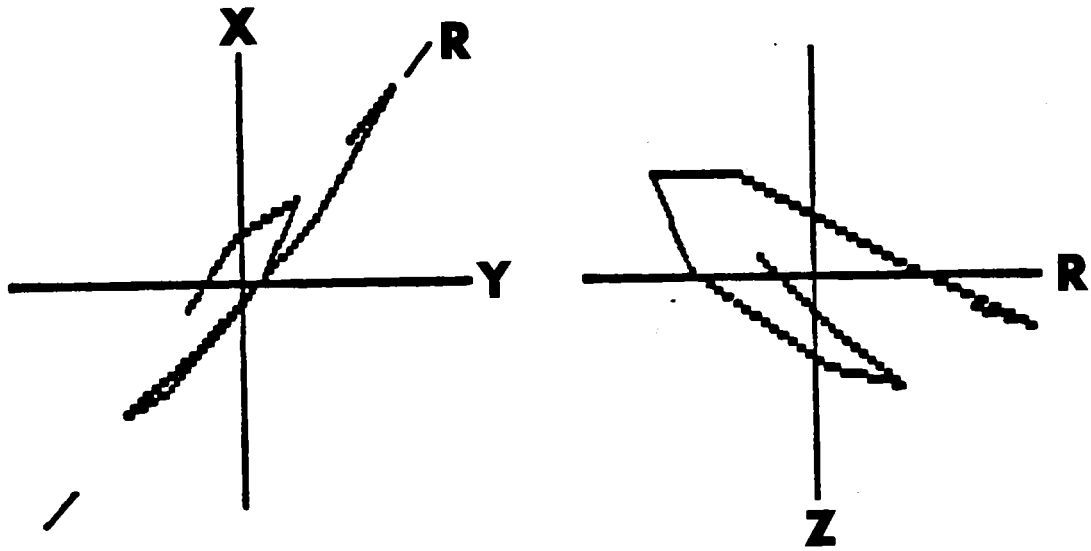

Figure 10.10. Polarization plots for the P arrival at MWX-3 from a perf shot in MWX-1, obtained from the seismograms in Figure 10.9.

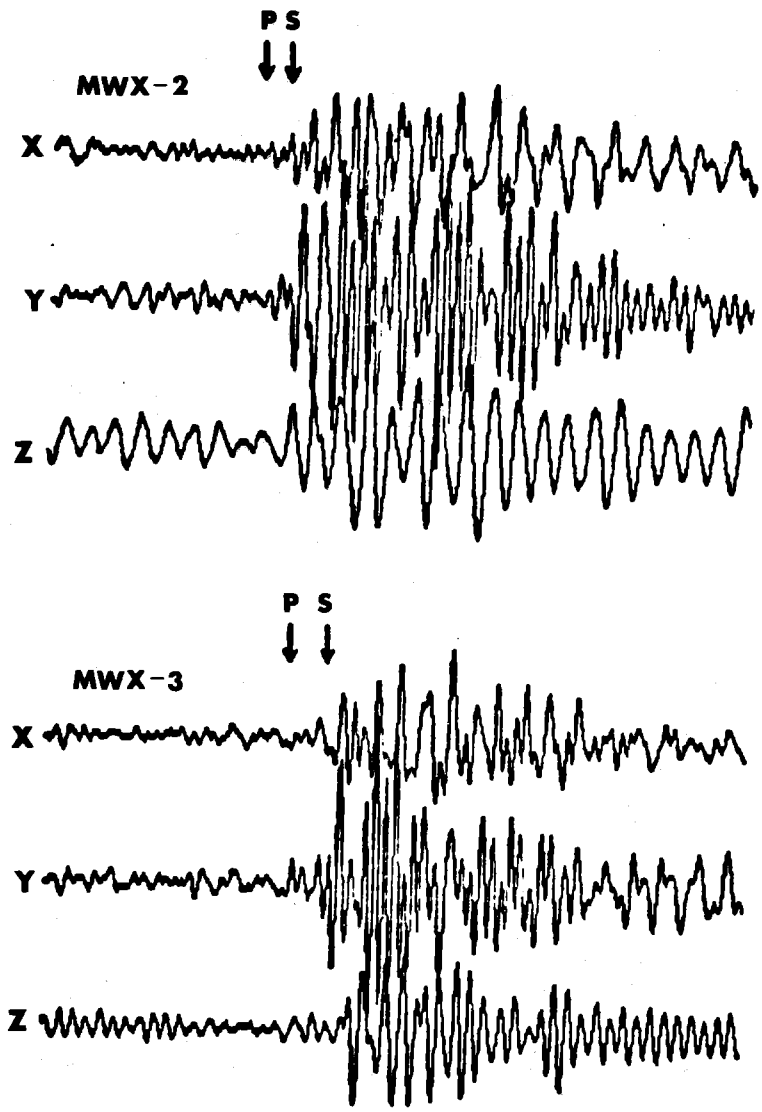

Figure 10.11. Microseismic event detected during hydrofracture monitoring. This event occurred after shut-in of the frac well.

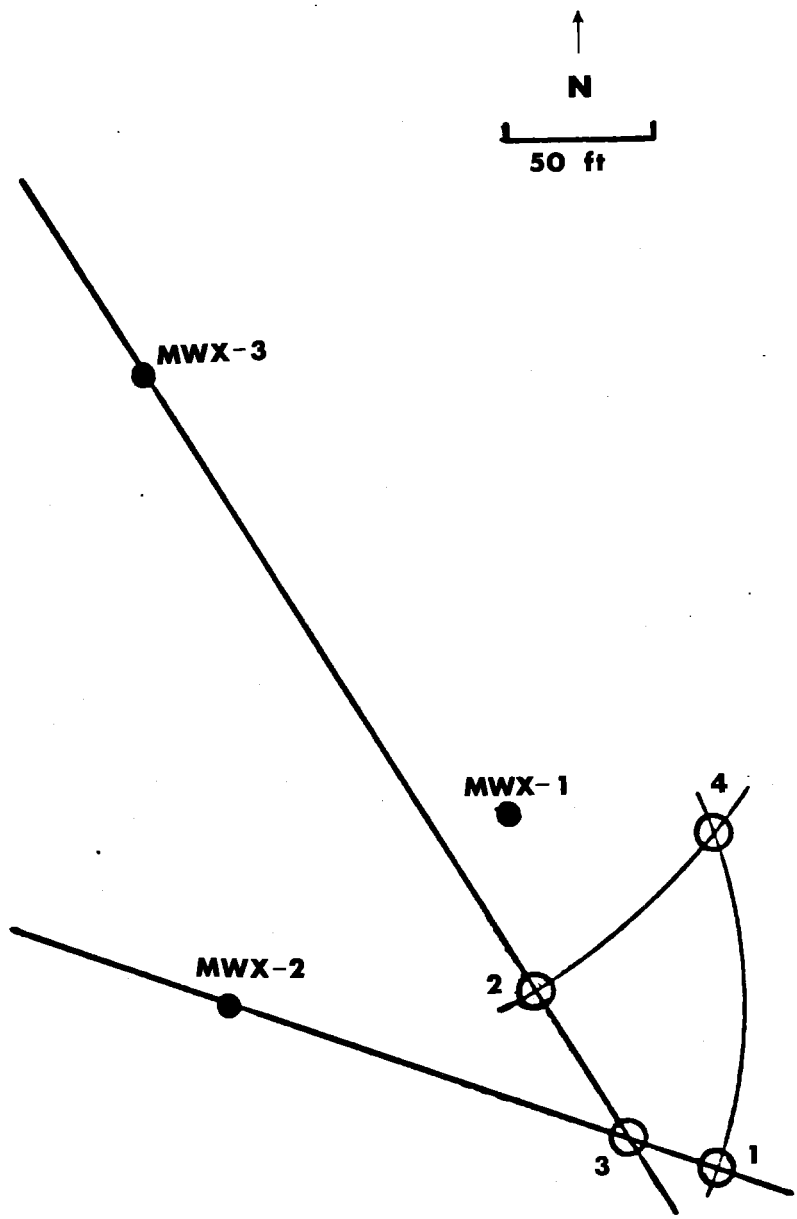

Figure 10.12. Locating scheme, using the data of Figure 10.16. Locations 1 and 2 rely on the MWX-2 and MWX-3 data independently. Location 3 is at the intersection of the polarization azimuths seen from the two wells (triangulated location). Location 4 lies at the distance from both observation wells indicated by the S-P times. Solid dots show the borehole geometry at 7000 ft.

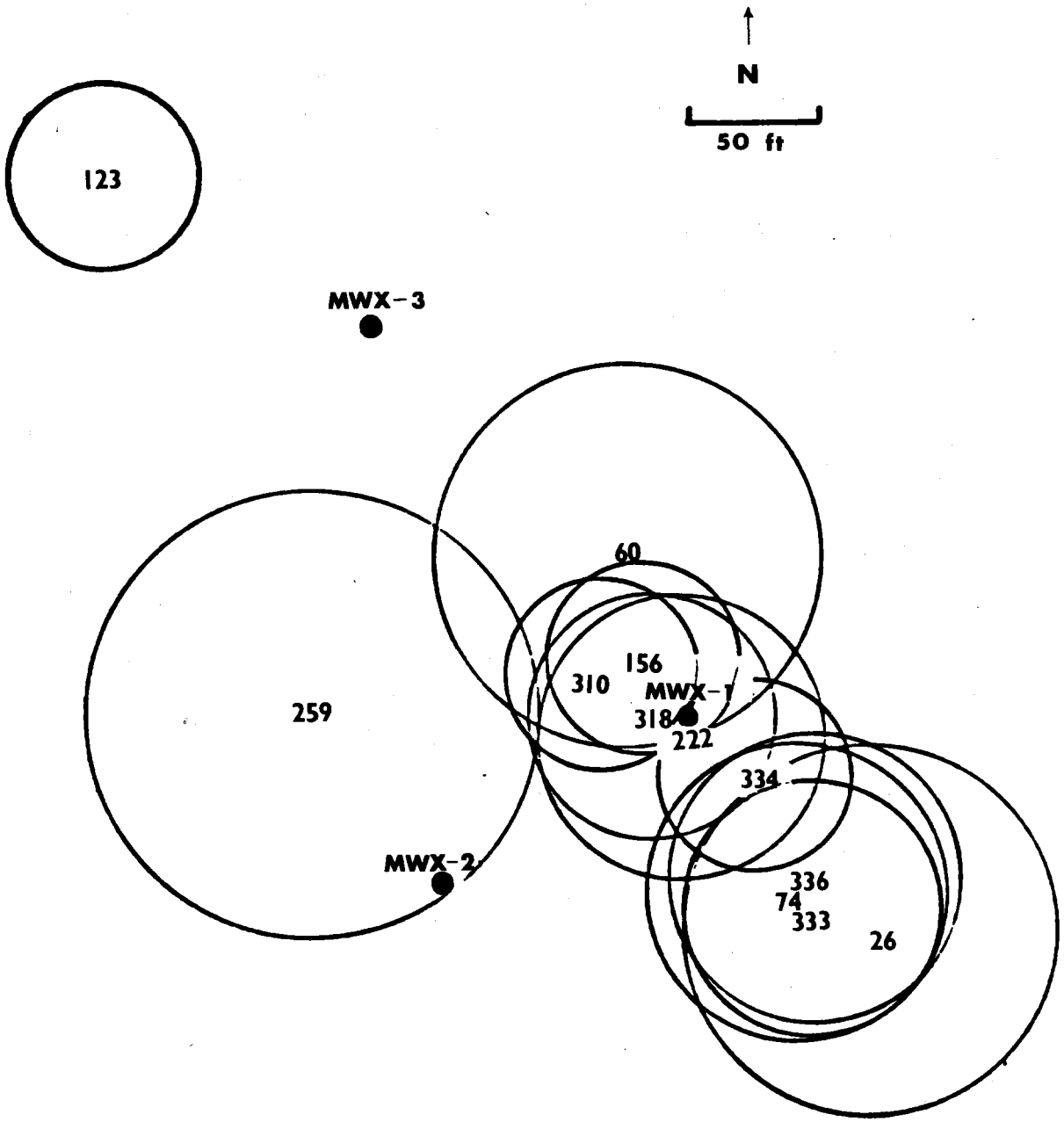

Figure 10.13. Event locations averaged from four methods. Radii of error circles are root mean squares of the deviations of the four contributing locations.

11.0 BIBLIOGRAPHY

S. J. Finley
Sandia National Laboratories

The technical output from the Multiwell Experiment resides in an MWX Data File which is maintained in the project office at Sandia National Laboratories in Albuquerque, NM.

The MWX Data File is intended to be "results-oriented." Thus, it includes such entries as (1) data reports from contractors and others, (2) memoranda, informal reports and compilations of results and analyses, (3) formal publications and reports, and (4) in limited cases, planning documents, review meeting summaries, etc. It is not intended to include every sheet of paper ever written on MWX or every bit of data taken. In general, these are entries which are referenceable and which convey data.

The MWX Data File has the following overall organization:

1.0 Well data by well
1.1 Well logs by well and logging program; analyses
1.2 Core and fluid analyses by type and performer
1.3 Core-log correlation
1.4 Geology by topic
1.5 Environmental
1.6 Geophysics by type
1.7 Stress testing by interval
1.8 Well testing by interval
1.9 Stimulation and fracture diagnostics by interval
3.1 General reviews and status reports
3.3 Quarterly reports
3.5 Topical meetings, displays and workshops
3.7 Technical Review Panel
3.8 Plans

A computer-based index to the MWX Data File is also maintained in which each entry is indexed by accession number, data file number, author(s), title, company, date, alternate report number, key word(s), and comments/notes. Thus, searches, retrieval, and summaries of various types can be made readily. Two listings from this index are presented:

(A) A listing is given in this section of publications and formal reports which include information on the paludal interval. (These are selected from the index through the key words "formal" and "paludal.")

(B) A listing of the complete MWX Data File index data is given in Appendix 12.9 for those entries which contain results for the paludal interval.

PALUDAL FORMAL REPORTS

****
ACCES NUM N00648
REPORT NUM 1.8.1.007
AUTHOR **BRANAGAN,P**
AUTHOR **CIPOLLA,C**
AUTHOR **LEE,SJ**
TITLE *COMPREHENSIVE WELL TESTING AND MODELING OF PRE AND POST FRACTURE WELL PERFORMANCE OF THE MWX LENTICULAR TIGHT GAS SANDS*
CORP AUTH CER
DATE 850519
ALT NUMBER SPEDOE13867
NOTES PRESENTED AT THE SPEDOE 1985 LOW PERMEABILITY GAS RESERVOIRS MEETING IN DENVER CO, MAY 19-22,1985
****
ACCES NUM N00318
REPORT NUM 1.8.0.007
AUTHOR **BRANAGAN,P**
AUTHOR **LEE,SJ**
AUTHOR **WILMER,R**
TITLE *WELL TESTING AND RESERVOIR EVALUATION (2.16)*
CORP AUTH CER
DATE 831018
ALT NUMBER DOEMETC843
NOTES TECHNICAL PROCEEDINGS OF THE WESTERN GAS SANDS SUBPROGRAM REVIEW, MORGANTOWN, WV, OCTOBER 18-19, 1983
****
ACCES NUM N00301
REPORT NUM 1.4.2.012
AUTHOR **EATOUGH,MO**
TITLE *MINERALOGIC AND PETROLOGIC OVERVIEW OF CORE SAMPLES FROM THE DEPT. OF ENERGY'S WESTERN GAS SANDS PROJECT MULTIWELL EXPERIMENT, PICEANCE BASIN, COLORADO*
CORP AUTH BENDIX
DATE 830300
ALT NUMBER SPEDOE11764
NOTES THIS PAPER WAS PRESENTED AT THE 1983 SPE/DOE SYMPOSIUM ON LOW PERMEABILITY HELD IN DENVER, COLORADO, MARCH 14-16, 1983
****
ACCES NUM N00657
REPORT NUM 1.9.1.023
AUTHOR **GALL,BL**
AUTHOR **RAIBLE,CJ**
TITLE *MOLECULAR SIZE STUDIES OF DEGRADED FRACTURING FLUID POLYMERS*
CORP AUTH NIPER
DATE 850409
ALT NUMBER SPE13566
NOTES PRESENTED AT THE INTERNATIONAL SYMPOSIUM ON OILFIELD AND GEOTHERMAL CHEMISTRY HELD IN PHOENIX, ARIZONA, APRIL 9-11,1985
****
ACCES NUM N00322
REPORT NUM 1.9.1.019
AUTHOR **HART,CM**
AUTHOR **ENGI,D**

AUTHOR **FLEMING,RP**
AUTHOR **MORRIS,HE**
TITLE *FRACTURE DIAGNOSTICS RESULTS FOR THE MULTIWELL EXPERIMENT'S PALUDAL ZONE STIMULATION*
CORP AUTH SAND
DATE 840513
ALT NUMBER SPEDOEGRI12852
NOTES PAPER WAS PRESENTED AT THE 1984 SPE/DOE/GRI UNCONVENTIONAL GAS RECOVERY SYMPOSIUM HELD IN PITTSBURGH, PA, MAY 13-15, 1984

****

ACCES NUM N00308
REPORT NUM 1.4.2.013
AUTHOR **HEINZE,DM**
TITLE *MINERALOGY AND PETROLOGY ASPECTS OF THE MESAVERDE FORMATION AT RIFLE GAP, COLORADO, SPECIFIC TO THE SEDIMENTOLOGY AND GAS-BEARING INTERVALS IN THE SUBSURFACE*
DATE 830300
ALT NUMBER SAND830287

****

ACCES NUM N00602
REPORT NUM 1.8.1.005
AUTHOR **HORTON,AI**
TITLE *STATUS OF MULTIWELL EXPERIMENT RESERVOIR MODELING ANALYSIS, VOL. 1*
CORP AUTH METC
DATE 850200
ALT NUMBER DOE/METC-85/4007

****

ACCES NUM N00630
REPORT NUM 3.1.004
AUTHOR **KOMAR,CA**
TITLE *PROCEEDINGS OF THE UNCONVENTIONAL GAS RECOVERY CONTRACTORS MEETING*
CORP AUTH DOE
DATE 851100
ALT NUMBER DOE/METC-86/6034

****

ACCES NUM N00575
REPORT NUM 1.1.4.012
AUTHOR **KUKAL,GC**
TITLE *A SYSTEMATIC APPROACH FOR THE EFFECTIVE LOG ANALYSIS OF TIGHT GAS SANDS*
CORP AUTH CER
DATE 840500
ALT NUMBER SPEDOE12851
NOTES PRESENTED AT SPE/DOE/GRI UNCONVENTIONAL GAS RECOVERY SYMPOSIUM, MAY 13-15, 1984, PITTSBURGH PA

****

ACCES NUM N00574
REPORT NUM 1.1.4.011
AUTHOR **KUKAL,GC**
AUTHOR **SIMONS,KE**
TITLE *LOG ANALYSIS TECHNIQUES FOR QUANTIFYING THE PERMEABILITY OF SUB-MILLIDARCY SANDSTONE RESERVOIRS*
CORP AUTH CER
DATE 850500
ALT NUMBER SPEDOE13880
NOTES PRESENTED AT THE SPE/DOE 1985 LOW PERMEABILITY GAS RESERVOIR SYMPOSIUM DENVER, COLORADO, MAY 19-22 1985.

****

ACCES NUM N00160

REPORT NUM 1.6.2.002
AUTHOR **LEE,MW**
TITLE *VERTICAL SEISMIC PROFILES AT MULTI-WELL EXPERIMENT SITE, GARFIELD COUNTY, COLORADO*
CORP AUTH USGS
DATE 831100
ALT NUMBER USGS OPEN FILE REPORT 84-168
****
ACCES NUM NO0511
REPORT NUM 1.4.3.030
AUTHOR **LORENZ,JC**
TITLE *PREDICTIONS OF SIZE AND ORIENTATIONS OF LENTICULAR RESERVOIRS IN THE MESAVERDE GROUP, NORTHWESTERN COLORADO*
CORP AUTH SAND
DATE 850519
ALT NUMBER SPEDOE13851
****
ACCES NUM NO0294
REPORT NUM 1.4.3.033
AUTHOR **LORENZ,JC**
TITLE *SEDIMENTOLOGY OF THE MESAVERDE FORMATION AT RIFLE GAP, COLORADO AND IMPLICATIONS FOR GAS-BEARING INTERVALS IN THE SUBSURFACE*
DATE 820300
ALT NUMBER SAND820604
****
ACCES NUM NO0309
REPORT NUM 1.4.3.037
AUTHOR **LORENZ,JC**
TITLE *RESERVOIR SEDIMENTOLOGY IN MESAVERDE ROCKS AT THE MULTI-WELL EXPERIMENT SITE*
DATE 830600
ALT NUMBER SAND83-1078
****
ACCES NUM NO0671
REPORT NUM 1.4.5.013
AUTHOR **LORENZ,JC**
AUTHOR **BRANAGAN,P**
AUTHOR **WARPINSKI,NR**
AUTHOR **SATTLER,AR**
TITLE *FRACTURE CHARACTERISTICS AND RESERVOIR BEHAVIOR OF STRESS-SENSITIVE FRACTURE SYSTEMS IN FLAT-LYING LENTICULAR FORMATIONS*
CORP AUTH SAND
CORP AUTH CER
DATE 860518
ALT NUMBER SPE 15244
NOTES PRESENTED AT THE UNCONVENTIONAL GAS TECHNOLOGY SYMPOSIUM OF THE SOCIETY OF PETROLEUM ENGINEERS, LOUISVILLE, KY, MAY 18-21,1986
****
ACCES NUM NO0328
REPORT NUM 1.2.55.005
AUTHOR **MORROW,NR**
TITLE *RELATIONSHIP OF PORE STRUCTURE TO FLUID BEHAVIOR IN LOW PERMEABILITY GAS SANDS*
CORP AUTH NMPRRC
DATE 840500
ALT NUMBER NMERDI2703303
****
ACCES NUM NO0705
REPORT NUM 1.2.55.012

AUTHOR **MORROW,NR**
TITLE *RELATIONSHIP OF PORE STRUCTURE TO FLUID BEHAVIOR IN LOW PERMEABILITY GAS SANDS: YEAR THREE*
CORP AUTH NMPRRC
DATE 850200
ALT NUMBER NMERDI 2-72-4309
****
ACCES NUM N00447
REPORT NUM 1.2.55.004
AUTHOR **MORROW,NR**
AUTHOR **BROWER,KR**
AUTHOR **KILMER,NH**
TITLE *RELATIONSHIP OF PORE STRUCTURE TO FLUID BEHAVIOR IN LOW PERMEABILITY GAS SANDS*
CORP AUTH NMPRRC
DATE 820000
ALT NUMBER DOE BC 10216-14
****
ACCES NUM N00704
REPORT NUM 1.2.55.011
AUTHOR **MORROW,NR**
AUTHOR **BROWER,KR**
AUTHOR **KILMER,NH**
TITLE *RELATIONSHIP OF PORE STRUCTURE TO FLUID BEHAVIOR IN LOW PERMEABILITY GAS SANDS, 1984 FINAL REPORT*
CORP AUTH NMPRRC
DATE 840900
ALT NUMBER DOEBC10216-13
****
ACCES NUM N00669
REPORT NUM 1.2.55.009
AUTHOR **MORROW,NR**
AUTHOR **WARD,J**
AUTHOR **BROWER,KR**
TITLE *ROCK MATRIX AND FRACTURE ANALYSIS OF FLOW IN TIGHT GAS SANDS, 1985 ANNUAL REPORT*
CORP AUTH NMPRRC
DATE 860200
ALT NUMBER DOEMC21179-2032
****
ACCES NUM N00320
REPORT NUM 1.9.5.001
AUTHOR **NORTHROP,DA**
TITLE *MWX STIMULATION EXPERIMENTS (2.19)*
CORP AUTH SAND
DATE 831018
ALT NUMBER DOEMETC843
NOTES PRESENTED AT WGSS PROGRAM REVIEW, OCTOBER 18-19, 1983, MORGANTOWN, WV
****
ACCES NUM N00325
REPORT NUM 3.1.011
AUTHOR **NORTHROP,DA**
AUTHOR **SATTLER,AR**
AUTHOR **MANN,RL**
AUTHOR **FROHNE,KH**
TITLE *CURRENT STATUS OF THE MULTIWELL EXPERIMENT*
CORP AUTH SAND
CORP AUTH DOE
CORP AUTH CER

DATE 840513
ALT NUMBER SPEDOEGRI12868
NOTES PAPER WAS PRESENTED AT THE 1984 SPE/DOE/GRI UNCONVENTIONAL GAS RECOVERY SYMPOSIUM HELD IN PITTSBURGH, PA, MAY 13-15, 1984

****

ACCES NUM NO0643
REPORT NUM 1.9.1.020
AUTHOR **PALMER,ID**
AUTHOR **CRAIG,HR**
TITLE *MODELING OF ASYMMETRIC VERTICAL GROWTH IN ELONGATED HYDRAULIC FRACTURES AND APPLICATION TO FIRST MWX STIMULATION*
CORP AUTH ORU
DATE 840513
ALT NUMBER SPEDOEGRIOR
NOTES PRESENTED AT 1984 SPEDOEGRI UNCONVENTIONAL GAS RECOVERY SYMPOSIUM HELD IN PITTSBURGH PA, MAY 13-15,1984

****

ACCES NUM NO0470
REPORT NUM 1.4.3.026
AUTHOR **PETERSON,RE**
TITLE *GEOLOGICAL AND PRODUCTION CHARACTERISTICS OF THE NON-MARINE PART OF THE MESAVERDE GROUP, RULISON FIELD AREA,PICEANCE BASIN, COLORADO*
CORP AUTH CER
DATE 840514
ALT NUMBER SPE 12835

****

ACCES NUM NO0295
REPORT NUM 1.4.3.034
AUTHOR **PETERSON,RE**
TITLE *WESTERN GAS SANDS PROJECT: AN APPROXIMATION OF CONTINUITY OF LENTICULAR MESAVERDE SANDSTONE LENSES, UTILIZING CLOSE WELL CORRELATIONS, PICEANCE BASIN, NORTHWEST COLORADO*
CORP AUTH CER
DATE 821100
ALT NUMBER DOENV102493

****

ACCES NUM NO0305
REPORT NUM 1.4.3.035
AUTHOR **PETERSON,RE**
AUTHOR **KOHOUT,J**
TITLE *AN APPROXIMATION OF CONTINIUITY OF LENTICULAR MESAVERDE SANDSTONE LENSES UTILIZING CLOSE-WELL CORRELATIONS, PICEANCE BASIN, NORTHWESTERN COLORADO*
CORP AUTH CER
DATE 830300
ALT NUMBER SPEDOE11610
NOTES THIS PAPER WAS PRESENTED AT THE 1983 SPE/DOE SYMPOSIUM ON LOW PERMEABILITY HELD IN DENVER, COLORADO, MARCH 14-16, 1983

****

ACCES NUM NO0300
REPORT NUM 1.2.12.020
AUTHOR **RANDOLPH,PL**
TITLE *POROSITY AND PERMEABILITY OF MESAVERDE SANDSTONE CORE FROM THE U.S. DOE MULTIWELL EXPERIMENT, GARFIELD COUNTRY, COLORADO*
CORP AUTH IGT
DATE 830300
ALT NUMBER SPEDOE11765
NOTES THIS PAPER WAS PRESENTED AT THE 1983 SPE/DOE SYMPOSIUM ON LOW PERMEABILITY HELD IN DENVER, COLORADO, MARCH 14-16, 1983

****
ACCES NUM NO0496
REPORT NUM 1.2.12.019
AUTHOR **RANDOLPH,PL**
AUTHOR **SOEDER,DJ**
AUTHOR **CHOWDIAH,P**
TITLE *EFFECTS OF WATER AND STRESS UPON PERMEABILITY TO GAS OF PALUDAL AND COASTAL SANDS; U.S. DOE MULTIWELL EXPERIMENT*
CORP AUTH IGT
DATE 850400
ALT NUMBER DOE/MC/20342-7
NOTES IGT PROJECT 61071 TOPICAL REPORT FOR USDOE/METC DECEMBER 1983-JULY 1984
****
ACCES NUM NO0326
REPORT NUM 1.2.12.021
AUTHOR **RANDOLPH,PL**
AUTHOR **SOEDER,DJ**
AUTHOR **CHOWDIAH,P**
TITLE *POROSITY AND PERMEABILITY OF TIGHT SANDS*
CORP AUTH IGT
DATE 840513
ALT NUMBER SPEDOEGRI12836
NOTES PRESENTED AT THE 1984 SPE/DOE/GRI UNCONVENTIONAL GAS RECOVERY SYMPOSIUM, PITTSBURGH, PENNSYLVANIA, MAY 13-15, 1984
****
ACCES NUM NO0672
REPORT NUM 1.2.62.017
AUTHOR **SATTLER,AR**
AUTHOR **HUDSON,PJ**
AUTHOR **RAIBLE,CJ**
AUTHOR **GALL,BL**
AUTHOR **MALONEY,D**
TITLE *LABORATORY STUDIES FOR THE DESIGN AND ANALYSIS OF HYDRAULIC FRACTURED STIMULATIONS IN LENTICULAR, TIGHT GAS RESERVOIRS*
CORP AUTH SAND
CORP AUTH DOWELL
CORP AUTH NIPER
DATE 860518
ALT NUMBER SPE 15245
NOTES THIS PAPER WAS PRESENTED AT THE UNCONVENTIONAL GAS TECHNOLOGY SYMPOSIUM OF THE SOCIETY OF PETROLEUM ENGINEERS HELD IN LOUISVILLE, KENTUCKY, MAY 1
****
ACCES NUM NO0512
REPORT NUM 1.2.61.011
AUTHOR **SATTLER,AR**
AUTHOR **RAIBLE,CJ**
AUTHOR **GALL,BL**
TITLE *INTEGRATION OF LABORATORY AND FIELD DATA FOR INSIGHT ON THE MULTIWELL EXPERIMENT PALUDAL STIMULATION*
CORP AUTH SAND
CORP AUTH NIPER
DATE 850519
ALT NUMBER SPEDOE 13891
****
ACCES NUM NO0572
REPORT NUM 1.6.4.002
AUTHOR **SEARLS,CA**
TITLE *THE MULTIWELL EXPERIMENT GEOPHYSICS PROGRAM FINAL REPORT*

CORP AUTH SAND
DATE 850900
ALT NUMBER SAND 85-1013
****
ACCES NUM N00297
REPORT NUM 1.6.4.003
AUTHOR SEARLS,CA
AUTHOR LEE,MW
AUTHOR MILLER,JJ
AUTHOR ALBRIGHT,JN
AUTHOR FRIED,J
AUTHOR APPLEGATE,JK
TITLE A COORDINATED SEISMIC STUDY OF THE MULTI-WELL EXPERIMENT SITE
CORP AUTH SAND
CORP AUTH USGS
CORP AUTH LANL
CORP AUTH CSM
DATE 830300
ALT NUMBER SPEDOE11613
NOTES THIS PAPER WAS PRESENTED AT THE 1983 SPE/DOE SYMPOSIUM ON LOW PERMEABILITY HELD IN DENVER, COLORADO, MARCH 14-16, 1983
****
ACCES NUM N00302
REPORT NUM 1.2.25.018
AUTHOR SENSENY,PE
TITLE LABORATORY MEASUREMENTS OF MECHANICAL PROPERTIES OF SANDSTONES AND SHALES
CORP AUTH RSI
ALT NUMBER SPEDOE11762
NOTES THIS PAPER WAS PRESENTED AT THE 1983 SPE/DOE SYMPOSIUM ON LOW PERMEABILITY HELD IN DENVER, COLORADO, MARCH 14-16, 1983
****
ACCES NUM N00329
REPORT NUM 1.2.12.022
AUTHOR SOEDER,DJ
AUTHOR RANDOLPH,PL
TITLE POROSITY, PERMEABILITY AND PORE STRUCTURE OF THE TIGHT MESA VERDE SANDSTONE, PICEANCE BASIN, COLORADO
CORP AUTH IGT
DATE 840916
ALT NUMBER SPE13134
NOTES PRESENTED AT THE 59TH ANNUAL TECHNICAL CONFERENCE AND EXHIBITION HELD IN HOUSTON, TEXAS, SEPTEMBER 16-19, 1984
****
ACCES NUM N00474
REPORT NUM 1.4.5.003
AUTHOR SPENCER,CW
AUTHOR KEIGHIN,CW
TITLE GEOLOGIC STUDIES IN SUPPORT OF THE U.S. DOE'S MULTI-WELL EXPERIMENT,GARFIELD COUNTY, COLORADO.
CORP AUTH USGS
DATE 841100
ALT NUMBER OFR 84757
NOTES SUMMARY OF USGS WORK ON MWX
****
ACCES NUM N00513
REPORT NUM 1.9.5.004
AUTHOR TEUFEL,LW
AUTHOR HART,CM
AUTHOR SATTLER,AR

AUTHOR **CLARK,JA**
TITLE *DETERMINATION OF HYDRAULIC FRACTURE AZIMUTH BY GEOPHYSICAL, GEOLOGICAL, AND ORIENTED CORE METHODS AT THE MULTI-WELL EXPERIMENT SITE, RIFLE, CO.*
CORP AUTH SAND
DATE 840916
ALT NUMBER SPE 13226
NOTES PRESENTED AT THE 59TH ANNUAL SPE MEETING HOUSTON TX, SEPTEMBER,1984

****

ACCES NUM N00444
REPORT NUM 1.2.55.003
AUTHOR **WARD,J**
AUTHOR **MORROW,NR**
TITLE *MULTI-WELL SPECIAL CORE ANALYSIS*
CORP AUTH NMPRRC
DATE 841001
ALT NUMBER PRRC 84-25

****

ACCES NUM N00647
REPORT NUM 1.2.55.006
AUTHOR **WARD,J**
AUTHOR **MORROW,NR**
TITLE *CAPILLARY PRESSURES AND GAS RELATIVE PERMEABILITIES OF LOW PERMEABILITY SANDSTONE*
CORP AUTH NMPRRC
DATE 850519
ALT NUMBER SPEDOE13882
NOTES PRESENTED AT THE SPEDOE 1985 LOW PERMEABILITY RESERVOIRS MEETING IN DENVER CO, MAY 19-22,1985

****

ACCES NUM N00311
REPORT NUM 1.7.0.008
AUTHOR **WARPINSKI,NR**
AUTHOR **BRANAGAN,P**
AUTHOR **WILMER,R**
TITLE *IN-SITU STRESS MEASUREMENTS AT DOE'S MULTIWELL EXPERIMENT SITE, MESAVERDE GROUP, RIFLE, COLORADO*
CORP AUTH CER
CORP AUTH SAND
DATE 831005
ALT NUMBER SPE12142
NOTES PRESENTED AT THE 58TH ANNUAL TECHNICAL CONFERENCE AND EXHIBITION HELD IN SAN FRANCISCO, CA, OCTOBER 5-8, 1983.

****

ACCES NUM N00267
REPORT NUM 1.7.0.004
AUTHOR **WARPINSKI,NR**
AUTHOR **BRANAGAN,P**
AUTHOR **WILMER,R**
TITLE *IN SITU STRESS MEASUREMENTS AT DOE'S MULTI-WELL EXPERIMENT*
CORP AUTH CER
CORP AUTH SAND
DATE 840100
NOTES WESTERN GAS SANDS SUBPROGRAM REVIEW TECHNICAL PROCEEDINGS DOE/METC/84-3, JANUARY 1984

****

ACCES NUM N00510
REPORT NUM 1.9.1.018
AUTHOR **WARPINSKI,NR**

AUTHOR **SATTLER,AR**
AUTHOR **BRANAGAN,P**
AUTHOR **LORENZ,JC**
AUTHOR **NORTHROP,DA**
AUTHOR **MANN,RL**
AUTHOR **FROHNE,KH**
TITLE *FRACTURING AND TESTING CASE STUDY OF PALUDAL, TIGHT, LENTICULAR GAS SANDS*
CORP AUTH SAND
CORP AUTH CER
CORP AUTH DOE
DATE 850519
ALT NUMBER SPE/DOE13876
****
ACCES NUM N00759
REPORT NUM 1.7.5.002
AUTHOR **WARPINSKI,NR**
AUTHOR **TEUFEL,LW**
TITLE *IN SITU STRESSES IN LOW PERMEABILITY, NONMARINE ROCKS*
CORP AUTH SANDIA
DATE 870518
ALT NUM SPEDOE 16402
NOTES PRESENTED AT THE 1987 SPEDOE JOINT SYMPOSIUM ON LOW PERMEABILITY RESERVOIRS, MAY 18-19,1987, DENVER,CO.

12.0 APPENDICES

The following appendices appear as microfiche in pocket on back cover:

12.1 Geophysics Final Report, C. A. Searls (Sandia)

12.2 Petrographic Data Sheets (Bendix)

12.3 Paludal Log Report, G. C. Kukal (CER)

12.3.1 Spectral Gamma Logs

12.4 Core Laboratories Data

12.5 Institute of Gas Technology (IGT) Data

12.6 RESPEC Data

12.7 Well Test Data (CER)

12.7.1 Zone 2

12.7.2 Zones 3 and 4: Prefrac

12.7.3 Zones 3 and 4: Interim

12.7.4 Zones 3 and 4: Postfrac

12.7.5 Zones 3 and 4: Reentry

12.8 Phase II Liquid Recovery and Analyses (CER)

12.9 Paludal MWX Data File Entries, S. J. Finley (Sandia)

DISTRIBUTION:

M. J. Singer
Deputy Assistant Secretary for Oil, Gas, Shale, and Special Technologies
US Department of Energy
D-121, FE/33 (GTN)
Washington, DC 20545

J. D. Batchelor
Office of Oil, Gas, and Shale Technologies
US Department of Energy
FE/25 (GTN)
Washington, DC 20545

J. R. White
Office of Oil, Gas and Shale Technologies
US Department of Energy
D-127 FE/33 (GTN)
Washington, DC 20545

US Department of Energy (9)
Morgantown Energy Technology Center
Box 880 Collins Ferry Road
Morgantown, WV 26505
Attn: A. A. Pitrolo
H. D. Guthrie
C. A. Komar
K-H. Frohne (3)
G. Latham
A. Layne
J. K. Westhusing

US Department of Energy (3)
Bartlesville Project Office
PO Box 1398
Bartlesville, OK 74005
Attn: T. C. Wesson

F. Heuze
Lawrence Livermore National Laboratory
MS L200
Livermore, CA 94550

J. A. Albright
Earth & Space Science Division
ESS-4
Los Alamos National Laboratory
Los Alamos, NM 87545

US Geological Survey (3)
Box 25046
Denver Federal Center
Denver, CO 80225
Attn: B. E. Law, MS 971
C. W. Spencer, MS 940
R. Johnson, MS 971

CER Corporation (30)
PO Box 15090
Las Vegas, NV 89114
Attn: R. L. Mann (25)
F. R. Myal
P. T. Branagan
G. C. Kukal
W. H. Mathis
C. Cipolla

L. F. Elkins
2615 Oak Drive, #28
Lakewood, CO 80215

J. L. Fitch
6034 Walnut Hill Circle
Dallas, TX 75230

T. Kirst
Mobil Oil Corp.
25737 Foothills Drive North
Golden, CO 80401

F. G. Martin
907 Glendell Drive
Irving, TX 75061

D. E. Nierode
Exxon Production Research Co.
PO Box 2189
Houston, TX 77001

R. J. Saucier
Shell Western E&P
Suite No. 7560
PO Box 576
Houston, TX 77001

Mobil Research and Development
Corp. (4)
PO Box 819047
Dallas, TX 75381
Attn: M. Strubhar
L. Medlin
E. Sprunt
I. Abou-Sayed

R. W. Veatch
Amoco Production Co.
Research Department
PO Box 3385
Tulsa, OK 74102

R. Veghte
Chandler & Associates
Suite 1400
1860 Lincoln Street
Denver, CO 80203

National Institute for Petroleum
and Energy Research (3)
PO Box 2128
Bartlesville, OK 74005
Attn: H. B. Carroll
C. J. Raible
B. L. Gall

Smith Energy Services (2)
R. D. Timberline Building
Junction Hwys 58 & 93
Golden, CO 80403
Attn: D. Holcomb
W. Holcomb

L. Harrington
The Western Company
PO Box 186
Fort Worth, TX 76101

Dowell Schlumberger
Research Center (4)
PO Box 2710
Tulsa, OK 74101
Attn: J. Elbel
J. McClennan
B. Ainley
K. Nimerick

P. Warembourg
Dowell Schlumberger
PO Box 5818
Denver, CO 80217

M. Brugler
Western Atlas International
Core Laboratories
7304 E 38th Street
Tulsa, OK 74145

S. Leeds
Western Atlas International
Core Laboratories
10703 E. Bethany Drive
Aurora, CO 80014

Western Atlas International (4)
Core Laboratories
1300 East Rochelle Blvd.
Irving, TX 75062
Attn: J. Walls
R. Jenkins
H. Hunt
E. York

P. Senseny
RE/SPEC, INC.
PO Box 725
Rapid City, SD 57701

United Nuclear Services (2)
PO Box 1569
Grand Junction, CO 81501
Attn: L. Fukui
R. Dayvault

Institute of Gas Technology (2)
3424 S. State Street
Chicago, IL 60616
Attn: P. L. Randolph
D. J. Soeder

Petroleum Recovery
Research Center (2)
NM Institute of Mining and
Technology
Socorro, NM 87801
Attn: F. D. Martin
N. R. Morrow

Gas Research Institute (4)
8600 West Bryn Mawr Avenue
Chicago, IL 60631
Attn: P. A. O'Shea
I. A. Salehi
C. F. Brandenberg
L. A. Rogers

S. A. Holditch
S. A. Holditch and Assoc. Inc.
3833 Texas Avenue, Suite 200
Bryan, TX 77801

C. Ossian
ARCO Oil & Gas
PRC G118
Research & Technical Services
2300 West Plano Parkway
Plano, TX 75075

B. McGlothlin
Chevron Geosciences Co.
PO Box 42832
Houston, TX 77242

CNG Producing Co. (2)
PO Box 2115
Tulsa, OK 74101-2115
Attn: B. Coffin
T. L. Reeves

D. Pellatz
Conoco Inc.
907 N. Poplar
Casper, WY 82601

D. Munson
David Munson Inc.
1525 Elm Street, Suite 1900
Dallas, TX 75201

M. Smith
NSI Technologies, Inc.
7030 Yale, Suite 502
Tulsa, OK 74136

J. Schwoebel
Resource Enterprises, Inc.
400 Wakara Way
Salt Lake City, UT 84108

D. L. Luffel
ResTech Houston
14411 Cornerstone Village Drive
Houston, TX 77014

R. E. Barba
Schlumberger
1031 Andrews Highway
Midland, TX 79701

R. A. Plumb
Schlumberger-Doll Research
Old Quarry Road
PO Box 307
Ridgefield, CT 06877

Shell Development Co. (2)
Bellaire Research Center
PO Box 481
Houston, TX 77001
Attn: K. Hansen
J. Shlyapobersky

M. Conway
Stim-Lab, Inc.
3445 N. Hwy 81
Duncan, OK 73534

G. R. Coulter
Sun Exploration and Production Company
Four NorthPark East
PO Box 2880
Dallas, TX 75221-2880

A. Jones
Terra Tek Inc.
420 Wakara Way
Salt Lake City, UT 84108

Union Oil Co. of California (4)
Research Department
PO Box 76
Brea, CA 92621
Attn: C. Allen
J. Smith
J. Cameron
W. Minner

W. Stoner
Universal Well Services, Inc.
159 Northwood Dr.
Box 1456
Meadville, PA 16335

R. E. Wyman
Canadian Hunter Exploration, Ltd.
435 4th Avenue SW
Calgary, Alberta T2P 3A8
Canada

R. Kry
Esso Resources Canada Limited
Research Department
339 50th Avenue SE
Calgary, Alberta T2G 2B3
Canada

L. Roodhart
Shell Candada Ltd.
PO Box 2506
Calgary, Alberta T2P 3S6
Canada

W. Hansen
Amoco Production Co.
1670 Broadway
Denver, CO 80202

S. Stone
Amoco Production Company
PO Box 800
Denver, CO 80201

D. O. Cox
Angus Petrotech
Corp.
14062 Denver West parkway
Suite 200
Golden, CO 80401

Barrett Energy Company (2)
1125 17th Street, Suite 2100
Denver, CO 80202
Attn: W. J. Barrett
K. Reinecke

J. N. Burkhalter
Burkhalter Engineering Inc.
715 Horizon Drive
Suite 330
Grand Junction, CO 81506

R. Martin
Coors Energy Company
PO Box 467
Golden, CO 80402

E. L. Sampson
Coseka Resources (USA) Ltd.
200 Writer Square
1512 Larimer Street
Denver, CO 80202-1602

R. Moore
Exxon Company USA
PO Box 120
Denver, CO 80201

F. M. Moore
Pancanadian Petroleum Co.
600 17th Street, Suite 1800
Denver, CO 80202

W. H. Pease, Jr.
Willard Pease Oil and Gas Company
PO Box 1874
Grand Junction, CO 81502

R. Poppe
Poppe Engineering
6066 E. Long Place
Englewood, CO 80112

T. Logan
Resource Enterprises, Inc.
743 Horizon Court, Suite 203
Grand Junction, CO 81506

R. E. Chancellor
Rio Blanco Natural Gas Company
621 17th Street, Suite 1255
Denver, CO 80293

S. M. Struna
Tenneco Oil Company
PO Box 3249
Englewood, CO 80293

T. Barrett
Terred Oil Company
518 17th Street, Suite 770
Denver, CO 80202

J. D. Haley
Van Pollen and Haley, Inc.
5601 S. Broadway, Suite 400
Littleton, CO 80121

M. Krey
133 N. 8th Street
Grand Junction, CO 81505

J. A. Morel
Consultant
2792 S. Fillmore Street
Denver, CO 80210

R. Hunter
Bureau of Land Management
Horizon Drive
Grand Junction, CO 81505

B. Kelso
Colorado Geological Survey
Department of Natural Resources
1313 Sherman Street Rm 715
Denver, CO 80203

Colorado Oil & Gas Commission
1580 Logan Street, Suite 380
Denver, CO 80203

Petroleum Information Services
PO Box 2610
Denver, CO 80201-2612

J. W. Crafton
Petroleum Engineering Dept.
Colorado School of Mines
Golden, CO 80401

J. Johnson
Department of Geology
Mesa College
Grand Junction, CO 81501

A. H. Harvey
Petroleum Engineering Dept.
University of Missouri at Rolla
Rolla, MO 65401

Department of Geology (2)
University of New Mexico
Albuquerque, NM 87131
Attn: L. Crossey
R. Wright

C. T. Luiskutty
Engineering and Physics Dept.
Oral Roberts University
Tulsa, OK 74171

N. Tyler
Bureau of Economic Geology
University of Texas at Austin
Austin, TX 78713

C. G. Guffey
Texas Tech University
PO Box 4099
Lubbock, TX 79409

E. Rybicki
Mechanical Engineering Dept.
University of Tulsa
Tulsa, OK 74104

K. Aminian
West Virginia University
PO Box 6070, 213 White Hall
Morgantown, WV 26506

D. Hambley
Argonne National Laboratory
EES-362, 9700 S. Cass Avenue
Argonne, IL 60439

P. L. Archer
Battelle
505 King Avenue
Columbus, OH 43201

W. K. Overby
BDM Corporation
789 South Hills Drive
Morgantown, WV 26505

V. A. Kuuskraa
ICF-Lewin Energy Division
9300 Lee Highway
Fairfax, VA 22031-1207

6000	D. L. Hartley
6200	V. L. Dugan
6210	B. W. Marshall
6213	D. Engi
6230	W. C. Luth
6232	W. R. Wawersik
6232	L. W. Teufel
6250	R. K. Traeger
6252	J. C. Dunn
6253	D. A. Northrop (30)
6253	S. J. Finley
6253	J. C. Lorenz (5)
6253	A. R. Sattler (5)
6253	N. R. Warpinski (5)
6253	MWX File
6257	J. K. Linn
6258	P. J. Hommert
6258	B. J. Thorne
6258	H. E. Morris
9114	C. A. Searls
3141	S. A. Landenberger (5)
3151	W. L. Garner (3)
3154-1	C. H. Dalin (8) for DOE/OSTI
8524	P. W. Dean